The background of the entire page features a stylized brain composed of various colored segments (yellow, orange, red, purple, blue, green) arranged in a circular pattern. Overlaid on this brain is a network of white lines connecting small grey dots, representing a neural or molecular network. The top half of the image has a solid blue background.

# NEURODEGENERATION: FROM GENETICS TO MOLECULES, VOLUME II

EDITED BY: Victoria Campos-Peña, Oscar Rosas-Carrasco,  
Karla Guadalupe Carvajal and Rocío Martínez De Pablos  
PUBLISHED IN: Frontiers in Cellular Neuroscience



# frontiers

## Frontiers eBook Copyright Statement

The copyright in the text of individual articles in this eBook is the property of their respective authors or their respective institutions or funders. The copyright in graphics and images within each article may be subject to copyright of other parties. In both cases this is subject to a license granted to Frontiers.

The compilation of articles constituting this eBook is the property of Frontiers.

Each article within this eBook, and the eBook itself, are published under the most recent version of the Creative Commons CC-BY licence.

The version current at the date of publication of this eBook is CC-BY 4.0. If the CC-BY licence is updated, the licence granted by Frontiers is automatically updated to the new version.

When exercising any right under the CC-BY licence, Frontiers must be attributed as the original publisher of the article or eBook, as applicable.

Authors have the responsibility of ensuring that any graphics or other materials which are the property of others may be included in the CC-BY licence, but this should be checked before relying on the CC-BY licence to reproduce those materials. Any copyright notices relating to those materials must be complied with.

Copyright and source acknowledgement notices may not be removed and must be displayed in any copy, derivative work or partial copy which includes the elements in question.

All copyright, and all rights therein, are protected by national and international copyright laws. The above represents a summary only. For further information please read Frontiers' Conditions for Website Use and Copyright Statement, and the applicable CC-BY licence.

ISSN 1664-8714

ISBN 978-2-88974-149-6

DOI 10.3389/978-2-88974-149-6

## About Frontiers

Frontiers is more than just an open-access publisher of scholarly articles: it is a pioneering approach to the world of academia, radically improving the way scholarly research is managed. The grand vision of Frontiers is a world where all people have an equal opportunity to seek, share and generate knowledge. Frontiers provides immediate and permanent online open access to all its publications, but this alone is not enough to realize our grand goals.

## Frontiers Journal Series

The Frontiers Journal Series is a multi-tier and interdisciplinary set of open-access, online journals, promising a paradigm shift from the current review, selection and dissemination processes in academic publishing. All Frontiers journals are driven by researchers for researchers; therefore, they constitute a service to the scholarly community. At the same time, the Frontiers Journal Series operates on a revolutionary invention, the tiered publishing system, initially addressing specific communities of scholars, and gradually climbing up to broader public understanding, thus serving the interests of the lay society, too.

## Dedication to Quality

Each Frontiers article is a landmark of the highest quality, thanks to genuinely collaborative interactions between authors and review editors, who include some of the world's best academicians. Research must be certified by peers before entering a stream of knowledge that may eventually reach the public - and shape society; therefore, Frontiers only applies the most rigorous and unbiased reviews.

Frontiers revolutionizes research publishing by freely delivering the most outstanding research, evaluated with no bias from both the academic and social point of view. By applying the most advanced information technologies, Frontiers is catapulting scholarly publishing into a new generation.

## What are Frontiers Research Topics?

Frontiers Research Topics are very popular trademarks of the Frontiers Journals Series: they are collections of at least ten articles, all centered on a particular subject. With their unique mix of varied contributions from Original Research to Review Articles, Frontiers Research Topics unify the most influential researchers, the latest key findings and historical advances in a hot research area! Find out more on how to host your own Frontiers Research Topic or contribute to one as an author by contacting the Frontiers Editorial Office: [frontiersin.org/about/contact](https://frontiersin.org/about/contact)



# NEURODEGENERATION: FROM GENETICS TO MOLECULES, VOLUME II

Topic Editors:

**Victoria Campos-Peña**, Manuel Velasco Suárez Instituto Nacional de Neurología y Neurocirugía, Mexico

**Oscar Rosas-Carrasco**, Ibero American University, Mexico

**Karla Guadalupe Carvajal**, National Institute of Pediatrics (Mexico), Mexico

**Rocío Martínez De Pablos**, Sevilla University, Spain

**Citation:** Campos-Peña, V., Rosas-Carrasco, O., Carvajal, K. G., De Pablos, R. M., eds. (2022). Neurodegeneration: From Genetics to Molecules, Volume II. Lausanne: Frontiers Media SA. doi: 10.3389/978-2-88974-149-6

# Table of Contents

- 05 Editorial: Neurodegeneration: From Genetics to Molecules (Part II)**  
Karla Guadalupe Carvajal, Rocío Martínez De Pablos and Victoria Campos-Peña
- 09 Early Post-stroke Activation of Vascular Endothelial Growth Factor Receptor 2 Hinders the Receptor 1-Dependent Neuroprotection Afforded by the Endogenous Ligand**  
Alfredo Cárdenas-Rivera, Aura N. Campero-Romero, Yessica Heras-Romero, Andrés Penagos-Puig, Ruth Rincón-Heredia and Luis B. Tovar-y-Romo
- 24 TMP21 in Alzheimer's Disease: Molecular Mechanisms and a Potential Target**  
Kaixin Qiu, Xiaojie Zhang, Shuai Wang, Chunyan Li, Xin Wang, Xuezhi Li and Yili Wu
- 32 Systemic L-Buthionine -S-R-Sulfoximine Treatment Increases Plasma NGF and Upregulates L-cys/L-cys2 Transporter and  $\gamma$ -Glutamylcysteine Ligase mRNAs Through the NGF/TrkA/Akt/Nrf2 Pathway in the Striatum**  
Cesar Valdovinos-Flores, Jorge H. Limón-Pacheco, Renato León-Rodríguez, Pavel Petrosyan, Carla Garza-Lombó and Maria E. Gonsebatt
- 45 RAD6B Plays a Critical Role in Neuronal DNA Damage Response to Resist Neurodegeneration**  
Zhao Guo, Yingxia Tian, Yingli Guo, Boya Li, Xiangwen Liu, Kun Xie, Yanfeng Song and Degui Wang
- 58 Distinct Signaling Pathways Regulate TREM2 Phagocytic and NF $\kappa$ B Antagonistic Activities**  
Hailan Yao, Kyle Coppola, Jonas Elias Schweig, Fiona Crawford, Michael Mullan and Daniel Paris
- 76 Maresin 1 Improves Cognitive Decline and Ameliorates Inflammation in a Mouse Model of Alzheimer's Disease**  
Ping Yin, Xu Wang, Shuang Wang, Yafen Wei, Jiachun Feng and Mingqin Zhu
- 89 Brainiac Caspases: Beyond the Wall of Apoptosis**  
Ana María Espinosa-Oliva, Juan García-Revilla, Isabel María Alonso-Bellido and Miguel Angel Burguillos
- 98 Pharmacological Targeting of Microglial Activation: New Therapeutic Approach**  
Cai-Yun Liu, Xu Wang, Chang Liu and Hong-Liang Zhang
- 117 The Rules of Engagement: Do Microglia Seal the Fate in the Inverse Relation of Glioma and Alzheimer's Disease?**  
Mathilde Cheray, Vassilis Stratoulis, Bertrand Joseph and Kathleen Grabert

- 126 ***Increased Inflammation and Unchanged Density of Synaptic Vesicle Glycoprotein 2A (SV2A) in the Postmortem Frontal Cortex of Alzheimer's Disease Patients***  
Athanasios Metaxas, Camilla Thygesen, Sanne R. R. Briting, Anne M. Landau, Sultan Darvesh and Bente Finsen
- 134 ***Neuroprotective Effect of AM404 Against NMDA-Induced Hippocampal Excitotoxicity***  
Soraya Wilke Saliba, Tiziana Bonifacino, Tsvetan Serchov, Giambattista Bonanno, Antônio Carlos Pinheiro de Oliveira and Bernd L. Fiebich
- 144 ***Early Neurotoxic Effects of Inorganic Arsenic Modulate Cortical GSH Levels Associated With the Activation of the Nrf2 and NF $\kappa$ B Pathways, Expression of Amino Acid Transporters and NMDA Receptors and the Production of Hydrogen Sulfide***  
Daniela Silva-Adaya, Lucio Antonio Ramos-Chávez, Pavel Petrosyan, Wendy Leslie González-Alfonso, Alegna Pérez-Acosta and Maria E. Gonsebatt
- 154 ***Application of Iron Oxide Nanoparticles in the Diagnosis and Treatment of Neurodegenerative Diseases With Emphasis on Alzheimer's Disease***  
Shen Luo, Chi Ma, Ming-Qin Zhu, Wei-Na Ju, Yu Yang and Xu Wang
- 165 ***Proteostasis of  $\alpha$ -Synuclein and Its Role in the Pathogenesis of Parkinson's Disease***  
Deqiang Han, Wei Zheng, Xueyao Wang and Zhiguo Chen
- 175 ***GSK3 $\beta$  and Tau Protein in Alzheimer's Disease and Epilepsy***  
Danira Toral-Rios, Pavel S. Pichardo-Rojas, Mario Alonso-Vanegas and Victoria Campos-Peña
- 184 ***Methylene Blue Preserves Cytochrome Oxidase Activity and Prevents Neurodegeneration and Memory Impairment in Rats With Chronic Cerebral Hypoperfusion***  
Allison M. Auchter, Douglas W. Barrett, Marie H. Monfils and F. Gonzalez-Lima
- 201 ***PHF-Core Tau as the Potential Initiating Event for Tau Pathology in Alzheimer's Disease***  
Nabil Itzi Luna-Viramontes, B. Berenice Campa-Córdoba, Miguel Ángel Ontiveros-Torres, Charles R. Harrington, Ignacio Villanueva-Fierro, Parménides Guadarrama-Ortiz, Linda Garcés-Ramírez, Fidel de la Cruz, Mario Hernandez-Alejandro, Sandra Martínez-Robles, Erik González-Ballesteros, Mar Pacheco-Herrero and José Luna-Muñoz



# Editorial: Neurodegeneration: From Genetics to Molecules (Part II)

Karla Guadalupe Carvajal<sup>1</sup>, Rocío Martínez De Pablos<sup>2</sup> and Victoria Campos-Peña<sup>3\*</sup>

<sup>1</sup> Laboratorio de Nutrición Experimental, Instituto Nacional de Pediatría, Mexico City, Mexico, <sup>2</sup> Department of Biochemistry and Molecular Biology, Faculty of Pharmacy, University of Seville, Seville, Spain, <sup>3</sup> Laboratorio Experimental de Enfermedades Neurodegenerativas, Instituto Nacional de Neurología y Neurocirugía, Manuel Velasco Suárez, Mexico City, Mexico

**Keywords:** neurodegeneration, oxidative stress, reactive oxygen species, dementia, inflammation

## Editorial on the Research Topic

### Neurodegeneration: From Genetics to Molecules (Part II)

Among non-transmissible chronic diseases, neurodegenerative complications have become a big challenge in public health. Elongation of human lifespan, due in part to better health services, lifestyle changes, and improvements in medicine and nutrition, has brought up in consequence, an emergence in growing scientific knowledge on fields related to aging and longevity physiology. This new social context faces human medicine to novel concerns that includes coping with chronic diseases that affect life quality at elderly and that increasingly, appear earlier in mid-age and young people.

This special issue offers a broad overview of current knowledge of the molecular and genetic mechanisms that underly neurodegenerative processes; present in various diseases of the central nervous system (CNS) such as Alzheimer's (AD), Parkinson's (PD), and temporal lobe epilepsy (TLE) among others. Here, we will address aspects such as the role of  $\beta$  amyloid ( $A\beta$ ) and tau protein in neurodegeneration, vascular endothelial growth factor (VEGF) in neuroprotection processes, signaling pathways such as NGF/TrkA/Akt/Nrf2 and AMPK/mTor, protein trafficking, DNA repair, apoptosis, inflammation, excitotoxicity, metal exposure, oxidative stress, and nanotechnology.

*Neurodegeneration: From Genetics to Molecules II*, is a multidisciplinary Research Topic that aims to interest basic researchers from several fields of neuroscience research, to seek and suggest new routes for the management of these diseases and help the development of more effective therapeutic approaches. Based on this, we selected this collection of manuscripts with the purpose of presenting the most innovative advances that help to solve unanswered questions and with this, opening new scenarios focused on the development of innovative strategies for learning and improving the treatment of neurodegenerative diseases.

Repair mechanisms in the brain play an important role; in this respect, Cardenas-Rivera et al. evaluated the neuroprotective mechanisms mediated by VEGF in the acute phase of stroke. To do this, they used an *in vivo* model produced by the transitory occlusion of the middle cerebral artery in the rat; the i.c.v. of VEGF favored an increase in neuronal survival, as well as a decrease in infarct volume. These results are directly related to the preferential activation of VEGF receptor 1 (VEGFR1), which has a significant role in the modulation of the inflammatory response and the polarization of the microglia toward a protective phenotype; suggesting, that this receptor could be a target for the development of therapeutic approaches during the acute phase post-stroke (Cardenas-Rivera et al.).

## OPEN ACCESS

### Edited and reviewed by:

Dirk M. Hermann,  
University of  
Duisburg-Essen, Germany

### \*Correspondence:

Victoria Campos-Peña  
neurovcp@gmail.com

### Specialty section:

This article was submitted to  
Cellular Neuropathology,  
a section of the journal  
Frontiers in Cellular Neuroscience

**Received:** 13 October 2021

**Accepted:** 26 October 2021

**Published:** 17 November 2021

### Citation:

Carvajal KG, De Pablos RM and  
Campos-Peña V (2021) Editorial:  
Neurodegeneration: From Genetics to  
Molecules (Part II).  
Front. Cell. Neurosci. 15:794630.  
doi: 10.3389/fncel.2021.794630

Glutathione (GSH) is an intracellular antioxidant molecule, which participates in several functions, such as proliferation, cell differentiation, and apoptosis. It is known that during aging, as well as in neurodegenerative and neuropsychiatric diseases, an alteration in the cellular GSH pools, and a downregulation of GSH-dependent enzymes are present. The increase in circulating nerve growth factor (NGF), an activator of antioxidant pathways, triggers a protective response, which involves an increase in GSH levels in CNS. Valdovinos-Flores et al. showed that peripheral administration of L-buthionine-S-R-sulfoximine (BSO) increases peripheral NGF, which activates the NGF/TrkA/Akt pathway in striatal neurons and leads to a neuroprotective response. Activation of this pathway induces an increase in the expression of genes involved in the uptake of the aminoacids L-cys and L-cys2, as well as glutamate-cysteine ligase modifier (gclm) subunit, which are related to GSH synthesis and transport from the blood to the neuronal parenchyma. The results obtained by these authors are of great importance since they demonstrate that the peripheral reduction of GSH significantly increases the circulating NGF, favoring the neuroprotective response; allowing the development of new studies to elucidate the role that peripheral NGF has on the modulation of GSH homeostasis in the CNS, and opening new possibilities in the progress of therapeutic strategies for neurodegenerative diseases (Valdovinos-Flores et al.).

Qiu et al. conducted a review of TPM21 evaluating the role of this protein in the development of AD. TMP21 is a type I transmembrane protein, which belongs to the p24 family. It is expressed in tissues such as the brain, heart, liver, lung, pancreas, etc. It has a significant role in protein trafficking and maturation, so it plays a critical role in maintaining physiological functions. The authors point out that the dysregulation of TMP21 is involved in the pathogenesis of AD. First, they indicate the regulation of TMP21 expression, whose gene is located on chromosome 14q24.3 and includes five exons and four introns, is positively regulated by nuclear factor of activated T-cells (NFAT), as well as another transcriptional factors such as CREB, AP1, and YY1F. The authors noted that TMP21 regulates A $\beta$ PP trafficking, affecting A $\beta$  production, thus, dysregulation of TMP21 promotes A $\beta$  generation by modulating APP trafficking/stability and regulating the processing of APP by  $\gamma$ -secretase activity, while it potentially regulates the expression and activity of BACE1. Finally, they mention that TMP21 dysregulation could promote tau phosphorylation and neuronal apoptosis, contributing to synaptic impairment and neuronal loss; therefore, modulating the expression of TMP21 could be a potential therapeutic target for the treatment of AD (Qiu et al.).

In recent years it has been documented that the CNS is exposed to constant oxidative damage, due to the presence of reactive oxygen species (ROS), which causes damage to the neuronal genome including double-stranded DNA breakage (DSBs). This DNA damage is not only related to the aging process, but also to neurodegenerative diseases. Guo et al. evaluated the role of RAD6 in double-stranded DNA repair, using RAD6-deficient mice and hippocampal cultures to which a siRNA against RAD6B was introduced. They compared RAD6-deficient mice with wild-type mice after DNA damage induced by

X-irradiation. The results obtained demonstrated that RAD6B-deficient mice exhibit deficits in learning and memory processes. It was also observed that RAD6 is essential for neuronal DNA damage response (DDR), since its deficiency causes defects in DSBs repair, generating genomic instability that leads to neurodegeneration (Guo et al.).

Yao et al. evaluated the phagocytic and anti-inflammatory functions dependent on TREM2 in a non-immune and non-phagocytic cell model, which does not express TREM2 or DAP12. To do this, they stably co-transfected HEK293 cells with TREM2 and DAP12 and evaluated the effects of some TREM2 mutations associated with AD. The results demonstrated that HEK293 cells had the ability to engulf bioparticles of *Escherichia coli*, only when they co-express TREM2 and DAP12, and that the presence of mutations in TREM2 significantly decreases the phagocytic process. In the same way, co-expression of TREM2 and DAP12 prevented NF $\kappa$ B activation in response to PMA treatment, and the TREM2 R47H mutation prevented PMA-induced TREM2-dependent inhibition of NF $\kappa$ B. Finally, TREM2-dependent phagocytosis requires the activation of SYK/PI3K/AKT/PLC $\gamma$  pathways, demonstrating that phagocytic and anti-inflammatory activities are mediated by different signaling pathways (Yao et al.).

Chronic inflammation is a feature present in many neurodegenerative diseases, such as, AD. The inflammatory process is controlled and culminated through negative feedback mechanisms that allow the restoration of the organism's homeostasis. When this does not occur, a detrimental process is generated that can lead to neurodegeneration. Inflammation resolution is an active process that involves not only the decrease in the proliferation and maturation of immune cells or the inhibition of the secretion of inflammatory mediators, as it also involves the repair of damaged tissues. This process is conducted by a group of specialized pro-resolving lipid mediators (SPMs) such as maresins (MaR1). Yin et al. investigated the effects of MaR1 on pathological changes and behavioral deficits in a mouse model of AD by A $\beta$ 42 microinjection. Their results showed that treatment with MaR1 decreased the activation of astrocytes and microglia, by decreasing the production of pro-inflammatory cytokines, induced by the microinjection of A $\beta$ 42. In the same way, it reduced the apoptosis pathways, and MaR1 significantly improved cognitive impairment and enhanced cell survival, suggesting that inflammation resolution may be a potential therapeutic target for AD (Yin et al.).

In recent years, new functions have been identified for caspases that go beyond being considered solely as regulators of apoptosis or inflammation. Espinosa-Oliva et al. conducted a mini-review focused on the "non-apoptotic" functions of caspases in the CNS. In this work, the participation of caspases in the activation of inflammasome, pyroptosis, and necroptosis in neuronal cells is discussed. The function of caspases in the synapse and the processing of aggregates, present in various neurodegenerative diseases, is also evaluated. These types of functions, other than apoptosis, may be related to the sequestration of effector caspases in different subcellular compartments and to the processing of substrates that are not related to cell death. An important example is procaspase-3, which can mediate mitochondrial biogenesis, regardless of its

enzymatic function. Caspase-3 also regulates embryonic stem cells (ESCs) differentiation through Nanog processing. Finally, they point out that the functions observed in caspase-3 can be investigated for other caspases, opening new lines of research to elucidate these functions beyond apoptosis and to evaluate them in other types of cells, different from those of the CNS (Espinosa-Oliva et al.).

Microglia, the immune cells of the CNS, play a fundamental role in brain homeostasis and in the neuroinflammation process. Liu et al. reviewed the role of microglia in the development of PD. They discuss that microglia have pro-inflammatory and anti-inflammatory activities, which depend on the stage and severity of the disease. Microglial polarization is a dynamic process that involves the release of inflammatory mediators such as cytokines, chemokines, ROS, growth factors, reactive nitrogen species (RNS), and prostaglandins (PG). In PD, damaged dopaminergic neurons are capable of causing neuroinflammation, oxidative stress, and cytokine-receptor-mediated apoptosis; this favors peripheral leukocyte recruitment, generating a feedback mechanism that results in exacerbation of the neurodegenerative process. Likewise, they indicate the interaction of microglia with other cell types such as neurons, astrocytes, mast cells, the microbiome-intestine-brain axis as well as  $\alpha$ -Synuclein-microglia interaction, which have a significant role in the regulation of microglial activation and neuroinflammation. Finally, they point out that since the activation of the microglia is a key point to understand PD, the therapeutic strategy should be focused at restoring the immune balance, instead of inhibiting the immune response (Liu et al.).

In the same way, Cheray et al. evaluated the role and functionality of microglia in primary brain tumors and AD. They reviewed several reports in the literature pointing out that there is an inverse relationship between AD and the appearance and development of glioblastoma mediated by microglia. The microglia triggers the activation of signaling cascades such as AKT-mTOR, PI3K, and PAM, that favor the tumor microenvironment, which are not present in AD. In AD, microglia is found around the amyloid plaques, while in cancer they constitute the tumor mass as well as support the expansion and invasion of glial cells into the tumor. The manuscript suggests that the key point that allows this inverse correlation is also found in the expression of specific proteins, the activation of some genes, and signaling pathways (Cheray et al.).

Metaxas et al. proposed new biomarkers for identifying early stages of AD progression, such as the synaptic vesicle glycoprotein 2A (SV2A), as a measure of neuronal density, inflammatory markers, and tau phosphorylation by using modern neuroimaging techniques. They found a positive correlation of these three biomarkers with the damage of the neuronal tissue, mainly in the frontal gyrus, a region that is vulnerable to A $\beta$  deposition, which could provide new approaches to early diagnosis of AD dementia. Although a small pilot study, the released results give new insights in the use of novel imaging technologies that could serve as tools in clinical diagnosis for opportune intervention and treatment of brain diseases (Metaxas et al.).

On the other hand, Silva-Adaya et al. showed in an integrative work, the role of environment metal pollution in the neurodegenerative processes, pointing out its importance on the growing incidence of chronic brain diseases such as AD. This work demonstrated that exposure to inorganic arsenic in healthy mice importantly affects the antioxidant capacity and amino acids transporter gene expression of brain tissues, which in turn, may predispose the organ to further damage or accelerate neurodegenerative pre-existing processes. These findings are valuable clues in preventing elderly complications, either by an opportune diagnosis, or by improving preventive therapies based on boosting the antioxidant capacity by nutritional support and healthier lifestyle. But, moreover, this work alerts about the imperative necessity of taking care of nature milieus, including food and tap water, from toxic pollutants derived from human activity, in order to preserve a healthful future in a context where longer lifespan has become a novel health challenge (Silva-Adaya et al.).

Concerning neurodegenerative chronic diseases, a novel proposal of treatment is presented by Saliba et al.. Here, they show the importance of cannabinoid receptors (CR) in the control of neuroinflammation and exocitotoxicity by using N-arachidonoylphenolamine (AM404) as a CR agonist. They also revealed the underlying mechanisms triggered by AM404, glutamate and calcium release that activate in turn the G-protein-related pathways that lead to cell death, and constitute one of the main causes of neurodegeneration in brain regions such as hippocampus and hypothalamus, often associated to mental and neuronal diseases such as AD, PD, and Huntington. They also found that modulation of CRs might reduce the pathways that conduce to inflammatory processes, by inhibiting the release of pro-inflammatory cytokine L-1 $\beta$  from microglia cells. Thus, they open new alternatives by targeting inflammation and neurotoxicity using CRs agonists, not only AM404, but many other, new and old molecules, that interact with these proteins (Saliba et al.).

Regarding pioneering strategies for diagnosis and therapy, Luo et al. in their review, present a detailed description of modern methods for the diagnosis of chronic CNS conditions, such as AD, PD, and amyotrophic lateral sclerosis (ALS), and propose a novel tool based on the use of iron oxide nanoparticles (IONPs), serving as highly sensitive drug carriers and contrast agent that reach specific brain regions affected in these diseases. They point out the advantage of IONPs vs. orthodox invasive techniques, such as biopsying and autopsy diagnosis, which present low sensitivity and are useful only during the late onset of the diseases, besides the little patient acceptance. By contrast, IONPs represent an innovative contrast agent tool that allows detections at early stages of neurodegenerative hallmarks by non-invasive imaging, thanks to their capacity to cross the blood-brain barrier (BBB) and relatively easy clearance, with a low grade of toxicity (Luo et al.).

More insights in the mechanisms involved in the neurodegenerative processes that accompany AD and epilepsy are revised in the work of Toral-Rios et al.. Here, they underline the role of the signaling pathway of glycogen synthase kinase 3 $\beta$  (GSK3 $\beta$ ) in leading the phosphorylation of key proteins



such as tau, the N-methyl-D-aspartate receptor (NMDAR), and pro-apoptotic molecules Bax and Bcl, which promote structural changes and organelle dysfunction that turn them into toxic components for the cell, such as neurofibrillary tangles (NFTs), excitotoxicity by the overstimulation of NMDAR and mitochondrial dysfunction. Detailed mechanisms of how GSK3 $\beta$  may interact with these pivotal proteins are discussed. The participation of upper signaling cascades, such as PI3K/Akt/mTor and Wnt/ $\beta$ -catenin, which are disrupted in some chronic metabolic conditions, may be involved in the overstimulation of GSK3 $\beta$ . These findings remark the importance of GSK3 $\beta$  modulation to maintain cellular homeostasis in neurodegenerative diseases, so that the proposal of this protein as a therapeutic target is open, in order to offer better alternatives for patients suffering from brain declining function. Besides, deeper studies about the nature of post-translational modification (PTM) of key proteins are encouraged, since, as pointed by the authors, they may play a significant role in modulating the function of the entire cell and thus, of the whole organ (Toral-Rios et al.).

In the same way, Han et al. extensively described the steps involved in aggregation of  $\alpha$ -Synuclein, and the effect on molecular components involved in the formation of toxic fibrils that damage neurons and lead to the progressive motor impairment in PD. Their discussion focuses on the local domains of the protein that mediate its aggregation, the physico-chemical determinants that undertake the phase separation and that finally lead to aggregation and fibrils formation. Cellular oxidative stress is commonly associated with chronic CNS diseases, standing out as the primary involved mechanism. Under this context, PTM such as phosphorylation, SUMOylation, nitration, and O-glcNacetylation in  $\alpha$ -Synuclein have been revealed as a critical step in the transition of the protein from a monomeric to an oligomeric toxic state. Also, interaction of  $\alpha$ -Synuclein with other cellular components such as mitochondria, lipid membranes, inflammatory cells, and genetic mutations are reviewed, warning the complex network of factors surrounding the role of this protein and its conversion into a toxic agent for PD, either by modifying its structure into an aggregating form, or by mediating signal cascades that evoke cell death (Han et al.).

Auchter et al. presented an alternative use of methylene blue (MB) as neuro-protective agent, facing diminished vascular perfusion that often precedes cerebral hypoperfusion in neurodegenerative processes. By using a model of permanent bilateral carotid artery occlusion (two-vessel occlusion; 2VO), Auchter et al. underlie the mechanistic effects of oxygen deprivation and their contribution to brain cellular damage. They monitor cytochrome c oxidase activity (CO) as a marker of mitochondrial electron chain function, over different regions of the brain, and demonstrated that low doses of MB may somewhat replace electron supply into the oxidative phosphorylation to maintain ATP production under brain ischemia and thus, preventing neurodegeneration and memory impairment. Therefore, regional CO activity impairment occurs in response to hypoperfusion, causing specific injury of brain regions that compromise cognition. However, electron donors such as MB may serve to reduce the extent of damage that could trigger neurodegeneration (Auchter et al.).

In the last review, Luna-Viramontes et al. revised the role of tau protein, the second element involved in tissue damage during AD. Tau protein belongs to the family of microtubule-associated proteins and undergoes PTMs that change its properties, such as hyperphosphorylation and cleavage, which render it less soluble and cause aggregation that forms fibrillar structures known as NFTs. The molecular mechanisms underlying the critical step on NFTs formation are the foundation of the minimal paired helical filaments, which serve as core for the growth of the NFTs. This mechanism takes place early during AD development, even before clinical symptoms appear. An important issue in NFTs formation are the signal pathways involved, mainly kinases such as GSK-3 $\beta$ , cell division protein kinase 5 (CDK5), AMP-activated protein kinase (AMPK), and protein kinase A, which are often affected by metabolic disturbances. Thus, the implication of preserving energy metabolism is relevant in the prevention of neurodegenerative processes. In brief, incipient steps in NFT formation appear to be a key control point in detection, prevention, and treatment of the AD and other related pathologies (Luna-Viramontes et al.).

Taken together, all the papers in this issue, present new insights on the cellular mechanisms that lead the subtle neurodegenerative progression behind chronic diseases such as AD, PD, Huntington, ALS, and epilepsy. They also reveal new biomarkers and protein targets aimed to help on early diagnosis, development of potential more effective drugs, and even preventive therapies that guarantee a higher quality of life. This is an issue especially important in a social context where longer life expectancy emerges along with new challenges imposed by the need of deep knowledge of CNS molecular physiology.

They also emphasize the importance of basic research that reveals at a molecular detail, the components and interactions among genes, external milieu, and lifestyle, that raise the perfect puzzle to damage or to heal the brain cells that control function in the aging brain, required to reduce the disability on sustaining longer lives from the future population.

## AUTHOR CONTRIBUTIONS

VC-P and KC prepared the editorial. RMP reviewed and edited the manuscript. VC-P, KC, and RMP contributed significantly to the review and editing of each manuscript accepted on this topic.

**Conflict of Interest:** The authors declare that the research was conducted in the absence of any commercial or financial relationships that could be construed as a potential conflict of interest.

**Publisher's Note:** All claims expressed in this article are solely those of the authors and do not necessarily represent those of their affiliated organizations, or those of the publisher, the editors and the reviewers. Any product that may be evaluated in this article, or claim that may be made by its manufacturer, is not guaranteed or endorsed by the publisher.

Copyright © 2021 Carvajal, De Pablos and Campos-Peña. This is an open-access article distributed under the terms of the Creative Commons Attribution License (CC BY). The use, distribution or reproduction in other forums is permitted, provided the original author(s) and the copyright owner(s) are credited and that the original publication in this journal is cited, in accordance with accepted academic practice. No use, distribution or reproduction is permitted which does not comply with these terms.



# Early Post-stroke Activation of Vascular Endothelial Growth Factor Receptor 2 Hinders the Receptor 1-Dependent Neuroprotection Afforded by the Endogenous Ligand

Alfredo Cárdenas-Rivera<sup>1</sup>, Aura N. Campero-Romero<sup>1</sup>, Yessica Heras-Romero<sup>1</sup>, Andrés Penagos-Puig<sup>1</sup>, Ruth Rincón-Heredia<sup>2</sup> and Luis B. Tovar-y-Romo<sup>1\*</sup>

<sup>1</sup> Division of Neuroscience, Instituto de Fisiología Celular, Universidad Nacional Autónoma de México, Mexico City, Mexico,

<sup>2</sup> Microscopy Core Unit, Instituto de Fisiología Celular, Universidad Nacional Autónoma de México, Mexico City, Mexico

## OPEN ACCESS

### Edited by:

Victoria Campos-Peña,  
National Institute of Neurology  
and Neurosurgery (INNN), Mexico

### Reviewed by:

Sharon DeMorrow,  
The University of Texas at Austin,  
United States  
Ertugrul Kilic,  
Istanbul Medipol University, Turkey

### \*Correspondence:

Luis B. Tovar-y-Romo  
ltovar@ifc.unam.mx

### Specialty section:

This article was submitted to  
Cellular Neuropathology,  
a section of the journal  
Frontiers in Cellular Neuroscience

**Received:** 21 March 2019

**Accepted:** 03 June 2019

**Published:** 02 July 2019

### Citation:

Cárdenas-Rivera A,  
Campero-Romero AN,  
Heras-Romero Y, Penagos-Puig A,  
Rincón-Heredia R and  
Tovar-y-Romo LB (2019) Early  
Post-stroke Activation of Vascular  
Endothelial Growth Factor Receptor 2  
Hinders the Receptor 1-Dependent  
Neuroprotection Afforded by  
the Endogenous Ligand.  
Front. Cell. Neurosci. 13:270.  
doi: 10.3389/fncel.2019.00270

Vascular endothelial growth factor (VEGF) has long been connected to the development of tissue lesion following ischemic stroke. Contradictory findings either situate VEGF as a promoter of large infarct volumes or as a potential attenuator of damage due to its well documented neuroprotective capability. The core of this discrepancy mostly lies on the substantial number of pleiotropic functions driven by VEGF. Mechanistically, these effects are activated through several VEGF receptors for which various closely related ligands exist. Here, we tested in an experimental model of stroke how the differential activation of VEGF receptors 1 and 2 would modify functional and histological outcomes in the acute phase post-ischemia. We also assessed whether VEGF-mediated responses would involve the modulation of inflammatory mechanisms and how this trophic factor acted specifically on neuronal receptors. We produced ischemic infarcts in adult rats by transiently occluding the middle cerebral artery and induced the pharmacological inhibition of VEGF receptors by i.c.v. administration of the specific VEGFR2 inhibitor SU1498 and the pan-VEGFR blocker Axitinib. We evaluated the neurological performance of animals at 24 h following stroke and the occurrence of brain infarctions analyzed at the gross metabolic and neuronal viability levels. We also assessed the induction of peripheral pro- and anti-inflammatory cytokines in the cerebrospinal fluid and blood and assessed the polarization of activated microglia. Finally, we studied the direct involvement of cortical neuronal receptors for VEGF with *in vitro* assays of excitotoxic damage. Preferential VEGFR1 activation by the endogenous ligand promotes neuronal protection and prevents the presentation of large volume infarcts that highly correlate with neurological performance, while the concomitant activation of VEGFR2 reduces this effect, even in the presence of exogenous ligand. This process partially involves the polarization of microglia to the state M2. At the cellular level, neurons also responded better to the preferential activation of VEGFR1 when challenged to *N*-methyl-D-aspartate-induced excitotoxicity.

Endogenous activation of VEGFR2 hinders the neuroprotective mechanisms mediated by the activation of VEGFR1. The selective modulation of these concurrent processes might enable the development of therapeutic approaches that target specific VEGFR1-mediated signaling during the acute phase post-stroke.

**Keywords:** Axitinib, ischemia, MCAO, stroke, SU1498, VEGF, VEGFR1, VEGFR2

## INTRODUCTION

The neuroprotective molecular mechanisms that drive endogenous adaptive responses to injury in the central nervous system (CNS) are mostly unknown, and their elucidation would ideally open new avenues for rehabilitation. A very promising process to target therapeutically is driven by vascular endothelial growth factor A (VEGF), which has long been implicated in the regulation of several events that take place following ischemic stroke, the leading cause of acquired disability in the developed world.

VEGF regulates a series of molecular processes that allow tissue to adapt to the conditions that prevail after stroke, such as neurovascular remodeling and repair, neuroprotection, brain plasticity and the recruitment and proliferation of neuronal precursors (Zhang et al., 2000; Ma et al., 2012; Dzierko et al., 2013; Greenberg and Jin, 2013). However, VEGF is also responsible for some damaging processes, such as cerebral edema and exacerbated blood-brain barrier leakage (Eliceiri et al., 1999; van Bruggen et al., 1999; Paul et al., 2001; Weis and Cheresch, 2005; Kim et al., 2018; Wu et al., 2018). Such opposing findings have, thus far, impeded the utilization of VEGF in a clinical setting aimed at alleviating the sequels of ischemic stroke.

VEGF acts by activating tyrosine kinase receptors 1 (VEGFR1, also known as FMS-like tyrosine kinase; Flt1) and 2 (VEGFR2, also known as kinase domain receptor; KRD, and fetal liver kinase 1; Flk-1). Both receptors are structurally closely related, each composed with seven immunoglobulin-like domains on the extracellular portion, a transmembrane motif, and an intracellular tyrosine kinase domain with conserved tyrosine phosphorylation sites (Grassot et al., 2006; Rahimi, 2006; Simons et al., 2016), although the ultimate biological actions driven by these receptors individually are somewhat different. Traditionally, VEGFR2 has been considered the canonical receptor for VEGF (Geiseler and Morland, 2018), and for a very long time, VEGFR1 has been thought to function as a decoy signal that counter-regulates VEGFR2 actions by sequestering the ligand, thus reducing its availability to binding VEGFR2 (Park et al., 1994; Meyer et al., 2006). Also, VEGFR1 is preferably activated by other members of the VEGF family, such as VEGF-B (Olsson et al., 2006).

An open question in all these molecular events is whether VEGF can also modulate the neuroinflammation elicited by ischemia (Geiseler and Morland, 2018). Neuroinflammation is an important component of the pathophysiology of stroke and other neurodegenerative processes where microglia, the resident macrophages of the CNS, play a central role.

Here we studied the mechanisms of VEGF-mediated neuroprotection in the acute phase of stroke using an *in vivo*

model produced by the transitory occlusion of the middle cerebral artery in the rat (MCAO). The i.c.v. administration of VEGF in the early phase after stroke results in a significant reduction of infarct volume and increased neuronal survival. We found that if VEGFR1 gets preferably activated when VEGFR2 is inhibited, there is a reduction of infarct volume and edema, and an increase of neuronal survival and neurological outcome. Given the role of VEGFR1 on microglial responses to altered brain homeostasis, the underlying mechanisms of the VEGFR1-mediated protection partially involve also the modulation of the inflammatory response and microglial polarization to a neuroprotector phenotype. These results point toward VEGFR1 as an attractive therapeutic target for stroke.

## MATERIALS AND METHODS

### Animals

In this study, we used young (1.5 months old; 270–290 g) Wistar rats that were subjected to MCAO as described below. Animals were housed in individual cages in a 12 h light/dark cycle with food and water *ad libitum*. All rats were killed at 24 h during the acute phase post-stroke. All experimental procedures were conducted under the current Mexican law for the use and care of laboratory animals (NOM-062-ZOO-1999) with the approval of the Institutional Animal Care and Use Committee (CICUAL-IFC-LTR93-16).

### Study Design

Animals were randomly divided into seven groups with an  $n = 10$ –13 for MCAO groups and 7 shams. The sample size was calculated *a priori* to detect a medium Cohen's  $d$  effect size  $> 0.3$ ,  $\beta$  power of 0.8 and significance of 0.05. Mortality rate was assumed to be 0.4 based on pilot experiments. These parameters were chosen to reduce the number of animals used. Inclusion criteria in analyzes considered the reduction of blood perfusion below 50% of basal values, which roughly corresponds to the effect of occluding the common carotid artery, no immediate recovery of reperfusion (above 50% baseline values within 3 min), total occlusion time between 90–95 min, absence of subarachnoid or intraparenchymal hemorrhages and survival at 24 h after stroke. This study is limited to assess effects on males.

### MCAO

Rats were put under isoflurane anesthesia (5% for induction followed by  $\leq 1.5\%$  during surgery) with oxygen as the carrier. Normal ventilation was autonomously maintained. Focal cerebral ischemia was induced with the Longa method (Longa et al., 1989) using a nylon monofilament with a silicone-dipped tip

(403734, Docol, Sharon, MA, United States) that was inserted in a stump created by cutting the ligated left external carotid artery and intraluminally advanced through the internal carotid artery until it reached and occluded the MCA at its inception in the Circle of Willis. MCA occlusion was kept for 90 min after which the monofilament was removed. Body temperature was maintained at 37°C with a heating pad for the duration of surgery. At the end of the procedure, the skin of the neck was sutured, and rats were returned to their cages. During the entire experimental procedure, the cerebral blood flow (CBF) was monitored in the territory irrigated by MCA with laser-Doppler flowmetry. For this, the parietal skull bone was thinned using a small mototool drill bit (Dremel, Racine, WI, United States) and a probe holder was glued onto it at stereotaxic coordinates (AP −1.5 L +3.5 from Bregma). A laser-Doppler probe (model 407, Perimed, Järfälla, Sweden) was inserted into the holder and connected to a Periflux System 5010 (Perimed). CBF was continuously monitored with an acquisition interval of 0.3 s using the Perisoft software (Perimed).

## Administration of VEGF and Pharmacological Inhibitors

VEGF and the VEGFRs inhibitors were administered by intracerebroventricular (i.c.v.) injections in the corresponding animal groups 30 min after intraluminal filament removal, which marked the beginning of reperfusion, with the following stereotaxic coordinates: AP −0.8 and L −1.5 from Bregma and V −4 from dura matter. Injections were performed with graduated glass microcapillary pipettes that were pulled to produce a tip < 50 µm in diameter (McCluskey et al., 2008) at a flux rate of 0.8 µL/min. Because of the non-polar nature of the inhibitors used in this study, we injected a corresponding volume of DMSO in all experimental groups to control for DMSO possible effects. Control sham- and MCAO-operated animals were injected with vehicle solutions consisting of 2 µL DMSO followed by 2 µL 0.1% BSA (4 µL final volume). Recombinant rat VEGF-A<sub>164</sub> (Sigma) was prepared in a 0.1% BSA at a final concentration of 25 ng/µL, 2 µL VEGF were injected followed by 2 µL DMSO. SU1498 and Axitinib (both from Sigma) were prepared in DMSO at a concentration of 6.4 mM. Two µL of each inhibitor were administered in the corresponding groups followed by 2 µL 0.1% BSA or 25 ng/µL VEGF depending on the experimental condition.

## Infarct Volume Calculation

Animals were sedated with sodium pentobarbital and transcardially perfused with 200 mL 0.9% NaCl at 4°C, after which brains were collected and immediately sectioned into seven coronal slices (2 mm thick) that were incubated in 2% 2,3,5-triphenyltetrazolium chloride (TTC) at 37°C for 10 min. Images of sections were digitally acquired with a Lexmark scanner (Lexmark X2650, Lexmark, Canada) using Imaging Studio software (Lexmark, Canada). The infarcted and individual hemisphere areas of each section were measured with a semi-automatized macro routine executed in Fiji (Fiji-ImageJ, version 1.52i, NIH, United States) (Schindelin et al., 2012).

Infarct volume was then calculated and corrected for edema with the following formula:

$$IV = \sum_{i=1}^n \left[ \left( \frac{clHA_i \times IA_i}{ilHA_i} \right) t \right]$$

Where IV is the volume of infarct in mm<sup>3</sup>, *n* is the number of sections, *clHA* is the area of the contralateral hemisphere in mm<sup>2</sup>, *IA* is the area of the damaged tissue in mm<sup>2</sup>, *ilHA* is the area of ipsilateral hemisphere in mm<sup>2</sup>, and *t* is the thickness of each section in mm.

## Post-stroke Neuronal Viability Evaluation

For histological analyses, three rats per group were transcardially perfused with 200 mL ice-cold 0.9% NaCl followed by 250 mL ice-cold 4% paraformaldehyde (PFA). Brains were collected and post-fixed in 4% PFA for 24 h and then cryoprotected in 30% sucrose. Whole PFA-fixed brains were cut into 40 µm thick sections in a cryostat to produce 10 series of consecutive sections that were 400 µm apart. An entire series was mounted on gelatin-coated slides and stained with 1% cresyl violet. Digital images of a section series were acquired in an Olympus IX71 microscope with a 20X magnification using a 12 Megapixel Evolution UVF camera (Media Cybernetics, Buckinghamshire, United Kingdom). Images were processed in Image-Pro Plus 6.0 (Media Cybernetics). Soma diameters and shapes of pyramidal neurons within an area of 250 × 350 µm in layers IV and V of the somatosensory cortex in 3 consecutive sections were analyzed with an automatized macro routine executed in Fiji. Healthy cells were defined by circularity values of 0.47 – 0.88 and area of 30 – 250 µm<sup>2</sup>. Neuronal viability is reported as a survival index, which was calculated from each count of ipsilateral live neurons expressed as a proportion of the count in the respective contralateral area. The resulting values were normalized to the pooled indexes of the sham group. This algorithm is calculated with the following formula:

$$SI = p \left( \sum_1^t \left( \frac{\sum_{i=1}^n (C_i^{il}/C_i^{cl})}{n} \right) \right)_t \bigg/ \left( \sum_1^p \left( \frac{\sum_{o=1}^m (S_o^{il}/S_o^{cl})}{m} \right) \right)_p$$

Where SI is the survival index, *C<sup>il</sup>* is the number of live neurons in the ipsilateral side, *C<sup>cl</sup>* is the number of live neurons in the respective contralateral side, *n* is the number of coronal sections analyzed for each brain, *t* is the number of animals analyzed per experimental group, *S<sup>il</sup>* is the number of neurons in the left side of the sham group, *S<sup>cl</sup>* is the number of neurons in the right side of the sham group and, *m* is the number of sections analyzed for each sham brain and *p* is the number of sham rats. No statistical differences were detected in absolute numbers of live neurons among contralateral sides across experimental groups.



## Behavioral Testing

Animals were evaluated with a battery of neurological tests to assess sensorimotor deficits 24 h after stroke. The severity of functional deficits was scored by assessing eight items described in **Table 1** with slight modifications from previous reports (Mattsson et al., 1997; Schallert et al., 2000; Burguete et al., 2006; Zhang et al., 2015). Maximum score (32 total) was assigned to animals without neurological deficits. All evaluations were cross-validated by a trained observer blinded to the experimental treatment that analyzed recorded videos of the tests.

## Peripheral Cytokines Determination

Blood samples were obtained by cardiac puncture right before transcardial perfusion to determine circulating cytokine levels 24 h after stroke. Plasma was prepared from blood by adding 50  $\mu$ L/mL 0.5 M EDTA and samples were stored at  $-80^{\circ}\text{C}$  until used. Cytokine detection was carried out with a custom-made rat cytokine/chemokine magnetic bead Milliplex MAP panel (Millipore, Temecula, CA, United States) following the manufacturer instructions. A 96-well plate was used to simultaneously determine the concentrations of IL-1 $\beta$ , IL-4, IL-6, IL-10, IL-12p70, IL-17, TNF- $\alpha$ , CCL11, INF $\gamma$ , CX3CL1, MIP-1 $\alpha$ , and VEGF. The plate was read on a MAGPIX system (EMD Millipore, Darmstadt, Germany). Results were analyzed using the xPONENT software (Luminex, Madison, WI, United States). Standards of 200–16,000 pg/mL were used for generating the corresponding concentration curve of each analyte. Determinations were done in duplicates per biological replicate ( $n = 3$ ).

## Cytokine mRNA Expression

Cytokine mRNA levels were determined 24 h after stroke by real-time quantitative PCR (RT-qPCR). For this, 1 mL of blood was combined with 50  $\mu$ L 0.5 M EDTA and 10 mL of red blood cells lysis buffer (155 mM NH $_4$ Cl, 12 mM NaCO $_3$ , 0.1M EDTA, pH 7). Samples were centrifuged at  $1,900 \times g$  for 8 min at RT in a Sorvall ST8 centrifuge (Thermo Fisher Scientific, Karlsruhe, Germany) to obtain white blood cells pellet. Total RNA was isolated with 5:1 TRIzol (Ambion Life Technologies, Austin, TX, United States)-chloroform by phase separation centrifugation at  $12,000 \times g$  for 15 min at  $4^{\circ}\text{C}$ . RNA was precipitated in 500  $\mu$ L isopropanol and washed in 75% ethanol. After air-drying, the pellet was reconstituted in RNase and DNase free ultrapure water (Thermo Scientific). RNA concentration and purity were assessed using OD 260/280 ratios and gel electrophoresis. RT-qPCR was performed with One-step NZYSpeed RT-qPCR Green kit, ROX (nzyTECH, Lisbon, Portugal) according to the manufacturer directions. RT-qPCRs were run in 96-well plates in an Applied Biosystems StepOne RT-qPCR System (Thermo Fisher) with the following parameters: 20 min reverse transcription at  $50^{\circ}\text{C}$ , 2 min cDNA denaturing at  $95^{\circ}\text{C}$ , 40 cycles of 5 s denaturation at  $95^{\circ}\text{C}$ , 30 s annealing/amplification at  $61^{\circ}\text{C}$ . Relative quantification of gene expression was performed using the  $2^{-\Delta\Delta C_T}$  method, with glyceraldehyde 3-phosphate dehydrogenase as a reference gene. Melting curve analyzes and gel electrophoresis evaluation of the RT-qPCR products were

routinely performed to determine the specificity of the RT-qPCR reaction. Primer information for each gene is contained in **Table 2**.

## Immunohistochemistry and Confocal Microscopy

PFA-fixed brain sections containing infarct core and penumbra were blocked with 5% bovine serum albumin in Tris-buffered saline with 0.5% v/v Triton X-100 (TBS-T) and incubated with anti-Iba-1 (1:200; Wako, Richmond, VA, United States) and anti-arginase-1 antibodies (1:200; Invitrogen) for 48 h. Sections were washed three times with TBS followed by 2 h incubation at RT with Alexa Fluor 488-conjugated anti-mouse and Alexa 546-conjugated anti-rabbit antibodies (1:2000 each; Invitrogen, Carlsbad, CA, United States) in TBS. Images were obtained in a Zeiss LSM 800 confocal microscope using a 63X objective. An average of 45 optical slices was obtained every 0.5  $\mu$ m for each Z-stack.

## Cortical Neuronal Cultures

Cortical neuronal cultures were prepared from embryonic day 17 Wistar rats as previously described (Tovar-y-Romo et al., 2012). Briefly, cortices were isolated and trypsinized, and cells were dissociated by trituration in a Ca $^{2+}$  and Mg $^{2+}$  free Hanks' balanced salt solution (Gibco, Carlsbad, CA, United States). Neurons were plated at a density of  $1.3 \times 10^5$  cells/cm $^2$  in polyethyleneimine-coated 24-well plates in Neurobasal medium supplemented with B-27 (Gibco) and 1% antibiotic/antimycotic solution (104 U of penicillin G/mL, 10 mg of streptomycin/mL, and 25  $\mu$ g of amphotericin B/mL) (Sigma). Ten  $\mu$ M cytosine  $\beta$ -D-arabinofuranoside (Sigma) was added on DIV 3 to prevent the proliferation of astrocytes.

Immunofluorescent staining was performed in cells plated on glass coverslips and fixed with 100% methanol for 10 min at  $-20^{\circ}\text{C}$  on DIV 7. Neurons were incubated with anti-VEGFR1 or anti-VEGFR2 (1:100 each, LifeSpan Biosciences, Seattle, WA, United States) and anti-microtubule-associated protein 2 (MAP2; 1:100, Sigma) overnight at  $4^{\circ}\text{C}$ . Labeled cells were incubated with Alexa Fluor 546- and Alexa Fluor 488-conjugated antibodies (1:200 each, Life Technologies), for 1 h at RT, after three washes, neurons were incubated with DAPI for 5 min and mounted on glass slides. Cells were imaged with confocal microscopy as described above with a 40X objective. An average of 30 optical slices was obtained every 0.5  $\mu$ m for each Z-stack.

## Cortical Neurons Excitotoxicity Assays

Neuronal cultures were challenged on DIV 11 with 1, 10, or 100  $\mu$ M NMDA + 1  $\mu$ M glycine for 24 h to induce excitotoxic damage or neuronal death. Rat recombinant VEGF-A $_{164}$  was added to some experimental wells at a concentration of 10 ng/mL for 24 h. In some experiments, we added, 2  $\mu$ M SU1498 or 2  $\mu$ M Axitinib for the same time. Neuronal viability was inferred from metabolic activity determined by standard 3-(4,5-dimethylthiazol-2-yl)-2,5-diphenyltetrazolium bromide (MTT) reduction. For this, neurons were incubated with 0.1 mg/mL

**TABLE 1 |** Items evaluated in neurofunctional assessments.

Neurological assessment	Reflex	Score	Previously reported
Spontaneous activity	Exploring an open arena more than 20 s	3	Burguete et al., 2006
	Exploring between 10 and 20 s	2	
	Exploring less than 10 s	1	
	Not exploring or moving only when stimulated	0	
Contralesioned- wise circling	None	3	Burguete et al., 2006
	Spontaneous circling	2	
	Stimulus-induced circling	1	
	Not moving	0	
Prehensile grip of forepaws to a wire	Symmetrical grip	4	Mattsson et al., 1997
	Asymmetrical, preferably use of non-lesioned forelimb	3	
	Asymmetrical, unable to hold body weight	2	
	Unable to hold grip with lesioned forelimb	1	
	Fall from wire	0	
Ability to rise while suspended from the tail	Unskewed side to rise	4	Zhang et al., 2015
	Rise preferably to the non-lesioned side	3	
	Able to rise only until reached the horizontal plane	2	
	Unable to rise	1	
	Unresponsive while suspended	0	
Cylinder test	Steading with both forelimbs at even height	4	Schallert et al., 2000
	Unable to bring lesioned forelimb to equal height of contralesioned forelimb	3	
	Does not support body weight on lesioned forelimb	2	
	Unable to rear	1	
	Unresponsive	0	
Protective retraction of forelimbs after poking	Symmetrical flex and move from the site	4	NA
	Asymmetrical flex of the ipsilateral forelimb and move from the site	3	
	Asymmetrical flex of the ipsilateral forelimb but stays on site	2	
	Slight movement of ipsilateral forelimb and stays on site	1	
	Does not flex forelimb and stays on site	0	
Body posture	Balanced	5	NA
	Head tilted to the right (lesioned flank)	4	
	Head tilted to the right and forearm extended	3	
	Body tilted to the right	2	
	Unable to keep posture with lesioned hindlimb	1	
March coordination	Unable to stand from lay down position	0	NA
	Symmetrical movement	5	
	Forepaws extended during march	4	
	Support on ulnar side of lesioned forelimb	3	
	Dragging fingers during march	2	
	Dragging lesioned forelimb on dorsal side	1	
	Does not stand on lesioned forelimb	0	

*The neurological performance of every individual was assessed 24 h after stroke in eight items, and for each one, a corresponding value was assigned. Behavioral evaluations were cross-validated by a trained analyst blind to the experimental conditions.*

**TABLE 2 |** Primer sequences for RT-PCR analyses of cytokine transcripts.

Gene	Primer sequence	Amplicon length (bp)	Accession number
IL-1b	F: 5'-CCCTGCAGCTGGAGAGTGTGG-3'	153	NM_031512.2
	R: 5'-TGTGCTCTGCTTGAGAGGTGCT-3'		
IL-6	F: 5'-CGAGCCACCAAGGAAACGAAAGTC-3'	84	M26744.1
	R: 5'-CTGGCTGGAAGTCTCTTGCGGAG-3'		
TGFB	F: 5'-ACCTGCAAGACCATCGACAT-3'	154	NM_021578.2
	R: 5'-TGTTGTACAAAGCGAGCACC-3'		
GAPDH	F: 5'-GCATCTTCTTGTGCAAGTGGC-3'	278	NM_017008.4
	R: 5'-GATCTCGCTCTGGAAGATGG-3'		



MTT for 2 h at 37°C at the end of the analyzed period. Media was removed, and formazan precipitations were dissolved in a 4 mM HCl isopropanol solution. The absorbance of cell debris-free supernatants was read in a spectrophotometer (Beckman Coulter) with a 570 nm wavelength. Data are presented as percentage relative to the absorbance of control conditions. In some experimental conditions we corroborated neuronal viability with the life/dead fluorescence assay (Thermo Fisher Scientific) that stain live cells with calcein AM (green) and dead cells with ethidium homodimer-1 (red), following manufacturers directions.

In an independent series of experiments, neurons were subjected to the same conditions and dendritic spines were stained with the Neurite Outgrowth Staining kit (Life Technologies, Carlsbad, CA, United States) following the manufacturer directions. Briefly, neurons plated on glass coverslips were fixed with 3.7% PFA for 30 min at RT, and 1X bright orange-fluorescent dye was added to stain the outer cell membrane surfaces. After incubation with a background suppression solution, coverslips were mounted on glass slides with a permanent mounting medium with antifading agents (DAKO, Santa Clara, CA, United States). Dendritic branches were visualized using a Leica DM1000 microscope under epifluorescence illumination (568-nm excitation and 580-nm emission) with a 40X objective. A minimum of 10 neurons from 3 independent experiments was analyzed for each condition. The number of dendritic spines, defined as thin protrusions emerging from dendritic processes, extending from two to five primary dendrites/neuron was quantified for a distance of approximately 20  $\mu$ m from the cell soma. Neurite lengths and spine numbers were quantified with ImageJ (NIH, United States). Spine density across all measured dendritic segments was normalized to the length of the primary dendrite.

## Statistics

R- Feather Spray version 3.5.1, (R Foundation for Statistical Computing, Vienna, Austria) was used to analyze all data from *in vivo* experiments. Normal distribution in each data set was corroborated using the Shapiro–Wilk normality test. Data were tested by one-way analysis of variance (ANOVA) followed by Tukey *post hoc* test. Data were considered significant at  $\alpha \leq 0.05$  level. All data are shown as mean  $\pm$  2SD. For *in vitro* experiments without normal distribution we did a Kruskal–Wallis, followed by Dunn *post hoc* test. Results are expressed as mean  $\pm$  SEM.

## RESULTS

### VEGF Mediates Neuroprotection in the Acute Phase of Stroke

There are contradictory findings on the neuroprotective effects of VEGF in stroke. Most of the reported discrepancies can be grounded on time, dose and route of administration of exogenous VEGF in several models of stroke (Ma et al., 2012; Tovar-y-Romo et al., 2016). Because of this, we first tested the effect of administering a single bolus of 50 ng rat recombinant

VEGF-A<sub>164</sub> by i.c.v. injection 30 min after the beginning of reperfusion (**Figure 1**), the dose was chosen based on pilot experiments, and also on a previous study showing that this dose and method of administration is protective in other models of neurodegeneration (Tovar-y-Romo and Tapia, 2012). This protocol was carried out using a pulled glass microcapillary pipette to minimize mechanical damage in order to prevent the activation of inflammatory processes merely associated with the injection procedure. Twenty four hours after stroke, animals were evaluated in a series of neurobehavioral and motor tasks to determine the level of neurological alterations produced by the stroke (**Figure 1A**). Animals that were injected with vehicle only (DMSO + 0.1% BSA; 4  $\mu$ l) showed a noticeable weakness and impaired movement of the lesioned side forelimb. These animals were unable to climb a grid and support their body weight and had a noticeable difficulty rising when placed on their sides, plus ~60% of animals had epileptiform seizures, mostly represented by tonic-clonic convulsions, barrel rolls and running fits. Stoked rats also displayed signs of neuropathic pain when stimulated by slightly poking the affected flank. Administration of 50 ng recombinant VEGF at the beginning of reperfusion did not improve significantly the neurological deficits presented after stroke and also failed to prevent seizures.

Nonetheless, VEGF did reduce infarct volumes by about 20% in comparison to the group that received vehicle only (**Figures 1B,C**). Moreover, neuronal viability was also preserved as revealed by analyzing the somatosensory region of the parietal cortex, in which ~50% neurons remain alive at 24 h post-stroke (**Figures 1D,E**). Therefore, with this experimental settings, we found a condition in which exogenous VEGF did produce a protective impact on brain tissue without translating into a better neurobehavioral outcome at this short time point after stroke.

### VEGFR2 Activation Hinders VEGFR1-Driven Neuroprotection Elicited by Endogenous Ligand in the Acute Phase Post-stroke

It has been known for a long time that VEGF synthesis is upregulated by ischemia immediately after an experimental stroke (Hayashi et al., 1997; Plate et al., 1999; Hai et al., 2003), and this phenomenon has also been reported to occur in human patients (Issa et al., 1999). It is suspected that such VEGF increase is mechanistically involved in neuroprotection. Considering the large body of evidence that involves VEGFR2 participation in neuroprotection (Olsson et al., 2006; Tovar-y-Romo et al., 2016; Geiseler and Morland, 2018), we set out to determine whether VEGFR2 would be primordially responsible for the protection seen here. For this, we administered i.c.v. 13 nmoles of SU1498, a selective VEGFR2 inhibitor (Strawn et al., 1996), 30 min after the beginning of reperfusion and analyzed the overall effects of this procedure 24 h after stroke. Animals in this group displayed signs of neurological deficits mainly characterized by paresis of the lesioned forelimb. However, all animals in this group performed better in the neurological tests and showed significantly fewer alterations than rats that were

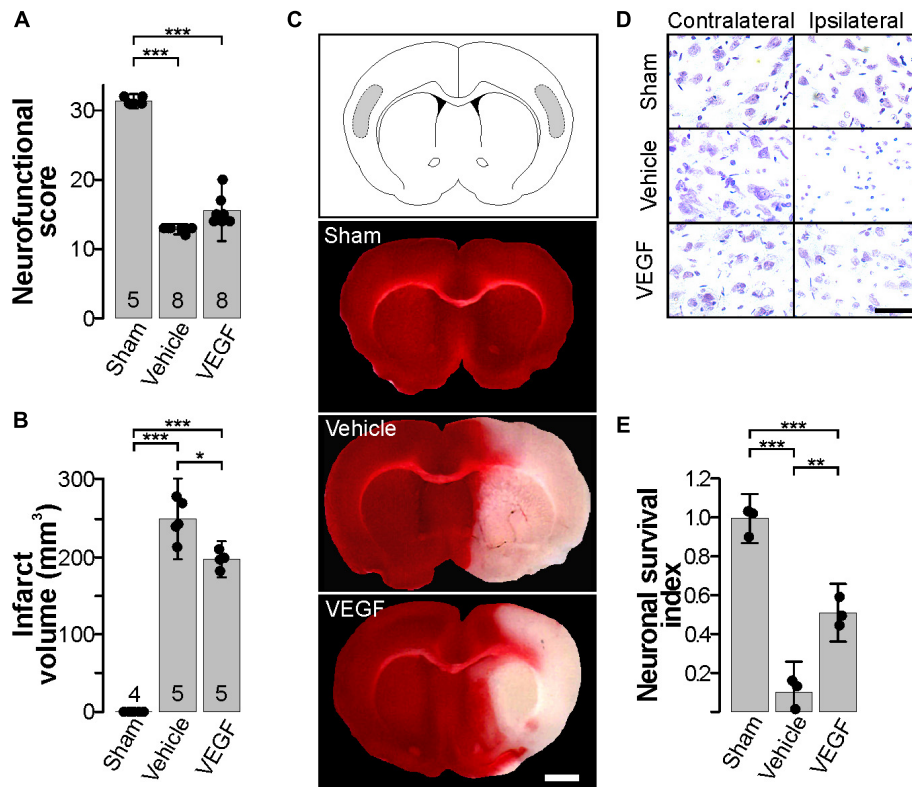


**FIGURE 1 |** Exogenous VEGF administration in the acute phase post-stroke is neuroprotective. **(A)** Behavioral performance of sham-operated animals and stroked rats treated with vehicle or VEGF 24 h post-stroke. Animals were assessed individually in 8 items with scoring values that added up to 32 points that corresponded to neurologically unaffected performance, see **Table 1**. **(B)** Mean infarct volume  $\pm$  2 SD of the indicated experimental groups. In **(A,B)**, the number of experiments analyzed in each group is indicated at the bottom of each column; individual data points are plotted for each group. **(C)** Representative images of thick coronal sections of brains stained with TTC from a sham-operated animal and stroked rats treated with vehicle or VEGF. The unstained (pinkish) portion of the tissue depicts the infarct. Images show brain structures at around Bregma level in the anteroposterior axis. Bar equals 2 mm. **(D)** Representative photomicrographs of Nissl-stained thin sections of the cortical areas shaded in the diagram in (top **C**). Alive neurons have a pyramidal morphology and cytosolic light violet stain, while damaged neurons appear as condensed pycnotic nuclei with enhanced concentration of the dye. Bar equals 50  $\mu$ m. **(E)** Survival index represents the portion of alive neurons present at 24 h post-stroke relative to the same region in the corresponding contralateral side normalized to the number of alive neurons in sham-operated animals. \* $p < 0.05$ , \*\* $p < 0.01$ , and \*\*\* $p < 0.001$  in one-way ANOVA followed by Tukey *post hoc* test.

administered with vehicle alone (**Figures 2A, 3**). Furthermore, co-administration of VEGFR2 antagonist together with a bolus of 50 ng exogenous agonist also resulted in a noticeable improvement in neurological function as compared to animals that received vehicle alone but also to the group that was administered with VEGF, which displayed better recoveries (**Figures 2A, 3**) – thus pointing to a VEGFR2-independent effect driven by the endogenous ligand.

Given the lack of a specific pharmacological inhibitor of VEGFR1, we employed the general VEGFR inhibitor Axitinib that blocks all VEGF receptors (Inai et al., 2004). The MCAO group that received 13 nmoles of Axitinib at 30 min of the beginning of reperfusion presented exacerbated neurological symptoms described above that were followed by a lethargic state in which animals laid on their right side. As expected, infarct volumes in this group were large and comparable to the vehicle group (**Figures 1B,C, 2B,C**). Finally, blocking all VEGFRs prevented any protection mediated by the i.c.v. administration of exogenous VEGF and animals displayed

neurological impairments characteristic of large infarctions (**Figures 2A–C**). Brain damage seen in TTC stainings in this group was of proportions similar to the ones seen in the control untreated group (**Figures 2B,C**). Accordingly, neuronal death was reduced in the animals that received SU1498 alone or in combination with VEGF and was increased in animals treated with Axitinib (**Figures 2D,E**).

Correlating the neurological performance of animals 24 h after stroke to the extent of brain tissue damage allowed us to clearly segregate groups by experimental treatment and show that blocking VEGFR2 and potentiating the activation of VEGFR1 by the administration of exogenous ligand, afforded the best level of neuroprotection, closely followed by only blocking VEGFR2 (**Figure 3**). This analysis shows a strong correlation of  $R^2 = 0.8747$  with a  $p = 3.33 \times 10^{-16}$ . The sole administration of the exogenous ligand, while still protective, does not result in a very different outcome as compared to all the non-protected experimental conditions, in which we either not treated animals or inhibited all VEGFRs (**Figure 3**).

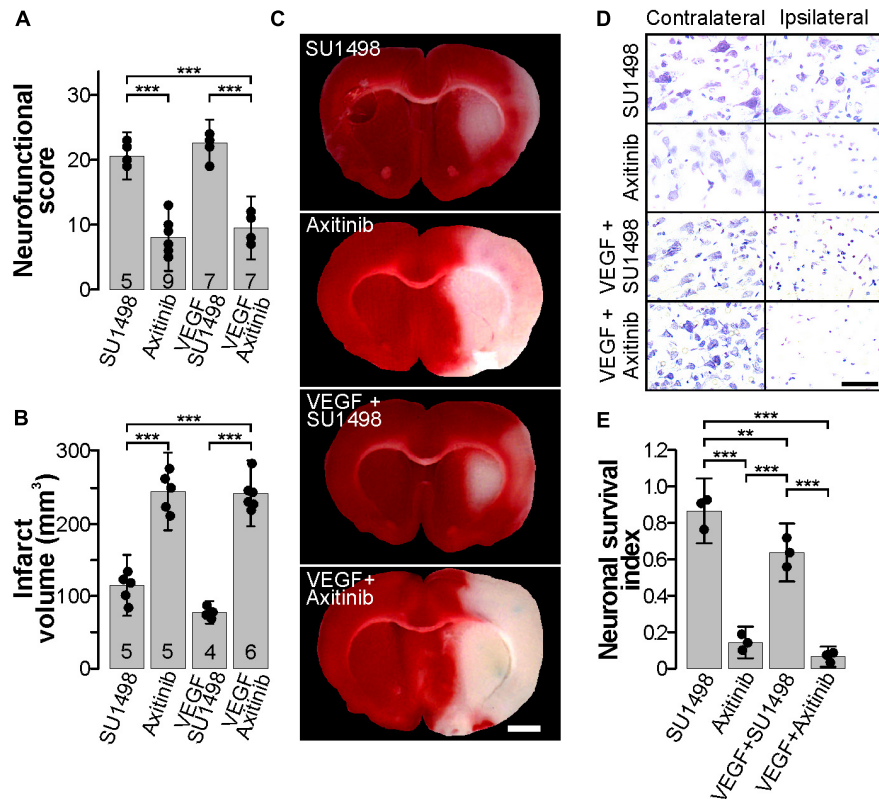


**FIGURE 2 |** Blocking the VEGFR2 in the acute phase post-stroke is neuroprotective. **(A)** Behavioral performance of stroked rats treated with the VEGFR2 specific inhibitor SU1498 and the pan-VEGFR inhibitor Axitinib with and without exogenous VEGF, 24 h post-stroke. **(B)** Mean infarct volume  $\pm$  2 SD of the indicated experimental groups treated with SU1498 or Axitinib alone or in combination with exogenous VEGF. In **(A,B)**, the number of experiments analyzed in each group is indicated at the bottom of each column; individual data points are plotted for each group. **(C)** Representative images of thick coronal sections of brains stained with TTC from stroked animals treated with SU1498 and Axitinib with or without exogenous VEGF. The unstained (pinkish) portion of the tissue depicts the infarct. Images show brain structures at around Bregma level in the anteroposterior axis. Bar equals 2 mm. **(D)** Representative photomicrographs of Nissl-stained thin sections of cortical areas in the somatosensory region. Alive neurons have a pyramidal morphology and cytosolic light violet stain, while damaged neurons appear as condensed pycnotic nuclei with enhanced concentration of the dye. Bar equals 50  $\mu$ m. **(E)** Survival index represents the portion of live neurons present at 24 h post-stroke relative to the same region in the corresponding contralateral side normalized to the number of live neurons in sham-operated animals. \*\* $p$  < 0.01 and \*\*\* $p$  < 0.001 in one-way ANOVA followed by Tukey *post hoc* test.

## VEGFR1-Mediated Neuroprotection Partially Involves M2 Polarization of Microglia With a Minimal Discernible Impact on Systemic Markers of Inflammation

VEGF drives the migration of macrophages and microglia to the damaged CNS through VEGFR1-mediated signaling (Forstreuter et al., 2002; Huang et al., 2013; Lelli et al., 2013). Therefore, we decided to study whether the neuroprotection exerted by the preferential activation of VEGFR1 would also involve the modulation of neuroinflammatory processes. We first assessed changes in inflammatory markers, both in CSF and in plasma, at 24 h post-stroke. We analyzed the content of IL-1 $\beta$ , IL-4, IL-6, IL-10, IL-12p70, IL-17, TNF- $\alpha$ , CCL11, INF $\gamma$ , CX3CL1, and MIP-1 $\alpha$  with a multiplex array for these cytokines in samples collected prior transcardial perfusion. None of the detected cytokines in CSF (IL-1 $\beta$ , INF $\gamma$ , CXCL-3) showed a significant change compared to the values seen in the vehicle-treated

group (Figure 4A). Likewise, for most of the peripheral markers of inflammation that produced a readable measurement in plasma, we did not find differences among experimental groups. However, we detected with this array that the inhibition of all VEGFRs with Axitinib blunted the release of peripheral markers of inflammation IL-12, TNF $\alpha$ , and CCL11. This blockade did not happen to the same degree when we selectively inhibited VEGFR2 (Figure 4B). Since under our experimental conditions we were not able to have reliable measurements of peripheral IL-1 $\beta$ , IL-6, and TGF $\beta$ , which have been previously identified as central players of the neuroinflammatory processes that happen after stroke, we decided to evaluate the levels of transcriptional expression of these cytokines in white blood cells collected 24 h after stroke. With RT-qPCR analyses, we determined that there are no significant changes in the level of transcription for neither of these molecules at the time point of our investigations and that VEGF or its receptors are not modifiers of these molecular responses (Figures 4C–E).

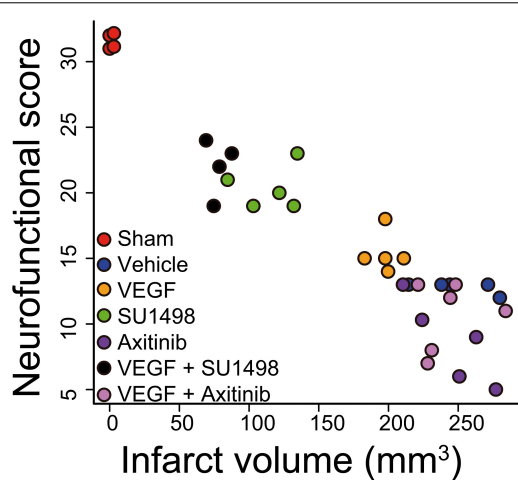


**FIGURE 3 |** Activation of VEGFR2 hinders VEGFR1-dependent neuroprotection afforded by the endogenous ligand. The plot shows the correlation of neurofunctional score to the infarct volume produced by MCAO in animals injected i.c.v. 30 min after the beginning of reperfusion with vehicle, or exogenous VEGF alone or in combination with VEGFR2 specific inhibitor SU1498 or VEGFR general inhibitor Axitinib. Two groups of animals that received the inhibitors individually are also presented. Each data point represents the values obtained in a single animal. Groups segregate by experimental condition and produce a strong correlation with an adjusted  $R^2 = 0.8747$ . Animals in which VEGFR2 early activation was prevented show the best levels of protection, both neurofunctional and histological, inhibiting VEGFR1 in addition to VEGFR2 blocked this effect.

Next, we looked into the polarization of microglial cells to the anti-inflammatory phenotype M2, which is known to occur in the first 24 h after stroke (Hu et al., 2012). For this, we co-stained brain sections for the microglial marker Iba-1 and the M2 marker arginase-1. Strikingly, resting state morphologically looking microglia were found to express arginase-1 in sham animals at 24 h of transiently occluding the common carotid artery (Figure 5). In the control MCAO group, microglia in the lesioned cortical region looked morphologically activated, mainly with shortened cellular processes and rounded somas but cells in these regions lacked the expression of arginase-1. VEGF-treated animals, however, showed activated microglia expressing the M2 polarization marker and this was also the scenario in the groups treated with the VEGFR2 inhibitor SU1498 with and without VEGF. In the case of animals injected with Axitinib, we found fewer activated microglia expressing arginase-1, suggesting that VEGFR1 blockade also reduced the polarization of microglia to the anti-inflammatory phenotype.

### VEGF Acts Directly on Neurons Through the Activation of VEGFR1

In the last part of our study, we analyzed whether the effects of preferentially activating VEGFR1 and the neuroprotection seen in the *in vivo* model of ischemic stroke were derived from the direct stimulation of neuronal receptors. Using an *in vitro* model of cultured cortical neurons we first determined the expression of both, VEGFR1 and VEGFR2 in these cells. Figure 6A shows

the expression of both TRKs at 7 DIV, specifically in neurons. Expression of both receptors is clear in neuronal somas as well as in neurites. Then, we tested whether the addition of VEGF to neuronal cultures could rescue neurons from excitotoxicity, one of the primary mechanisms underlying neuronal death after ischemia. For this, we incubated the neurons with different concentrations of the glutamatergic agonist NMDA for 24 h in the same culture media in which cells were grown for 11 days. At the lowest concentration assayed (1  $\mu$ M), neuronal death is not apparent and increasing the concentration of NMDA to 10, and 100  $\mu$ M gradually increased the level of neuronal death (Figures 6B,C). Addition of 10 ng/mL recombinant VEGF reduced in about 20% the loss of metabolic activity in the neuronal cultures, which relates to the overall health of the cells and their survivability.

Even though the lower concentrations of NMDA tested here did not produce a substantial decrease of neuronal viability, neurons exposed to these conditions developed morphological signs of structural damage, mainly characterized by dendritic spine loss. Addition of VEGF to the culture media also prevented this morphological change and preserved spine structures although it did not modify the length of primary neurites (Figures 6D–F). With these experiments, we showed that VEGF executes trophic effects on cortical neurons to allow them to grow healthy in culture and make them less susceptible to excitotoxic death.

Finally, in an independent set of experiments, we tested the role of VEGFR1 and VEGFR2 in driving the pro-survival effects. Strikingly, blocking VEGFR2 activation by addition of SU1498 also resulted in a significant increase in neuronal protection, which was further potentiated by the co-administration of VEGF (Figure 6G). By contrast, inhibiting the activation of both receptors with Axitinib prevented entirely the neuroprotection exerted by VEGF (Figure 6G). These results replicated well the effects that we described first with the *in vivo* model, therefore, proving that the mechanisms of protection seen partially encompassed a direct involvement of neuronal receptors.

## DISCUSSION

Since VEGF is a molecule with pleiotropic actions that can execute its functions by binding a number of different receptors, the exact role of VEGF increased expression after stroke in neuroprotective mechanisms has been the core of a controversy. The prevailing idea on the dual effects exerted by VEGF states that the dominant actions of this trophic factor, whether neuroprotective or detrimental, are chiefly dictated by the timing, dosage, and route of administration in experimental models of stroke (Wittko-Schneider et al., 2013; Geiseler and Morland, 2018). Moreover, it has been amply described that excessive levels of VEGF in the early phase following stroke promote BBB alterations and a general state that favors neurodegeneration. Interestingly, delayed administration of VEGF is more likely to result in neuroprotection (Sun et al., 2003; Dzielko et al., 2013), even though, others have also reported the protective effect of an early VEGF i.c.v. administration (Kaya et al., 2005).



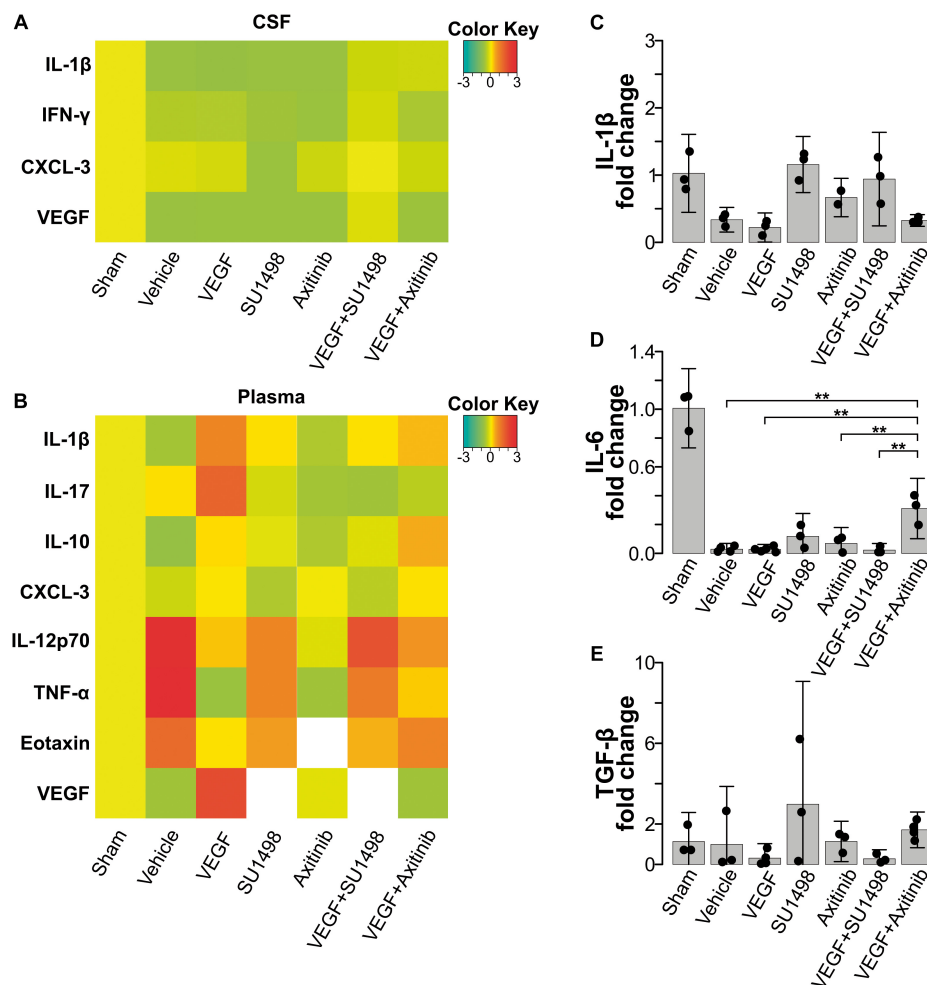


**FIGURE 4 |** VEGFR1-dependent neuroprotection does not reflect on changes in peripheral inflammatory markers. **(A)** Heatmap of cytokines and VEGF detected in CSF 24 h after stroke. **(B)** Heatmap of peripheral cytokines and VEGF detected in plasma 24 h after stroke. No significant differences were detected in these markers in the acute phase following stroke. White colored areas are from groups with undetectable readings. Changes in transcriptional expression of **(C)** IL-1 $\beta$ , **(D)** IL-6, and **(E)** TGF- $\beta$ , determined by RT-qPCR relative to GAPDH in blood 24 h following stroke. No differences were found among experimental groups.

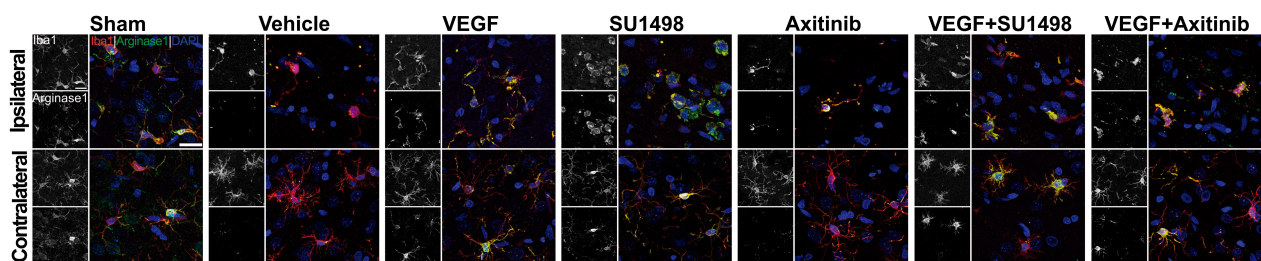


**FIGURE 5 |** Blockade of VEGFR1 impedes the polarization of microglia to the M2 phenotype. Representative images of brain sections co-labeled with the microglia marker Iba-1 (red) and the M2 phenotype indicator arginase-1 (green). Images were taken from the somatosensory cortex adjacent to infarct core. Ameboid-like activated morphology is present under all MCAO conditions in the ipsilateral side. M2 polarizations are evident in most of the Iba-1 positive cells in the MCAO groups treated with vehicle, VEGF, SU1498 and the combination of VEGF and SU1498. Animals injected with the pan-VEGFR blocker Axitinib do not show labeling of M2 polarization in the activated microglia on the ipsilateral side. Bar equals 20  $\mu$ m.

In the brain, VEGFR1 and VEGFR2 are the most expressed receptors, with VEGFR1 showing a higher density in neurons (Yang et al., 2003; Du et al., 2010). Several reports have

been published over the years indicating that VEGFR2 is the receptor predominantly responsible for neuroprotective actions, mainly by driving pro-survival signaling mediated by

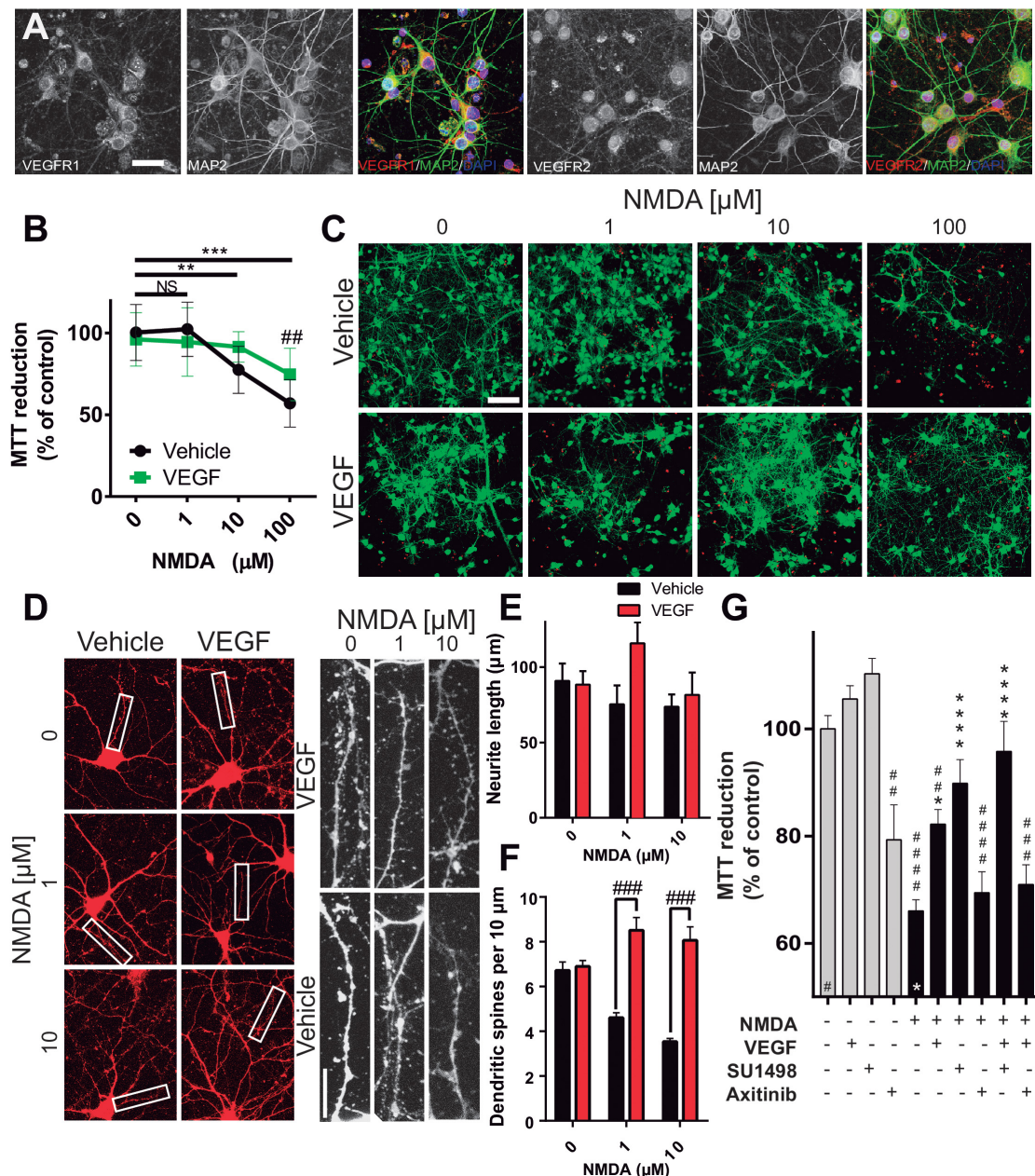


**FIGURE 6 | Neuronal VEGFR1 drives neuroprotection under excitotoxic stress. (A)** Representative photomicrographs of cultured cortical neurons labeled with the neuronal marker MAP2 (green), and VEGFR1 and VEGFR2 (red). Bar equals 25  $\mu\text{m}$ . **(B)** Neuronal survival assessed by MTT reduction of cultures exposed to increasing concentrations of NMDA for 24 h and 10 ng/mL VEGF. The graph shows the mean  $\pm$  SEM of three independent experiments. **(C)** Representative images of cortical neurons exposed to increasing concentrations of NMDA for 24 h with or without 10 ng/mL VEGF, calcein stain labels alive neurons green, while dead cells are marked by the nuclear staining of bromide homodimer in red. Bar equals 200  $\mu\text{m}$ . **(D)** Representative micrographs of neurons exposed to sublethal concentrations of NMDA for 24 h and stained with a membrane dye. VEGF preserved the structural integrity of neurites and dendritic spines. Images on the right are magnifications of the indicated areas on the left. Scale bar equals 10  $\mu\text{m}$ . Quantifications of neurite length **(E)** and dendritic spines **(F)** of the experiments described in **(D)**. Each column represents the mean  $\pm$  SEM of the neurites of 5 neurons analyzed in three independent experiments. **(G)** Neuronal survival assessed by MTT reduction of cultures exposed to 100  $\mu\text{M}$  NMDA for 24 h and 10 ng/mL VEGF alone or in combination with 2  $\mu\text{M}$  SU1498 and 0.2  $\mu\text{M}$  Axitinib. The graph shows the mean  $\pm$  SEM of three independent experiments. \* $p < 0.05$ , \*\* $p < 0.01$ , \*\*\* $p < 0.001$ , and \*\*\*\* $p < 0.0001$  compared to NMDA alone, and ## $p < 0.01$ , ### $p < 0.001$ , and #### $p < 0.0001$  compared to untreated neurons in Kruskal–Wallis followed by Dunn *post hoc* test.

PI-3K/PKB and MEK/Erk pathways (Greenberg and Jin, 2013). Here, we found that the preferential activation of VEGFR1 by the endogenous ligand promotes neuronal protection and

prevents the presentation of large volume infarcts; this is highly correlated with neurological performance. Of note, the concurrent activation of VEGFR2 prevents this effect, even in the



presence of excess ligand. Strikingly, such protection still happens at the cellular level, where neurons are better protected when challenged to NMDA-induced excitotoxicity by the activation of VEGFR1 if VEGFR2 is blocked.

VEGF along with its receptors 1 and 2 are transcriptionally upregulated following stroke (Hayashi et al., 1997; Issa et al., 1999; Plate et al., 1999; Marti et al., 2000; Hai et al., 2003; Stowe et al., 2007, 2008) in a long-lasting fashion (Zhang et al., 2002), through the stabilization and subsequent binding of hypoxia-inducible factor 1 (HIF-1) to the hypoxia response element sequence in their promoters (Forsythe et al., 1996). Also, it has been shown that exogenous administration of VEGF causes the upregulation of VEGFR1 and VEGFR2 (Krum et al., 2008). Cellular distribution of VEGFRs might be key in understanding the temporal regulation of vasculature adaptations in the acute phase post-stroke. In this regard, the apicobasal localization of VEGFR1 and VEGFR2 is different, where VEGFR2 is predominantly expressed in the basal side and VEGFR1 in the apical pole that produces a differential response when the ligand acts at the circulation or the parenchymal sides of endothelial cells (Hudson et al., 2014). It has also been reported that the expression of VEGFR1 is upregulated while VEGFR2 is downregulated in endothelial cells following hypoxia, which changes the VEGFR1:VEGFR2 ratio altering the ultimate responses on cell viability and recovery (Ulyatt et al., 2011). It is also important to point out that the affinity of VEGFR1 for VEGF is about 1 order of magnitude higher than the one for VEGFR2 ( $K_d$  2–10 pM for VEGFR1 and 75–250 pM for VEGFR2) (de Vries et al., 1992; Ferrara, 2004; Shibuya, 2006). Although VEGFR3 is expressed in the adult rat brain (Hou et al., 2011), we ruled out the participation of this receptor in the neuroprotection seen here, even when it can also be inhibited by Axitinib, because it does not get activated by VEGF-A (Olsson et al., 2006; Leppänen et al., 2013) and its expression is primarily restricted to lymphatic endothelial cells (Iljin et al., 2001), which have a very low relative abundance in the brain (Louveau et al., 2015).

Our observations lead to reaffirm the critical role of VEGFR1 in the endogenous neuroprotective mechanisms elicited after ischemic insults to the brain. In this regard, it is known that the deletion of VEGF-B, a specific ligand for VEGFR1, produces 50% larger infarcts in mice when subjected to the permanent occlusion of the MCA in comparison to WT animals, by inhibition of apoptotic executioner molecules (Li et al., 2008). Protein analysis identified a significant increase of VEGF-B in CSF and the ischemic hemispheres, with increased VEGFR1 activation that also correlated with an increase in Akt phosphorylation, whereas an increase in VEGF in the contralateral hemisphere correlates with a significant increase in vascular density 7 days post-stroke (Guan et al., 2011). VEGFR1 activation in pericytes promotes the formation of stable new vessels in a mechanistic way independent of endothelial cells, and also slightly attenuated inflammation when administered in the sub-acute phase post-stroke (Jean LeBlanc et al., 2018). In this sense, it has also been shown that PlGF, a specific ligand for VEGFR1, is the most efficient promoter of angiogenesis, which produces mature non-leaky new vessels (Luttun et al., 2002; Gaál et al., 2013).

The direct VEGFR1 activation in neurons might be a mechanism more relevant than promoting healthy angiogenesis (Poesen et al., 2008; Dhondt et al., 2011; Ishrat et al., 2018). In this regard, it is noteworthy that VEGF associates to neurons in infarct and peri-infarct brain regions in a non-human primate model of stroke (Stowe et al., 2007), and interestingly, such association can even be more relevant than the interaction of this growth factor with astrocytes (Shen et al., 2018). Our results, however, indicate that all these neuroprotective mechanisms driven by VEGFR1 are suppressed in the first hours following stroke by the activation of VEGFR2. The exact mechanisms underlying this phenomenon are not fully elucidated, but they might involve the suppression of endoplasmic reticulum stress and apoptosis (Feng et al., 2019).

VEGF has some interesting roles in regulating neuroinflammation. It has been shown that macrophages express more VEGF in response to disturbances in brain metabolic homeostasis, especially responding to decreased glucose incorporation (Jais et al., 2016), and microglia in chronically affected regions of CNS upregulate their expression of VEGF (Nikodemova et al., 2014). However, not much is known about the involvement of VEGF, or its receptors, in the polarization of macrophages/microglia under inflammation. Interestingly, very recent evidence indicates that the antiangiogenic VEGF isoform VEGF<sub>164b</sub> is capable of blocking VEGFR1 prompting the M1 polarization of peripheral macrophages (Ganta et al., 2019), although it is known that this form of VEGF has neuroprotective effects in the CNS (Beazley-Long et al., 2013). Also, M2-polarized peripheral macrophages in culture are known to upregulate their VEGFR1 mRNA expression (Melton et al., 2015), which in microglial cells could lead to the inhibition of the expression of the scavenger receptor A following stroke (Xu et al., 2017). With the determinations carried out in the present study, we were unable to obtain reliable readings of the levels of soluble mediators of inflammation poured on CSF and plasma, however, many of these markers, like IL-6, have been disregarded as important predictors of the outcome (Clark Wayne et al., 2000; Worthmann et al., 2010). Nonetheless, we could characterize the overall response of microglia polarizing to the anti-inflammatory phenotype under the experimental conditions that allow the activation of VEGFR1. More detailed analyses are required to characterize these responses at the molecular and cellular levels.

## CONCLUSION

We found that the activation of VEGFR2 in the first hours post-stroke obstructs endogenously-coded mechanisms of adaptation to injury in the brain. We propose here the existence of a VEGFR2-mediated antagonism of VEGFR1, which has not been reported previously. This process would constitute a fundamental mechanism of endogenous operations that drive adaptive responses in the brain after stroke that is worthy of further exploration. Our results also strengthen the notion that VEGFR1 has a critical role in neuroprotection, and that targeting this receptor would be useful at developing restorative therapies for stroke.

## DATA AVAILABILITY

The datasets used and/or analyzed during the current study are available from the corresponding author on reasonable request.

## ETHICS STATEMENT

This study was carried out in accordance with the Mexican law for the use and care of laboratory animals (NOM-062-ZOO-1999) with the approval of the Institutional Animal Care and Use Committee (CICUAL-IFC-LTR93-16).

## AUTHOR CONTRIBUTIONS

AC-R and LT-y-R conceived the project and designed the experiments. AC-R conducted the *in vivo* experiments, wrote the R-based scripts to process data, and carried out statistical analyses. YH-R cross-validated the neurological assessments. ANC-R and AP-P conducted the *in vitro* experiments. RR-H was responsible for confocal microscopy acquisition and analyses. AC-R, ANC-R, YH-R, and LT-y-R analyzed the data. LT-y-R wrote the manuscript. All authors read and approved the final version of the manuscript.

## REFERENCES

- Beazley-Long, N., Hua, J., Jehle, T., Hulse, R. P., Dersch, R., Lehrling, C., et al. (2013). VEGF-A165b is an endogenous neuroprotective splice isoform of vascular endothelial growth factor A *in vivo* and *in vitro*. *Am. J. Pathol.* 183, 918–929. doi: 10.1016/j.ajpath.2013.05.031
- Burguete, M. C., Torregrosa, G., Pérez-Asensio, F. J., Castelló-Ruiz, M., Salom, J. B., Gil, J. V., et al. (2006). Dietary phytoestrogens improve stroke outcome after transient focal cerebral ischemia in rats. *Eur. J. Neurosci.* 23, 703–710. doi: 10.1111/j.1460-9568.2006.04599.x
- Clark Wayne, M., Rinker Lisa, G., Lessov Nikola, S., Hazel, K., Hill, J. K., Stenzel-Poore, M., et al. (2000). Lack of interleukin-6 expression is not protective against focal central nervous system ischemia. *Stroke* 31, 1715–1720. doi: 10.1161/01.STR.31.7.1715
- de Vries, C., Escobedo, J. A., Ueno, H., Houck, K., Ferrara, N., and Williams, L. T. (1992). The fms-like tyrosine kinase, a receptor for vascular endothelial growth factor. *Science* 255, 989–991. doi: 10.1126/science.1312256
- Dhondt, J., Peeraer, E., Verheyen, A., Nuydens, R., Buysschaert, I., Poesen, K., et al. (2011). Neuronal FLT1 receptor and its selective ligand VEGF-B protect against retrograde degeneration of sensory neurons. *FASEB J.* 25, 1461–1473. doi: 10.1096/fj.10-170944
- Du, H., Li, P., Pan, Y., Li, W., Hou, J., Chen, H., et al. (2010). Vascular endothelial growth factor signaling implicated in neuroprotective effects of placental growth factor in an *in vitro* ischemic model. *Brain Res.* 1357, 1–8. doi: 10.1016/j.brainres.2010.07.015
- Dzietko, M., Derugin, N., Wendland, M. F., Vexler, Z. S., and Ferriero, D. M. (2013). Delayed VEGF treatment enhances angiogenesis and recovery after neonatal focal rodent stroke. *Transl. Stroke Res.* 4, 189–200. doi: 10.1007/s12975-012-0221-6
- Eliceiri, B. P., Paul, R., Schwartzberg, P. L., Hood, J. D., Leng, J., and Cheresh, D. A. (1999). Selective requirement for Src kinases during VEGF-induced angiogenesis and vascular permeability. *Mol. Cell* 4, 915–924. doi: 10.1016/S1097-2765(00)80221-X
- Feng, S.-Q., Zong, S.-Y., Liu, J.-X., Chen, Y., Xu, R., Yin, X., et al. (2019). VEGF antagonism attenuates cerebral ischemia/reperfusion-induced injury via inhibiting endoplasmic reticulum stress-mediated apoptosis. *Biol. Pharm. Bull.* 42, 692–702. doi: 10.1248/bpb.b18-00628

## FUNDING

This work was supported by the Programa de Apoyo a Proyectos de Investigación e Innovación Tecnológica, Dirección General de Asuntos del Personal Académico (IN226617), Consejo Nacional de Ciencia y Tecnología (CONACYT; CB219542/13219), and the Committee for Aid and Education in Neurochemistry of the International Society for Neurochemistry and the International Brain Research Organization Return Home Program (2014) grants to LT-y-R. AC-R, ANC-R, and YH-R are recipients of doctoral scholarships from the CONACYT (280986/277660/428473).

## ACKNOWLEDGMENTS

We thank Jaime Rogerio Ríos for his contribution with microglia immunofluorescence stainings, Cristina Aranda Fraustro for administrative assistance, Dr. Laura Ongay-Larios for her expert aid with RT-qPCR, and Gabriela Meneses and Dr. Edda Sciutto for their helpful assistance with the MAGPIX system. AC-R conducted this study in partial fulfillment of the requirements of the Programa de Doctorado en Ciencias Biomédicas of Universidad Nacional Autónoma de México.

- Ferrara, N. (2004). Vascular endothelial growth factor: basic science and clinical progress. *Endocr. Rev.* 25, 581–611. doi: 10.1210/er.2003-0027
- Forstreuter, F., Lucius, R., and Mentlein, R. (2002). Vascular endothelial growth factor induces chemotaxis and proliferation of microglial cells. *J. Neuroimmunol.* 132, 93–98. doi: 10.1016/s0165-5728(02)00315-6
- Forsythe, J. A., Jiang, B. H., Iyer, N. V., Agani, F., Leung, S. W., Koos, R. D., et al. (1996). Activation of vascular endothelial growth factor gene transcription by hypoxia-inducible factor 1. *Mol. Cell. Biol.* 16, 4604–4613. doi: 10.1128/mcb.16.9.4604
- Gaál, E. I., Tammela, T., Anisimov, A., Marbacher, S., Honkanen, P., Zarkada, G., et al. (2013). Comparison of vascular growth factors in the murine brain reveals placenta growth factor as prime candidate for CNS revascularization. *Blood* 122, 658–665. doi: 10.1182/blood-2012-07-441527
- Ganta, V. C., Choi, M., Farber, C. R., and Annex, B. H. (2019). Antiangiogenic VEGF165b regulates macrophage polarization via S100A8/S100A9 in peripheral artery disease. *Circulation* 139, 226–242. doi: 10.1161/CIRCULATIONAHA.118.034165
- Geiseler, S. J., and Morland, C. (2018). The janus face of VEGF in stroke. *Int. J. Mol. Sci.* 19:1362. doi: 10.3390/ijms19051362
- Grassot, J., Gouy, M., Perrière, G., and Mouchiroud, G. (2006). Origin and molecular evolution of receptor tyrosine kinases with immunoglobulin-like domains. *Mol. Biol. Evol.* 23, 1232–1241. doi: 10.1093/molbev/msk007
- Greenberg, D. A., and Jin, K. (2013). Vascular endothelial growth factors (VEGFs) and stroke. *Cell. Mol. Life Sci.* 70, 1753–1761. doi: 10.1007/s00018-013-1282-8
- Guan, W., Somanath, P. R., Kozak, A., Goc, A., El-Remessy, A. B., Ergul, A., et al. (2011). Vascular protection by angiotensin receptor antagonism involves differential VEGF expression in both hemispheres after experimental stroke. *PLoS One* 6:e24551. doi: 10.1371/journal.pone.0024551
- Hai, J., Li, S.-T., Lin, Q., Pan, Q.-G., Gao, F., and Ding, M.-X. (2003). Vascular endothelial growth factor expression and angiogenesis induced by chronic cerebral hypoperfusion in rat brain. *Neurosurgery* 53, 963–970; discussion 970–972.
- Hayashi, T., Abe, K., Suzuki, H., and Itoyama, Y. (1997). Rapid induction of vascular endothelial growth factor gene expression after transient middle cerebral artery occlusion in rats. *Stroke* 28, 2039–2044. doi: 10.1161/01.str.28.10.2039

- Hou, Y., Shin, Y.-J., Han, E. J., Choi, J.-S., Park, J.-M., Cha, J.-H., et al. (2011). Distribution of vascular endothelial growth factor receptor-3/Flt4 mRNA in adult rat central nervous system. *J. Chem. Neuroanat.* 42, 56–64. doi: 10.1016/j.jchemneu.2011.06.001
- Hu, X., Li, P., Guo, Y., Wang, H., Leak, R. K., Chen, S., et al. (2012). Microglia/macrophage polarization dynamics reveal novel mechanism of injury expansion after focal cerebral ischemia. *Stroke* 43, 3063–3070. doi: 10.1161/STROKEAHA.112.659656
- Huang, H., Parlier, R., Shen, J.-K., Luty, G. A., and Vinore, S. A. (2013). VEGF receptor blockade markedly reduces retinal microglia/macrophage infiltration into laser-induced CNV. *PLoS One* 8:e71808. doi: 10.1371/journal.pone.0071808
- Hudson, N., Powner, M. B., Sarker, M. H., Burgoyne, T., Campbell, M., Ockrim, Z. K., et al. (2014). Differential apical/basal VEGF signaling at vascular blood-neural barriers. *Dev. Cell* 30, 541–552. doi: 10.1016/j.devcel.2014.06.027
- Iljin, K., Karkkainen, M. J., Lawrence, E. C., Kimak, M. A., Uutela, M., Taipale, J., et al. (2001). VEGFR3 gene structure, regulatory region, and sequence polymorphisms. *FASEB J.* 15, 1028–1036. doi: 10.1096/fj.00-0383com
- Inai, T., Mancuso, M., Hashizume, H., Baffert, F., Haskell, A., Baluk, P., et al. (2004). Inhibition of vascular endothelial growth factor (VEGF) signaling in cancer causes loss of endothelial fenestrations, regression of tumor vessels, and appearance of basement membrane ghosts. *Am. J. Pathol.* 165, 35–52. doi: 10.1016/s0002-9440(10)63273-7
- Ishrat, T., Soliman, S., Eldahshan, W., Pillai, B., Ergul, A., and Fagan, S. C. (2018). Silencing VEGF-B diminishes the neuroprotective effect of candesartan treatment after experimental focal cerebral ischemia. *Neurochem. Res.* 43, 1869–1878. doi: 10.1007/s11064-018-2604-x
- Issa, R., Krupinski, J., Bujny, T., Kumar, S., Kaluza, J., and Kumar, P. (1999). Vascular endothelial growth factor and its receptor, KDR, in human brain tissue after ischemic stroke. *Lab. Invest.* 79, 417–425.
- Jais, A., Solas, M., Backes, H., Chaurasia, B., Kleinridders, A., Theurich, S., et al. (2016). Myeloid-cell-derived VEGF maintains brain glucose uptake and limits cognitive impairment in obesity. *Cell* 165, 882–895. doi: 10.1016/j.cell.2016.03.033
- Jean LeBlanc, N., Guruswamy, R., and ElAli, A. (2018). Vascular endothelial growth factor isoform-B stimulates neurovascular repair after ischemic stroke by promoting the function of pericytes via vascular endothelial growth factor receptor-1. *Mol. Neurobiol.* 55, 3611–3626. doi: 10.1007/s12035-017-0478-6
- Kaya, D., Gürsoy-Ozdemir, Y., Yemisci, M., Tuncer, N., Aktan, S., and Dalkara, T. (2005). VEGF protects brain against focal ischemia without increasing blood-brain permeability when administered intracerebroventricularly. *J. Cereb. Blood Flow Metab.* 25, 1111–1118. doi: 10.1038/sj.jcbfm.9600109
- Kim, E., Yang, J., Park, K. W., and Cho, S. (2018). Inhibition of VEGF signaling reduces diabetes-exacerbated brain swelling, but not infarct size, in large cerebral infarction in mice. *Transl. Stroke Res.* 9, 540–548. doi: 10.1007/s12975-017-0601-z
- Krum, J. M., Mani, N., and Rosenstein, J. M. (2008). Roles of the endogenous VEGF receptors flt-1 and flk-1 in astroglial and vascular remodeling after brain injury. *Exp. Neurol.* 212, 108–117. doi: 10.1016/j.expneurol.2008.03.019
- Lelli, A., Gervais, A., Colin, C., Chéret, C., Ruiz de Almodovar, C., Carmeliet, P., et al. (2013). The NADPH oxidase Nox2 regulates VEGFR1/CSF-1R-mediated microglial chemotaxis and promotes early postnatal infiltration of phagocytes in the subventricular zone of the mouse cerebral cortex. *Glia* 61, 1542–1555. doi: 10.1002/glia.22540
- Leppänen, V.-M., Tvorogov, D., Kisko, K., Prota, A. E., Jeltsch, M., Anisimov, A., et al. (2013). Structural and mechanistic insights into VEGF receptor 3 ligand binding and activation. *Proc. Natl. Acad. Sci. U.S.A.* 110, 12960–12965. doi: 10.1073/pnas.1301415110
- Li, Y., Zhang, F., Nagai, N., Tang, Z., Zhang, S., Scotney, P., et al. (2008). VEGF-B inhibits apoptosis via VEGFR-1-mediated suppression of the expression of BH3-only protein genes in mice and rats. *J. Clin. Invest.* 118, 913–923. doi: 10.1172/JCI33673
- Longa, E. Z., Weinstein, P. R., Carlson, S., and Cummins, R. (1989). Reversible middle cerebral artery occlusion without craniectomy in rats. *Stroke* 20, 84–91. doi: 10.1161/01.str.20.1.84
- Louveau, A., Smirnov, I., Keyes, T. J., Eccles, J. D., Rouhani, S. J., Peske, J. D., et al. (2015). Structural and functional features of central nervous system lymphatic vessels. *Nature* 523, 337–341. doi: 10.1038/nature14432
- Luttun, A., Tjwa, M., and Carmeliet, P. (2002). Placental growth factor (PlGF) and its receptor Flt-1 (VEGFR-1): novel therapeutic targets for angiogenic disorders. *Ann. N. Y. Acad. Sci.* 979, 80–93. doi: 10.1111/j.1749-6632.2002.tb04870.x
- Ma, Y., Zechariah, A., Qu, Y., and Hermann, D. M. (2012). Effects of vascular endothelial growth factor in ischemic stroke. *J. Neurosci. Res.* 90, 1873–1882. doi: 10.1002/jnr.23088
- Marti, H. J. H., Bernaudin, M., Bellail, A., Schoch, H., Euler, M., Petit, E., et al. (2000). Hypoxia-induced vascular endothelial growth factor expression precedes neovascularization after cerebral ischemia. *Am. J. Pathol.* 156, 965–976. doi: 10.1016/s0002-9440(10)64964-4
- Mattsson, B., Sørensen, J. C., Zimmer, J., and Johansson, B. B. (1997). Neural grafting to experimental neocortical infarcts improves behavioral outcome and reduces thalamic atrophy in rats housed in enriched but not in standard environments. *Stroke* 28, 1225–1231; discussion 1231–1232.
- McCluskey, L., Campbell, S., Anthony, D., and Allan, S. M. (2008). Inflammatory responses in the rat brain in response to different methods of intra-cerebral administration. *J. Neuroimmunol.* 194, 27–33. doi: 10.1016/j.jneuroim.2007.11.009
- Melton, D. W., McManus, L. M., Gelfond, J. A. L., and Shireman, P. K. (2015). Temporal phenotypic features distinguish polarized macrophages in vitro. *Autoimmunity* 48, 161–176. doi: 10.3109/08916934.2015.1027816
- Meyer, R. D., Mohammadi, M., and Rahimi, N. (2006). A single amino acid substitution in the activation loop defines the decoy characteristic of VEGFR-1/FLT-1. *J. Biol. Chem.* 281, 867–875. doi: 10.1074/jbc.M506454200
- Nikodemova, M., Small, A. L., Smith, S. M. C., Mitchell, G. S., and Watters, J. J. (2014). Spinal but not cortical microglia acquire an atypical phenotype with high VEGF, galectin-3 and osteopontin, and blunted inflammatory responses in ALS rats. *Neurobiol. Dis.* 69, 43–53. doi: 10.1016/j.nbd.2013.11.009
- Olsson, A.-K., Dimberg, A., Kreuger, J., and Claesson-Welsh, L. (2006). VEGF receptor signalling? in control of vascular function. *Nat. Rev. Mol. Cell Biol.* 7, 359–371. doi: 10.1038/nrm1911
- Park, J. E., Chen, H. H., Winer, J., Houck, K. A., and Ferrara, N. (1994). Placenta growth factor. Potentiation of vascular endothelial growth factor bioactivity, in vitro and in vivo, and high affinity binding to Flt-1 but not to Flk-1/KDR. *J. Biol. Chem.* 269, 25646–25654.
- Paul, R., Zhang, Z. G., Eliceiri, B. P., Jiang, Q., Boccia, A. D., Zhang, R. L., et al. (2001). Src deficiency or blockade of Src activity in mice provides cerebral protection following stroke. *Nat. Med.* 7, 222–227. doi: 10.1038/84675
- Plate, K. H., Beck, H., Danner, S., Allegrini, P. R., and Wiessner, C. (1999). Cell type specific upregulation of vascular endothelial growth factor in an MCA-occlusion model of cerebral infarct. *J. Neuropathol. Exp. Neurol.* 58, 654–666. doi: 10.1097/00005072-199906000-00010
- Poesen, K., Lambrechts, D., Van Damme, P., Dhondt, J., Bender, F., Frank, N., et al. (2008). Novel role for vascular endothelial growth factor (VEGF) receptor-1 and its ligand VEGF-B in motor neuron degeneration. *J. Neurosci.* 28, 10451–10459. doi: 10.1523/JNEUROSCI.1092-08.2008
- Rahimi, N. (2006). VEGFR-1 and VEGFR-2: two non-identical twins with a unique physiognomy. *Front. Biosci.* 11, 818–829.
- Schallert, T., Fleming, S. M., Leasure, J. L., Tillerson, J. L., and Bland, S. T. (2000). CNS plasticity and assessment of forelimb sensorimotor outcome in unilateral rat models of stroke, cortical ablation, parkinsonism and spinal cord injury. *Neuropharmacology* 39, 777–787. doi: 10.1016/s0028-3908(00)00005-8
- Schindelin, J., Arganda-Carreras, I., Frise, E., Kaynig, V., Longair, M., Pietzsch, T., et al. (2012). Fiji: an open-source platform for biological-image analysis. *Nat. Methods* 9, 676–682. doi: 10.1038/nmeth.2019
- Shen, Y., Gu, J., Liu, Z., Xu, C., Qian, S., Zhang, X., et al. (2018). Inhibition of HIF-1 $\alpha$  reduced blood brain barrier damage by regulating MMP-2 and VEGF during acute cerebral ischemia. *Front. Cell. Neurosci.* 12:288. doi: 10.3389/fncel.2018.00288
- Shibuya, M. (2006). Vascular endothelial growth factor receptor-1 (VEGFR-1/Flt-1): a dual regulator for angiogenesis. *Angiogenesis* 9, 225–230; discussion 231.
- Simons, M., Gordon, E., and Claesson-Welsh, L. (2016). Mechanisms and regulation of endothelial VEGF receptor signalling. *Nat. Rev. Mol. Cell Biol.* 17, 611–625. doi: 10.1038/nrm.2016.87
- Stowe, A. M., Plautz, E. J., Eisner-Janowicz, I., Frost, S. B., Barbay, S., Zoubina, E. V., et al. (2007). VEGF protein associates to neurons in remote regions following cortical infarct. *J. Cereb. Blood Flow Metab.* 27, 76–85. doi: 10.1038/sj.jcbfm.9600320

- Stowe, A. M., Plautz, E. J., Nguyen, P., Frost, S. B., Eisner-Janowicz, I., Barbay, S., et al. (2008). Neuronal HIF-1 alpha protein and VEGFR-2 immunoreactivity in functionally related motor areas following a focal M1 infarct. *J. Cereb. Blood Flow Metab.* 28, 612–620. doi: 10.1038/sj.jcbfm.9600560
- Strawn, L. M., McMahon, G., App, H., Schreck, R., Kuchler, W. R., Longhi, M. P., et al. (1996). Flk-1 as a target for tumor growth inhibition. *Cancer Res.* 56, 3540–3545.
- Sun, Y., Jin, K., Xie, L., Childs, J., Mao, X. O., Logvinova, A., et al. (2003). VEGF-induced neuroprotection, neurogenesis, and angiogenesis after focal cerebral ischemia. *J. Clin. Invest.* 111, 1843–1851. doi: 10.1172/JCI17977
- Tovar-y-Romo, L. B., Bumpus, N. N., Pomerantz, D., Avery, L. B., Sacktor, N., McArthur, J. C., et al. (2012). Dendritic spine injury induced by the 8-hydroxy metabolite of efavirenz. *J. Pharmacol. Exp. Ther.* 343, 696–703. doi: 10.1124/jpet.112.195701
- Tovar-y-Romo, L. B., Penagos-Puig, A., and Ramírez-Jarquín, J. O. (2016). Endogenous recovery after brain damage: molecular mechanisms that balance neuronal life/death fate. *J. Neurochem.* 136, 13–27. doi: 10.1111/jnc.13362
- Tovar-y-Romo, L. B., and Tapia, R. (2012). Delayed administration of VEGF rescues spinal motor neurons from death with a short effective time frame in excitotoxic experimental models in vivo. *ASN Neuro* 4:e00081. doi: 10.1042/AN20110057
- Ulyatt, C., Walker, J., and Ponnambalam, S. (2011). Hypoxia differentially regulates VEGFR1 and VEGFR2 levels and alters intracellular signaling and cell migration in endothelial cells. *Biochem. Biophys. Res. Commun.* 404, 774–779. doi: 10.1016/j.bbrc.2010.12.057
- van Bruggen, N., Thibodeaux, H., Palmer, J. T., Lee, W. P., Fu, L., Cairns, B., et al. (1999). VEGF antagonism reduces edema formation and tissue damage after ischemia/reperfusion injury in the mouse brain. *J. Clin. Invest.* 104, 1613–1620. doi: 10.1172/JCI8218
- Weis, S. M., and Cheresch, D. A. (2005). Pathophysiological consequences of VEGF-induced vascular permeability. *Nature* 437, 497–504. doi: 10.1038/nature03987
- Wittko-Schneider, I. M., Schneider, F. T., and Plate, K. H. (2013). Brain homeostasis: VEGF receptor 1 and 2-two unequal brothers in mind. *Cell. Mol. Life Sci.* 70, 1705–1725. doi: 10.1007/s00018-013-1279-3
- Worthmann, H., Tryc, A. B., Goldbecker, A., Ma, Y. T., Tountopoulou, A., Hahn, A., et al. (2010). The temporal profile of inflammatory markers and mediators in blood after acute ischemic stroke differs depending on stroke outcome. *Cerebrovasc. Dis.* 30, 85–92. doi: 10.1159/000314624
- Wu, L., Ye, Z., Pan, Y., Li, X., Fu, X., Zhang, B., et al. (2018). Vascular endothelial growth factor aggravates cerebral ischemia and reperfusion-induced blood-brain-barrier disruption through regulating LOC102640519/HOXC13/ZO-1 signaling. *Exp. Cell Res.* 369, 275–283. doi: 10.1016/j.yexcr.2018.05.029
- Xu, Z., Han, K., Chen, J., Wang, C., Dong, Y., Yu, M., et al. (2017). Vascular endothelial growth factor is neuroprotective against ischemic brain injury by inhibiting scavenger receptor A expression on microglia. *J. Neurochem.* 142, 700–709. doi: 10.1111/jnc.14108
- Yang, S.-Z., Zhang, L.-M., Huang, Y.-L., and Sun, F.-Y. (2003). Distribution of Flk-1 and Flt-1 receptors in neonatal and adult rat brains. *Anat. Rec. A Discov. Mol. Cell. Evol. Biol.* 274, 851–856. doi: 10.1002/ar.a.10103
- Zhang, H., Shen, Y., Wang, W., and Gao, H. (2015). Rat model of focal cerebral ischemia in the dominant hemisphere. *Int. J. Clin. Exp. Med.* 8, 504–511.
- Zhang, Z. G., Zhang, L., Jiang, Q., Zhang, R., Davies, K., Powers, C., et al. (2000). VEGF enhances angiogenesis and promotes blood-brain barrier leakage in the ischemic brain. *J. Clin. Invest.* 106, 829–838. doi: 10.1172/JCI9369
- Zhang, Z. G., Zhang, L., Tsang, W., Soltanian-Zadeh, H., Morris, D., Zhang, R., et al. (2002). Correlation of VEGF and angiopoietin expression with disruption of blood-brain barrier and angiogenesis after focal cerebral ischemia. *J. Cereb. Blood Flow Metab.* 22, 379–392. doi: 10.1097/00004647-200204000-00002

**Conflict of Interest Statement:** The authors declare that the research was conducted in the absence of any commercial or financial relationships that could be construed as a potential conflict of interest.

Copyright © 2019 Cárdenas-Rivera, Campero-Romero, Heras-Romero, Penagos-Puig, Rincón-Heredia and Tovar-y-Romo. This is an open-access article distributed under the terms of the Creative Commons Attribution License (CC BY). The use, distribution or reproduction in other forums is permitted, provided the original author(s) and the copyright owner(s) are credited and that the original publication in this journal is cited, in accordance with accepted academic practice. No use, distribution or reproduction is permitted which does not comply with these terms.





# TMP21 in Alzheimer's Disease: Molecular Mechanisms and a Potential Target

Kaixin Qiu<sup>1,2,3†</sup>, Xiaojie Zhang<sup>4,5,6†</sup>, Shuai Wang<sup>2,3†</sup>, Chunyan Li<sup>1,2,3</sup>, Xin Wang<sup>2,3</sup>, Xuezhi Li<sup>2,3</sup> and Yili Wu<sup>2,3\*</sup>

<sup>1</sup> Cheeloo College of Medicine, Shandong University, Jinan, China, <sup>2</sup> Shandong Collaborative Innovation Center for Diagnosis, Treatment and Behavioral Interventions, Institute of Mental Health, Jining Medical University, Jining, China, <sup>3</sup> Shandong Key Laboratory of Behavioral Medicine, School of Mental Health, Jining Medical University, Jining, China, <sup>4</sup> Department of Psychiatry, The Second Xiangya Hospital, Central South University, Changsha, China, <sup>5</sup> National Clinical Research Center for Mental Disorders, Changsha, China, <sup>6</sup> National Technology Institute on Mental Disorders, Changsha, China

## OPEN ACCESS

### Edited by:

Rocio Martínez De Pablos,  
University of Seville, Spain

### Reviewed by:

María V. Sánchez Micó,  
University of Seville, Spain

Sebastian Jimenez,  
Network Biomedical Research Center  
on Neurodegenerative Diseases  
(CIBERNED), Spain

### \*Correspondence:

Yili Wu  
yili\_wu2004@yahoo.ca;  
wuyili@mail.jnmc.edu.cn

<sup>†</sup> These authors have contributed  
equally to this work

### Specialty section:

This article was submitted to  
Cellular Neuropathology,  
a section of the journal  
Frontiers in Cellular Neuroscience

**Received:** 23 April 2019

**Accepted:** 03 July 2019

**Published:** 17 July 2019

### Citation:

Qiu K, Zhang X, Wang S, Li C,  
Wang X, Li X and Wu Y (2019) TMP21  
in Alzheimer's Disease: Molecular  
Mechanisms and a Potential Target.  
Front. Cell. Neurosci. 13:328.  
doi: 10.3389/fncel.2019.00328

Alzheimer's disease (AD) is the most common form of dementia in the elderly, which is characterized by progressive cognitive impairment. Neuritic plaques, neurofibrillary tangles and neuronal loss are the major neuropathological hallmarks in AD brains. TMP21 is a key molecule for protein trafficking in cells. Growing evidence indicates that TMP21 is dysregulated in AD, which plays a pivotal role in neuritic plaque formation. Therefore, we aim to review the dysregulation of TMP21 in AD, the role of TMP21 in neuritic plaque formation and underlying mechanisms. Moreover, the potential role of TMP21 in neurofibrillary tangle formation, synaptic impairment and neuronal loss is discussed. It will provide an outlook into the potential of regulating TMP21 as a therapeutic approach for AD treatment.

**Keywords:** Alzheimer's disease, TMP21, A $\beta$ , Tau phosphorylation, neuronal loss

## INTRODUCTION

Alzheimer's disease (AD) is the most common form of neurodegenerative disorders leading to dementia in the elderly. Neuritic plaques, neurofibrillary tangles and neuronal loss are the major neuropathological in the brain of patients with AD (Wu et al., 2014b; Wang et al., 2017). Clinical manifestations of AD are characterized by progressive memory loss, cognitive impairment and psychosis (Walsh and Selkoe, 2004; Sorbi et al., 2012). With the aggravation of aging population, the incidence of AD is increasing year by year. According to World Alzheimer Report 2018, 50 million people worldwide are living with dementia in 2018, and the number will be tripled to more than 152 million by 2050 (Patterson, 2018). The total estimated worldwide cost of dementia is US\$1 trillion in 2018, and it will rise to 2 trillion dollars by 2030. Therefore, it is urgent to elucidate the pathogenesis of AD and develop effective treatments.

Growing evidence indicates that transmembrane protein, 21KD (TMP21), also known as transmembrane emp24 domain-containing protein 10 (TMED10), is a member of p24 family. It is dysregulated in AD and play a pivotal role in the pathogenesis of AD (Chen et al., 2006; Pardossi-Piquard et al., 2009; Zhang et al., 2019). Therefore, this review aims to describe the dysregulation of TMP21 in AD and its role in the pathogenesis of AD. Moreover, the underlying mechanisms

are discussed. Furthermore, we provide an outlook into the potential of regulating TMP21 as a therapeutic approach for AD treatment.

## CHARACTERISTICS OF TMP21

### p24 Family Proteins

p24 family proteins are type I transmembrane proteins with molecular weight of 22–24 KD (Stamnes et al., 1995). Based on sequence homology, p24 proteins are classified into four subfamilies, i.e.,  $\alpha$ ,  $\beta$ ,  $\gamma$ , and  $\delta$  (Dominguez et al., 1998; Strating et al., 2009; Pastor-Cantizano et al., 2016). In human,  $\alpha$  subfamily consists of TMED9 and TMED11, and  $\beta$  subfamily consists of TMED2 and TMED4.  $\gamma$  family is the largest subfamily of p24 family, including TMED1, TMED3, TMED5, TMED6, and TMED7, while TMP21 belongs to  $\delta$  subfamily. They share the conserved architecture, including luminal N-terminus, transmembrane (TM) region and cytosolic C-terminus. Generally, the luminal region contains a Golgi dynamic (GOLD) domain and a coiled-coil (CC) domain, while the cytosolic tail contains dilysine or dibasic (KKXX) motif and diaromatic (FF) motif. GOLD domain acts as a cargo receptor by mediating diverse protein-protein interactions, while CC domain mainly contributes to the oligomerization of p24 family members although a recent study showed that it does play a key role in recognition and transport of GPI-anchored proteins (Theiler et al., 2014). Oligomerization of p24 family members may affect their stabilization, localization, and expression levels (Carney and Bowen, 2004). For example, co-expression of TMED2 and TMP21 is necessary and sufficient for *cis*-Golgi/Golgi localization of each protein, while deleting each member individually leads to a general decrease of the other protein and loss function of the complex (Emery et al., 2000; Jenne et al., 2002). The cytosolic tail of p24 proteins contains signals for the binding of coat protein complex I (COPII) and coat protein complex I (COPI) contributing to the transport of cargo proteins between endoplasmic reticulum (ER) and Golgi apparatus in the early secretory pathway (Schimmöller et al., 1995; Muñiz et al., 2000; Barr et al., 2001; Belden and Barlowe, 2001; Gommel et al., 2001).

### Regulation of TMP21 Expression

Human TMP21 gene is located on chromosome 14q24.3, including 5 exons and 4 introns (Liu et al., 2011; Zhang et al., 2018), which is transcribed into two transcripts, Tmp21-I and Tmp21-II. With a nonsense mutation and a reading frame jump in comparison to Tmp21-I, Tmp21II was demonstrated to be derived from a pseudogene as the consequence of a duplication and diversification of hum-Tmp21-I. Thus, only Tmp21-I encodes a functional TMP21 (Blum et al., 1996; Horer et al., 1999). The expression of TMP21 is regulated at multiple levels. First, TMP21 is positively regulated by nuclear factor of activated T-cells (NFAT) at transcriptional level. In addition, sequence analysis showed that a number of putative *cis*-acting elements, e.g., CREB, YY1F, AP1 etc., are located in TMP21 promoter region, suggesting that TMP21 might be regulated by multiple transcriptional factors (Liu et al., 2011). Moreover,

TMP21 expression could be regulated at post-transcriptional level. For example, the single-nucleotide polymorphism (SNP) rs12435391 in intron 4 significantly increases TMP21 expression by increasing the splicing efficiency of *TMP21* pre-mRNA (Zhang et al., 2018). Furthermore, TMP21 is degraded through ubiquitin-proteasome pathway with a short half-life of approximately 3hs, indicating that TMP21 could be regulated at post-translational level (Liu et al., 2008).

### Tissue-Specific Expression and Functions *in vivo*

TMP21 is ubiquitously expressed in different tissues in mammals. It was reported that TMP21 transcript is expressed in brain, pancreas, lung, liver, spleen etc. multiple organs of rats (Blum et al., 1996; Hosaka et al., 2007; Vetrivel et al., 2008). In human, both TMP21 mRNA and protein are highly expressed in heart, liver, spleen etc., whereas they are moderately expressed in brain, pancreas, colon etc. (Xie et al., 2014). In addition, TMP21 is expressed in most regions of the brain including septum, striatum, cortex, hippocampus, amygdala, thalamus, hypothalamus, cerebellum, and brainstem (Vetrivel et al., 2008). It shows stronger expression in neuronal cells than in glial cells (Vetrivel et al., 2008). Importantly, temporal expression of TMP21 was observed in mouse brain (Vetrivel et al., 2008). High level of TMP21 was detected in embryonic mouse brain, however, the expression of TMP21 gradually declined in brains of postnatal mice and reached lower level in adult brains. The evidence suggests that TMP21 expression is stringently regulated, which might play a pivotal role in development and maintenance of physiological functions. Consistently, complete deletion of TMP21 results in embryonic lethality at very early stage, while transgenic mice with neuron-specific increase of TMP21 expression display post-natal growth retardation and severe neurological problems including tremors, seizure, ataxia, uncoordinated movements and premature death (Denzel et al., 2000; Gong et al., 2011).

### Subcellular Distribution and Molecular Functions

TMP21 is a protein with 219 amino acids, including a signal peptide with 31 amino acids and a mature peptide with 188 amino acids. The signal peptide directs the newly synthesized TMP21 translocating into the ER, where it is cleaved and the mature TMP21 is generated. The mature TMP21 consists of N-terminal luminal region (32–185 aa), transmembrane region (186–206 aa) and C-terminal cytoplasmic region (207–219 aa), while the GOLD domain (41–193 aa) contains part of luminal region and part of transmembrane region, respectively (Anantharaman and Aravind, 2002; Nagae et al., 2016). TMP21 is enriched in the membrane of ER, plasma and Golgi apparatus. In addition, it was also reported to be located in ER-Golgi intermediate compartment (ERGIC) membrane and secretory vesicle membrane (Emery et al., 2000; Hosaka et al., 2007; Langhans et al., 2008; Strating and Martens, 2009). As a vesicle trafficking protein, the main function of TMP21 is for protein transport. First, TMP21 serves as a cargo receptor



protein contributing to uptaking cargo proteins into COP vesicles, which is mainly mediated by GOLD domain (Muñiz et al., 2000; Anantharaman and Aravind, 2002; Castillon et al., 2009). The cytoplasmic tail of TMP21 is responsible for its binding to the subunits of COPI or COPII contributing to the transport of cargo proteins between ER and Golgi apparatus (Muñiz et al., 2000; Belden and Barlowe, 2001; Gommel et al., 2001; Blum and Lepier, 2008). Secondly, TMP21 cytoplasmic tail combined with the Golgi matrix proteins has an effect on the transport of cargo proteins to the cell surface or the efficient retention of them in the Golgi apparatus (Barr et al., 2001; Blum and Lepier, 2008). In addition, TMP21 also selectively interacts with glycosylphosphatidylinositol-anchored proteins contributing to their ER export and lipid rafts translocation. Moreover, TMP21 is a major component of Golgi apparatus and *cis*-Golgi network (CGN), which is essential for the integrity and proper organization of Golgi structure. Furthermore, TMP21 is a modulator of  $\gamma$ -secretase, which is implicated in various physiological and pathological processes by cleaving its substrates, e.g., APP and Notch.  $\gamma$ -secretase is a protein complex consisting of the core catalytic components, presenilin1 (PSEN1) and presenilin2 (PSEN2), and the regulatory components, nicastrin, APH-1 and PEN-2. TMP21 is a non-essential component of the complex (Pardossi-Piquard et al., 2009; Wang et al., 2017). Importantly, TMP21 regulates  $\gamma$ -secretase cleavage at the  $\gamma$ -site but not at the  $\epsilon$ -site, indicating that TMP21 selectively regulates  $\gamma$ -secretase cleavage on its substrate. For example, TMP21 regulates  $\gamma$ -secretase cleavage of APP at the  $\gamma$ -site, however, it has no effect on the  $\gamma$ -secretase cleavage of Notch at the  $\epsilon$ -site (Chen et al., 2006; Bromley-Brits and Song, 2012). Compared with other p24 members, it is a specific feature of TMP21 to regulate  $\gamma$ -secretase activity.

## ABERRANT EXPRESSION OF TMP21 IN AD

Increased evidence indicates that TMP21 is dysregulated in AD. First, Chr14q24.3 is defined as a minimal co-segregating region by linkage studies, which contains the major genes predisposing to early onset AD. *TMP21* gene is located in this region. Secondly, the expression of TMP21 are significantly reduced in brains of both sporadic AD cases and familial AD cases compared with age-matched controls, which is consistent with the previous study that knockdown of TMP21 increases A $\beta$  expression (Chen et al., 2006; Vetrivel et al., 2008). In addition, the SNP rs12435391 in intron 4 of *TMP21* gene is associated with increased AD risk by accelerating *TMP21* pre-mRNA splicing leading to increased expression of TMP21 (Zhang et al., 2018). It seems contradictory that both reduced and increased TMP21 levels are associated with AD. However, two issues need to be considered. First, it has to be noted that the latter experiment was done in HEK293 cells but not in neurons. The exact role of SNP rs12435391 in the regulation of TMP21 expression in neuronal cells or brains needs to be further investigated. Secondly, the precise control of TMP21 expression is crucial to maintain the physiological functions as both increased and decreased TMP21 expression is

lethal in mice (Denzel et al., 2000; Gong et al., 2012). It suggests that TMP21 might has bidirectional roles, which is common for many important molecules, such as regulator of calcineurin 1 (Wu and Song, 2013; Yan et al., 2014; Duan et al., 2015; Wu et al., 2015). Thus, it highly indicates that the precise control of TMP21 expression is crucial to maintain its physiological functions, avoiding the pathogenic effects.

Dysregulated calcineurin-NFAT signaling might be implicated in the dysregulation of TMP21 in AD as TMP21 is positively regulated by NFAT at transcriptional level (Abdul et al., 2009; Liu et al., 2011; Sun et al., 2014; Wu et al., 2014a). First, the regulator of calcineurin 1 (RCAN1) is significantly increased in AD brains, which inhibits calcineurin-NFAT signaling (Wu and Song, 2013). It suggests that increased RCAN1 may contribute to the reduction of TMP21 expression in AD. In addition, elevated oligomeric A $\beta$  stimulates calcineurin-NFAT signaling in neurons and astrocytes, which might promote TMP21 expression in AD (Shankar et al., 2007; Abdul et al., 2009). Moreover, a number of putative *cis*-acting elements located in TMP21 promoter region might be implicated in the dysregulation of TMP21 transcription as various transcriptional factors are altered in AD, such as CREB (Liu et al., 2011; Pugazhenthir et al., 2011; Bartolotti et al., 2016; Ettcheto et al., 2018). Furthermore, impairment of ubiquitin-proteasome system in AD might contribute to TMP21 upregulation as TMP21 is degraded through ubiquitin-proteasome pathway (Liu et al., 2008). Therefore, aberrant expression TMP21 in AD is a combined effect by various regulation mechanisms, and differential alteration of TMP21 observed in AD might be associated with the progress or stages of AD.

## TMP21 IN THE PATHOGENESIS OF AD

Neuritic plaques, neurofibrillary tangles and neuronal loss are the characteristic neuropathological features in AD brains (Wu et al., 2014a,b; Wang et al., 2017). Increased evidence indicates that dysregulated TMP21 promotes neuritic plaque formation. Moreover, TMP21 dysregulation potentially contributes to neurofibrillary tangle formation, synaptic impairment and neuronal loss.

### Aberrant Expression of TMP21 Promotes A $\beta$ Generation

Neuritic plaques are only observed in AD while neurofibrillary tangles, synaptic impairment and neuronal loss also exist in many other neurodegenerative disorders. Thus, neuritic plaques are the only neuropathological hallmark to distinguish AD from other neurodegenerative disorders. Amyloid  $\beta$ -protein (A $\beta$ ) is the major component of neuritic plaques, which is derived from sequential cleavages of APP by  $\beta$ - and  $\gamma$ -secretase. However, the majority of APP undergoes non-amyloidogenic pathway. First, APP is cleaved by  $\alpha$ -secretase to generate a C-terminal fragment (CTF) of 83 amino acids (C83), excluding A $\beta$  generation (Wang et al., 2017). In addition, beta-site APP cleaving enzyme 2 (BACE2) and  $\eta$ -secretase are also involved in non-amyloidogenic

pathway although our recent work showed that BACE2 is a conditional  $\beta$ -secretase under specific conditions (Willem et al., 2015; Wang et al., 2019). The minority of APP is cleaved by beta-site APP cleaving enzyme 1 (BACE1) at Asp1 ( $\beta$  site) and Glu11 ( $\beta'$  site, numbering for A $\beta$ ) sites, respectively. Glu11 is the major  $\beta$ -cleavage site to yield a CTF with 89 amino acids (C89). C89 is further cleaved by  $\gamma$ -secretase to produce a truncated A $\beta_{11-40/42}$ , excluding A $\beta$  generation. Asp1 is the minor  $\beta$ -cleavage site to generate a CTF with 99 amino acids (C99) which is further cleaved by  $\gamma$ -secretase to produce A $\beta$  (Liu et al., 2002; Deng et al., 2013).

Increased evidence indicates that dysregulated TMP21 is implicated in increased A $\beta$  generation in AD (Figure 1A). First,  $\gamma$ -secretase is a protein complex consisting of PSEN1 or PSEN2, nicastrin, APH-1 and PEN-2, while TMP21 is a non-essential component of the complex (Wang et al., 2017). As a modulator of  $\gamma$ -secretase, reduced TMP21 expression promotes A $\beta$  generation by increasing  $\gamma$ -secretase cleavage of APP at  $\gamma$ -site (Chen et al., 2006; Bromley-Brits and Song, 2012). Secondly, TMP21, likely other p24 family proteins, regulates the trafficking of APP, which further affects A $\beta$  production. For example, knockdown of TMP21 expression by specific siRNA increases the stability and maturation of nascent APP in both non-neuronal and neuroblastoma cell lines, contributing to increased APP level and A $\beta$  generation. Moreover, TMP21 suppression compromises bidirectional transport of APP in the ER/Golgi,

resulting in more APP undergoing amyloidogenic cleavage in endocytic compartments, as well as secretion of sAPP, A $\beta_{40}$  and A $\beta_{42}$  (Vetrivel et al., 2007). Our recent work showed that reduced TMP21 inhibits the expression of phosphoinositide-3-kinase regulatory subunit 1 (PI3K $\alpha$ ) in mouse brains, which might release the inhibitory effect of PI3K/AKT on GSK3 $\beta$  contributing to increased activity of GSK3 $\beta$  (Zhang et al., 2019). Increased GSK3 $\beta$  activity promotes APP phosphorylation facilitating APP stability and A $\beta$  generation (Wang et al., 2017). On the other hand, increased GSK3 $\beta$  activity facilitates NF- $\kappa$ B-mediated BACE1 expression and activity, which further promotes APP processing and A $\beta$  generation (Ly et al., 2013).

AD-associated SNP rs12435391 in intron 4 of *TMP21* gene increases TMP21 expression, which promotes A $\beta$  generation (Zhang et al., 2018). It remains unknown that this effect is mediated by regulating  $\gamma$ -secretase activity or modification/trafficking of APP or BACE1 activity. In addition, as a vesicle trafficking protein, aberrant expression of TMP21 might also regulate the trafficking and stability of multiple proteins involved in APP processing (e.g., APP,  $\alpha$ -secretase, BACE1, BACE2), leading to increased A $\beta$  generation. For example, TMP21 does affect APP stability contributing to the alteration of A $\beta$  production (Vetrivel et al., 2007). Furthermore, TMP21 might be implicated in mTOR- or PI3K-mediated GSK3 $\beta$  activation, which subsequently contributes to increased A $\beta$  generation by upregulating APP expression, BACE1 expression

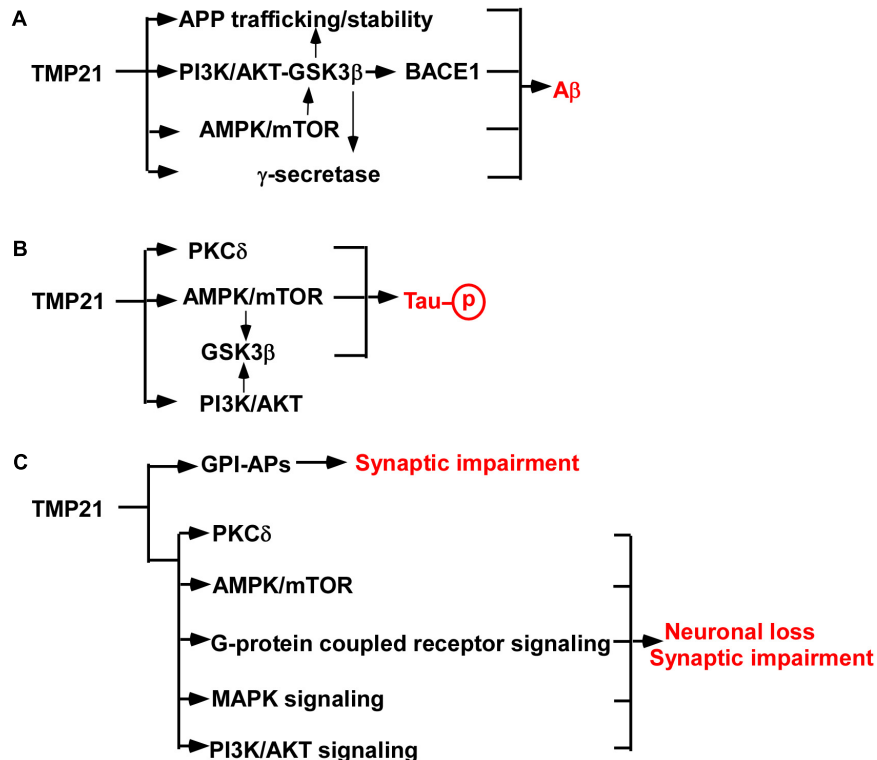


**FIGURE 1 |** TMP21 in the pathogenesis of AD. **(A)** TMP21 dysregulation promotes A $\beta$  generation. **(B)** TMP21 dysregulation might increase Tau phosphorylation. **(C)** TMP21 dysregulation might contribute to synaptic impairment and neuronal loss.

and  $\gamma$ -secretase activity (Qing et al., 2008; Caccamo et al., 2013; Ly et al., 2013; Yang et al., 2013; Xu et al., 2015; Wang et al., 2017; Zhang et al., 2019). However, it has to be noted that the effect of increased TMP21 on promoting A $\beta$  generation was determined in HEK293 cells but not in neurons. The exact role of SNP rs12435391 in A $\beta$  generation in brain or neuronal cells needs to be further investigated.

TMP21 possibly plays a bidirectional role in A $\beta$  production as both upregulation and downregulation of TMP21 promotes A $\beta$  generation in HEK293. In addition, TMP21 dysregulation does show bidirectional functions in mice as both the increase and decrease of TMP21 expression is lethal in mice (Denzel et al., 2000; Gong et al., 2012). Moreover, the bidirectional roles are common for many important molecules. For example, both upregulation and downregulation of regulator of calcineurin 1 facilitates neuronal apoptosis (Wu and Song, 2013; Yan et al., 2014; Duan et al., 2015; Wu et al., 2015). Thus, the effect of TMP21 dysregulation on A $\beta$  generation in neuronal cells and underlying mechanisms need to be further investigated.

## Potential Roles of Dysregulated TMP21 in Tau Phosphorylation and Neuronal Loss

The major component of neurofibrillary tangles is hyperphosphorylated Tau. Increased Tau phosphorylation promotes neurofibrillary tangle formation (Wu et al., 2014b). Although no direct evidence supports that TMP21 plays a role in Tau phosphorylation, a couple of studies indicates that TMP21 might contribute to the regulation of Tau phosphorylation (**Figure 1B**) (Tsujo et al., 2000; Wang et al., 2011; Caccamo et al., 2013; Xu et al., 2015; Lee et al., 2017; Zhang et al., 2019). First, increased A $\beta$  promotes Tau hyperphosphorylation via various mechanisms, e.g., oxidative stress, while TMP21 dysregulation contributes to A $\beta$  generation (Wu et al., 2014b). It suggests that dysregulated TMP21 might promote Tau hyperphosphorylation mediated by increasing A $\beta$  generation. In addition, increasing mTOR activity promotes Tau phosphorylation, while reduced TMP21 expression facilitates the activation of mTOR (Caccamo et al., 2013; Xu et al., 2015). It suggests that reduced TMP21 might promote mTOR-mediated Tau phosphorylation contributing to neurofibrillary tangle formation in AD (Lee et al., 2017). Moreover, protein kinase C delta (PKC $\delta$ ) inactivates GSK3 $\beta$ -mediated Tau phosphorylation, while TMP21 inhibits PKC $\delta$  activation (Tsujo et al., 2000; Wang et al., 2011). Consistently, our recent work indicates that reduced TMP21 might increase GSK3 $\beta$  activity by downregulating PiK3r1 expression (Zhang et al., 2019). It suggests that aberrant expression TMP21 might play a role in Tau hyperphosphorylation contributing to neurofibrillary tangle formation in AD via various mechanisms.

Synaptic impairment and neuronal loss is the major cause leading to cognitive impairment and psychosis in AD. However, the role of aberrant expression of TMP21 in synaptic dysfunction and neuronal loss is elusive. Growing evidence indicates that TMP21 might be involved in synaptic dysfunction

and neuronal loss in AD (**Figure 1C**). First, changes in TMP21 expression might be implicated in the dysfunction of ER processing and export of glycosylphosphatidylinositols-associated proteins (GPI-APs), which acts as a modulator of synapse development via direct interactions with key synapse-organizing proteins (Um and Ko, 2017; Kim et al., 2019). TMP21 is a member of p24 protein which specifically recognizes GPI-APs and is essential for GPI-APs quality control. Either dysregulation or dysfunction of TMP21 may lead to abnormal synaptic stability via faulty quality-control of GPI-APs, which has been reported in the frontal cortex of elderly subjects with schizophrenia (Kim et al., 2019). Consistently, TMP21 reduction significantly affects synapse-associated biological processes and pathways in mouse brains, e.g., synaptic development, synapse organization and synaptic vesicle cycle etc. (Zhang et al., 2019). Moreover, TMP21 inhibits mTOR- and PKC $\delta$ -mediated apoptosis in cancer cells, while dysfunction of mTOR- and PKC $\delta$  is implicated in synaptic impairment and neuronal apoptosis (Caccamo et al., 2010; Wang et al., 2011; Xu et al., 2015). It suggests that dysregulation of TMP21 might be implicated in synaptic impairment and neuronal apoptosis. In addition, TMP21 reduction could lead to the dysregulation of multiple pathways, e.g., G-protein coupled receptor signaling pathway, MAPK signaling pathway, PI3K-AKT pathway etc., which play an important role in synaptic impairment and neuronal apoptosis, such as apelin and apelin receptor system (Franco et al., 2017; Qiu et al., 2017; Wu et al., 2017, 2018; Zhang et al., 2019). Furthermore, TMP21 dysregulation facilitates A $\beta$  generation and potentially increases Tau hyperphosphorylation, which subsequently promotes synaptic impairment and neuronal loss. For example, A $\beta$ -induced dysregulation of an NMDA-type glutamate receptor-dependent signaling promotes synapse loss, while TMP21 dysregulation promotes A $\beta$  generation. It suggests that dysregulated TMP21 might trigger synapse loss through A $\beta$ -induced dysfunction of the NMDA-type glutamate receptor (Shankar et al., 2007). Hyperphosphorylation of Tau promotes neuronal apoptosis, while TMP21 potentially increases Tau phosphorylation, suggesting that dysregulated TMP21 might promote neuronal apoptosis by increasing Tau phosphorylation (Lee et al., 2017). Therefore, TMP21 dysregulation might contribute to synaptic impairment and neuronal loss, which is mediated by the direct effect of TMP21 dysregulation or the indirect effect of TMP21 dysregulation-induced increased A $\beta$  generation and Tau phosphorylation.

## CONCLUSION

Growing evidence indicates that TMP21 might play a central role in the pathogenesis of AD and it might be a specific and effective target for AD treatment. First, dysregulated TMP21 promotes A $\beta$  generation by modulating APP trafficking/stability and  $\gamma$ -secretase activity, while it potentially regulates BACE1 expression and activity. Importantly, TMP21 regulates  $\gamma$ -secretase cleavage of APP at the  $\gamma$ -site, however, it has no effect on the  $\gamma$ -secretase cleavage of Notch at the  $\epsilon$ -site.

It is well-known that inhibiting Notch cleavage and its functions is a major obstacle to develop  $\gamma$ -secretase inhibitors for AD treatment. The specific feature of TMP21, inhibiting  $\gamma$ -cleavage but sparing  $\epsilon$ -cleavage, makes it as a potential target to reduce A $\beta$  generation and avoid toxic effects. Although no direct evidence shows that TMP21 plays a role in Tau pathology and synaptic/neuronal loss, a number of studies suggest that TMP21 dysregulation might be implicated in Tau pathology and synaptic/neuronal loss. Above evidence indicates that modulating TMP21 expression is a potential target for AD treatment. However, targeting TMP21 for AD treatment is limited by the following reasons. First, developing an approach to precisely controlling TMP21 expression is crucial for clinical application. Moreover, elucidating a number of issues is critical for developing effective TMP21-targeting approaches, e.g., the consistence of TMP21 regulation in neurons and non-neuronal cells, the physiological function of TMP21, temporal regulation of TMP21 during AD progress etc.

## REFERENCES

- Abdul, H. M., Sama, M. A., Furman, J. L., Mathis, D. M., Beckett, T. L., Weidner, A. M., et al. (2009). Cognitive decline in alzheimer's disease is associated with selective changes in calcineurin/NFAT signaling. *J. Neurosci.* 29, 12957–12969. doi: 10.1523/JNEUROSCI.1064-09.2009
- Anantharaman, V., and Aravind, L. (2002). The gold domain, a novel protein module involved in golgi function and secretion. *Genome Biol.* 3:research0023.
- Barr, F. A., Preisinger, C., Kopajtich, R., and Körner, R. (2001). Golgi matrix proteins interact with p24 cargo receptors and aid their efficient retention in the golgi apparatus. *J. Cell Biol.* 155, 885–892. doi: 10.1083/jcb.2001.08102
- Bartolotti, N., Bennett, D. A., and Lazarov, O. (2016). Reduced pCREB in alzheimer's disease prefrontal cortex is reflected in peripheral blood mononuclear cells. *Mol. Psychiatry* 21, 1158–1166. doi: 10.1038/mp.2016.111
- Belden, W. J., and Barlowe, C. (2001). Distinct roles for the cytoplasmic tail sequences of Emp24p and Erv25p in transport between the endoplasmic reticulum and golgi complex. *J. Biol. Chem.* 276, 43040–43048. doi: 10.1074/jbc.M108113200
- Blum, R., Feick, P., Puype, M., Vandekerckhove, J., Klengel, R., Nastainczyk, W., et al. (1996). Tmp21 and p24A, two type I proteins enriched in pancreatic microsomal membranes, are members of a protein family involved in vesicular trafficking. *J. Biol. Chem.* 271, 17183–17189. doi: 10.1074/jbc.271.29.17183
- Blum, R., and Lepier, A. (2008). The luminal domain of p23 (Tmp21) plays a critical role in p23 cell surface trafficking. *Traffic* 9, 1530–1550. doi: 10.1111/j.1600-0854.2008.00784.x
- Bromley-Brits, K., and Song, W. (2012). The role of TMP21 in trafficking and amyloid- $\beta$  precursor protein (APP) processing in alzheimer's disease. *Curr. Alzheimer Res.* 9, 411–424. doi: 10.2174/156720512800492521
- Caccamo, A., Magri, A., Medina, D. X., Wisely, E. V., Lopez-Aranda, M. F., Silva, A. J., et al. (2013). mTOR regulates tau phosphorylation and degradation: implications for alzheimer's disease and other tauopathies. *Aging Cell* 12, 370–380. doi: 10.1111/acle.12057
- Caccamo, A., Majumder, S., Richardson, A., Strong, R., and Oddo, S. (2010). Molecular interplay between mammalian target of rapamycin (mTOR), amyloid-beta, and tau: effects on cognitive impairments. *J. Biol. Chem.* 285, 13107–13120. doi: 10.1074/jbc.M110.100420
- Carney, G. E., and Bowen, N. J. (2004). p24 proteins, intracellular trafficking, and behavior: *Drosophila melanogaster* provides insights and opportunities. *Biol. Cell* 96, 271–278. doi: 10.1111/j.1768-322x.2004.tb01415.x
- Castillon, G. A., Watanabe, R., Taylor, M., Schwabe, T. M., and Riezman, H. (2009). Concentration of GPI-anchored proteins upon ER exit in yeast. *Traffic* 10, 186–200. doi: 10.1111/j.1600-0854.2008.00857.x
- Chen, F., Hasegawa, H., Schmitt-Ulms, G., Kawai, T., Bohm, C., Katayama, T., et al. (2006). TMP21 is a presenilin complex component that modulates gamma-secretase but not epsilon-secretase activity. *Nature* 440, 1208–1212. doi: 10.1038/nature04667
- Deng, Y., Wang, Z., Wang, R., Zhang, X., Zhang, S., Wu, Y., et al. (2013). Amyloid-beta protein (A $\beta$ ) Glu11 is the major beta-secretase site of beta-site amyloid-beta precursor protein-cleaving enzyme 1 (BACE1), and shifting the cleavage site to A $\beta$  Asp1 contributes to alzheimer pathogenesis. *Eur. J. Neurosci.* 37, 1962–1969. doi: 10.1111/ejn.12235
- Denzel, A., Otto, F., Girod, A., Pepperkok, R., Watson, R., Rosewell, I., et al. (2000). The p24 family member p23 is required for early embryonic development. *Curr. Biol.* 10, 55–58. doi: 10.1016/S0960-9822(99)00266-3
- Dominguez, M., Deigaard, K., Füllekrug, J., Dahan, S., Fazel, A., Paccaud, J. P., et al. (1998). gp25L/emp24/p24 protein family members of the cis-golgi network bind both COP I and II coatomer. *J. Cell Biol.* 140, 751–765. doi: 10.1083/jcb.140.4.751
- Duan, H., Li, Y., Yan, L., Yang, H., Wu, J., Qian, P., et al. (2015). Rcan1-1L overexpression induces mitochondrial autophagy and improves cell survival in angiotensin II-exposed cardiomyocytes. *Exp. Cell Res.* 335, 99–106. doi: 10.1016/j.yexcr.2015.05.003
- Emery, G., Rojo, M., and Gruenberg, J. (2000). Coupled transport of p24 family members. *J. Cell Sci.* 113(Pt 13), 2507–2516.
- Ettcheto, M., Abad, S., Petrov, D., Pedros, I., Busquets, O., Sanchez-Lopez, E., et al. (2018). Early preclinical changes in hippocampal creb-binding protein expression in a mouse model of familial alzheimer's disease. *Mol. Neurobiol.* 55, 4885–4895. doi: 10.1007/s12035-017-0690-4
- Franco, R., Martinez-Pinilla, E., Navarro, G., and Zamarbide, M. (2017). Potential of GPCRs to modulate MAPK and mTOR pathways in alzheimer's disease. *Prog. Neurobiol.* 149–150, 21–38. doi: 10.1016/j.pneurobio.2017.01.004
- Gommel, D. U., Memon, A. R., Heiss, A., Lottspeich, F., Pfannstiel, J., Lechner, J., et al. (2001). Recruitment to golgi membranes of ADP-ribosylation factor 1 is mediated by the cytoplasmic domain of p23. *EMBO J.* 20, 6751–6760. doi: 10.1093/emboj/20.23.6751
- Gong, P., Roseman, J., Fernandez, C. G., Vetrivel, K. S., Bindokas, V. P., Zitzow, L. A., et al. (2011). Transgenic neuronal overexpression reveals that stringently regulated p23 expression is critical for coordinated movement in mice. *Mol. Neurodegener.* 6:87. doi: 10.1186/1750-1326-6-87
- Gong, P., Roseman, J., Vetrivel, K. S., Bindokas, V. P., Zitzow, L. A., Kar, S., et al. (2012). Stringently regulated p23 expression is critical for coordinated movement in mice: implications for alzheimer's disease. *Mol. Neurodegener.* 7(Suppl. 1):L2. doi: 10.1186/1750-1326-6-87
- Horer, J., Blum, R., Feick, P., Nastainczyk, W., and Schulz, I. (1999). A comparative study of rat and human Tmp21 (p23) reveals the pseudogene-like features

## AUTHOR CONTRIBUTIONS

YW conceived and formulated the manuscript. KQ, XZ, SW, CL, XW, and YW wrote the manuscript. XZ, XL, and YW revised the manuscript.

## FUNDING

This work was supported by the National Natural Science Foundation of China (NSFC) Grant 81771147 to YW, Grant 81501108 to XZ, Grant 31701247 to XL, Science and Technology Bureau of Jining City Grant 2017SMNS006 to SW, Teacher Research Support Foundation of Jining Medical University Grant JY2017JS001 to XW, and Research Fund for Lin He's Academician Workstation of New Medicine and Clinical Translation in Jining Medical University Grant JYHL2018MS07 to XW.



- of human Tmp21-II. *DNA Seq.* 10, 121–126. doi: 10.3109/1042517990908429
- Hosaka, M., Watanabe, T., Yamauchi, Y., Sakai, Y., Suda, M., Mizutani, S., et al. (2007). A subset of p23 localized on secretory granules in pancreatic beta-cells. *J. Histochem. Cytochem.* 55, 235–245. doi: 10.1369/jhc.6a7093.2006
- Jenne, N., Frey, K., Brugger, B., and Wieland, F. T. (2002). Oligomeric state and stoichiometry of p24 proteins in the early secretory pathway. *J. Biol. Chem.* 277, 46504–46511. doi: 10.1074/jbc.M206989200
- Kim, P., Scott, M. R., and Meador-Woodruff, J. H. (2019). Abnormal ER quality control of neural GPI-anchored proteins via dysfunction in ER export processing in the frontal cortex of elderly subjects with schizophrenia. *Transl. Psychiatry* 9:6. doi: 10.1038/s41398-018-0359-4
- Langhans, M., Marcote, M. J., Pimpl, P., Virgili-López, G., Robinson, D. G., and Aniento, F. (2008). In vivo trafficking and localization of p24 proteins in plant cells. *Traffic* 9, 770–785. doi: 10.1111/j.1600-0854.2008.00719.x
- Lee, K. H., Lee, S. J., Lee, H. J., Choi, G. E., Jung, Y. H., Kim, D. I., et al. (2017). Amyloid beta1-42 (Aβeta1-42) induces the cdk2-mediated phosphorylation of tau through the activation of the mtorc1 signaling pathway while promoting neuronal cell death. *Front. Mol. Neurosci.* 10:229. doi: 10.3389/fnmol.2017.00229
- Liu, K., Doms, R. W., and Lee, V. M. (2002). Glu11 site cleavage and n-terminally truncated a beta production upon bace overexpression. *Biochemistry* 41, 3128–3136. doi: 10.1021/bi015800g
- Liu, S., Bromley-Brits, K., Xia, K., Mittelholtz, J., Wang, R., and Song, W. (2008). TMP21 degradation is mediated by the ubiquitin-proteasome pathway. *Eur. J. Neurosci.* 28, 1980–1988. doi: 10.1111/j.1460-9568.2008.06497.x
- Liu, S., Zhang, S., Bromley-Brits, K., Cai, F., Zhou, W., Xia, K., et al. (2011). Transcriptional regulation of TMP21 by NFAT. *Mol. Neurodegener.* 6:21. doi: 10.1186/1750-1326-6-21
- Ly, P. T., Wu, Y., Zou, H., Wang, R., Zhou, W., Kinoshita, A., et al. (2013). Inhibition of GSK3beta-mediated BACE1 expression reduces alzheimer-associated phenotypes. *J. Clin. Invest.* 123, 224–235. doi: 10.1172/JCI64516
- Muñiz, M., Nuoffer, C., Hauri, H. P., and Riezman, H. (2000). The Emp24 complex recruits a specific cargo molecule into endoplasmic reticulum-derived vesicles. *J. Cell Biol.* 148, 925–930. doi: 10.1083/jcb.148.5.925
- Nagae, M., Hirata, T., Morita-Matsumoto, K., Theiler, R., Fujita, M., Kinoshita, T., et al. (2016). 3D structure and interaction of p24β and p24δ golgi dynamics domains: implication for p24 complex formation and cargo transport. *J. Mol. Biol.* 428, 4087–4099. doi: 10.1016/j.jmb.2016.08.023
- Pardossi-Piquard, R., Böhm, C., Chen, F., Kanemoto, S., Checler, F., Schmitt-Ulms, G., et al. (2009). TMP21 transmembrane domain regulates gamma-secretase cleavage. *J. Biol. Chem.* 284, 28634–28641. doi: 10.1074/jbc.M109.059345
- Pastor-Cantizano, N., Montesinos, J. C., Bernat-Silvestre, C., Marcote, M. J., and Aniento, F. (2016). p24 family proteins: key players in the regulation of trafficking along the secretory pathway. *Protoplasma* 253, 967–985. doi: 10.1007/s00709-015-0858-6
- Patterson, C. (2018). *World Alzheimer Report 2018*. London: Alzheimer's Disease International (ADI).
- Pugazhenth, S., Wang, M., Pham, S., Sze, C. I., and Eckman, C. B. (2011). Downregulation of CREB expression in alzheimer's brain and in abeta-treated rat hippocampal neurons. *Mol. Neurodegener.* 6:60. doi: 10.1186/1750-1326-6-60
- Qing, H., He, G., Ly, P. T., Fox, C. J., Staufienbiel, M., Cai, F., et al. (2008). Valproic acid inhibits abeta production, neuritic plaque formation, and behavioral deficits in alzheimer's disease mouse models. *J. Exp. Med.* 205, 2781–2789. doi: 10.1084/jem.20081588
- Qiu, J., Wang, X., Wu, F., Wan, L., Cheng, B., Wu, Y., et al. (2017). Low dose of apelin-36 attenuates er stress-associated apoptosis in rats with ischemic stroke. *Front. Neurol.* 8:556. doi: 10.3389/fneur.2017.00556
- Schimmöller, F., Singer-Krüger, B., Schröder, S., Krüger, U., Barlowe, C., and Riezman, H. (1995). The absence of Emp24p, a component of ER-derived COPII-coated vesicles, causes a defect in transport of selected proteins to the golgi. *EMBO J.* 14, 1329–1339. doi: 10.1002/j.1460-2075.1995.tb07119.x
- Shankar, G. M., Bloodgood, B. L., Townsend, M., Walsh, D. M., Selkoe, D. J., and Sabatini, B. L. (2007). Natural oligomers of the alzheimer amyloid-beta protein induce reversible synapse loss by modulating an NMDA-type glutamate receptor-dependent signaling pathway. *J. Neurosci.* 27, 2866–2875. doi: 10.1523/jneurosci.4970-06.2007
- Sorbi, S., Hort, J., Erkinjuntti, T., Fladby, T., Gainotti, G., Gurvit, H., et al. (2012). EFNS-ENS guidelines on the diagnosis and management of disorders associated with dementia. *Eur. J. Neurol.* 19, 1159–1179. doi: 10.1111/j.1468-1331.2012.03784.x
- Stammes, M. A., Craighead, M. W., Hoe, M. H., Lampen, N., Geromanos, S., Tempst, P., et al. (1995). An integral membrane component of coatamer-coated transport vesicles defines a family of proteins involved in budding. *Proc. Natl. Acad. Sci. U.S.A.* 92, 8011–8015. doi: 10.1073/pnas.92.17.8011
- Strating, J. R., and Martens, G. J. (2009). The p24 family and selective transport processes at the ER-golgi interface. *Biol. Cell* 101, 495–509. doi: 10.1042/BC20080233
- Strating, J. R., Van Bakel, N. H., Leunissen, J. A., and Martens, G. J. (2009). A comprehensive overview of the vertebrate p24 family: identification of a novel tissue-specifically expressed member. *Mol. Biol. Evol.* 26, 1707–1714. doi: 10.1093/molbev/msp099
- Sun, X., Wu, Y., Herculan, B., and Song, W. (2014). RCAN1 overexpression exacerbates calcium overloading-induced neuronal apoptosis. *PLoS One* 9:e95471. doi: 10.1371/journal.pone.0095471
- Theiler, R., Fujita, M., Nagae, M., Yamaguchi, Y., Maeda, Y., and Kinoshita, T. (2014). The alpha-helical region in p24gamma2 subunit of p24 protein cargo receptor is pivotal for the recognition and transport of glycosylphosphatidylinositol-anchored proteins. *J. Biol. Chem.* 289, 16835–16843. doi: 10.1074/jbc.M114.568311
- Tsujo, I., Tanaka, T., Kudo, T., Nishikawa, T., Shinozaki, K., Grundke-Iqbal, I., et al. (2000). Inactivation of glycogen synthase kinase-3 by protein kinase c delta: implications for regulation of tau phosphorylation. *FEBS Lett.* 469, 111–117. doi: 10.1016/s0014-5793(00)01234-5
- Um, J. W., and Ko, J. (2017). Neural glycosylphosphatidylinositol-anchored proteins in synaptic specification. *Trends Cell Biol.* 27, 931–945. doi: 10.1016/j.tcb.2017.06.007
- Vettrivel, K. S., Gong, P., Bowen, J. W., Cheng, H., Chen, Y., Carter, M., et al. (2007). Dual roles of the transmembrane protein p23/TMP21 in the modulation of amyloid precursor protein metabolism. *Mol. Neurodegener.* 2:4.
- Vettrivel, K. S., Kodam, A., Gong, P., Chen, Y., Parent, A. T., Kar, S., et al. (2008). Localization and regional distribution of p23/TMP21 in the brain. *Neurobiol. Dis.* 32, 37–49. doi: 10.1016/j.nbd.2008.06.012
- Walsh, D. M., and Selkoe, D. J. (2004). Deciphering the molecular basis of memory failure in alzheimer's disease. *Neuron* 44, 181–193. doi: 10.1016/j.neuron.2004.09.010
- Wang, H., Xiao, L., and Kazanietz, M. G. (2011). p23/Tmp21 associates with protein kinase c delta (PKCdelta) and modulates its apoptotic function. *J. Biol. Chem.* 286, 15821–15831. doi: 10.1074/jbc.M111.227991
- Wang, X., Zhou, X., Li, G., Zhang, Y., Wu, Y., and Song, W. (2017). Modifications and trafficking of APP in the pathogenesis of Alzheimer's Disease. *Front. Mol. Neurosci.* 10:294. doi: 10.3389/fnmol.2017.00294
- Wang, Z., Xu, Q., Cai, F., Liu, X., Wu, Y., and Song, W. (2019). BACE2, a conditional beta-secretase, contributes to alzheimer's disease pathogenesis. *JCI Insight* doi: 10.1172/jci.insight.123431 [Epub ahead of print].
- Willem, M., Tahirovic, S., Busche, M. A., Ovsepian, S. V., Chafai, M., Kootar, S., et al. (2015). eta-secretase processing of APP inhibits neuronal activity in the hippocampus. *Nature* 526, 443–447. doi: 10.1038/nature14864
- Wu, F., Qiu, J., Fan, Y., Zhang, Q., Cheng, B., Wu, Y., et al. (2018). Apelin-13 attenuates ER stress-mediated neuronal apoptosis by activating Galphai/Galphaq-CK2 signaling in ischemic stroke. *Exp. Neurol.* 302, 136–144. doi: 10.1016/j.expneurol.2018.01.006
- Wu, Y., Deng, Y., Zhang, S., Luo, Y., Cai, F., Zhang, Z., et al. (2015). Amyloid-beta precursor protein facilitates the regulator of calcineurin 1-mediated apoptosis by downregulating proteasome subunit alpha type-5 and proteasome subunit beta type-7. *Neurobiol. Aging* 36, 169–177. doi: 10.1016/j.neurobiolaging.2014.07.029
- Wu, Y., Ly, P. T., and Song, W. (2014a). Aberrant expression of rcn1 in alzheimer's pathogenesis: a new molecular mechanism and a novel drug target. *Mol. Neurobiol.* 50, 1085–1097. doi: 10.1007/s12035-014-8704-y

- Wu, Y., Xu, Q., and Song, W. (2014b). "Oxidative stress and alzheimer's disease," in *Systems Biology of Free Radicals and Antioxidants*, ed. I. Laher (Berlin: Springer), 2147–2174.
- Wu, Y., and Song, W. (2013). Regulation of rcan1 translation and its role in oxidative stress-induced apoptosis. *FASEB J.* 27, 208–221. doi: 10.1096/fj.12-213124
- Wu, Y., Wang, X., Zhou, X., Cheng, B., Li, G., and Bai, B. (2017). Temporal expression of apelin/apelin receptor in ischemic stroke and its therapeutic potential. *Front. Mol. Neurosci.* 10:1. doi: 10.3389/fnmol.2017.00001
- Xie, J., Yang, Y., Li, J., Hou, J., Xia, K., Song, W., et al. (2014). Expression of tmp21 in normal adult human tissues. *Int. J. Clin. Exp. Med.* 7, 2976–2983.
- Xu, X., Gao, H., Qin, J., He, L., and Liu, W. (2015). TMP21 modulates cell growth in papillary thyroid cancer cells by inducing autophagy through activation of the AMPK/mTOR pathway. *Int. J. Clin. Exp. Pathol.* 8, 10824–10831.
- Yan, L., Yang, H., Li, Y., Duan, H., Wu, J., Qian, P., et al. (2014). Regulator of calcineurin 1-1L protects cardiomyocytes against hypoxia-induced apoptosis via mitophagy. *J. Cardiovasc. Pharmacol.* 64, 310–317. doi: 10.1097/FJC.0000000000000121
- Yang, Y., Wu, Y., Zhang, S., and Song, W. (2013). High glucose promotes abeta production by inhibiting APP degradation. *PLoS One* 8:e69824. doi: 10.1371/journal.pone.0069824
- Zhang, X., Wu, Y., Cai, F., Liu, S., Bromley-Brits, K., Xia, K., et al. (2018). A novel alzheimer-associated snp in tmp21 increases amyloidogenesis. *Mol. Neurobiol.* 55, 1862–1870. doi: 10.1007/s12035-017-0459-9
- Zhang, X., Wu, Y., Cai, F., and Song, W. (2019). Regulation of global gene expression in brain by TMP21. *Mol. Brain* 12:39. doi: 10.1186/s13041-019-0460-5

**Conflict of Interest Statement:** The authors declare that the research was conducted in the absence of any commercial or financial relationships that could be construed as a potential conflict of interest.

Copyright © 2019 Qiu, Zhang, Wang, Li, Wang, Li and Wu. This is an open-access article distributed under the terms of the Creative Commons Attribution License (CC BY). The use, distribution or reproduction in other forums is permitted, provided the original author(s) and the copyright owner(s) are credited and that the original publication in this journal is cited, in accordance with accepted academic practice. No use, distribution or reproduction is permitted which does not comply with these terms.





# Systemic L-Buthionine-S-R-Sulfoximine Treatment Increases Plasma NGF and Upregulates L-cys/L-cys<sub>2</sub> Transporter and $\gamma$ -Glutamylcysteine Ligase mRNAs Through the NGF/TrkA/Akt/Nrf2 Pathway in the Striatum

## OPEN ACCESS

### Edited by:

Rocío Martínez De Pablos,  
University of Seville, Spain

### Reviewed by:

Toshio Nakaki,  
Teikyo University, Japan  
Yun Zhou,  
University of Oslo, Norway

Abel Santamaria,  
National Institute of Neurology  
and Neurosurgery (INNN), Mexico

### \*Correspondence:

Maria E. Gensebatt  
margen@unam.mx

### Specialty section:

This article was submitted to  
Cellular Neurophysiology,  
a section of the journal  
Frontiers in Cellular Neuroscience

**Received:** 15 May 2019

**Accepted:** 03 July 2019

**Published:** 23 July 2019

### Citation:

Valdovinos-Flores C,  
Limón-Pacheco JH,  
León-Rodríguez R, Petrosyan P,  
Garza-Lombó C and Gensebatt ME  
(2019) Systemic L-Buthionine  
-S-R-Sulfoximine Treatment Increases  
Plasma NGF and Upregulates  
L-cys/L-cys<sub>2</sub> Transporter  
and  $\gamma$ -Glutamylcysteine Ligase  
mRNAs Through  
the NGF/TrkA/Akt/Nrf2 Pathway  
in the Striatum.  
*Front. Cell. Neurosci.* 13:325.  
doi: 10.3389/fncel.2019.00325

Cesar Valdovinos-Flores, Jorge H. Limón-Pacheco, Renato León-Rodríguez,  
Pavel Petrosyan, Carla Garza-Lombó and Maria E. Gensebatt\*

Departamento de Medicina Genómica y Toxicología Ambiental, Instituto de Investigaciones Biomédicas, Universidad  
Nacional Autónoma de México, Ciudad de México, Mexico

Glutathione (GSH) is the most abundant intracellular antioxidant. GSH depletion leads to oxidative stress and neuronal damage in the central nervous system (CNS). In mice, the acute systemic inhibition of GSH synthesis by L-buthionine-S-R-sulfoximine (BSO) triggers a protective response and a subsequent increase in the CNS GSH content. This response might be modulated by a peripheral increment of circulating nerve growth factor (NGF). NGF is an important activator of antioxidant pathways mediated by tropomyosin-related kinase receptor A (TrkA). Here, we report that peripheral administration of BSO increased plasma NGF levels. Additionally, BSO increased NGF levels and activated the NGF/TrkA/Akt pathway in striatal neurons. Moreover, the response in the striatum included an increased transcription of *nrf2*, *gclm*, *lat1*, *eaac1*, and *xct*, all of which are involved in antioxidant responses, and L-cys/L-cys<sub>2</sub> and glutamate transporters. Using antibody against NGF confirmed that peripheral NGF activated the NGF/TrkA/Akt/Nrf2 pathway in the striatum and subsequently increased the transcription of *gclm*, *nrf2*, *lat1*, *eaac1*, and *xct*. These results provide evidence that the reduction of peripheral GSH pools increases peripheral NGF circulation that orchestrates a neuroprotective response in the CNS, at least in the striatum, through the NGF/TrkA/Akt/Nrf2 pathway.

**Keywords:** GSH synthesis inhibition, BSO, brain protection, xCT, Nrf2

## INTRODUCTION

Reactive oxygen species (ROS) are products of aerobic metabolism. Even in resting cells, up to 2% of oxygen uptake is converted into ROS (Bridges et al., 2012). Some of these intracellular ROS activate cellular signals involved in the protection against oxidative stress, such as the synthesis of glutathione (GSH), thioredoxin (Trx-1) and antioxidant enzymes. In an organism, tissues and

organs contain specific antioxidant reservoirs, likely due to their different metabolic rates, which are reflected by their blood supply and oxygen consumption (Limón-Pacheco and Gonsébat, 2009). These distinct features cause some organs, such as the brain, to be susceptible to oxidative injury.

GSH not only participates in protection against oxidative stress but also performs relevant functions in various cellular processes, such as cell proliferation, apoptosis and differentiation, and the inactivation of toxic electrophilic compounds (Valdovinos-Flores and Gonsébat, 2013). Hence, alterations in GSH homeostasis due to impaired synthesis/recycling or increased consumption are associated with disease. In fact, aging as well as degenerative and neuropsychiatric diseases, such as Parkinson's disease, Alzheimer's disease, autism and schizophrenia, are associated with increased ROS production, the disruption of cellular GSH pools, and downregulation of GSH-dependent enzymes (Ballatori et al., 2009; Johnson et al., 2012; Gu et al., 2015).

Because GSH does not readily penetrate the blood-brain barrier (BBB) (Anderson et al., 1989), central nervous system (CNS) GSH levels depend on *de novo* synthesis by two enzymes:  $\gamma$ -glutamate-cysteine ligase (GCL) and glutathione synthetase (GS) (Valdovinos-Flores and Gonsébat, 2012).

Glutamate-cysteine ligase catalyzes the first rate-limiting enzymatic step, which is limited by the availability of the sulfhydryl amino acid (AA) L-cysteine (L-cys) (Valdovinos-Flores and Gonsébat, 2012). L-cystine, the disulfide form of L-cysteine, is transported across the CSF-brain barrier via the  $\text{Na}^+$ -independent L-cystine/L-glutamate exchanger system  $x_c^-$  (Shih et al., 2006). L-cystine is reduced in the BBB, and the resulting cysteine is transported out of the endothelial cells into the brain via L-type amino acid transporter 1 (LAT1) (Sánchez del Pino et al., 1995). Extracellular L-cysteine is oxidized to L-cystine and transported through the  $x_c^-$  system into astrocytes (Shih et al., 2006), which release GSH via the multidrug resistance protein 1 (MRP1) as the first step in supplying cysteine for GSH synthesis in neurons (Minich et al., 2006). Neurons take up cysteine via excitatory amino acid carrier 1 (EAAC1/EAAT3), which is a glutamate/cysteine transporter that is part of the  $x_{AG}^-$  system (Zerangue and Kavanaugh, 1996).

The systemic inhibition of GSH synthesis by L-buthionine-S-R-sulfoximine (BSO, Meister, 1995) in liver and kidneys or the exposure to a toxic metalloid such as arsenite, rose brain GSH pools in mice. Simultaneously, we observed an up-regulation of amino acid transporters, such as xCT and EAAT3 (Limón-Pacheco et al., 2007; Ramos-Chávez et al., 2015; Garza-Lombó et al., 2018), which were associated with a disruption of glutamate disposition and potentially leading to neurotoxicity (Nelson-Mora et al., 2018).

In the cerebellum, EAAT3 up-regulation and increased GSH levels were associated with an earlier activation of the NGF/TrkA and mTOR signaling pathways in neurons (Garza-Lombó et al., 2018).

Nerve growth factor is a neurotrophin (NT) that regulates neuronal development, differentiation, plasticity, cell death and survival (Lu et al., 2005). NGF binds to two distinct

classes of transmembrane receptors, the low-affinity p75 neurotrophin receptor (p75NTR), a member of the tumor necrosis receptor superfamily, and high-affinity tropomyosin-related kinase receptor A (TrkA) (Lu et al., 2005).

In the human and murine CNS, NGF- and TrkA-positive regions correlate with the anatomical distribution of cholinergic neurons in the basal forebrain and striatum (Bizon et al., 1999). Moreover, NTs and their receptors are expressed in non-neural tissues (Yamamoto et al., 1996). The NGF/TrkA pathway participates in the induction of antioxidant responses in both the CNS and non-neural tissues (Pan and Perez-Polo, 1993, 1996; Sampath et al., 1994; Guégan et al., 1999; Salinas et al., 2003; Podratz and Windebank, 2005). Furthermore, exogenous NGF increases the activity of the major antioxidant enzymes in brain tissues and attenuates neuronal injuries induced by traumatic brain injury, such as the quinolinic acid induced decline in glutathione reductase activity and GSH content in striatum (Cruz-Aguado et al., 2000; Zhou et al., 2003).

Also, NGF synthesis and the NGF/TrkA pathway are activated by oxidative stress in non-neural tissues (Caporali et al., 2008; Wang et al., 2013). We have also gathered evidence suggesting that NGF plays a relevant role in maintaining reduced thiol levels and protecting the liver from oxidative stress and xenobiotic injury through the NGF/TrkA/PI3K/AKT/nuclear factor kappa B (NF $\kappa$ B) pathway (Valdovinos-Flores and Gonsébat, 2013). In fact, transgenic mice overexpressing NGF display elevated GSH concentrations in the plasma, brain, and liver (Arsenijevic et al., 2007).

Here, we document that a systemic reduction of GSH levels, up-regulates the transcription of L-cys/L-cys<sub>2</sub> and glutamate AA transporters and antioxidant genes in the striatum through the TrkA/Akt pathway, which was mediated, at least in part, by peripheral NGF levels.

## MATERIALS AND METHODS

### Chemicals and Antibodies

All chemicals were purchased from Sigma (St. Louis, MO, United States) unless otherwise indicated. The neutralizing anti-NGF antibody (Cat No. ab16161) and the TrkA (Cat. No. ab76291), proNGF (Cat. No. ab52918), transferrin (Cat. No. ab82411), and NeuN (Cat. No. ab5541) antibodies were purchased from Abcam (Cambridge, MA, United States). The primary antibody against native glyceraldehyde-3-phosphate dehydrogenase (GAPDH; Cat. No. MAB374) was purchased from Millipore (Bedford, MA, United States);  $\beta$ -tubulin (Cat. No. T4026) from Sigma-Aldrich. Antibodies against phospho-TrkA (Tyr 490; Cat. No. 9141), Akt (Cat. No. 9272), NGF (Cat. No. 2046) and nucleophosmin (NPM; Cat. No. 3542) and the secondary anti-rabbit antibody used for western blotting were obtained from Cell Signaling Technology (Danvers, MA, United States). DyLight 649-labeled Lycopersicon esculentum (Tomato) lectin (Vector Laboratories, Burlingame, CA; Cat. No. DL-1178) and the Alexa Fluor 546-conjugated anti-rabbit (Invitrogen, Carlsbad, CA, United States; Cat. No.

A10040) and Alexa Fluor 488-conjugated anti-mouse (Invitrogen; Cat. No. A21202) secondary antibodies were used for immunofluorescence.

## Animal Use and Treatments

Six-week-old male BALB/c mice were obtained from the animal care facility at the Instituto de Investigaciones Biomédicas at Universidad Nacional Autónoma de México. The animals were housed on a 12-h light/dark cycle. Intraperitoneal (i.p.) injections of 6 mmol kg<sup>-1</sup> BSO or 14 mg kg<sup>-1</sup> iAs dissolved in a 0.9% saline solution or 0.9% saline solution alone were administered to mice. Control and treated mice were sacrificed via cervical dislocation at 0.5, 2, 6, or 24 h after treatment. To examine the role of systemic NGF, the animals were pretreated with 1 mg kg<sup>-1</sup> neutralizing anti-NGF antibody dissolved in saline solution 1 h prior to BSO administration and sacrificed after 2 h (Valdovinos-Flores and Gonshebbat, 2013). The striatum and liver were harvested and washed with ice-cold PBS to remove blood and tissue debris. Then, the tissues were immediately frozen in liquid nitrogen and stored at -70°C until use in RT-PCR experiments or processed immediately for protein studies.

## Glutathione Determination

Glutathione and GSH disulfide (GSSG) contents were assayed using the fluorometric o-phthalaldehyde (OPA) method (Senft et al., 2000), which was previously proven in our laboratory by HPLC [18], using 96-well black microplates. Fluorescence readings were taken at 365-nm excitation and 430-nm emission with a Beckman Coulter DTX 800/880 Multimode Detector (Beckman Coulter, Fullerton, CA, United States). The final values were calculated as the fluorescence of unit B minus the fluorescence of unit A ( $UF_B - UF_A = UF_F$ ).

## Western Blotting

To evaluate NGF levels in the striatum and for phosphorylation levels, fresh tissue was homogenized at a 30% ratio (w v<sup>-1</sup>) in kinase extraction buffer A (10 mM HEPES, pH 7.9, 10 mM KCl, 10 mM EDTA, 1 mM DTT, 0.4% v v<sup>-1</sup> IGEPAL, 1 mM Na<sub>3</sub>VO<sub>4</sub>, 1 mM PMSF, and 10 mg mL<sup>-1</sup> aprotinin and leupeptin) using a previously described method (Kaneko et al., 2004). The samples were incubated on ice for 10 min and then centrifuged at 4000 g for 15 min at 4°C. The supernatant fractions (cytoplasmic soluble proteins) were collected. The nuclear pellet was washed and then lysed in buffer C (20 mM HEPES, pH 7.9, 200 mM NaCl, 1 mM EDTA, 5% v v<sup>-1</sup> glycerol, 1 mM DTT, 1 mM Na<sub>3</sub>VO<sub>4</sub>, 1 mM PMSF, and 10 mg mL<sup>-1</sup> aprotinin and leupeptin). The lysates were incubated on ice for 2 h and then centrifuged at maximum speed for 15 min. Protein concentrations were determined using the micro Bradford method (Bio-Rad, Hercules, CA, United States), according to the manufacturer's protocol. Peripheral blood was collected after the mice were sacrificed via cervical dislocation; the blood was stored at 4°C overnight and then centrifuged at 4000 g for 15 min at 4°C to obtain plasma. The supernatant fractions were collected. Protease inhibitors

(1 mM PMSF and 10 mg mL<sup>-1</sup> aprotinin and leupeptin) were added to the plasma fraction and samples were stored at -70°C until the Western blot analysis. Lysates and plasma samples were separated on 10% SDS-PAGE gels and transferred to a Hybond-ECL nitrocellulose membrane (Amersham Biosciences, Piscataway, NJ, United States). Membranes were blocked overnight at 4°C with Tris-buffered saline containing 5% non-fat milk and then incubated with the primary antibody against the phosphorylated kinase. An antibody against the native form was used to detect the total protein content. For the analysis of transcription factor translocation, both the nuclear and cytoplasmic extracts were utilized, and NPM and GAPDH, respectively, were used as loading controls. For the evaluation of the plasma and striatal NGF levels, ferritin and  $\beta$ -tubulin, respectively, were used as loading controls. Proteins were visualized via chemiluminescence using the ECL Advance Western Blotting Detection Kit (Amersham Biosciences), and images were captured and analyzed by densitometry using a Kodak ID Version 3.6 Image Analyzer (Kodak, NY, United States).

## Immunofluorescence Staining

Control and BSO-treated mice were transcardially perfused with a cold saline solution followed by buffered paraformaldehyde (4%). The brains of the mice were removed, postfixed with the same fixative for 24 h at 4°C, and then cryoprotected using a graded series of buffered sucrose solutions (20% and 30%). Sections (50  $\mu$ m thick) were cut using a cryostat and individually collected in 96-well culture plates filled with 0.1 M phosphate buffer (PB). After three washes with PB supplemented with 0.3% Triton X-100 (PBT), the sections were incubated overnight at 4°C in PBT containing 0.3% BSA (Santa Cruz), 2% normal horse serum (Vector Laboratories), and the mouse anti-NeuN and rabbit anti-TrkA or anti-NGF primary antibodies (at a dilution of 1:200 in all cases except for NeuN, which was used at a dilution of 1:600). After three washes with PBT, the sections were incubated with the Alexa Fluor 546-conjugated anti-rabbit (1:600) and Alexa Fluor 488-conjugated anti-mouse (1:400) secondary antibodies for 2 h at room temperature in the dark. Then, the sections were washed with 0.1 M PB, endothelial cells were counterstained with lectin, and nuclei were counterstained with 4',6-diamidino-2-phenylindole (DAPI, Invitrogen), according to the manufacturer's protocols. Finally, liver sections were mounted in Fluorescent Mounting Medium (DAKO, Glostrup, Denmark). Fluorescence images were sequentially acquired with a Nikon A1R+ laser scanning confocal Eclipse Ti-E inverted microscope (Nikon Corporation, Tokyo, Japan) equipped with a motorized stage (TI-S-E, Nikon). Imaging was performed with a CFI Plan Apo VC 60xA WI DIC N2 objective (N.A. 1.2) using 3 mW of 405 nm laser power, 0.77 mW of 488 nm laser power, 0.7 mW of 561 nm laser power and 125 mW of 647 nm laser power, a pinhole aperture of 12.77 mm and both PMT and GaAsP detectors, all of which were controlled using NIS Elements C software v4.50 (Nikon). ImageJ version 1.46r software (U.S. National Institutes

of Health, Bethesda, MD, United States) was used to analyze the final images.

## Real-Time RT-PCR Analysis

Total RNA was isolated using TRIzol (Invitrogen). RNA concentrations were determined by measuring the absorbance at 260 nm. RNA integrity was verified via electrophoresis on 1% agarose gels. One microgram of total RNA was reverse-transcribed to cDNA using M-MLV reverse transcriptase (Invitrogen). For the real-time RT-PCR analysis, a Rotor-Gene Q PCR cycler (Qiagen GmbH, Hilden, Germany) was used. Previously prepared cDNA was diluted 1:125 and used as a template for real-time PCR. PCR products were detected using the Kapa SYBR FAST qPCR kit (Kapa Biosystems, Woburn, MA, United States). Each reaction included 8  $\mu$ L of diluted cDNA, 10  $\mu$ L of Kapa SYBR FAST qPCR kit reagents and 1  $\mu$ L each of 5  $\mu$ M stocks of the forward and reverse primers in a total reaction volume of 20  $\mu$ L. The following reaction conditions were used: an initial cycle at 94°C for 3 min, 30 cycles of 94°C for 5 s and 60°C for 20 s and a final melting curve from 73°C to 93°C to ensure that only one product was amplified. The primers used are shown in **Table 1**. The mean amplification efficiency  $\pm$  standard deviation (SD) was  $0.995 \pm 0.011$ , and the mean correlation coefficient  $\pm$  SD was  $0.992 \pm 0.006$ . The results were analyzed using the  $2^{-\Delta\Delta CT}$  method with *gapdh* as a reference gene (Livak and Schmittgen, 2001).

## Data Analysis

Each assay was performed in triplicate unless otherwise indicated. Data are presented as the means  $\pm$  S.E., and significance was analyzed using one-way ANOVA with Tukey's *post hoc* analysis, as indicated in each case. A *p*-value  $\leq 0.05$  was considered significant in all cases.

## Ethics Statement

The experiments reported in this manuscript were conducted according to the guidelines stated in the Principles of Laboratory Animal Care (Institute for Laboratory Animal Research, 2011) and the Norma Oficial Mexicana de la Secretaría de Agricultura, Ganadería, Desarrollo Rural, Pesca y Alimentación (SAGARPA, México) Especificaciones técnicas para la

producción, Cuidado y uso de los animales de laboratorio (Agricultura y Ganadería, 2001).

## RESULTS

### NGF Protein Levels Are Increased in the Plasma and Striatum, and NGF/TrkA Pathway Is Activated in the Striatum After BSO Treatment Which Depletes Liver GSH

The protein expression of *ngfb* was investigated in the plasma after the intraperitoneal (i.p.) administration of BSO or iAs. Both agents diminish GSH levels (Rodríguez et al., 2005; Valdovinos-Flores and Gensebatt, 2013 and **Table 2**). Increased levels of NGF were observed in the plasma from 0.5 to 2 h after BSO injection and 6 h after iAs administration (**Figure 1A**), suggesting the participation of tissues in a systemic response. In fact, under the same experimental conditions, *ngfb* transcription and the TrkA/PI3K/Akt/NF $\kappa$ B pathway are activated in the liver (Valdovinos-Flores and Gensebatt, 2013).

In addition, we observed an upregulation of NGF protein in the striatum at 0.5 and 2 h after BSO injection. Increased NGF and TrkA protein levels in striatal neurons were confirmed at 0.5 h via immunofluorescence (**Figure 2**). Furthermore, increased TrkA phosphorylation was detected from 0.5 h after BSO injection (**Figure 3**), suggesting that the TrkA pathway is activated, despite the impermeability of BSO to the BBB. The response observed here was according to the previous report. Under the same exposure protocol, we observed the activation of the NGF/TrkA pathways in the cerebellum (Garza-Lombó et al., 2018).

These results indicate that systemic treatment with BSO induces the synthesis of NGF by peripheral tissues, as well as the NGF and TrkA protein levels and TrkA phosphorylation in the striatum, possibly as a response to systemic oxidative stress induced by GSH depletion after BSO treatment (**Table 2**), suggesting that NGF is a redox sensor in both the peripheral tissues and striatum.

**TABLE 1** | Primers used for PCR and real-time PCR.

Gene	Primers	Product (bp)	Acc. No.	References
<i>lat1</i> ( <i>Slc7a5</i> )	F: 5' AGC TTC TTC AAC TGG CTG TGT 3' R: 5' AGA GGC AGG CCA GGA TAA A 3'	133	NM_011404.3	
<i>xct</i> ( <i>Slc7a11</i> )	F: 5' AGC CAG TCG GTG ATA GCA AAG 3' R: 5' AGG GGG AAA AAC AAA ACA AGA C 3'	122	NM_011990.2	Limón-Pacheco et al., 2007
<i>eaac1</i> ( <i>Slc1a1</i> )	F: 5' CGC AAA CGT CAG TGC TCA 3' R: 5' CCA CGA CTC CTA AGA CAA TTC C 3'	132	NM_009199.2	
<i>gapdh</i> ( <i>gapdh</i> )	F: 5' ACC ACC AAC TGC TTA GCC CC 3' R: 5' CAG CTC TGG GAT GAC CTT GC 3'	216	NM_008084.2	
<i>gclm</i> ( <i>gclm</i> )	F: 5' CAG TTG GAG CAG CTG TAT CAG T 3' R: 5' CAG TCA AAT CTG GTG GCA TC 3'	91	NM_008129.4	
<i>nrf2</i> ( <i>Nfe2l2</i> )	F: 5' CAC CAG TGG ATC CGC CAG CTA 3' R: 5' TAT CCA GGG CAA GCG ACT CA 3'	134	NM_010902.3	



**TABLE 2 |** L-Buthionine-S-R-sulfoximine modulates the redox state in the liver.

Treatment	GSH ( $\mu\text{mol/g}$ tissue)	GSSG ( $\mu\text{mol/g}$ tissue)	GSH/GSSG
Control	7.296 ( $\pm 0.312$ )	0.134 ( $\pm 0.0101$ )	54.193 ( $\pm 3.524$ )
BSO (6 mmol/kg)	3.521 ( $\pm 0.312$ )*	0.127 ( $\pm 0.0090$ )	27.653 ( $\pm 0.979$ )*

GSH and GSSG levels in the liver after 2 h of 6 mmol/kg of and i.p. BSO injection. Control mice were injected with a saline solution. Means ( $\pm$ S.E.)  $n = 5$ . Student's *t*-test. The symbol "\*" indicates statistical significance difference vs. control;  $P \leq 0.05$ .

## Peripheral NGF "Informs" the CNS (Striatum) of Systemic Oxidative Stress

The results described above suggest that NGF is positively modulated systemically in peripheral tissues and in the striatum after an oxidative insult. Thus, changes in peripheral NGF levels may constitute a molecular signal that induces the NGF/ TrkA pathway in the striatum (CNS). Consequently, we investigated whether peripheral NGF was responsible for these effects on the striatum.

We evaluated the effect of neutralizing peripheral NGF using an anti-NGF antibody that does not permeate the BBB as a pretreatment before the i.p. injection of BSO. Mice were treated with a neutralizing anti-NGF antibody for 1 h prior to the BSO injection and sacrificed 2 h later. In these animals, TrkA phosphorylation, Akt nuclear translocation were prevented in the striatum (Figure 4). Suggesting that peripheral NGF is a critical modulator of the NGF/TrkA/Akt/ pathway in the striatum.

## The Expression of the L-cys and L-cys<sub>2</sub>/Glutamate Amino Acid Transporters mRNA Is Upregulated in the Striatum After BSO and Is Mediated by the NGF/TrkA/Akt/Nrf2 Pathway

We previously found that *xct* mRNA is upregulated in whole brain homogenates after GSH depletion (Limón-Pacheco et al., 2007), and more recently we have shown that EAAT3 protein levels are upregulated after the i.p. injection of BSO via the NGF/TrkA and mTOR signaling in the cerebellum (Garza-Lombó et al., 2018). Thus, we next examined the modulatory effects of BSO on the mRNA expression of CNS AA transporters that provide L-cys, such as *lat1* and *eaac1*, and L-cys<sub>2</sub>/glutamate, such as *xct*, in the striatum. A significant increase in mRNA levels was detected for all the genes evaluated after BSO injection (Figure 5). These results show that BSO treatment modulates the levels of the transcripts encoding AA transporters related to L-cys/L-cys<sub>2</sub> availability in the striatum.

Furthermore, the anti-NGF antibody pretreatment abrogated the BSO-induced changes in the levels of the *xct*, *lat1*, and *eaac1* mRNA (Figure 5). In addition, the anti-NGF antibody pretreatment abolished the previously observed changes in the levels of the *gclm* and *nrf2* mRNAs (Limón-Pacheco et al., 2007). Thus, peripheral NGF is a critical modulator of the NGF/TrkA/Akt/Nrf2 pathway in the striatum and participates in

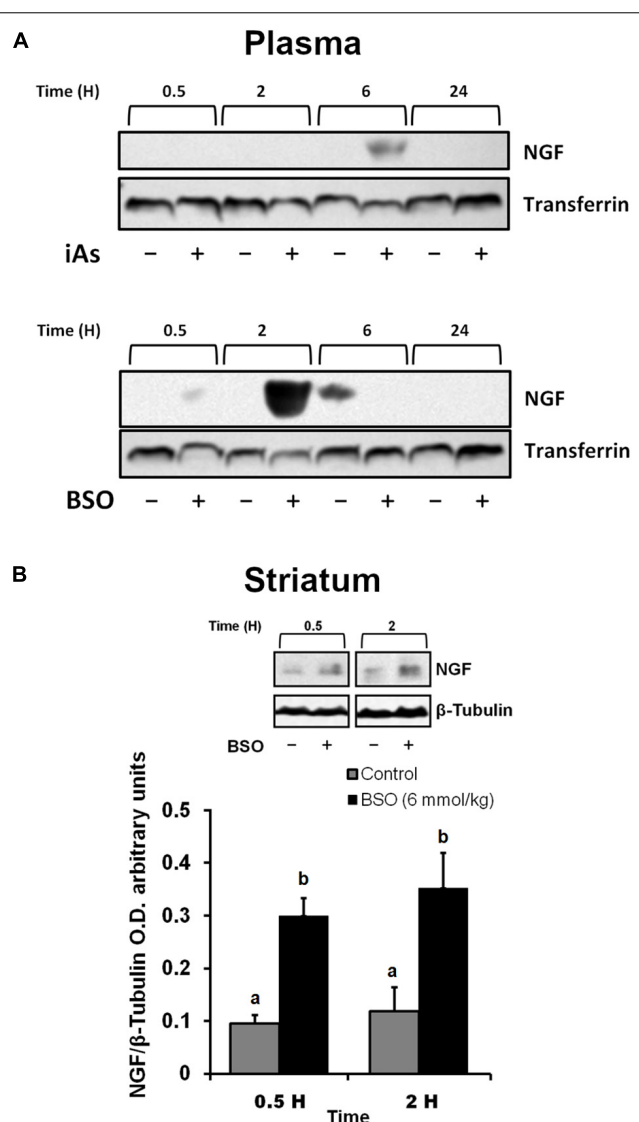


**FIGURE 1 |** L-Buthionine-S-R-sulfoximine or iAs i.p. injection increased NGF protein levels in the plasma, and BSO treatment increased NGF protein levels in the striatum. **(A)** Increased NGF protein levels in the plasma. Western blots were performed using transferrin as a loading control. The upper image is a representative western blot of NGF in the plasma of mice treated with 14 mg  $\text{kg}^{-1}$  iAs or saline solution. The lower image is a representative western blot of NGF in the plasma of mice treated with 6 mmol  $\text{kg}^{-1}$  BSO or saline solution. **(B)** Increased NGF protein levels in the striatum. The upper panel shows a representative western blot of NGF in the striatum. Densitometric evaluations of the western blot images were performed using  $\beta$ -tubulin as a loading control. The bars represent the mean  $\pm$  S.E. of triplicate experiments and were calculated from the densitometry data ( $n = 9$ ). The data were analyzed using one-way ANOVA with Tukey's *post hoc* analysis. Different letters in the superscript above each column indicate statistically significant differences;  $P \leq 0.05$ .

modulating the transcription of *gclm*, *nrf2*, and genes involved in AA transport systems that are responsible for the uptake of L-cys/L-cys<sub>2</sub> in the striatum in different cell types such as endothelial, astrocytes, microglia, and neurons.

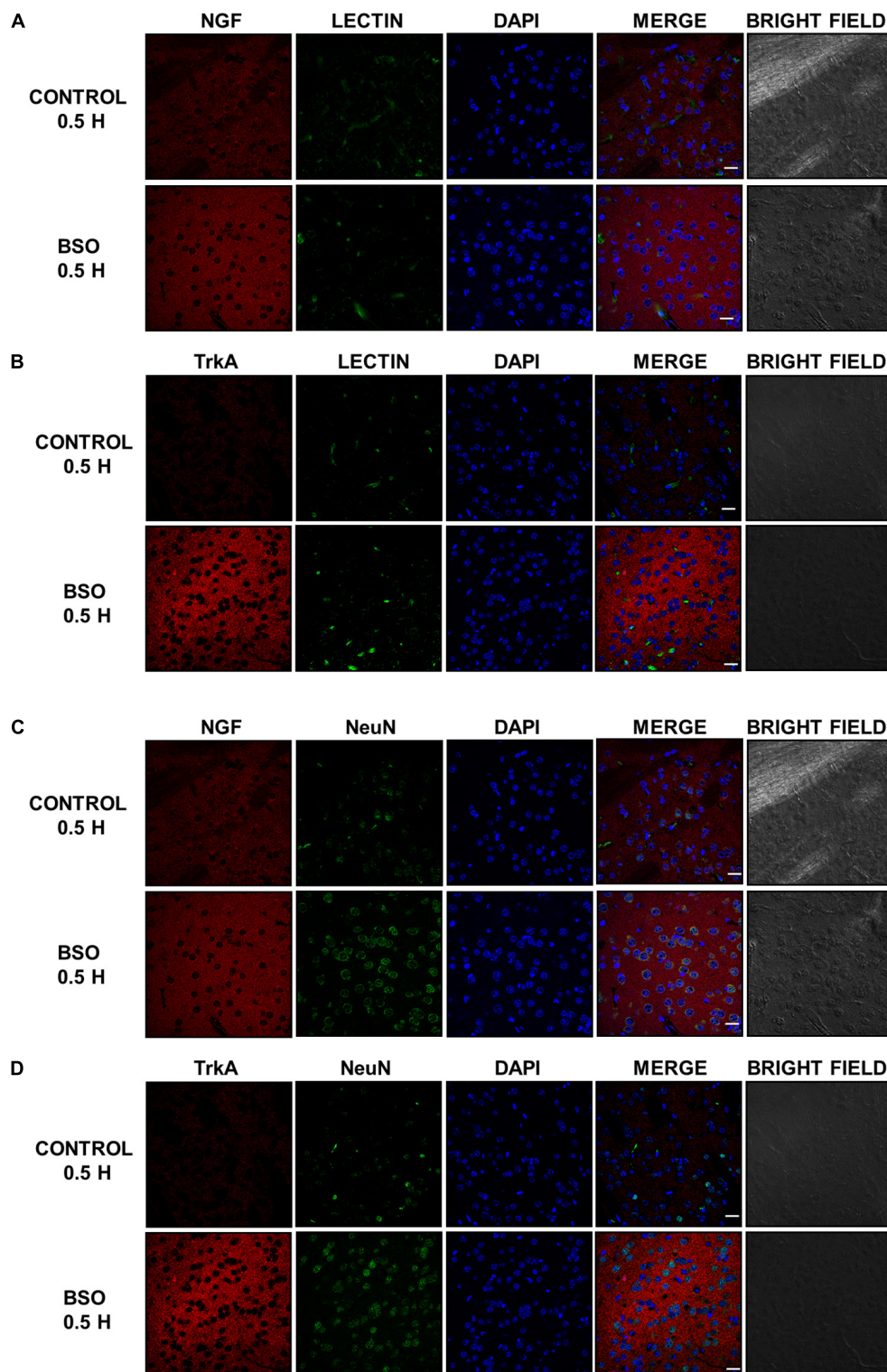
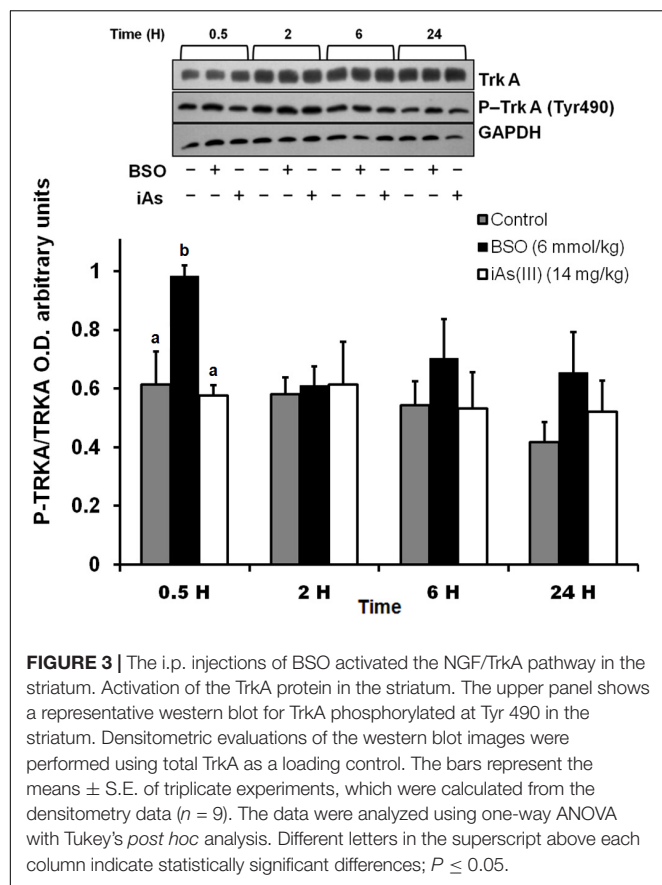


**FIGURE 2 |** The i.p. injections of BSO increased the levels of the NGF and TrkA proteins in the mouse striatum. Immunostained and bright field confocal images of striata sections of control and BSO-injected mice. **(A)** Images of immunofluorescence staining of NGF (red) endothelial cells (lectin, green), and nuclei (DAPI, blue) in control and treated mice. **(B)** Images of immunofluorescence staining of endothelial cells (lectin, green), TrkA (red), and nuclei (DAPI, blue) in control and treated mice. **(C)** Images of immunofluorescence staining of NGF (red), neurons (NeuN, green), and nuclei (DAPI, blue) in control and treated mice. **(D)** Images of immunofluorescence staining of TrkA (red), neurons (NeuN, green), and nuclei (DAPI, blue) in control and treated mice. Scale bar: 20 microns.



## DISCUSSION

Glutathione is an essential peptide not only for the cellular redox homeostasis but also for the metabolism/elimination of metabolites and chemicals including drugs. Environmental exposure to metals, pesticides, ionizing radiation, U.V., or some pharmaceutical drugs, diminishes GSH pools in target tissues (Limón-Pacheco and Gonsébat, 2009). In the CNS, low levels of GSH have been associated with neuropsychiatric disorders such as Parkinson's and Alzheimer's disease, and schizophrenia (Ballatori et al., 2009; Do et al., 2009). Here, we used a murine model to explore the protective response observed in the CNS after a systemic inhibition of GSH synthesis.

The role of NGF in the CNS has been studied and reviewed extensively. Furthermore, NGF and its receptors are expressed, and in many cases, modulated during stress in non-neural tissues, such as epithelial cells, fibroblasts, lymphocytes, activated macrophages, the pancreas, the heart and the liver (Yamamoto et al., 1996; Micera et al., 2001; Caporali et al., 2008; Abram et al., 2009). Moreover, it has been demonstrated that NGF levels are increased in the plasma after social and physical stress (see a previous review: Alleva and Santucci, 2001). These studies suggest a systemic role for this NT as a neuro-immune-endocrine modulator with fundamental functions in the regulation of homeostatic processes, as was first proposed by Levi-Montalcini and Aloe (1997).

Previous *in vivo* and *in vitro* studies have revealed a role for NGF in the activation of the antioxidant response in the CNS in regions such as the cerebellum (Pan and Perez-Polo, 1993; Guégan et al., 1999; Garza-Lombó et al., 2018). This cell survival response occurs as a consequence of the activation of the TrkA receptor (Sofroniew et al., 2001; Lu et al., 2005). The pathways activated by TrkA include Ras, Rac, PI3K, and PLC- $\gamma$ 1, which in turn activate mitogen-activated protein kinase (MAPK) cascades and Akt to generate inositol triphosphate and diacylglycerol (Sofroniew et al., 2001).

On the other hand, the  $p75^{NTR}$  receptor has been reported to either induce or prevent apoptosis upon oxidative insult in both *in vivo* and *in vitro* models. Nevertheless, Tyurina et al. (2005) showed that the role of the  $p75^{NTR}$  antioxidant response is not related to its extracellular receptor domain or to extracellular ligands of this NT receptor. Moreover, the increase in GSH levels induced by Nrf2 activation prevents the  $p75^{NTR}$ -mediated apoptosis of neurons *in vitro* (Vargas et al., 2006).

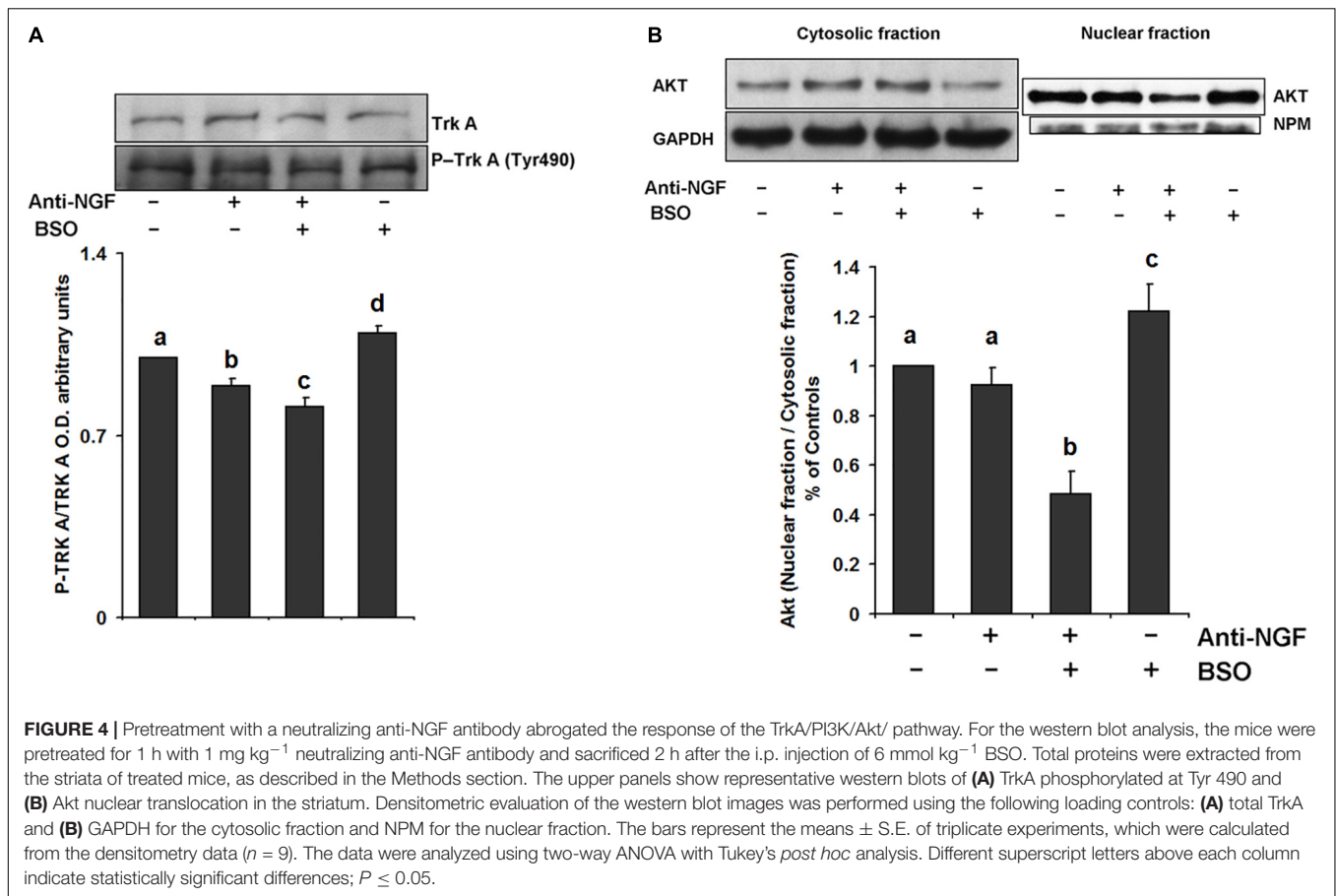
In our mouse model, BSO and iAs up-regulated NGF protein levels in plasma although in the case of iAs, at a delayed time scale (Figure 1) that was not associated with TrkA activation in the striatum (Figure 3). These results suggest that NGF synthesis is modulated by changes in the redox cellular state, despite the differences in the time scales of these responses, probably due to the specific characteristics of the target organ, drug mechanisms of action and kinetic disparities. Because we were searching for early responses, we decided to continue only with BSO treatments.

Similarly to the results obtained here, earlier works have reported oxidative stress-related NGF up-regulation in peripheral tissues such as heart (Caporali et al., 2008) and liver (Valdovinos-Flores and Gonsébat, 2013), that could lead to the observed increase in plasma NGF protein levels after treatment with BSO and iAs (Figure 1).

L-Buthionine-S-R-sulfoximine also induced the expression of NGF and TrkA protein levels in the striatum, as well as TrkA phosphorylation at Tyr 490 (Figures 1, 2, 3). These results suggest that NGF levels are positively modulated systemically in peripheral tissues and the striatum after an oxidative insult. Thus, changes in peripheral NGF levels may constitute a molecular signal to induce NGF and TrkA transcription in the striatum (CNS). To evaluate this hypothesis, we inhibited the NGF/TrkA pathway by using an anti-NGF antibody, which does not permeate the BBB, as a pretreatment before the i.p. injection of BSO. The administration of a neutralizing anti-NGF antibody abrogated signaling through the NGF/TrkA/Akt pathway in the liver in our previous study (Valdovinos-Flores and Gonsébat, 2013). Here, the neutralizing anti-NGF antibody prevented the activation of the NGF/TrkA/Akt pathway in the striatum (Figure 4), according to our hypothesis.

The fact that transgenic mice overexpressing NGF exhibit elevated GSH concentrations in the brain, plasma, and liver (Arsenijevic et al., 2007) supports our hypothesis that NGF plays a key role as a systemic redox sensor in both the CNS and peripheral tissues and integrates homeostatic systemic responses. In that respect, we have observed that agents that diminish the levels of cellular GSH, such as BSO, iAs, and





APAP, induce *ngfb* transcription in the mouse liver. Additionally, the use of a neutralizing anti-NGF antibody diminished GSH levels and downregulated *trx-1* mRNA levels in the liver (Valdovinos-Flores and Gonsbatt, 2013).

Glutathione does not penetrate the BBB easily (Anderson et al., 1989), therefore GSH synthesis in the brain is limited by the availability of the sulfhydryl AAs L-cys and L-cys<sub>2</sub> (Shih et al., 2006). We hypothesized that the activation of the NGF/TrkA signaling pathway in the striatum after BSO, might be associated with the transcriptional upregulation of the amino acid transporters genes related to the availability of L-cys and L-cys<sub>2</sub>.

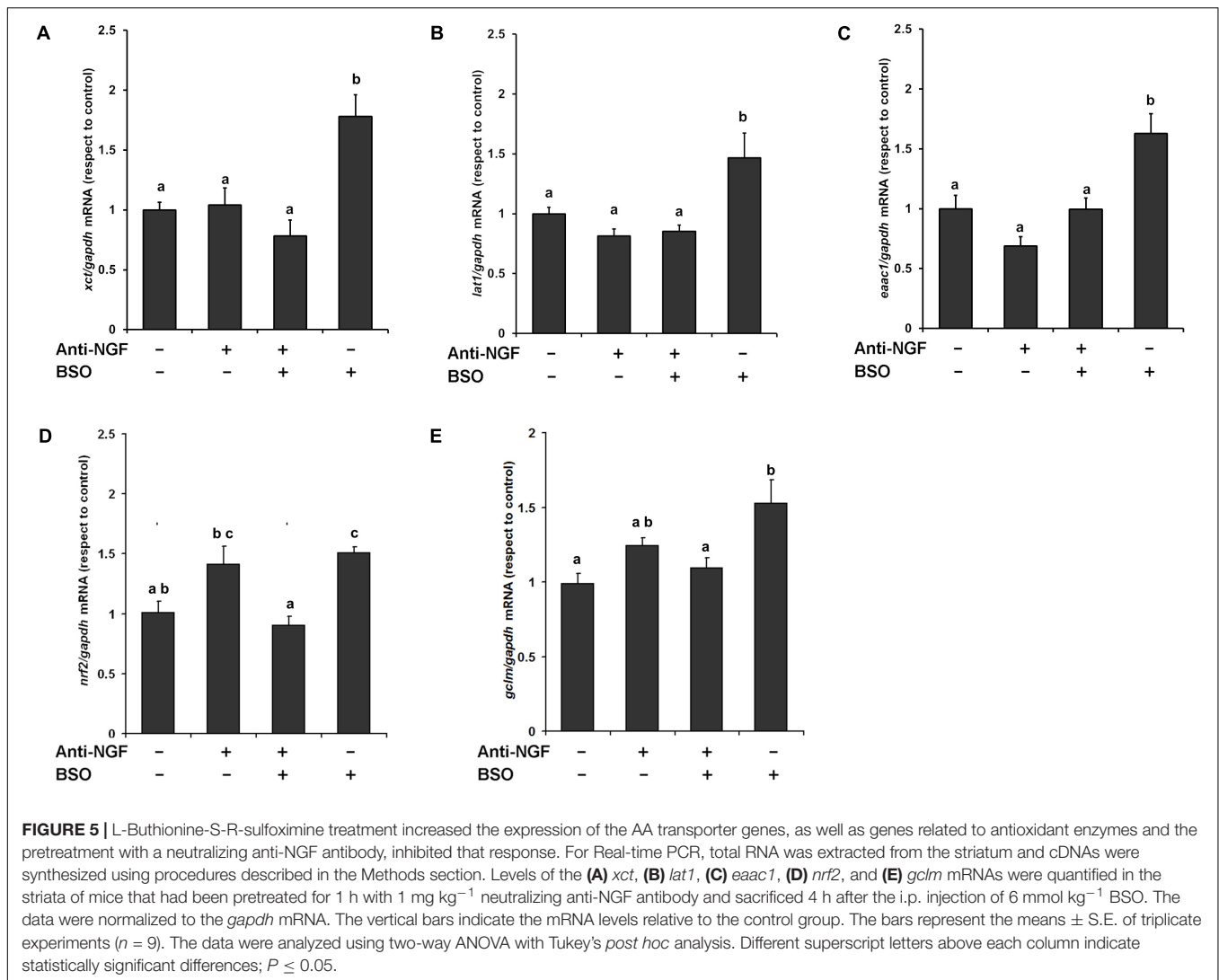
Thus, we evaluated the modulation of the *xct*, *lat1* and *eaac1* mRNA levels in the striatum. BSO treatment increased the transcription of these transporters (Figure 5). *In vivo* and *in vitro* models, the modulation of xCT and EAAC1 expression by oxidative stress stimuli has been widely reported (Kim et al., 2001; Muguruma et al., 2007; Escartin et al., 2011; Ramos-Chávez et al., 2015; Nelson-Mora et al., 2018). The genes that encode xCT, EAAC1 and LAT1 contain putative antioxidant response element (ARE) motifs in their proximal promoter sequences (Diah et al., 2001; Sasaki et al., 2002; Escartin et al., 2011), suggesting that the transcription factor Nrf2 participates in the upregulation of the transcription of the AA transporters. In fact, we found an upregulation of *nrf2* mRNA levels in response to BSO treatment (Figure 5) as was previously reported under the

same experimental conditions (Limón-Pacheco et al., 2007). It has been reported that *nrf2* mRNA levels correlated with its protein levels and have been observed as part of antioxidant enzyme regulation (Frohlich et al., 2008). Another antioxidant gene positively modulated include the gene that codified to the regulatory subunit of the first rate-limiting enzyme of glutathione synthesis, *gclm*, which mRNA level was increased after BSO treatment.

This finding is consistent with the observations reported by Kosaka et al. (2010) and Mimura et al. (2011), who showed that TrkA activation via NGF induces the nuclear translocation of Nrf2 and subsequently induces the transcription of ARE-containing genes, including *ngfb*, in PC12 cells. Notably, the mRNA increase of all the genes evaluated was abolished by the use of a neutralizing anti-NGF antibody (Figure 5).

The induction of the L-cys<sub>2</sub>/L-glu exchange transporter, which is mediated by system x<sub>c</sub><sup>-</sup>, represents potentially a source of excitotoxic extracellular L-glu in the striatal parenchyma (Bridges et al., 2012; Ramos-Chávez et al., 2015; Nelson-Mora et al., 2018). Thus, we evaluated whether, along with *xct*, the levels of the *glt-1* mRNA, which is a member of the system x<sub>AG</sub><sup>-</sup> transporter and is important for the clearance of L-glu (Pines et al., 1992), were increased. However, we did not detect any changes in the transcription of *glt-1* after treatment with BSO (data not shown), suggesting that *xct* upregulation could lead to increased





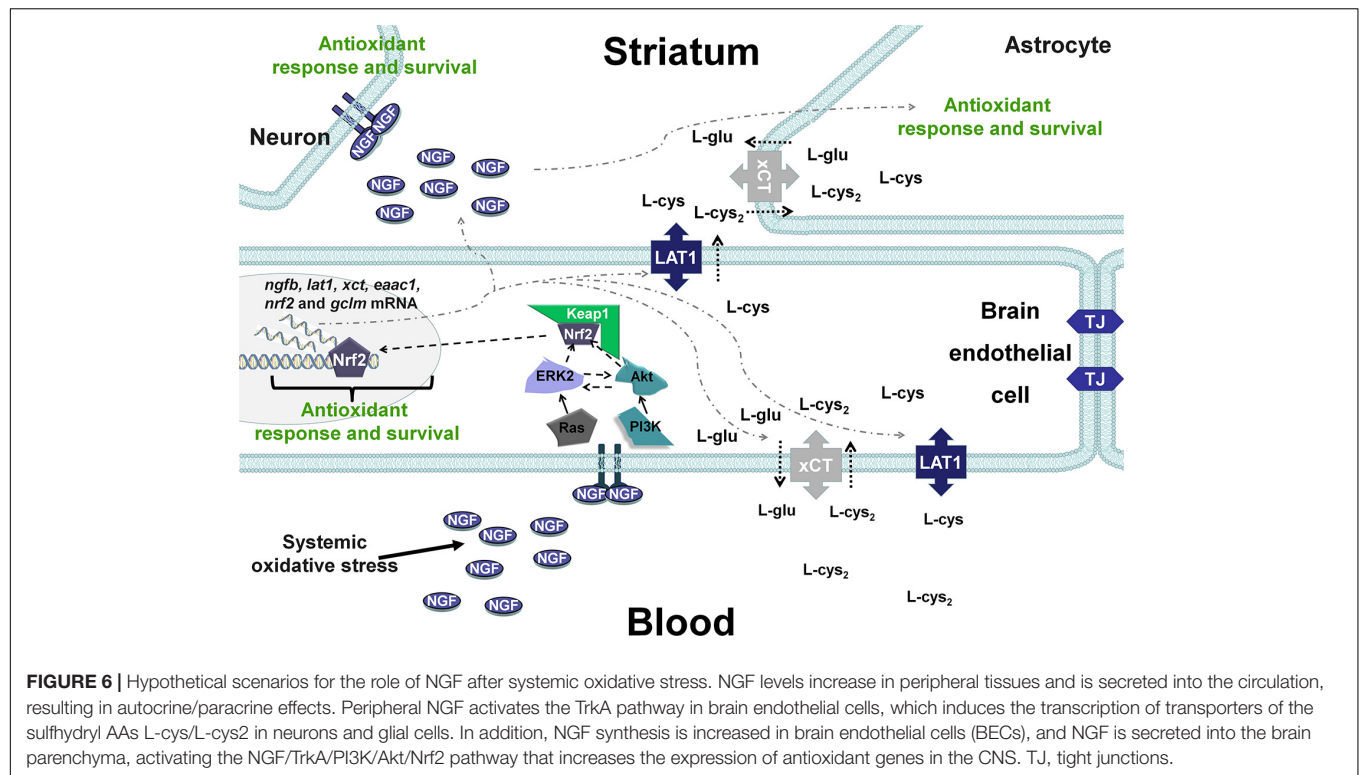
extracellular glutamate levels, as observed in mice that have been gestationally exposed to arsenic (Ramos-Chávez et al., 2015; Nelson-Mora et al., 2018).

Because NGF induces an antioxidant response via TrkA/Akt or MAPK signaling pathway, these data support our previous finding that increased levels of GSH in the brain are associated with ERK2 activation (Limón-Pacheco et al., 2007), as well as the association of TrkA and mTOR signaling pathways with the increased levels of the EAAC1 protein in the cerebellum (Garza-Lombó et al., 2018).

Our findings suggest that systemic NGF helps to maintain redox homeostasis, which would explain why NGF and TrkA levels are increased in both the plasma and brain during the systemic oxidative stress generated by physical activity (Alleva and Santucci, 2001; Ang et al., 2003; Chung et al., 2010), as well as the neuroprotective effect of physical activity on murine models of brain damage (Ding et al., 2004; Matsuda et al., 2011). However, an increase in plasma NGF levels due to excess physical activity is also associated with the occurrence of a Th2

response in subjects with allergic diseases (Bonini et al., 2013). Moreover, the experimental use of NGF antibodies as pain-relieving drugs might cause joint destruction and autonomic dysfunction by inducing changes in GSH homeostasis (Miller et al., 2017; Mullard, 2018).

Taking into account these results and our previous studies (Limón-Pacheco et al., 2007; Valdovinos-Flores and Gensebatt, 2013; Garza-Lombó et al., 2018), it is possible that changes in the systemic redox state induce tissue-specific responses through Nrf2 or NF- $\kappa$ B that include the synthesis of NGF, which increases circulating NGF levels in the blood. Then, although at the time evaluated here it was not observed, it is possible that peripheral NGF activates the NGF/TrkA signaling pathway in brain endothelial cells and enables the entrance of the sulfhydryl AAs L-cys/L-cys2 into the brain parenchyma and the subsequent secretion of NGF in the brain, where it plays a critical role in the antioxidant response via the NGF/TrkA pathway (Figure 6) in neurons and glial cells. In fact, xCT mRNA and protein expression have been shown along brain blood vessels, including



endothelial cells, meninges and astrocytes, EAAC1 is expressed in neurons and LAT1 in microvascular cells of the BBB and neurons (Burdo et al., 2006; Muller and Heuer, 2014; Ottestad-Hansen et al., 2018). Another possibility is that peripheral NGF could enter directly to the CNS as was proposed for (Levi-Montalcini and Aloe, 1985), although the mechanisms underlying this phenomenon are unknown.

The present study supports a systemic role for this NT as a neuro-immune-endocrine modulator, with fundamental functions in the regulation of homeostatic processes, as proposed by Levi-Montalcini (Levi-Montalcini and Aloe, 1997). However, further investigations of the specific responses of other organs to NGF are needed, because the increased expression of NGF is associated with allergic and inflammatory reactions in the lungs and the bladder, respectively (Pines et al., 1992; Guerios et al., 2006; Bonini et al., 2013). In addition, the upregulation of *xct* expression in astrocytes might increase extracellular glutamate concentrations in some brain regions, generating excitotoxicity (Nelson-Mora et al., 2018).

## CONCLUSION

In conclusion, we provide evidence that changes in the redox cellular state induce increases in peripheral NGF levels that orchestrate a neuroprotective response in the CNS, at least in the striatum, through the NGF/TrkA/Akt/Nrf2 pathway, including increased expression of genes involved in the uptake of the AAs L-cys and L-cys<sub>2</sub> and *gclm*, all of which are related to GSH synthesis and transport from the blood to

the neuronal parenchyma. Recently, the hNGPp peptide that harbors a mutation reducing the pro-nociceptive activity of NGF, delivered intranasally in mice, activated the TrkA and downstream Erk1/2, Akt pathways leading to neuroprotective and anti-amyloidogenic actions (Cattaneo and Capsoni, 2019). These findings prompt further studies of the role of peripheral NGF in the modulation of GSH homeostasis in the CNS and generate new perspectives for therapies that target ROS in patients with neurodegenerative diseases.

## DATA AVAILABILITY

All datasets generated for this study are included in the manuscript and/or the supplementary files.

## ETHICS STATEMENT

The animal study was reviewed and approved by The CICUAL Comision at the Instituto de Investigaciones Biomédicas, UNAM.

## AUTHOR CONTRIBUTIONS

CV-F designed the study, performed the experiments, and prepared the manuscript draft. JHL-P and CG-L contributed with important intellectual inputs. RL-R performed Western blot analysis for NGF determination in plasma. PP helped in animal treatments and protein determinations. MEG designed the

study, applied for approval from the Research Ethics Board, and reviewed the manuscript draft.

## FUNDING

This work was supported by grants from the Consejo Nacional de Ciencia y Tecnología in México (Grant No. 102287) and the Dirección General de Asuntos del Personal Académico, Universidad Nacional Autónoma de México (UNAM) (Grant No. PAPIIT IN207611). CV-F and CG-L were fellows in the Programa de Doctorado en Ciencias Biomédicas and at the UNAM and were

supported by the CONACYT fellowship Nos. 17407 and 290116.

## ACKNOWLEDGMENTS

The authors thank Miguel Tapia Rodríguez, Ph.D. for his assistance in the analysis of immunofluorescence staining; Luis Angel Albarrán-Ponce, M.Sc., Daniel Garzón, Ph.D. MVZs, Jorge Omar García Rebollar, and Georgina Diaz Herrera for their assistance in animal experiments; and Lourdes Massieu, Ph.D. for providing helpful comments and participating in helpful discussions.

## REFERENCES

- Abram, M., Wegmann, M., Fokuhl, V., Sonar, S., Luger, E. O., Kerzel, S., et al. (2009). Nerve growth factor and neurotrophin-3 mediate survival of pulmonary plasma cells during the allergic airway inflammation. *J. Immunol.* 182, 4705–4712. doi: 10.4049/jimmunol.0802814
- Agricultura y Ganadería, D. R. (2001). *Norma Oficial Mexicana, NOM -062-ZOO- 1999, Especificaciones Técnicas Para la Producción, Cuidado y uso de los Animales de Laboratorio*. México: SAGARPA.
- Alleva, E., and Santucci, D. (2001). Psychosocial vs. “physical” stress situations in rodents and humans: role of neurotrophins. *Physiol. Behav.* 73, 313–320. doi: 10.1016/S0031-9384(01)00498-X
- Anderson, E. M., Underwood, M., Bridges, R. J., and Meister, A. (1989). Glutathione metabolism at the blood-cerebrospinal fluid barrier. *J. Fed. Am. Soc. Exp. Biol.* 3, 2527–2531. doi: 10.1096/fasebj.3.13.2572501
- Ang, E. T., Wong, P. T. H., Mochhala, S., and Ng, Y. K. (2003). Neuroprotection associated with running: is it a result of increased endogenous neurotrophic factors? *Neuroscience* 118, 335–345. doi: 10.1016/S0306-4522(02)00989-2
- Arsenijevic, D., Hernadfalvi, N., Von Meyenburg, C., Onteniente, B., Richard, D., and Langhans, W. (2007). Role for nerve growth factor in the in vivo regulation of glutathione in response to LPS in mice. *Eur. Cytokine Netw.* 18, 93–101. doi: 10.1684/ecr.2007.0091
- Ballatori, N., Krance, S. M., Notenboom, S., Shi, S., Tieu, K., and Hammond, C. L. (2009). Glutathione dysregulation and the etiology and progression of human diseases. *Biol. Chem.* 390, 191–214. doi: 10.1515/BC.2009.033
- Bizon, J. L., Lauterborn, J. C., and Gall, C. M. (1999). Subpopulations of striatal interneurons can be distinguished on the basis of neurotrophic factor expression. *J. Comp. Neurol.* 408, 283–298. doi: 10.1002/(sici)1096-9861(19990531)408:2<283::aid-cne9>3.0.co;2-2
- Bonini, M., Fioretti, D., Sargentini, V., Del Giacco, S., Rinaldi, M., Tranquilli, C., et al. (2013). Increased nerve growth factor serum levels in top athletes. *Clin. J. Sport Med.* 23, 228–231. doi: 10.1097/JSM.0b013e31827ee6d5
- Bridges, R. J., Natale, N. R., and Patel, S. A. (2012). System x c- cystine/glutamate antiporter: an update on molecular pharmacology and roles within the CNS. *Br. J. Pharmacol.* 195, 20–34. doi: 10.1111/j.1476-5381.2011.01480.x
- Burdo, J., Dargusch, R., and Schubert, D. (2006). Distribution of the cystine/glutamate antiporter system xc- in the brain, kidney, and duodenum. *J. Histochem. Cytochem.* 54, 549–557. doi: 10.1369/jhc.5a6840.2006
- Caporali, A., Sala-Newby, G. B., Meloni, M., Graiani, G., Pani, E., Cristofaro, B., et al. (2008). Identification of the prosurvival activity of nerve growth factor on cardiac myocytes. *Cell Death Differ.* 15, 299–311. doi: 10.1038/sj.cdd.4402263
- Cattaneo, A., and Capsoni, S. (2019). Painless nerve growth factor: a TrkA biased agonist mediating a broad neuroprotection via its actions on microglia cells. *Pharmacol. Res.* 139, 17–25. doi: 10.1016/j.phrs.2018.10.028
- Chung, J. Y., Kim, M. W., Bang, M. S., and Kim, M. (2010). The effect of exercise on trkA in the contralateral hemisphere of the ischemic rat brain. *Brain Res.* 1353, 187–193. doi: 10.1016/j.brainres.2010.06.057
- Cruz-Aguado, R., Turner, L. F., Diaz, C. M., and Pinero, J. (2000). Nerve growth factor and striatal glutathione metabolism in a rat model of Huntington's disease. *Restor. Neurol. Neurosci.* 17, 217–221.
- Diah, S. K., Padbury, J. F., Campbell, W. A., Britt, D., and Thompson, N. L. (2001). Molecular cloning of the rat TA1/LAT-1/CD98 light chain gene promoter. *Biochim. Biophys. Acta* 1518, 267–270. doi: 10.1016/S0167-4781(01)00202-0
- Ding, Y., Li, J., Luan, X., Ding, Y. H., Lai, Q., Rafols, J. A., et al. (2004). Exercise pre-conditioning reduces brain damage in ischemic rats that may be associated with regional angiogenesis and cellular overexpression of neurotrophin. *Neuroscience* 124, 583–591. doi: 10.1016/j.neuroscience.2003.12.029
- Do, K. Q., Cabungcal, J. H., Frank, A., Steullet, P., and Cuenod, M. (2009). Redox dysregulation, neurodevelopment, and schizophrenia. *Curr. Opin. Neurobiol.* 19, 220–230. doi: 10.1016/j.conb.2009.05.001
- Escartin, C., Joon Won, S., Malmgren, C., Auregan, G., Berman, A. E., Chen, P.-C., et al. (2011). Nuclear factor erythroid 2-related factor 2 facilitates neuronal glutathione synthesis by upregulating neuronal excitatory amino acid transporter 3 expression. *J. Neurosci.* 31, 7392–7401. doi: 10.1523/JNEUROSCI.6577-10.2011
- Frohlich, D. A., McCabe, M. T., Arnold, R. S., and Day, M. L. (2008). The role of Nrf2 in increased reactive oxygen species and DNA damage in prostate tumorigenesis. *Oncogene* 27, 4353–4362. doi: 10.1038/onc.2008.79
- Garza-Lombó, C., Petrosyan, P., Tapia-Rodríguez, M., Valdovinos-Flores, C., and Gonshebbat, M. E. (2018). Systemic L-buthionine-S-R-sulfoximine administration modulates glutathione homeostasis via NGF/TrkA and mTOR signaling in the cerebellum. *Neurochem. Int.* 121, 8–18. doi: 10.1016/j.neuint.2018.10.007
- Gu, F., Chauhan, V., and Chauhan, A. (2015). Glutathione redox imbalance in brain disorders. *Curr. Opin. Clin. Nutr. Metab. Care* 18, 89–95. doi: 10.1097/MCO.0000000000000134
- Guégan, C., Ceballos-Picot, I., Chevalier, E., Nicole, A., Onténiente, B., and Sola, B. (1999). Reduction of ischemic damage in NGF-transgenic mice: correlation with enhancement of antioxidant enzyme activities. *Neurobiol. Dis.* 6, 180–189. doi: 10.1006/nbdi.1999.0240
- Guerios, S. D., Wang, Z. Y., and Bjorling, D. E. (2006). Nerve growth factor mediates peripheral mechanical hypersensitivity that accompanies experimental cystitis in mice. *Neurosci. Lett.* 392, 193–197. doi: 10.1016/j.neulet.2005.09.026
- Institute for Laboratory Animal Research. (2011). *Guide for the Care and Use of Laboratory Animals*. 8th Edn. Washington, WA: National Academies Press, doi: 10.2307/1525495
- Johnson, W. M., Wilson-Delfosse, A. L., and Mieyal, J. J. (2012). Dysregulation of glutathione homeostasis in neurodegenerative diseases. *Nutrients* 4, 1399–1440. doi: 10.3390/nu4101399
- Kaneko, Y., Kitazato, K., and Basaki, Y. (2004). Integrin-linked kinase regulates vascular morphogenesis induced by vascular endothelial growth factor. *J. Cell Sci.* 117, 407–415. doi: 10.1242/jcs.00871
- Kim, J. Y., Kanai, Y., Chairoungdua, A., Cha, S. H., Matsuo, H., Kim, D. K., et al. (2001). Human cystine/glutamate transporter: cDNA cloning and upregulation by oxidative stress in glioma cells. *Biochim. Biophys. Acta Biomembr.* 1512, 335–344. doi: 10.1016/S0005-2736(01)00338-8

- Kosaka, K., Mimura, J., Itoh, K., Satoh, T., Shimojo, Y., Kitajima, C., et al. (2010). Role of Nrf2 and p62/ZIP in the neurite outgrowth by carnosic acid in PC12h cells. *J. Biochem.* 147, 73–81. doi: 10.1093/jb/mvp149
- Levi-Montalcini, R., and Aloe, L. (1985). Differentiating effects of murine nerve growth factor in the peripheral and central nervous systems of *Xenopus laevis* tadpoles. *Proc. Nat. Acad. Sci. U.S.A.* 82, 7111–7115. doi: 10.1073/pnas.82.20.7111
- Levi-Montalcini, R., and Aloe, L. (1997). A Role for Nerve Growth Factor in Nervous, Endocrine and Immune Systems, in: *The Saga of the Nerve Growth Factor: Preliminary Studies, Discovery, Further Development*. Singapore: World Scientific.
- Limón-Pacheco, J., and Gonshebbat, M. E. (2009). The role of antioxidants and antioxidant-related enzymes in protective responses to environmentally induced oxidative stress. *Mutat. Res. Genet. Toxicol. Environ. Mutagen.* 674, 137–147. doi: 10.1016/j.mrgentox.2008.09.015
- Limón-Pacheco, J. H., Hernández, N. A., Fanjul-Moles, M. L., and Gonshebbat, M. E. (2007). Glutathione depletion activates mitogen-activated protein kinase (MAPK) pathways that display organ-specific responses and brain protection in mice. *Free Radic. Biol. Med.* 43, 1335–1347. doi: 10.1016/j.freeradbiomed.2007.06.028
- Livak, K. J., and Schmittgen, T. D. (2001). Analysis of relative gene expression data using real-time quantitative PCR and the 2<sup>-</sup>(Delta Delta C(T)) Method. *Methods* 25, 402–408. doi: 10.1006/meth.2001.1262
- Lu, B., Pang, P. T., and Woo, N. H. (2005). The yin and yang of neurotrophin action. *Nat. Rev. Neurosci.* 6, 603–614. doi: 10.1038/nrn1726
- Matsuda, F., Sakakima, H., and Yoshida, Y. (2011). The effects of early exercise on brain damage and recovery after focal cerebral infarction in rats. *Acta Physiol.* 201, 275–287. doi: 10.1111/j.1748-1716.2010.02174.x
- Meister, A. (1995). Glutathione biosynthesis and its inhibition. *Methods Enzymol.* 252, 26–30. doi: 10.1016/0076-6879(95)52005-8
- Micera, A., Vigneti, E., Pickholtz, D., Reich, R., Pappo, O., Bonini, S., et al. (2001). Nerve growth factor displays stimulatory effects on human skin and lung fibroblasts, demonstrating a direct role for this factor in tissue repair. *Proc. Natl. Acad. Sci. U.S.A.* 98, 6162–6167. doi: 10.1073/pnas.101130898
- Miller, R. E., Malfait, A. M., and Block, J. A. (2017). Current status of nerve growth factor antibodies for the treatment of osteoarthritis pain. *Clin. Exp. Rheumatol.* 29, 110–118. doi: 10.1097/BOR.0000000000000354
- Mimura, J., Kosaka, K., Maruyama, A., Satoh, T., Harada, N., Yoshida, H., et al. (2011). Nrf2 regulates NGF mRNA induction by carnosic acid in T98G glioblastoma cells and normal human astrocytes. *J. Biochem.* 150, 209–217. doi: 10.1093/jb/mvr065
- Minich, T., Riemer, J., Schulz, J. B., Wielinga, P., Wijnholds, J., and Dringen, R. (2006). The multidrug resistance protein 1 (Mrp1), but not Mrp5, mediates export of glutathione and glutathione disulfide from brain astrocytes. *J. Neurochem.* 97, 373–384. doi: 10.1111/j.1471-4159.2006.03737.x
- Muguruma, M., Unami, A., Kanki, M., Kuroiwa, Y., Nishimura, J., Dewa, Y., et al. (2007). Possible involvement of oxidative stress in piperonyl butoxide induced hepatocarcinogenesis in rats. *Toxicology* 236, 61–75. doi: 10.1016/j.tox.2007.03.025
- Mullard, A. (2018). Painkilling anti-NGF antibodies stage phase III comeback. *Nat. Rev. Drug Discov.* 17:697. doi: 10.1038/nrd.2018.177
- Muller, J., and Heuer, H. (2014). Expression pattern of thyroid hormone transporters in the postnatal mouse brain. *Front. Endocrinol.* 5:92. doi: 10.3389/fendo.2014.00092
- Nelson-Mora, J., Escobar, M. L., Rodríguez-Durán, L., Massieu, L., Montiel, T., Rodríguez, V. M., et al. (2018). Gestational exposure to inorganic arsenic (iAs3+) alters glutamate disposition in the mouse hippocampus and ionotropic glutamate receptor expression leading to memory impairment. *Arch. Toxicol.* 92, 1037–1048. doi: 10.1007/s00204-017-2111-x
- Ottestad-Hansen, S., Hu, Q. X., Follin-Arbelet, V. V., Bentea, E., Sato, H., Massie, A., et al. (2018). The cystine-glutamate exchanger (xCT, Slc7a11) is expressed in significant concentrations in a subpopulation of astrocytes in the mouse brain. *Glia* 66, 951–970. doi: 10.1002/glia.23294
- Pan, Z., and Perez-Polo, R. (1993). Role of nerve growth factor in oxidant homeostasis: glutathione metabolism. *J. Neurochem.* 61, 1713–1721. doi: 10.1111/j.1471-4159.1993.tb09808.x
- Pan, Z., and Perez-Polo, R. (1996). Increased uptake of L-cysteine and L-cystine by nerve growth factor in rat pheochromocytoma cells. *Brain Res.* 740, 21–26. doi: 10.1016/s0006-8993(96)00844-x
- Pines, G., Danbolt, N. C., Bjoras, M., Zhang, Y., Bendahan, A., Eide, L., et al. (1992). Cloning and expression of a rat brain L-glutamate transporter. *Nature* 360, 464–467. doi: 10.1038/360464a0
- Podratz, J. L., and Windebank, A. J. (2005). NGF rescues DRG neurons in vitro from oxidative damage produced by hemodialyzers. *Neurotoxicology* 26, 343–350. doi: 10.1016/j.neuro.2005.01.003
- Ramos-Chávez, L. A., Rendón-López, C. R. R., Zepeda, A., Silva-Adaya, D., Del Razo, L. M., and Gonshebbat, M. E. (2015). Neurological effects of inorganic arsenic exposure: altered cysteine/glutamate transport, NMDA expression and spatial memory impairment. *Front. Cell. Neurosci.* 9:21. doi: 10.3389/fncel.2015.00021
- Rodríguez, V. M., Del Razo, L. M., Limón-Pacheco, J. H., Giordano, M., Sánchez-Peña, L. C., Uribe-Querol, E., et al. (2005). Glutathione reductase inhibition and methylated arsenic distribution in Cd1 mice brain and liver. *Toxicol. Sci.* 84, 157–166. doi: 10.1093/toxsci/kfi057
- Salinas, M., Diaz, R., Abraham, N. G., De Galarreta, C. M. R., and Cuadrado, A. (2003). Nerve growth factor protects against 6-hydroxydopamine-induced oxidative stress by increasing expression of heme oxygenase-1 in a phosphatidylinositol 3-kinase-dependent manner. *J. Biol. Chem.* 278, 13898–13904. doi: 10.1074/jbc.M209164200
- Sampath, D., Jackson, G. R., Werbach-Perez, K., and Perez-Polo, J. R. (1994). Effects of nerve growth factor on glutathione peroxidase and catalase in PC12 cells. *J. Neurochem.* 62, 2476–2479. doi: 10.1046/j.1471-4159.1994.6206.2476.x
- Sánchez del Pino, M. M., Peterson, D. R., and Hawkins, R. A. (1995). Neutral amino acid transport characterization of isolated luminal and abluminal membranes of the blood-brain barrier. *J. Biol. Chem.* 270, 14913–14918. doi: 10.1074/jbc.270.25.14913
- Sasaki, H., Sato, H., Kuriyama-Matsumura, K., Sato, K., Maebara, K., Wang, H., et al. (2002). Electrophile response element-mediated induction of the cystine/glutamate exchange transporter gene expression. *J. Biol. Chem.* 277, 44765–44771. doi: 10.1074/jbc.M208704200
- Senft, A. P., Dalton, T. P., and Shertzer, H. G. (2000). Determining glutathione, and glutathione disulfide using the fluorescence probe o-phthalaldehyde. *Anal. Biochem.* 280, 80–86. doi: 10.1006/abio.2000.4498
- Shih, A. Y., Erb, H., Sun, X., Toda, S., Kalivas, P. W., and Murphy, T. H. (2006). Cystine/glutamate exchange modulates glutathione supply for neuroprotection from oxidative stress and cell proliferation. *J. Neurosci.* 26, 10514–10523. doi: 10.1523/JNEUROSCI.3178-06.2006
- Sofroniew, M. V., Howe, C. L., and Mobley, W. C. (2001). Nerve growth factor signaling, neuroprotection, and neural repair. *Annu. Rev. Neurosci.* 24, 1217–1281. doi: 10.1146/annurev.neuro.24.1.1217
- Tyurina, Y. Y., Nylander, K. D., Mirnics, Z. K., Portugal, C., Yan, C., Zaccaro, C., et al. (2005). The intracellular domain of p75NTR as a determinant of cellular reducing potential and response to oxidant stress. *Aging Cell* 4, 187–196. doi: 10.1111/j.1474-9726.2005.00160.x
- Valdovinos-Flores, C., and Gonshebbat, M. E. (2012). The role of amino acid transporters in GSH synthesis in the blood-brain barrier and central nervous system. *Neurochem. Int.* 61, 405–414. doi: 10.1016/j.neuint.2012.05.019
- Valdovinos-Flores, C., and Gonshebbat, M. E. (2013). Nerve growth factor exhibits an antioxidant and an autocrine activity in mouse liver that is modulated by buthionine sulfoximine, arsenic, and acetaminophen. *Free Radic. Res.* 47, 404–412. doi: 10.3109/10715762.2013.783210
- Vargas, M. R., Pehar, M., Cassina, P., Beckman, J. S., and Barbeito, L. (2006). Increased glutathione biosynthesis by Nrf2 activation in astrocytes prevents p75NTR-dependent motor neuron apoptosis. *J. Neurochem.* 97, 687–696. doi: 10.1111/j.1471-4159.2006.03742.x
- Wang, F., Li, C., Liu, W., Jin, Y., and Guo, L. (2013). Effects of subchronic exposure to low-dose volatile organic compounds on lung inflammation in mice. *Env. Toxicol.* 29, 1089–1097. doi: 10.1002/tox.21844



- Yamamoto, M., Sobue, G., Yamamoto, K., Terao, S., and Mitsuma, T. (1996). Expression of mRNAs for neurotrophic factors (NGF, BDNF, NT-3, and GDNF) and their receptors (p75NGFR, TrkA, TrkB, and TrkC) in the adult human peripheral nervous system and nonneural tissues. *Neurochem. Res.* 21, 929–938. doi: 10.1007/BF02532343
- Zerangue, N., and Kavanaugh, M. P. (1996). Interaction of L-cysteine with a human excitatory amino acid transporter. *J. Physiology.* 493, 419–423. doi: 10.1113/jphysiol.1996.sp021393
- Zhou, Z., Chen, H., Zhang, K., Yang, H., Liu, J., and Huang, Q. (2003). Protective effect of nerve growth factor on neurons after traumatic brain injury. *J. Basic Clin. Physiol. Pharmacol.* 14, 217–224.

**Conflict of Interest Statement:** The authors declare that the research was conducted in the absence of any commercial or financial relationships that could be construed as a potential conflict of interest.

Copyright © 2019 Valdovinos-Flores, Limón-Pacheco, León-Rodríguez, Petrosyan, Garza-Lombó and Gonsebatt. This is an open-access article distributed under the terms of the Creative Commons Attribution License (CC BY). The use, distribution or reproduction in other forums is permitted, provided the original author(s) and the copyright owner(s) are credited and that the original publication in this journal is cited, in accordance with accepted academic practice. No use, distribution or reproduction is permitted which does not comply with these terms.



# RAD6B Plays a Critical Role in Neuronal DNA Damage Response to Resist Neurodegeneration

Zhao Guo<sup>1†</sup>, Yingxia Tian<sup>2†</sup>, Yingli Guo<sup>1</sup>, Boya Li<sup>1</sup>, Xiangwen Liu<sup>1</sup>, Kun Xie<sup>1</sup>, Yanfeng Song<sup>1\*</sup> and Degui Wang<sup>1\*</sup>

<sup>1</sup> Department of Anatomy and Histology, School of Basic Medical Sciences, Lanzhou University, Lanzhou, China,

<sup>2</sup> Department of Internal Medicine, Gansu Provincial Academic Institute for Medical Research, Lanzhou, China

## OPEN ACCESS

### Edited by:

Rocio Martínez De Pablos,  
University of Seville, Spain

### Reviewed by:

Fabrizio Palitti,  
Università degli Studi della Toscana, Italy  
Ray Truant,  
McMaster University, Canada

### \*Correspondence:

Yanfeng Song  
songyanfeng@lzu.edu.cn  
Degui Wang  
wangdegui@lzu.edu.cn

<sup>†</sup>These authors have contributed  
equally to this work

### Specialty section:

This article was submitted to  
Cellular Neuropathology,  
a section of the journal  
Frontiers in Cellular Neuroscience

**Received:** 10 April 2019

**Accepted:** 09 August 2019

**Published:** 23 August 2019

### Citation:

Guo Z, Tian Y, Guo Y, Li B, Liu X,  
Xie K, Song Y and Wang D (2019)  
RAD6B Plays a Critical Role  
in Neuronal DNA Damage Response  
to Resist Neurodegeneration.  
Front. Cell. Neurosci. 13:392.  
doi: 10.3389/fncel.2019.00392

RAD6 participates in DNA double-strand breaks (DSBs) repair by ubiquitinating histone H2B in mitotic cells. In terminally differentiated cells, however, the mechanisms of DNA damage repair are less well known. In this study, we investigate whether RAD6B is involved in DSBs repair in neurons and effects of RAD6B deficiency on neuronal survival. We compared neurons of RAD6B-deficient mice with those of littermate wild type (WT) mice and induced DNA damage by X-ray irradiation. We provide evidence that RAD6B is essential for neural DDR and RAD6B deficiency results in increased genomic instability and neurodegeneration. Moreover, higher levels of p53 and p21 are present in the brains of RAD6B-deficient mice, which may be responsible for neuronal senescence, and degeneration. In addition, behavioral experiments show that RAD6B-deficient mice exhibit marked learning and memory deficits. In conclusion, these findings suggest that RAD6B is critical for neural integrity and that the absence of RAD6B accelerates neurodegeneration in mice.

**Keywords:** RAD6B, aging, histone ubiquitination, DNA damage, neurodegeneration, senescence

## INTRODUCTION

Biological cells are affected by various genotoxic stressors from endogenous and exogenous sources, and it is estimated that a typical mammalian cell undergoes  $\sim 2 \times 10^5$  lesions per day (Harper and Elledge, 2007; Ouyang et al., 2015; White and Vijg, 2016; Hegde et al., 2017). DNA DSBs are the most harmful to cells (Jackson and Bartek, 2009; Ouyang et al., 2015), which often lead to chromosomal rearrangements, senescence, tumorigenesis, or cell death (Lee and Mckinnon, 2007; White and Vijg, 2016). To avert those potentially devastating consequences, cells initiate highly evolved DNA damage response (DDR), and detect and repair damaged DNA. DSBs always occur when cells are exposed to genotoxic agents such as ionizing radiation and oxidative stress and are detected by two sensor proteins, the MRE11/RAD50/NBS1 (MRN) complex and the Ku70/Ku80 heterodimer (White and Vijg, 2016). Then ATM is activated and phosphorylates histone variant H2AX to form  $\gamma$ -H2AX and bind to the break sites.  $\gamma$ -H2AX also forms a binding site for MDC1, which recruits additional downstream repair factors, such as RNF8, 53BP1 and BRCA1, to gather at the sites and repair these breaks (Harper and Elledge, 2007; Marteijn et al., 2009; Liu et al., 2013; Ouyang et al., 2015). Based on different factors, including the cell type, cell-cycle stage and the severity of the damage, accurate repair leads to restoration of an intact double helix, while failed repair often cause apoptosis, and senescence or even tumor formation (Barzilai, 2010).

Protein ubiquitination is a series of complex cascade reactions including three enzymes: ubiquitin activating enzymes (E1s), ubiquitin conjugating enzymes (E2s), and ubiquitin ligases (E3s) (Walden et al., 2003; Chen et al., 2012). Along with other modifications such as methylation, acetylation and phosphorylation, ubiquitination plays important roles in many cellular processes (Kim et al., 2009), including the regulation of cell cycle, apoptosis, gene expression, transcription regulation, DNA damage repair, and protein degradation (Ciechanover, 1994; Biochem, 1998; Varshavsky, 2005; Chen et al., 2012). RAD6 is first identified as an important E2 in yeast and interacts with three separate E3s (Ubr1, Rad18, and Bre1) to participate in DDR. However, there are still some problems to be clarified for RAD6-mediated DNA repair involving its function with Bre1 in mono-ubiquitinating the histone H2B residue lysine 123. RAD6 mutation causes yeasts to be highly sensitive to ultraviolet light (Game and Chernikova, 2009; Chen et al., 2012). In addition, *Saccharomyces* mutants deficient in H2B mono-ubiquitination also shown irradiation-sensitive and abortive DNA damage repair, gene silencing, and cell-cycle checkpoints (Game and Chernikova, 2009; Chernikova et al., 2012). RAD6A and RAD6B are two homologs of yeast RAD6 and mice are non-viable if both homologs are absent (Chen et al., 2012).

While in the central nervous system, protected by the skull and blood-brain barrier, the most common threat to the neuronal genome comes from metabolic reactive oxygen species (ROS), which cause oxidative DNA damage, including single strand breaks (SSBs) (Madabhushi et al., 2014). However, under certain conditions, SSBs may be converted to DSBs, such as two SSBs that are in close proximity to each other (Madabhushi et al., 2014). And recent studies have shown that DNA DSBs are also formed in normal physiological/metabolic processes. On the other hand, the ability of neurons to repair damage decreases with aging. Thus, appropriate responses to DNA DSBs and accurate repair of broken DNA are required to maintain homeostasis and organismic survival (Lee and McKinnon, 2007).

In recent years, there has been a continuous stream of evidences that mutations of DNA repair genes frequently cause severe defects in the central nervous system (Herrup et al., 2013) and that DNA damage is not only correlated with the aging process but also proposed to accelerate it (Barzilai and McKinnon, 2013; Canugovi et al., 2013; Hegde et al., 2017). Furthermore, several neurodegenerative diseases, such as ataxia-telangiectasia (A-T), Alzheimer's disease (AD), and Parkinson's disease (PD), are closely related to DNA damage repair (Jackson and Bartek, 2009; Reynolds and Stewart, 2013). Our latest experiments have shown that loss of the ubiquitin ligase RNF8 leads to neurodegeneration in mice and DNA damage preceding dopamine neuron degeneration in PD mice (Ouyang et al., 2015; Wang et al., 2016). Bioinformatics analysis also indicates that 293T cells with RAD6B deficiency express higher levels of mRNA involving neurodegeneration. To further explore the effect of RAD6B deficiency on neurons, we focus on the function of RAD6B in neural DDR and phenotypes of neurons in RAD6B-deficient mice.

## RESULTS

### RAD6B Is Essential for Neural DNA DSBs Repair

To compare the repair processes for DSBs in the neurons of RAD6B-deficient mice with those in the neurons of WT mice, we observed the formation of ionizing radiation-induced nuclear foci (IRIF) at the broken sites after inducing damage by X-ray irradiation.  $\gamma$ -H2AX foci were used as a marker of DNA damage, while MDC1, 53BP1, RNF8, and BRCA1 were co-stained with  $\gamma$ -H2AX as repair factors. As shown in **Figure 1**, there were numerous 53BP1, BRCA1, RNF8, and MDC1 foci in the neurons of WT mice. In addition, most of them colocalized with the corresponding  $\gamma$ -H2AX foci, indicating that they were recruited to the broken sites after X-ray irradiation. By contrast, 53BP1 and BRCA1 foci were decreased dramatically in the neurons of RAD6B-deficient mice after X-ray irradiation, suggesting that RAD6B deficiency caused them to be recruited less to the break sites. However, in the neurons of RAD6B-deficient mice, almost the same proportions of MDC1 and RNF8 foci of were detected as in the neurons of WT mice, respectively (**Figures 1A,B**). These results suggest that RAD6B is involved in the repair process for DNA DSBs in neurons. Deficiency of RAD6B leads to incomplete recruitment of downstream repair factors, including 53BP1 and BRCA1, but the upstream proteins MDC1 and RNF8 are not affected.

### Loss of RAD6B Leads to Decreased H2B Ubiquitination

Post-translational modifications (PTMs) of histones are important regulators of the structure of chromosomes. We next focused on the substrate histones of RAD6B ubiquitination in neurons and measured the ubiquitination levels of the histones H2A and H2B. As shown in **Figures 2A,B**, knockout of RAD6B leads to significant reduction in the ubiquitination of H2B compared with the WT mouse brains. No evident increase was detected in the expression of ubH2B in RAD6B-deficient mouse brains, while ubH2B in the WT mouse brains increased obviously after X-ray irradiation. However, ubH2A in the brains of WT mice and RAD6B-deficient mice both increased after IR, and higher level of ubH2A was observed in the brains of RAD6B-deficient mice. The relative expression levels of H2A and H2B did not show clear changes between groups (**Figures 2A,B**). Consistent with ubH2B, the level of H3K79me2 in RAD6B-deficient mouse brains decreased significantly (**Figures 2C,D**).

### RAD6B Deficiency Leads to Increased Genomic Instability and Neurodegeneration

While knocking down RAD6B did not significantly influence cell proliferation compared with siNeg treated cells within 72 h, cell growth was obviously inhibited with 2Gy of X-ray treatment (**Figure 3A**). To determine the effect of RAD6B deficiency on neuronal genomic integrity, we evaluated the

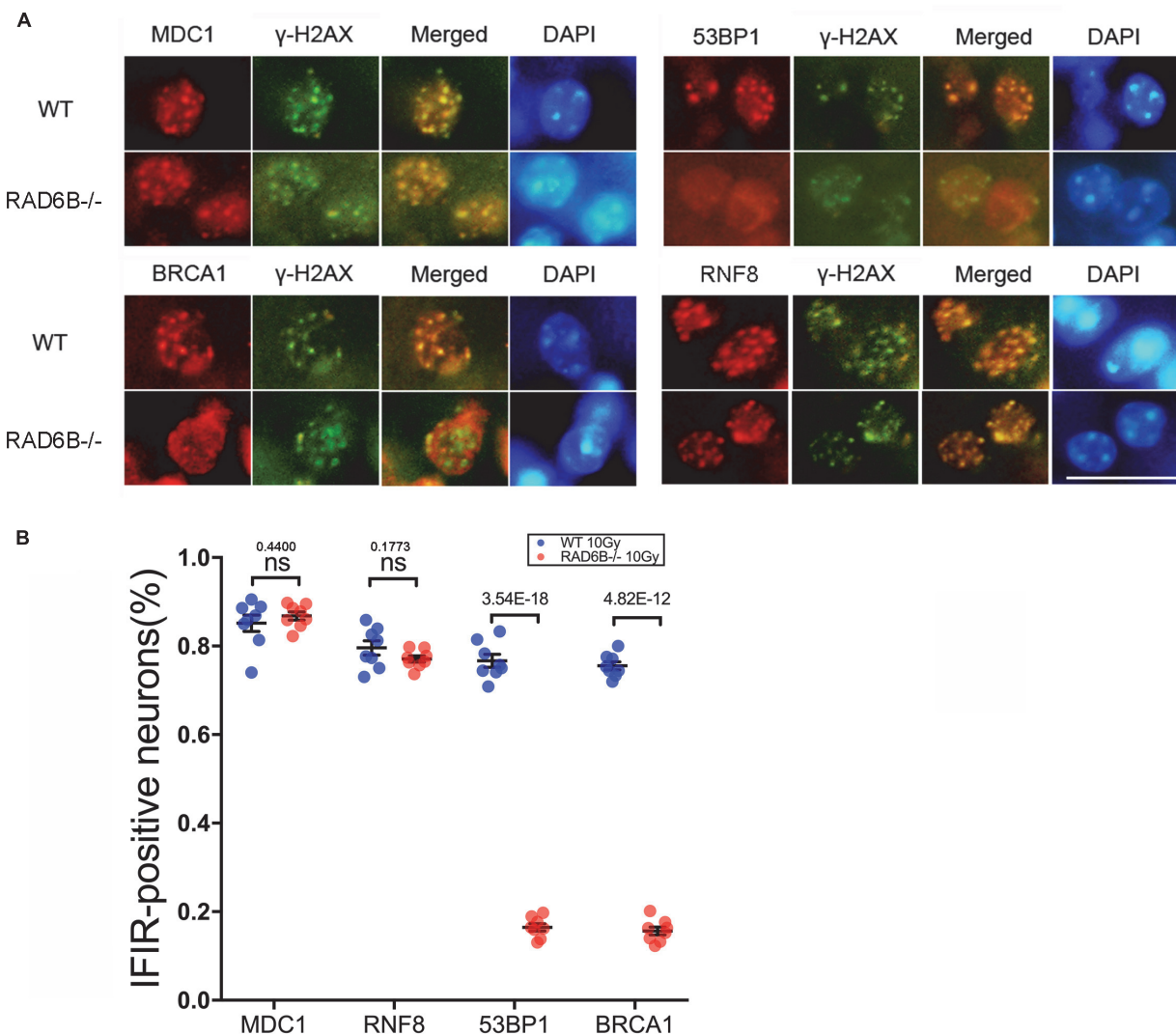


**FIGURE 1 |** RAD6B is involved in DNA damage repair in neurons after IR. **(A)** RAD6B-deficient mice and control mice were simultaneously exposed to X-rays at a dose of 10 Gy. After 2 h of recovery, frozen sections of brain tissues were obtained and immunofluorescence was used to detect the formation of IRIF. Anti-MDC1, anti-53BP1, anti-BRCA1, and anti-RNF8 antibodies were applied separately for co-immunostaining with anti-γ-H2AX antibody. Scale bar = 20 μm. **(B)** The average percentages of IRIF-positive neurons were analyzed and are displayed with scatter diagrams. All values are presented as the mean ± SEM ( $n = 8$ ). Student's *t*-test.

formation of MN. A total of 1000 binucleated cells in six separate experiments for each group were scored to evaluate the frequency of MN induction and cells contained at least one MN were counted as MN-positive. Shin Koyama reported that there was a threshold of dose of X-rays for MN induction and no significant difference at doses lower than 0.05Gy was detected compared with the control. Interestingly, a small amount of MN was also detected in siRAD6B-treated RPE1 cells without X-ray irradiation. However, in the case of X-ray treatment, a large amount of MN was produced, about four folds as much as that of siNeg treated cells (Figures 3B,C). Generally, MN originate from chromosome fragments or whole chromosomes lagging behind during anaphase of mitosis. Therefore, these results suggest that RAD6B deficiency causes increase of genomic instability in neurons due to the defect of DSBs repair.

Analysis of the nuclei and neurites in neurons of the RAD6B-deficient mice with silver staining revealed that more nuclei in RAD6B-deficient mice became irregular and deeply stained, while neurons in the WT mice had relatively regular morphology and included only a few deeply stained cells. X-ray irradiation increased the staining of some nuclei, but the neurons in RAD6B-deficient mice were more pronounced (Figures 3D,E). More degenerated neurites (tangles, thickening, and deeper staining) were also observed in the brains of RAD6B-deficient mice (Supplementary Figure S2C).

Astrocytes, as the most important supporting cells in the central nervous system, become larger and grow longer protrusions with more branches when activated. Furthermore, upregulation of glial fibrillary acidic protein (GFAP) in activated astrocytes indicates neuronal injury and degeneration. We



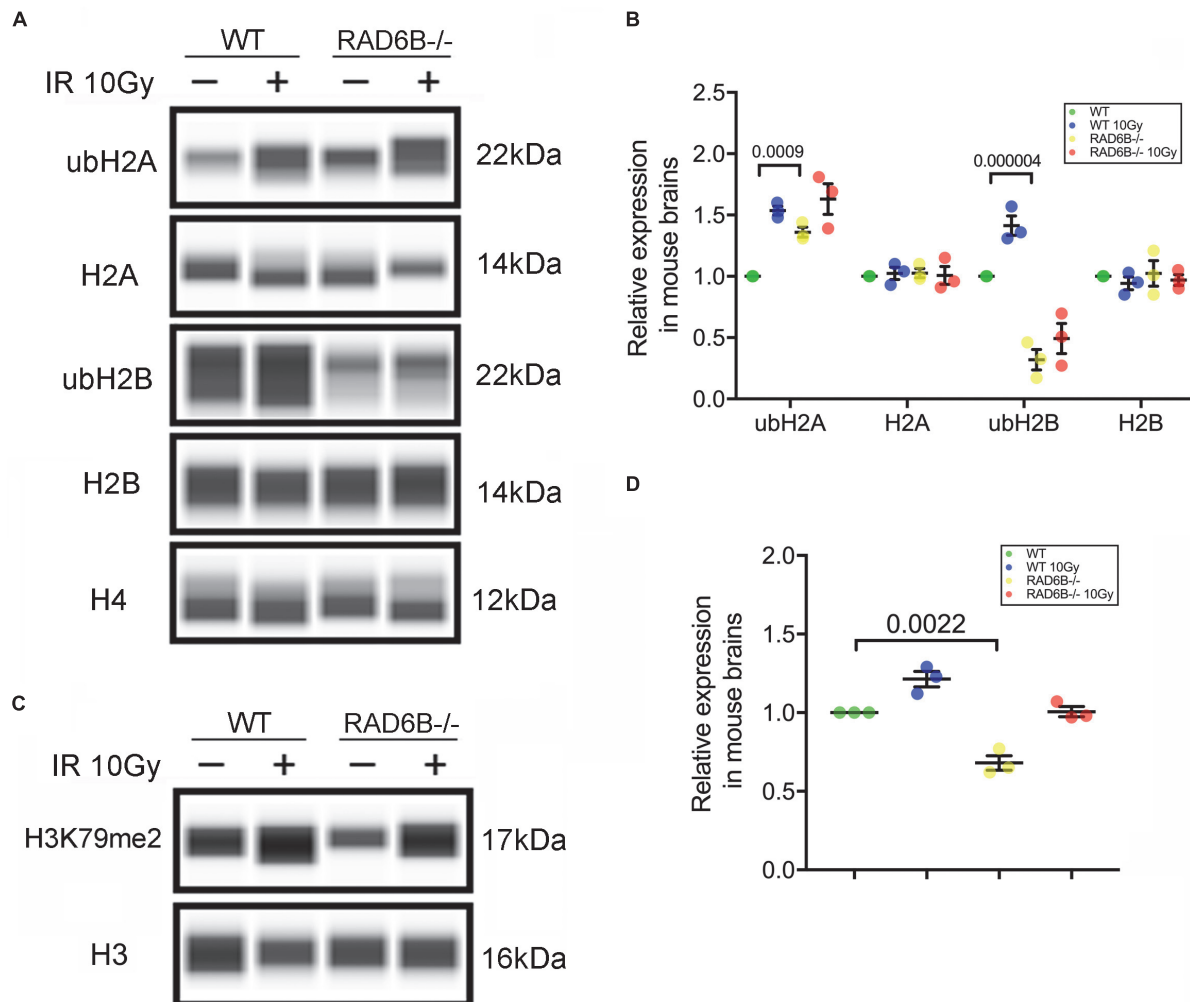


**FIGURE 2 |** Loss of RAD6B causes decreased H2B ubiquitination. **(A)** RAD6B-deficient mice and control mice were treated with 10 Gy of X-rays or not. After recovery, histones were extracted from the brain in diluted hydrochloric acid, and the relative levels of ub-H2A, ub-H2B, H2A, H2B, and H4 were detected through western blotting. **(B)** The gray values of each group were measured, and the relative expression is displayed with a scatter diagram. All values are presented as the mean  $\pm$  SEM ( $n = 3$ ). Student's *t*-test. **(C)** The relative levels of dimethylation of histone H3K79 were detected through western blotting. **(D)** The scatter diagram showing the relative expression of dimethylation of histone H3K79. All values are presented as the mean  $\pm$  SEM ( $n = 3$ ). Student's *t*-test.

measured GFAP and found that there were more astrocytes activated in RAD6B-deficient mice than in WT mice. X-ray irradiation also increased the activation of astrocytes in the brains of RAD6B-deficient mice and WT mice, and RAD6B-deficient mice showed significantly more astrocytic activation after X-ray irradiation (Figures 3F,G). In addition, there were more degenerated neurons surrounded by microglial cells in RAD6B-deficient mice (Supplementary Figures S2D,E).

Analysis of immunohistochemistry with anti-NeuN revealed that the number of neurons in the RAD6B-deficient mice was significantly reduced compared with homologous 12-month-old WT mice; the RAD6B mutants had approximately 3/4 as many neurons as the WT mice. In addition, RAD6B-deficient mice lost more neurons than WT mice after X-ray irradiation (Supplementary Figures S2A,B). We further performed CV staining to investigate neuronal loss in those knockout mice

over time. The loss of pyramidal neurons resulting from RAD6B deficiency gradually increased, and those mice lost more neurons than homologous WT mice from 6 to 12 months of age (Figures 3H,I). Above all, changes in brain slices demonstrate that RAD6B deficiency results in a reduction in the number of neurons.

Argyrophilic grain disease, characterized by the presence of argyrophilic grains, is a progressive degenerative disorder of neurons and becomes increasingly prevalent with advancing age (Braak and Braak, 1998; Yoshida et al., 2017). Unexpectedly, we found a large number of argyrophilic grains (AGs) in the hippocampus and dentate gyrus in 9-month-old RAD6B-deficient mice (Figures 4A,B). Moreover, there was no significant change in the number of AGs after X-ray irradiation. After a further study of age-related changes in AGs, we noticed that numerous AG deposits were present in the hippocampus and

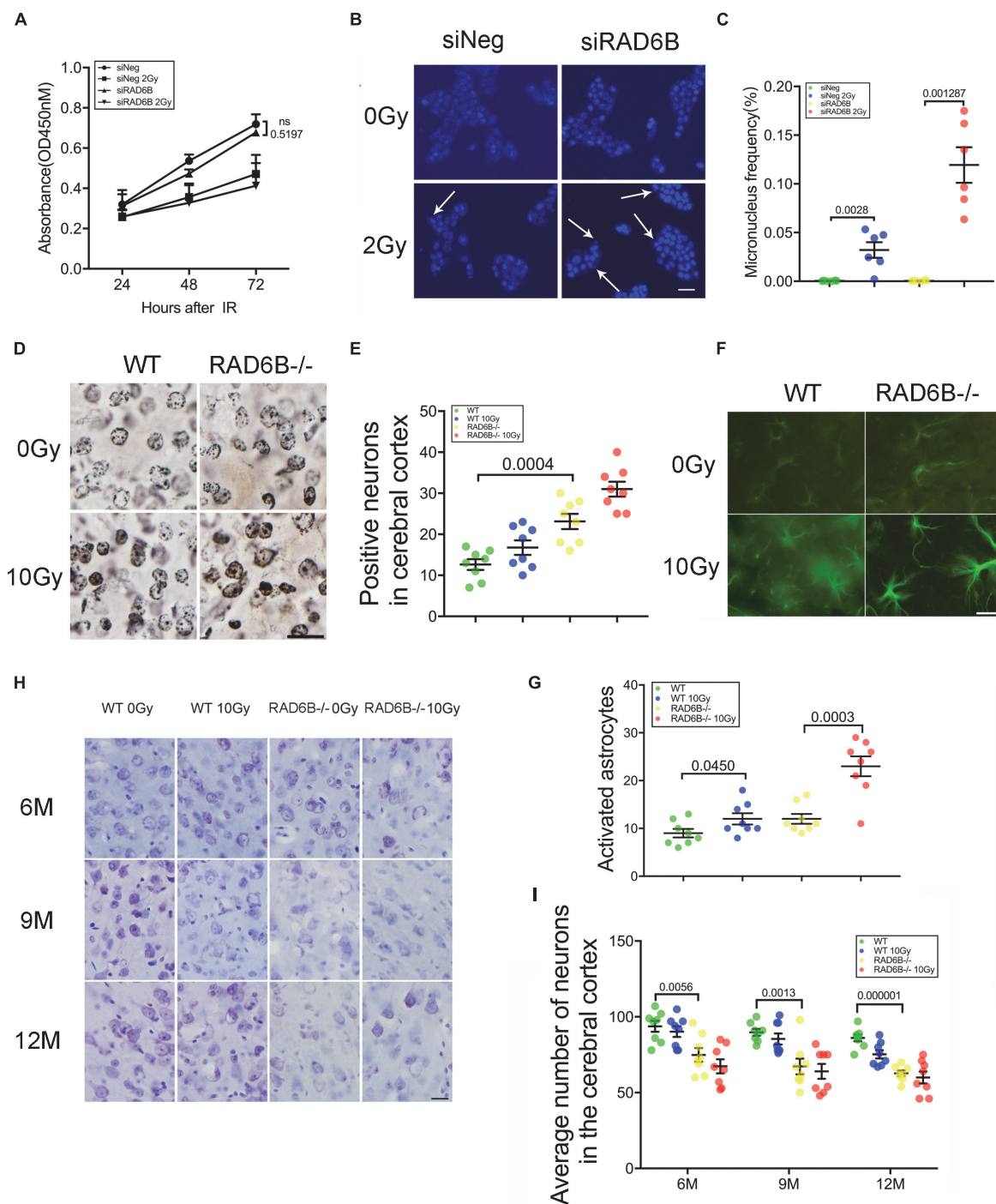


**FIGURE 3 |** Deficiency of RAD6B leads to neurodegeneration and loss of neurons. **(A)** Proliferation of siNeg or siRAD6B-treated RPE1 cells after 2Gy of X-ray irradiation or not. All values are presented as the mean  $\pm$  SEM ( $n = 3$ ). Two-way ANOVA. **(B)** Photomicrographs of siNeg or siRAD6B-treated RPE1 cells scored in the MN test, the arrow indicating the representative MN. Scale bar = 50  $\mu$ m. **(C)** The frequency of MN formation in RPE1 cells, the data are presented as means  $\pm$  SEM ( $n = 6$ ). Student's *t*-test. **(D)** Plot of neurons in silver-stained slices from 12-month-old mice. Scale bar = 20  $\mu$ m. **(E)** Scatter diagram displaying the average density of abnormal neurons in the cerebral cortex of 12-month-old mice. All values are presented as the mean  $\pm$  SEM ( $n = 8$ ). Student's *t*-test. **(F)** Two hours after X-ray irradiation, the brain slices of 6-month-old mice underwent immunofluorescence staining of GFAP to show astrocytes. Scale bar = 20  $\mu$ m. **(G)** A scatter diagram showing the relative activation of astrocytes in the brains of mice in each group after 2 h of recovery. All values are presented as the mean  $\pm$  SEM ( $n = 8$ ). Student's *t*-test. **(H)** CV staining of slices from mice of different ages; the mice were treated with X-rays and allowed to recover for days or were not treated with X-rays. Scale bar = 20  $\mu$ m. **(I)** Scatter diagrams indicating the average number of neurons in each group at different ages. All values are presented as the mean  $\pm$  SEM ( $n = 8$ ). Student's *t*-test.

dentate gyrus in 6-month-old RAD6B-deficient mice. However, there were only sporadic deposits in brain slices from 12-month-old WT mice. RAD6B-deficient mice had more AG aggregates than their WT littermates at different ages (**Figures 4C–E**). These results further suggest that RAD6B deficiency accelerates neuronal senescence.

## RAD6B Deficiency Results in Neuronal Senescence

DNA damage repair defects lead to accumulation of damages, resulting in apoptosis and senescence, which are widely accepted as the major mechanisms inhibiting tumor formation mediated by p53 (Campisi, 2005; Li et al., 2012). To evaluate the effects of RAD6B deficiency on neuron survival, we compared the senescence of neurons in the four groups of mice. Senescent cells are usually larger in size and express  $\beta$ -galactosidase with high enzyme activity at pH 6.0. The senescent neurons in the RAD6B-deficient mice were slightly more numerous than those in the WT mice, and greater numbers of senescent neurons were observed after X-ray irradiation in 12-month-old mice (**Figures 5A,B**). Similarly, RAD6B silencing also causes RPE1 cells to show increased activity of SA- $\beta$ -gal as more senescent cells were detected compared to control cells 7 days after X-ray treatment (**Figures 5C,D**). Next, we compared the levels of activated caspase-3 and mature form of AIF in WT mice and RAD6B-deficient mice to assess apoptosis, but no significant difference was detected (**Figures 5E,F**). These results suggest that inhibition of RAD6B induces defects in DNA damage repair and that neurons are more susceptible to senescence.

## Activation of P53 and P21 Contributes to the Senescence of RAD6B Deficient Neurons

Failure of DNA damage repair leads to senescence, usually through two signaling pathways: the p53–p21 pathway and the p16–Rb pathway (Sherr and McCormick, 2002; Campisi, 2005; Cao and Li, 2015; Gil and Withers, 2016). To investigate the causes of neuronal senescence in RAD6B-deficient mice, we examined key factors in these two pathways. As shown in **Figures 5G,H**, the levels of p21 increased in both groups after X-ray irradiation. Meanwhile, in the absence of X-ray irradiation, the levels of p21 in RAD6B-deficient mice also increased significantly. In addition, changes in the expression of p53 protein were similar to the changes in p21. However, p53 had relative markedly higher expression than p21 in RAD6B-deficient mouse brains. The levels of p16 did not vary obviously between groups (**Figures 5G,H**). Those results suggest that deficiency of RAD6B leads to increased expression of p53 and p21, which may contribute to neural senescence in RAD6B-deficient mice.

## RAD6B Deficient Mice Exhibit Learning and Memory Impairment

As the command center of the nervous system, the brain controls a number of functions, including learning and memory, motor control, homeostasis, information processing, and perception (Rulten and Caldecott, 2013). Interesting, we noticed that the

learning and memory abilities of RAD6B-deficient mice were significantly lower than those of WT mice. To identify whether these changes were caused by RAD6B systemic knockout, we used RAD6B neuron-conditional knockout mice (ncKO) and their WT littermate controls to evaluate the differences in motor performance and learning and memory through avoidance experiments and Morris water maze. RAD6B ncKO mice looked more inactive and exhibited slow behavior and decreased movement, and the two genotypes showed apparent difference in motor ability (**Figures 6A,B**). In addition, RAD6B ncKO mice were smaller in size than the WT mice and weighed significantly less (**Supplementary Figures S1C,D**).

We subjected both genotypes to a spatial exploration experiment to evaluate their spatial learning and memory ability in the Morris water maze. The WT mice were more likely to enter the target region to find the escape platform, with shorter latency to enter the target region, a longer total duration of time spent there, and more entries into the region (**Figures 6C–E**).

In the passive avoidance response test, RAD6B ncKO mice made twice as many errors as WT mice (**Figure 6F**). In addition, their error latency was significantly shorter than that of WT mice (**Figure 6G**). These results indicate that the learning and memory abilities of RAD6B-deficient mice are lower than those of WT mice during the early learning process.

## DISCUSSION

Maintaining genetic stability, especially in the central nervous system, is vital to individual survival and reproduction. Most neurons in human beings are developed within 3 years and survive for the individual's lifetime (Hegde et al., 2017). As DNA DSBs usually threaten cell survival, eukaryotic organisms will mainly repair the injury in two conservative ways: homologous recombination (HR) and non-homologous end joining (NHEJ) (Escobedo-Díaz et al., 2013; Iyama, 2013). NHEJ can occur at any stage of the cell cycle, although it is not as precise as HR (Iyama, 2013; Rulten and Caldecott, 2013; Ouyang et al., 2015). Since neurons are terminally differentiated cells and cannot re-enter the cell cycle, there is no template for homologous recombination repair. NHEJ is the primary mechanism involved in neuronal DDR 4–6 h after X-ray irradiation and repairs 80–85% of DNA DSBs (Löbrich et al., 2010; Jeggo et al., 2011; Reynolds and Stewart, 2013; Ouyang et al., 2015). However, the mechanisms underlying this repair are less well known in terminally differentiated cells.

In response to DNA DSBs, the MRN complex and KU proteins will sense this fragmentation damage and rapidly recruit and activate downstream ATM and DNA-PKcs, respectively (Assenmacher and Hopfner, 2004; Jackson, 2005; Bartkova et al., 2008). ATM is phosphorylated at Ser1981 and binds to the break sites, where it assembles the histone variant H2AX and phosphorylates it at Ser139 (Lavin, 2007; Marteijn et al., 2009; Rulten and Caldecott, 2013). Subsequently, MDC1 recognizes and binds to  $\gamma$ -H2AX via the BRCT domains and recruits downstream two important cell cycle checkpoint mediators: 53BP1 and BRCA1, both of which are also involved in many



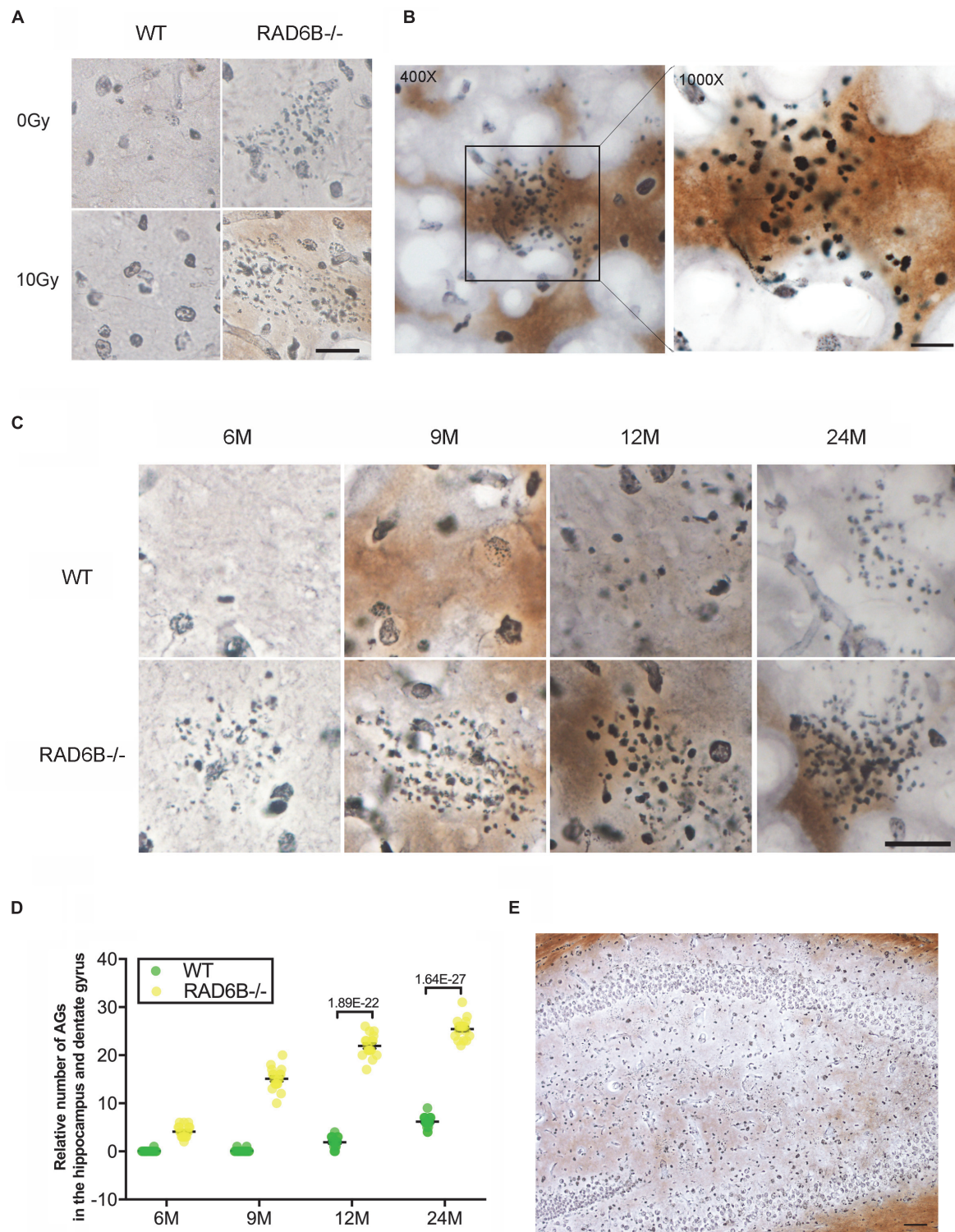


**FIGURE 4 |** RAD6B deficiency leads to abnormal accumulation of argyrophilic grains (AGs) in the hippocampus and dentate gyrus. **(A)** Brain slices were stained with silver, showing abnormal accumulation of AGs in the hippocampus. RAD6B-deficient mice and control mice were treated with 10 Gy of X-rays or left untreated. Scale bar = 20  $\mu$ m. **(B)** A representative image shows the abnormal accumulation of AGs in the hippocampus and a magnified detail of the image. **(C)** Aggregation of AGs in hippocampus of WT mice and RAD6B-deficient mice at different ages. Scale bar = 10  $\mu$ m. **(D)** The scatter diagram shows the relative number of AGs abnormally aggregated in the hippocampus of mice of different ages. All values are presented as the mean  $\pm$  SEM ( $n = 18$ ). Student's  $t$ -test. **(E)** The silver-stained brain slices show that AGs are widely distributed in the hippocampus and dentate gyrus. Scale bar = 100  $\mu$ m.



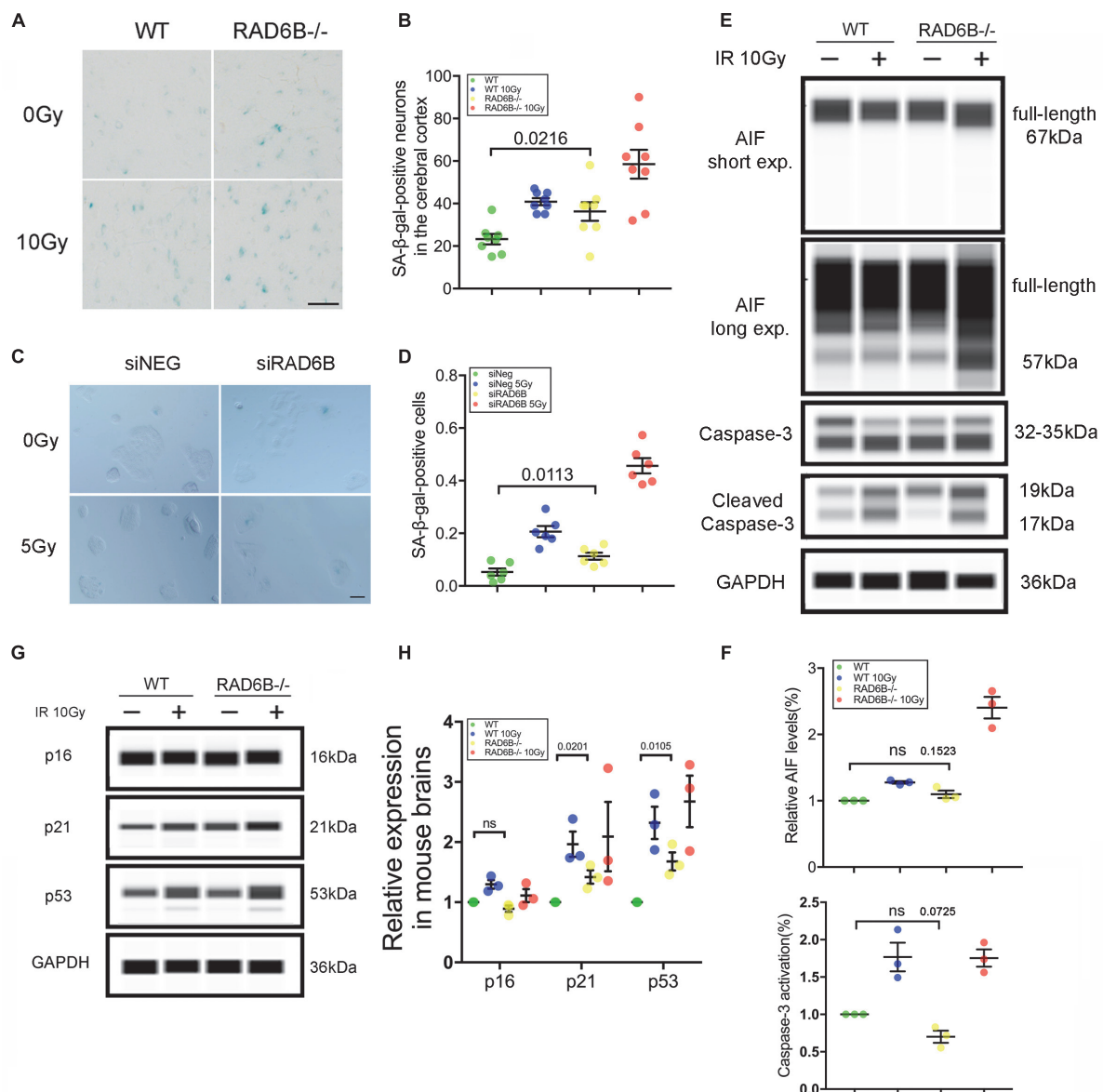


**FIGURE 5 |** RAD6B deficiency leads to increased neuronal senescence. **(A)**  $\beta$ -Galactosidase staining of slices from 12-month-old mice; the mice were either treated with X-rays and allowed to recover for 10 days or not treated with X-rays. Scale bar = 20  $\mu$ m. **(B)** The scatter diagram showing the average number of senescent neurons in the cortex. All values are presented as the mean  $\pm$  SEM ( $n = 8$ ). Student's  $t$ -test. **(C)** Photomicrographs of  $\beta$ -Galactosidase staining of siNEG or siRAD6B-treated RPE1 cells. Scale bar = 50  $\mu$ m. **(D)** The bar chart displaying the percentage of senescent RPE1 cells, the data are presented as means  $\pm$  SEM ( $n = 6$ ). Student's  $t$ -test. **(E)** The representative blot presenting caspase-3 and AIF levels analyzed through simple western. **(F)** A scatter diagram displaying the relative levels of cleaved caspase-3 and mature form of AIF (57 kDa) in each group. All values are presented as the mean  $\pm$  SEM ( $n = 3$ ). Student's  $t$ -test. **(G)** RAD6B-deficient mice and control mice, treated with 10 Gy of X-rays, or not. After a 2 h recovery period, the total protein of the brain was extracted, and a western blot was performed with the following primary antibodies: p16, p53, p21, and GAPDH. **(H)** The gray values of each group were measured, and the scatter diagram indicates the relative levels of these proteins. All values are presented as the mean  $\pm$  SEM ( $n = 3$ ). Student's  $t$ -test.

aspects of DNA repair. While 53BP1 mainly acts through its effector Rif1 to promote NHEJ, BRCA1 facilitates homologous recombination after resection of the broken ends (Bunting et al., 2010; Escribano-Díaz et al., 2013). Interestingly, deficiency of RAD6B caused mice to form fewer 53BP1 and BRCA1 foci in neurons with X-ray treatment, while the underlying mechanism needs further study. Previous studies reported that MDC1

recruits RNF8 at damage sites through the interaction between RNF8 and UBC13, which would ubiquitinate H1 and initiate subsequent ubiquitination events, including ubiquitylation of H2A-type histones mediated by RNF168 (Marteijn et al., 2009; Fradet-Turcotte et al., 2013; Thorslund et al., 2015; Mandemaker et al., 2017). BRE1 facilitates mono-ubiquitination of H2B by RAD6 through its ring finger domain. In addition, ubH2B is

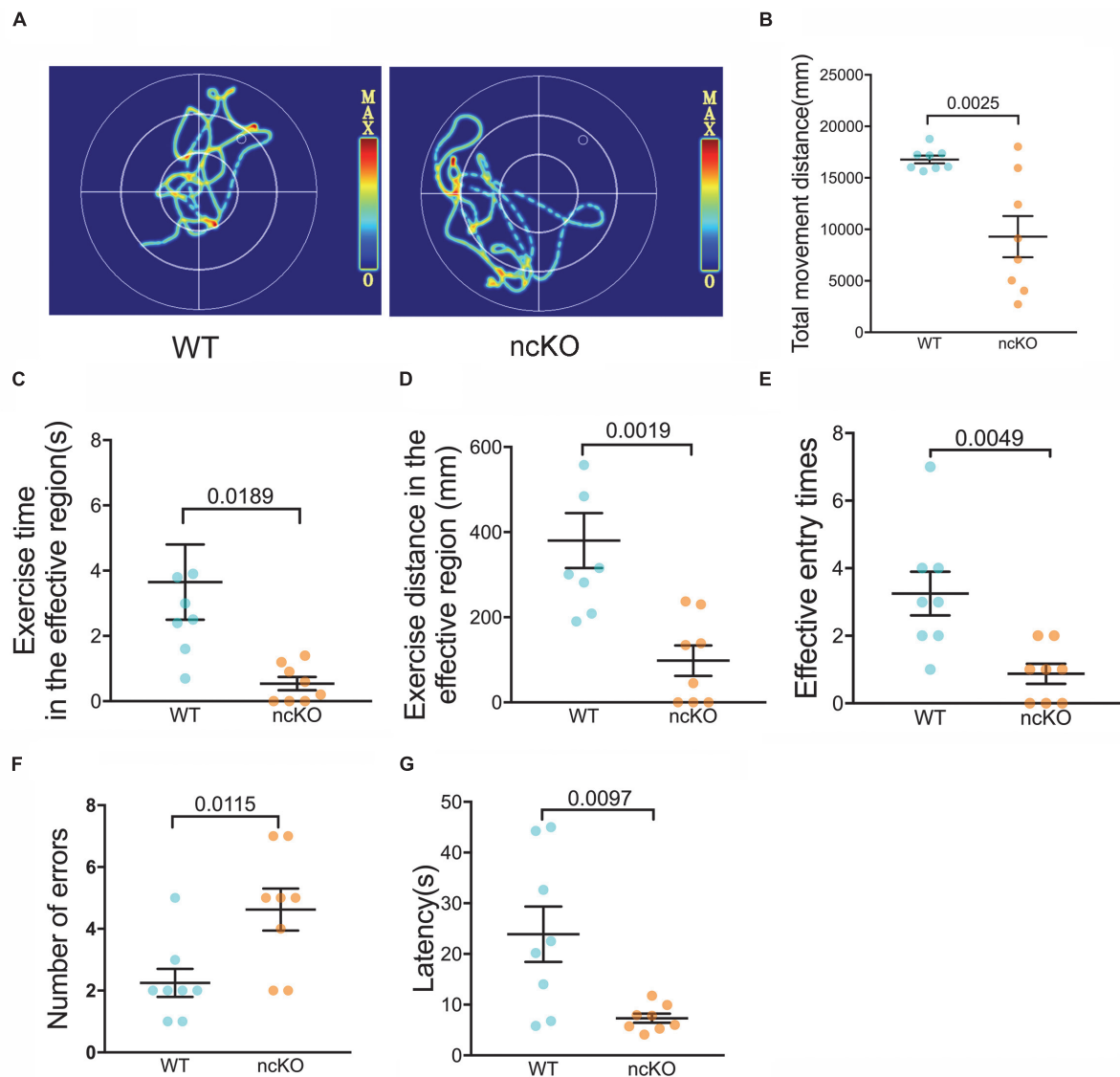


**FIGURE 6 |** RAD6B-deficient mice exhibit weight loss accompanied by learning and memory deficits. **(A)** Motion paths of RAD6B ncKO mice and normal mice in the Morris water maze **(B–E)**. The scatter diagrams show total movement distance, time and distance in the target region and the frequency with which the two genotypes entered the target region in the Morris water maze. All values are presented as the mean  $\pm$  SEM ( $n = 8$ ). Student's *t*-test. **(F,G)** The number of errors and the latency of the first error on the passive avoidance response test are summarized and displayed in scatter diagrams. All values are presented as the mean  $\pm$  SEM ( $n = 8$ ). Student's *t*-test.

essential for the dimethylation and trimethylation of histones H3K4 and H3K79 (Ng et al., 2002; Kim et al., 2009; Chen et al., 2012; Kleiner et al., 2015; Van Oss et al., 2016), which are required for activation of chromatin, remodeling, and activation of transcription of corresponding genes. Our results demonstrated that the ubiquitination level of H2B showed significant difference between RAD6B-deficient mouse brains and WT mouse brains, resulting in subsequent repair failures in neurons.

The developing and mature central nervous system responds differently to DNA damage, with the former tending to apoptosis, while the consequences of latter is less known (Lee and Mckinnon, 2007). Duchaud, E. et al. reported that

mutations in ATM gene result in increased sensitivity of cells to ionizing radiation, however, they show less apoptosis than normal cells after irradiation (Roos and Kaina, 2006). Similarly, in this study, we noticed a remarkable increase in genomic instability in RAD6B deficient neurons, but no significant apoptosis compared with neurons from WT mice. Unrepaired DBSs caused by NHEJ deficiency have been reported to accelerate aging in mice and analysis of DSBs during aging revealed that cells from older mice contained more DSB than those from younger mice (Reynolds and Stewart, 2013; Rulten and Caldecott, 2013; Madabhushi et al., 2014). In addition, Approximately 20–40% of the cerebral cortex and hippocampus region in the brains

of older C57BL/6 mice has been observed to have severe DNA damage, heterochromatin formation, and senescence-associated  $\beta$ -galactosidase activation (Jurk et al., 2012). Jurk et al. (2012) reported that neurons develop a p21-dependent senescence-like phenotype mediated by failed DNA damage response. Western blot showed elevated expression of p53 and p21 which may stimulate subsequent responses and cause senescence. And slices from RAD6B-deficient mice exhibit more deeply stained nuclei and increased activation of astrocytes compared to those from WT mice, suggesting more unrepaired lesions in those neurons and more neurons undergoing neurodegeneration associated with aging. Further, the loss of neurons was more severe in RAD6B-deficient mice than in WT mice, which corresponded to the decrease in ubiquitination of H2B and an increase in p53 and p21 expression. In combination with these results, the absence of RAD6B was responsible for the failure of repair, leading to neuronal senescence, and neurodegeneration.

As the mice grew, we observed physical and behavioral differences between mice; the RAD6B-deficient mice were lighter in body weight than the WT mice and appeared less active than the WT mice. We further explored the changes in their learning and memory through behavioral experiments. RAD6B-deficient mice showed reduced learning and memory ability in behavioral tests, indicating impairment in learning, and memory. In combination with neuronal changes in the mutant mice, we suggest that neurodegeneration may lead to these behavioral differences between RAD6B-deficient and wild-type mice.

Collectively, our data indicate that, in the central nervous system, RAD6B is essential for DDR and RAD6B deficiency causes defects in DNA DSBs repair and increased genome instability, which accelerates neuronal senescence and leads to neurodegeneration.

## MATERIALS AND METHODS

### Generation of RAD6B KO Mice and X-Ray Irradiation

RAD6B knockout C57BL/6 embryonic stem (ES) cells were generated by the knockout mouse project (KOMP) repository (UC Davis). The ES cells contained an allele [Ube2btm1 (KOMP) Vlcg] with an ablating deletion of the RAD6B gene, inserted in place of the WT allele by an expression-selection cassette (VelociGene KOMP definitive null allele design). The ES cells were implanted in the uteri of mice to produce transgenic mice. RAD6B knockout mice were obtained by crossing the mice with lines containing CMV-cre for systemic knockout and Nes-cre for neuron-conditional knockout (**Supplementary Figures S1A,B**). All mice were fed and bred in an SPF laboratory at the animal center of Lanzhou University. We randomly selected RAD6B<sup>−/−</sup> mice and homologous WT mice and divided them into four groups [WT, WT IR (with X-ray irradiation treatment), RAD6B<sup>−/−</sup> and RAD6B<sup>−/−</sup> IR]; each group contained 30 mice. X-ray irradiation was performed with an X-ray biological irradiation system (X-RAD 225 Cx, Pxinc). All experiments involved in this study were approved by the ethics committee of Lanzhou University.

### Tissues Sampling and Frozen Sections

Mice from each group were anesthetized with isoflurane, then perfused and fixed with 4% neutral formaldehyde. The brains were totally dissected and soaked in 20% and 30% sucrose solution for gradient dehydration. All the sections were cut at a thickness of 25  $\mu$ m on a freezing microtome.

### Cells Culture

The immortalized mouse hippocampal neuronal RPE1 cells were purchased from ATCC and cultured in DMEM with high glucose supplemented with 10% fetal bovine serum (Gibco, Frederick, MD, United States) at 37°C in a humidified incubator with 5% CO<sub>2</sub> and 95% air. While for SA- $\beta$ -Gal staining and micronucleus test, cells were seeded into coverslip in Petri dishes at a density of  $1 \times 10^5$  cells per mL and grown for days until 70–80% confluent.

### Silencing of RAD6B Gene

RPE1 cells between passages 5 and 15 were infected with lentivirus particles (GeneChem Co., Shanghai, China) at a multiplicity of infection (MOI) of approximately 50 to generate siRNA against RAD6B (siRAD6B) or non-targeting siRNA (siNeg) [siRAD6B: 5' ACCAGAAGGGAC ACCCTTTGAAGATG3'; siNeg: negative control (GeneChem)]. 12 h after infection, the medium was replaced by complete medium, and cultured for subsequent days. The RNA interference efficiency was confirmed by western blot.

### Immunofluorescence Staining

Brain slices from 6-month-old WT IR and RAD6B<sup>−/−</sup> IR mice were subjected to immunofluorescence staining as described by Liu et al. (2013). The primary antibodies used were anti- $\gamma$ -H2AX (ab26350, Abcam; 1:200), anti-GFAP (BA0056, BOSTER; 1:150), anti-BRCA1 (ab26350, Abcam; 1:200), anti-53BP1 (ab36823, Abcam; 1:200), anti-MDC1 (ab11169, Abcam; 1:200), and anti-RNF8 (ab26350, Abcam; 1:200). After the nuclei were stained with DAPI, photomicrographs were captured with an olympus fluorescence microscope (BX53).

### Western Blot Assay

Brain tissues from 6-month-old mice were frozen quickly in liquid nitrogen, after which histones, and total protein were extracted according to the standard methods provided by Abcam. The concentration of each protein of interest was measured with an ultra-microspectrophotometer (DS-11 FX, DeNovix). We performed automated western blots with Simple Western according to the manufacturer's instructions. And histones were detected with primary antibodies against H1.2 (19649, Proteintech; 1:500), ub-H2A (clone E6C5, Millipore; 1:500), H2A (ab36823, Abcam; 1:200), ub-H2B (clone 56, Millipore; 1:500), H2B (15857, Proteintech; 1:1000) and H4 (16047, Proteintech; 1:2000), while total protein was reacted with antibodies against p21 (ab109199, Abcam; 1:1000), p16 (ab108349, Abcam; 1:1000), p53 (10442-1-AP, Proteintech; 1:500), AIF (17984-1-AP, Proteintech; 1:500), caspase-3 (19677-1-AP, Proteintech; 1:500), and GAPDH (10494-1-AP, Proteintech; 1:2000).

## Cell Proliferation

RPE1 cells were seeded at 1000 cells/well in 96-well dishes. After having been incubated for 12 h, cells were irradiated at dose of 2Gy or not. Following 24, 48, and 72 h of incubation, cell proliferation was measured by CCK-8 assay.

## Micronucleus Test

Following irradiation at a dose of 2Gy, cells were washed three times with phosphate buffer saline (PBS) and continued to culture in DMEM containing cytochalasin B at a concentration of 3  $\mu$ g/ml for 16h to prevent cell division. After incubation, cells were washed and fixed with 10% neutral formaldehyde for at least 30 min. The cells were washed gently with PBS and stained with DAPI, and photomicrographs were captured with an BX53.

## Cresyl Violet (CV) Staining

After X-ray irradiation at a dose of 10Gy and days of recovery, slices from 6-, 9-, and 12-month-old mice were stained with 0.5% CV for 15 min and differentiated in 0.25% glacial acetic acid ethanol solution for 15 s, until the slices turned light blue. The slices were dehydrated with graded ethanol, cleared in xylene and covered with neutral balsam.

## Silver Staining

Brain slices from 12-month-old mice were incubated in 20% silver nitrate for 30 min at 37°C. After being washed 3 times in 0.01 M PBS, they were reduced in 10% neutral formaldehyde for 3 min, until they had turned brown. Following incubation in silver ammonia solution for 5 min at 37°C, slices were placed in 10% neutral formaldehyde for 40 s and toned with 0.2% gold chloride solution. Finally, the slices were rinsed in 5% sodium thiosulfate solution for 2 min. After being washed adequately with distilled water, all slices were dehydrated and covered with neutral gum.

## SA- $\beta$ -GAL Staining

Senescent cells were stained with a Senescence  $\beta$ -Galactosidase Staining Kit (C0602, Beyotime) according to the standard procedures. The slices were fixed at room temperature for 20 min. After being washed three times, each slice was stained with the dyeing solution and incubated at 37°C overnight. The positive cells were observed by microscope after routine dehydration and mounting. Detection of senescence-associated  $\beta$ -galactosidase in RPE1 cells was also performed following the instructions.

## Behavioral Tests

RAD6B nKO mice were subjected to the Morris water maze and a passive avoidance response test. For the Morris water maze, all mice were trained for 5 min on 7 consecutive days and assessed on the eighth day. The escape latency, total distance and time spent in the effective region were recorded automatically by a monitoring system (WMT-100, TECHMAN SOFT).

Passive avoidance response was performed with a video analysis system (PAT-8, TECHMAN SOFT). After the mice were allowed to move freely between the light chamber and the dark chamber for 3 min, the metal grids of the dark chamber

were electrified with a voltage of 24 volts for 5 min. Prior to the formal test, all mice underwent two consecutive days of regular exposure and training. The Error counts and latency were recorded every 3 s.

## DATA AVAILABILITY

All datasets generated for this study are included in the manuscript and/or the **Supplementary Files**.

## ETHICS STATEMENT

All experiments involved in this study were approved by the ethics committee of Lanzhou University.

## AUTHOR CONTRIBUTIONS

ZG and DW initiated the project and wrote the manuscript. ZG, YS, YT, and YG designed the experiments. ZG, YS, YT, YG, and BL performed the experiments. XL, YT, YG, and BL analyzed the data. KX, YG, and DW constructed the figures.

## FUNDING

This work was supported by the National Natural Science Foundation of China (Grant Nos. 81472541 and 81772907 to DW and No. 81571362 to YS) and the Fundamental Research Funds for the Central Universities (Grant lzujbky-2017-k12 to DW).

## SUPPLEMENTARY MATERIAL

The Supplementary Material for this article can be found online at: <https://www.frontiersin.org/articles/10.3389/fncel.2019.00392/full#supplementary-material>

**FIGURE S1 |** Implementation of RAD6B-deficient mice. **(A)** Editing the RAD6B gene through the Cre-loxP recombination system. CMV-cre and Nes-cre were used to produce systemic knockout mice and nKO mice, respectively. **(B)** Identification of the genotypes of some offspring mice obtained from RAD6B heterozygous mice. Primers were designed for genome amplification. **(C)** Physical comparison of 4-month-old WT mice and RAD6B nKO mice. **(D)** The scatter diagram shows weight differences between 18-month-old WT mice and RAD6B nKO mice, each group containing 8 mice. All values are presented as the mean  $\pm$  SEM ( $n = 8$ ). Student's *t*-test.

**FIGURE S2 |** More neurodegeneration was observed in the brains of RAD6B-deficient mice. **(A)** Immunofluorescence was performed with anti-NeuN in the brain slices from RAD6B-deficient mice and control mice that were treated with 10Gy of X-rays or not. Scale bar = 20  $\mu$ m. **(B)** The scatter diagram displays the relative density of neurons in the cerebral cortex of mice from each group. All values are presented as the mean  $\pm$  SEM ( $n = 18$ ). Student's *t*-test. **(C)** Degeneration of nerve fibers (tangling, thickening, and staining) was observed in the silver-stained brain slices from RAD6B-deficient mice. Scale bar = 10  $\mu$ m. **(D)** In lipofuscin staining of brain slices from RAD6B-deficient mice, microglia clustered around degenerated neurons. Scale bar = 10  $\mu$ m. **(E)** The scatter diagram displays the proportion of abnormal neurons. All values are presented as the mean  $\pm$  SEM ( $n = 18$ ). Student's *t*-test.



## REFERENCES

- Assenmacher, N., and Hopfner, K.-P. (2004). MRE11/RAD50/NBS1: complex activities. *Chromosoma* 113, 157–166. doi: 10.1007/s00412-004-0306-304
- Bartkova, J., Tommiska, J., Oplustilova, L., Aaltonen, K., Tamminen, A., Heikkinen, T., et al. (2008). Aberrations of the MRE11-RAD50-NBS1 DNA damage sensor complex in human breast cancer: mre11 as a candidate familial cancer-predisposing gene. *Mol. Oncol.* 2, 296–316. doi: 10.1016/j.molonc.2008.09.007
- Barzilai, A. (2010). DNA damage, neuronal and glial cell death and neurodegeneration. *Apoptosis* 15, 1371–1381. doi: 10.1007/s10495-010-0501-0
- Barzilai, A., and Mckinnon, P. J. (2013). Genome maintenance in the nervous system; insight into the role of the DNA damage response in brain development and disease. *DNA Repair* 12, 541–542. doi: 10.1016/j.dnarep.2013.06.005
- Biochem, A. R. (1998). The ubiquitin system. *Annu. Rev. Biochem.* 67, 425–479.
- Braak, H., and Braak, E. (1998). Argyrophilic grain disease: frequency of occurrence in different age categories and neuropathological diagnostic criteria. *J. Neural Transm.* 105, 801–819. doi: 10.1007/s007020050096
- Bunting, S. F., Callen, E., Wong, N., Chen, H. T., Polato, F., Gunn, A., et al. (2010). 53BP1 inhibits homologous recombination in Brca1-deficient cells by blocking resection of DNA breaks. *Cell* 141, 243–254. doi: 10.1016/j.cell.2010.03.012
- Campisi, J. (2005). Senescent cells, tumor suppression, and organismal aging: good citizens, bad neighbors. *Cell* 120, 513–533.
- Canugovi, C., Misiak, M., Ferarelli, L. K., Croteau, D. L., and Bohr, V. A. (2013). The role of DNA repair in brain related disease pathology. *DNA Repair* 12, 578–587. doi: 10.1016/j.dnarep.2013.04.010
- Cao, X., and Li, M. (2015). A new pathway for senescence regulation. *Genomics Proteomics Bioinformatics* 13, 333–335. doi: 10.1016/j.gpb.2015.11.002
- Chen, S., Wang, D. L., Liu, Y., Zhao, L., and Sun, F. L. (2012). RAD6 regulates the dosage of p53 by a combination of transcriptional and posttranscriptional mechanisms. *Mol. Cell. Biol.* 32, 576–587. doi: 10.1128/MCB.05966-11
- Chernikova, S. B., Razorenova, O. V., Higgins, J. P., Sishc, B. J., Nicolau, M., Dorth, J. A., et al. (2012). Deficiency in mammalian histone H2B ubiquitin ligase Bre1 (Rnf20/Rnf40) leads to replication stress and chromosomal instability. *Cancer Res.* 72, 2111–2119. doi: 10.1158/0008-5472.CAN-11-2209
- Ciechanover, A. (1994). The ubiquitin-proteasome proteolytic pathway. *Cell* 79, 13–21. doi: 10.1016/0092-8674(94)90396-4
- Escribano-Díaz, C., Orthwein, A., Fradet-Turcotte, A., Xing, M., Young, J. F., Tkàè, J., et al. (2013). A cell cycle-dependent regulatory circuit composed of 53BP1-RIF1 and BRCA1-CtIP controls DNA repair pathway choice. *Mol. Cell* 49, 872–883. doi: 10.1016/j.molcel.2013.01.001
- Fradet-Turcotte, A., Canny, M. D., Escribano-Díaz, C., Orthwein, A., Leung, C. C. Y., Huang, H., et al. (2013). 53BP1 is a reader of the DNA-damage-induced H2A Lys 15 ubiquitin mark. *Nature* 499, 50–54. doi: 10.1038/nature12318
- Game, J. C., and Chernikova, S. B. (2009). The role of RAD6 in recombinational repair, checkpoints and meiosis via histone modification. *DNA Repair* 8, 470–482. doi: 10.1016/j.dnarep.2009.01.007
- Gil, J., and Withers, D. J. (2016). Ageing: out with the old. *Nature* 530, 164–165. doi: 10.1038/nature16875
- Harper, J. W., and Elledge, S. J. (2007). The DNA damage response: ten years after. *Mol. Cell* 28, 739–745. doi: 10.1016/j.molcel.2007.11.015
- Hegde, M. L., Bohr, V. A., and Mitra, S. (2017). DNA damage responses in central nervous system and age-associated neurodegeneration. *Mech. Ageing Dev.* 161(Pt A), 1–3. doi: 10.1016/j.mad.2017.01.010
- Herrup, K., Li, J., and Chen, J. (2013). The role of ATM and DNA damage in neurons: upstream and downstream connections. *DNA Repair* 12, 600–604. doi: 10.1016/j.dnarep.2013.04.012
- Iyama, T. (2013). DNA repair mechanisms in dividing and non-dividing cells. *DNA Repair* 12, 620–636. doi: 10.1016/j.dnarep.2013.04.015
- Jackson, S. P. (2005). Conserved modes of recruitment of ATM, ATR and DNA-PKcs to sites of DNA damage. *Nature* 434, 605–611. doi: 10.1038/nature03442
- Jackson, S. P., and Bartek, J. (2009). The DNA-damage response in human biology and disease. *Nature* 461, 1071–1078. doi: 10.1038/nature08467
- Jeggo, P. A., Geuting, V., and Löbrich, M. (2011). The role of homologous recombination in radiation-induced double-strand break repair. *Radiother. Oncol.* 101, 7–12. doi: 10.1016/j.radonc.2011.06.019
- Jurk, D., Wang, C., Miwa, S., Maddick, M., Korolchuk, V., Tzolou, A., et al. (2012). Postmitotic neurons develop a p21-dependent senescence-like phenotype driven by a DNA damage response. *Aging Cell* 11, 996–1004. doi: 10.1111/j.1474-9726.2012.00870.x
- Kim, J., Guermah, M., McGinty, R. K., Lee, J. S., Tang, Z., Milne, T. A., et al. (2009). RAD6-Mediated transcription-coupled H2B ubiquitylation directly stimulates H3K4 methylation in human cells. *Cell* 137, 459–471. doi: 10.1016/j.cell.2009.02.027
- Kleiner, R. E., Verma, P., Molloy, K. R., Chait, B. T., and Kapoor, T. M. (2015). Chemical proteomics reveals a [gamma]H2AX-53BP1 interaction in the DNA damage response. *Nat. Chem. Biol.* 11, 807–814. doi: 10.1038/nchembio.1908
- Lavin, M. (2007). ATM and the Mre11 complex combine to recognize and signal DNA double-strand breaks. *Oncogene* 26, 7749–7758. doi: 10.1038/sj.onc.1210880
- Lee, Y., and Mckinnon, P. J. (2007). Responding to DNA double strand breaks in the nervous system. *Neuroscience* 145, 1365–1374. doi: 10.1016/j.neuroscience.2006.07.026
- Li, T., Kon, N., Jiang, L., Tan, M., Ludwig, T., Zhao, Y., et al. (2012). Tumor suppression in the absence of p53-mediated cell-cycle arrest, apoptosis, and senescence. *Cell* 149, 1269–1283. doi: 10.1016/j.cell.2012.04.026
- Liu, C., Wang, D., Wu, J., Keller, J., Ma, T., and Yu, X. (2013). RNF168 forms a functional complex with RAD6 during the DNA damage response. *J. Cell Sci.* 126(Pt 9), 2042–2051. doi: 10.1242/jcs.122945
- Löbrich, M., Shibata, A., Beucher, A., Fisher, A., Ensminger, M., Goodarzi, A. A., et al. (2010). γH2AX foci analysis for monitoring DNA double-strand break repair: strengths, limitations and optimization. *Cell Cycle* 9, 662–669. doi: 10.4161/cc.9.4.10764
- Madabhushi, R., Pan, L., and Tsai, L.-H. (2014). DNA damage and its links to neurodegeneration. *Neuron* 83, 266–282. doi: 10.1016/j.neuron.2014.06.034
- Mandemaker, I. K., Van, C. L., Janssens, R. C., Lans, H., Bezstarosti, K., Hoeijmakers, J. H., et al. (2017). DNA damage-induced histone H1 ubiquitylation is mediated by HUWE1 and stimulates the RNF8-RNF168 pathway. *Sci. Rep.* 7:15353. doi: 10.1038/s41598-017-15194-y
- Marteijn, J. A., Bekker-Jensen, S., Mairland, N., Lans, H., Schwertman, P., Gourdin, A. M., et al. (2009). Nucleotide excision repair-induced H2A ubiquitination is dependent on MDC1 and RNF8 and reveals a universal DNA damage response. *J. Cell Biol.* 186, 835–847. doi: 10.1083/jcb.200902150
- Ng, H. H., Xu, R. M., Zhang, Y., and Struhl, K. (2002). Ubiquitination of histone H2B by Rad6 is required for efficient dot1-mediated methylation of histone H3 lysine 79. *J. Biol. Chem.* 277, 34655–34657. doi: 10.1074/jbc.C200432000
- Ouyang, S., Song, Y., Tian, Y., Chen, Y., Yu, X., and Wang, D. (2015). RNF8 deficiency results in neurodegeneration in mice. *Neurobiol. Aging* 36, 2850–2860. doi: 10.1016/j.neurobiolaging.2015.07.010
- Reynolds, J. J., and Stewart, G. S. (2013). A nervous predisposition to unrepaired DNA double strand breaks. *DNA Repair* 12, 588–599. doi: 10.1016/j.dnarep.2013.04.011
- Roos, W. P., and Kaina, B. (2006). DNA damage-induced cell death by apoptosis. *Trends Mol. Med.* 12, 440–450. doi: 10.1016/j.molmed.2006.07.007
- Rulten, S. L., and Caldecott, K. W. (2013). DNA strand break repair and neurodegeneration. *DNA Repair* 12, 558–567. doi: 10.1016/j.dnarep.2013.04.008
- Sherr, C. J., and McCormick, F. (2002). The RB and p53 pathways in cancer. *Cancer Cell* 2, 103–112. doi: 10.1016/s1535-6108(02)00102-2
- Thorslund, T., Ripplinger, A., Hoffmann, S., Wild, T., Uckelmann, M., Villumsen, B., et al. (2015). Histone H1 couples initiation and amplification of ubiquitin signalling after DNA damage. *Nature* 527, 389–393. doi: 10.1038/nature15401

- Van Oss, S. B., Shirra, M. K., Bataille, A. R., Wier, A. D., Yen, K., Vinayachandran, V., et al. (2016). The histone modification domain of Paf1 complex subunit Rtf1 directly stimulates H2B ubiquitylation through an interaction with Rad6. *Mol. Cell* 64, 815–825. doi: 10.1016/j.molcel.2016.10.008
- Varshavsky, A. (2005). Regulated protein degradation. *Trends Biochem. Sci.* 30, 283–286.
- Walden, H., Podgorski, M. S., and Schulman, B. A. (2003). Insights into the ubiquitin transfer cascade from the structure of the activating enzyme for NEDD8. *Nature* 422, 330–332.
- Wang, D., Yu, T., Liu, Y., Yan, J., Guo, Y., Jing, Y., et al. (2016). DNA damage preceding dopamine neuron degeneration in A53T human alpha-synuclein transgenic mice. *Biochem. Biophys. Res. Commun.* 481, 104–110. doi: 10.1016/j.bbrc.2016.11.008
- White, R. R., and Vijg, J. (2016). Do DNA double-strand breaks drive aging? *Mol. Cell* 63, 729–738. doi: 10.1016/j.molcel.2016.08.004
- Yoshida, K., Hata, Y., Kinoshita, K., and Nishida, N. (2017). Argyrophilic grain disease in a 46-year-old male suicide victim. *J. Neurol. Sci.* 380, 223–225. doi: 10.1016/j.jns.2017.07.043
- Conflict of Interest Statement:** The authors declare that the research was conducted in the absence of any commercial or financial relationships that could be construed as a potential conflict of interest.

Copyright © 2019 Guo, Tian, Guo, Li, Liu, Xie, Song and Wang. This is an open-access article distributed under the terms of the Creative Commons Attribution License (CC BY). The use, distribution or reproduction in other forums is permitted, provided the original author(s) and the copyright owner(s) are credited and that the original publication in this journal is cited, in accordance with accepted academic practice. No use, distribution or reproduction is permitted which does not comply with these terms.



# Distinct Signaling Pathways Regulate TREM2 Phagocytic and NF $\kappa$ B Antagonistic Activities

Hailan Yao<sup>1,2\*</sup>, Kyle Coppola<sup>1,2</sup>, Jonas Elias Schweig<sup>1,2</sup>, Fiona Crawford<sup>1,2</sup>, Michael Mullan<sup>1,2</sup> and Daniel Paris<sup>1,2</sup>

<sup>1</sup> The Roskamp Institute, Sarasota, FL, United States, <sup>2</sup> James A. Haley Veterans' Hospital, Tampa, FL, United States

## OPEN ACCESS

### Edited by:

Rocio Martínez De Pablos,  
University of Seville, Spain

### Reviewed by:

Miguel Angel Burguillos,  
University of Seville, Spain  
Antonio Boza Serrano,  
Lund University, Sweden

### \*Correspondence:

Hailan Yao  
hyao@roskampinstitute.net

### Specialty section:

This article was submitted to  
Cellular Neuropathology,  
a section of the journal  
Frontiers in Cellular Neuroscience

**Received:** 08 July 2019

**Accepted:** 25 September 2019

**Published:** 10 October 2019

### Citation:

Yao H, Coppola K, Schweig JE, Crawford F, Mullan M and Paris D (2019) Distinct Signaling Pathways Regulate TREM2 Phagocytic and NF $\kappa$ B Antagonistic Activities. *Front. Cell. Neurosci.* 13:457. doi: 10.3389/fncel.2019.00457

Several genetic variants of the Triggering Receptor Expressed on Myeloid Cells-2 (TREM2) have been shown to increase the risk of developing Alzheimer's disease (AD) supporting a role of microglia and immune cells in the pathobiology of AD. We have employed an ectopic model of TREM2 and DAP12 expression in HEK293 cells to study selectively TREM2 dependent signaling and phagocytic functions and evaluated the effects of some of the TREM2 mutations associated with AD. We show that shedding of the TREM2 N-terminal domain does not affect the inhibition of NF $\kappa$ B activation induced by TREM2 while it completely blocks phagocytosis suggesting that TREM2 anti-inflammatory properties can be mediated by the TREM2 C-terminal fragment while the phagocytic activity requires the full-length receptor. In addition, we confirm in that model that apolipoprotein E (APOE) is a ligand for TREM2 and triggers TREM2 signaling. In particular, we show that APOE4 stimulates spleen tyrosine kinase (SYK) activation more potently than APOE2 in a TREM2 dependent manner. Interestingly, TREM2 appears to antagonize NF $\kappa$ B activation induced by phorbol ester but is unable to prevent TNF $\alpha$  induction of NF $\kappa$ B activation suggesting that TREM2 antagonizes inflammatory events triggered downstream of PKC. TREM2 mutations drastically impact TREM2 phagocytosis as well as its ability to antagonize NF $\kappa$ B activation and notably prevent the activation of the PI3K/AKT pathway observed with wild-type TREM2. Overall our data suggest that TREM2 dependent phagocytosis requires an activation of the SYK/PI3K/AKT/PLC $\gamma$  pathways while the suppression of NF $\kappa$ B activation by TREM2 is independent of SYK, PI3K, and PLC $\gamma$  activities. This model of ectopic TREM2-DAP12 co-expression appears suitable to study TREM2 signaling as several biological functions of TREM2 and TREM2 mutations that have been previously described in myeloid and microglial cells were also replicated in this model.

**Keywords:** Alzheimer's disease, TREM2, inflammation, signaling pathways, phagocytosis, SYK, DAP12, APOE

## INTRODUCTION

The brain of Alzheimer's disease (AD) patients is characterized by the presence of three pathologies that are central to the AD process: extracellular accumulation of cerebral  $\beta$ -amyloid ( $A\beta$ ); intraneuronal accumulation of hyperphosphorylated and aggregated tau, and; inflammation (Hardy and Selkoe, 2002; De Strooper and Karran, 2016; Hammond et al., 2019). Much evidence, from many groups, suggests that these three AD pathologies interact synergistically each exacerbating the others resulting in synaptic and neuronal loss (Yoshiyama et al., 2007; Gorlovoy et al., 2009; Roe et al., 2011).

Genetic studies have identified variants in the gene TREM2 (triggering receptor expressed on myeloid cells 2) that confer increased risk for developing AD (Guerreiro et al., 2013; Jonsson et al., 2013), directly implicating immunoinflammatory responses in AD pathobiology as TREM2 encodes a receptor that is exclusively expressed on immune cells within the CNS including infiltrating monocytes/macrophages and microglia (Colonna, 2003; Hickman et al., 2013; Fahrenhold et al., 2018). Although, TREM2 mutations are rare, their observed effect size is comparable to the *APOE* $\epsilon$ 4 allele, which represents the strongest genetic risk factor for late onset AD (Ulrich et al., 2017; Yeh et al., 2017; Carmona et al., 2018). The most common AD TREM2 variant results from a single nucleotide polymorphism encoding an arginine to histidine missense substitution at the amino acid 47 (R47H) (Guerreiro et al., 2013; Jonsson et al., 2013).

Interestingly, APOE is a known ligand for TREM2 and several AD-associated mutations in TREM2 impair APOE binding (Atagi et al., 2015; Yeh et al., 2016) suggesting that these two AD risk genes could be mechanistically linked.  $A\beta$  oligomers have also been shown to interact with TREM2 with high affinity and to induce NFAT (nuclear factor of activated T cell) signaling while in TREM2 AD variants, although the  $A\beta$  affinity for TREM2 remains unchanged, NFAT signaling induced by  $A\beta$  oligomers is reduced suggesting a partial loss of TREM2 function (Lessard et al., 2018). TREM2 is involved in microglia phagocytosis and activation as TREM2 knockdown inhibits phagocytosis and stimulates the production of inflammatory cytokines by microglia while TREM2 overexpression has the opposite effect (Takahashi et al., 2005). BV2 microglial cells expressing AD TREM2 variants show impaired phagocytic activity suggesting TREM2 loss of function for these variants (Kleinberger et al., 2014).

TREM2 signals through its association with TYRO protein tyrosine kinase binding protein (TYROBP), also known as DNAX-activating protein of 12 kDa (DAP12), which recruits the spleen tyrosine kinase (SYK) through its cytosolic immunoreceptor tyrosine-based activation motifs (ITAMs) (Peng et al., 2010). SYK has been therefore postulated to be a key kinase required to transduce TREM2 signaling pathways. TREM2 signaling has anti-inflammatory consequences and has been shown to antagonize Toll-like receptor (TLR-4) mediated inflammation by modulating the JNK and NF $\kappa$ B signaling pathways (Takahashi et al., 2005; Hamerman et al., 2006; Zhong et al., 2017a). Most of the studies on TREM2 signaling have used anti-TREM2 antibodies to stimulate the TREM2 receptor

promoting the interaction between TREM2 and DAP12 and the recruitment of SYK (Varnum et al., 2017). So far, the only attempts to study TREM2 signaling in response to receptor ligation with APOE have been conducted by using indirect calcium-driven reporter systems without clearly delineating which signaling pathways are triggered or antagonized upstream of the reporter. Such functional analyses have however, suggested that APOE is an agonist of TREM2 (Jendresen et al., 2017) and that several TREM2 variants associated with AD impair TREM2 activation whereas other variants oppositely increase TREM2 activation in response to phosphatidylcholine and other lipid ligands (Song et al., 2017) suggesting that AD TREM2 mutations are not simply loss of function mutations as previously thought.

To investigate the functional role of TREM2 on AD pathology, several studies have tested the impact of TREM2 deficiency on  $A\beta$  accumulation and tau pathology using various transgenic mouse models of AD as AD associated TREM2 mutations were assumed to result from TREM2 loss-of-function phenotype (Cheng-Hathaway et al., 2018; Song et al., 2018). The studies conducted using models of  $A\beta$  accumulation gave puzzling results and suggest that TREM2 deficiency reduces the  $A\beta$  pathology early on Jay et al. (2015, 2017) but increases  $A\beta$  deposition in older mice (Wang et al., 2016; Jay et al., 2017). Other studies show opposite data with increased  $A\beta$  deposition in younger TREM2 deficient mice and no change in  $A\beta$  deposition in older animals (Parhizkar et al., 2019). Similarly, the impact of TREM2 deficiency on tau pathology is unclear with studies suggesting that TREM2 deficiency exacerbates the tau pathology (Bemiller et al., 2017) or on the opposite prevents the neurodegeneration induced by the tauopathy (Leyns et al., 2017). In addition, differential effects of partial and complete loss of TREM2 have been observed in a mouse model of tauopathy showing protective effects of complete TREM2 deficiency but exacerbation of the tau pathology in TREM2 haploinsufficient mice (Sayed et al., 2018). Therefore, it is not settled whether TREM2 plays a beneficial or detrimental role in AD and these studies do not shed light on the exact molecular mechanisms that link TREM2 variants to the AD pathobiology.

TREM2 deficiency consistently leads to a reduction in myeloid cell accumulation around  $A\beta$  deposits supporting a possible role of TREM2 in myeloid cell survival, proliferation, and chemotaxis (Jay et al., 2015, 2017; Wang et al., 2016; Yuan et al., 2016). It has been suggested that TREM2-dependent microglial functions limit amyloid plaques growth early by promoting  $A\beta$  phagocytosis but not late during the disease by increasing the levels of APOE around amyloid deposits, hence promoting further  $A\beta$  aggregation (Parhizkar et al., 2019) given the known role of APOE on  $A\beta$  deposition. AD TREM2 mutants may therefore enhance  $A\beta$  deposition during the early stage of AD while leading to a reduction in APOE production by microglia and decreased APOE levels in senile plaques suggesting that TREM2 may have protective functions early during amyloidogenesis (Parhizkar et al., 2019).

As indicated earlier, DAP12 is a signaling adapter protein that pairs with TREM2 and is required to mediate TREM2 signaling. Interestingly, DAP12 deletion has been shown to improve learning behavior and synaptic function in a mouse model of



tauopathy (Audrain et al., 2018) and to reverse the behavioral, electrophysiological alterations and neuro-inflammation in a mouse model of  $\beta$ -amyloidosis (Haure-Mirande et al., 2019). It remains possible that aberrant TREM2 signaling induced by TREM2 mutations plays a key role in the development of AD suggesting that the study of TREM2 signaling may lead to the discovery of therapeutic targets downstream of TREM2 that could be manipulated to reverse the effects of TREM2 mutations.

TREM2 is a negative regulator of TLR4 mediated inflammation (Takahashi et al., 2005; Hamerman et al., 2006; Zhong et al., 2017a; Li and Zhang, 2018) but the exact molecular mechanisms responsible for this effect are not fully understood. In addition, the impact of TREM2/DAP12 on inflammation mediated by other inflammatory stimuli beside LPS (TLR-4 agonist) remains to be examined.

The study of TREM2 signaling in immune cells or microglia is particularly challenging because these cells express many receptors, besides TREM2, that are also signaling by engaging DAP12. Therefore, it is particularly complex to delineate specific TREM2 signaling pathways from pathways influenced by other receptors recruiting DAP12 in these cells. In addition, immune cells and microglia express multiple phagocytic receptors which complicates the study of TREM2-dependent phagocytic activity and the signaling mechanisms involved in this process. To overcome these difficulties and allow to assess selectively TREM2 dependent phagocytic and anti-inflammatory functions, we elected to express TREM2 and DAP12 in HEK293 cells that do not express DAP12 or TREM2 and are non-phagocytic. Several groups have used similar TREM2 and DAP12 co-expression in HEK293 cells to study TREM2 biology including TREM2 signal transduction and function as well as TREM2 shedding (Kleinberger et al., 2014; Feuerbach et al., 2017; Thornton et al., 2017). In this study, we investigated the impact of TREM2/DAP12 on PMA (phorbol-12-myristate-13-acetate) and TNF $\alpha$  induction of NF $\kappa$ B and assessed the impact of TREM2 processing on inflammation and phagocytosis. In addition, we determined whether SYK stimulation by TREM2/DAP12 was required to mediate TREM2 dependent phagocytic and anti-inflammatory activities. Our data differentiate TREM2 signaling events responsible for its anti-inflammatory and phagocytic activities and reveal the impact of the AD associated TREM2 R47H variant on these events. Overall our data show that TREM2/DAP12 anti-inflammatory activity is mediated by signaling events distinct from those required to mediate TREM2 dependent phagocytic activity. In addition, we show that TREM2 processing has no influence on TREM2 anti-inflammatory activity but greatly impacts TREM2 dependent phagocytosis.

## MATERIALS AND METHODS

### Reagents

12-*O*-Tetradecanoylphorbol 13-acetate (PMA), human recombinant TNF- $\alpha$ , dimethyl sulfoxide (DMSO), 2-mercaptoethanol, sodium chloride, phenylmethylsulfonyl fluoride (PMSF), TAPI-1, DAPT, and  $\beta$ -secretase inhibitor IV (C3) were purchased from Sigma-Aldrich (St. Louis, MO,

United States). APOE2 and APOE4 were obtained from Biovision (Milpitas, CA, United States). Go 6983, Ro 32-0432, Wortmannin and LY294002 were purchased from Tocris (Minneapolis, MN, United States). All antibiotics, fungizone, PBS, culture media, and fetal bovine serum were purchased from Invitrogen (Carlsbad, CA, United States). The MPER reagent and the cocktail of protease/phosphatase inhibitors were purchased from Thermo Fisher Scientific (Waltham, MA, United States).

### DNA Constructs

A multicistronic vector with “self-cleaving” 2A peptide sequence (pcDNA 3.1-P2A, GenScript) has been used to co-express human TREM2 and DAP12 genes from a single mRNA. Human TREM2 and DAP12 cDNA sequences were amplified by PCR, digested with restriction enzymes and sequentially inserted into the pcDNA3.1-P2A vector to develop the pcDNA3.1-TREM2-P2A-DAP12 plasmid. TREM2 mutants (Y38C and R47H) were generated in the pcDNA3.1-TREM2-P2A-DAP12 construct by using the Q5 site-directed mutagenesis kit (New England BioLabs), according to the manufacturer’s instructions. All constructs were confirmed by DNA sequencing. SYK shRNAs(E9) and a scrambled control shRNA (NS) were cloned into the GIPZ lentiviral vector and were purchased from Origene (Rockville, MD, United States).

### Cell Culture and Transfection

HEK293 cells were purchased from American Type Culture Collection (ATCC, Manassas, VA, United States) and maintained in DMEM medium supplemented with 10% fetal bovine serum, GlutaMAX, and 1% penicillin/streptomycin/fungizone (Thermo Fisher Scientific, Waltham, MA, United States). For stable transfection, HEK293 cells and a stable NF $\kappa$ B luciferase reporter cell line of HEK293 (Panomics, Fremont, CA, United States) were grown on 6-well plates until reaching 70–80% confluence and transfected using lipofectamine 2000 (Invitrogen, Carlsbad, CA, United States). After 48 h, transfected cells were placed into fresh medium in the presence of 500  $\mu$ g/ml G418 (Invitrogen, Carlsbad, CA, United States) or 500  $\mu$ g/ml G418 plus 100  $\mu$ g/ml hygromycin B for the NF $\kappa$ B luciferase cells for selection. After 14 days in culture, resistant cells were trypsinized and expanded.

### Immunoblotting

HEK293 cells were lysed in mammalian protein extraction reagent (MPER, Thermo Fisher Scientific, Waltham, MA, United States) containing Halt protease and phosphatase single use inhibitor (Thermo Fisher Scientific, Waltham, MA, United States). Lysates were separated by SDS-PAGE using Criterion TGX gels (Bio-Rad, Berkeley, CA, United States), and transferred onto 0.2  $\mu$ M PVDF membranes (Bio-Rad, Berkeley, CA, United States). Membrane were blocked with 5% non-fat milk in TBS for 1 h, incubated with anti-TREM2, anti-DAP12, anti-Phospho-Akt (Ser473), anti-AKT, anti-I $\kappa$ B $\alpha$ , anti-Phospho-NF- $\kappa$ B p65 (Ser536), anti-NF- $\kappa$ B p65, anti-Phospho-MARCKS (Ser167/170), anti-MARCKS, anti-Actin (1:1000, Cell Signaling, Danvers, MA, United States), anti-Phospho-Syk (Tyr525/526) (1:1000, Abgent, United States), or anti-SYK (4D10, 1:1000, Santa Cruz, CA, United States) primary antibody overnight

at 4°C, and incubated in HRP-conjugated anti-Rabbit or anti-Mouse secondary antibody (1:3000, Cell Signaling, Danvers, MA, United States) at room temperature for 1 h. Western blots were visualized using SuperSignal West Femto Maximum Sensitivity Substrate (Thermo Fisher Scientific, Waltham, MA, United States). Signals were quantified using ChemiDoc XRS (Bio-Rad, Berkeley, CA, United States) and densitometric analysis were performed using Image Lab (Bio-Rad, Berkeley, CA, United States).

## Cell Immunostaining

HEK293 cells, grown on poly-D-lysine coated coverslips, were washed with PBS and fixed in 4% formaldehyde in PBS for 10 min. Cells were then washed three times in PBS, permeabilized and blocked using 5% BSA, 0.3% Triton X-100 in PBS at room temperature for 1 h. Cells were then incubated with anti-TREM2 (1:100, R&D, United States), anti-DAP12 (1:100, Santa Cruz, CA, United States), and anti-Phospho-Akt (Ser473) (1:100, Cell Signaling, Danvers, MA, United States) primary antibodies overnight at 4°C. Cells were then washed three times and anti-goat secondary Alexa Fluor 488 conjugate, anti-mouse secondary Alexa Fluor 555, and anti-rabbit secondary Alexa Fluor 647 (1:1000, Invitrogen, United States) antibodies were added at room temperature for 1 h. Cells were washed three times and then mounted in Fluoroshield with DAPI (Sigma-Aldrich, St. Louis, MO, United States). Confocal microscopy was carried out using the LSM800 Laser Confocal Scanning Microscope (Carl Zeiss Microscopy, Thornwood, NY, United States), the ZEN Blue 2.1 software (Carl Zeiss AG, Germany) and a 63 × objective.

## Phagocytosis Assays

All cells were plated at a density of 100,000 cells in 96-well cell culture plates and cultured for 24 h. pHrodo *Escherichia coli* bioparticles were dissolved in live cell imaging buffer (Invitrogen, Carlsbad, CA, United States) at a concentration of 1 µg/ml and incubated at 37°C with the different cell lines in a Biotek Synergy HT reader. The uptake of *E. coli* bioparticles was measured by quantifying fluorescent emission (Ex 560 nm/Em 585 nm) every 10 min for 2 h. Phagocytosis was quantified by measuring the average amount of bioparticles uptake in mFU/min during the 2 h incubation period.

## NFκB Luciferase Activity Measurements

NFκB activation was triggered with 200 nM PMA or 10 µg/ml TNFα for 4 h, and NFκB luciferase activity was quantified by chemiluminescence using the Luc-Screen Extended Glow kit (Applied Biosystems, Foster City, CA, United States) with a Synergy HT chemiluminescence reader (Biotek) as we previously described (Paris et al., 2011).

## Statistical Analysis

Data were analyzed and plotted with GraphPad Prism (GraphPad Software, Inc., San Diego, CA, United States). The Shapiro–Wilk test for normality was used to test for Gaussian distribution. Statistical significance was determined by either one-way ANOVA (for comparisons of three or more groups), two-way ANOVA followed by *post hoc* analysis using Bonferroni's

correction or *t*-test where appropriate. All data are presented as mean ± standard deviation (SD) and  $p < 0.05$  was considered significant (\* $p < 0.05$ , \*\* $p < 0.01$ , \*\*\* $p < 0.001$ , \*\*\*\* $p < 0.0001$ ).

## RESULTS

### Generation of HEK293 Stable Cell Lines Co-expressing TREM2 and DAP12

TREM2 is a phagocytic receptor exclusively expressed in myeloid cells which signals through the adaptor protein DAP12 following the binding of ligands to TREM2. It has been shown that some TREM2 ligands induce the phosphorylation of two tyrosine residues within the ITAM domain of DAP12 resulting in the recruitment and activation of SYK and downstream signaling molecules including PI3K and PLCγ (Takahashi et al., 2005; Otero et al., 2009; Peng et al., 2010; Wang et al., 2015; Colonna and Wang, 2016). In microglia and myeloid cells, DAP12 also form complexes with multiple receptors beside TREM2 which complicates the study of TREM2 signaling as signals attributed to TREM2 may emerge from other receptors that associate with DAP12. In addition, multiple phagocytic receptors are also expressed by myeloid cells which render difficult the study of specific TREM2 phagocytic functions. To overcome these difficulties and examine more selectively the role of TREM2 signaling in inflammation and phagocytosis, we induced an ectopic expression of TREM2 and DAP12 in non-immune and non-phagocytic HEK293 cells. We also selected HEK293 cells because they express SYK, PI3K, and PLCγ which are signaling molecules known to be recruited following TREM2 ligation in myeloid cells (Kleinberger et al., 2014; Licona-Limon et al., 2015).

To ensure co-expression of TREM2 and DAP12 in HEK293 cells, we inserted TREM2 and DAP12 cDNAs into a bicistronic vector, which contains 2A peptides to allow the co-expression of multiple genes from a single transcript using a single vector. We also established a stable cell line expressing TREM2 with the AD R47H mutation and DAP12. Anti-TREM2 and anti-DAP12 immunoblotting confirmed the co-expression of TREM2 and DAP12 in the HEK293 cells (Figure 1A). Laser confocal imaging following immunostaining with TREM2 and DAP12 antibodies reveals that HEK293 cells stably expressing DAP12 and TREM2 or the TREM R47H mutation display both cell surface and cytosolic expression of TREM2 as well as a colocalization between TREM2 and DAP12 for membrane associated TREM2 (Figure 1C). These data suggest that TREM2 and DAP12 undergo normal trafficking when stably expressed in HEK 293 cells and that the TREM2 R47H mutation does not impair the recruitment of DAP12 by TREM2. TREM2 R47H mutant has previously been shown to affect TREM2 maturation (Park et al., 2015, 2016; Kober et al., 2016; Sirkis et al., 2017). We confirmed this phenomenon, in our HEK293 cells expressing wild-type and mutant TREM2 by showing that the TREM2 R47H mutation reduces the maturation of TREM2 resulting in a greater amount of immature TREM2 and a lower level of mature TREM2 compared to cell expressing wild-type TREM2 (Figure 1A).

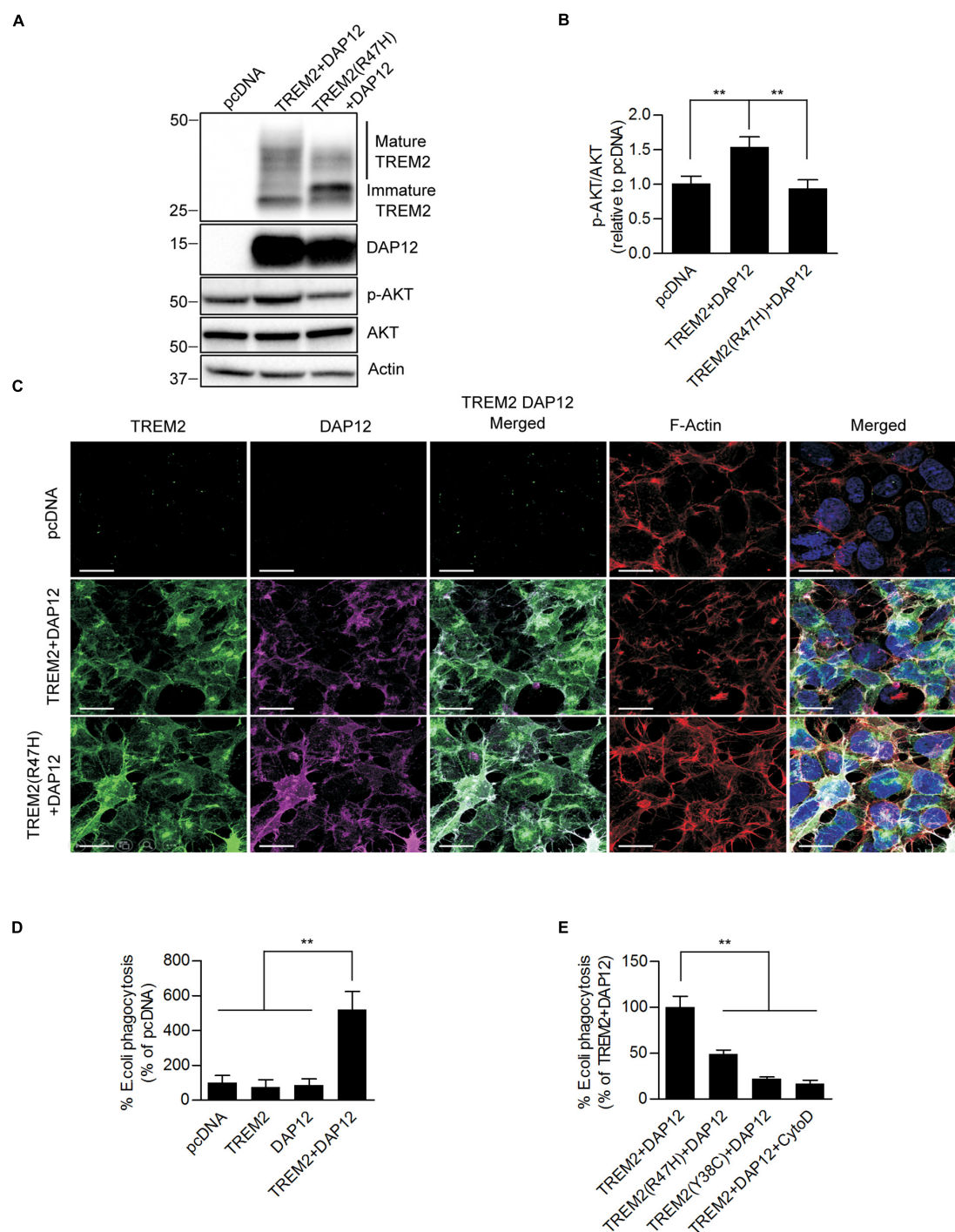


**FIGURE 1 |** Ectopic expression of TREM2 and DAP12 induces AKT activation and phagocytosis in HEK293 cells. **(A)** Western-blot analysis of lysates from HEK293 cells transfected with pcDNA (control empty vector), TREM2 + DAP12 and TREM2 (R47H) + DAP12 constructs. A representative western-blot showing the impact of TREM2 + DAP12 and TREM2(R47H) + DAP12 expression on p-AKT(Ser473) compared to HEK293 cells transfected with the empty pcDNA vector (control) is shown. **(B)** Histogram representing the quantification by western-blots of p-AKT(Ser473) normalized to total AKT in HEK293 cells transfected with pcDNA (empty vector), TREM2 + DAP12 and TREM2(R47H) + DAP12 constructs. Data represent the average  $\pm$  SD p-AKT/Total AKT levels standardized to values obtained in HEK293 cells transfected with the pcDNA empty vector; ( $n = 4$ ) for each experimental condition; statistical significance (\*\* $p < 0.01$ ) was evaluated by ANOVA followed by *post hoc* analysis using Bonferroni corrections. **(C)** Representative laser confocal images of HEK293 cells transfected with pcDNA (empty vector), TREM2 + DAP12 and TREM2(R47H) + DAP12 following immunostaining with N-terminal TREM2 (green), DAP12 (purple) antibodies. Cells were counterstained with DAPI (blue) and fluorescent phalloidin (red) to stain F-actin. TREM2 and DAP12 expression was detected in HEK293 cells transfected with TREM2 + DAP12 and TREM2(R47H) + DAP12 constructs while no expression of TREM2 and DAP12 was observed in HEK293 cells transfected with the empty vector (pcDNA).

(Continued)



**FIGURE 1 | Continued**

Colocalization between TREM2 and DAP12 was observed both in cells co-expressing wild-type TREM2 and DAP12 and in cell co-expressing the TREM2 R47H mutation and DAP12. The white scale bar represents 20  $\mu\text{m}$ . **(D)** Phagocytosis of pHrodo *E. coli* bioparticles conjugate in pcDNA, TREM2, DAP12, or TREM2 + DAP12 transfected HEK293 cells. Data are represented as mean  $\pm$  SD from at least two independent cell culture experiments and expressed relative to data obtained in HEK293 transfected with the pcDNA empty vector; ( $n = 6$ ) for each experimental condition; statistical significance ( $**p < 0.01$ ) was evaluated by ANOVA followed by *post hoc* analysis using Bonferroni corrections. Data show that the co-expression of DAP12 with TREM2 significantly stimulates the phagocytosis of pHrodo *E. coli* bioparticles whereas DAP12 or TREM2 expression alone are not sufficient to promote phagocytic activity compared to HEK293 transfected with the empty vector pcDNA (control). **(E)** Phagocytosis of pHrodo *E. coli* bioparticles conjugate in TREM2 + DAP12, TREM2(R47H) + DAP12, and TREM2(Y38C) + DAP12 transfected HEK293 cells. TREM2 + DAP12 transfected HEK293 cells were also treated with cytochalasin D (10  $\mu\text{M}$ ), an inhibitor of actin polymerization which blocks phagocytosis (positive control). Data are represented as means  $\pm$  SD from at least two independent cell culture experiments and expressed as a percentage of the amount of phagocytosis quantified in TREM2 + DAP12 transfected HEK293 cells; ( $n = 6$ ) for each experimental condition; statistical significance ( $**p < 0.01$ ) was evaluated by ANOVA followed by *post hoc* analysis using Bonferroni corrections. Data show that that cytochalasin D antagonizes TREM2 + DAP12 dependent phagocytic activity while TREM2(R47H) reduced phagocytosis by 50% and TREM2(Y38C) by 80% compared to wild-type TREM2.

We further assessed the functionality of TREM2/DAP12 in HEK293 cell lines stably transfected with DAP12, wild-type TREM2 and TREM2 R47H by analyzing AKT activation by immunoblotting. We found that AKT phosphorylation at Ser473 was significantly increased in cells stably transfected with wild-type TREM2 and DAP12 but not in TREM2 R47H mutant cells suggesting a loss of function of the TREM2 R47H mutation as previously observed (Figures 1A,B). We next investigated whether the co-expression of TREM2-DAP12 was sufficient to transform HEK293 cells into phagocytic cells and whether the TREM2 R47H mutation was able to impact the phagocytosis activity of TREM2 as previously shown in myeloid cells (Kleinberger et al., 2014; Kober et al., 2016). Phagocytic activity was investigated by measuring the internalization of *E. coli* conjugated to a pH-sensitive pHrodo dye (pHrodo *E. coli*) that only yields a fluorescent signal in an acidic compartment. The phagocytosis of pHrodo *E. coli* bioparticles was evaluated in HEK293 cells expressing TREM2 only (TREM2), DAP12 (DAP12) only and in cells co-expressing TREM2 and DAP12 (TREM2 + DAP12). We show that the phagocytosis of *E. coli* bioparticles is only induced in HEK293 cells co-expressing TREM2 and DAP12 but is not observed in cells singly expressing either TREM2 or DAP12 showing that TREM2 dependent phagocytic activity requires DAP12 (Figure 1D). In addition, as a positive control, we used cytochalasin D (Cyto D), which inhibits phagocytosis in myeloid cells including microglia (N'Diaye et al., 2009) and demonstrated that Cyto D effectively abolishes the phagocytosis of pHrodo *E. coli* in TREM2 + DAP12 cells (Figure 1E). Expression of the AD-associated R47H variant and Nasu-Hakola disease (NHD)-associated TREM2 mutants Y38C also strongly reduced the phagocytic activity of TREM2 in HEK293 cells (Figure 1E) mimicking previous observations in microglial cells expressing TREM2 mutations (Kleinberger et al., 2014). Our data suggest that the co-expression of TREM2 and DAP12 in HEK293 cells is functional and can induce AKT activation which is one of the downstream TREM2 signaling molecule previously identified in immune cells (Peng et al., 2010). In addition, our HEK293 cell lines stably co-expressing DAP12 and wild-type TREM2 elicit phagocytic activity while the HEK293 cell lines expressing AD TREM2 R47H mutation or the NHD TREM2 Y38C demonstrate a reduced phagocytic activity reproducing previously described phagocytic dysfunction of TREM2 mutations observed in microglial cells (Kleinberger et al., 2014; Kober et al., 2016). Overall, these data suggest

that our HEK293 cell lines co-expressing wild-type or mutant TREM2 with DAP12 constitute a suitable model to investigate TREM2 functions.

## TREM2 and DAP12 Coexpression Inhibits NF $\kappa$ B Activation in Response to PMA Treatment

Previous studies have shown that TREM2 can modulate inflammatory signaling in immune cells including microglia (Hamerman et al., 2006; Turnbull et al., 2006). In particular, TREM2 has been shown to inhibit the NF $\kappa$ B pathway resulting in reduced pro-inflammatory cytokines production (Ren et al., 2018; Li et al., 2019). We therefore examined whether TREM2 and DAP12 co-expression was able to impact NF $\kappa$ B activation in our HEK293 cell lines. To induce NF $\kappa$ B, we treated HEK293 cells stably transfected with the pcDNA empty vector (pcDNA; control cells), TREM2 and DAP12 co-expression vector (TREM2 + DAP12) and TREM2 R47H mutant and DAP12 co-expression vector [TREM2(R47H) + DAP12] with Phorbol 12-myristate 13-acetate (PMA) and with TNF $\alpha$ . PMA treatment resulted in an increase in p65 NF $\kappa$ B (Ser536) phosphorylation and I $\kappa$ B $\alpha$  degradation in pcDNA cells but not in TREM2 + DAP12 cells, showing that TREM2 and DAP12 co-expression prevented NF $\kappa$ B activation in response to PMA treatment (Figure 2A). Interestingly, TREM2(R47H) + DAP12 cells showed an increased in p65 NF $\kappa$ B (Ser536) phosphorylation and I $\kappa$ B $\alpha$  degradation after PMA treatment, which was similar to that observed in control pcDNA cells. These results indicate that the AD-associated TREM2 R47H mutation results in a loss-of-function of TREM2 preventing TREM2 dependent inhibition of NF $\kappa$ B activation induced by PMA. We further examined the effect of TREM2 and DAP12 co-expression on PMA induced NF $\kappa$ B promoter luciferase activity in HEK293 NF $\kappa$ B -luciferase cells. We found that TREM2 and DAP12 overexpression significantly inhibited NF $\kappa$ B luciferase activation induced by PMA (Figure 2B) further confirming an inhibition of the NF $\kappa$ B pathway. By contrast, TNF $\alpha$  treatment increased p65 (Ser536) phosphorylation and I $\kappa$ B $\alpha$  degradation in all pcDNA, TREM2 + DAP12 and TREM2(R47H) + DAP12 cells (Figure 2C) to a similar extent showing that TREM2-DAP12 co-expression is unable to suppress NF $\kappa$ B activation induced by TNF $\alpha$ . This was further supported by the fact that TREM2 and DAP12 co-expression was also unable to block NF $\kappa$ B luciferase



activation induced by TNF $\alpha$  in our NF $\kappa$ B luciferase reporter cells further suggesting that TREM2 does not affect the NF $\kappa$ B activation induced by TNF $\alpha$  (Figure 2D).

## Shedding of the TREM2 Ectodomain Does Not Prevent the Anti-inflammatory Function of TREM2

It has been shown recently that TREM2 is cleaved by ADAM10 and ADAM17 resulting in the production of soluble TREM2 (sTREM2) and a membrane-retained C-terminal fragment (TREM2-CTF) (Feuerbach et al., 2017; Schlepckow et al., 2017; Thornton et al., 2017). TREM2-CTF is then cleared by an intramembranous cleavage by the  $\gamma$ -secretase (Wunderlich et al., 2013). Since PMA is a strong activator of ADAM17, we investigated whether proteolytic processing of TREM2 was induced by PMA and determined the impact of TREM2 processing on phagocytic and anti-inflammatory functions of TREM2. We treated pcDNA and TREM2 + DAP12 cells with PMA and examined the levels of full length TREM2 (fTREM2) and of TREM2-CTF generated by ectodomain shedding at different time points. As expected, PMA treatment drastically lowered fTREM2 level and increased the generation of TREM2-CTF accordingly (Figures 3A–C). The level of DAP12 did not change after the PMA treatment (Figure 3D). We further examined the effect of TNF $\alpha$  treatment on TREM2 processing. We found that the levels of fTREM2 and DAP12 remained the same after TNF $\alpha$  treatment and that TREM2-CTF was not induced by the TNF $\alpha$  treatment showing that TNF $\alpha$  does not impact the processing of TREM2 (Figures 3E–G).

We further examined the effect of a blockade of the proteolytic processing of TREM2 on the anti-inflammatory functions of TREM2 by using the broad-spectrum inhibitor of the ADAM family of proteases, tumor necrosis factor- $\alpha$  protease inhibitor (TAPI-1) in TREM2 + DAP12 cells. TAPI-1 treatment was able to effectively increase the steady state level of TREM2 in TREM2 + DAP12 cells, indicating that TAPI-1 is blocking the shedding of fTREM2 (Figure 4A). TAPI-1 also blocked the effects of the PMA treatment on fTREM2 degradation and TREM2-CTF generation in a dose dependent manner but did not affect the inhibition of p65 NF $\kappa$ B(Ser536) phosphorylation and I $\kappa$ B $\alpha$  degradation in TREM2 + DAP12 cells (Figures 4A–C). Moreover, we confirmed by laser confocal imaging following TREM2 immunostaining with an antibody detecting the N-terminal domain of TREM2 that TAPI-1 protected TREM2 from the shedding induced by PMA treatment in TREM2 + DAP12 cells (Figure 4D). These results suggest that blocking the ectodomain shedding of TREM2 with TAPI-1 does not affect the anti-inflammatory functions of TREM2. The fact that the NF $\kappa$ B activation induced by PMA in TREM2-DAP12 co-expressing cells is blocked even after complete shedding of TREM2 suggest that the anti-inflammatory functions of TREM2 may be exerted by TREM2-CTF under these circumstances and therefore do not require the N-terminal domain of TREM2.

We also investigated the effects of an inhibition of the proteolytic processing of TREM2 on TREM2 phagocytic functions. We found that TAPI-1 was significantly increasing

the phagocytosis of pHrodo *E. coli*, whereas PMA was completely antagonizing TREM2 dependent phagocytic activity (Figures 4E,F). Interestingly, the amount of phagocytosis stimulation induced by TAPI-1 in our TREM2 + DAP12 HEK293 cells is similar to the increased in phagocytosis induced by a broad-spectrum ADAM protease inhibitor (GM6001) in a microglial cell line (Kleinberger et al., 2014). We also tested in the phagocytosis assay the impact of DAPT, an inhibitor of the  $\gamma$ -secretase which has been shown previously to prevent the clearance of the TREM2-CTF (Feuerbach et al., 2017) and of C3, an inhibitor of the  $\beta$ -secretase (Kleinberger et al., 2014). We found that DAPT did not affect the phagocytosis of pHrodo *E. coli* in TREM2 + DAP12 cells (Figure 4E) suggesting that TREM2 dependent phagocytosis is not influenced by the  $\gamma$ -secretase processing of TREM2-CTF. The increased phagocytosis induced by TAPI-1 is paralleled by an increased in fTREM2 levels observed after TAPI-1 treatment. We found that TAPI-1 was able to completely reverse the inhibition of TREM2 dependent phagocytosis induced by PMA as well as the shedding of TREM2 in TREM2 + DAP12 cells indicating that the phagocytic functions of TREM2 are correlated with the levels of fTREM2 and require fTREM2.

## APOE Induces SYK Activation in a TREM2 Dependent Manner

It has been reported that TREM2 binds to apolipoproteins including APOE, which is the strongest genetic risk factor for late-onset Alzheimer disease. We next investigated whether APOE was able to affect TREM2 signaling. It has been shown that upon TREM2 binding with a TREM2 activating antibody that tyrosine residues in the ITAM domain of DAP12 are phosphorylated allowing the recruitment and activation of the SYK in myeloid cells (Yeh et al., 2017). We therefore examined whether APOE2 and APOE4 were able to induce an activation of SYK in HEK293 cells co-expressing TREM2 and DAP12. We show that both APOE2 and APOE4 effectively activates SYK in HEK293 cells stably overexpressing TREM2 and DAP12 (Figures 5A,B). This effect of APOE was mediated by TREM2 since it was not observed in cells that did not express TREM2 (pcDNA empty vector control cells). These data therefore confirm in our model that APOE is an agonist of TREM2. Interestingly, our data suggest that APOE4 is able to induce SYK activation more potently than APOE2 (Figures 5A,B), supporting a differential effect of ApoE isoforms on TREM2 signaling. We further examined whether APOE was affecting NF $\kappa$ B activation and phagocytosis in TREM2 + DAP12 cells. We found that APOE2 and APOE4 had no effect on PMA induced NF $\kappa$ B activation in pcDNA and did not block the anti-inflammatory activity of TREM2 in TREM2 + DAP12 cells (Figure 5C). In the phagocytosis assay, TREM2 + DAP12 cells showed a decreasing trend in phagocytic activity after APOE2 and APOE4 treatment (Figure 5D). Overall these results show that APOE does not affect the anti-inflammatory and has only a marginal impact on the phagocytic activity of TREM2 in TREM2 + DAP12 cells.

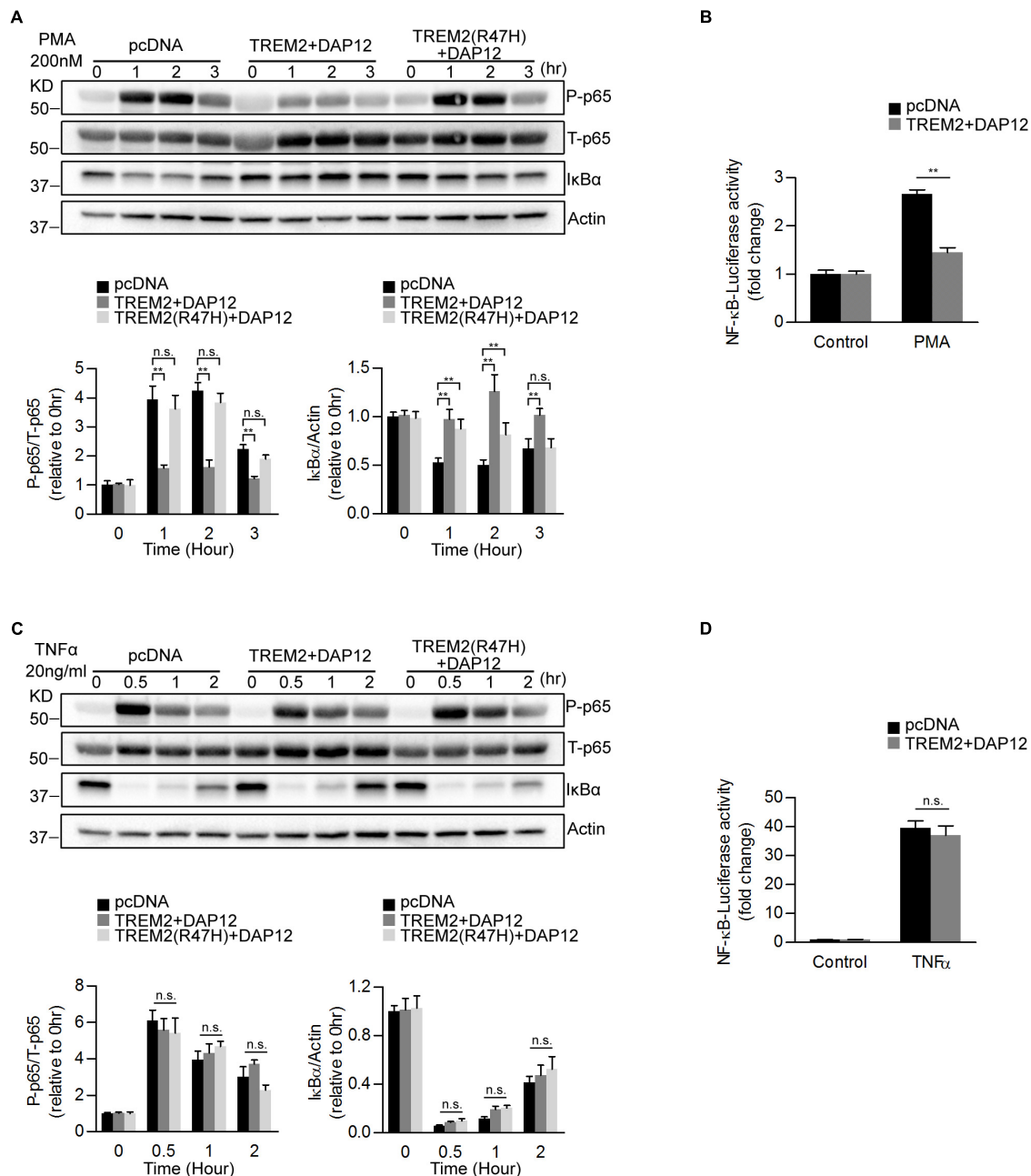


**FIGURE 2 |** Overexpression of TREM2 and DAP12 in HEK 293 cells antagonizes PMA induced p65 NFκB phosphorylation and NFκB transactivity. **(A)** Western blot analysis of lysates from TREM2 + DAP12 and TREM2 (R47H) + DAP12 transfected HEK293 cells treated with PMA (200 nM) for different timepoints (0, 1, 2, and 3 h). Lower panel: the histogram represents the western-blot quantification of P-p65 NFκB (Ser536) normalized to total p65 NFκB (T-p65) levels and IκBα levels normalized to Actin levels. Data are represented as means ± SD and expressed relative to the 0-h timepoint;  $n = 4$  for each experimental condition; statistical significance (\*\* $p < 0.01$ ; n.s., not significant) were evaluated by ANOVA followed by *post hoc* analyses with Bonferroni corrections. **(B)** The histogram represents the amount NFκB activation measured by quantifying PMA-induced intracellular luciferase activity in NFκB luciferase reporter HEK293 cell line transfected with pcDNA (empty vector) and TREM2 + DAP12. Data are represented as means ± SD from at least two independent cell culture experiments and expressed relative to NFκB luciferase activity measured in control cells transfected with the empty vector (pcDNA);  $n = 6$  for each experimental condition; statistical significance (\*\* $p < 0.01$ ) was evaluated with ANOVA followed by *post hoc* analysis with Bonferroni corrections. **(C)** Western-blot analyses of lysates from TREM2 + DAP12 and TREM2 (R47H) + DAP12 transfected HEK293 cells treated with TNFα (20 ng/ml) for different timepoints (0, 0.5, 1, and 2 h). Lower panel: the histogram represents the western-blot quantification of P-p65 NFκB (Ser536)/total p65 NFκB (T-p65), and IκBα levels normalized to Actin. Data are represented as means ± SD and expressed relative to the 0-h timepoint;  $n = 4$  for each experimental condition; statistical significance (n.s., not significant) was evaluated with ANOVA followed by *post hoc* analyses using Bonferroni correction. **(D)** The histogram represents the amount of NFκB activation measured by quantifying TNFα-induced intracellular luciferase activity in NFκB luciferase reporter HEK293 cells transfected with pcDNA (empty vector) and TREM2 + DAP12. Data are represented as means ± SD from at least two independent cell culture experiments and expressed relative to control HEK293 NFκB luciferase cells transfected with the empty vector;  $n = 6$  for each experimental condition; statistical significance (n.s., not significant) was evaluated by ANOVA.

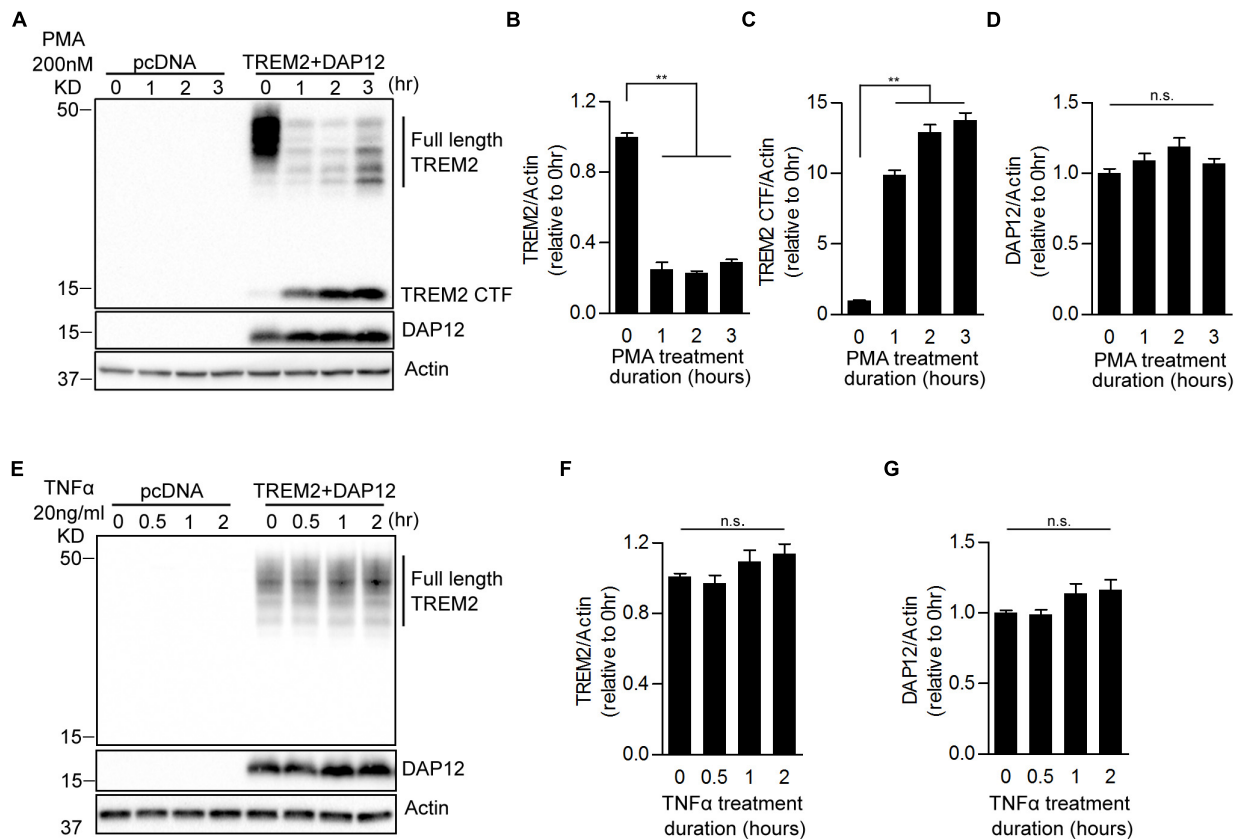


**FIGURE 3 |** Effects of PMA and  $\text{TNF}\alpha$  treatments on the shedding of TREM2 in HEK293 cells overexpressing TREM2 + DAP12. **(A)** A representative western-blot showing the effects of PMA on full length TREM2 and TREM2-CTF is shown. Control pcDNA (empty vector) and TREM2 + DAP12 transfected HEK293 cells were treated with PMA (200 nM) for different timepoints (0, 1, 2, and 3 h). The histograms represent the quantification of western-blot data and show the amount of full length TREM2 normalized to Actin **(B)**, TREM2-CTF levels normalized to Actin **(C)**, and DAP12 levels normalized to Actin **(D)**. Data are represented as means  $\pm$  SD and expressed relative to the 0-h timepoint;  $n = 4$  for each experimental condition; statistical significance (\*\* $p < 0.01$ ; n.s., not significant) was evaluated by ANOVA followed by *post hoc* analyses using Bonferroni corrections. **(E)** Western blot analysis of lysates from TREM2 + DAP12 transfected HEK293 cells treated with  $\text{TNF}\alpha$  (20 ng/ml) for different timepoints (0, 0.5, 1, and 2 h). The histograms depict the quantification of full length TREM2 levels normalized to Actin **(F)** and DAP12 levels normalized to Actin **(G)**. Data are represented as means  $\pm$  SD and expressed relative to 0-h timepoint;  $n = 4$  for each experimental condition; statistical significance (n.s., not significant) was evaluated by ANOVA.

## SYK Kinase Is Required for TREM2 Dependent Phagocytosis but Not for the Suppression of $\text{NF}\kappa\text{B}$ Activation

We further examined the possible contribution of SYK in regulating the phagocytic and the inhibition of  $\text{NF}\kappa\text{B}$  activation by TREM2. We used short hairpin RNAs (shRNAs) to stably knockdown the SYK gene expression in pcDNA and TREM2 + DAP12 cells (**Figures 6A,B**). We then measured the effect of SYK knockdown on PMA-induced  $\text{NF}\kappa\text{B}$  activation and phagocytosis of pHrodo *E. coli*. We found that the suppression of SYK expression was slightly reducing PMA stimulation of  $\text{NF}\kappa\text{B}$  p65 phosphorylation in pcDNA cells but had no effect on the inhibition of p65  $\text{NF}\kappa\text{B}$  phosphorylation in TREM2 + DAP12 cells with or without PMA treatment (**Figures 6C,D**). Interestingly, the phagocytic activity of TREM2 was partially prevented by the suppression of SYK expression (**Figure 6E**). Collectively, these data suggest that the inhibition of  $\text{NF}\kappa\text{B}$  activation by TREM2 is SYK independent whereas

its phagocytic functions are partially mediated via a SYK dependent pathway.

## PI3K/AKT Signaling Differently Affects the Anti-inflammatory and Phagocytic Functions of TREM2

PMA is a diacylglycerol (DAG) analog known to activate protein kinase C (PKC) resulting in the activation of the  $\text{NF}\kappa\text{B}$  pathway and inflammation (Holden et al., 2008). Our data therefore suggest that inhibition of  $\text{NF}\kappa\text{B}$  activation induced by TREM2 in response to PMA is mediated by a suppression of the PKC pathway. To investigate whether PKC activation induced by PMA was affected in TREM2 + DAP12 cells, we monitored the phosphorylation of Myristoylated Alanine Rich Protein Kinase C Substrate (MARCKs), the most prominent cellular substrate for PKC. In addition, we also inhibited PKC using two different PKC inhibitors, Go 6983 or Ro 32-0432. We found as expected that PKC inhibitors can totally block PMA-induced

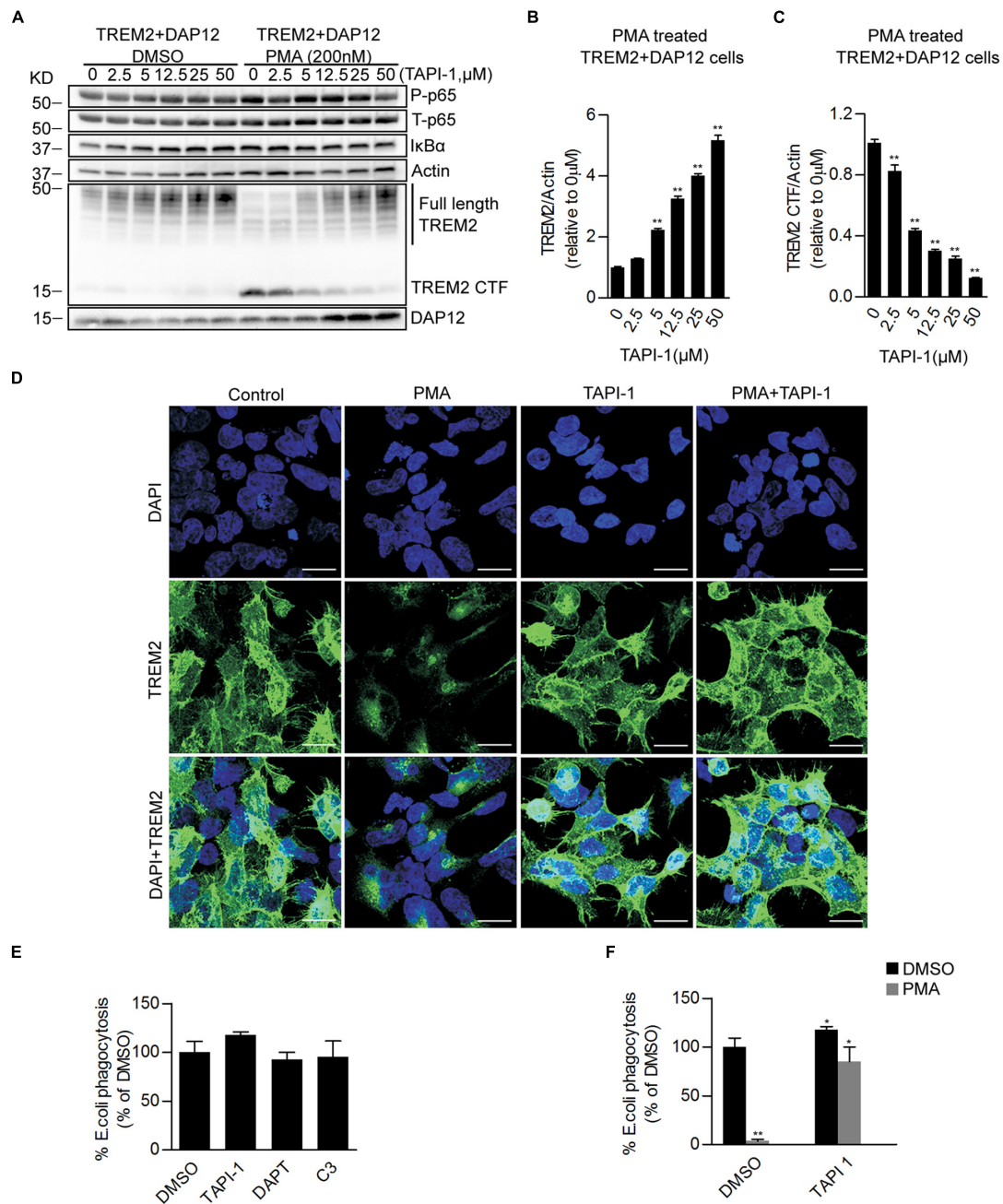


**FIGURE 4 |** Pharmacological inhibition of ADAM proteases prevents PMA induced TREM2 shedding and increases phagocytosis in TREM2 + DAP12 HEK293 cells. **(A)** Western blot analysis of lysates from TREM2 + DAP12 HEK293 cells pretreated with different doses of TAPI-1 (0, 2.5, 5, 12.5, 25, and 50 μM) for 1 h, and then challenged with PMA (200 nM) for 1 h. The histograms represent the quantification of full length TREM2 levels normalized to Actin **(B)** and TREM2 CTF levels normalized to Actin used as a reference protein **(C)**. Data are represented as means ± SD and expressed relatively to the level of full length TREM2 quantified in TREM2 + DAP12 HEK293 cells prior to TAPI-1 treatment;  $n = 4$  for each experimental condition; statistical significance (\*\* $p < 0.01$ ) was evaluated by ANOVA followed by *post hoc* analyses with Bonferroni corrections. **(D)** Representative laser confocal images obtained following immunostaining with an N-terminal TREM2 antibody (green) and counterstaining with DAPI (blue) in HEK293 cells transfected with TREM2 + DAP12. Cells were pretreated with or without TAPI-1 (25 μM) for 1 h, and then challenged with PMA (200 nM) for 1 h prior to immunostaining. The white scale bar represents 20 μm. **(E)** Phagocytosis of pHrodo *E. coli* bioparticles conjugate in TREM2 + DAP12 transfected HEK293 cells treated with TAPI-1 (25 μM), DAPT (10 μM), or C3 (10 μM) for 1 h. Data are represented as means ± SD from at least two independent cell culture experiments and expressed as a percentage of the values obtained in DMSO (vehicle used to dissolve TAPI-1, DAPT, and C3) treatment conditions (control);  $n = 6$  for each experimental condition; statistical significance (\* $p < 0.05$ ) was evaluated by ANOVA followed by *post hoc* analyses with Bonferroni corrections. **(F)** Phagocytosis of pHrodo *E. coli* bioparticles conjugate in TREM2 + DAP12 transfected HEK293 cells pretreated with TAPI-1 (25 μM) for 1 h and then challenged with PMA (200 nM) for 1 h. Data are represented as means ± SD from at least two independent cell culture experiments and expressed as a percentage of the values obtained in TREM2 + DAP12 HEK293 cells following DMSO treatment;  $n = 6$  for each experimental condition; statistical significance (\* $p < 0.05$ ; \*\* $p < 0.01$ ) was evaluated by ANOVA followed by *post hoc* analyses with Bonferroni correction.



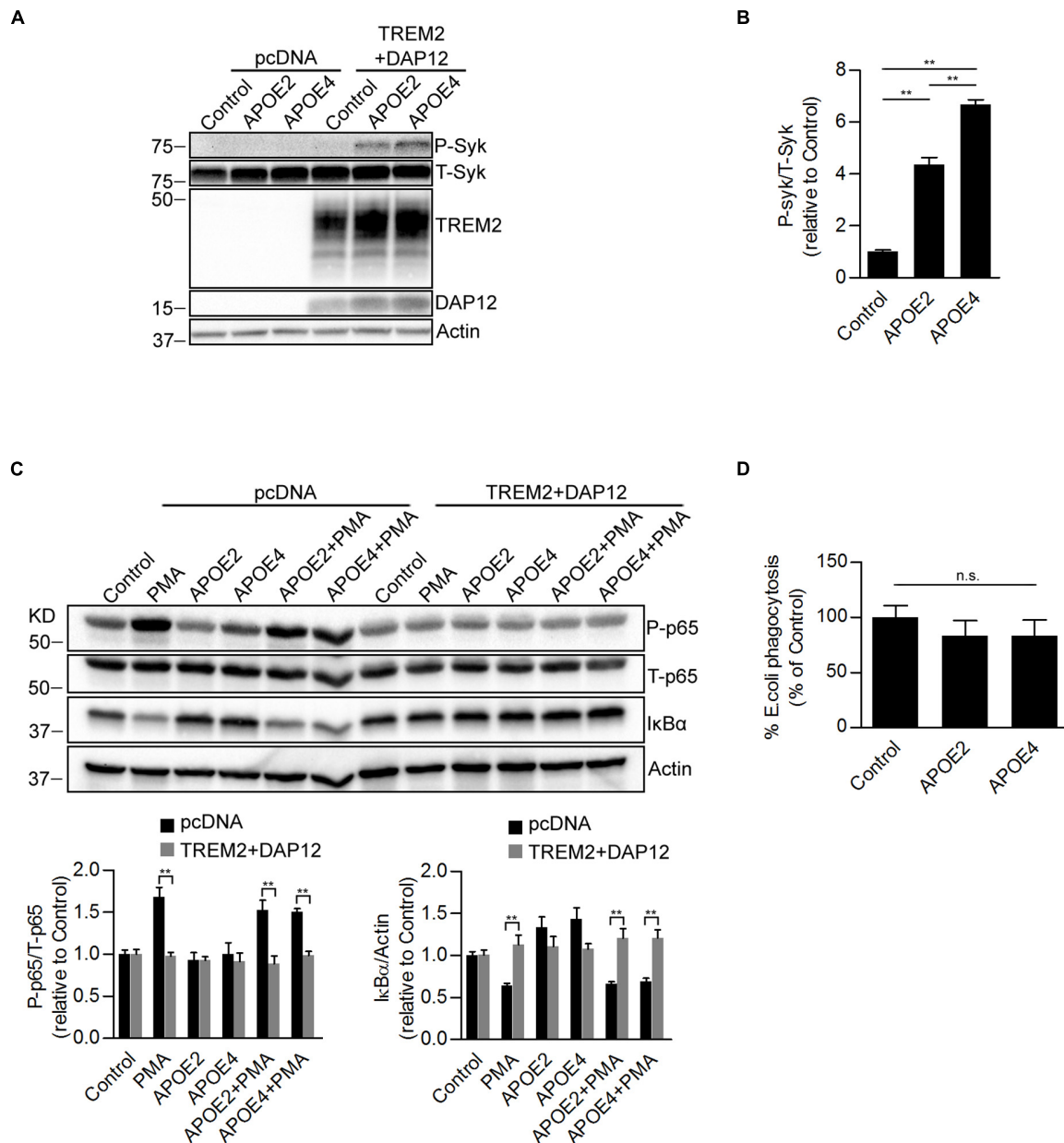


**FIGURE 5 |** Effects of ApoE isoforms on SYK kinase phosphorylation, *NF-κB* activation, and phagocytosis in TREM2 + DAP12 transfected HEK293 cells.

(A) Western blot analysis of lysates from pcDNA and TREM2 + DAP12 transfected HEK293 cells following treatment with APOE2 (10 μg/ml) and APOE4 (10 μg/ml) for 12 h. (B) The histogram represents the quantification of P-Syk (Tyr525/526)/total Syk(T-Syk) ratios in TREM2 + DAP12 HEK293 cells with and without treatment with ApoE isoforms. Data are represented as means ± SD and expressed relative to TREM2 + DAP12 cells untreated with ApoE isoforms;  $n = 4$  for each treatment condition; statistical significance (\*\* $p < 0.01$ ) was evaluated by ANOVA followed by *post hoc* analyses with Bonferroni correction. (C) Western blot analysis of lysates from pcDNA (empty vector) or TREM2 + DAP12 transfected HEK293 cells pretreated with APOE2 (10 μg/ml) and APOE4 (10 μg/ml) for 12 h, and then challenged with PMA (200 nM) for 1 h. Lower panel: the histograms represent the quantification of P-p65 (Ser536)/total P65 (T-p65) ratios and IκBα levels normalized to Actin. Data are represented as means ± SD and expressed relative to untreated pcDNA (empty vector) control cells;  $n = 4$  for each treatment condition; statistical significance (\*\* $p < 0.01$ ) was evaluated by ANOVA followed by *post hoc* analysis with Bonferroni correction. (D) Phagocytosis of pHrodo *E. coli* bioparticles conjugate in TREM2 + DAP12 transfected HEK293 cells pretreated with APOE2 (10 μg/ml) and APOE4 (10 μg/ml) for 12 h. Data are represented as means ± SD from at least two independent cell culture experiments and expressed as a percentage of the phagocytic activity measured in TREM2 + DAP12 HEK293 cells without APOE treatment;  $n = 6$  for each experimental condition; ANOVA reveals no significant main effect of APOE4 and APOE2 on phagocytosis (n.s., not significant).

NFκB activation and phosphorylation of MARCKs in pcDNA cells (Figure 7A) showing that the stimulation of NFκB induced by PMA is effectively driven by an activation of PKC enzymes.

There was however no difference in the phosphorylation of MARCKs between pcDNA and TREM2 + DAP12 cells after PMA treatment, indicating that PKC activation was

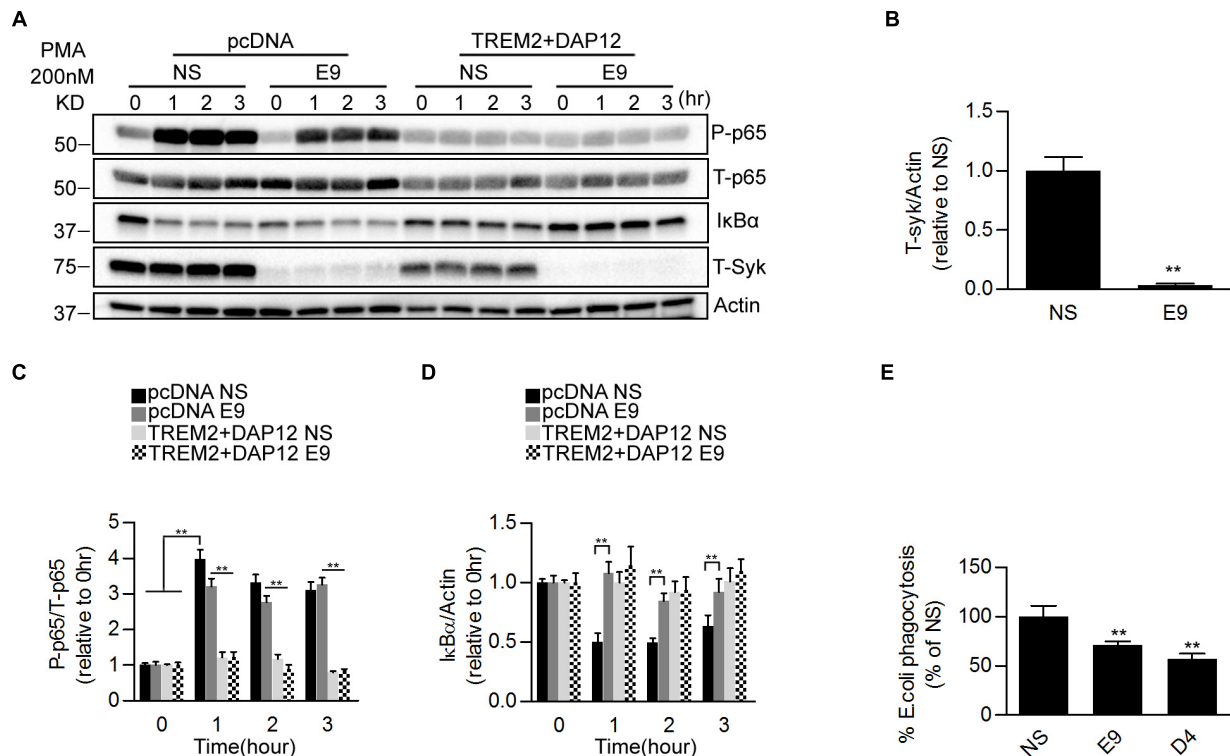


**FIGURE 6 |** Effects of genetic suppression of SYK kinase expression on *NFκB* activation and phagocytosis in TREM2 + DAP12 transfected HEK293 cells.

**(A)** Western blot analysis of lysates from pcDNA or TREM2 + DAP12 transfected HEK293 cells, with or without silencing of the Syk gene [lentiviral vector expressing Syk specific shRNA(E9) or nonsense control shRNAs(NS)], following treatment with PMA (200 nM) for the indicated timepoints (0, 1, 2, and 3 h). **(B)** The histogram represents the quantification of Syk levels normalized to Actin in control TREM2 + DAP12 HEK293 cells transfected with the nonsense shRNA (NS) and in TREM2 + DAP12 cells in which the Syk gene was silenced (shRNA E9). Data are represented as means  $\pm$  SD and expressed relative to RNAi the amount of SYK quantified in shRNA nonsense (NS) transfected cells;  $n = 4$  for each experimental condition; statistical significance (\*\* $p < 0.01$ ) was evaluated with two-tailed Student's *t*-test. **(C,D)** The histograms represent the ratios of P-p65 *NFκB* (Ser536)/total p65 *NFκB* (T-p65) and IκBα levels normalized to Actin. Data are represented as means  $\pm$  SD and expressed relative to pcDNA (empty vector) shRNA nonsense (NS) transfected cells;  $n = 4$  for each treatment condition; statistical significance (\*\* $p < 0.01$ ; n.s., not significant) was evaluated by ANOVA followed by *post hoc* analyses with Bonferroni correction. **(E)** Phagocytosis of pHrodo *E. coli* bioparticles conjugate in TREM2 + DAP12 transfected HEK293 cells with or without silencing of the Syk gene [lentiviral vector expressing Syk specific shRNA (E9 and D4) or nonsense control shRNAs(NS)]. Data are represented as means  $\pm$  SD from at least two independent cell culture experiments and expressed relative to shRNA nonsense (NS) transfected cells TREM2 + DAP12 HEK293 cells;  $n = 6$  for each experimental condition; statistical significance (\*\* $p < 0.01$ ) was evaluated by ANOVA followed by *post hoc* analyses with Bonferroni correction.

similar in pcDNA and TREM2 + DAP12 cells (**Figure 7B**) suggesting that TREM2 is acting downstream of PKC to block *NFκB* activation.

As shown earlier, AKT activation was observed in TREM2 + DAP12 cells, which is consistent with previous reports demonstrating an activation of the PI3K/AKT pathway by TREM2 in myeloid cells (Peng et al., 2010). To examine the role of PI3K/AKT signaling on TREM2 functions, we used two different PI3K inhibitors, wortmannin and LY294002. As shown by immunoblotting and immunostaining, AKT phosphorylation was effectively blocked by the two inhibitors of PI3K in TREM2 + DAP12 cells confirming that TREM2 activates PI3K (**Figures 7C,D**). Interestingly, inhibiting PI3K/AKT signaling had no effect on the inhibition of *NFκB* activation induced by TREM2 since PMA-induced *NFκB* activation was still suppressed in TREM2-DAP12 cells when PI3K was inhibited (**Figure 7C**). By contrast, inhibition of PI3K/AKT signaling largely decreased the phagocytosis of pHrodo *E. coli* in

TREM2 + DAP12 cells, suggesting that phagocytic functions of TREM2 require PI3K/AKT signaling (**Figure 7E**).

## DISCUSSION

TREM2 signals through the intracellular adaptor DAP12 (Lanier et al., 1998; Bouchon et al., 2001; Daws et al., 2001) also known as TYRO protein- TYROBP. TREM2 ligation promotes the phosphorylation of its ITAMS by Src kinases creating a docking site for the SH2 domains of several proteins including SYK (Takahashi et al., 2005; Mocsai et al., 2010; Yu et al., 2013). Upon ligation of TREM2, downstream signaling molecules including phosphatidyl inositol 3-kinase (PI3K) and phospholipase Cγ (PLCγ) have been shown to be activated (Takahashi et al., 2005; Otero et al., 2009; Peng et al., 2010; Wang et al., 2015; Colonna and Wang, 2016; Zhao et al., 2018). It remains unclear how TREM2 exerts an anti-inflammatory activity as TREM2 ligands

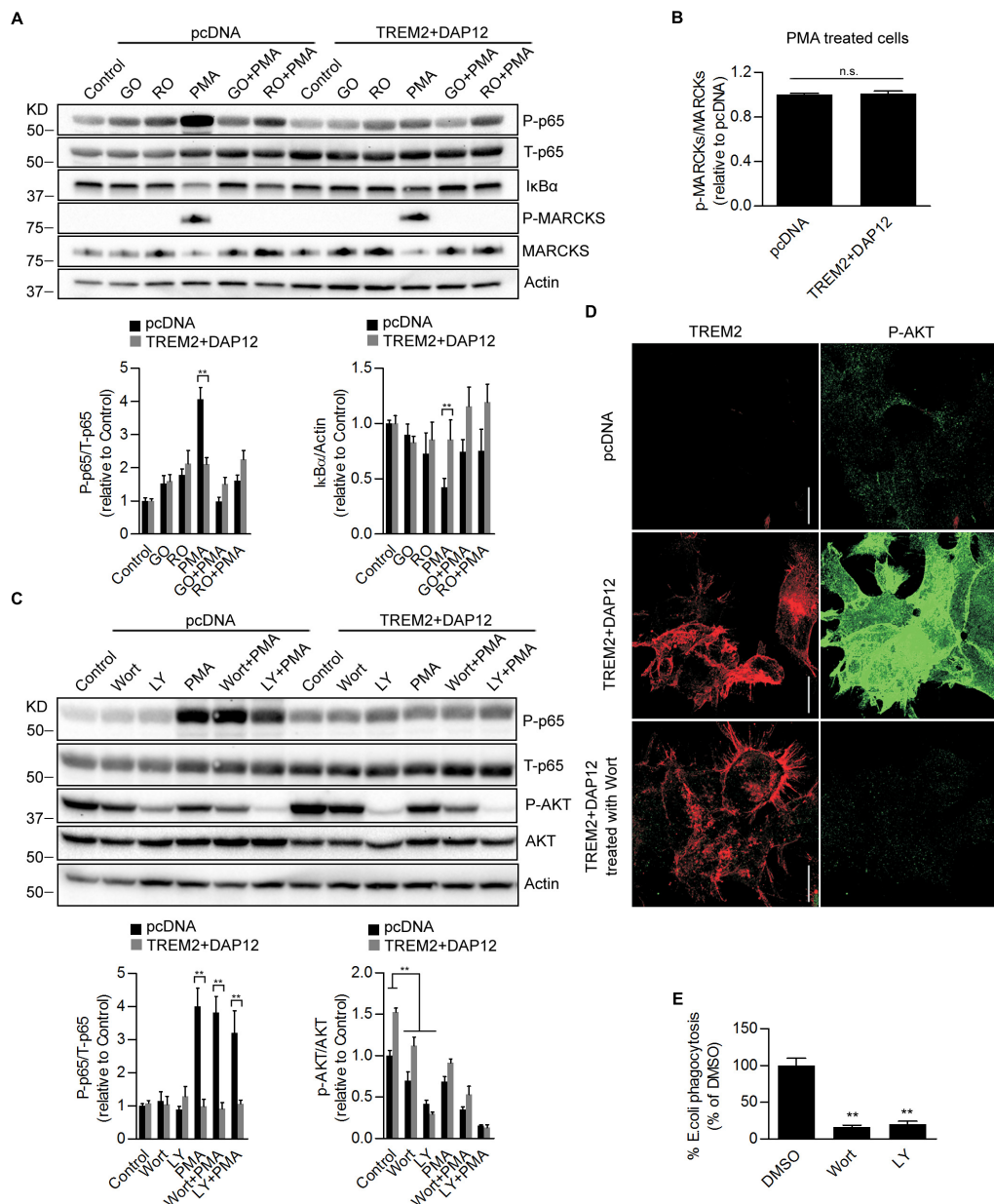


**FIGURE 7 |** Effects of Pharmacological inhibition of PI3K/AKT signaling on *NFκB* activation and phagocytosis in TREM2 + DAP12 HEK293 cells. **(A)** Western-blot analysis of lysates from TREM2 + DAP12 transfected HEK293 cells pretreated with different PKC inhibitors Go 6983 (Go; 5 μM), Ro 32-0432 (Ro; 10 μM) for 1 h, and then challenged with PMA (200 nM) for 1 h. Lower panel: the histograms represent the ratios of P-p65 NFκB (Ser536)/total p65 NFκB and IκBα levels normalized to Actin in control pcDNA (empty vector) cells and in TREM2 + DAP12 HEK293 cells. Data are represented as means ± SD and expressed relative to control pcDNA transfected cells;  $n = 4$  for each experimental condition; statistical significance (\*\* $p < 0.01$ ) was evaluated by ANOVA followed by *post hoc* analyses with Bonferroni correction. **(B)** The histogram represents the ratios of p-MARCKS/total MARCKS in PMA treated pcDNA (control cells) and TREM2 + DAP12 transfected HEK293 cells. Data are represented as means ± SD and expressed relative to pcDNA transfected cells;  $n = 4$  for each experimental condition; no statistical significance (n.s.;  $p > 0.05$ ) was found using a two-tailed Student's *t*-test. **(C)** Western blot analysis of lysates from pcDNA (empty vector) and TREM2 + DAP12 transfected HEK293 cells pretreated with different PI3K inhibitors: wortmannin (wort; 200 nM) and LY 294002 (LY; 20 μM) for 1 h, and then challenged with PMA (200 nM) for 1 h. Lower panel: the histograms represent the ratios of P-p65 NFκB (Ser536)/total p65 NFκB (T-p65) and p-AKT (Ser473)/Total AKT levels normalized to Actin quantified in control pcDNA (empty vector) and TREM2 + DAP12 HEK293 cells. Data are represented as means ± SD and expressed relative to control pcDNA (empty vector) transfected HEK293 cells;  $n = 4$  for each experimental condition; statistical significance (\*\* $p < 0.01$ ) was evaluated by ANOVA followed by *post hoc* analyses with Bonferroni corrections. **(D)** Representative laser confocal images obtained following immunostaining of HEK293 cells transfected with pcDNA (empty vector) and TREM2 + DAP12 HEK293 cells using an N-terminal TREM2 antibody (red), and a p-AKT (Ser473) antibody (green) following treatment of the cells with the PI3K inhibitor wortmannin (wort; 200 nM) for 1 h. The white scale bar represents 20 μm. **(E)** Phagocytosis of pHrodo *E. coli* bioparticles conjugate in TREM2 + DAP12 transfected HEK293 cells treated with the PI3K inhibitors wortmannin (wort; 200 nM) and LY 294002 (LY; 20 μM) for 1 h. Data are represented as means ± SD from at least two independent cell culture experiments and expressed relative to DMSO (vehicle) conditions in TREM2 + DAP12 HEK293 cells;  $n = 6$  for each treatment condition; statistical significance (\*\* $p < 0.01$ ) was evaluated by one-way ANOVA followed by *post hoc* analyses with Bonferroni corrections.

are known to promote SYK signaling which has been shown to mediate inflammation notably in microglia and myeloid cells (McDonald et al., 1997; Combs et al., 2001; Sondag et al., 2009; Zeng et al., 2014; Xie et al., 2017). TREM2 ligation with A $\beta$  oligomers has been shown to promote SYK activation and NFAT signaling (Lessard et al., 2018). The activation of NFAT signaling could be mediated by SYK which is known to activate the PLC $\gamma$ -calcineurin-NFAT pathway (Mocsai et al., 2010). We therefore investigated here whether SYK, PLC $\gamma$ , and PI3K were required to mediate the inhibition of NF $\kappa$ B activation and phagocytic functions of TREM2. In addition, we tested the impact of TREM2 ligation with ApoE2 and ApoE4 isoforms on SYK and NF $\kappa$ B activation.

Our data show that TREM2 inhibits NF $\kappa$ B activation only when DAP12 is co-expressed with TREM2. Similarly, we show that TREM2 dependent phagocytic activity also requires DAP12. Interestingly, HEK293 cells co-expressing the AD variant TREM2 R47H with DAP12 are unable to suppress NF $\kappa$ B activation induced by PMA and to phagocytose *E. coli* bioparticles suggesting that the TREM2 R47H variant confers loss-of-function-like phenotypes. Our data further suggest that the inhibition of NF $\kappa$ B activation by TREM2/DAP12 originates from a decreased degradation of I $\kappa$ B $\alpha$  (which inhibits NF $\kappa$ B). Following PMA stimulation, I $\kappa$ B $\alpha$  degradation and NF $\kappa$ B activation induced by PMA are not inhibited by the TREM2 AD variant R47H suggesting a loss of TREM2 function. We show that PMA stimulates PKC activity to a similar extent in TREM2/DAP12 overexpressing cells and control HEK293 cells as the phosphorylation of myristoylated Alanine-rich C Kinase substrate (MARCKS), substrate of PKC, was similar in these cells. As expected, PKC inhibition was able to prevent NF $\kappa$ B activation induced by PMA in control HEK293 cells and did not suppress the inhibition of NF $\kappa$ B activation in TREM2/DAP12 overexpressing cells. These data therefore suggest that TREM2/DAP12 antagonizes signaling elements downstream of PKC that are required to mediate NF $\kappa$ B activation. For instance, PKC has been shown to direct the assembly of the CARMA1-BCL10-MALT1 (CBM complex) which is essential to mediate NF $\kappa$ B activation and JNK signaling pathways (Matsumoto et al., 2005; Hara et al., 2008; So et al., 2011). It is interesting to note that both JNK and NF $\kappa$ B signaling have been shown to be affected by TREM2/DAP12 in microglia (Zhong et al., 2017b) which could result from a diminished CBM complex formation. More work will be required to determine whether TREM2/DAP12 can effectively impact the formation of the CBM complex. Interestingly, genetic variations that enhance PKC $\alpha$  activity have been identified in patients with AD (Alfonso et al., 2016) whereas inhibition of PKC has been shown to reduce amyloid- $\beta$  levels and neuroinflammation in an AD mouse model (Du et al., 2018) suggesting that PKC activation has a deleterious impact in AD. Our data showing that TREM2 can negate PKC induced NF $\kappa$ B activation could therefore support a positive role of TREM2 for alleviating neuroinflammation triggered by PKC stimulation in AD.

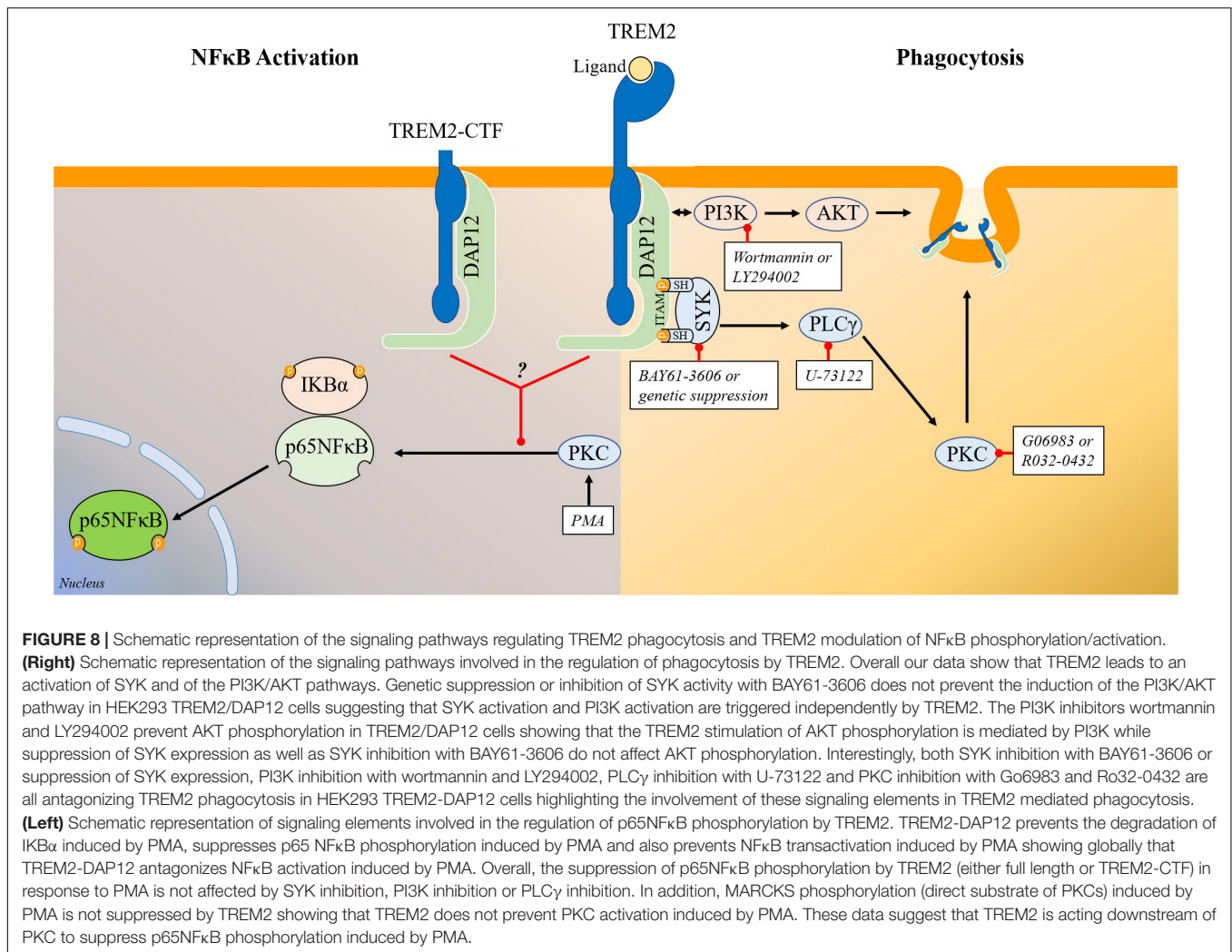
The inhibition of NF $\kappa$ B activation by TREM2/DAP12 in response to PMA was observed without the need to add an exogenous ligand for TREM2 which could suggest that TREM2

ligation is not required for its anti-inflammatory activity or that HEK293 cells produce an endogenous TREM2 ligand. We found that PMA induces a rapid cleavage of full length TREM2 resulting in a decreased cell surface expression of the TREM2 N-terminal domain and an increased production of the TREM2 C-terminal fragment (TREM2-CTF) while the inhibition of NF $\kappa$ B activation was still observed. These data further suggest that the N-terminal portion of the TREM2 receptor is not required to mediate the anti-inflammatory activity of TREM2 and therefore that TREM2 ligation is not necessary for that effect. TREM2 N-terminal domain undergoes shedding by proteases in the ADAM (a disintegrin and metalloproteinase) family including ADAM10 and ADAM17 (Kleinberger et al., 2014; Feuerbach et al., 2017; Schlepckow et al., 2017; Thornton et al., 2017) resulting in the production of soluble TREM2 (sTREM2) and TREM2-CTF. sTREM2 has been postulated to act as a decoy receptor that could bind TREM2 ligands and antagonize TREM2 signaling (Piccio et al., 2008; Zhong et al., 2017a). We found that in presence of the ADAM10/ADAM17 inhibitor TAPI-1 (which blocked the shedding of TREM2 following PMA treatment) that there was no modulation of the TREM2/DAP12 inhibition of NF $\kappa$ B activation suggesting that both the full length TREM2 receptor and the TREM2-CTF are capable of inhibiting NF $\kappa$ B. These data further imply that TREM2 suppression of NF $\kappa$ B activation is not dependent on the presence of sTREM2 as TAPI-1 treatment which inhibits the production of sTREM2 did not affect the inhibition of NF $\kappa$ B by TREM2. It has been shown that TREM2-CTF inhibits LPS induced inflammation in microglial cells (Zhong et al., 2015) showing also that the full-length receptor and TREM2 ligation are not required for the anti-inflammatory activity of TREM2 in myeloid cells which is consistent with our observations.

We found that TREM2/DAP12 overexpression led to a stimulation of AKT phosphorylation which was blocked by the PI3K inhibitors wortmannin and LY294002 showing that the PI3K/AKT pathway is triggered by TREM2/DAP12. We found however that there was no activation of PI3K/AKT in cells co-expressing the TREM2 AD mutation R47H with DAP12. Additionally, we observed that PI3K inhibition is unable to suppress the inhibition of NF $\kappa$ B activation following PMA stimulation in TREM2/DAP12 cells showing that the PI3K/AKT activation is probably not responsible for the inhibition of NF $\kappa$ B activation in TREM2/DAP12 cells.

TREM2 ligation with a stimulating antibody or with A $\beta$  oligomers has been shown to trigger SYK activation (Zhao et al., 2018; Zhong et al., 2018). However, SYK activation has been shown to promote inflammation and NF $\kappa$ B activation (McDonald et al., 1997; Combs et al., 2001; Sondag et al., 2009) while SYK inhibition is anti-inflammatory (Zeng et al., 2014; Xie et al., 2017; Sahan-Firat et al., 2019). These data could therefore suggest that upon ligation, TREM2 may have a proinflammatory activity and therefore that TREM2 could have both anti-inflammatory and pro-inflammatory functions depending on the presence and nature of TREM2 ligands. For example, intrathecal injection of an agonistic TREM2 antibody has been shown to result in microglial activation and increased proinflammatory cytokines production (Kobayashi et al., 2016).





Similarly, myelin lipids following demyelination have been shown to trigger TREM2 signaling resulting in microglial activation and upregulation of proinflammatory genes (Cantoni et al., 2015; Poliani et al., 2015) which could support that hypothesis. It remains also possible that different TREM2 ligands may have different activities toward TREM2 signaling as previously postulated (Turnbull et al., 2006; Kober and Brett, 2017). To further analyze the possible involvement of SYK in the regulation of NFκB activation in TREM2/DAP12 cells, we generated TREM2/DAP12 overexpressing HEK293 cells that are also knockdown for SYK. We found that in absence of SYK expression, TREM2/DAP12 still dampen PMA induction of NFκB activation showing that SYK is not required to mediate TREM2 suppression of NFκB activation. In cells that do not express TREM2/DAP12, we observed that downregulation of SYK expression was partially suppressing PMA induction of p65NFκB phosphorylation further confirming a pro-inflammatory function of SYK. In addition, we found that PI3K/AKT stimulation induced by TREM2/DAP12 overexpression was not suppressed in SYK knockdown cells showing that SYK does not mediate the PI3K/AKT

stimulation observed in TREM2/DAP12 overexpressing cells which could suggest that DAP12 could also directly recruit PI3K independently of SYK as previously thought (Peng et al., 2010). We tested the possible contribution of PLCγ in mediating the anti-inflammatory activity of TREM2 as previous data have suggested that TREM2 ligation can activate PLCγ (Takahashi et al., 2005; Otero et al., 2009; Peng et al., 2010; Wang et al., 2015; Colonna and Wang, 2016; Zhao et al., 2018). We found that PLCγ inhibition has no impact on the suppression of NFκB activation observed in TREM2/DAP12 overexpressing cells following challenge with PMA. In addition, PLCγ inhibition did not impact NFκB activation induced by PMA in control HEK293 cells further suggesting that the inhibition of NFκB activation observed in TREM2/DAP12 co-expressing cells following PMA challenge is PLCγ independent. We evaluated the possible effect of APOE on NFκB in TREM2/DAP12 as we have shown that APOE stimulation of TREM2 results in the activation of SYK. We observed that APOE did not trigger NFκB activation or affect basal p65NFκB phosphorylation in TREM2/DAP12 cells. Overall, these data show that the inhibition of NFκB activation by

TREM2/DAP12 is SYK, PLC $\gamma$ , and PI3K/AKT independent and does not require the stimulation of TREM2 by a ligand. **Figure 8** provides a schematic representation of the signaling pathways regulating TREM2 phagocytosis and TREM2 suppression of NF $\kappa$ B activation.

Protein binding assays suggest that APOE binds to TREM2 (Atagi et al., 2015; Bailey et al., 2015; Yeh et al., 2016) raising the possibility that APOE-TREM2 interactions may trigger TREM2 signaling. We analyzed this possibility in HEK293 cells expressing TREM2/DAP12 and TREM2 R47H/DAP12 constructs. We show that treatment of TREM2/DAP12 overexpressing cells with APOE induces SYK activation. Interestingly, APOE4 appears to stimulate SYK activation with greater potency than APOE2. This effect of APOE is TREM2 mediated as no stimulation of SYK phosphorylation by APOE was observed in control HEK293 cells that do not express TREM2. In cells expressing the TREM2 AD variant R47H, APOE was still able to stimulate SYK phosphorylation although to a lesser extent than in wild-type TREM2 expressing cells suggesting a subtle loss of function of TREM2 R47H for that particular outcome.

We found that TREM2 phagocytosis was partially prevented in SYK knockdown cells and was antagonized by PI3K inhibition. Although treatment of TREM2/DAP12 cells with APOE stimulates SYK activation, APOE isoforms do not appear to significantly impact the phagocytosis of *E. coli* bioparticles. In addition, we found that PLC $\gamma$  inhibition potently suppresses TREM2/DAP12 phagocytic activity. These data therefore demonstrate that TREM2/DAP12 phagocytic and anti-inflammatory activities are mediated by distinct signaling pathways. Interestingly, stimulation of TREM2 processing by PMA completely antagonizes TREM2 dependent phagocytosis. A phenomenon which was reverted using the ADAM10/ADAM17 inhibitor TAPI-1 showing that full length TREM2 receptor is required for its phagocytic activity.

HEK293 are not immune cells and therefore may not react like immune cells to inflammatory challenges. This is a limitation of the ectopic HEK293 cell model to study TREM2 biology and the findings observed in this cellular model will require validation in immune cells such as microglia cells. In summary, our data show that TREM2 suppression of NF $\kappa$ B activation induced by PMA is not mediated by a stimulation of the PI3K/AKT pathway which occurs following TREM2/DAP12 overexpression. In addition, our data suggest that TREM2 ligation, PLC $\gamma$ , SYK or the N-terminal domain of TREM2 are not necessary to mediate the suppression of NF $\kappa$ B activation mediated by TREM2 whereas TREM2 dependent phagocytosis requires the full-length TREM2 receptor, SYK, PLC $\gamma$ , and PI3K/AKT activities.

## DATA AVAILABILITY STATEMENT

All datasets generated for this study are included in the manuscript/supplementary files.

## AUTHOR CONTRIBUTIONS

HY, KC, JS, and DP performed the research. HY and DP designed the research and wrote the manuscript. HY, DP, MM, and FC analyzed the data. All the authors read and approved the final manuscript.

## FUNDING

Funding for these studies was provided in part by the Department of Veterans Affairs VA Merit 1I01BX002572 (FC). The contents of this manuscript do not represent the views of the Department of Veterans Affairs or the United States Government. We are thankful to the Roskamp Foundation for providing additional funding which helped to make this study possible.

## REFERENCES

- Alfonso, S. I., Callender, J. A., Hooli, B., Antal, C. E., Mullin, K., Sherman, M. A., et al. (2016). Gain-of-function mutations in protein kinase Calpha (PKCalpha) may promote synaptic defects in Alzheimer's disease. *Sci. Signal.* 9:ra47. doi: 10.1126/scisignal.aaf6209
- Atagi, Y., Liu, C. C., Painter, M. M., Chen, X. F., Verbeeck, C., Zheng, H., et al. (2015). Apolipoprotein E is a ligand for triggering receptor expressed on myeloid cells 2 (TREM2). *J. Biol. Chem.* 290, 26043–26050. doi: 10.1074/jbc.m115.679043
- Audrain, M., Haure-Mirande, J. V., Wang, M., Kim, S. H., Fanutza, T., Chakrabarty, P., et al. (2018). Integrative approach to sporadic Alzheimer's disease: deficiency of TYROBP in a tauopathy mouse model reduces C1q and normalizes clinical phenotype while increasing spread and state of phosphorylation of tau. *Mol. Psychiatry* 24, 1383–1397. doi: 10.1038/s41380-018-0258-3
- Bailey, C. C., DeVaux, L. B., and Farzan, M. (2015). The triggering receptor expressed on myeloid cells 2 binds apolipoprotein E. *J. Biol. Chem.* 290, 26033–26042. doi: 10.1074/jbc.M115.677286
- Bemiller, S. M., McCray, T. J., Allan, K., Formica, S. V., Xu, G., Wilson, G., et al. (2017). TREM2 deficiency exacerbates tau pathology through dysregulated kinase signaling in a mouse model of tauopathy. *Mol. Neurodegener.* 12:74. doi: 10.1186/s13024-017-0216-6
- Bouchon, A., Hernandez-Munain, C., Cella, M., and Colonna, M. (2001). A DAP12-mediated pathway regulates expression of CC chemokine receptor 7 and maturation of human dendritic cells. *J. Exp. Med.* 194, 1111–1122. doi: 10.1084/jem.194.8.1111
- Cantoni, C., Bollman, B., Licastro, D., Xie, M., Mikesell, R., Schmidt, R., et al. (2015). TREM2 regulates microglial cell activation in response to demyelination in vivo. *Acta Neuropathol.* 129, 429–447. doi: 10.1007/s00401-015-1388-1
- Carmona, S., Zahs, K., Wu, E., Dakin, K., Bras, J., and Guerreiro, R. (2018). The role of TREM2 in Alzheimer's disease and other neurodegenerative disorders. *Lancet Neurol.* 17, 721–730. doi: 10.1016/S1474-4422(18)30232-1
- Cheng-Hathaway, P. J., Reed-Geaghan, E. G., Jay, T. R., Casali, B. T., Bemiller, S. M., Puntambekar, S. S., et al. (2018). The Trem2 R47H variant confers loss-of-function-like phenotypes in Alzheimer's disease. *Mol. Neurodegener.* 13:29. doi: 10.1186/s13024-018-0262-8
- Colonna, M. (2003). TREMs in the immune system and beyond. *Nat. Rev. Immunol.* 3, 445–453. doi: 10.1038/nri1106
- Colonna, M., and Wang, Y. (2016). TREM2 variants: new keys to decipher Alzheimer disease pathogenesis. *Nat. Rev. Neurosci.* 17, 201–207. doi: 10.1038/nrn.2016.7

- Combs, C. K., Karlo, J. C., Kao, S. C., and Landreth, G. E. (2001). beta-Amyloid stimulation of microglia and monocytes results in TNF $\alpha$ -dependent expression of inducible nitric oxide synthase and neuronal apoptosis. *J. Neurosci.* 21, 1179–1188. doi: 10.1523/jneurosci.21-04-01179.2001
- Daws, M. R., Lanier, L. L., Seaman, W. E., and Ryan, J. C. (2001). Cloning and characterization of a novel mouse myeloid DAP12-associated receptor family. *Eur. J. Immunol.* 31, 783–791. doi: 10.1002/1521-4141(200103)31:3<783::aid-immu783>3.0.co;2-u
- De Strooper, B., and Karran, E. (2016). The Cellular Phase of Alzheimer's Disease. *Cell* 164, 603–615. doi: 10.1016/j.cell.2015.12.056
- Du, Y., Zhao, Y., Li, C., Zheng, Q., Tian, J., Li, Z., et al. (2018). Inhibition of PKC $\delta$  reduces amyloid-beta levels and reverses Alzheimer disease phenotypes. *J. Exp. Med.* 215, 1665–1677. doi: 10.1084/jem.20171193
- Fahrenhold, M., Rakic, S., Classey, J., Brayne, C., Ince, P. G., Nicoll, J. A. R., et al. (2018). TREM2 expression in the human brain: a marker of monocyte recruitment? *Brain Pathol.* 28, 595–602. doi: 10.1111/bpa.12564
- Feuerbach, D., Schindler, P., Barske, C., Joller, S., Beng-Louka, E., Worringer, K. A., et al. (2017). ADAM17 is the main sheddase for the generation of human triggering receptor expressed in myeloid cells (hTREM2) ectodomain and cleaves TREM2 after Histidine 157. *Neurosci. Lett.* 660, 109–114. doi: 10.1016/j.neulet.2017.09.034
- Gorlovoy, P., Larionov, S., Pham, T. T., and Neumann, H. (2009). Accumulation of tau induced in neurites by microglial proinflammatory mediators. *FASEB J.* 23, 2502–2513. doi: 10.1096/fj.08-123877
- Guerreiro, R., Wojtas, A., Bras, J., Carrasquillo, M., Rogaeva, E., Majounie, E., et al. (2013). TREM2 variants in Alzheimer's disease. *N. Engl. J. Med.* 368, 117–127. doi: 10.1056/NEJMoa1211851
- Hamerman, J. A., Jarjoura, J. R., Humphrey, M. B., Nakamura, M. C., Seaman, W. E., and Lanier, L. L. (2006). Cutting edge: inhibition of TLR and FcR responses in macrophages by triggering receptor expressed on myeloid cells (TREM)-2 and DAP12. *J. Immunol.* 177, 2051–2055. doi: 10.4049/jimmunol.177.4.2051
- Hammond, T. R., Marsh, S. E., and Stevens, B. (2019). Immune signaling in neurodegeneration. *Immunity* 50, 955–974. doi: 10.1016/j.immuni.2019.03.016
- Hara, H., Ishihara, C., Takeuchi, A., Xue, L., Morris, S. W., Penninger, J. M., et al. (2008). Cell type-specific regulation of ITAM-mediated NF- $\kappa$ B activation by the adaptors, CARMA1 and CARD9. *J. Immunol.* 181, 918–930. doi: 10.4049/jimmunol.181.2.918
- Hardy, J., and Selkoe, D. J. (2002). The amyloid hypothesis of Alzheimer's disease: progress and problems on the road to therapeutics. *Science* 297, 353–356. doi: 10.1126/science.1072994
- Haure-Mirande, J. V., Wang, M., Audrain, M., Fanutza, T., Kim, S. H., Heja, S., et al. (2019). Correction: integrative approach to sporadic Alzheimer's disease: deficiency of TYROBP in cerebral abeta amyloidosis mouse normalizes clinical phenotype and complement subnetwork molecular pathology without reducing abeta burden. *Mol. Psychiatry* 24, 431–446. doi: 10.1038/s41380-018-0301-4
- Hickman, S. E., Kingery, N. D., Ohsumi, T. K., Borowsky, M. L., Wang, L. C., Means, T. K., et al. (2013). The microglial sensome revealed by direct RNA sequencing. *Nat. Neurosci.* 16, 1896–1905. doi: 10.1038/nn.3554
- Holden, N. S., Squires, P. E., Kaur, M., Bland, R., Jones, C. E., and Newton, R. (2008). Phorbol ester-stimulated NF- $\kappa$ B-dependent transcription: roles for isoforms of novel protein kinase C. *Cell Signal.* 20, 1338–1348. doi: 10.1016/j.cellsig.2008.03.001
- Jay, T. R., Hirsch, A. M., Broihier, M. L., Miller, C. M., Neilson, L. E., Ransohoff, R. M., et al. (2017). Disease progression-dependent effects of TREM2 deficiency in a mouse model of Alzheimer's disease. *J. Neurosci.* 37, 637–647. doi: 10.1523/JNEUROSCI.2110-16.2016
- Jay, T. R., Miller, C. M., Cheng, P. J., Graham, L. C., Bemiller, S., Broihier, M. L., et al. (2015). TREM2 deficiency eliminates TREM2<sup>+</sup> inflammatory macrophages and ameliorates pathology in Alzheimer's disease mouse models. *J. Exp. Med.* 212, 287–295. doi: 10.1084/jem.20142322
- Jendresen, C., Arskog, V., Daws, M. R., and Nilsson, L. N. (2017). The Alzheimer's disease risk factors apolipoprotein E and TREM2 are linked in a receptor signaling pathway. *J. Neuroinflamm.* 14:59. doi: 10.1186/s12974-017-0835-4
- Jonsson, T., Stefansson, H., Steinberg, S., Jonsson, P. V., Snaedal, J., et al. (2013). Variant of TREM2 associated with the risk of Alzheimer's disease. *N. Engl. J. Med.* 368, 107–116. doi: 10.1056/NEJMoa1211103
- Kleinberger, G., Yamanishi, Y., Suarez-Calvet, M., Czirr, E., Lohmann, E., Cuyvers, E., et al. (2014). TREM2 mutations implicated in neurodegeneration impair cell surface transport and phagocytosis. *Sci. Transl. Med.* 6:243ra286. doi: 10.1126/scitranslmed.3009093
- Kobayashi, M., Konishi, H., Sayo, A., Takai, T., and Kiyama, H. (2016). TREM2/DAP12 Signal Elicits Proinflammatory Response in Microglia and Exacerbates Neuropathic Pain. *J. Neurosci.* 36, 11138–11150. doi: 10.1523/jneurosci.1238-16.2016
- Kober, D. L., Alexander-Brett, J. M., Karch, C. M., Cruchaga, C., Colonna, M., Holtzman, M. J., et al. (2016). Neurodegenerative disease mutations in TREM2 reveal a functional surface and distinct loss-of-function mechanisms. *Elife* 5:e20391. doi: 10.7554/eLife.20391
- Kober, D. L., and Brett, T. J. (2017). TREM2-Ligand Interactions in Health and Disease. *J. Mol. Biol.* 429, 1607–1629. doi: 10.1016/j.jmb.2017.04.004
- Lanier, L. L., Corliss, B. C., Wu, J., Leong, C., and Phillips, J. H. (1998). Immunoreceptor DAP12 bearing a tyrosine-based activation motif is involved in activating NK cells. *Nature* 391, 703–707. doi: 10.1038/35642
- Lessard, C. B., Malnik, S. L., Zhou, Y., Ladd, T. B., Cruz, P. E., Ran, Y., et al. (2018). High-affinity interactions and signal transduction between Abeta oligomers and TREM2. *EMBO Mol. Med.* 10:e9027. doi: 10.15252/emmm.201809027
- Leyns, C. E. G., Ulrich, J. D., Finn, M. B., Stewart, F. R., Koscal, L. J., Remolina Serrano, J., et al. (2017). TREM2 deficiency attenuates neuroinflammation and protects against neurodegeneration in a mouse model of tauopathy. *Proc. Natl. Acad. Sci. U.S.A.* 114, 11524–11529. doi: 10.1073/pnas.1710311114
- Li, C., Zhao, B., Lin, C., Gong, Z., and An, X. (2019). TREM2 inhibits inflammatory responses in mouse microglia by suppressing the PI3K/NF- $\kappa$ B signaling. *Cell Biol. Int.* 43, 360–372. doi: 10.1002/cbin.10975
- Li, J. T., and Zhang, Y. (2018). TREM2 regulates innate immunity in Alzheimer's disease. *J. Neuroinflamm.* 15:107. doi: 10.1186/s12974-018-1148-y
- Licon-Limon, I., Garay-Canales, C. A., Munoz-Paleta, O., and Ortega, E. (2015). CD13 mediates phagocytosis in human monocytic cells. *J. Leukoc. Biol.* 98, 85–98. doi: 10.1189/jlb.2A0914-458R
- Matsumoto, R., Wang, D., Blonska, M., Li, H., Kobayashi, M., Pappu, B., et al. (2005). Phosphorylation of CARMA1 plays a critical role in T Cell receptor-mediated NF- $\kappa$ B activation. *Immunity* 23, 575–585. doi: 10.1016/j.immuni.2005.10.007
- McDonald, D. R., Brunden, K. R., and Landreth, G. E. (1997). Amyloid fibrils activate tyrosine kinase-dependent signaling and superoxide production in microglia. *J. Neurosci.* 17, 2284–2294. doi: 10.1523/jneurosci.17-07-02284.1997
- Mocsa, A., Ruland, J., and Tybulewicz, V. L. (2010). The SYK tyrosine kinase: a crucial player in diverse biological functions. *Nat. Rev. Immunol.* 10, 387–402. doi: 10.1038/nri2765
- N'Diaye, E. N., Branda, C. S., Branda, S. S., Nevarez, L., Colonna, M., Lowell, C., et al. (2009). TREM-2 (triggering receptor expressed on myeloid cells 2) is a phagocytic receptor for bacteria. *J. Cell Biol.* 184, 215–223. doi: 10.1083/jcb.200808080
- Otero, K., Turnbull, I. R., Poliani, P. L., Vermi, W., Cerutti, E., Aoshi, T., et al. (2009). Macrophage colony-stimulating factor induces the proliferation and survival of macrophages via a pathway involving DAP12 and beta-catenin. *Nat. Immunol.* 10, 734–743. doi: 10.1038/ni.1744
- Parhizkar, S., Arzberger, T., Brendel, M., Kleinberger, G., Deussing, M., Focke, C., et al. (2019). Loss of TREM2 function increases amyloid seeding but reduces plaque-associated ApoE. *Nat. Neurosci.* 22, 191–204. doi: 10.1038/s41593-018-0296-9
- Paris, D., Beaulieu-Abdelahad, D., Bachmeier, C., Reed, J., Ait-Ghezala, G., Bishop, A., et al. (2011). Anatabine lowers Alzheimer's Abeta production in vitro and in vivo. *Eur. J. Pharmacol.* 670, 384–391. doi: 10.1016/j.ejphar.2011.09.019
- Park, J. S., Ji, I. J., An, H. J., Kang, M. J., Kang, S. W., Kim, D. H., et al. (2015). Disease-associated mutations of TREM2 alter the processing of N-linked oligosaccharides in the golgi apparatus. *Traffic* 16, 510–518. doi: 10.1111/tra.12264
- Park, J. S., Ji, I. J., Kim, D. H., An, H. J., and Yoon, S. Y. (2016). The Alzheimer's disease-associated R47H variant of TREM2 has an altered glycosylation pattern and protein stability. *Front. Neurosci.* 10:618. doi: 10.3389/fnins.2016.00618
- Peng, Q., Malhotra, S., Torchia, J. A., Kerr, W. G., Coggeshall, K. M., and Humphrey, M. B. (2010). TREM2- and DAP12-dependent activation of PI3K requires DAP10 and is inhibited by SHIP1. *Sci. Signal.* 3:ra38. doi: 10.1126/scisignal.2000500



- Piccio, L., Buonsanti, C., Cella, M., Tassi, I., Schmidt, R. E., Fenoglio, C., et al. (2008). Identification of soluble TREM-2 in the cerebrospinal fluid and its association with multiple sclerosis and CNS inflammation. *Brain* 131, 3081–3091. doi: 10.1093/brain/awn217
- Pollani, P. L., Wang, Y., Fontana, E., Robinette, M. L., Yamanishi, Y., Gilfillan, S., et al. (2015). TREM2 sustains microglial expansion during aging and response to demyelination. *J. Clin. Invest.* 125, 2161–2170. doi: 10.1172/JCI77983
- Ren, M., Guo, Y., Wei, X., Yan, S., Qin, Y., Zhang, X., et al. (2018). TREM2 overexpression attenuates neuroinflammation and protects dopaminergic neurons in experimental models of Parkinson's disease. *Exp. Neurol.* 302, 205–213. doi: 10.1016/j.expneurol.2018.01.016
- Roe, C. M., Fagan, A. M., Grant, E. A., Marcus, D. S., Benzinger, T. L., Mintun, M. A., et al. (2011). Cerebrospinal fluid biomarkers, education, brain volume, and future cognition. *Arch. Neurol.* 68, 1145–1151. doi: 10.1001/archneurol.2011.192
- Sahan-Firat, S., Temiz-Resitoglu, M., Guden, D. S., Senol, S. P., Sari, A. N., Cil, M., et al. (2019). NF-kappaB activation mediates LPS-or zymosan-induced hypotension and inflammation reversed by BAY61-3606, a selective Syk inhibitor, in rat models of septic and non-septic shock. *Clin. Exp. Pharmacol. Physiol.* 46, 173–182. doi: 10.1111/1440-1681.13045
- Sayed, F. A., Telpoukhovskaia, M., Kodama, L., Li, Y., Zhou, Y., Le, D., et al. (2018). Differential effects of partial and complete loss of TREM2 on microglial injury response and tauopathy. *Proc. Natl. Acad. Sci. U.S.A.* 115, 10172–10177. doi: 10.1073/pnas.1811411115
- Schlepckow, K., Kleinberger, G., Fukumori, A., Feederle, R., Lichtenthaler, S. F., Steiner, H., et al. (2017). An Alzheimer-associated TREM2 variant occurs at the ADAM cleavage site and affects shedding and phagocytic function. *EMBO Mol. Med.* 9, 1356–1365. doi: 10.15252/emmm.201707672
- Sirkis, D. W., Aparicio, R. E., and Schekman, R. (2017). Neurodegeneration-associated mutant TREM2 proteins abortively cycle between the ER and ER-Golgi intermediate compartment. *Mol. Biol. Cell* 28, 2723–2733. doi: 10.1091/mbc.E17-06-0423
- So, T., Soroosh, P., Eun, S. Y., Altman, A., and Croft, M. (2011). Antigen-independent signalosome of CARMA1, PKCtheta, and TNF receptor-associated factor 2 (TRAF2) determines NF-kappaB signaling in T cells. *Proc. Natl. Acad. Sci. U.S.A.* 108, 2903–2908. doi: 10.1073/pnas.1008765108
- Sondag, C. M., Dhawan, G., and Combs, C. K. (2009). Beta amyloid oligomers and fibrils stimulate differential activation of primary microglia. *J. Neuroinflamm.* 6:1. doi: 10.1186/1742-2094-6-1
- Song, W., Hooli, B., Mullin, K., Jin, S. C., Cella, M., Ulland, T. K., et al. (2017). Alzheimer's disease-associated TREM2 variants exhibit either decreased or increased ligand-dependent activation. *Alzheimers Dement.* 13, 381–387. doi: 10.1016/j.jalz.2016.07.004
- Song, W. M., Joshita, S., Zhou, Y., Ulland, T. K., Gilfillan, S., and Colonna, M. (2018). Humanized TREM2 mice reveal microglia-intrinsic and -extrinsic effects of R47H polymorphism. *J. Exp. Med.* 215, 745–760. doi: 10.1084/jem.20171529
- Takahashi, K., Rochford, C. D., and Neumann, H. (2005). Clearance of apoptotic neurons without inflammation by microglial triggering receptor expressed on myeloid cells-2. *J. Exp. Med.* 201, 647–657. doi: 10.1084/jem.20041611
- Thornton, P., Sevalle, J., Deery, M. J., Fraser, G., Zhou, Y., Stahl, S., et al. (2017). TREM2 shedding by cleavage at the H157-S158 bond is accelerated for the Alzheimer's disease-associated H157Y variant. *EMBO Mol. Med.* 9, 1366–1378. doi: 10.15252/emmm.201707673
- Turnbull, I. R., Gilfillan, S., Cella, M., Aoshi, T., Miller, M., Piccio, L., et al. (2006). Cutting edge: TREM-2 attenuates macrophage activation. *J. Immunol.* 177, 3520–3524. doi: 10.4049/jimmunol.177.6.3520
- Ulrich, J. D., Ulland, T. K., Colonna, M., and Holtzman, D. M. (2017). Elucidating the Role of TREM2 in Alzheimer's Disease. *Neuron* 94, 237–248. doi: 10.1016/j.neuron.2017.02.042
- Varnum, M. M., Clayton, K. A., Yoshii-Kitahara, A., Yonemoto, G., Koro, L., Ikezu, S., et al. (2017). A split-luciferase complementation, real-time reporting assay enables monitoring of the disease-associated transmembrane protein TREM2 in live cells. *J. Biol. Chem.* 292, 10651–10663. doi: 10.1074/jbc.M116.759159
- Wang, Y., Cella, M., Mallinson, K., Ulrich, J. D., Young, K. L., Robinette, M. L., et al. (2015). TREM2 lipid sensing sustains the microglial response in an Alzheimer's disease model. *Cell* 160, 1061–1071. doi: 10.1016/j.cell.2015.01.049
- Wang, Y., Ulland, T. K., Ulrich, J. D., Song, W., Tzaferis, J. A., Hole, J. T., et al. (2016). TREM2-mediated early microglial response limits diffusion and toxicity of amyloid plaques. *J. Exp. Med.* 213, 667–675. doi: 10.1084/jem.20151948
- Wunderlich, P., Glebov, K., Kemmerling, N., Tien, N. T., Neumann, H., and Walter, J. (2013). Sequential proteolytic processing of the triggering receptor expressed on myeloid cells-2 (TREM2) protein by ectodomain shedding and gamma-secretase-dependent intramembranous cleavage. *J. Biol. Chem.* 288, 33027–33036. doi: 10.1074/jbc.M113.517540
- Xie, Y., Guo, H., Wang, L., Xu, L., Zhang, X., Yu, L., et al. (2017). Human albumin attenuates excessive innate immunity via inhibition of microglial Mincle/Syk signaling in subarachnoid hemorrhage. *Brain Behav. Immun.* 60, 346–360. doi: 10.1016/j.bbi.2016.11.004
- Yeh, F. L., Hansen, D. V., and Sheng, M. (2017). TREM2, microglia, and neurodegenerative diseases. *Trends Mol. Med.* 23, 512–533. doi: 10.1016/j.molmed.2017.03.008
- Yeh, F. L., Wang, Y., Tom, I., Gonzalez, L. C., and Sheng, M. (2016). TREM2 binds to apolipoproteins, including APOE and CLU/APOJ, and thereby facilitates uptake of amyloid-beta by microglia. *Neuron* 91, 328–340. doi: 10.1016/j.neuron.2016.06.015
- Yoshiyama, Y., Higuchi, M., Zhang, B., Huang, S. M., Iwata, N., Saido, T. C., et al. (2007). Synapse loss and microglial activation precede tangles in a P301S tauopathy mouse model. *Neuron* 53, 337–351. doi: 10.1016/j.neuron.2007.01.010
- Yu, S., Huang, H., Iliuk, A., Wang, W. H., Jayasundera, K. B., Tao, W. A., et al. (2013). Syk inhibits the activity of protein kinase A by phosphorylating tyrosine 330 of the catalytic subunit. *J. Biol. Chem.* 288, 10870–10881. doi: 10.1074/jbc.M112.426130
- Yuan, P., Condello, C., Keene, C. D., Wang, Y., Bird, T. D., Paul, S. M., et al. (2016). TREM2 haploinsufficiency in mice and humans impairs the microglia barrier function leading to decreased amyloid compaction and severe axonal dystrophy. *Neuron* 92, 252–264. doi: 10.1016/j.neuron.2016.09.016
- Zeng, K. W., Wang, S., Dong, X., Jiang, Y., Jin, H. W., and Tu, P. F. (2014). Sesquiterpene dimmer (DSF-27) inhibits the release of neuroinflammatory mediators from microglia by targeting spleen tyrosine kinase (Syk) and Janus kinase 2 (Jak2): two major non-receptor tyrosine signaling proteins involved in inflammatory events. *Toxicol. Appl. Pharmacol.* 275, 244–256. doi: 10.1016/j.taap.2014.01.014
- Zhao, Y., Wu, X., Li, X., Jiang, L. L., Gui, X., Liu, Y., et al. (2018). TREM2 is a receptor for beta-amyloid that mediates microglial function. *Neuron* 97, 1023.e7–1031.e7. doi: 10.1016/j.neuron.2018.01.031
- Zhong, L., Chen, X. F., Wang, T., Wang, Z., Liao, C., Huang, R., et al. (2017a). Soluble TREM2 induces inflammatory responses and enhances microglial survival. *J. Exp. Med.* 214, 597–607. doi: 10.1084/jem.20160844
- Zhong, L., Zhang, Z. L., Li, X., Liao, C., Mou, P., Wang, T., et al. (2017b). TREM2/DAP12 complex regulates inflammatory responses in microglia via the JNK signaling pathway. *Front. Aging Neurosci.* 9:204. doi: 10.3389/fnagi.2017.00204
- Zhong, L., Chen, X. F., Zhang, Z. L., Wang, Z., Shi, X. Z., Xu, K., et al. (2015). DAP12 Stabilizes the C-terminal fragment of the triggering receptor expressed on myeloid cells-2 (TREM2) and protects against lps-induced pro-inflammatory response. *J. Biol. Chem.* 290, 15866–15877. doi: 10.1074/jbc.M115.645986
- Zhong, L., Wang, Z., Wang, D., Martens, Y. A., Wu, L., Xu, Y., et al. (2018). Amyloid-beta modulates microglial responses by binding to the triggering receptor expressed on myeloid cells 2 (TREM2). *Mol. Neurodegener.* 13:15. doi: 10.1186/s13024-018-0247-7

**Conflict of Interest:** The authors declare that the research was conducted in the absence of any commercial or financial relationships that could be construed as a potential conflict of interest.

Copyright © 2019 Yao, Coppola, Schweig, Crawford, Mullan and Paris. This is an open-access article distributed under the terms of the Creative Commons Attribution License (CC BY). The use, distribution or reproduction in other forums is permitted, provided the original author(s) and the copyright owner(s) are credited and that the original publication in this journal is cited, in accordance with accepted academic practice. No use, distribution or reproduction is permitted which does not comply with these terms.





# Maresin 1 Improves Cognitive Decline and Ameliorates Inflammation in a Mouse Model of Alzheimer's Disease

Ping Yin<sup>1,2†</sup>, Xu Wang<sup>1†</sup>, Shuang Wang<sup>1</sup>, Yafen Wei<sup>1,2</sup>, Jiachun Feng<sup>1\*</sup> and Mingqin Zhu<sup>1\*</sup>

<sup>1</sup> Department of Neurology and Neuroscience Center, The First Hospital of Jilin University, Changchun, China, <sup>2</sup> Department of Neurology, Heilongjiang Provincial Hospital, Harbin, China

## OPEN ACCESS

### Edited by:

Rocío Martínez De Pablos,  
University of Seville, Spain

### Reviewed by:

Shafiq Ur. Rehman,  
Gyeongsang National University,  
South Korea  
Antonio Boza Serrano,  
Lund University, Sweden

### \*Correspondence:

Jiachun Feng  
fjcfank@qq.com  
Mingqin Zhu  
mingqin.zhu@hotmail.com

<sup>†</sup>These authors have contributed  
equally to this work

### Specialty section:

This article was submitted to  
Cellular Neuropathology,  
a section of the journal  
Frontiers in Cellular Neuroscience

**Received:** 09 May 2019

**Accepted:** 30 September 2019

**Published:** 15 October 2019

### Citation:

Yin P, Wang X, Wang S, Wei Y,  
Feng J and Zhu M (2019) Maresin 1  
Improves Cognitive Decline  
and Ameliorates Inflammation in a  
Mouse Model of Alzheimer's Disease.  
Front. Cell. Neurosci. 13:466.  
doi: 10.3389/fncel.2019.00466

Alzheimer's disease (AD) is one of the most common neurodegenerative disease. Accumulating evidences suggest an active role of inflammation in the pathogenesis of AD. Inflammation resolution is an active process that terminates inflammation and facilitates the restoration of inflamed tissue to homeostasis. Resolution of inflammation has been shown to be conducted by a group of specialized pro-resolving lipid mediators (SPMs) including lipoxins, resolvins, protectins, and maresins (MaRs). Recent studies have demonstrated that failure of inflammation resolution can lead to chronic inflammation and, hence, contribute to AD progression. We have previously shown that MaR1 can improve neuronal survival and increase microglial phagocytosis of A $\beta$ . However, the effects of MaR1 on animal models of AD have not been reported. In this study, we aim to investigate the effects of MaR1 on behavioral deficits and pathological changes in a mouse model of AD. Mice received bilateral injections of A $\beta$ <sub>42</sub> protein into the hippocampus, followed by administration of MaR1 by intra-cerebroventricular injection. The behavioral changes in the mice were analyzed using Morris water maze. Immunohistochemistry, Fluoro-Jade B (FJB) staining, cytometric beads array (CBA), and western blot analysis were used to demonstrate molecular changes in the mice hippocampus and cortex. Our results showed that MaR1 treatment significantly improved the cognitive decline, attenuated microglia and astrocyte activation. In addition, we found that MaR1 decreased the pro-inflammatory cytokines TNF- $\alpha$ , IL-6, and MCP-1 production induced by A $\beta$ <sub>42</sub> and increased the anti-inflammatory cytokines IL-2, IL-10 secretion with or without A $\beta$ <sub>42</sub> stimulation. Moreover, western blot results showed that MaR1 up-regulated the levels of proteins related to survival pathway including PI3K/AKT, ERK and down-regulated the levels of proteins associated with inflammation, autophagy, and apoptosis pathways such as p38, mTOR and caspase 3. To conclude, MaR1 improved the cognitive decline, ameliorated pro-inflammatory glia cells activation via improving survival, enhancing autophagy, inhibiting inflammation and apoptosis pathways. In conclusion, this study shows that inflammation resolution may be a potential therapeutic target for AD.

**Keywords:** Alzheimer's disease, resolution of inflammation, maresin 1, neuroinflammation, memory

## INTRODUCTION

Alzheimer's disease (AD) is the most common cause of dementia, with no existing treatment that can significantly delay or reverse AD-associated cognitive decline or pathological changes. The gross histopathology of AD is characterized by brain atrophy, deepening of the cerebral grooves and the enlargement of the cerebral ventricles. Histologically, AD is characterized by extracellular deposition of amyloid- $\beta$  (A $\beta$ ), intracellular accumulation of neurofibrillary tangles (NFTs) (Alzheimer et al., 1995), and chronic inflammation (McGeer et al., 1987, 1988; Griffin et al., 1989; Cacabelos et al., 1994). A $\beta$  has been considered as a main culprit of AD, and the A $\beta$  hypothesis has been dominant for explaining the pathogenesis of AD (Hardy, 2009). There is a plethora of evidence that support the A $\beta$  hypothesis: patients with an extra copy of chromosome 21, where the APP gene locates, develop dementia at an early age; APP transgenic mice exhibit significant cognitive impairment; the toxicity of A $\beta$  has been documented extensively in *in vitro* studies (Del Bo et al., 1995; Combs et al., 2001; Wicklund et al., 2010). Results from genetic studies have shown an association of inflammation-related genes with AD (Griciuc et al., 2013). Further, microglia activation as well as elevated pro-inflammatory mediators observed in postmortem AD brains and in AD mice models support that chronic inflammation is an integral part of AD pathogenesis (Heppner et al., 2015). Inflammation resolution is an active regulatory process in the end stage of inflammatory reaction that can terminate inflammation and initiate repair of damaged tissues rather than passive disappearance of inflammatory mediators as previously believed (Serhan, 2017). Inflammation resolution is mediated by a group of lipid mediators called specialized pro-resolving lipid mediators (SPMs) including lipoxins (LXs), resolvins (Rvs), protectins (NPDs), and maresins (MaRs), all of which are biosynthesized from polyunsaturated fatty acids (PUFAs) via cyclooxygenases (COXs) and lipoxygenases (LOXs) (Serhan, 2014). In humans, studies have found that reduced SPMs lead to failure of inflammation resolution that can contribute to chronic inflammation diseases such as atherosclerosis (Fredman et al., 2016), dry eye pathogenesis (Gao et al., 2015) as well as AD (Wang et al., 2015).

Evidences from recent studies demonstrate that inflammation resolution is impaired in AD and stimulation of inflammation resolution showed beneficial effects in AD related *in vivo* and *in vitro* models (Wang et al., 2015; Zhu et al., 2016). The conversion from dietary FAs to  $\omega$ -3 FAs, which are precursors of SPMs has been reported to be decreased in the liver of AD patients (Kang and Rivest, 2012). Accordingly, we have previously found that the levels of SPMs were lower in different areas of the postmortem AD brains including the hippocampus and the entorhinal cortex (Lukiw et al., 2005; Wang et al., 2015). Interestingly, results from clinical trials using PUFAs to treat AD patients showed that  $\omega$ -3 FAs treatment has beneficial effects only on the patients with mild cognitive impairment (MCI) (Yurko-Mauro et al., 2010) but not on late stage AD patients. Therefore, it is plausible that SPMs are the effective factors mediating the protective effects of  $\omega$ -3 FAs, however, the conversion from

FAs to SPMs is decreased in late stage AD patients. Hence, we hypothesized that SPMs treatment is more effective for AD patients. Afterward, we tested this hypothesis on AD related cellular models including neuronal and microglia models and observed that all the types of SPMs could improve neuronal survival, and MaR1 was more effective in microglial phagocytosis of amyloid- $\beta$ (A $\beta$ )<sub>42</sub> (Zhu et al., 2016), indicating that inducing inflammation resolution by SPMs especially by MaR1 could be a novel therapeutic strategy for AD. MaR1 synthesis is initiated by the 14-lipoxygenation of DHA to yield 14S-hydro(peroxy)-4Z,7Z,10Z,12E,14S,16Z,19Z-docosahexaenoic acid and then to 13S, 14S-e MaR. This intermediate is then enzymatically hydrolyzed to MaR1 (Deng et al., 2014; Dalli et al., 2016). The biological functions of MaR1 have been showed in various disease models: MaR1 has to stimulate the pro-inflammatory M1 to anti-inflammatory M2 macrophage phenotype shifts and tissue regenerative actions of MaR1 have also been reported (Dalli et al., 2013). Moreover, MaR1 has been reported suppressed oxidative stress in a left pulmonary hilum I/R mouse model (Sun et al., 2017).

However, the effects of MaR1 on AD animal models have not been studied, and the mechanisms underlying the protective effects of MaR1 remain less understood. The aim of this study was to investigate the effects of MaR1 on behavioral deficits and pathological changes induced by intra-hippocampal injection of A $\beta$ <sub>42</sub> protein in a mouse model along with the molecular mechanisms of action of MaR1.

## MATERIALS AND METHODS

### Animals

Forty C57BL/6 mice (male, 3–4 months old, weight 26–31 g) were obtained from animal experiment center of Jilin University. The animals were housed at controlled room temperature (22  $\pm$  2°C) and humidity (50–60%) under a 12h:12h light-dark cycle. Free access to water and food was provided. All procedures used in the present study followed the “National Institutes of Health Guide for Care and Use of Laboratory Animals” (Publication No. 85–23, revised 1985) and were approved by the Animal Ethics Committee of Jilin University. Efforts were also made to minimize animal suffering and to reduce the number of animals used.

### A $\beta$ <sub>42</sub> and MaR1 Preparation

A $\beta$ <sub>42</sub> (Abcam, United Kingdom, ab120301) was prepared as a stock solution at a final concentration of 1 mg/ml in sterile 0.1 M phosphate-buffered saline (PBS), and aliquots were stored at –20°C. A $\beta$ <sub>42</sub> solution was aggregated by incubation at 37°C for 4 days before use. MaR1 (Cayman Chemical, United States) was dissolved in alcohol at the concentration of 0.1  $\mu$ g/ $\mu$ l and was further diluted with PBS to 0.01  $\mu$ g/ $\mu$ l solution before use.

### Primary Culture of Microglia

Mouse brain mixed glial cells were prepared from whole brains of 1–3 day postnatal C57BL/6/J mice and dissociated with a mild mechanical trituration. Cells were seeded in the cell culture

bottles (75 cm<sup>2</sup>) pre-coated with poly-D-lysine. The culture medium was DMEM-High glucose supplemented with 10% fetal bovine serum, 1% penicillin/streptomycin (all from Life Sciences, United States) and 0.8% insulin. Microglia were further extracted from the mixed glial cell cultures by mild trypsinization digestion method as previously described (Saura et al., 2003).

## HT22 Cell Culture

HT22 mouse hippocampal neuronal cell line were cultured at 37°C in Dulbecco's modified Eagle's medium (DMEM) supplied with 10% fetal bovine serum (FBS) and antibiotic solution (100 U/ml penicillin, 0.1 mg/ml streptomycin) in a humidified atmosphere in the presence of 5% CO<sub>2</sub> until they reached confluence, when reached 90% confluence, cells were subcultured after treatment with 0.25% trypsin-EDTA mixture.

## Cell Viability Assay

Cell Counting Kit-8 (CCK-8, meilunbio) was used to assess the viability of HT22 neuronal cell and microglia. Cells were seeded in 96-well plates and cultured for 24 h (5000/well). After treatment with different concentrations of MaR1 (0.005 μM MaR1, 0.05 μM MaR1, 0.5 μM MaR1) for 6 h, 10 μL CCK-8 solution were added into each well. The optical density values were measured by microplate reader (Bio-Rad iMark) at 490 nm.

## Stereotaxic Intra-Hippocampal Aβ42 Injection and Drug Treatments

Mice were randomly divided into 4 groups: (1) Vehicle group ( $n = 10$ ): bilateral injections of 1 μl PBS in the hippocampus and intra-cerebroventricular injection of 1 μl solvent of MaR1; (2) Aβ42 group ( $n = 10$ ): bilateral hippocampal injections of 1 μl Aβ42 solution and intra-cerebroventricular injection of 1 μl solvent of MaR1; (3) MaR1 group ( $n = 10$ ): bilateral hippocampal injections of 1 μl PBS and intra-cerebroventricular injection of 1 μl MaR1 solution; and (4) Aβ42 + MaR1 group ( $n = 10$ ): bilateral hippocampal injections of 1 μl Aβ42 solution and intra-cerebroventricular injection of 1 μl MaR1 solution.

Mice were anesthetized with isoflurane and the heads were fixed on a stereo locator. A volume of 1 μl of MaR1 solution or MaR1 solvent was injected into the ventricle of mouse brains at the following stereotaxic coordinates using a microsyringe: anteroposterior, −0.3 mm from bregma; mediolateral, +1.00 mm from midline; and dorsoventral, −2.2 mm from dura. The needle was removed after 20 min using three intermediate steps with a 1 min inter-step delay to minimize backflow.

Then, the same procedure was used for bilateral hippocampal injections of Aβ42. A volume of 1 μl of Aβ42 solution or PBS was injected into each side at the following stereotaxic coordinates: anteroposterior, −2.46 mm from bregma; mediolateral, ±1.5 mm from midline; and dorsoventral, −2.0 mm from dura. The needle was removed after 5 min. Mice were placed on a thermal pad (32–33°C) till they were awake.

## Morris Water Maze (MWM) Test

To assess the memory and spatial learning ability of mice, MWM test was conducted 7 days after Aβ42 and MaR1

administration. The experimental apparatus consisted of a circular tank (diameter = 100 cm, height = 50 cm) that was divided into four quadrants. It was filled with water and was maintained at 22 ± 2°C. A platform (diameter = 9 cm) was placed in the pool approximately 1.0 cm below the surface of the water in one of the four quadrants. On the four sides of MWM apparatus, different shapes of visual cues were placed on the inside wall of the pool in a diagonal pattern. A non-toxic white food additive titanium dioxide was added to the water in the pool to contrast with the mice color. We used tracking software (Viewer 2 Tracking Software, Ji Liang Instruments, China) to monitor and record each trial. The MWM paradigm consisted of four 90 s trials per day for 5 consecutive days followed by the probe test on the sixth day. At the end of each trial, the mice were dried with a dry cloth and returned back to the home cages, which were kept on a thermal pad. The interval between each trial for a mouse was more than 30 min. For each trial, starting position was different and the mice were allowed to swim while being tracked by the software. The trial ended when the animal reached the platform or when 90 s had elapsed. If the mouse did not reach the platform, it was directed and placed onto the platform for 10 s. A 90 s probe trial was performed on the sixth day to determine memory retention. For this single trial, the submerged platform was removed and each mouse was placed into the quadrant opposite to the quadrant that formerly contained the platform. The number of platform crossing, the time spent in the quadrant containing the platform previously, and escape latency were recorded.

## Immunohistochemistry

Mice were deeply anesthetized with isoflurane and were sacrificed 1 day after they took MWM test. The brains were harvested, fixed in paraformaldehyde, and then saturated with increasing sucrose concentrations (10%, 20%, 30%) in PBS. Brains were frozen and sectioned coronally at 10 μm thickness using a microtome. Fixed sections were incubated at room temperature for 1 h in 5% normal goat serum in PBS, followed by overnight incubation at 4°C with Iba-1 antibody (1:100; Abcam, ab178847) for microglia and GFAP antibody (1:300; Cell Signaling, 3670) for astrocytes. Thereafter, the sections were washed three times with PBS and incubated for 1 h with Goat Anti-Rabbit IgG (1:500; Abcam, ab150080) and Goat Anti-Mouse IgG (1:500; Abcam, ab150113). Sections were then rinsed with PBS three times. For nucleus labeling, the sections were incubated with DAPI (1:1000; Beyotime, C1006). Positive cells were quantified under a Laser scanning confocal microscope in stained sections in the hippocampus and cortex.

ImageJ software (NIH, Bethesda, MD, United States) was used to measure Iba-1 and GFAP immune-positive staining in the CA1 region and cortex. Four sections per brain were analyzed, and multiple images were taken within each section to cover the CA1 region and cortex. Threshold was equally adjusted across all brain sections to highlight the stained area, and particles were analyzed to determine the total stained area. Results were expressed as total area stained per total area analyzed (area fraction).

## Fluoro-Jade B (FJB) Staining

Prior to immunostaining, fixed sections described above were mounted onto slides from distilled water and then air-dried for at least 30 min on a slide warmer at 50°C. Then, the tissue sections were immersed in a basic alcohol solution of 1% sodium hydroxide in 80% ethanol for 5 min. They were then rinsed in 70% ethanol for 2 min, followed by distilled water for 2 min, and then incubated in 0.06% potassium permanganate solution for 10 min. After a water rinse for 1–2 min, the slides were then transferred to a 0.0004% solution of Fluoro-Jade B (EMD Millipore, United States) dissolved in 0.1% acetic acid for 20 min. The slides were then rinsed thrice in distilled water, ensuring that each rinse lasted for 1 min. The slides were dried by paper towel and then air-dried on a slide at 50°C for at least 5 min. The air-dried slides were then immersed in xylene for at least 1 min and coverslipped using DPX mounting medium. FJB-positive cells were quantified under a microscope (Olympus BX51, Japan) in stained sections in the hippocampus and cortex. Four sections per animal were viewed. Results were expressed as the number of FJB positive cells per section.

## Tissue Processing for Western Blot and Cytometric Beads Array (CBA)

For western blot and CBA, anesthetized mice were subjected to cervical dislocation, the hippocampus and cortex were dissected out and immediately frozen in liquid nitrogen. Proteins were extracted in 10X volume/weight with radio-immuno precipitation assay (RIPA) buffer, supplemented with 1% protease inhibitor cocktail and 1% phosphatase inhibitor cocktail (Sigma-Aldrich, United States), and centrifuged at 12,000 rpm at 4°C for 20 min. The supernatant was collected and stored for further analyses.

## Cytometric Beads Array (CBA)

The levels of tumor necrosis factor (TNF)- $\alpha$ , interleukin (IL)-2, IL-4, IL-6, IL-10, Interferon (IFN)- $\gamma$  and IL-17A in the hippocampus and cortex tissues were analyzed by CBA (BD Biosciences, United States) according to the manufacturer's manual. Cytokine levels were then quantified using flow cytometry.

## Enzyme-Linked Immunosorbent Assay (ELISA)

The cortex and hippocampus of mice were homogenized with 10X volume/weight normal saline. The levels of monocyte chemoattractant protein (MCP)-1 were measured by ELISA kit (Shanghai Yuan-ye Bioengineering Institute, China) according to the manufacturer's manual.

## Western Blot

Analysis of proteins by western blot was performed using proteins extracted from the hippocampus. Total protein concentration was determined by a BCA assay kit. Briefly, samples containing 40  $\mu$ g protein each were mixed with an equal volume of 2X Laemmli sample buffer, and were boiled at 95°C for 5 min. The denatured samples were then loaded on a

10% SDS-PAGE gel, after which the proteins were transferred to a nitrocellulose membrane under 85 mA current overnight at 4°C. The membranes were blocked with 5% non-fatty dry milk at room temperature for 45 min, and then incubated with the following antibodies: anti-actin (1:2500; Abcam, ab8224), anti-LaminA (1:1000; Abcam, ab26300), Anti-GAPDH (1:10000; Abcam, ab181602), anti-phospho-PI3K (1:1000; Abcam, ab182651), anti-PI3K (1:1000; Abcam, ab191606), anti-phospho-AKT (1:5000; Abcam, ab81283), anti-AKT (1:2000; Abcam, ab28422), anti-phospho-p38 (1:1000; Abcam, ab195049), anti-p38 (1:2000; Abcam, ab170099), anti-phospho-ERK1 + ERK2 (1:1000; Abcam, ab201015), anti-ERK1 + ERK2 (1:10000; Abcam, ab184699), anti-caspase 3 (1:5000; Abcam, ab184737), anti-phospho-mTOR (1:1000; Cell signaling, 2971), anti-mTOR (1:1000; Cell signaling, 2972), anti-LC3B (1:3000; Abcam, ab51520), Anti-SQSTM1/p62 (1:500; Abcam, ab56416) Anti-Beclin 1 (1:2000; Abcam, ab62557), in Tris-buffered saline with 0.1% Tween 20 (TBS-T) at 4°C overnight. After incubation with appropriate secondary antibody, the antigen-antibody complexes were visualized with the ECL chemiluminescence system (Amersham, United Kingdom). The relative densities of bands were analyzed using the ImageJ software.

## Statistical Analysis

All values are expressed as the mean  $\pm$  SEM. Normal distributions and homogeneity of variance were found for all analyzed categories. All statistical analyses were conducted using GraphPad Prism 7 software (GraphPad Software, La Jolla, CA, United States). Independent *t*-test was used to compare between the two groups, and one-way-ANOVA was used in multi-group pairwise comparison. In all instances, statistical significance was defined as follows: \**P* < 0.05, \*\**P* < 0.01, \*\*\**P* < 0.001.

## RESULTS

### MaR1 Ameliorated A $\beta$ 42 Protein-Induced Cognitive Decline

The escape latency for all the groups gradually decreased during 5 consecutive training days, as indicated by **Figures 1A,B**. Differences gradually became larger in the mean latency between the 4 groups. On the fifth day, the escape latency of A $\beta$ 42 group was significantly longer than that of Vehicle group (*P* < 0.05), and the escape latency of A $\beta$ 42 + MaR1 group was significantly shorter than that of A $\beta$ 42 group (*P* < 0.05). There was no significant difference in escape latency between Vehicle group and MaR1 group. In the probe test, the number of platform crossing and the time spent in the target quadrant by the A $\beta$ 42 group were significantly less than those in Vehicle group (*P* < 0.001), and the number of platform crossing and the time spent in the target quadrant by the A $\beta$ 42 + MaR1 group were more than those in A $\beta$ 42 group (*P* < 0.05). There was no significant difference between Vehicle group and MaR1 group in the platform crossing and the time spent in the target quadrant (**Figures 1C,D**).



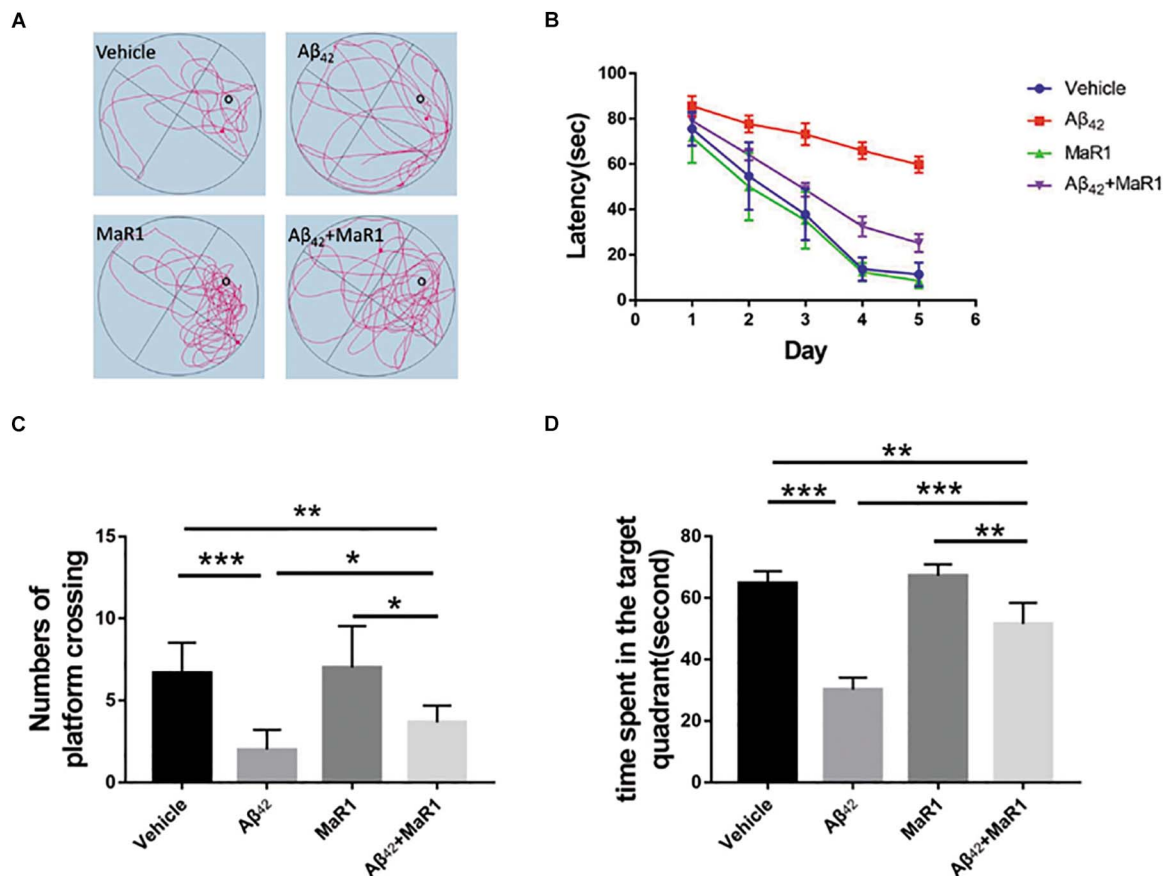


**FIGURE 1 |** MaR1 improved learning and memory deficits in Aβ<sub>42</sub> treated mice. **(A)** Typical swimming tracks of the four groups on the sixth day after drug treatment. **(B)** Escape latency gradually decreased with time in all the four groups. On the sixth day after drug treatment, Aβ<sub>42</sub> treatment group showed significantly increased escape latency compared to Vehicle group, however, Aβ<sub>42</sub> + MaR1 treatment reversed the changes induced by Aβ<sub>42</sub> ( $P < 0.05$ ). **(C)** Numbers of platform crossing on the sixth day after drug treatment in probe test. Aβ<sub>42</sub> treatment significantly decreased the number of platform crossing compared to Vehicle group, while Aβ<sub>42</sub> + MaR1 treatment attenuated the changes induced by Aβ<sub>42</sub> ( $P < 0.05$ ). **(D)** Time spent in the target quadrant in the probe test on the sixth day after drug treatment. Aβ<sub>42</sub> treatment significantly decreased the time spent in the target quadrant compared to Vehicle group, while Aβ<sub>42</sub> + MaR1 treatment attenuated the changes induced by Aβ<sub>42</sub> ( $P < 0.001$ ). Data are expressed as mean  $\pm$  SEM, 10 mice in each group, and statistical significance is defined as follows: \* $P < 0.05$ , \*\* $P < 0.01$ , \*\*\* $P < 0.001$ .

## MaR1 Attenuated Neuronal Degeneration and Glia Activation in the Hippocampus and Cortex of Mice Treated With Aβ<sub>42</sub>

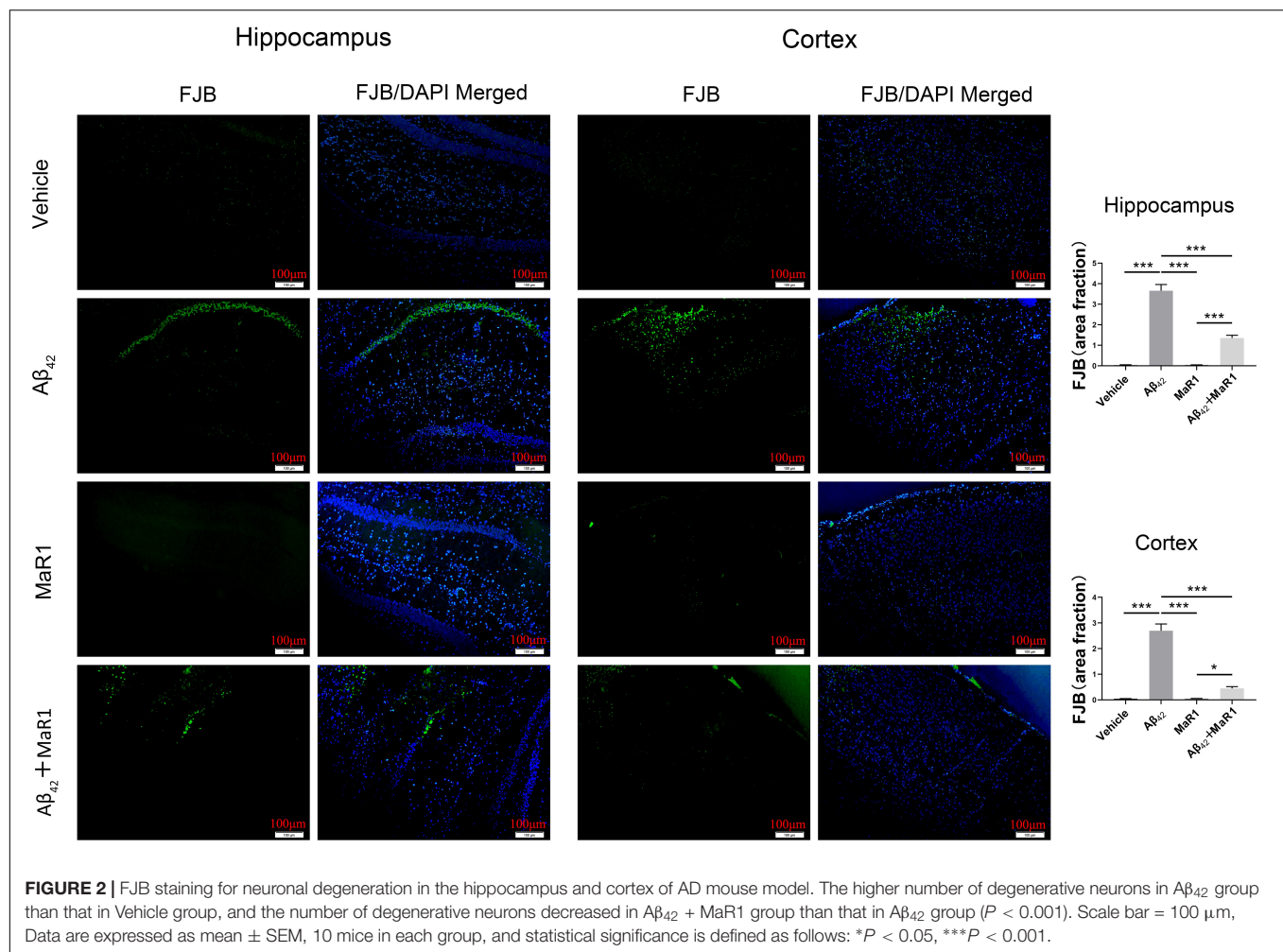
Neurodegenerative neurons were revealed by FJB staining (Figure 2). In the hippocampus and cortex, the number of degenerative neurons in Aβ<sub>42</sub> group was more than that in Vehicle group ( $P < 0.001$ ), while the number of degenerative neurons in Aβ<sub>42</sub> + MaR1 group was less than that in Aβ<sub>42</sub> group ( $P < 0.001$ ). No significant difference was observed in the number of degenerative neurons between Vehicle group and MaR1 group.

Iba-1 and GFAP were used to demonstrate microglia and astrocytes, respectively (Figure 3). In the hippocampus and cortex, the percentage of area with Iba-1 and GFAP positive staining cells in Aβ<sub>42</sub> group was higher than that in Vehicle group ( $P < 0.001$ ), and the percentage of area with Iba-1 and GFAP positive staining cells in Aβ<sub>42</sub> + MaR1 group was lower than that in Aβ<sub>42</sub> group ( $P < 0.001$ ). There was no significant difference in

the percentage of area with Iba-1 or GFAP positive staining cells between Vehicle group and MaR1 group.

## MaR1 Reduced Pro-inflammatory Cytokine and Chemokine Production and Increased Anti-inflammatory Cytokine Production

The production of different cytokines was examined to further investigate the effect of MaR1 on neuroinflammation in AD. The levels of TNF-α, IL-6 and MCP-1 in Aβ<sub>42</sub> group were significantly higher than those in Vehicle group ( $P < 0.05$ ), while treatment of Aβ<sub>42</sub> + MaR1 significantly decreased the levels of TNF-α, IL-6 and MCP-1 induced by Aβ<sub>42</sub> ( $P < 0.05$ ). There was no significant difference in TNF-α, IL-6 and MCP-1 between Vehicle group and MaR1 group (Figures 4A–F). The levels of IL-2 and IL-10 in Aβ<sub>42</sub> group were significantly higher than those in Vehicle group in the hippocampus and cortex ( $P < 0.05$ );



MaR1 treatment increased the production of IL-2 and IL-10 in the hippocampus ( $P < 0.05$ ); the levels of IL-2 and IL-10 in Aβ<sub>42</sub> + MaR1 group were higher than those in Vehicle group in the cortex but not in the hippocampus ( $P < 0.05$ ) (Figures 4G–J). No difference was observed in the levels of IL-4, IFN-γ and IL-17A among the four groups (data not shown).

### MaR1 Exerted Neuroprotection and Suppressed Neuroinflammation by Modulating Autophagy, Apoptosis, and MAPK Signal Pathways

Compared with Vehicle group, the ratio of p-PI3K/t-PI3K and p-AKT/t-AKT were down-regulated (Figures 5A,B), while the ratio of p-mTOR/t-mTOR, p-p38/t-p38, as well as the levels of caspase 3 were up-regulated in Aβ<sub>42</sub> group ( $P < 0.01$ ) (Figures 5C–E), however, these Aβ<sub>42</sub> induced changes were reversed by Aβ<sub>42</sub> + MaR1 treatment ( $P < 0.05$ ). The ratio of p-ERK/t-ERK was increased by both, Aβ<sub>42</sub> ( $P < 0.001$ ) and MaR1 ( $P < 0.01$ ) alone, and was further increased by their co-stimulation as compared to Vehicle group ( $P < 0.01$ ) and Aβ<sub>42</sub> group ( $P < 0.05$ ) (Figure 5F).

### MaR1 Exerted Neuroprotection and Suppressed Neuroinflammation by Modulating Autophagy Signal Pathways

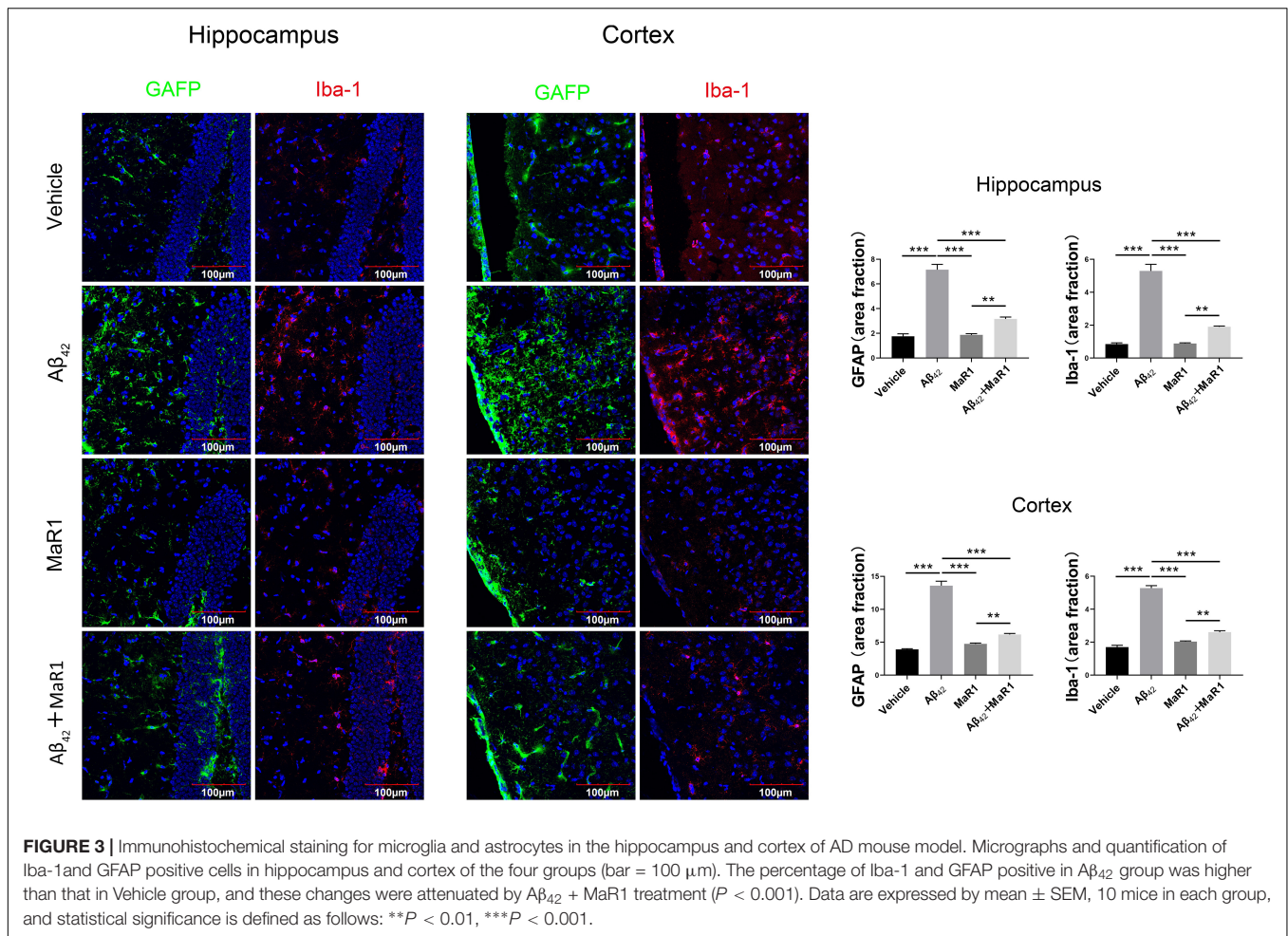
Compared with Vehicle and MaR1 group, the ratio of LC3-II/LC3-I was down-regulated ( $P < 0.01$ ,  $P < 0.05$ ), while the levels of p62 was up-regulated in Aβ<sub>42</sub> group ( $P < 0.01$ ), however, these Aβ<sub>42</sub> induced changes were reversed by Aβ<sub>42</sub> + MaR1 treatment ( $P < 0.01$ ). Compared with MaR1 group, the level of Beclin-1 was decreased in Aβ<sub>42</sub> group ( $P < 0.01$ ), and increased by Aβ<sub>42</sub> + MaR1 treatment ( $P < 0.01$ ) (Figure 6).

### In vitro Cytotoxicity Analysis

The cell proliferation rate was at a normal level in HT22 neuronal cell and microglia after MaR1 treatment. There was no significant difference in cell proliferation after treatment with different MaR1 concentrations (Figure 7).

## DISCUSSION

We have previously showed that inflammation resolution is impaired in the AD brains and stimulating resolution



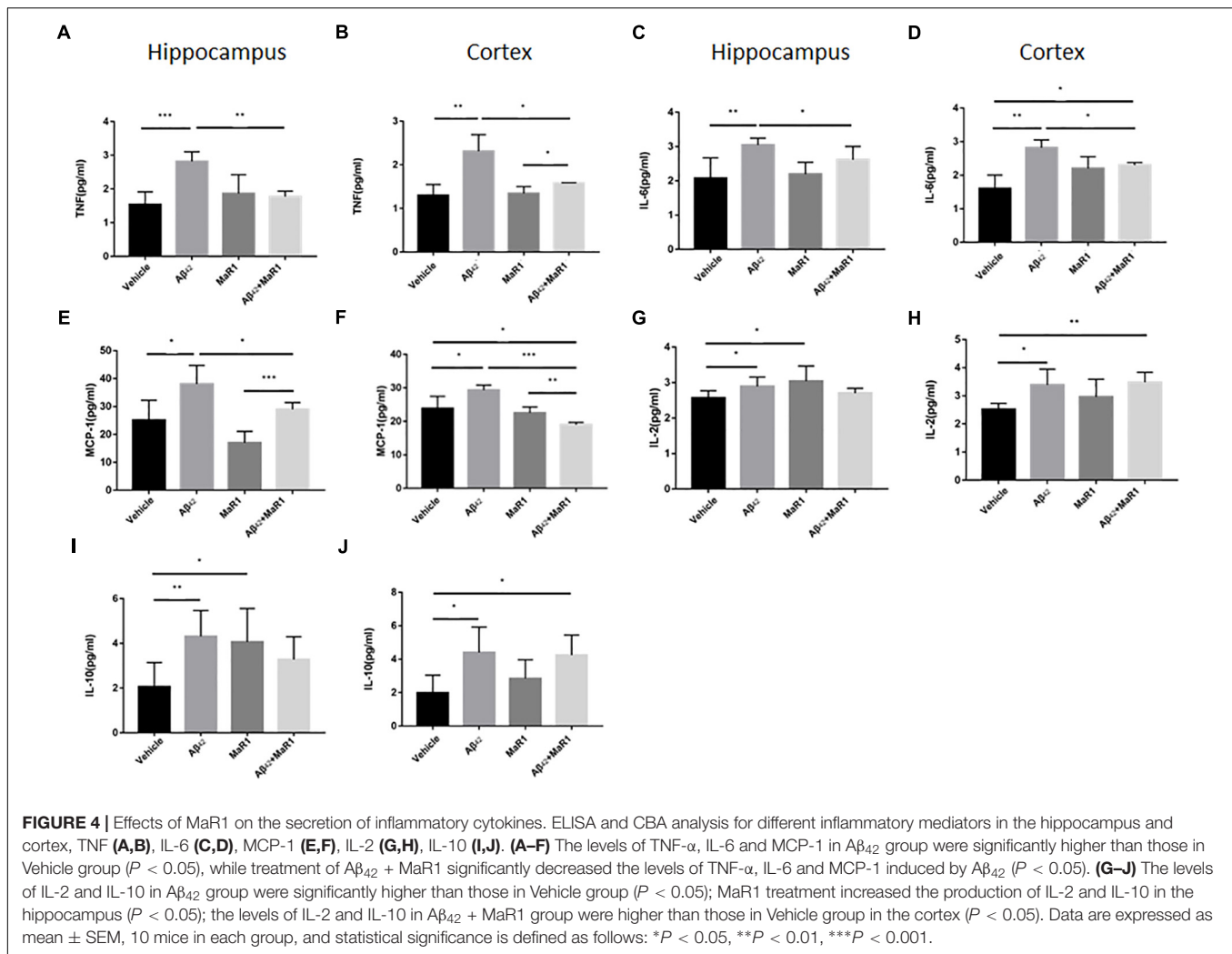
of inflammation by SPMs has proved to be beneficial in cellular models of AD, therefore, indicating that resolution of inflammation by SPMs may be a potential therapeutic target for AD (Wang et al., 2015; Zhu et al., 2016). Aspirin-triggered LXA4 (ATL) has been shown to alleviate AD related pathological changes and improve the cognitive impairment in AD animal models (Medeiros et al., 2013; Dunn et al., 2015). However, there is no study regarding the effects of SPMs on *in vivo* AD models. In this study, we have investigated the effects of MaR1 on the behavioral and pathological changes as well as the molecular pathways affected by MaR1 in AD mouse model.

Administering Aβ<sub>42</sub> peptide to hippocampus can induce behavioral changes specific to learning and memory (Colaianna et al., 2010; Passos et al., 2010). In the MWM tests, a decrease in the escape latency in all the four groups was observed as the training proceeded, indicating an ongoing spatial learning and memory in the mice. However, the escape latency in Aβ<sub>42</sub> group was significantly longer compared with Vehicle group on the fifth day, suggesting that mice treated with Aβ<sub>42</sub> developed learning and memory deficits. But co-stimulation with MaR1 and Aβ<sub>42</sub> ameliorated the cognitive decline indicated by our observation that the escape latency in Aβ<sub>42</sub> + MaR1 group was shorter than that in Aβ<sub>42</sub> group on the fifth day. Similar trends were also found

in the probe test, as the number of platform crossings and the time spent in the target quadrant by Aβ<sub>42</sub> + MaR1 group were longer than those in Aβ<sub>42</sub> group. All these results suggest that MaR1 could improve behavioral dysfunction induced by Aβ<sub>42</sub>. We also noticed that there were no significant differences in escape latency, cross times, and time spent in target quadrant between Vehicle and MaR1 group. The possible explanation might be that MaR1 alone does not have any effect on normal mice, however, it promotes inflammation resolution only when there are ongoing inflammatory changes.

Consistent with the results of behavioral test, the injection of Aβ<sub>42</sub> into hippocampus caused neuronal degeneration revealed by FJB staining, which resulted in memory deficits. The number of degenerative neurons in the hippocampus and cortex of Aβ<sub>42</sub> and MaR1 co-stimulation group was significantly lower than that of Aβ<sub>42</sub> group, suggesting that MaR1 could restore the behavioral deficits by protecting the neurons from Aβ<sub>42</sub> toxicity. Increased number of microglia and astrocytes have been observed in postmortem AD brain (Medeiros et al., 2013). Moreover, it has been demonstrated that activation of glia cells including microglia and astrocytes by Aβ leads to elevated production of pro-inflammatory mediators, chronic inflammation, neurodegeneration, decreased glutamate uptake,





loss of neuronal synapses, and ultimately cognitive deficits in AD (Prokop et al., 2013; Michaud and Rivest, 2015). In addition, increased cytokines can down-regulate the expression of A $\beta$  phagocytosis receptors on microglia and ultimately result in insufficient microglial phagocytic activity (Hickman et al., 2008). The weakening of A $\beta$  clearance further aggravates the inflammatory response and forms a vicious circle. The immunohistochemical experiments showed that the number of Iba-1 and GFAP positive cells were elevated after A $\beta_{42}$  treatment, however, this trend was reversed by combination treatment of A $\beta_{42}$  and MaR1, suggesting that MaR1 could attenuate inflammation by inhibiting pro-inflammatory activation of microglia and astrocytes. We also observed that the level of MCP-1 was higher in the hippocampus and cortex of A $\beta_{42}$  injected mice, which decreased when mice received combined treatment of A $\beta_{42}$  and MaR1. Therefore, MaR1 may inhibit the chemotaxis of glia by decreasing the secretion of chemokines, which in turn reduces the inflammatory response. Fibrillar A $\beta$  in plaques has been shown to stimulate microglia to secrete pro-inflammatory cytokines, including IL-1, IL-6 and TNF- $\alpha$  (Murphy et al., 1998; Combs et al., 2001). There

are reports indicating that MaR1 reduces TNF- $\alpha$  and IL-6 secretion in peripheral inflammation disease models such as septic mouse model (Hao et al., 2019), and human periodontal ligament cell model. In line with previous reports, we found MaR1 could reverse the increased levels of TNF- $\alpha$  and IL-6 induced by A $\beta_{42}$  in the central nervous system. The increased levels of IL-6, TNF- $\alpha$  are associated with increased A $\beta$  production, decreased A $\beta$  clearance, tau hyperphosphorylation (Ringheim et al., 1998; Zilka et al., 2012), synaptic dysfunction, and cognitive deficits (Singh-Manoux et al., 2014; Chang et al., 2017). In an aspergillus fumigatus keratitis mouse model, MaR1 was found to increase the expression of anti-inflammatory cytokine IL-10 (Tang et al., 2019). We also observed that both A $\beta_{42}$  and MaR1 could induce the secretion of anti-inflammatory cytokines, IL-2 and IL-10. It has been reported that IL-2 and IL-10 and their signaling pathways are elevated in the brain of AD patients (Strle et al., 2001; Gezen-Ak et al., 2013; Guillot-Sestier et al., 2015a). Some researchers hypothesize that the increase in IL-10 levels may lead to innate immunity repression and microglia dysfunction in A $\beta$  clearance (Guillot-Sestier et al.,



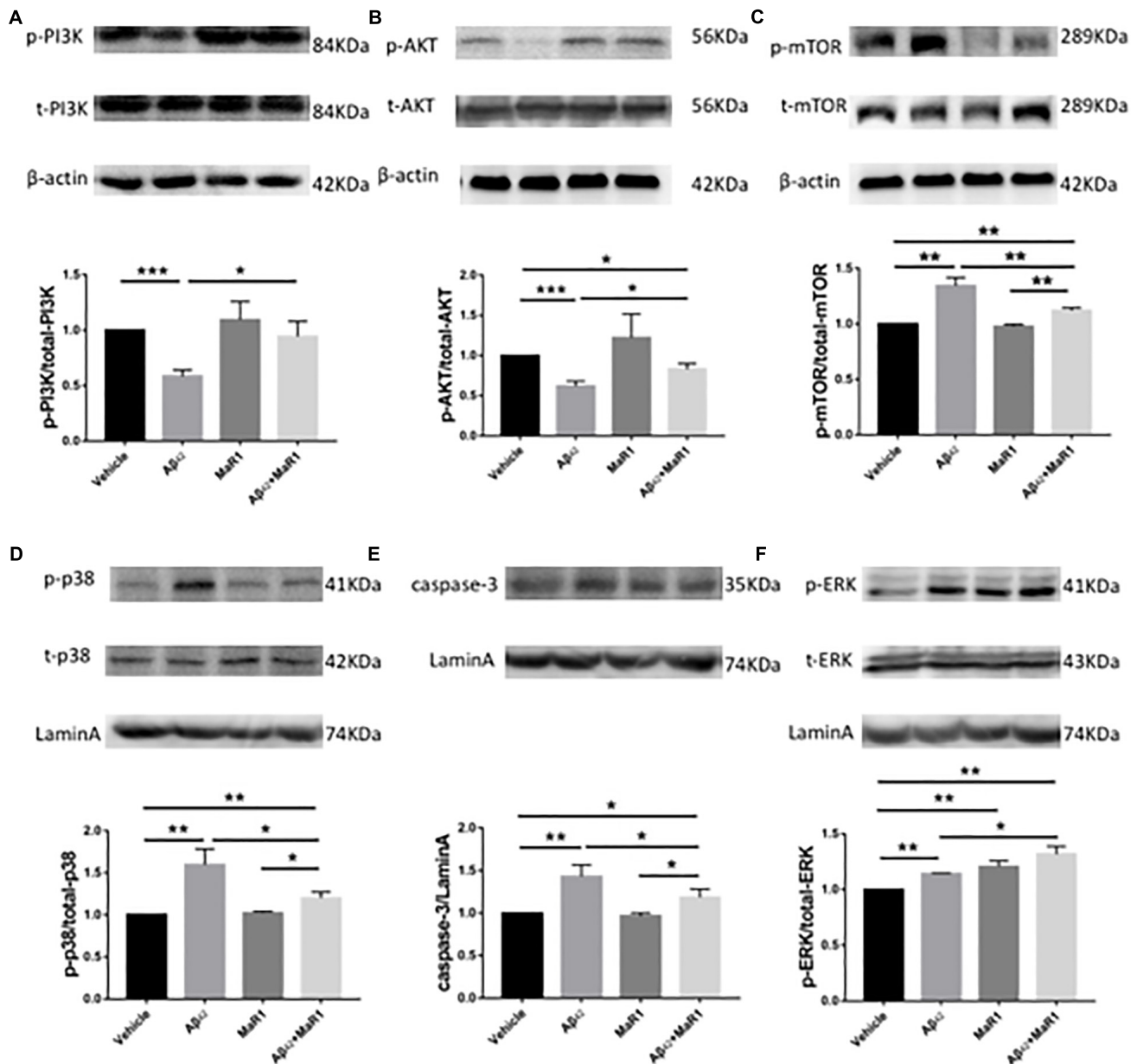


**FIGURE 5 |** MaR1 altered survival, autophagy, apoptosis, and MAPK signal pathways. Western blots for different proteins and its quantitation in the four groups, PI3K (A), AKT (B), mTOR (C), p38 (D), caspase 3 (E), ERK (F). Compared with Vehicle group, the ratio of p-PI3K/t-PI3K and p-AKT/t-AKT were down-regulated (A,B), while the ratio of p-mTOR/t-mTOR, p-p38/t-p38, as well as the levels of caspase 3 were up-regulated in Aβ<sub>42</sub> group ( $P < 0.01$ ) (C–E), however, these Aβ<sub>42</sub> induced changes were reversed by Aβ<sub>42</sub> + MaR1 treatment. (F) The ratio of p-ERK/t-ERK was increased by both, Aβ<sub>42</sub> ( $P < 0.001$ ) and MaR1 ( $P < 0.01$ ) alone, and was further increased by their co-stimulation compared to Vehicle group ( $P < 0.01$ ) and compared to Aβ<sub>42</sub> group ( $P < 0.05$ ). Data are expressed as mean  $\pm$  SEM, 10 mice in each group, and statistical significance is defined as follows: \* $P < 0.05$ , \*\* $P < 0.01$ , \*\*\* $P < 0.001$ .

2015b), while the others argue that elevated anti-inflammatory cytokines levels is beneficial in decreasing amyloid plaque load, improving synaptic plasticity, and rescuing spine density (Dansokho et al., 2016; Alves et al., 2017). However, it may also be explained by third possibility that Aβ<sub>42</sub> induces inflammation in the brain, which in turn stimulates IL-10 secretion that plays an immunomodulatory role and facilitates the resolution of inflammatory cascades (Garcia et al., 2017). In summary,

MaR1 plays neuroprotective role by down-regulating pro-inflammatory activation of microglia and astrocytes, decreasing pro-inflammatory while increasing anti-inflammatory cytokines production, and promoting resolution of inflammation.

Even though beneficial effects have been reported in a different study using other SPMs in AD mice models (Zhu et al., 2016), there is no research that demonstrates the effects of MaR1 on AD animal models. Moreover, the underlying

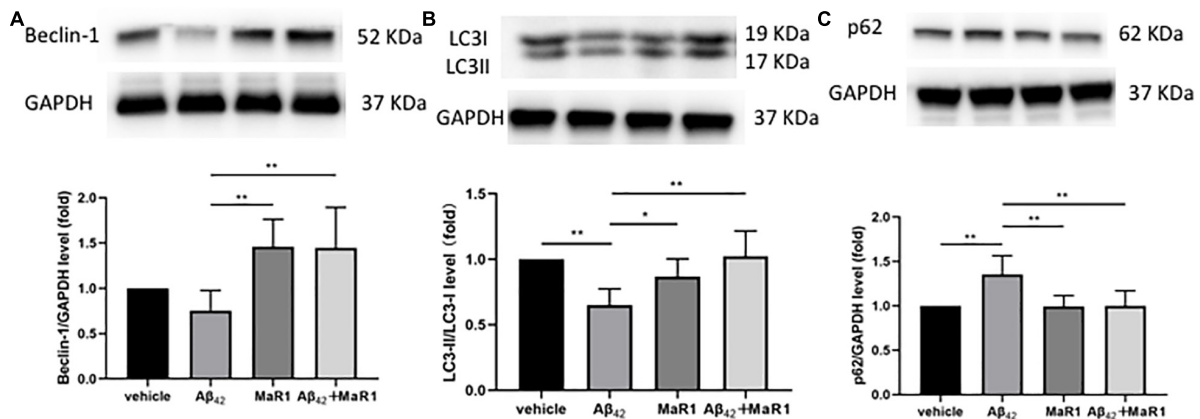


**FIGURE 6 |** MaR1 altered autophagy signal pathways. Compared with MaR1 group, the level of Beclin-1 (A) was decreased in Aβ<sub>42</sub> group ( $P < 0.01$ ), and increased by Aβ<sub>42</sub> + MaR1 treatment ( $P < 0.01$ ). Compared with Vehicle and MaR1 group, the ratio of LC3-II/LC3-I (B) was down-regulated ( $P < 0.01$ ,  $P < 0.05$ ), while the levels of p62 (C) was up-regulated in Aβ<sub>42</sub> group ( $P < 0.01$ ), however, these Aβ<sub>42</sub> induced changes were reversed by Aβ<sub>42</sub> + MaR1 treatment ( $P < 0.01$ ). Data are expressed as mean ± SEM, 10 mice in each group, and statistical significance is defined as follows: \* $P < 0.05$ , \*\* $P < 0.01$ .

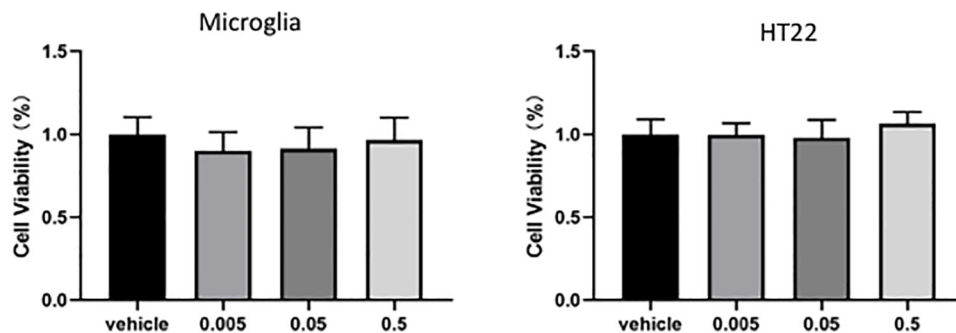


**FIGURE 7 |** *In vitro* cytotoxicity analysis. There was no significant difference in cell proliferation after treatment with different concentrations MaR1 both in HT22 and in microglia cells.

mechanisms are less understood and the receptor of MaR1 has not been identified. However, in this study, we observed that several signaling pathways involved in inflammation, cellular survival, proliferation, autophagy, apoptosis, and axon formation were altered by MaR1, including PI3K/AKT, ERK1/2, mTOR, p38, and caspase 3.

PI3K/AKT signaling pathway plays an important role in cellular proliferation, growth, survival, motility, and metabolic functions (Kriplani et al., 2015). It has been demonstrated that PI3K/AKT can activate its downstream factors mTOR and Nrf2 (Kim et al., 2013), which are involved in axon branching, autophagy, alleviating oxidative damage, and down-regulating tau protein phosphorylation as well as apoptosis of neurons via inhibiting caspase 3 and glycogen synthase kinase (GSK) -3β (Chami et al., 2016). PI3K/AKT signaling has been found to be impaired in AD patients in previous studies (Wang et al., 2016). Besides AD, the same results have also been observed in other neurodegenerative diseases such as amyotrophic lateral sclerosis (ALS) and Parkinson's disease (PD) (Recabarren and Alarcon, 2017). All four types of SPMs have been reported to affect the expression of PI3K/AKT pathway and hence, play a

protective role: LXA4 protected human or murine macrophages from apoptosis through activation of PI3K/AKT and ERK/Nrf2 pathways (Prieto et al., 2010); RvD1 reduced myocardial infarct size by increasing PI3K/AKT expression (Gilbert et al., 2015); NPD1 induced retinal pigment epithelial cell survival by activating PI3K/AKT signal pathway (Halapin and Bazan, 2010); MaR1 activated PI3K/AKT pathway to down-regulate Nedd4-2 protein and improve Na, K-adenosine triphosphatase (ATPase) activity, and then stimulate alveolar fluid clearance (Zhang et al., 2017). In line with previous findings, we found that PI3K/AKT signaling was down-regulated in Aβ<sub>42</sub> induced AD mouse model, while MaR1 administration enhanced PI3K/AKT signaling pathway and promoted cell survival, indicating that the protective role of MaR1 is partly due to activation of PI3K/AKT signaling pathway. Furthermore, similar to previous studies in humans and mouse models, we also observed that the mTOR signaling was enhanced in the Aβ<sub>42</sub> induced AD mouse model. The up-regulation of mTOR could result in reduction of autophagy, which probably is the main cause for abnormal protein aggregation in AD (O'Neill, 2013; Tramutola et al., 2017). This is further supported by studies that show that treatment

with mTOR inhibitors improves the cognitive impairment in AD (Tramutola et al., 2017, 2018). Interestingly, previous studies have verified that precursors of SPMs, omega-3 PUFAs, are beneficial for chronic pathological conditions by inhibiting mTOR expression (Kim et al., 2018). In the present study, we observed that MaR1, the downstream product of PUFAs, could also down-regulate the elevated mTOR levels induced by A $\beta$ <sub>42</sub> treatment, indicating that MaR1 could enhance autophagy by inhibiting mTOR pathway.

The reason for up-regulation of mTOR in AD maybe partly attributed to Ras/ERK, which is an up-stream activating factor for mTOR. Extracellular signal-regulated kinase (ERK) has been found to be elevated in the brain of AD patients (Russo et al., 2002). We observed that ERK signaling pathway was enhanced by both, A $\beta$ <sub>42</sub> and MaR1 treatment alone or by their combination. Another mitogen-activated protein kinases (MAPKs) family member, p38 signaling pathway, was also enhanced by A $\beta$ <sub>42</sub> treatment that was reversed by MaR1 treatment. ERK can activate AKT, hence it is the key regulator for neuronal plasticity and survival. In addition, ERK can also activate its downstream effector, cAMP response element binding protein (CREB) (Dineley et al., 2001; Bell et al., 2004), which is involved in synaptic plasticity. However, A $\beta$ -induced activation of ERK pathway in the hippocampus also leads to caspase activation (Chong et al., 2006) and aberrant hyper-phosphorylation of tau protein (Arora et al., 2015). Therefore, subsequent cellular response induced by ERK activation is complicated and can trigger both beneficial and detrimental effects on neuronal cells. The p38 MAPK activation leads to microglia and astrocyte activation and subsequently promotes neuroinflammation in AD (Hensley et al., 1999; Sun et al., 2003; Schnoder et al., 2016). Inhibition of p38 MAPK by p38 MAPK inhibitors can effectively alleviate chronic inflammatory diseases such as rheumatoid arthritis, cardiovascular disease, and inflammatory pain (Cohen et al., 2009; Marber et al., 2011; Arthur and Ley, 2013; Lin et al., 2014), and therefore, may be potential therapies for neurodegenerative diseases including AD (Lee and Kim, 2017). We found p38 signaling was activated in AD by A $\beta$ <sub>42</sub> and down-regulated after MaR1 treatment, indicating that MaR1 may also play protective role via inhibiting p38 MAPK mediated inflammation.

The down-regulated PI3K/AKT and up-regulated p38 and ERK signaling in AD can induce caspase 3 expression, which is closely related to neuronal apoptosis and is considered as the terminal event preceding cell death. Caspase 3 levels have been demonstrated to be higher in AD brains than in age-matched controls (Shimohama et al., 1999), the same as we have observed in the present study. However, we found that caspase 3 was down-regulated after MaR1 treatment, suggesting that MaR1 plays a protective role by inhibiting apoptosis. To sum up, MaR1 promotes neuronal survival and ameliorates inflammation by up-regulating PI3K/AKT, ERK pathway while down-regulating mTOR, p38, and caspase 3 pathway.

There are some limitations in the current study that can be addressed in further investigations. Firstly, in this study, AD animal model used was made by injecting A $\beta$ <sub>42</sub> into the

hippocampus. Although this method is simple and economical, it could not imitate the pathological changes of AD patients completely, and AD transgenic mice may be a better choice. Secondly, the pathways affected by MaR1 are not only limited to inflammatory pathways, but also other proteins that affect cell survival, axonal growth, and apoptosis, other proteins besides inflammatory cytokines should also be investigated. Thirdly, MaR1 was administered intraventricularly to avoid the restriction of blood-brain barrier (BBB). However, the capacity of MaR1 across the BBB needs to be further studied.

To conclude, resolution of inflammation is impaired in AD, MaR1 could ameliorate memory dysfunction, improve neuronal survival, and reduce secretion of pro-inflammatory while promote anti-inflammatory mediators. MaR1 is beneficial in AD via pathways not only restricted to inflammation, but also through pathways involved in cellular survival, autophagy, axon formation, and apoptosis.

## DATA AVAILABILITY STATEMENT

All datasets generated for this study are included in the manuscript/supplementary files.

## ETHICS STATEMENT

All procedures used in the present study followed the “National Institutes of Health Guide for Care and Use of Laboratory Animals” (Publication No. 85–23, revised 1985) and were approved by the Animal Ethics Committee of Jilin University. Efforts were also made to minimize animal suffering and to reduce the number of animals used.

## AUTHOR CONTRIBUTIONS

MZ, JF, PY, and XW designed the research. PY, XW, and YW performed the experiments. MZ and PY analyzed the data. MZ, JF, PY, and XW wrote the manuscript. All authors reviewed the manuscript.

## FUNDING

This study was supported by grants from the National Natural Science Foundation of China (Nos. 31600820 and 81701158), the Health and Family Planning Commission of Jilin Province (No. 2016Q036), the Science and Technology Planning Project of Jilin Province (No. 20180520110JH), the First Hospital of Jilin University (JDYY52015016) as well as from the Norman Bethune Program of Jilin University (No. 2015335).

## ACKNOWLEDGMENTS

We would like to thank Editage for English language editing.

## REFERENCES

- Alves, S., Churlaud, G., Audrain, M., Michaelsen-Preusse, K., Fol, R., Souchet, B., et al. (2017). Interleukin-2 improves amyloid pathology, synaptic failure and memory in Alzheimer's disease mice. *Brain* 140, 826–842. doi: 10.1093/brain/aww330
- Alzheimer, A., Stelzmann, R. A., Schnitzlein, H. N., and Murtagh, F. R. (1995). An english translation of Alzheimer's 1907 paper, "Über eine eigenartige Erkrankung der Hirnrinde". *Clin. Anat.* 8, 429–431. doi: 10.1002/ca.980080612
- Arora, K., Cheng, J., and Nichols, R. A. (2015). Nicotinic acetylcholine receptors sensitize a MAPK-linked toxicity pathway on prolonged exposure to beta-amyloid. *J. Biol. Chem.* 290, 21409–21420. doi: 10.1074/jbc.M114.634162
- Arthur, J. S., and Ley, S. C. (2013). Mitogen-activated protein kinases in innate immunity. *Nat. Rev. Immunol.* 13, 679–692. doi: 10.1038/nri3495
- Bell, K. A., O'Riordan, K. J., Sweatt, J. D., and Dineley, K. T. (2004). MAPK recruitment by beta-amyloid in organotypic hippocampal slice cultures depends on physical state and exposure time. *J. Neurochem.* 91, 349–361. doi: 10.1111/j.1471-4159.2004.02722.x
- Cacabelos, R., Alvarez, X. A., Fernandez-Novoa, L., Franco, A., Mangues, R., Pellicer, A., et al. (1994). Brain interleukin-1 $\beta$  in Alzheimer's disease and vascular dementia. *Methods Find Exp. Clin. Pharmacol.* 16, 141–151.
- Chami, B., Steel, A. J., De La Monte, S. M., and Sutherland, G. T. (2016). The rise and fall of insulin signaling in Alzheimer's disease. *Metab. Brain Dis.* 31, 497–515. doi: 10.1007/s11011-016-9806-1
- Chang, R., Yee, K. L., and Sumbria, R. K. (2017). Tumor necrosis factor alpha inhibition for Alzheimer's disease. *J. Cent. Nerv. Syst. Dis.* 9, 1179573517709278. doi: 10.1177/1179573517709278
- Chong, Y. H., Shin, Y. J., Lee, E. O., Kaye, R., Glabe, C. G., and Tenner, A. J. (2006). ERK1/2 activation mediates A $\beta$  oligomer-induced neurotoxicity via caspase-3 activation and tau cleavage in rat organotypic hippocampal slice cultures. *J. Biol. Chem.* 281, 20315–20325. doi: 10.1074/jbc.M601016200
- Cohen, S. B., Cheng, T. T., Chindalore, V., Damjanov, N., Burgos-Vargas, R., Delora, P., et al. (2009). Evaluation of the efficacy and safety of pamapimod, a p38 MAP kinase inhibitor, in a double-blind, methotrexate-controlled study of patients with active rheumatoid arthritis. *Arthritis Rheum.* 60, 335–344. doi: 10.1002/art.24266
- Colaïanna, M., Tucci, P., Zotti, M., Morgese, M. G., Schiavone, S., Govoni, S., et al. (2010). Soluble beta amyloid(1–42): a critical player in producing behavioural and biochemical changes evoking depressive-related state? *Br. J. Pharmacol.* 159, 1704–1715. doi: 10.1111/j.1476-5381.2010.00669.x
- Combs, C. K., Karlo, J. C., Kao, S. C., and Landreth, G. E. (2001). beta-Amyloid stimulation of microglia and monocytes results in TNF $\alpha$ -dependent expression of inducible nitric oxide synthase and neuronal apoptosis. *J. Neurosci.* 21, 1179–1188. doi: 10.1523/jneurosci.21-04-01179.2001
- Dalli, J., Vlasakov, I., Riley, I. R., Rodriguez, A. R., Spur, B. W., Petasis, N. A., et al. (2016). Maresin conjugates in tissue regeneration biosynthesis enzymes in human macrophages. *Proc. Natl. Acad. Sci. U.S.A.* 113, 12232–12237. doi: 10.1073/pnas.1607003113
- Dalli, J., Zhu, M., Vlasenko, N. A., Deng, B., Haeggstrom, J. Z., Petasis, N. A., et al. (2013). The novel 13S,14S-epoxy-maresin is converted by human macrophages to maresin 1 (MaR1), inhibits leukotriene A4 hydrolase (LTA4H), and shifts macrophage phenotype. *FASEB J.* 27, 2573–2583. doi: 10.1096/fj.13-227728
- Dansokho, C., Ait Ahmed, D., Aid, S., Toly-Ndour, C., Chaigneau, T., Calle, V., et al. (2016). Regulatory T cells delay disease progression in Alzheimer-like pathology. *Brain* 139(Pt 4), 1237–1251. doi: 10.1093/brain/aww408
- Del Bo, R., Angeretti, N., Lucca, E., De Simoni, M. G., and Forloni, G. (1995). Reciprocal control of inflammatory cytokines, IL-1 and IL-6, and A $\beta$  production in cultures. *Neurosci. Lett.* 188, 70–74. doi: 10.1016/0304-3940(95)11384-9
- Deng, B., Wang, C. W., Arnardottir, H. H., Li, Y., Cheng, C. Y., Dalli, J., et al. (2014). Maresin biosynthesis and identification of maresin 2, a new anti-inflammatory and pro-resolving mediator from human macrophages. *PLoS One* 9:e102362. doi: 10.1371/journal.pone.0102362
- Dineley, K. T., Westerman, M., Bui, D., Bell, K., Ashe, K. H., and Sweatt, J. D. (2001). Beta-amyloid activates the mitogen-activated protein kinase cascade via hippocampal alpha7 nicotinic acetylcholine receptors: in vitro and in vivo mechanisms related to Alzheimer's disease. *J. Neurosci.* 21, 4125–4133. doi: 10.1523/jneurosci.21-12-04125.2001
- Dunn, H. C., Ager, R. R., Baglietto-Vargas, D., Cheng, D., Kitazawa, M., Cribbs, D. H., et al. (2015). Restoration of lipoxin A4 signaling reduces Alzheimer's disease-like pathology in the 3xTg-AD mouse model. *J. Alzheimers Dis.* 43, 893–903. doi: 10.3233/JAD-141335
- Fredman, G., Hellmann, J., Proto, J. D., Kuriakose, G., Colas, R. A., Dorweiler, B., et al. (2016). An imbalance between specialized pro-resolving lipid mediators and pro-inflammatory leukotrienes promotes instability of atherosclerotic plaques. *Nat. Commun.* 7:12859. doi: 10.1038/ncomms12859
- Gao, Y., Min, K., Zhang, Y., Su, J., Greenwood, M., and Gronert, K. (2015). Female-specific downregulation of tissue polymorphonuclear neutrophils drives impaired regulatory T cell and amplified effector T cell responses in autoimmune dry eye disease. *J. Immunol.* 195, 3086–3099. doi: 10.4049/jimmunol.1500610
- Garcia, J. M., Stillings, S. A., Leclerc, J. L., Phillips, H., Edwards, N. J., Robicsek, S. A., et al. (2017). Role of interleukin-10 in acute brain injuries. *Front. Neurol.* 8:244. doi: 10.3389/fneur.2017.00244
- Gezen-Ak, D., Dursun, E., Hanagasi, H., Bilgic, B., Lohman, E., Araz, O. S., et al. (2013). BDNF, TNF $\alpha$ , HSP90, CFH, and IL-10 serum levels in patients with early or late onset Alzheimer's disease or mild cognitive impairment. *J. Alzheimers Dis.* 37, 185–195. doi: 10.3233/JAD-130497
- Gilbert, K., Bernier, J., Bourque-Riel, V., Malick, M., and Rousseau, G. (2015). Resolvin D1 reduces infarct size through a phosphoinositide 3-kinase/protein kinase b mechanism. *J. Cardiovasc. Pharmacol.* 66, 72–79. doi: 10.1097/FJC.0000000000000245
- Grieco, A., Serrano-Pozo, A., Parrado, A. R., Lesinski, A. N., Asselin, C. N., Mullin, K., et al. (2013). Alzheimer's disease risk gene CD33 inhibits microglial uptake of amyloid- $\beta$ . *Neuron* 78, 631–643. doi: 10.1016/j.neuron.2013.04.014
- Griffin, W. S., Stanley, L. C., Ling, C., White, L., MacLeod, V., Perrot, L. J., et al. (1989). Brain interleukin 1 and S-100 immunoreactivity are elevated in down syndrome and Alzheimer disease. *Proc. Natl. Acad. Sci. U.S.A.* 86, 7611–7615. doi: 10.1073/pnas.86.19.7611
- Guillot-Sestier, M. V., Doty, K. R., Gate, D., Rodriguez, J. Jr., Leung, B. P., Rezai-Zadeh, K., et al. (2015a). IL10 deficiency rebalances innate immunity to mitigate Alzheimer-like pathology. *Neuron* 85, 534–548. doi: 10.1016/j.neuron.2014.12.068
- Guillot-Sestier, M. V., Doty, K. R., and Town, T. (2015b). Innate immunity fights Alzheimer's disease. *Trends Neurosci.* 38, 674–681. doi: 10.1016/j.tins.2015.08.008
- Halapin, N. A., and Bazan, N. G. (2010). NPD1 induction of retinal pigment epithelial cell survival involves PI3K/Akt phosphorylation signaling. *Neurochem. Res.* 35, 1944–1947. doi: 10.1007/s11064-010-0351-358
- Hao, Y., Zheng, H., Wang, R. H., Li, H., Yang, L. L., Bhandari, S., et al. (2019). Maresin1 alleviates metabolic dysfunction in septic mice: a (1)H NMR-based metabolomics analysis. *Mediators Inflamm.* 2019:2309175. doi: 10.1155/2019/2309175
- Hardy, J. (2009). The amyloid hypothesis for Alzheimer's disease: a critical reappraisal. *J. Neurochem.* 110, 1129–1134. doi: 10.1111/j.1471-4159.2009.06181.x
- Hensley, K., Floyd, R. A., Zheng, N. Y., Nael, R., Robinson, K. A., Nguyen, X., et al. (1999). p38 kinase is activated in the Alzheimer's disease brain. *J. Neurochem.* 72, 2053–2058.
- Heppner, F. L., Ransohoff, R. M., and Becher, B. (2015). Immune attack: the role of inflammation in Alzheimer disease. *Nat. Rev. Neurosci.* 16, 358–372. doi: 10.1038/nrn3880
- Hickman, S. E., Allison, E. K., and El Khoury, J. (2008). Microglial dysfunction and defective beta-amyloid clearance pathways in aging Alzheimer's disease mice. *J. Neurosci.* 28, 8354–8360. doi: 10.1523/JNEUROSCI.0616-08.2008
- Kang, J., and Rivest, S. (2012). Lipid metabolism and neuroinflammation in Alzheimer's disease: a role for liver X receptors. *Endocr. Rev.* 33, 715–746. doi: 10.1210/er.2011-1049
- Kim, K. C., Lee, I. K., Kang, K. A., Cha, J. W., Cho, S. J., Na, S. Y., et al. (2013). 7,8-Dihydroxyflavone suppresses oxidative stress-induced base modification in DNA via induction of the repair enzyme 8-oxoguanine DNA glycosylase-1. *Biomed. Res. Int.* 2013:863720. doi: 10.1155/2013/863720
- Kim, S., Jing, K., Shin, S., Jeong, S., Han, S. H., Oh, H., et al. (2018). omega3-polyunsaturated fatty acids induce cell death through apoptosis and autophagy in glioblastoma cells: in vitro and in vivo. *Oncol. Rep.* 39, 239–246. doi: 10.3892/or.2017.6101



- Kriplani, N., Hermida, M. A., Brown, E. R., and Leslie, N. R. (2015). Class I PI 3-kinases: function and evolution. *Adv. Biol. Regul.* 59, 53–64. doi: 10.1016/j.bior.2015.05.002
- Lee, J. K., and Kim, N. J. (2017). Recent advances in the inhibition of p38 MAPK as a potential strategy for the treatment of Alzheimer's disease. *Molecules* 22:E1287. doi: 10.3390/molecules22081287
- Lin, X., Wang, M., Zhang, J., and Xu, R. (2014). p38 MAPK: a potential target of chronic pain. *Curr. Med. Chem.* 21, 4405–4418. doi: 10.2174/0929867321666140915143040
- Lukiw, W. J., Cui, J. G., Marcheselli, V. L., Bodker, M., Botkjaer, A., Gotlinger, K., et al. (2005). A role for docosahexaenoic acid-derived neuroprotectin D1 in neural cell survival and Alzheimer disease. *J. Clin. Invest.* 115, 2774–2783. doi: 10.1172/JCI25420
- Marber, M. S., Rose, B., and Wang, Y. (2011). The p38 mitogen-activated protein kinase pathway—a potential target for intervention in infarction, hypertrophy, and heart failure. *J. Mol. Cell Cardiol.* 51, 485–490. doi: 10.1016/j.yjmcc.2010.10.021
- McGeer, P. L., Itagaki, S., Boyes, B. E., and McGeer, E. G. (1988). Reactive microglia are positive for HLA-DR in the substantia nigra of Parkinson's and Alzheimer's disease brains. *Neurology* 38, 1285–1291.
- McGeer, P. L., Itagaki, S., Tago, H., and McGeer, E. G. (1987). Reactive microglia in patients with senile dementia of the Alzheimer type are positive for the histocompatibility glycoprotein HLA-DR. *Neurosci. Lett.* 79, 195–200. doi: 10.1016/0304-3940(87)90696-3
- Medeiros, R., Kitazawa, M., Passos, G. F., Baglietto-Vargas, D., Cheng, D., Cribbs, D. H., et al. (2013). Aspirin-triggered lipoxin A4 stimulates alternative activation of microglia and reduces Alzheimer disease-like pathology in mice. *Am. J. Pathol.* 182, 1780–1789. doi: 10.1016/j.ajpath.2013.01.051
- Michaud, J. P., and Rivest, S. (2015). Anti-inflammatory signaling in microglia exacerbates Alzheimer's disease-related pathology. *Neuron* 85, 450–452. doi: 10.1016/j.neuron.2015.01.021
- Murphy, G. M. Jr., Yang, L., and Cordell, B. (1998). Macrophage colony-stimulating factor augments beta-amyloid-induced interleukin-1, interleukin-6, and nitric oxide production by microglial cells. *J. Biol. Chem.* 273, 20967–20971. doi: 10.1074/jbc.273.33.20967
- O'Neill, C. (2013). PI3-kinase/Akt/mTOR signaling: impaired on/off switches in aging, cognitive decline and Alzheimer's disease. *Exp. Gerontol.* 48, 647–653. doi: 10.1016/j.exger.2013.02.025
- Passos, G. F., Figueiredo, C. P., Prediger, R. D., Silva, K. A., Siqueira, J. M., Duarte, F. S., et al. (2010). Involvement of phosphoinositide 3-kinase gamma in the neuro-inflammatory response and cognitive impairments induced by beta-amyloid 1-40 peptide in mice. *Brain Behav. Immun.* 24, 493–501. doi: 10.1016/j.bbi.2009.12.003
- Prieto, P., Cuenca, J., Traves, P. G., Fernandez-Velasco, M., Martin-Sanz, P., and Bosca, L. (2010). Lipoxin A4 impairment of apoptotic signaling in macrophages: implication of the PI3K/Akt and the ERK/Nrf-2 defense pathways. *Cell Death Differ.* 17, 1179–1188. doi: 10.1038/cdd.2009.220
- Prokop, S., Miller, K. R., and Heppner, F. L. (2013). Microglia actions in Alzheimer's disease. *Acta Neuropathol.* 126, 461–477. doi: 10.1007/s00401-013-1182-x
- Recabarren, D., and Alarcon, M. (2017). Gene networks in neurodegenerative disorders. *Life Sci.* 183, 83–97. doi: 10.1016/j.lfs.2017.06.009
- Ringheim, G. E., Szczepanik, A. M., Petko, W., Burgher, K. L., Zhu, S. Z., and Chao, C. C. (1998). Enhancement of beta-amyloid precursor protein transcription and expression by the soluble interleukin-6 receptor/interleukin-6 complex. *Brain Res. Mol. Brain Res.* 55, 35–44. doi: 10.1016/s0169-328x(97)00356-2
- Russo, C., Dolcini, V., Salis, S., Venezia, V., Zambrano, N., Russo, T., et al. (2002). Signal transduction through tyrosine-phosphorylated C-terminal fragments of amyloid precursor protein via an enhanced interaction with Shc/Grb2 adaptor proteins in reactive astrocytes of Alzheimer's disease brain. *J. Biol. Chem.* 277, 35282–35288. doi: 10.1074/jbc.M110785200
- Saura, J., Tusell, J. M., and Serratos, J. (2003). High-yield isolation of murine microglia by mild trypsinization. *Glia* 44, 183–189. doi: 10.1002/glia.10274
- Schnoder, L., Hao, W., Qin, Y., Liu, S., Tomic, I., Liu, X., et al. (2016). Deficiency of neuronal p38alpha MAPK attenuates amyloid pathology in Alzheimer disease mouse and cell models through facilitating lysosomal degradation of BACE1. *J. Biol. Chem.* 291, 2067–2079. doi: 10.1074/jbc.M115.695916
- Serhan, C. N. (2014). Pro-resolving lipid mediators are leads for resolution physiology. *Nature* 510, 92–101. doi: 10.1038/nature13479
- Serhan, C. N. (2017). Treating inflammation and infection in the 21st century: new hints from decoding resolution mediators and mechanisms. *FASEB J.* 31, 1273–1288. doi: 10.1096/fj.201601222R
- Shimohama, S., Tanino, H., and Fujimoto, S. (1999). Changes in caspase expression in Alzheimer's disease: comparison with development and aging. *Biochem. Biophys. Res. Commun.* 256, 381–384. doi: 10.1006/bbrc.1999.0344
- Singh-Manoux, A., Dugravot, A., Brunner, E., Kumari, M., Shipley, M., Elbaz, A., et al. (2014). Interleukin-6 and C-reactive protein as predictors of cognitive decline in late midlife. *Neurology* 83, 486–493. doi: 10.1212/WNL.0000000000000665
- Strle, K., Zhou, J. H., Shen, W. H., Broussard, S. R., Johnson, R. W., Freund, G. G., et al. (2001). Interleukin-10 in the brain. *Crit. Rev. Immunol.* 21, 427–449.
- Sun, A., Liu, M., Nguyen, X. V., and Bing, G. (2003). P38 MAP kinase is activated at early stages in Alzheimer's disease brain. *Exp. Neurol.* 183, 394–405. doi: 10.1016/s0014-4886(03)00180-8
- Sun, Q., Wu, Y., Zhao, F., and Wang, J. (2017). Maresin 1 ameliorates lung ischemia/reperfusion injury by suppressing oxidative stress via activation of the Nrf-2-mediated HO-1 signaling pathway. *Oxid. Med. Cell Longev.* 2017:9634803. doi: 10.1155/2017/9634803
- Tang, Q., Che, C., Lin, J., He, H., Zhao, W., Lv, L., et al. (2019). Maresin1 regulates neutrophil recruitment and IL-10 expression in *Aspergillus fumigatus* keratitis. *Int. Immunopharmacol.* 69, 103–108. doi: 10.1016/j.intimp.2019.01.032
- Tramutola, A., Lanzillotta, C., Barone, E., Arena, A., Zuliani, I., Mosca, L., et al. (2018). Intranasal rapamycin ameliorates Alzheimer-like cognitive decline in a mouse model of down syndrome. *Transl. Neurodegener.* 7:28. doi: 10.1186/s40035-018-0133-9
- Tramutola, A., Lanzillotta, C., and Di Domenico, F. (2017). Targeting mTOR to reduce Alzheimer-related cognitive decline: from current hits to future therapies. *Expert Rev. Neurother.* 17, 33–45. doi: 10.1080/14737175.2017.1244482
- Wang, X., Zhu, M., Hjorth, E., Cortes-Toro, V., Eyjolfssdottir, H., Graff, C., et al. (2015). Resolution of inflammation is altered in Alzheimer's disease. *Alzheimers Dement.* 11:40–50.e1–2. doi: 10.1016/j.jalz.2013.12.024
- Wang, Y., Wu, C., Han, B., Xu, F., Mao, M., Guo, X., et al. (2016). Dexmedetomidine attenuates repeated propofol exposure-induced hippocampal apoptosis, PI3K/Akt/Gsk-3beta signaling disruption, and juvenile cognitive deficits in neonatal rats. *Mol. Med. Rep.* 14, 769–775. doi: 10.3892/mmr.2016.5321
- Wicklund, L., Leao, R. N., Stromberg, A. M., Mousavi, M., Hovatta, O., Nordberg, A., et al. (2010). Aβ42 oligomers impair function of human embryonic stem cell-derived forebrain cholinergic neurons. *PLoS One* 5:e15600. doi: 10.1371/journal.pone.0015600
- Yurko-Mauro, K., McCarthy, D., Rom, D., Nelson, E. B., Ryan, A. S., Blackwell, A., et al. (2010). Beneficial effects of docosahexaenoic acid on cognition in age-related cognitive decline. *Alzheimers Dement.* 6, 456–464. doi: 10.1016/j.jalz.2010.01.013
- Zhang, J. L., Zhuo, X. J., Lin, J., Luo, L. C., Ying, W. Y., Xie, X., et al. (2017). Maresin1 stimulates alveolar fluid clearance through the alveolar epithelial sodium channel Na,K-ATPase via the ALX/PI3K/Nedd4-2 pathway. *Lab. Invest.* 97, 543–554. doi: 10.1038/labinvest.2016.150
- Zhu, M., Wang, X., Hjorth, E., Colas, R. A., Schroeder, L., Granholm, A. C., et al. (2016). Pro-resolving lipid mediators improve neuronal survival and increase Abeta42 phagocytosis. *Mol. Neurobiol.* 53, 2733–2749. doi: 10.1007/s12035-015-9544-0
- Zilka, N., Kazmerova, Z., Jadhav, S., Neradil, P., Madari, A., Obetkova, D., et al. (2012). Who fans the flames of Alzheimer's disease brains? Misfolded tau on the crossroad of neurodegenerative and inflammatory pathways. *J. Neuroinflamm.* 9:47. doi: 10.1186/1742-2094-9-47

**Conflict of Interest:** The authors declare that the research was conducted in the absence of any commercial or financial relationships that could be construed as a potential conflict of interest.

Copyright © 2019 Yin, Wang, Wang, Wei, Feng and Zhu. This is an open-access article distributed under the terms of the Creative Commons Attribution License (CC BY). The use, distribution or reproduction in other forums is permitted, provided the original author(s) and the copyright owner(s) are credited and that the original publication in this journal is cited, in accordance with accepted academic practice. No use, distribution or reproduction is permitted which does not comply with these terms.



# Brainiac Caspases: Beyond the Wall of Apoptosis

Ana María Espinosa-Oliva, Juan García-Revilla, Isabel María Alonso-Bellido and Miguel Angel Burguillos\*

Departamento de Bioquímica y Biología Molecular, Facultad de Farmacia, Universidad de Sevilla, and Instituto de Biomedicina de Sevilla (IBiS), Hospital Universitario Virgen del Rocío/CSIC, Seville, Spain

## OPEN ACCESS

### Edited by:

Victoria Campos-Peña,  
National Institute of Neurology  
and Neurosurgery (INNN), Mexico

### Reviewed by:

Jorge Matias-Guiu,  
Complutense University of Madrid,  
Spain

Dwayne G. Stupack,  
University of California, San Diego,  
United States

### \*Correspondence:

Miguel Angel Burguillos  
maburguillos@us.es

### Specialty section:

This article was submitted to  
Cellular Neuropathology,  
a section of the journal  
Frontiers in Cellular Neuroscience

**Received:** 27 June 2019

**Accepted:** 22 October 2019

**Published:** 05 November 2019

### Citation:

Espinosa-Oliva AM,  
García-Revilla J, Alonso-Bellido IM  
and Burguillos MA (2019) Brainiac  
Caspases: Beyond the Wall  
of Apoptosis.  
Front. Cell. Neurosci. 13:500.  
doi: 10.3389/fncel.2019.00500

For the last two decades, caspases, a family of cysteine-aspartic proteases, have evolved from being considered solely as regulators of apoptosis or inflammation to having a wider range of functions. In this mini review, we focus on the most recent “non-apoptotic” roles of caspases in the CNS, particularly in neurons, astrocytes and oligodendrocytes. Non-apoptotic caspase functions in microglia have already been reviewed extensively elsewhere. Here we discuss the involvement of caspases in the activation of the inflammasome, autophagy, and non-apoptotic forms of cell death such as necroptosis and pyroptosis. Also, we review the involvement of caspases in synapses and the processing of aggregates key to neurodegenerative diseases such as Parkinson’s, Alzheimer’s and Huntington’s diseases. Likewise, we mention the recently described involvement of caspases in mitochondrial biogenesis, which is a function independent of the enzymatic activity. We conclude discussing the relevance that “new” functions of caspases have in the CNS and the future of this field of research.

**Keywords:** caspase, neuron, astrocytes, oligodendrocytes, inflammasome, necroptosis, neurodegeneration, pyroptosis

## INTRODUCTION

Caspases are a family of proteins belonging to the cysteine aspartate proteases classically associated with different forms of programmed cell death (Stennicke and Salvesen, 1999; Hyman and Yuan, 2012; Tummers and Green, 2017).

Since the discovery of CED-3 in *Caenorhabditis elegans* (Ellis and Horvitz, 1986) and the caspase-1/Interleukin-1 converting enzyme (ICE) (Thornberry et al., 1992; Yuan et al., 1993), caspases were grouped based on their function as “apoptotic” or “inflammatory.” This classification has remained useful to some extent until recently, since new non-apoptotic or non-inflammatory roles have surfaced for caspases (Shalini et al., 2015; Baena-Lopez et al., 2018; Hollville and Deshmukh, 2018). Besides, over the last decade, evidence has been gathered detailing non-apoptotic roles for caspases in astrocytes, neurons, oligodendrocytes (ODCs) and microglia (Acarin et al., 2007; Li et al., 2010; Burguillos et al., 2011; Wagner et al., 2011).

The aim of this mini-review is to provide an update on the various functions of caspases (from those described over two decades ago, to recent functions described within the last 5 years) in the CNS, focusing mainly on neurons, astrocytes and ODCs (see **Table 1**). We will only briefly discuss microglia cells as we recently published an in-depth review on this topic (Shen et al., 2018).

**TABLE 1 |** Non-apoptotic functions of caspases in different cell types.

	Cell type	Model and caspase involved	References
<b>Inflammasome</b>	<b>Astrocytes</b>	Primary cortical astrocytes from mice with $A\beta_{1-42}$ ( <b>caspase-1</b> )	Ebrahimi et al., 2018
		Primary glial cultures from WT, $Nlrp3^{-/-}$ , $Nlrp3^{-/-}$ and $Asc^{-/-}$ mice with LPC( <b>caspase-1</b> )	Freeman et al., 2017;
		Human primary astrocytes with ATP ( <b>caspase-1</b> )	Minkiewicz et al., 2013
		SOD1 mouse model/ALS patients ( <b>caspase-1</b> )	Johann et al., 2015
		Intracerebral hemorrhage mouse model ( <b>caspase-1</b> )	Wang et al., 2017
		Mouse primary astrocytes with methamphetamine ( <b>caspase-11</b> )	Du et al., 2017
	<b>Microglia</b>	EAE mouse model ( <b>caspase-8</b> )	Zhang et al., 2018
	<b>Neurons</b>	Primary cultures of human neurons under serum-deprived conditions ( <b>caspase-1</b> )	Kaushal et al., 2015
		APP <sup>Swe</sup> /PS1 <sup>dE9</sup> transgenic mice ( <b>caspase-1</b> )	Tan et al., 2014
	<b>ODCs</b>	Dopaminergic neurons from PD patients ( <b>caspase-1</b> )	von Herrmann et al., 2018
<b>Pyroptosis</b>	<b>Astrocytes</b>	Administration prenatal of dexamethasone to mice ( <b>caspase-1</b> )	Maturana et al., 2017
		Ischemia induced by the oxygen-glucose deprivation in primary cultured astrocytes from rats ( <b>caspase-1</b> )	Xia et al., 2018
		Stroke model in rats ( <b>caspase-1</b> )	
		Cultured rat cortical astrocytes with bilirubin ( <b>caspase-1</b> )	Feng et al., 2018
		Sepsis model in mice and rats induced by LPS ( <b>caspase-1</b> )	Li et al., 2019; Sun et al., 2019
		Primary cultures of human neurons under serum-deprived conditions ( <b>caspase-1</b> )	Kaushal et al., 2015
	<b>Neurons Neurons</b>	Cultured cortical neurons from rats with $A\beta$ ( <b>caspase-1</b> )	Tan et al., 2014
		SCI model in rats ( <b>caspase-1, caspase-11</b> )	Lin et al., 2016; de Rivero Vaccari et al., 2008
		Caspase-1 <sup>-/-</sup> mice subjected to controlled cortical impact injury ( <b>caspase-1</b> )	Liu et al., 2018
		Ischemic stroke model in mice ( <b>caspase-1, caspase-11</b> )	Fann et al., 2018
<b>Necroptosis</b>	<b>ODCs</b>	Ocular hypertension-injured retina in mice ( <b>caspase-1</b> )	Pronin et al., 2019
		EAE mouse model ( <b>caspase-1</b> )	McKenzie et al., 2018
		MS patients ( <b>caspase-1</b> )	
		MS patients ( <b>caspase-1</b> )	
	<b>ODCs</b>	EAE and Cuprizone mouse models of MS and in MS patients ( <b>caspase-8</b> )	Ofengeim et al., 2015
		Osmotic demyelination syndrome model in mice ( <b>caspase-8</b> )	Bouchat et al., 2018
		Neonatal rats subjected to hypoxia-ischemia ( <b>caspase-8</b> )	Qu et al., 2017
		Global cerebral ischemia/reperfusion in CA1 neurons in rats ( <b>caspase-8</b> )	Xu et al., 2016
	<b>Neurons</b>	Subarachnoid hemorrhage induced brain injury model in rats ( <b>caspase-8</b> )	Chen et al., 2018; Yuan et al., 2019
		Models of retinal degeneration in rats ( <b>caspase-8</b> )	Jang et al., 2019
<b>Synapses</b>	<b>Astrocytes</b>	Mouse spinal cord astrocytes with LPS or TNF- $\alpha$ with zVAD ( <b>caspase-8</b> )	Fan et al., 2016
		SCI model in mice ( <b>caspase-8</b> )	
		Mice stereotactically injected with LPC ( <b>caspase-8</b> )	Lloyd et al., 2019
		Cultured neurons subjected to neurotrophic factor deprivation ( <b>caspase-3, caspase-6, caspase-9</b> )	Simon et al., 2012
	<b>Microglia</b>	Caspase-3 knockout mice ( <b>caspase-3</b> )	Ertürk et al., 2014
		J20 APP transgenic mice ( <b>caspase-2</b> )	Pozueta et al., 2013
		Caspase-9 <sup>-/-</sup> mice ( <b>caspase-9</b> )	Ohsawa et al., 2010
		Caspase-3 <sup>-/-</sup> neonatal mice ( <b>caspase-3</b> )	Gu et al., 2017
		Caspase-3 knockout mice and rats ( <b>caspase-3</b> )	Li et al., 2010
		Tg2576-APP <sup>Swe</sup> mice ( <b>caspase-3</b> )	D'Amelio et al., 2011
<b>Autophagy</b>	<b>Neurons</b>	Primary cortical neurons from wt and $casp2^{-/-}$ mice with rotenone ( <b>caspase-2</b> )	Tiwari et al., 2011
		PC12 cells and cortical neurons from rats with $A\beta_{1-42}$ ( <b>caspase-3</b> )	Wang et al., 2017
		APP <sup>Swe</sup> /PS1 <sup>dE9</sup> transgenic mice ( <b>caspase-3</b> )	
<b>Mitochondria Biogenesis</b>	<b>Neurons</b>	Dopaminergic cell line ( <b>procaspase-3</b> )	Kim et al., 2018

## Caspases Inflammasome and Pyroptosis

The inflammasome (Martinon et al., 2002) is a multiprotein intracellular complex that senses pathogenic microorganisms and sterile stressors, which ultimately processes and releases IL-1 $\beta$

and IL-18. The activation of the inflammasome consists of a two-step pathway (First step: TLR activation; Second step: e.g., ATP). This leads to caspase-1, caspase-11 (de Rivero Vaccari et al., 2014; Walsh et al., 2014; Broz and Dixit, 2016;

Voet et al., 2019) and caspase-8 (Zhang et al., 2018) activation. Also intracellular lipopolysaccharide (LPS) may bind directly to caspase-11, promoting its activation (Shen et al., 2018). Inflammasomes are categorized as canonical (caspase-1) or non-canonical (caspase-11) (Broz and Dixit, 2016) (for the general signaling pathway, see **Figure 1A**). In microglia cells, a recent study described a non-canonical inflammasome associated to caspase-8 (and independently of caspase-1), in which microglia were able to generate IL-1 $\beta$  in an Experimental autoimmune encephalomyelitis (EAE) mouse model (Zhang et al., 2018). This finding is contradictory of a previous study done in Bone Marrow Derived Macrophages (BMDM), where caspase-1 deficiency is necessary for caspase-8 processing and release of IL-1 $\beta$  (Schneider et al., 2017).

The activation of the inflammasome can evolve into a process of regulated cell death termed pyroptosis, which acts as a defense mechanism against infection by inducing pathological inflammation (Tait et al., 2014). In pyroptosis, both caspase-1 and caspase-11 (caspase-4 and caspase-5 in humans) have been described as mediators of this type of cell death (for the general signaling pathway, see **Figure 1A**; Aglietti et al., 2016; Pronin et al., 2019).

Inflammasomes were originally described in immune cells (Shen et al., 2018) though the presence of the inflammasome in other cells than microglia in the CNS has been reported too. In astrocytes, crucial regulators of the immune responses in the injured CNS, the presence of canonical and non-canonical inflammasomes occurs upon treatment with different stimuli *in vitro* (Minkiewicz et al., 2013; Du et al., 2017; Freeman et al., 2017; Ebrahimi et al., 2018). *In vivo*, high expression levels of nucleotide-binding oligomerization domain-like receptor protein (NLRP) 3 related to the neuroinflammatory response has been found in astrocytes of SOD1 mice and in Amyotrophic lateral sclerosis (ALS) patients (Johann et al., 2015). Also, different studies showed astrocytic pyroptosis in animal models of sepsis induced by LPS (Li et al., 2019; Sun et al., 2019).

Besides microglia and astrocytes, the presence of different types of inflammasomes have been reported in non-immune related cells, such as neurons (**Figure 1B** and **Table 1**). Over 10 years ago, the existence of NACHT leucine-rich-repeat protein 1 (NALP1) neuronal inflammasome was reported (Kummer et al., 2007). Since then, several studies have demonstrated that activation of the inflammasome occurs in neurons, followed normally by cell death induced by pyroptosis. In the context of Alzheimer's disease (AD), pyroptosis occurs upon amyloid- $\beta$  (A $\beta$ ) treatment *in vitro*, as well as *in vivo* in the APPSwe/PS1dE9 mice. In both cases, either knockdown of NLRP1 (another type of inflammasome) or caspase-1 conferred neuroprotection (Tan et al., 2014). Interestingly, in a recent study, NLRP3 inflammasome was characterized in dopaminergic neurons from Parkinson's disease (PD) patients (von Herrmann et al., 2018). In this study the authors identified, via exome sequencing, a single-nucleotide polymorphisms (SNPs) for NLRP3 which results in a less soluble form of NLRP3 protein than NLRP3 wild-type. This less soluble form was associated with a significantly reduced risk of developing PD, highlighting the relevance

of NLRP3 inflammasome in dopaminergic neurons in PD (von Herrmann et al., 2018).

In a recent study by Tsuchiya et al. (2019), the authors described how it was possible to alter the type of neuronal death (from pyroptosis to apoptosis), based on the levels of expression of Gasdermin D (GSDMD). GSDMD is a specific substrate for caspase-1, -4, -5 and -11, whose N-terminal cleavage product has a pore-forming activity that causes cell swelling and lysis via pyroptosis. In this sense, cortical neurons may die through apoptosis instead of pyroptosis after oxygen-glucose deprivation (OGD) and nigericin stimulation due to low expression of GSDMD (Tsuchiya et al., 2019).

Finally, in ODCs, the relevance of inflammasome activation has not been as well documented, with only a few reports published. For instance, prenatal administration of dexamethasone to mice, a treatment that promotes demyelination, induces NLRP3, caspase-1 and Apoptosis-associated speck-like protein containing a CARD (ASC) expression in ODCs, which the authors suggested could be contributing to demyelination (Maturana et al., 2017). Also, pyroptosis has been observed in myelin-forming ODCs in the EAE mice and in patients with Multiple sclerosis (MS) (McKenzie et al., 2018). In this case, inhibition of caspase-1, using the inhibitor VX-756, reduced pyroptosis in ODCs and microglia and promoted neuroprotection and improved performance in different neurobehavioral tests. In this case is hard to distinguish if VX-756 beneficial effect over behavior is based on inhibition of inflammasome and/or pyroptosis or both.

## Caspases and Necroptosis

Originally necroptosis was considered a passive death of cells under pathological conditions, where the cellular contents are released and cause an immune response. However, currently it is considered a cell death pathway regulated through the interaction of different molecules including receptor-interacting protein kinase (RIPK)-1 and RIPK3, mixed lineage kinase domain-like protein (MLKL), and caspase-8 (whose activity is inhibited for instance by caspase-8 or pan-caspase inhibitors) (**Figure 1A**; Tait et al., 2014; Ofengeim et al., 2015).

Necroptosis mediates ODC degeneration induced by TNF- $\alpha$ , whose binding to TNFR1 triggers caspase-8 activation, and the inhibition of RIPK1 protects against ODC cell death in two animal models to study MS, and also in cell culture (Ofengeim et al., 2015). In the same paper, the authors found in cortical lesions of human MS samples defective caspase-8 activation and activation of RIPK1, RIPK3, and MLKL. Also in a different *in vivo* model of osmotic demyelination syndrome, ODC cell death has been linked to necroptosis based on an increase of phospho-MLKL immunoreactivity (Bouchat et al., 2018), but further experiments are needed to confirm this result.

In the developing brain, a study showed that neonatal rats subjected to hypoxia-ischemia (HI) and ODCs from neonatal rats treated with OGD together with the pan-caspase activity inhibitor zVAD die via necroptosis (Qu et al., 2017). Treatments aimed to block the interaction of RIPK3 with MLKL or CaMKII $\delta$ , a new described substrate of RIPK3, managed to decrease necroptosis under these conditions (Qu et al., 2017).



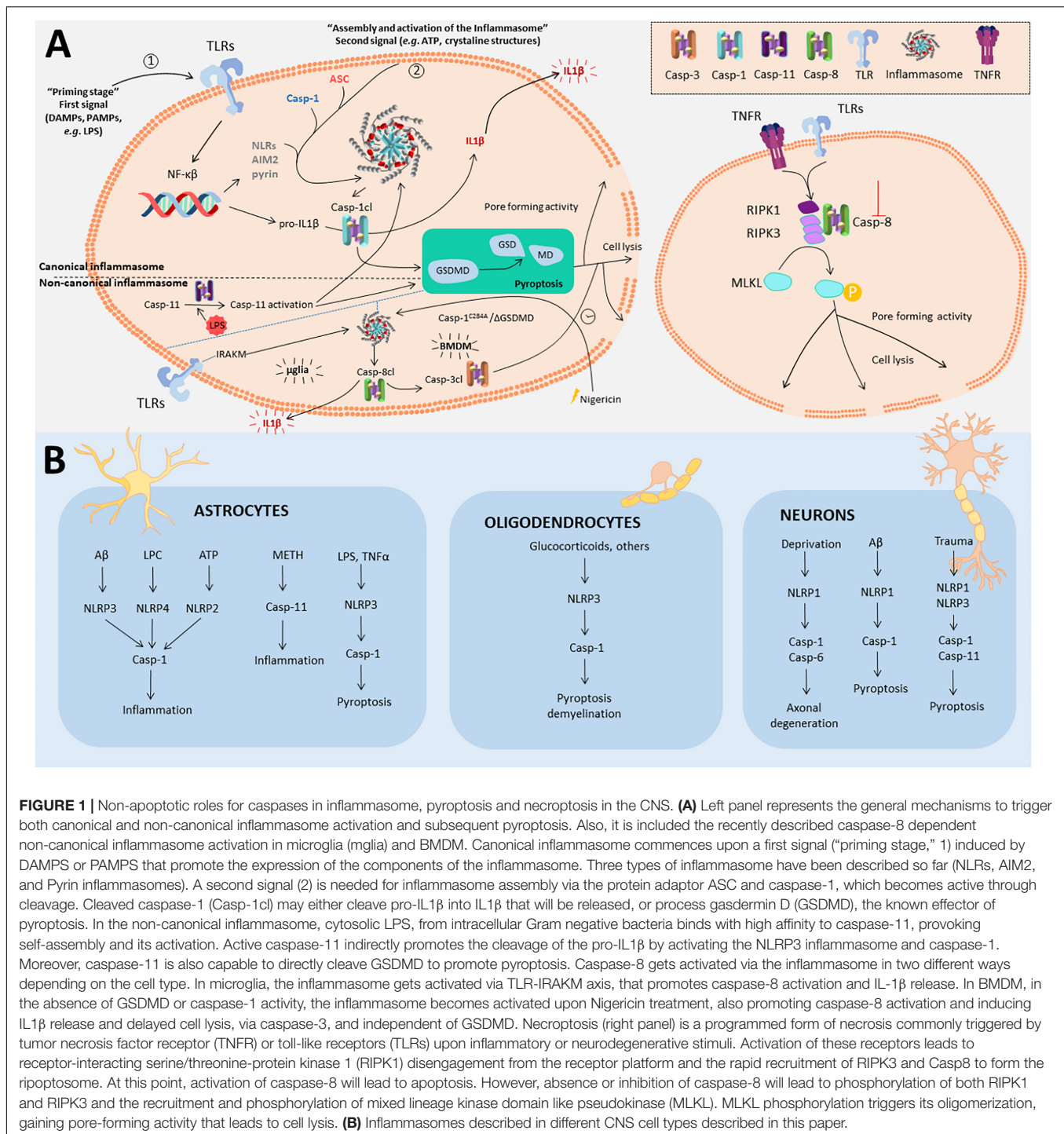


**FIGURE 1 |** Non-apoptotic roles for caspases in inflammasome, pyroptosis and necroptosis in the CNS. **(A)** Left panel represents the general mechanisms to trigger both canonical and non-canonical inflammasome activation and subsequent pyroptosis. Also, it is included the recently described caspase-8 dependent non-canonical inflammasome activation in microglia (mglia) and BMDM. Canonical inflammasome commences upon a first signal ("priming stage," 1) induced by DAMPs or PAMPs that promote the expression of the components of the inflammasome. Three types of inflammasome have been described so far (NLRs, AIM2, and Pyrin inflammasomes). A second signal (2) is needed for inflammasome assembly via the protein adaptor ASC and caspase-1, which becomes active through cleavage. Cleaved caspase-1 (Casp-1cl) may either cleave pro-IL1 $\beta$  into IL1 $\beta$  that will be released, or process gasdermin D (GSDMD), the known effector of pyroptosis. In the non-canonical inflammasome, cytosolic LPS, from intracellular Gram negative bacteria binds with high affinity to caspase-11, provoking self-assembly and its activation. Active caspase-11 indirectly promotes the cleavage of the pro-IL1 $\beta$  by activating the NLRP3 inflammasome and caspase-1. Moreover, caspase-11 is also capable to directly cleave GSDMD to promote pyroptosis. Caspase-8 gets activated via the inflammasome in two different ways depending on the cell type. In microglia, the inflammasome gets activated via TLR-IRAKM axis, that promotes caspase-8 activation and IL-1 $\beta$  release. In BMDM, in the absence of GSDMD or caspase-1 activity, the inflammasome becomes activated upon Nigericin treatment, also promoting caspase-8 activation and inducing IL1 $\beta$  release and delayed cell lysis, via caspase-3, and independent of GSDMD. Necroptosis (right panel) is a programmed form of necrosis commonly triggered by tumor necrosis factor receptor (TNFR) or toll-like receptors (TLRs) upon inflammatory or neurodegenerative stimuli. Activation of these receptors leads to receptor-interacting serine/threonine-protein kinase 1 (RIPK1) disengagement from the receptor platform and the rapid recruitment of RIPK3 and Casp8 to form the ripoptosome. At this point, activation of caspase-8 will lead to apoptosis. However, absence or inhibition of caspase-8 will lead to phosphorylation of both RIPK1 and RIPK3 and the recruitment and phosphorylation of mixed lineage kinase domain like pseudokinase (MLKL). MLKL phosphorylation triggers its oligomerization, gaining pore-forming activity that leads to cell lysis. **(B)** Inflammasomes described in different CNS cell types described in this paper.

Interestingly in neurons, a new interaction of RIPK3 with the protein apoptosis-inducing factor (AIF) has been reported. Their interaction and translocation into the nucleus in a model of 20-min global cerebral ischemia/reperfusion (I/R) has been described in CA1 neurons, which was critical to ischemic DNA degradation and programmed necrosis (Xu et al., 2016). The fact that these CA1 neurons lack caspase-8 expression, facilitates necroptosis in these cells.

In astrocytes, a study performed in mouse spinal cord astrocytes treated with LPS or TNF- $\alpha$  with zVAD *in vitro*, and subjected to spinal cord injury (SCI) *in vivo*, showed an increase in the expression of RIPK3 and MLKL proteins (Fan et al., 2016). Treatment with the chemical inhibitor of RIPK1 (Necrostatin-1) or RIPK3 genetic ablation (Fan et al., 2016) rescued the cells.

In the case of neurons, in a model of subarachnoid hemorrhage it has been reported that neuronal death occurs

via RIPK3 and MKLK (Chen et al., 2018; Yuan et al., 2019). Moreover, inhibition of RIPK1 [using RIPK1-inhibitory compound (RIC)] in retinal degenerative diseases induced by glaucomatous insult has been proved to exert a neuroprotective effect (Jang et al., 2019).

Intriguingly, while necroptosis of neurons, ODCs and astrocytes is associated normally with demyelination and neurodegeneration, a new report in microglia cells (Lloyd et al., 2019) proposes that the remyelination process in white matter is driven by proinflammatory microglia necroptosis and the subsequent repopulation of positively regulated by type-1 IFN signaling microglia.

## Caspases and Synapses

In the mature CNS, caspases are not only involved in mediating cell death but also regulatory events that are important for neuronal functions, such as, axon pruning and synapse elimination (D'Amelio et al., 2010; Hyman and Yuan, 2012; Hollville and Deshmukh, 2018).

During axonal pruning, the absence of neurotrophic factors provokes caspase-3/6 activation via JNK that facilitates mitochondrial depolarization (Hollville and Deshmukh, 2018). The role of caspases in axon pruning has also been studied in the context of axon degeneration induced by neurotrophic factor deprivation in sympathetic neurons. Caspase-3, caspase-6 or caspase-9 are required for the axon selective degeneration or pruning (Simon et al., 2012) but not Apaf-1 (Cusack et al., 2013), which is required for triggering cell death upon axonal Neuronal Growth Factor (NGF) deprivation. Caspase-3 was also found to control spine density and dendrite morphology in specific areas within the cell generating supernumerary spines in caspase-3 knockout mice (Ertürk et al., 2014). Caspase-2 participates in the control of dendrite spine density via activation of the RhoA/ROCK-II signaling pathway (Pozueta et al., 2013). Caspase-2 deficiency in J20 APP transgenic mice did not thwart cognitive function despite having similar A $\beta$  load and neuroinflammatory response to wild type animals (Pozueta et al., 2013).

Caspases are also involved in axonal guidance and synaptogenesis like for instance caspase-9-mediated cleavage of Semaphorin 7 mediates the proper projection of axons in sensory neurons (Ohsawa et al., 2010). In the spinal cord of neonatal mice, caspase-3 regulates the number of axonal branches via Bax/Bak in the axons of corticospinal neurons. Early postnatal inactivation of Bax/Bak in motor cortex results in increased axonal branches in the spine of these animals when they reach adulthood. As a consequence, connectivity's fine-tuning is lost and animals fail to acquire fine voluntary movements (Gu et al., 2017).

Normal brain functions depend on proper synaptic activity. Long-term potentiation (LTP) and long-term depression (LTD) are long-lasting modifications of synapses in the hippocampus region. Activation of caspase-3 during LTD occurs without cell death (Li et al., 2010; Simon et al., 2012) and facilitates the internalization of AMPA receptor in the postsynaptic membrane. Furthermore, caspase-3 promotes modifications in

AMPA-type receptor that lead to alterations of glutamatergic synaptic transmission and plasticity in Tg2576-APP<sup>Swe</sup> mice. Notably, pharmacological inhibition of caspase-3 activity in these mice rescued the observed AD-like phenotypes (D'Amelio et al., 2011).

## Caspases and Neurotoxic Protein Aggregates

Caspases play a significant role in the pathogenesis of different neurodegenerative diseases including AD, PD and Huntington's disease (HD), since they are able to modify the properties of different neurotoxic proteins aggregates (amyloid precursor protein (APP), Tau,  $\alpha$ -synuclein ( $\alpha$ -Syn) and huntingtin (htt) through cleavage.

Under apoptotic conditions, caspases cleave APP, either directly or following  $\gamma$ -secretase generation of the AICD fragment, to generate the C31 and Jcasp peptides [for more information see review (Nhan et al., 2015)]. While AICD and C31 are associated with cell death *in vitro* (Lu et al., 2000; Bertrand et al., 2001; Park et al., 2009), the impact of this *in vivo* may be minimal, since mice bearing mutant caspase-resistant APP displayed no rescue in learning or memory in a mouse model of AZ (Harris et al., 2010).

Tau is another substrate processed by caspases early in the progression of AD (Rissman et al., 2004). Cleaved Tau promotes nucleation-dependent filament formation which is phosphorylated by glycogen synthase kinase-3b in a process mediated by caspase-3 (Chu et al., 2017). Recently, it has been shown that caspase-2 specific cleavage in Tau provokes an inadequate sorting of Tau toward the dendritic spines, promoting cognitive impairment and synaptic dysfunction (Zhao et al., 2016). Interestingly, cleavage of APP promotes phosphorylation of Tau in different residues, in a process where C31 binds to the asparagine, proline, threonine, tyrosine (NPTY) motif of the catalytic subunit of the phosphatase PP2A, repressing its activity (Park et al., 2012).

$\alpha$ -Syn is an abundantly expressed neuronal protein localized in the presynaptic terminals of neurons.  $\alpha$ -Syn is key to understanding the etiology of a group of overlapping neurodegenerative disorders called  $\alpha$ -synucleinopathies, including PD.  $\alpha$ -Syn is processed through caspase-1 forming a truncated protein whose effect is to accelerate the formation of aggregates as compared to the full-length form of  $\alpha$ -Syn (Wang et al., 2016). Interestingly, truncated  $\alpha$ -Syn itself stimulates caspase-1 activation which promotes more cleavage of  $\alpha$ -Syn, in a positive feedback loop (Ma et al., 2018).

Finally, caspase cleavage of htt induces its accumulation in the nuclei of neurons of HD patients (Graham et al., 2010). Caspase-6 cleaves htt, and caspase-6 activation has been observed before the onset of motor abnormalities both in mouse and human HD brains (Graham et al., 2010). Strikingly, *in vivo* experiments using YAC mice expressing caspase-6-resistant cleavage of htt, showed no striatal neurodegeneration. Recently a new caspase cleavage site of htt has been described, in this case depending on caspase-1 activity that promotes aggregation of mutant htt (Martin et al., 2019).

While the evidence gathered in PD and HD studies suggests that caspase-dependent processing of  $\alpha$ -Syn and htt may play a role in the pathogenesis of the diseases, conflicting results for APP *in vitro* and *in vivo* have been observed in AD models, requiring further investigation.

Also, the experiments to study cleavage of APP by caspases have been performed under apoptotic conditions, which makes difficult to conclude if the caspase cleavage of APP plays any pathological role or is just “collateral damage” that occurs during apoptosis. Further experiments under non-cell death conditions should be performed to resolve this issue.

## Caspases and Autophagy and Mitochondria Biogenesis

Autophagy is a catabolic process that delivers cytoplasmic constituents into lysosome for degradation and eventual recycling. Under physiological conditions, autophagy promotes cell survival by elimination of damaged organelles and proteins aggregates (Zare-Shahabadi et al., 2015). However, autophagy has also been linked to cell death, either promoting it (Das et al., 2012) or at least being associated with it (Kroemer and Levine, 2008). Evidence suggests that autophagy may be controlled by caspases during apoptosis (Tsapras and Nezis, 2017). However, evidence of the interaction between autophagy-related proteins and caspases in the CNS are still scarce. In primary cultures of cortical neurons treated with rotenone, lack of caspase-2 prolonged cell survival by enhancing autophagy. However, the cells die eventually via necrosis (Tiwari et al., 2011).

A recent study showed that caspase-3-induced Beclin-1 cleavage and subcellular redistribution of the Beclin-1 N-terminal into the nucleus has been shown in neuron-glia co-cultures with A $\beta$ <sub>1–42</sub> and APPSwe/PS1dE9 mice. The authors hypothesized that cleavage of Beclin-1 by caspase-3 could affect autophagy and lead to defective protein clearance and neuronal death (Wang et al., 2017).

Despite all these roles that we have discussed in this mini-review, new and exciting roles are still emerging for caspases in the CNS. For instance, in a recent study performed by Kim et al. (2018) in dopaminergic neurons, the authors described how procaspase-3 acts as a regulator for mitochondria biogenesis without affecting autophagy. They showed that TFAM, Nrf-1, and PGC-1 $\alpha$  (transcriptional activators of mitochondrial biogenesis) are regulated by procaspase-3. Furthermore, in the same study, the authors show that lack of procaspase-3 in dopaminergic neurons dramatically reduced electron transport chain complex I, II, and IV activity. Interestingly, treatment with caspase-3 inhibitor failed to mimic the observed effects thus raising the view that caspase-3-dependent mitochondrial biogenesis is independent of its catalytic activity.

## DISCUSSION

Within the last decade, there has been an exponential growth in the number of studies of non-apoptotic functions of caspases.

Some of these non-apoptotic roles have been extensively studied in specific cell types, such as the inflammasome in immune cells (Martinon et al., 2002). In the CNS, while many of these non-apoptotic functions have been studied in microglia cells, few reports have been published for neurons, astrocytes and ODCs in comparison. Here we attempt to shed light onto some “old and new” non-apoptotic functions for caspases in these cell types, which have been gathering momentum in recent years and their relevance under pathological conditions.

Why does the activation of executioner caspases not translate always into an apoptotic process? A possible explanation could be sequestration of effector caspases into different subcellular compartments (Li et al., 2010; Kavanagh et al., 2014; Amcheslavsky et al., 2018) and/or cleavage of non-cell death related substrates (Acarin et al., 2007).

Different manners in which caspases affect cellular signaling continue to emerge. Besides the diverse mechanisms employed to activate different caspases already commented in this mini-review, it has been shown that the reduction of the basal activity of caspase-3 promotes a change toward a tumor supportive phenotype in microglia cells in contact with glioma cells (Shen et al., 2016). Also, and in agreement with this, in embryonic stem cells (ESCs), basal caspase-3 activity regulates cell differentiation of these cells through Nanog processing (Baena-Lopez et al., 2018). We have also discussed previously in this mini-review how the zymogen (procaspase-3) mediates the mitochondrial biogenesis independently of its enzymatic activity (Kim et al., 2018). It is possible that these functions of caspase-3 can be extended to other caspases, opening new possibilities in the field of caspase biology, for new mechanistic roles of caspases with relevance not only limited to the CNS but applicable to all cell types.

## AUTHOR CONTRIBUTIONS

MB and AE-O conceived the main outline. MB wrote the manuscript. All authors searched the references and decided the contents of the mini review.

## FUNDING

JG-R has been funded by a grant from the Spanish Ministerio de Economía y Competitividad SAF2015-64171-R (MINECO/FEDER, EU). MB has been funded by the Spanish Ministerio de Economía y Competitividad (Programa Ramón y Cajal: RYC-2017-21804).

## ACKNOWLEDGMENTS

We apologize to colleagues whose work we have not cited here as a result of space limitations.



## REFERENCES

- Acarin, L., Villapol, S., Faiz, M., Rohn, T. T., Castellano, B., and Gonzalez, B. (2007). Caspase-3 activation in astrocytes following postnatal excitotoxic damage correlates with cytoskeletal remodeling but not with cell death or proliferation. *Glia* 55, 954–965. doi: 10.1002/glia.20518
- Aglietti, R. A., Estevez, A., Gupta, A., Ramirez, M. G., Liu, P. S., Kayagaki, N., et al. (2016). GsdmD p30 elicited by caspase-11 during pyroptosis forms pores in membranes. *Proc. Natl. Acad. Sci. U.S.A.* 113, 7858–7863. doi: 10.1073/pnas.1607769113
- Amcheslavsky, A., Wang, S., Fogarty, C. E., Lindblad, J. L., Fan, Y., and Bergmann, A. (2018). Plasma membrane localization of apoptotic caspases for non-apoptotic functions. *Dev. Cell* 45, 450–464.e3. doi: 10.1016/j.devcel.2018.04.020
- Baena-Lopez, L. A., Arthunrton, L., Xu, D. C., and Galasso, A. (2018). Non-apoptotic caspase regulation of stem cell properties. *Semin. Cell Dev. Biol.* 82, 118–126. doi: 10.1016/j.semcdb.2017.10.034
- Bertrand, E., Brouillet, E., Caillé, I., Bouillot, C., Cole, G. M., Prochiantz, A., et al. (2001). A short cytoplasmic domain of the amyloid precursor protein induces apoptosis *in vitro* and *in vivo*. *Mol. Cell. Neurosci.* 18, 503–511. doi: 10.1006/mcne.2001.1030
- Bouchat, J., Couturier, B., Marneffe, C., Gankam-Kengne, F., Balau, B., De Swert, K., et al. (2018). Regional oligodendrocytopathy and astrocytopathy precede myelin loss and blood-brain barrier disruption in a murine model of osmotic demyelination syndrome. *Glia* 66, 606–622. doi: 10.1002/glia.23268
- Broz, P., and Dixit, V. M. (2016). Inflammasomes: mechanism of assembly, regulation and signalling. *Nat. Rev. Immunol.* 16, 407–420. doi: 10.1038/nri.2016.58
- Burguillos, M. A., Deierborg, T., Kavanagh, E., Persson, A., Hajji, N., Garcia-Quintanilla, A., et al. (2011). Caspase signalling controls microglia activation and neurotoxicity. *Nature* 472, 319–324. doi: 10.1038/nature09788
- Chen, T., Pan, H., Li, J., Xu, H., Jin, H., Qian, C., et al. (2018). Inhibiting of RIPK3 attenuates early brain injury following subarachnoid hemorrhage: possibly through alleviating necroptosis. *Biomed. Pharmacother.* 107, 563–570. doi: 10.1016/j.biopha.2018.08.056
- Chu, J., Lauretti, E., and Praticò, D. (2017). Caspase-3-dependent cleavage of Akt modulates tau phosphorylation via GSK3 $\beta$  kinase: implications for Alzheimer's disease. *Mol. Psychiatry* 22, 1002–1008. doi: 10.1038/mp.2016.214
- Cusack, C. L., Swahari, V., Hampton Henley, W., Michael Ramsey, J., and Deshmukh, M. (2013). Distinct pathways mediate axon degeneration during apoptosis and axon-specific pruning. *Nat. Commun.* 4:1876. doi: 10.1038/ncomms2910
- D'Amelio, M., Cavallucci, V., and Cecconi, F. (2010). Neuronal caspase-3 signaling: not only cell death. *Cell Death Differ.* 17, 1104–1114. doi: 10.1038/cdd.2009.180
- D'Amelio, M., Cavallucci, V., Middei, S., Marchetti, C., Pacioni, S., Ferri, A., et al. (2011). Caspase-3 triggers early synaptic dysfunction in a mouse model of Alzheimer's disease. *Nat. Neurosci.* 14, 69–76. doi: 10.1038/nn.2709
- Das, G., Shrivastava, B. V., and Baehrecke, E. H. (2012). Regulation and function of autophagy during cell survival and cell death. *Cold Spring Harb. Perspect. Biol.* 4:a008813. doi: 10.1101/cshperspect.a008813
- de Rivero Vaccari, J. P., Dietrich, W. D., and Keane, R. W. (2014). Activation and regulation of cellular inflammasomes: gaps in our knowledge for central nervous system injury. *J. Cereb. Blood Flow Metab.* 34, 369–375. doi: 10.1038/jcbfm.2013.227
- de Rivero Vaccari, J. P., Lotocki, G., Marcillo, A. E., Dietrich, W. D., and Keane, R. W. (2008). A molecular platform in neurons regulates inflammation after spinal cord injury. *J. Neurosci.* 28, 3404–3414. doi: 10.1523/JNEUROSCI.0157-08.2008
- Du, S. H., Qiao, D. F., Chen, C. X., Chen, S., Liu, C., Lin, Z., et al. (2017). Toll-like receptor 4 mediates methamphetamine-induced neuroinflammation through Caspase-11 signaling pathway in astrocytes. *Front. Mol. Neurosci.* 10:409. doi: 10.3389/fnmol.2017.00409
- Ebrahimi, T., Rust, M., Kaiser, S. N., Slowik, A., Beyer, C., Koczulla, A. R., et al. (2018).  $\alpha$ 1-antitrypsin mitigates NLRP3-inflammasome activation in amyloid  $\beta$ 1–42-stimulated murine astrocytes. *J. Neuroinflammation* 15:282. doi: 10.1186/s12974-018-1319-x
- Ellis, H. M., and Horvitz, H. R. (1986). Genetic control of programmed cell death in the nematode *C. elegans*. *Cell* 44, 817–829. doi: 10.1016/0092-8674(86)90004-8
- Ertürk, A., Wang, Y., and Sheng, M. (2014). Local pruning of dendrites and spines by caspase-3-dependent and proteasome-limited mechanisms. *J. Neurosci.* 34, 1672–1688. doi: 10.1523/JNEUROSCI.3121-13.2014
- Fan, H., Zhang, K., Shan, L., Kuang, F., Chen, K., Zhu, K., et al. (2016). Reactive astrocytes undergo M1 microglia/macrophages-induced necroptosis in spinal cord injury. *Mol. Neurodegener.* 11:14. doi: 10.1186/s13024-016-0081-8
- Fann, D. Y., Lim, Y. A., Cheng, Y. L., Lok, K. Z., Chunduri, P., Baik, S. H., et al. (2018). Evidence that NF- $\kappa$ B and MAPK signaling promotes NLRP inflammasome activation in neurons following ischemic stroke. *Mol. Neurobiol.* 55, 1082–1096. doi: 10.1007/s12035-017-0394-9
- Feng, J., Li, M., Wei, Q., Li, S., Song, S., and Hua, Z. (2018). Unconjugated bilirubin induces pyroptosis in cultured rat cortical astrocytes. *J. Neuroinflammation* 15:23. doi: 10.1186/s12974-018-1064-1
- Freeman, L., Guo, H., David, C. N., Brickey, W. J., Jha, S., and Ting, J. P. (2017). NLR members NLRC4 and NLRP3 mediate sterile inflammasome activation in microglia and astrocytes. *J. Exp. Med.* 214, 1351–1370. doi: 10.1084/jem.20150237
- Graham, R. K., Deng, Y., Carroll, J., Vaid, K., Cowan, C., Pouladi, M. A., et al. (2010). Cleavage at the 586 amino acid caspase-6 site in mutant huntingtin influences caspase-6 activation *in vivo*. *J. Neurosci.* 30, 15019–15029. doi: 10.1523/JNEUROSCI.2071-10.2010
- Gu, Z., Serradi, N., Ueno, M., Liang, M., Li, J., Baccei, M. L., et al. (2017). Skilled movements require non-apoptotic Bax/Bak pathway-mediated corticospinal circuit reorganization. *Neuron* 94, 626–641.e4. doi: 10.1016/j.neuron.2017.04.019
- Harris, J. A., Devidze, N., Halabisky, B., Lo, I., Thwin, M. T., Yu, G. Q., et al. (2010). Many neuronal and behavioral impairments in transgenic mouse models of Alzheimer's disease are independent of caspase cleavage of the amyloid precursor protein. *J. Neurosci.* 30, 372–381. doi: 10.1523/JNEUROSCI.5341-09.2010
- Hollville, E., and Deshmukh, M. (2018). Physiological functions of non-apoptotic caspase activity in the nervous system. *Semin. Cell Dev. Biol.* 82, 127–136. doi: 10.1016/j.semcdb.2017.11.037
- Hyman, B. T., and Yuan, J. (2012). Apoptotic and non-apoptotic roles of caspases in neuronal physiology and pathophysiology. *Nat. Rev. Neurosci.* 13, 395–406. doi: 10.1038/nrn3228
- Jang, K. H., Do, Y. J., Koo, T. S., Choi, J. S., Song, E. J., Hwang, Y., et al. (2019). Protective effect of RIPK1-inhibitory compound in *in vivo* models for retinal degenerative disease. *Exp. Eye Res.* 180, 8–17. doi: 10.1016/j.exer.2018.11.026
- Johann, S., Heitzer, M., Kanagaratnam, M., Goswami, A., Rizo, T., Weis, J., et al. (2015). NLRP3 inflammasome is expressed by astrocytes in the SOD1 mouse model of ALS and in human sporadic ALS patients. *Glia* 63, 2260–2273. doi: 10.1002/glia.22891
- Kaushal, V., Dye, R., Pakavathkumar, P., Foveau, B., Flores, J., Hyman, B., et al. (2015). Neuronal NLRP1 inflammasome activation of Caspase-1 coordinately regulates inflammatory interleukin-1-beta production and axonal degeneration-associated Caspase-6 activation. *Cell Death Differ.* 22, 1676–1686. doi: 10.1038/cdd.2015.16
- Kavanagh, E., Rodhe, J., Burguillos, M. A., Venero, J. L., and Joseph, B. (2014). Regulation of caspase-3 processing by cIAP2 controls the switch between pro-inflammatory activation and cell death in microglia. *Cell Death Dis.* 5:e1565. doi: 10.1038/cddis.2014.514
- Kim, J. S., Ha, J. Y., Yang, S. J., and Son, J. H. (2018). A novel non-apoptotic role of procaspase-3 in the regulation of mitochondrial biogenesis activators. *J. Cell. Biochem.* 119, 347–357. doi: 10.1002/jcb.26186
- Kroemer, G., and Levine, B. (2008). Autophagic cell death: the story of a misnomer. *Nat. Rev. Mol. Cell Biol.* 9, 1004–1010. doi: 10.1038/nrm2529
- Kummer, J. A., Broekhuizen, R., Everett, H., Agostini, L., Kuijk, L., Martinon, F., et al. (2007). Inflammasome components NALP 1 and 3 show distinct but separate expression profiles in human tissues suggesting a site-specific role in the inflammatory response. *J. Histochem. Cytochem.* 55, 443–452. doi: 10.1369/jhc.6a7101.2006
- Li, L., Shu, M. Q., and Chen, J. (2019). CYLD deficiency exacerbates lipopolysaccharide (LPS)-induced pyroptosis in astrocytes of mice with sepsis. *Biochem. Biophys. Res. Commun.* 514, 1066–1073. doi: 10.1016/j.bbrc.2019.05.033
- Li, Z., Jo, J., Jia, J. M., Lo, S. C., Whitcomb, D. J., Jiao, S., et al. (2010). Caspase-3 activation via mitochondria is required for long-term depression



- and AMPA receptor internalization. *Cell* 141, 859–871. doi: 10.1016/j.cell.2010.03.053
- Lin, W. P., Xiong, G. P., Lin, Q., Chen, X. W., Zhang, L. Q., Shi, J. X., et al. (2016). Heme oxygenase-1 promotes neuron survival through down-regulation of neuronal NLRP1 expression after spinal cord injury. *J. Neuroinflammation* 13:52. doi: 10.1186/s12974-016-0521-y
- Liu, W., Chen, Y., Meng, J., Wu, M., Bi, F., Chang, C., et al. (2018). Ablation of caspase-1 protects against TBI-induced pyroptosis in vitro and in vivo. *J. Neuroinflammation* 15:48. doi: 10.1186/s12974-018-1083-y
- Lloyd, A. F., Davies, C. L., Holloway, R. K., Labrak, Y., Ireland, G., Carradori, D., et al. (2019). Central nervous system regeneration is driven by microglia necroptosis and repopulation. *Nat. Neurosci.* 22, 1046–1052. doi: 10.1038/s41593-019-0418-z
- Lu, D. C., Rabizadeh, S., Chandra, S., Shayya, R. F., Ellerby, L. M., Ye, X., et al. (2000). A second cytotoxic proteolytic peptide derived from amyloid  $\beta$ -protein precursor. *Nat. Med.* 6, 397–404. doi: 10.1038/74656
- Ma, L., Yang, C., Zhang, X., Li, Y., Wang, S., Zheng, L., et al. (2018). C-terminal truncation exacerbates the aggregation and cytotoxicity of  $\alpha$ -Synuclein: a vicious cycle in Parkinson's disease. *Biochim. Biophys. Acta Mol. Basis Dis.* 1864, 3714–3725. doi: 10.1016/j.bbdis.2018.10.003
- Martin, D. D. O., Schmidt, M. E., Nguyen, Y. T., Lazic, N., and Hayden, M. R. (2019). Identification of a novel caspase cleavage site in huntingtin that regulates mutant huntingtin clearance. *FASEB J.* 33, 3190–3197. doi: 10.1096/fj.201701510RRR
- Martinon, F., Burns, K., and Tschopp, J. (2002). The inflammasome: a molecular platform triggering activation of inflammatory caspases and processing of proIL- $\beta$ . *Mol. Cell.* 10, 417–426.
- Maturana, C. J., Aguirre, A., and Sáez, J. C. (2017). High glucocorticoid levels during gestation activate the inflammasome in hippocampal oligodendrocytes of the offspring. *Dev. Neurobiol.* 77, 625–642. doi: 10.1002/dneu.22409
- McKenzie, B. A., Mamik, M. K., Saito, L. B., Boghazian, R., Monaco, M. C., Major, E. O., et al. (2018). Caspase-1 inhibition prevents glial inflammasome activation and pyroptosis in models of multiple sclerosis. *Proc. Natl. Acad. Sci. U.S.A.* 115, E6065–E6074. doi: 10.1073/pnas.1722041115
- Minkiewicz, J., de Rivero Vaccari, J. P., and Keane, R. W. (2013). Human astrocytes express a novel NLRP2 inflammasome. *Glia* 61, 1113–1121. doi: 10.1002/glia.22499
- Nhan, H. S., Chiang, K., and Koo, E. H. (2015). The multifaceted nature of amyloid precursor protein and its proteolytic fragments: friends and foes. *Acta Neuropathol.* 129, 1–19. doi: 10.1007/s00401-014-1347-2
- Ofengeim, D., Ito, Y., Najafav, A., Zhang, Y., Shan, B., DeWitt, J. P., et al. (2015). Activation of necroptosis in multiple sclerosis. *Cell Rep.* 10, 1836–1849.
- Ohsawa, S., Hamada, S., Kuida, K., Yoshida, H., Igaki, T., and Miura, M. (2010). Maturation of the olfactory sensory neurons by Apaf-1/caspase-9-mediated caspase activity. *Proc. Natl. Acad. Sci. U.S.A.* 107, 13366–13371. doi: 10.1073/pnas.0910488107
- Park, S. A., Shaked, G. M., Bredesen, D. E., and Koo, E. H. (2009). Mechanism of cytotoxicity mediated by the C31 fragment of the amyloid precursor protein. *Biochem. Biophys. Res. Commun.* 388, 450–455. doi: 10.1016/j.bbrc.2009.08.042
- Park, S. S., Jung, H. J., Kim, Y. J., Park, T. K., Kim, C., Choi, H., et al. (2012). Asp664 cleavage of amyloid precursor protein induces tau phosphorylation by decreasing protein phosphatase 2A activity. *J. Neurochem.* 123, 856–865. doi: 10.1111/jnc.12032
- Pozueta, J., Lefort, R., Ribe, E. M., Troy, C. M., Arancio, O., and Shelanski, M. (2013). Caspase-2 is required for dendritic spine and behavioural alterations in J20 APP transgenic mice. *Nat. Commun.* 4:1939. doi: 10.1038/ncomms2927
- Pronin, A., Pham, D., An, W., Dvorianchikova, G., Reshetnikova, G., Qiao, J., et al. (2019). Inflammasome activation induces pyroptosis in the retina exposed to ocular hypertension injury. *Front. Mol. Neurosci.* 12:36. doi: 10.3389/fnmol.2019.00036
- Qu, Y., Tang, J., Wang, H., Li, S., Zhao, F., Zhang, L., et al. (2017). RIPK3 interactions with MLKL and CaMKII mediate oligodendrocytes death in the developing brain. *Cell Death Dis.* 8:e2629. doi: 10.1038/cddis.2017.54
- Rissman, R. A., Poon, W. W., Blurton-Jones, M., Oddo, S., Torp, R., Vitek, M. P., et al. (2004). Caspase-cleavage of tau is an early event in Alzheimer disease tangle pathology. *J. Clin. Invest.* 114, 121–130. doi: 10.1172/jci20640
- Schneider, K. S., Groß, C. J., Dreier, R. F., Saller, B. S., Mishra, R., Gorka, O., et al. (2017). The inflammasome drives GSDMD-independent secondary pyroptosis and IL-1 release in the absence of Caspase-1 protease activity. *Cell Rep.* 21, 3846–3859. doi: 10.1016/j.celrep.2017.12.018
- Shalini, S., Dorstyn, L., Dawar, S., and Kumar, S. (2015). Old, new and emerging functions of caspases. *Cell Death Differ.* 22, 526–539. doi: 10.1038/cdd.2014.216
- Shen, X., Burguillos, M. A., Osman, A. M., Frijhoff, J., Carrillo-Jiménez, A., Kanatani, S., et al. (2016). Glioma-induced inhibition of caspase-3 in microglia promotes a tumor-supportive phenotype. *Nat. Immunol.* 17, 1282–1290. doi: 10.1038/ni.3545
- Shen, X., Venero, J. L., Joseph, B., and Burguillos, M. A. (2018). Caspases orchestrate microglia instrumental functions. *Prog. Neurobiol.* 171, 50–71. doi: 10.1016/j.pneurobio.2018.09.007
- Simon, D. J., Weimer, R. M., McLaughlin, T., Kallop, D., Stanger, K., Yang, J., et al. (2012). A caspase cascade regulating developmental axon degeneration. *J. Neurosci.* 32, 17540–17553. doi: 10.1523/JNEUROSCI.3012-12.2012
- Stennicke, H. R., and Salvesen, G. S. (1999). Catalytic properties of the caspases. *Cell Death Differ.* 6, 1054–1059. doi: 10.1038/sj.cdd.4400599
- Sun, Y. B., Zhao, H., Mu, D. L., Zhang, W., Cui, J., Wu, L., et al. (2019). Dexmedetomidine inhibits astrocyte pyroptosis and subsequently protects the brain in vitro and in vivo models of sepsis. *Cell Death Dis.* 10:167. doi: 10.1038/s41419-019-1416-5
- Tait, S. W., Ichim, G., and Green, D. R. (2014). Die another way—non-apoptotic mechanisms of cell death. *J. Cell Sci.* 127, 2135–2144. doi: 10.1242/jcs.093575
- Tan, M. S., Tan, L., Jiang, T., Zhu, X. C., Wang, H. F., Jia, C. D., et al. (2014). Amyloid- $\beta$  induces NLRP1-dependent neuronal pyroptosis in models of Alzheimer's disease. *Cell Death Dis.* 5:e1382. doi: 10.1038/cddis.2014.348
- Thornberry, N. A., Bull, H. G., Calaycay, J. R., Chapman, K. T., Howard, A. D., Kostura, M. J., et al. (1992). A novel heterodimeric cysteine protease is required for interleukin-1  $\beta$  processing in monocytes. *Nature* 356, 768–774. doi: 10.1038/356768a0
- Tiwari, M., Lopez-Cruzan, M., Morgan, W. W., and Herman, B. (2011). Loss of caspase-2-dependent apoptosis induces autophagy after mitochondrial oxidative stress in primary cultures of young adult cortical neurons. *J. Biol. Chem.* 286, 8493–8506. doi: 10.1074/jbc.M110.163824
- Tsaprass, P., and Nezis, I. P. (2017). Caspase involvement in autophagy. *Cell Death Differ.* 24, 1369–1379. doi: 10.1038/cdd.2017.43
- Tsuchiya, K., Nakajima, S., Hosojima, S., Thi Nguyen, D., Hattori, T., Manh Le, T., et al. (2019). Caspase-1 initiates apoptosis in the absence of gasdermin D. *Nat. Commun.* 10:2091. doi: 10.1038/s41467-019-09753-2
- Tummers, B., and Green, D. R. (2017). Caspase-8: regulating life and death. *Immunol. Rev.* 277, 76–89. doi: 10.1111/imr.12541
- Voet, S., Srinivasan, S., Lamkanfi, M., and van Loo, G. (2019). Inflammasomes in neuroinflammatory and neurodegenerative diseases. *EMBO Mol. Med.* 11:e10248. doi: 10.15252/emmm.201810248
- von Herrmann, K. M., Salas, L. A., Martinez, E. M., Young, A. L., Howard, J. M., Feldman, M. S., et al. (2018). NLRP3 expression in mesencephalic neurons and characterization of a rare. *NPJ Parkinsons Dis.* 4:24. doi: 10.1038/s41531-018-0061-5
- Wagner, D. C., Riegelsberger, U. M., Michalk, S., Hartig, W., Kranz, A., and Boltze, J. (2011). Cleaved caspase-3 expression after experimental stroke exhibits different phenotypes and is predominantly non-apoptotic. *Brain Res.* 1381, 237–242. doi: 10.1016/j.brainres.2011.01.041
- Walsh, J. G., Muruve, D. A., and Power, C. (2014). Inflammasomes in the CNS. *Nat. Rev. Neurosci.* 15, 84–97. doi: 10.1038/nrn3638
- Wang, L., Xu, X. B., You, W. W., Lin, X. X., Li, C. T., Qian, H. R., et al. (2017). The cytoplasmic nuclear shuttling of Beclin 1 in neurons with Alzheimer's disease-like injury. *Neurosci. Lett.* 661, 63–70. doi: 10.1016/j.neulet.2017.09.055
- Wang, W., Nguyen, L. T., Burlak, C., Chugini, F., Guo, F., Chataway, T., et al. (2016). Caspase-1 causes truncation and aggregation of the Parkinson's disease-associated protein  $\alpha$ -synuclein. *Proc. Natl. Acad. Sci. U.S.A.* 113, 9587–9592. doi: 10.1073/pnas.1610099113
- Xia, P., Pan, Y., Zhang, F., Wang, N., Wang, E., Guo, Q., et al. (2018). Pioglitazone confers neuroprotection against ischemia-induced pyroptosis due to its inhibitory effects on HMGB-1/RAGE and Rac1/ROS pathway by activating PPAR- $\gamma$ . *Cell. Physiol. Biochem.* 45, 2351–2368. doi: 10.1159/000488183
- Xu, Y., Wang, J., Song, X., Qu, L., Wei, R., He, F., et al. (2016). RIP3 induces ischemic neuronal DNA degradation and programmed necrosis in rat via AIF. *Sci. Rep.* 6:29362. doi: 10.1038/srep29362

- Yuan, J., Shaham, S., Ledoux, S., Ellis, H. M., and Horvitz, H. R. (1993). The *C. elegans* cell death gene *ced-3* encodes a protein similar to mammalian interleukin-1 beta-converting enzyme. *Cell* 75, 641–652. doi: 10.1016/0092-8674(93)90485-9
- Yuan, S., Yu, Z., Zhang, Z., Zhang, J., Zhang, P., Li, X., et al. (2019). RIP3 participates in early brain injury after experimental subarachnoid hemorrhage in rats by inducing necroptosis. *Neurobiol. Dis.* 129, 144–158. doi: 10.1016/j.nbd.2019.05.004
- Zare-Shahabadi, A., Masliah, E., Johnson, G. V., and Rezaei, N. (2015). Autophagy in Alzheimer's disease. *Rev. Neurosci.* 26, 385–395. doi: 10.1515/revneuro-2014-0076
- Zhang, C. J., Jiang, M., Zhou, H., Liu, W., Wang, C., Kang, Z., et al. (2018). TLR-stimulated IRAKM activates caspase-8 inflammasome in microglia and promotes neuroinflammation. *J. Clin. Invest.* 128, 5399–5412. doi: 10.1172/JCI121901
- Zhao, X., Kotilinek, L. A., Smith, B., Hlynialuk, C., Zahs, K., Ramsden, M., et al. (2016). Caspase-2 cleavage of tau reversibly impairs memory. *Nat. Med.* 22, 1268–1276. doi: 10.1038/nm.4199
- Conflict of Interest:** The authors declare that the research was conducted in the absence of any commercial or financial relationships that could be construed as a potential conflict of interest.
- Copyright © 2019 Espinosa-Oliva, García-Revilla, Alonso-Bellido and Burguillos. This is an open-access article distributed under the terms of the Creative Commons Attribution License (CC BY). The use, distribution or reproduction in other forums is permitted, provided the original author(s) and the copyright owner(s) are credited and that the original publication in this journal is cited, in accordance with accepted academic practice. No use, distribution or reproduction is permitted which does not comply with these terms.



# Pharmacological Targeting of Microglial Activation: New Therapeutic Approach

Cai-Yun Liu<sup>1\*</sup>, Xu Wang<sup>1</sup>, Chang Liu<sup>1</sup> and Hong-Liang Zhang<sup>1,2\*</sup>

<sup>1</sup> Department of Neurology, The First Hospital of Jilin University, Changchun, China, <sup>2</sup> Department of Life Sciences, National Natural Science Foundation of China, Beijing, China

## OPEN ACCESS

### Edited by:

Victoria Campos-Peña,  
National Institute of Neurology  
and Neurosurgery (INNN), Mexico

### Reviewed by:

Lorenzo Di Cesare Mannelli,  
University of Florence, Italy  
Veronica Ghiglieri,  
University of Perugia, Italy

### \*Correspondence:

Cai-Yun Liu  
caiyun\_0770@163.com  
Hong-Liang Zhang  
drzhl@hotmail.com

### Specialty section:

This article was submitted to  
Cellular Neuropathology,  
a section of the journal  
Frontiers in Cellular Neuroscience

**Received:** 21 August 2019

**Accepted:** 31 October 2019

**Published:** 19 November 2019

### Citation:

Liu C-Y, Wang X, Liu C and  
Zhang H-L (2019) Pharmacological  
Targeting of Microglial Activation: New  
Therapeutic Approach.  
Front. Cell. Neurosci. 13:514.  
doi: 10.3389/fncel.2019.00514

Mounting evidence suggests that neuroinflammation is not just a consequence but a vital contributor to the development and progression of Parkinson's disease (PD). Microglia in particular, may contribute to the induction and modulation of inflammation in PD. Upon stimulation, microglia convert into activated phenotypes, which exist along a dynamic continuum and bear different immune properties depending on the disease stage and severity. Activated microglia release various factors involved in neuroinflammation, such as cytokines, chemokines, growth factors, reactive oxygen species (ROS), reactive nitrogen species (RNS), and prostaglandins (PGs). Further, activated microglia interact with other cell types (e.g., neurons, astrocytes and mast cells) and are closely associated with  $\alpha$ -synuclein ( $\alpha$ -syn) pathophysiology and iron homeostasis disturbance. Taken together, microglial activation and microglia-mediated inflammatory responses play essential roles in the pathogenesis of PD and elucidation of the complexity and imbalance of microglial activation may shed light on novel therapeutic approaches for PD.

**Keywords:** Parkinson's disease, microglia, neuroinflammation, microglial activation, polarization

**Abbreviations:**  $\alpha$ -syn,  $\alpha$ -synuclein; 6-OHDA, 6-hydroxydopamine; AAV2-hIL-10, adeno-associated viral vector containing the cDNA for human interleukin-10; AD, Alzheimer's disease; BBB, blood-brain barrier; BDNF, brain-derived neurotrophic factor; bFGF, basic fibroblast growth factor; CB2, cannabinoid type 2; CNS, central nervous system; COX, cyclooxygenase; CX3CR1, CX3C chemokine receptor 1; CXCL, chemokine (C-X-C motif) ligand; cyclic AMP, cyclic adenosine monophosphate; DA, dopamine; DAPI12, DNAX activation protein 12; DMT1, divalent metal transporter 1; DN-TNF, dominant-negative tumor necrosis factor; EAA, excitatory amino acids; EAE, experimental autoimmune encephalomyelitis; EGF, epidermal growth factor; ERK, extracellular signal-regulated kinase; GSH, glutathione; GWAS, genome-wide association studies; H<sub>4</sub>R, histamine-4 receptor; HLA, human leucocyte antigen; I $\kappa$ B $\alpha$ , inhibitory protein- $\kappa$ -B $\alpha$ ; IFN, interferon; IGF-1, insulin-like growth factor-1; IKK, I $\kappa$ B kinase; IL, interleukin; iNOS, inducible nitric oxide synthase; IP-10, interferon-gamma-induced protein-10; IRAK, interleukin-1 receptor-associated kinase; IRF, interferon regulatory factor; IRP1, iron regulatory protein 1; JAK, Janus kinase; LPS, lipopolysaccharide; MAPK, mitogen-activated protein kinase; MHC, major histocompatibility complex; MMP, matrix metalloproteinase; MPTP, 1-methyl-4-phenyl-1,2,3,6-tetrahydropyridine; MS, multiple sclerosis; NADPH, nicotinamide adenine dinucleotide phosphate; NF- $\kappa$ B, nuclear factor kappa B; NGF, nerve growth factor; NLRP3, NLR family pyrin domain containing 3; NO, nitric oxide; NSAID, nonsteroidal anti-inflammatory drug; NSPC, neural stem/progenitor cell; PAR-1, protease-activated receptor-1; PARP, poly ADP ribose polymerase; PD, Parkinson's disease; PDE, phosphodiesterase; PET, positron emission tomography; PG, prostaglandins; PPAR, peroxisome proliferator-activated receptor; P-SAPK/JNK, phospho-stress-activated protein kinases/c-Jun N-terminal kinases; RNS, reactive nitrogen species; ROS, reactive oxygen species; rTMS, repetitive transcranial magnetic stimulation; SCFAs, short-chain fatty acids; SN, substantia nigra; SNpc, substantia nigra (SN) pars compacta; SOCS3, suppressor of cytokine signaling 3; soluble TNF, soluble tumor necrosis factor; SR, scavenger receptor; STAT, signal transducer and activator of transcription; TAK1, TGF- $\beta$ -activated protein kinase 1; Tem, effector/memory T cells; TGF, transforming growth factor; TIR, toll-interleukin 1 receptor; TLR, toll-like receptor; TNF, tumor necrosis factor; TRAF6, TNF receptor-associated factor 6; TREM2, triggering receptor expressed on myeloid cells 2; TRPC1, transient receptor potential canonical 1; UPDRS-III, Unified Parkinson's Disease Rating Scale III.

## GENERIC VIEW OF PD PATHOGENESIS

Parkinson's disease, a prevalent movement disorder which affects almost 2% of the aged population worldwide, is the second most common neurodegenerative disease (Hirsch et al., 2016). Pathologically, PD is characterized by the selective and progressive degeneration of dopaminergic neurons in the SNpc and dopaminergic terminals in the striatum. The exact molecular mechanisms of neuronal loss are not fully understood, but several pathways and mechanisms are known to be implicated in PD pathophysiology, including neuroinflammation, impairment of autophagy, oxidative stress, severe endoplasmic reticulum stress, mitochondrial dysfunction, dysfunction of axonal transport, motor circuit pathophysiology,  $\alpha$ -syn aggregation, and prion-like cell-to-cell transmission of  $\alpha$ -syn (Charvin et al., 2018). Although it may not be the initial trigger of PD, neuroinflammation is considered to be a vital promoter to the development of PD, in which microglia perform significant roles (Hirsch and Hunot, 2009; Wang et al., 2015c; Skaper et al., 2018).

McGeer et al. (1988) first proposed that innate immunity was involved in PD in 1988 when a substantial number of HLA-DR-positive reactive microglia were detected in the SN of brains from post-mortem PD patients using immunohistochemical staining. Another neuropathologic study showed that the number of reactive microglia expressing MHC class II molecules not only in the SN and putamen but also in the hippocampus, cingulate cortex, temporal cortex and transentorhinal cortex was increased as the neuronal degeneration proceeded (Imamura et al., 2003). Similar up-regulated expression of MHC, as well as T-cell infiltration, has been reported in the SN and striatum of MPTP mouse model of PD (Kurkowska-Jastrzebska et al., 1999). Moreover, GWAS further indicated that common genetic variation in the HLA region was related to sporadic PD (Hamza et al., 2010; Hill-Burns et al., 2011; Nalls et al., 2011). *In vivo* studies using PET confirmed that microglia were widespread activated at the early stage of PD and levels remained relatively stable, possibly driving the disease process via inflammatory reaction (Ouchi et al., 2005; Gerhard et al., 2006; Edison et al., 2013; Iannaccone et al., 2013; Femminella et al., 2016; Ghadery et al., 2017).

The brain of PD patients and animal models induced by MPTP or 6-OHDA showed several signs of increased inflammatory reaction and programmed cell death (or apoptosis) of neurons and/or neuroglia (Nagatsu et al., 2000; Hunot and Hirsch, 2003): (a) microgliosis which was observed in various toxin-based models, such as MPTP, 6-OHDA, and rotenone (Marinova-Mutafchieva et al., 2009; Fricke et al., 2016; Ojha et al., 2016; Manocha et al., 2017), as well as in mutant  $\alpha$ -syn transgenic models of PD (Lee et al., 2002; Su et al., 2009); (b) elevated levels of inflammatory cytokines (Mogi et al., 1994a,b, 1996), such as IL-1 $\beta$ , IL-2, IL-4, IL-6, IFN- $\gamma$  and TNF- $\alpha$ , TGF- $\alpha$ , TGF- $\beta$ 1, TGF- $\beta$ 2, EGF, bFGF; (c) increased levels of cytokine receptors, such as TNF- $\alpha$  receptor R1 (p55); (d) increased levels of caspase activities, such as caspase-1 and caspase-3; (e) enzymes related to inflammation (Knott et al., 2000), such as COX-1, COX-2, and iNOS (Knott et al., 2000; Iravani et al., 2002; Ruano et al., 2006); (f) reduced levels of neurotrophins, such as NGF and BDNF; (g)

elevated levels of bcl-2 and soluble Fas, which could protect and promote apoptosis, respectively.

A remarkable percentage of monocytic precursors were found in the peripheral blood of patients with PD (Funk et al., 2013). Moreover, increased effector/memory T cells (Tem), defined as CD45RO<sup>+</sup> and FAS<sup>+</sup> CD4<sup>+</sup> T cells, and decreased CD31<sup>+</sup> and  $\alpha$ 4 $\beta$ 7<sup>+</sup> CD4<sup>+</sup> T cells were associated with progressive Unified PD Rating Scale III (UPDRS-III) scores (Saunders et al., 2012). Collectively, the immune responses, notably the CD4<sup>+</sup>-cell subset imbalance and Tem activation, may mirror the pathobiology of PD in the CNS.

Several meta-analyses revealed the association between the use of NSAIDs and the risk of PD (Samii et al., 2009; Gagne and Power, 2010; Gao et al., 2011; Rees et al., 2011; Poly et al., 2019), whereas the relationship was inconclusive. NSAIDs as a whole seemed not to be related to the risk of PD (Samii et al., 2009; Poly et al., 2019). Interestingly, subgroup analysis indicated that use of nonaspirin NSAIDs may have a protective effect, though not shared by aspirin (Gagne and Power, 2010; Rees et al., 2011) or acetaminophen (Gagne and Power, 2010; Gao et al., 2011). One prospective study suggested that the use of nonaspirin NSAIDs may reduce PD risk in males but not in females (Hernan et al., 2006). One population-based study reported that the effect of aspirin also differed by gender, namely a protective role only in females, especially for longer duration of use ( $\geq 24$  months) or at higher doses ( $\geq 14$  pills/week) (Wahner et al., 2007). This gender-specific association between NSAIDs and lower PD risk warrants further investigation. As regards ibuprofen, whether there is a potential therapeutic effect or not is still controversial (Chen et al., 2005; Samii et al., 2009; Gao et al., 2011). Further, in MPTP-induced mouse models, indomethacin exerted anti-inflammatory effects and promoted survival of new neurons in the hippocampus without reversing dopaminergic neuronal loss (Hain et al., 2018). Rofecoxib and ibuprofen were also shown to directly protect MPTP-induced damage (Gupta et al., 2009; Swiatkiewicz et al., 2013). In an *in vitro* study, 6-OHDA-induced PC12 cells pretreated with celecoxib, indomethacin and ibuprofen for 24 h showed significantly increased cell viability, GSH content, and cytoplasmic level of NF- $\kappa$ B, as well as decreased levels of ROS and several apoptosis biomarkers, including cleaved caspase-3, Bax, P-SAPK/JNK and cleaved PARP (Ramazani et al., 2019). Further studies are still needed to elucidate the underlying inflammation process in PD and possible protective effects of NSAIDs.

Taken together, neuroinflammation appears to play central roles in the development of PD. Glial cells, particularly microglia, are involved in this scenario.

## GENERIC VIEW OF MICROGLIAL FUNCTIONS

Microglia are resident macrophage-like immune cells in the CNS (Lawson et al., 1990). "Resting" microglia exhibit a ramified morphology with elongated motile cytoplasmic protrusions and processes; they constantly survey the CNS microenvironment



and dynamically interact with other neighboring elements, such as neuronal cell bodies, astrocytes, and blood vessels (Davalos et al., 2005; Nimmerjahn et al., 2005; Szalay et al., 2016; Catalin et al., 2017).

Microglia actively contribute to brain development, injury repair, as well as homeostasis maintenance and surveillance (Michell-Robinson et al., 2015; Colonna and Butovsky, 2017). In the developing CNS, microglia control its patterning by regulating apoptosis of neuronal subpopulations (Wakselman et al., 2008) as well as neuron survival and proliferation (Ueno et al., 2013), and control the wiring of neurons by modulating synapse function and maturation, activity-dependent synaptic pruning, as well as synapse number (Wake et al., 2009; Paolicelli et al., 2011; Schafer et al., 2012; Kierdorf and Prinz, 2017). Acting similarly to peripheral macrophages, microglia in the mature CNS are able to phagocytize excess synapses, dead cells, protein aggregates, pathogens, and other particulate and dissolvable antigens that may endanger the CNS (Neumann et al., 2009; Sierra et al., 2010; Kettenmann et al., 2011; Colonna and Butovsky, 2017). Moreover, microglia secrete cytokines, chemokines, growth factors, ROS and RNS, and PGs (Gonzalez et al., 2014). These functions of microglia can be regulated by interactions with the BBB and other cellular elements, including astrocytes, neurons, infiltrating T cells and mast cells (Gonzalez et al., 2014; **Figure 1**). Microglia show brain region-dependent diversity and selective regional sensitivities to aging, which could underlie region-specific sensitivities to microglial dysregulation and involvement in age-related neurodegeneration (Grabert et al., 2016).

## POLARIZATION OF MICROGLIA AND ITS ROLES IN NEUROINFLAMMATION

In various neurodegenerative diseases or in response to any insult, microglia become activated, including morphological changes, alterations of gene expression and surface markers, and proliferation (Wolf et al., 2017). Activated microglia may present epithelioid, rod, amoeboid, multinucleated or “dystrophic” morphological appearance (Boche et al., 2013). Growing evidence shows that microglial activation in the CNS is heterogeneous, similarly to peripheral macrophages, which is often simplified into two polarization states: the M1 phenotype (known as “classical activation”) and the M2 phenotype (known as “alternative activation”) (Orihuela et al., 2016). Activation of microglia can be induced by various factors through numerous pattern recognition receptors like TLRs, SRs and cytokine receptors and chemokine receptors. Microglial cells may present distinctive phenotypes and exhibit specific effects depending on the nature, intensity and duration of the stimulus (Ransohoff and Perry, 2009; Gosselin et al., 2017; Joers et al., 2017; **Figure 1**).

The M1 polarized microglia with an IL-12<sup>high</sup>, IL-23<sup>high</sup>, IL-10<sup>low</sup> phenotype, present markers such as MHC-II, COX-2, iNOS, and CD86 (Martinez et al., 2006; Chhor et al., 2013), which are associated with the production of pro-inflammatory

cytokines (IL-1 $\beta$ , IL-6, IL-12, IFN- $\gamma$ , and TNF- $\alpha$ ), chemokines (CCL-2, CCL-20), CXCL-10, cytotoxic substances (ROS, RNS, NO, EAA), and prostaglandin E2 (PGE2) (Le et al., 2001; Mantovani et al., 2005; Pais et al., 2008). M1 microglia are able to promote neurogenesis and astrocytogenesis from NSPCs (Butovsky et al., 2006; Vay et al., 2018), participate as inducer and effector cells in polarized Th1 responses, and mediate resistance against tumor cells and intracellular parasites (Mantovani et al., 2005). This polarized phenotype can be induced in experimental animals by using IFN- $\gamma$  or LPS. IFN- $\gamma$  mediates M1 polarization of microglia mainly through the JAK/STAT intracellular signal transduction pathway; also by “priming”, enhancing TLR-activated signal transduction and then reinforcing microglial responsiveness to inflammatory stimuli (e.g., TLR ligands and TNF- $\alpha$ ) (Hu and Ivashkiv, 2009). Studies *in vivo* and *in vitro* on macrophage showed that TRPC1-mediated Ca<sup>2+</sup> influx is crucial for IFN- $\gamma$ -induced polarization to the M1 phenotype (Chauhan et al., 2018). LPS, an endotoxin in the outer membrane of Gram-negative bacteria, induces M1 polarization via binding to TLR4, which is coupled to myeloid differentiation protein 2, with participation of LPS-binding protein and co-receptors CD14 (Chow et al., 1999; Takeda and Akira, 2004). The TLR4-mediated signaling typically involves an MyD88-dependent pathway, in which activation of transcription factor NF- $\kappa$ B is followed by production of several inflammatory cytokines (e.g., IL-1 $\beta$ , IL-6, TNF- $\alpha$ ), and an MyD88-independent pathway, in which activation of transcription factors NF- $\kappa$ B and IRF-3 is followed by the production of IFN- $\beta$  mediating IFN- $\beta$ -induced STAT1-dependent gene expression (Chow et al., 1999; Kawai et al., 2001; Toshchakov et al., 2002; Takeda and Akira, 2004). In this way, expressions of numerous M1-associated cytokines, chemokines and other inflammatory factors are increased. These cytokines activate iNOS and NADPH oxidase, leading to the production of NO, ROS, and RNS (Bove and Perier, 2012; Zeng et al., 2012).

The mechanism of M2 polarization in microglia, as compared to macrophages, is much less clear. The characteristics of M2 microglia may parallel those of macrophages to some extent (Chhor et al., 2013; Miron et al., 2013). The M2 state in macrophages can be divided into three sub-classes named M2a, M2b, and M2c, respectively (Martinez and Gordon, 2014), which might be extrapolated to microglia. The M2 polarized microglia with an IL-12<sup>low</sup>, IL-23<sup>low</sup>, IL-10<sup>high</sup> phenotype, generally present high levels of scavenger, mannose-type and galactose-type receptors (Mantovani et al., 2005), which are associated with the production of anti-inflammatory cytokines (e.g., IL-4, IL-10, and TGF- $\beta$ ), glucocorticoids, neurotrophic factors (e.g., BDNF and IGF-1), and extracellular matrix proteins (e.g., fibronectin) (Subramaniam and Federoff, 2017). M2 microglia are able to promote oligodendrogenesis and neurogenesis (especially oligodendrogenesis) from NSPCs via the PPAR- $\gamma$  signaling pathway (Butovsky et al., 2006; Vay et al., 2018) and perform vital roles in various situations, such as immune regulation, inflammation inhibition and tissue repair (Michell-Robinson et al., 2015). The activation mechanisms

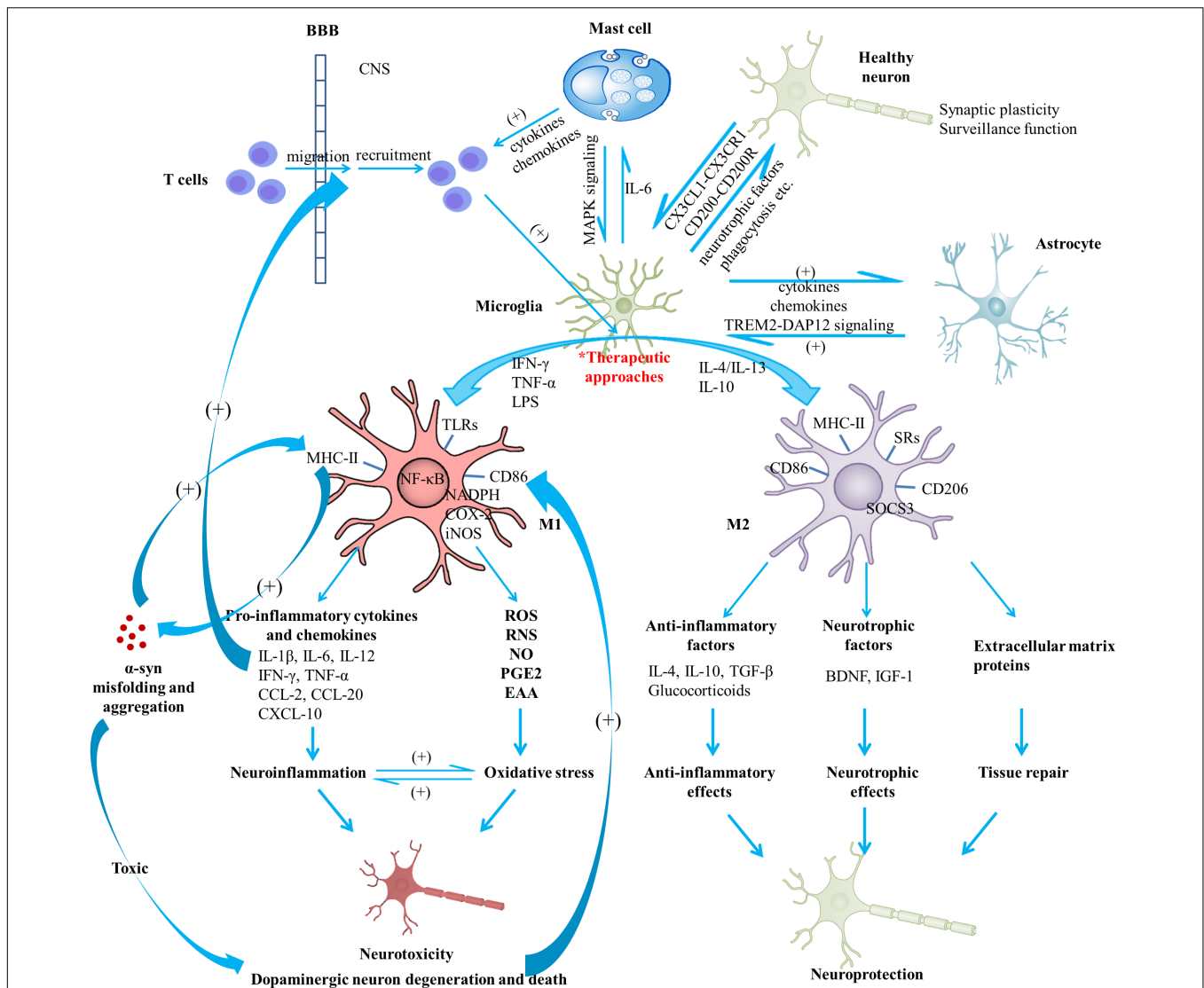


**FIGURE 1 |** Schematic view of microglial activation and cross-talks between microglia and other immune factors in the pathogenesis of Parkinson's disease. With regard to PD pathogenesis, microglial activation and microglia-mediated inflammatory responses play essential roles. The M1 polarized state can be induced by TNF- $\alpha$ , IFN- $\gamma$ , and LPS; present phenotype markers such as MHC-II and CD86; are associated with the production of pro-inflammatory cytokines (IL-1 $\beta$ , IL-6, IL-12, IFN- $\gamma$ , and TNF- $\alpha$ ), chemokines (CCL-2, CCL-20) and CXCL-10; are capable of releasing cytotoxic substances (ROS, RNS, NO, PGE2, EAA) due to the activation of NADPH oxidase, iNOS, as well as expression of COX-2, contributing to the enhanced oxidative stress. Neuroinflammation and oxidative stress interact with each other to engender a vicious cycle, exerting toxic effects on dopaminergic neurons and leading to the exacerbation of the neurodegenerative process. On the other hand, M2 can be induced by IL-4, IL-10, and IL-13; generally present intracellular components (e.g., SOCS3), cell surface markers (SRs, CD206, CD86, and MHC-II); are capable of producing mediators such as anti-inflammatory cytokines (e.g., IL-4, IL-10, and TGF- $\beta$ ), glucocorticoids, neurotrophic factors (e.g., BDNF and IGF-1), and extracellular matrix proteins; exert anti-inflammatory and neurotrophic effects and play vital roles in tissue repair. Notably, activated microglia may exist along a dynamic continuum rather than be simply polarized into two categories, which is regulated by interactions with other cellular elements, including astrocytes, neurons, infiltrating T cells and mast cells. TREM2-DAP12 signaling complex, the CD200-CD200R and the CX3CL1-CX3CR1 axes are considered to be involved in the astrocyte-microglia and neuron-glia cross-talks. Activated mast cells could induce microglial activation via the MAPK signaling pathway. In turn, microglia-derived IL-6 could induce surface TLR2 and TLR4 expression and consequent cytokine release of mast cells, which contribute to the recruitment of immune cells to the injured areas. In addition, microglial activation has been indicated to promote the prion-like behavior of  $\alpha$ -syn misfolding and aggregation. In turn, misfolded  $\alpha$ -syn act as chemoattractants to direct microglial migration toward damaged neurons, promote the pro-inflammatory microglia, and exert toxic effects on neurons. Dopaminergic neurons in a death process can trigger microglial activation and inflammatory factor production which can promote recruitment of peripheral leucocytes (mainly T cells). In this way, a complex inflammatory network forms and aggravates degeneration of dopaminergic neurons. A variety of agents or approaches might exert neuroprotective effects due to their regulatory roles on microglial activation. BBB, blood-brain barrier; BDNF, brain-derived neurotrophic factor; COX, cyclooxygenase; CXCL, chemokine (C-X-C motif) ligand; DAP12, DNAX activation protein 12; EAA, excitatory amino acids; IFN, interferon; IGF-1, insulin-like growth factor-1; IL, interleukin; iNOS, inducible nitric oxide synthase; LPS, lipopolysaccharide; MAPK, mitogen-activated protein kinase; NADPH, nicotinamide adenine dinucleotide phosphate; NO, nitric oxide; PD, Parkinson's disease; PGE2, prostaglandin E2; RNS, reactive nitrogen species; ROS, reactive oxygen species; SOCS3, suppressor of cytokine signaling 3; SR, scavenger receptor; TGF, transforming growth factor; TLR, toll-like receptor; TNF, tumor necrosis factor; TREM2, triggering receptor expressed on myeloid cells 2;  $\alpha$ -syn,  $\alpha$ -synuclein.

of these three sub-classes as well as their functions are different. The M2a activation state, which performs phagocytosis, functions to suppress inflammation, and contributes to tissue repair, can be induced by IL-4 or IL-13 (Stein et al., 1992; Joers et al., 2017; Subramaniam and Federoff, 2017). IL-4 *per se* mediates M2a polarization through binding to various receptor pairs, then stimulating JAK1 or JAK3, activating STAT6 and resulting in expression of M2a-associated genes, such as intracellular components (e.g., SOCS3), cell surface markers (SRs and CD206), Ym1 (chitinase-like protein), Fizz1 (found in inflammatory zone) and IL-10 (Stein et al., 1992; Joers et al., 2017; Subramaniam and Federoff, 2017). The M2b polarized state, which is involved in inflammation regulation and selective phagocytosis, can be induced by agonists of TLRs and IL-1 receptors. TLRs become activated by fusing Fc gamma receptors, which bind to immunoglobulin G complexes, resulting in macrophage/microglia polarization to an M2b phenotype and then leading to the secretion of IL-10 and the production of cell surface markers (MHC-II, CD86) (Franco and Fernandez-Suarez, 2015). The M2c polarized state, which plays vital roles in immune regulation, matrix deposition and tissue remodeling, can be induced by IL-10 and glucocorticoid hormones (Subramaniam and Federoff, 2017). IL-10 can activate JAK1 through binding to IL-10 receptor 1 and 2 subunits, then resulting in the translocation of STAT3 to the nucleus, which consequently inhibits the production of M1-associated pro-inflammatory cytokines (Subramaniam and Federoff, 2017).

In general, the M1 phenotype is considered to be the first line of defense with pro-inflammatory roles, while the M2 phenotype to suppress inflammation and to promote tissue repair. Of note is that activated microglia may exist along a dynamic continuum and get different profiles depending on their surrounding microenvironment, rather than be simply polarized into either category (Figure 1).

As mentioned above, the over-simplified “polarization” designation of activated microglia is still controversial. Additional microglia phenotypes which do not align with the traditional binary classification have been discovered (Holtman et al., 2015; Szulzewsky et al., 2015; Morganti et al., 2016; Cho et al., 2019). Therefore, polarization of microglia or the continuum from M1 to M2 state has not been fully supported by experimental data; more importantly, the microglial polarization paradigm may impede rather than facilitate research progress as this schema tends to simplify data interpretation (Ransohoff, 2016). Current research is focused on the characterization of activated microglia for discovering new drug target.

## ACTIVATION OF MICROGLIA AND PATHOGENESIS OF PD, WHAT HAVE WE LEARNED?

The complexity and imbalance of microglial activation has become an area of intense focus, aiming to elucidate a potential mechanism of PD pathogenesis and to

identify potential targets for anti-inflammatory treatment (Du et al., 2017).

## Microglial Activation and Associated Neuroinflammation and Oxidative Stress

Studies in PD patients, alongside with mounting data in experimental models of this disease, clearly indicate that microglial activation and microglia-mediated inflammation exert dual (beneficial/harmful) effects in PD pathophysiology, as discussed above. A variant in the TREM2 gene of microglia, p.R47H, is a risk factor for PD (Rayaprolu et al., 2013). In the MPTP-induced mouse models of progressive PD, the degeneration of dopaminergic neurons was associated with gradual polarization of microglia to an M1 (pro-inflammatory) phenotype (Pisanu et al., 2014), which could become even more obvious with age (Yao and Zhao, 2018). Furthermore, microglia seemed to present dynamically changing phenotypes depending on disease-stage, accounting for the dynamic changes of pro-inflammatory and anti-inflammatory cytokines (Pisanu et al., 2014; Joers et al., 2017).

Activated microglia proliferate and exhibit a stage- and region-specific secretion of cytokines and mediators (neurotoxic molecules including NO, ROS, RNS and pro-inflammatory cytokines), leading to progressive degeneration of dopaminergic neurons, while microglia in the SNpc are more abundant (approximately 4.5 times) than in other brain regions (Grabert et al., 2016; Lopez Gonzalez et al., 2016). In addition, dopaminergic neurons in the SNpc have decreased anti-oxidant potentials, while the redox reaction of DA could be enhanced by the intensified generation of ROS, resulting in the production of toxic DA metabolites (Whitton, 2007; Tansey and Goldberg, 2010; L'Episcopo et al., 2018). All these features render midbrain dopaminergic neurons more susceptible to oxidative/inflammatory attacks (Whitton, 2007; Tansey and Goldberg, 2010; L'Episcopo et al., 2018). Hence, neuroinflammatory mechanisms could contribute to neuronal degeneration via cascade events.

With regard to the mechanism(s) of dopaminergic neuron degeneration and death, non-cell-autonomous mechanisms might play vital roles as well (Hirsch and Hunot, 2009). Activation of glial cells (especially microglia), triggered by dopaminergic neurons in a death process, could induce inflammatory responses as well as oxidative stress and cytokine-receptor-mediated apoptosis, which in turn promote recruitment of peripheral leucocytes (mainly T cells) and lead to an inflammatory network around neuronal injury (Hirsch and Hunot, 2009). The non-cell-autonomous mechanism is considered to drive dopaminergic cell death and hence neurodegeneration in PD (Hirsch and Hunot, 2009). During microglial activation, activation of NADPH oxidase, iNOS, as well as expression of COX-2 results in the synthesis of high levels of ROS, RNS, NO, and PGE2, contributing to the enhanced oxidative stress, which not only exerts toxic effects on dopaminergic neurons but also further amplifies the pro-inflammatory microenvironment (Taylor et al., 2013). Peroxynitrite, a potent toxin produced when NADPH oxidase

and iNOS are present together, promotes the nitration of proteins (e.g., tyrosine) and further production of hydroxyl radicals, which can damage lipids, proteins, DNA and RNA, resulting in dysfunction and eventual death of neurons (Gao and Hong, 2008; Taylor et al., 2013; L'Episcopo et al., 2018). In this way, neuroinflammation and oxidative stress interact to engender a vicious cycle, leading to the exacerbation of neurodegeneration (**Figure 1**). However, microgliosis and increase of pro-inflammatory molecules could be detected at the early stage and well before dopaminergic neuron death in the  $\alpha$ -syn transgenic models (Su et al., 2009), implying that cell death is not necessarily a prerequisite for the activation of microglia and mutated  $\alpha$ -syn could also initiate the vicious cycle.

The interaction between  $\alpha$ -syn and microglia is considered to be vital in the pathogenesis of PD (**Figure 1**).  $\alpha$ -syn, a presynaptic protein secreted by neurons in small amounts which prevalently exists as monomers in physiology, is over-expressed and aggregates into oligomers or protofibrils in PD (Theillet et al., 2016). Oligomers/protofibrils could propagate between cells as free floating proteins or via extracellular vesicles (Li et al., 2008; Ingelsson, 2016), exert toxic effects on the synapses, resulting in disruption of electrophysiological properties (Calo et al., 2016; Ingelsson, 2016; Bridi and Hirth, 2018; La Vitola et al., 2018; Prots et al., 2018; Longhena et al., 2019), and act as chemoattractants to direct microglial migration toward damaged neurons (Wang et al., 2015a). In addition,  $\alpha$ -syn over-expression promotes the polarization of microglia to the pro-inflammatory phenotype with elevated production of cytokines such as IL-1 $\beta$ , IL-6, and TNF- $\alpha$  as well as COX-2, iNOS and free radicals (Zhang et al., 2005, 2017; Austin et al., 2006; Su et al., 2008, 2009; Theodore et al., 2008; Sacino et al., 2014; Ferreira and Romero-Ramos, 2018). Oligomeric  $\alpha$ -syn induces the M1 phenotype by directly engaging the TLR1/2 heterodimer, resulting in the nuclear translocation of NF- $\kappa$ B and the elevated production of these cytokines by an MyD88-dependent pathway (Kim et al., 2013; Daniele et al., 2015; Ho, 2019; Kouli et al., 2019): After  $\alpha$ -syn activates TLR1/2 heterodimer, the C-terminal intracellular TIR domains of TLR interact with MyD88, activating the IRAK complex (Lin et al., 2010), which in return activates the TRAF6 via its K63-linked auto-ubiquitination. Then, the subsequent activation of the TAK1 complex and its downstream effector IKK complex lead to the degradation of I $\kappa$ B $\alpha$  and the production of pro-inflammatory cytokines via the activation of MAPK and translocation of NF- $\kappa$ B, p38 and JNK (Symons et al., 2006; Kawai and Akira, 2007, 2010). TLR4 could also mediate  $\alpha$ -syn-dependent activation of microglia, including the production of ROS and pro-inflammatory cytokines as well as the phagocytic activity of microglia (Fellner et al., 2013; Janda et al., 2018; Hughes et al., 2019). Scavenger receptor CD36 and P2X7 receptor are also involved in  $\alpha$ -syn-mediated microglial activation (Su et al., 2008; Jiang et al., 2015). Moreover,  $\alpha$ -syn-stimulated microglia secrete MMPs, activating PAR-1 and amplifying microglial inflammatory signals (Lee et al., 2010). In this way,  $\alpha$ -syn is a vital regulator of microglial activation and phagocytosis. Activated microglia which exert enhanced phagocytosis of  $\alpha$ -syn in turn, could on one hand directly play a beneficial role in controlling  $\alpha$ -syn spread (Stefanova et al., 2011),

and on the other hand, notably, promote the prion-like behavior of  $\alpha$ -syn misfolding, aggregation and spread (Hansen et al., 2011; George et al., 2019; Olanow et al., 2019). This may be associated with the increased accumulation of intracellular  $\alpha$ -syn in microglia and accelerated secretion of  $\alpha$ -syn into extracellular space via exosomal pathways (Porro et al., 2019; Xia et al., 2019), as well as the toxic effects of cytokines generated from activated microglia on the vulnerable neuronal cells (Olanow et al., 2019). Taken together, microglia-derived oxidative stress is considered to bridge  $\alpha$ -syn pathogenic alteration and neuroinflammation, contributing to chronic progression of neurodegeneration in PD (Lawand et al., 2015). Those mentioned receptors on microglia could be therapeutic targets for microglial activation and  $\alpha$ -syn pathogenesis.

## Cross-Talks Between Microglia and Other Cell Types

The microglial polarization status and associated neuroinflammation are tightly connected with astrocyte-microglia and neuron-glia interactions via ligand-receptor pairings (**Figure 1**). TREM2, exclusively expressed by microglia, could enhance the phagocytosis function of microglia (Takahashi et al., 2005, 2007; Kawabori et al., 2015), and attenuate inflammatory responses by negatively regulating the TLR4-mediated activation of NF- $\kappa$ B signaling and shifting M1 polarization to the M2 phenotype (Jiang et al., 2016; Ren et al., 2018; Zhang et al., 2018). In addition, TREM2-DAP12 signaling complex exerts vital roles in promoting phagocytosis, microglial activation, as well as microglial survival (Belloli et al., 2017; Konishi and Kiyama, 2018; Mecca et al., 2018). The fractalkine receptor CX3CR1, another receptor specifically expressed in microglia, plays a fundamental role in the communication between microglia and neurons by binding to neuronal fractalkine, namely CX3CL1 (Harrison et al., 1998). Accumulating evidence suggests that the CX3CL1-CX3CR1 axis is involved in homeostatic suppression of microglial activation and regulation of chemoattraction and synaptic plasticity, inhibiting microglia-mediated inflammatory responses and neurotoxicity (Cardona et al., 2006; Pabon et al., 2011; Sheridan and Murphy, 2013; Mecca et al., 2018). CD200, a transmembrane glycoprotein present on neurons, can regulate microglial activation status by binding to microglial CD200R. Deficits in the CD200-CD200R axis could exacerbate activation of microglia and dopaminergic neurodegeneration (Wang et al., 2011; Zhang et al., 2011).

Notably, the mast cell-glia cross-talk is also involved in regulation of neuroinflammation (Skaper et al., 2017, 2018; **Figure 1**). In inflammatory tissues, the expression of ligand-receptor pairings is increased, enhancing chemotactic actions of glial cells and mast cells and facilitating intercellular communication. Activated mast cells could induce microglial activation and subsequent production of TNF- $\alpha$  and IL-6 via the MAPK signaling pathway (Zhang et al., 2016). In turn, microglia-derived IL-6 could induce expression of surface TLR2 and TLR4 and consequent release of cytokines by mast cells, which recruit immune cells (including microglia) to the injured areas (Pietrzak



et al., 2011; Aguirre et al., 2013). Conceivably, these two cell types form a feedback loop in concert to promote neuroinflammation.

## Activation of Microglia and Imbalance of Iron Metabolism

Importantly, disturbance of iron homeostasis is a cardinal feature and contributes to the pathogenesis of multiple neurodegenerative diseases including PD, and microglia are capable of modulating the neuronal iron metabolism (Song et al., 2018). Iron is essential for oxygen transport and the related metabolic activities, especially for brain, the highest oxygen-consuming organ. In addition, iron is necessary for various activities exclusively in the brain, such as the maintenance of myelin, the synthesis and metabolism of neurotransmitters including serotonin, norepinephrine and DA (Ward et al., 2014; Crielgaard et al., 2017). Iron accumulation is a physiological feature of aging brain, the degree of which seems to be even greater in PD (Ward et al., 2014). The first observation of abnormal deposits of iron in post-mortem brain especially in the basal ganglia of one PD patient was reported by Lhermitte et al. (1924) in 1924, and was later verified by pathological studies (Sofic et al., 1988; Riederer et al., 1989), magnetic resonance imaging studies (Zhang J. et al., 2010; Wang C. et al., 2013; Lehericy et al., 2014) and transcranial ultrasound (Becker and Berg, 2001; Zecca et al., 2005). However, there has long been a debate as to whether iron is a cause or a consequence of this disorder. Abnormal iron accumulation can induce oxidative stress via ROS, especially hydroxyl radical production, leading to the oxidation and modification of proteins, carbohydrates, lipids, and DNA (Ward et al., 2014). Loss of transferrin receptor 1 (involved in iron uptake) rather than ferroportin could cause age-progressive degeneration of dopaminergic neurons and motor deficits in mice (Matak et al., 2016). Iron might modulate the expression of  $\alpha$ -syn and facilitate its aggregation and toxicity via oxidative stress-induced nitration and phosphorylation, contributing to degeneration of dopaminergic neurons (Song et al., 2018). Furthermore, neurodegeneration in the injured regions could be exacerbated by the strong redox coupling of iron and DA (Hare and Double, 2016). Regarding microglial contributions to the disturbance of iron metabolism in PD, the expressed transporters/molecules and the released factors such as pro-inflammatory factors, neurotropic factors and lactoferrin, exert fundamental roles (Song et al., 2018). Microglia are more efficient to accumulate and safely store abundant iron than astrocytes and neurons (Bishop et al., 2011), as evidenced by the finding that ferritin was abundant in microglia while rarely detected in astrocytes and neurons (Healy et al., 2016). Even in the case of acute oxidative stress-induced ferritin reduction, the increased iron storage capacity of microglia might be achieved by elevated iron saturation of the existing ferritin molecules (Mehlhasse et al., 2005), coupled with the aggregation of activated microglia around degenerative neurons. Further, pro-inflammatory factors released by activated microglia (e.g., IL-1 $\beta$ , IL-6, and TNF- $\alpha$ ) contribute to the iron deposition by up-regulating the expression of IRP1 and iron transporters (e.g., DMT1) through production of ROS and RNS (Urrutia et al., 2013;

Wang J. et al., 2013). These findings provide compelling evidence that microglia could aggravate iron-mediated neurodegeneration in PD. Understanding iron metabolism and roles of microglia in iron dyshomeostasis might provide new therapeutic strategies for PD via restoring brain iron homeostasis.

## Microbiome-Gut-Brain Axis

In the last decade, the microbiome-gut-brain axis in the pathogenesis of neurodegenerative disorders has attracted increasingly more attention. The gut microbiota could affect BBB permeability (Braniste et al., 2014), and microbiome-derived SCFAs were involved in regulation of microglia homeostasis (Erny et al., 2015). Further, a multi-faceted TLR signaling network is essential for the immune-mediated processes both in the gut and in the CNS, exerting inflammatory or regulatory effects in the pathogenesis of PD (Houser and Tansey, 2017; Caputi and Giron, 2018). Dietary tryptophan metabolites produced by symbiotic microbiota could influence microglial activities, TGF- $\alpha$  production, and neuroinflammatory pathology in EAE, a mouse model of MS (Rothhammer et al., 2018). Future investigations should be focused on whether probiotics or antibiotics or dietary protocols can be utilized to modulate microglial function and to alleviate progress of neurodegenerative diseases including PD.

In brief, as far as PD pathogenesis is concerned, microglial activation and microglia-mediated inflammatory responses play essential roles. Further,  $\alpha$ -syn-microglia, neuron-glia, astrocyte-microglia, and mast cell-glia cross-talks (Figure 1), as well as the microbiome-gut-brain axis, are considered to be involved in the regulation of these processes.

## POTENTIALS OF MICROGLIA AS A THERAPEUTIC TARGET FOR PD

Drugs are currently available to relieve PD symptoms by limiting the extent of inflammation (Glass et al., 2010), and thus to enhance the life quality of patients. Nevertheless, these drugs are incapable of repairing or regenerating the damaged neurons (Song and Suk, 2017). Given that the balance of M1/M2 polarization states of microglia has been concerned in connection with the pathogenesis of neurodegenerative disorders, including PD, some small molecular compounds have been studied to determine their potentials to modulate the balance and to elucidate the underlying mechanisms.

## Novel Agents or Approaches Targeting the M1 Polarization State

Drugs targeting pro-inflammatory and pro-killing M1 polarization state could potentially help reduce neuronal damage caused by inflammation. These drugs listed in Table 1 can be divided into several categories:

Firstly, regulation or modification of receptors on microglia, such as TLRs and CB2 receptors, provides a novel pharmacological target for neurodegenerative disorders including PD (Maresz et al., 2005; Cassano et al., 2017; Fiebich et al., 2018; Navarro et al., 2018). In patients with PD,

**TABLE 1 |** Novel agents or approaches targeting M1 polarization state.

Target	Agent or approach	Description	Effects
TLR2	Candesartan cilexetil (Dasu et al., 2009; Daniele et al., 2015)	A drug approved for cerebrovascular diseases	Inhibit TLR2 and TLR4 expression; reverse M1 phenotype activated by $\alpha$ -syn
	Rifampicin and its autooxidation product rifampicin quinone (Acuna et al., 2019)	Antibiotic	Prevent $\alpha$ -syn-induced TLR2- and P2X7-dependent microglial inflammatory responses <i>in vitro</i>
	Endurance exercise (Jang et al., 2017; Koo et al., 2017)		Regulate TLR2 and its downstream signaling (MyD88, TRAF6 and TAK-1)
TLR4	TAK-242 or RSLA (Hughes et al., 2019)	Small molecule antagonists of TLR4	Attenuate $\alpha$ -syn-mediated oxidative stress, TNF- $\alpha$ production by microglia and neuronal death <i>in vitro</i>
CB2	$\beta$ -caryophyllene (Javed et al., 2016; Ojha et al., 2016)	A agonist of CB2 receptors	Suppress microglial activation; inhibit pro-inflammatory cytokine expression
	JWH133 (Chung et al., 2016)	A selective CB2 receptor agonist	Alleviate BBB disruption; suppress peripheral immune cell infiltration; inhibit iNOS and pro-inflammatory cytokine production
JAK/STAT or NF- $\kappa$ B signaling	$\alpha$ -asarone (Kim et al., 2015)	A chemical component found in Annonaceae and Araceae species	Inhibit the NF- $\kappa$ B signaling; inhibit pro-inflammatory factor production; reserve anti-inflammatory factor expression; eventually mitigate behavioral anomalies
NADPH oxidase	Tanshinone I (Wang et al., 2015b)	A bioactive flavonoid	Inhibit microglial activation; suppress the generation of ROS, RNS and pro-inflammatory cytokines; promote anti-inflammatory state
	Apocynin (Choi et al., 2012; Sharma and Nehru, 2016)	Extracted from <i>Apocynum cannabinum</i> etc.	
	Resveratrol (Zhang F. et al., 2010)	Extracted from reynoutria etc.	
Cytokines	Diphenyleneiodonium (Wang et al., 2014, 2015d)	A bivalent iodine compound	Alleviate glial activation; attenuate dopaminergic neuron loss; finally mitigate behavioral deficits
	DN-TNF	Intranigral lentiviral delivery of DN-TNF (McCoy et al., 2008; Harms et al., 2011); nigral infusion of XENP345 (McCoy et al., 2006); peripheral application of XPro <sup>®</sup> 1595 (Barnum et al., 2014)	
GHS-R1a	Ghrelin (Jiang et al., 2008; Moon et al., 2009)	An endogenous ligand for GHS-R1a	Prevent the activation of microglia; inhibit production of pro-inflammatory factors (TNF- $\alpha$ and IL-1 $\beta$ , NO); attenuate dopaminergic neuron loss
unclear	Lenalidomide (Valera et al., 2015)	Drugs approved for other distinct diseases	Inhibit activation of microglia; attenuate production of pro-inflammatory cytokines
unclear	Zonisamide (Hossain et al., 2018)		Inhibit activation of microglia; attenuate production of pro-inflammatory cytokines
	Minocycline (Wu et al., 2002; Kobayashi et al., 2013)		
	Dimethyl fumarate (Campolo et al., 2017)		
	Ginsenoside Rg1 (Zhou et al., 2015; Heng et al., 2016)	Bioactive compounds extracted from various plants	
	Piperine (Yang et al., 2015)		
	Curcumin (Ghasemi et al., 2019)		
	Rosmarinic acid (Lv et al., 2019)		
H <sub>4</sub> R	Astilbin (Zhu et al., 2019)		Suppress pro-inflammatory activation; prevent dopaminergic neuron degeneration; reduce Lewy body-like neuropathology; improve Parkinson-like behavior
	JNJ7777120 (Zhou et al., 2019)	H <sub>4</sub> R antagonist	
NLRP3	MCC950 (Gordon et al., 2018)	A small-molecule inhibitor of NLRP3 inflammasome	Inhibit NLRP3 inflammasome activation; prevent dopaminergic degeneration and $\alpha$ -syn pathology; alleviate motor behaviors

stage and region-dependent TLR2 expression is consistent with region-specific polarization states of microglia, indicating that TLR2 plays a critical role in the microglia-associated responses in this disorder (Doorn et al., 2014). Candesartan cilexetil, an FDA-approved drug for treating cerebrovascular diseases, hypertension, and chronic heart failure, also able to inhibit the expression of TLR2 and TLR4 (Dasu et al., 2009), might reverse the pro-inflammatory phenotype of microglia activated by oligomeric  $\alpha$ -syn (Daniele et al., 2015). Moreover, one recent study showed that the antibiotic rifampin and its autooxidation product rifampicin quinone prevented  $\alpha$ -syn-induced TLR2- and P2X7-dependent microglial inflammatory responses *in vitro* (Acuna et al., 2019), which needs further investigation to confirm their potentials as anti-parkinsonian drugs. Interestingly, endurance exercise could exert neuroprotective effects in MPTP-induced PD mice by regulating the expression of TLR2 and its downstream signaling such as MyD88, TRAF6, and TAK1 (Jang et al., 2017; Koo et al., 2017). As previously discussed, TLR4, another receptor involved in microglial activation, is a potential therapeutic target. Hughes et al. found that pretreatment with TAK-242 or RSLA, small molecule antagonists of TLR4, significantly attenuated  $\alpha$ -syn-mediated oxidative stress, TNF- $\alpha$  production by microglia and neuronal death *in vitro* (Hughes et al., 2019), but has not been tested *in vivo*. The endocannabinoid system is considered to be closely associated with the neuropathological processes of PD (Navarrete et al., 2018). A naturally occurring agonist of CB2 receptors,  $\beta$ -caryophyllene, could negatively regulate microglial activation and suppress expressions of pro-inflammatory cytokines, whereby eliciting significant neuroprotective effects on nigral dopaminergic neurons (Javed et al., 2016; Ojha et al., 2016). JWH133, another selective CB2 receptor agonist, could protect the MPTP induced PD mice by alleviating BBB disruption and by suppressing the peripheral immune cell infiltration as well as by reducing the M1 microglia-production of iNOS and pro-inflammatory cytokines (Chung et al., 2016).

Secondly, the JAK/STAT signaling pathway and the NF- $\kappa$ B signaling pathway are vital for the polarization of microglia to the M1 state. Targeting these signaling pathways may serve as a potential to regulate M1 activation. For example,  $\alpha$ -asarone, a chemical component found in various plants (e.g., Annonaceae and Araceae species), was shown to significantly suppress M1 polarization and to attenuate the production of pro-inflammatory cytokines by inhibiting the NF- $\kappa$ B signaling, and to eventually mitigate PD-like behavioral anomalies in the MPTP-induced mouse model (Kim et al., 2015). Tanshinone I, a bioactive flavonoid, could selectively inhibit the activation of NF- $\kappa$ B signaling and the production of M1-pro-inflammatory molecules including IL-1 $\beta$ , IL-6, TNF- $\alpha$  and NO, partially reverse the expression of M2-anti-inflammatory markers such as IL-10, and prevent nigrostriatal dopaminergic neurodegeneration (Wang et al., 2015b).

Thirdly, some compounds targeting NADPH oxidase, such as apocynin, resveratrol and diphenyleneiodonium, could inhibit microglial activation, suppress the generation of various toxic factors (e.g., ROS, RNS, and pro-inflammatory cytokines), and promote microglial phenotype toward anti-inflammatory state,

thereby offering promising candidates for clinical trials in patients with neurodegenerative diseases including PD and AD (Zhang F. et al., 2010; Choi et al., 2012; Wang et al., 2014, 2015d; Sharma and Nehru, 2016).

Finally, targeting pro-inflammatory cytokines (e.g., IL-1 $\beta$  and TNF- $\alpha$ ) may provide new possibilities to inhibit M1 polarization. In mouse models induced by MPTP or 6-OHDA, selective suppression of solTNF via intranigral lentiviral delivery of DN-TNF (McCoy et al., 2008; Harms et al., 2011) or nigral infusion of DN-TNF compound XENP345 (McCoy et al., 2006) or peripheral application of DN-TNF inhibitor XPro1595 (Barnum et al., 2014) could alleviate glial activation, dopaminergic neuron loss and final behavioral deficits, suggesting that blocking the solTNF signaling by DN-TNF gene transfer or novel agents is therapeutically feasible for PD.

Interestingly, ghrelin, an endogenous ligand for growth hormone secretagogue receptor 1a, was demonstrated to prevent the activation of microglia, the production of pro-inflammatory factors (e.g., TNF- $\alpha$  and IL-1 $\beta$ ) and the activation of iNOS, and to attenuate dopaminergic neuron loss in the MPTP-induced mouse models of PD (Jiang et al., 2008; Moon et al., 2009). The inhibitory effect of ghrelin seems to be exerted by suppressing the expression of MMP-3 in stressed dopaminergic neurons (Moon et al., 2009).

In addition, several drugs approved for other distinct diseases [e.g., lenalidomide for multiple myeloma or myelodysplastic syndrome (Valera et al., 2015), zonisamide for epilepsy (Hossain et al., 2018), minocycline for infectious diseases (Wu et al., 2002; Kobayashi et al., 2013), dimethyl fumarate for MS (Campolo et al., 2017)] and some bioactive compounds [e.g., ginsenoside Rg1 (Zhou et al., 2015; Heng et al., 2016), piperine (Yang et al., 2015), curcumin (Ghasemi et al., 2019), rosmarinic acid (Lv et al., 2019), astilbin (Zhu et al., 2019)] are capable of inhibiting activation of microglia and attenuating production of pro-inflammatory cytokines in mouse models of PD. These drugs might offer novel alternative therapeutic approaches for PD. However, the underlying mechanisms or involved signaling pathways are not fully understood and require further investigations.

Several promising targets have been proposed to modulate microglial activation. For example, microglia-mediated immune responses could be enhanced by CD73-derived adenosine A2A signaling. CD73 inactivation substantially limited adenosine production, inhibited A2A receptor (A2AR)-mediated pro-inflammatory state of microglia, enhanced the activity of dopaminergic neurons, and mitigated the motor symptoms in animal models of PD (Meng et al., 2019). Histamine-4 receptor is another regulator of microglial activation. Lateral ventricle infusion of H4R antagonist JNJ777120 could suppress the pro-inflammatory activation of microglia, prevent the degeneration of dopaminergic neurons, reduce the Lewy body-like neuropathology, and improve parkinsonian behaviors (Zhou et al., 2019). Another potential target for PD, NLRP3 inflammasome in microglia can be activated by fibrillar  $\alpha$ -syn (Gordon et al., 2018). Oral administration of a small-molecule inhibitor of NLRP3 inflammasome, MCC950, effectively prevented dopaminergic degeneration and  $\alpha$ -syn

pathology, and alleviated motor behaviors in PD models (Gordon et al., 2018).

## Novel Agents or Approaches Capable of Enhancing the M2 Phenotype or Induce the Phenotypic Switch From M1 to M2

Some molecules (e.g., IL-10, cyclic AMP, and vitamin D), which have the capability of enhancing the anti-inflammatory phenotype or of inducing the phenotypic switch from pro-inflammatory to anti-inflammatory, may have therapeutic feasibility for PD (Table 2).

IL-10 is a potent anti-inflammatory cytokine capable of suppressing iNOS expression via the inhibition of the NF- $\kappa$ B activity (Schwenkgrub et al., 2013). Several studies have demonstrated that intracerebral injection of AAV2-hIL-10 in MPTP-induced mouse models of PD could enhance the expression of the striatal tyrosine hydroxylase protein associated with down-regulated expressions of pro-inflammatory iNOS, and promote the production of anti-inflammatory factors like TGF- $\beta$ , suggesting the neuroprotective properties of AAV2-hIL-10 (Schwenkgrub et al., 2013; Joniec-Maciejak et al., 2014).

Cyclic AMP is considered to be a key intracellular regulator of microglial phenotypic conversion (Ghosh et al., 2016). The M1 to M2a conversion could be promoted by cyclic AMP combined with IL-4, but neither alone, in *in vitro* microglia cell culture. The M2a-converted microglia showed abated production of oxidative molecules (e.g., ROS) and pro-inflammatory factors (e.g., TNF- $\alpha$  and IP-10), as well as improved phagocytic properties. The cyclic AMP-protein kinase A signaling pathway was involved in the conversion process (Ghosh et al., 2016). Based on this finding, application of synthetic analogs of cyclic AMP, activators of adenylyl cyclase, or inhibitors of PDE might suppress the pro-inflammatory phenotype of microglial cells via elevation of cyclic AMP. Notably, PDE inhibitors, such as rolipram for PDE4, sildenafil and yonkenafil for PDE5 (Zhao et al., 2016), and non-selective PDE inhibitors (e.g., ibudilast), have been proposed as potential therapeutic drugs for neurodegenerative disorders, including MS (Pifarre et al., 2011), AD (Myeku et al., 2016; Kumar and Singh, 2017; Rabal et al., 2018; Xu et al., 2018), and PD (Kinoshita et al., 2017; Schwenkgrub et al., 2017).

Vitamin D is capable of protecting dopaminergic neurons against neuroinflammation and oxidative stress via inhibition of microglial activation, shifting M1 to M2 polarized states, which has been demonstrated in mouse models of PD induced by 6-OHDA/MPTP (Kim et al., 2006; Calvellido et al., 2017; Lima et al., 2018) and in microglial HMO6/BV-2 cells (Boontanrart et al., 2016; Dulla et al., 2016; Verma and Kim, 2016). Vitamin D treatment could attenuate M1 polarization with decreased expression of iNOS and TLR4 and reduced production of pro-inflammatory factors (IL-1 $\beta$ , IL-6, IL-12, TNF- $\alpha$ , and NO), and facilitate M2 polarization with elevated expression of TLR10 and increased generation of anti-inflammatory mediators (IL-4, IL-10, TGF- $\beta$ , and chemokine CCL17) and typical hallmarks of M2 microglia (CD163, CD204, and CD206) (Kim et al., 2006; Dulla et al., 2016; Verma and Kim, 2016; Calvellido et al., 2017). Regulatory effects of vitamin D on microglial activation

might be associated with suppression of ERK activation (Dulla et al., 2016) and an IL-10 dependent SOCS3 mechanism (Boontanrart et al., 2016).

Peroxisome proliferator-activated receptors, nuclear receptors involved in the pathogenesis of neurodegenerative disorders, have garnered much attention as a promising therapeutic target. PPARs down-regulate microglial activation, neuroinflammation and oxidative stress (Agarwal et al., 2017). PPAR- $\gamma$  agonists, such as pioglitazone and rosiglitazone, could modulate microglial polarization, thus playing neuroprotective roles on dopaminergic neurons. Oral administration of pioglitazone improved motor symptoms of parkinsonian rhesus monkeys induced by MPTP via anti-inflammatory and neuroprotective effects (Swanson et al., 2011). Pioglitazone might sequentially act via activation of PPAR- $\gamma$ , induction of I $\kappa$ B $\alpha$ , blockade of NF- $\kappa$ B activation, iNOS induction and NO-mediated toxicity in an MPTP-induced mouse model of PD (Dehmer et al., 2004). In addition, an *in vitro* study indicated that the anti-inflammatory and neuroprotective effects of PPAR- $\gamma$  agonists might be closely associated with the interaction between CD200 and CD200R1 (Dentesano et al., 2014). Similarly, rosiglitazone could boost the M2 (anti-inflammatory) phenotype, and regulate cytokine production, whereby alleviating the degeneration of dopaminergic neurons in both SNpc and striatum (Pisanu et al., 2014). However, clinical studies as to whether glitazone protected against PD yielded controversial results (Brauer et al., 2015; Connolly et al., 2015; Ninds Exploratory Trials in Parkinson Disease (Net-Pd) Fs-Zone Investigators., 2015; Brakedal et al., 2017). Notably, a phase 2, multi-center, double-blind, placebo-controlled, randomized clinical trial reported that pioglitazone seemed incapable of modifying progression in early PD (Ninds Exploratory Trials in Parkinson Disease (Net-Pd) Fs-Zone Investigators., 2015). Some novel PPAR- $\gamma$  agonists, such as an N-carbamylated urethane compound SNU-BP (Song et al., 2016), may inhibit M1-pro-inflammatory cytokine and NO production, and enhance M2 marker expression. Further studies are still needed to confirm the therapeutic potentials of PPAR agonists in neurodegeneration and to explore the underlying mechanisms.

In summary, a variety of drugs may play neuroprotective roles in PD by regulating microglial activation and microglia-induced inflammation; nevertheless, the therapeutic mechanisms are not fully understood (Tables 1, 2). In view of roles of iron metabolism in PD pathogenesis, the protective effects of iron chelation has been explored in the MPTP mouse model by both genetic (transgenic expression of the iron binding protein ferritin) and pharmacological (oral administration of the bioavailable metal chelator clioquinol) means (Kaur et al., 2003). Deferiprone, another oral iron chelator used to treat systemic iron overload diseases, was demonstrated to increase hippocampal BDNF levels, rescue memory deficits and ameliorate iron-induced harmful effects (Alcalde et al., 2018). Further investigations are warranted to explore the underlying mechanisms of beneficial effects of these drugs and to discover other novel potentially therapeutic approaches. It is noteworthy, however, that the pharmacological modulation of microglia could also have adverse effects as microglia



**TABLE 2 |** Novel agents or approaches capable of enhancing M2 phenotype or induce the phenotypic switch from M1 to M2.

Key molecule	Agent or approach	Mechanism	Effects
IL-10	Intracerebral injection of AAV2-hIL-10 (Schwenkgrub et al., 2013; Joniec-Maciejak et al., 2014)	IL-10 is capable of suppressing iNOS expression via the inhibition of NF- $\kappa$ B activity (Schwenkgrub et al., 2013).	Enhance tyrosine hydroxylase protein expression; inhibit iNOS expression; promote anti-inflammatory factor production (e.g., TGF- $\beta$ and IFN- $\gamma$ )
Cyclic AMP	PDE4 inhibitor rolipram (Kinoshita et al., 2017)  PDE5 inhibitors sildenafil and yonkenafil (Zhao et al., 2016)  Non-selective PDE inhibitor ibudilast (Schwenkgrub et al., 2017)	PDE inhibitors elevate production of cyclic AMP; cyclic AMP is considered to be a key intracellular regulator of microglial phenotypic conversion in the presence of IL-4 (Ghosh et al., 2016).	Abate production of oxidative molecules (e.g., ROS) and pro-inflammatory factors (e.g., TNF- $\alpha$ and IP-10); improve phagocytic properties
Vitamin D (Kim et al., 2006; Dulla et al., 2016; Verma and Kim, 2016; Calvello et al., 2017)		Vitamin D is capable of inhibiting microglial activation, shifting M1 to M2 polarized states via suppression of ERK activation (Dulla et al., 2016) and an IL-10 dependent SOCS3 mechanism (Boontanrart et al., 2016).	Attenuate M1 with decreased iNOS and TLR4 expression and reduced pro-inflammatory factor production (IL-1 $\beta$ , IL-6, IL-12, TNF- $\alpha$ , and NO); facilitate M2 with elevated TLR10 expression and increased anti-inflammatory mediator generation (IL-4, IL-10, TGF- $\beta$ , and CCL17)
PPAR- $\gamma$ agonists	Pioglitazone (Dehmer et al., 2004; Swanson et al., 2011)  Rosiglitazone (Pisanu et al., 2014)  An N-carbamoylated urethane compound SNU-BP (Song et al., 2016)	PPARs play vital roles in the down-regulation of microglial activation, neuroinflammation, oxidative stress, proteasomal dysfunction, and mitochondrial dysfunction via regulation of CD200 and CD200R1 expression (Dentesano et al., 2014).	Act via activation of PPAR- $\gamma$ , induction of I $\kappa$ B $\alpha$ , block of NF- $\kappa$ B activation, iNOS induction and NO-mediated toxicity; shift M1 to M2; improve motor symptoms

have such physiological functions mentioned above. One recent study found that blockade of CD22, a canonical B-cell receptor which is up-regulated on aged microglia, reprogrammed microglia toward a homeostatic transcriptional state and restored homeostatic microglial phagocytosis of  $\alpha$ -syn fibrils (Pluvinage et al., 2019).

Apart from these pharmacological treatments, rTMS have been reported to have modulating effect (promoting/suppressing) on microglial activation, which may depend on the intensity and frequency of rTMS (Cullen and Young, 2016; Sasso et al., 2016; Cacace et al., 2017). Further research are needed to clarify the specific effect of rTMS on microglia as well as on astrocytes and neurons. In addition, accumulating evidence indicates that physical exercise could inhibit microglial activation and regulate neuroinflammation as well as improve the synaptic plasticity, whereby enhancing brain function and attenuating neurodegeneration (Mee-Inta et al., 2019).

## FUTURE PERSPECTIVES

Accumulating studies on PD pathogenesis have focused on activation of microglia and cross-talks between microglia and other immune factors. Activated microglia bear pro-inflammatory or anti-inflammatory properties depending on the nature, intensity and duration of the stimulus and associated

with disease stage and severity. Importantly, activated microglia may exist along a dynamic continuum rather than be simply polarized into two categories. Activation of microglia triggered by damaged dopaminergic neurons could cause neuroinflammation, oxidative stress and cytokine-receptor-mediated apoptosis, which in turn enhance peripheral leucocyte recruitment. In this way, a vicious cycle comes into being, resulting in the exacerbation of the neurodegenerative process. In addition, cross-talks of  $\alpha$ -syn-microglia, neuron-glia, astrocyte-microglia, and mast cell-glia as well as the microbiome-gut-brain axis are thought to be involved in the regulation of microglial activation and neuroinflammation. The existing available drugs of PD are able to mitigate symptoms by limiting the extent of inflammation (Glass et al., 2010). Remarkably, the strategy of the biological therapy should be to restore the immune balance, rather than simply inhibit the immune responses. A variety of agents or approaches, including candesartan cilexetil, rifampicin/rifampicin quinone, TAK-242, RSLA,  $\beta$ -caryophyllene, JWH133,  $\alpha$ -asarone, tanshinone I, apocynin, resveratrol, diphenyleneiodonium, DN-TNF, lenalidomide, zonisamide, minocycline, dimethyl fumarate, some bioactive compounds extracted from various plants, JNJ7777120, MCC950, AAV2-hIL-10, Vitamin D, PDE inhibitors (rolipram, ibudilast), and PPAR- $\gamma$  agonists (pioglitazone, rosiglitazone), might exert neuroprotective effects due to their regulatory effects on microglial activation. In addition, intervention of iron metabolism balance or microbiome-gut-brain axis as well as

rTMS and physical exercise may offer emerging therapeutic strategies. In conclusion, microglial activation is a key point to understand the pathogenesis of PD and a potential therapeutic target for PD. Further investigations should focus on the dual role of reactive microglia to elucidate PD pathogenesis and detect emerging agents/approaches for PD.

## REFERENCES

- Acuna, L., Hamadat, S., Corbalan, N. S., Gonzalez-Lizarraga, F., Dos-Santos-Pereira, M., Rocca, J., et al. (2019). Rifampicin and its derivative rifampicin quinone reduce microglial inflammatory responses and neurodegeneration induced in vitro by alpha-synuclein fibrillary aggregates. *Cells* 8:E776. doi: 10.3390/cells8080776
- Agarwal, S., Yadav, A., and Chaturvedi, R. K. (2017). Peroxisome proliferator-activated receptors (PPARs) as therapeutic target in neurodegenerative disorders. *Biochem. Biophys. Res. Commun.* 483, 1166–1177. doi: 10.1016/j.bbrc.2016.08.043
- Aguirre, A., Maturana, C. J., Harcha, P. A., and Saez, J. C. (2013). Possible involvement of TLRs and hemichannels in stress-induced CNS dysfunction via mastocytes, and glia activation. *Mediators Inflamm.* 2013:893521. doi: 10.1155/2013/893521
- Alcalde, L. A., de Freitas, B. S., Machado, G. D. B., de Freitas Crivelaro, P. C., Dornelles, V. C., Gus, H., et al. (2018). Iron chelator deferiprone rescues memory deficits, hippocampal BDNF levels and antioxidant defenses in an experimental model of memory impairment. *Biometals* 31, 927–940. doi: 10.1007/s10534-018-0135-1
- Austin, S. A., Floden, A. M., Murphy, E. J., and Combs, C. K. (2006). Alpha-synuclein expression modulates microglial activation phenotype. *J. Neurosci.* 26, 10558–10563. doi: 10.1523/jneurosci.1799-06.2006
- Barnum, C. J., Chen, X., Chung, J., Chang, J., Williams, M., Grigoryan, N., et al. (2014). Peripheral administration of the selective inhibitor of soluble tumor necrosis factor (TNF) XPro(R)1595 attenuates nigral cell loss and glial activation in 6-OHDA hemiparkinsonian rats. *J. Parkinsons Dis.* 4, 349–360. doi: 10.3233/jpd-140410
- Becker, G., and Berg, D. (2001). Neuroimaging in basal ganglia disorders: perspectives for transcranial ultrasound. *Mov. Disord.* 16, 23–32. doi: 10.1002/1531-8257(200101)16:1<23::aid-mds1003>3.0.co;2-2
- Belloli, S., Pannese, M., Buonsanti, C., Maiorino, C., Di Grigoli, G., Carpinelli, A., et al. (2017). Early upregulation of 18-kDa translocator protein in response to acute neurodegenerative damage in TREM2-deficient mice. *Neurobiol. Aging* 53, 159–168. doi: 10.1016/j.neurobiolaging.2017.01.010
- Bishop, G. M., Dang, T. N., Dringen, R., and Robinson, S. R. (2011). Accumulation of non-transferrin-bound iron by neurons, astrocytes, and microglia. *Neurotox. Res.* 19, 443–451. doi: 10.1007/s12640-010-9195-x
- Boche, D., Perry, V. H., and Nicoll, J. A. (2013). Review: activation patterns of microglia and their identification in the human brain. *Neuropathol. Appl. Neurobiol.* 39, 3–18. doi: 10.1111/nan.12011
- Boontanart, M., Hall, S. D., Spanier, J. A., Hayes, C. E., and Olson, J. K. (2016). Vitamin D3 alters microglia immune activation by an IL-10 dependent SOCS3 mechanism. *J. Neuroimmunol.* 292, 126–136. doi: 10.1016/j.jneuroim.2016.01.015
- Bove, J., and Perier, C. (2012). Neurotoxin-based models of Parkinson's disease. *Neuroscience* 211, 51–76. doi: 10.1016/j.neuroscience.2011.10.057
- Brakedal, B., Flones, I., Reiter, S. F., Torkildsen, O., Dolle, C., Assmus, J., et al. (2017). Glitazone use associated with reduced risk of Parkinson's disease. *Mov. Disord.* 32, 1594–1599. doi: 10.1002/mds.27128
- Braniste, V., Al-Asmakh, M., Kowal, C., Anuar, F., Abbaspour, A., Toth, M., et al. (2014). The gut microbiota influences blood-brain barrier permeability in mice. *Sci. Transl. Med.* 6:263ra158. doi: 10.1126/scitranslmed.3009759
- Brauer, R., Bhaskaran, K., Chaturvedi, N., Dexter, D. T., Smeeth, L., and Douglas, I. (2015). Glitazone Treatment and incidence of Parkinson's Disease among people with diabetes: a retrospective cohort study. *PLoS Med.* 12:e1001854. doi: 10.1371/journal.pmed.1001854
- Bridi, J. C., and Hirth, F. (2018). Mechanisms of alpha-synuclein induced synaptopathy in Parkinson's Disease. *Front. Neurosci.* 12:80. doi: 10.3389/fnins.2018.00080
- Butovsky, O., Ziv, Y., Schwartz, A., Landa, G., Talpalar, A. E., Pluchino, S., et al. (2006). Microglia activated by IL-4 or IFN-gamma differentially induce neurogenesis and oligodendrogenesis from adult stem/progenitor cells. *Mol. Cell. Neurosci.* 31, 149–160. doi: 10.1016/j.mcn.2005.10.006
- Cacace, F., Mineo, D., Viscomi, M. T., Latagliata, E. C., Mancini, M., Sasso, V., et al. (2017). Intermittent theta-burst stimulation rescues dopamine-dependent corticostriatal synaptic plasticity and motor behavior in experimental parkinsonism: possible role of glial activity. *Mov. Disord.* 32, 1035–1046. doi: 10.1002/mds.26982
- Calo, L., Wegrynowicz, M., Santivanez-Perez, J., and Grazia Spillantini, M. (2016). Synaptic failure and alpha-synuclein. *Mov. Disord.* 31, 169–177. doi: 10.1002/mds.26479
- Calvello, R., Cianciulli, A., Nicolardi, G., De Nuccio, F., Giannotti, L., Salvatore, R., et al. (2017). Vitamin D treatment attenuates neuroinflammation and dopaminergic neurodegeneration in an animal model of Parkinson's Disease. Shifting M1 to M2 microglia responses. *J. Neuroimmune Pharmacol.* 12, 327–339. doi: 10.1007/s11481-016-9720-7
- Campolo, M., Casili, G., Biundo, F., Crupi, R., Cordaro, M., Cuzzocrea, S., et al. (2017). The Neuroprotective Effect of Dimethyl Fumarate in an MPTP-Mouse Model of Parkinson's Disease: involvement of Reactive Oxygen Species/Nuclear Factor-kappaB/Nuclear Transcription Factor Related to NF-E2. *Antioxid. Redox Signal.* 27, 453–471. doi: 10.1089/ars.2016.6800
- Caputi, V., and Giron, M. C. (2018). Microbiome-gut-brain axis and toll-like receptors in Parkinson's Disease. *Int. J. Mol. Sci.* 19:E1689. doi: 10.3390/ijms19061689
- Cardona, A. E., Pioro, E. P., Sasse, M. E., Kostenko, V., Cardona, S. M., Dijkstra, I. M., et al. (2006). Control of microglial neurotoxicity by the fractalkine receptor. *Nat. Neurosci.* 9, 917–924. doi: 10.1038/nn1715
- Cassano, T., Calcagnini, S., Pace, L., De Marco, F., Romano, A., and Gaetani, S. (2017). Cannabinoid receptor 2 signaling in neurodegenerative disorders: from pathogenesis to a promising therapeutic target. *Front. Neurosci.* 11:30. doi: 10.3389/fnins.2017.00030
- Catalin, B., Stopper, L., Balseanu, T. A., and Scheller, A. (2017). The in situ morphology of microglia is highly sensitive to the mode of tissue fixation. *J. Chem. Neuroanat.* 86, 59–66. doi: 10.1016/j.jchemneu.2017.08.007
- Charvin, D., Medori, R., Hauser, R. A., and Rascol, O. (2018). Therapeutic strategies for Parkinson disease: beyond dopaminergic drugs. *Nat. Rev. Drug Discov.* 17, 804–822. doi: 10.1038/nrd.2018.136
- Chauhan, A., Sun, Y., Sukumaran, P., Quenum Zangbede, F. O., Jondle, C. N., Sharma, A., et al. (2018). M1 macrophage polarization is dependent on TRPC1-mediated calcium entry. *Science* 8, 85–102. doi: 10.1016/j.isci.2018.09.014
- Chen, H., Jacobs, E., Schwarzschild, M. A., McCullough, M. L., Calle, E. E., Thun, M. J., et al. (2005). Nonsteroidal antiinflammatory drug use and the risk for Parkinson's disease. *Ann. Neurol.* 58, 963–967. doi: 10.1002/ana.20682
- Chhor, V., Le Charpentier, T., Lebon, S., Ore, M. V., Celador, I. L., Josseland, J., et al. (2013). Characterization of phenotype markers and neuronotoxic potential of polarized primary microglia in vitro. *Brain Behav. Immun.* 32, 70–85. doi: 10.1016/j.bbi.2013.02.005
- Cho, C. E., Damle, S. S., Wancewicz, E. V., Mukhopadhyay, S., Hart, C. E., Mazur, C., et al. (2019). A modular analysis of microglia gene expression, insights into the aged phenotype. *BMC Genomics* 20:164. doi: 10.1186/s12864-019-5549-9
- Choi, S. H., Aid, S., Kim, H. W., Jackson, S. H., and Bosetti, F. (2012). Inhibition of NADPH oxidase promotes alternative and anti-inflammatory microglial activation during neuroinflammation. *J. Neurochem.* 120, 292–301. doi: 10.1111/j.1471-4159.2011.07572.x

## AUTHOR CONTRIBUTIONS

C-YL, XW, and CL searched the literature and drafted the manuscript. C-YL and H-LZ critically revised the manuscript. All authors listed have made a substantial, direct, and intellectual contribution to the work, and approved it for publication.

- Chow, J. C., Young, D. W., Golenbock, D. T., Christ, W. J., and Gusovsky, F. (1999). Toll-like receptor-4 mediates lipopolysaccharide-induced signal transduction. *J. Biol. Chem.* 274, 10689–10692. doi: 10.1074/jbc.274.16.10689
- Chung, Y. C., Shin, W. H., Baek, J. Y., Cho, E. J., Baik, H. H., Kim, S. R., et al. (2016). CB2 receptor activation prevents glial-derived neurotoxic mediator production, BBB leakage and peripheral immune cell infiltration and rescues dopamine neurons in the MPTP model of Parkinson's disease. *Exp. Mol. Med.* 48:e205. doi: 10.1038/emmm.2015.100
- Colonna, M., and Butovsky, O. (2017). Microglia function in the central nervous system during health and neurodegeneration. *Annu. Rev. Immunol.* 35, 441–468. doi: 10.1146/annurev-immunol-051116-052358
- Connolly, J. G., Bykov, K., and Gagne, J. J. (2015). Thiazolidinediones and parkinson disease: a cohort study. *Am. J. Epidemiol.* 182, 936–944. doi: 10.1093/aje/kwv109
- Crielaard, B. J., Lammers, T., and Rivella, S. (2017). Targeting iron metabolism in drug discovery and delivery. *Nat. Rev. Drug Discov.* 16, 400–423. doi: 10.1038/nrd.2016.248
- Cullen, C. L., and Young, K. M. (2016). How Does Transcranial Magnetic Stimulation Influence Glial Cells in the Central Nervous System? *Front. Neural Circuits* 10:26. doi: 10.3389/fncir.2016.00026
- Daniele, S. G., Beraud, D., Davenport, C., Cheng, K., Yin, H., and Maguire-Zeiss, K. A. (2015). Activation of MyD88-dependent TLR1/2 signaling by misfolded alpha-synuclein, a protein linked to neurodegenerative disorders. *Sci. Signal.* 8:ra45. doi: 10.1126/scisignal.2005965
- Dasu, M. R., Riosvelasco, A. C., and Jialal, I. (2009). Candesartan inhibits Toll-like receptor expression and activity both in vitro and in vivo. *Atherosclerosis* 202, 76–83. doi: 10.1016/j.atherosclerosis.2008.04.010
- Davalos, D., Grutzendler, J., Yang, G., Kim, J. V., Zuo, Y., Jung, S., et al. (2005). ATP mediates rapid microglial response to local brain injury in vivo. *Nat. Neurosci.* 8, 752–758. doi: 10.1038/nn1472
- Dehmer, T., Heneka, M. T., Sastre, M., Dichgans, J., and Schulz, J. B. (2004). Protection by pioglitazone in the MPTP model of Parkinson's disease correlates with I kappa B alpha induction and block of NF kappa B and iNOS activation. *J. Neurochem.* 88, 494–501. doi: 10.1046/j.1471-4159.2003.02210.x
- Dentesano, G., Serratos, J., Tusell, J. M., Ramon, P., Valente, T., Saura, J., et al. (2014). CD200R1 and CD200 expression are regulated by PPAR-gamma in activated glial cells. *Glia* 62, 982–998. doi: 10.1002/glia.22656
- Doorn, K. J., Moors, T., Drukarch, B., van de Berg, W., Lucassen, P. J., and van Dam, A. M. (2014). Microglial phenotypes and toll-like receptor 2 in the substantia nigra and hippocampus of incidental Lewy body disease cases and Parkinson's disease patients. *Acta Neuropathol. Commun.* 2:90. doi: 10.1186/s40478-014-0090-1
- Du, L., Zhang, Y., Chen, Y., Zhu, J., Yang, Y., and Zhang, H. L. (2017). Role of microglia in neurological disorders and their potentials as a therapeutic target. *Mol. Neurobiol.* 54, 7567–7584. doi: 10.1007/s12035-016-0245-0
- Dulla, Y. A., Kurauchi, Y., Hisatsune, A., Seki, T., Shudo, K., and Katsuki, H. (2016). Regulatory mechanisms of vitamin D3 on production of nitric oxide and pro-inflammatory cytokines in microglial BV-2 cells. *Neurochem. Res.* 41, 2848–2858. doi: 10.1007/s11064-016-2000-3
- Edison, P., Ahmed, I., Fan, Z., Hinz, R., Gelosa, G., Ray Chaudhuri, K., et al. (2013). Microglia, amyloid, and glucose metabolism in Parkinson's disease with and without dementia. *Neuropsychopharmacology* 38, 938–949. doi: 10.1038/npp.2012.255
- Erny, D., Hrabec, de Angelis, A. L., Jaitin, D., Wieghofer, P., Staszewski, O., et al. (2015). Host microbiota constantly control maturation and function of microglia in the CNS. *Nat. Neurosci.* 18, 965–977. doi: 10.1038/nn.4030
- Fellner, L., Irshick, R., Schanda, K., Reindl, M., Klimaschewski, L., Poewe, W., et al. (2013). Toll-like receptor 4 is required for alpha-synuclein dependent activation of microglia and astroglia. *Glia* 61, 349–360. doi: 10.1002/glia.22437
- Femminella, G. D., Ninan, S., Atkinson, R., Fan, Z., Brooks, D. J., and Edison, P. (2016). Does microglial activation influence hippocampal volume and neuronal function in alzheimer's disease and parkinson's disease dementia? *J. Alzheimers Dis.* 51, 1275–1289. doi: 10.3233/jad-150827
- Ferreira, S. A., and Romero-Ramos, M. (2018). Microglia response during parkinson's disease: alpha-synuclein intervention. *Front. Cell. Neurosci.* 12:247. doi: 10.3389/fncel.2018.00247
- Fiebig, B. L., Batista, C. R. A., Saliba, S. W., Yousif, N. M., and de Oliveira, A. C. P. (2018). Role of Microglia TLRs in neurodegeneration. *Front. Cell. Neurosci.* 12:329. doi: 10.3389/fncel.2018.00329
- Franco, R., and Fernandez-Suarez, D. (2015). Alternatively activated microglia and macrophages in the central nervous system. *Prog. Neurobiol.* 131, 65–86. doi: 10.1016/j.pneurobio.2015.05.003
- Fricke, I. B., Viel, T., Worlitz, M. M., Collmann, F. M., Vrachimis, A., Faust, A., et al. (2016). 6-hydroxydopamine-induced Parkinson's disease-like degeneration generates acute microgliosis and astrogliosis in the nigrostriatal system but no bioluminescence imaging-detectable alteration in adult neurogenesis. *Eur. J. Neurosci.* 43, 1352–1365. doi: 10.1111/ejn.13232
- Funk, N., Wieghofer, P., Grimm, S., Schaefer, R., Buhning, H. J., Gasser, T., et al. (2013). Characterization of peripheral hematopoietic stem cells and monocytes in Parkinson's disease. *Mov. Disord.* 28, 392–395. doi: 10.1002/mds.25300
- Gagne, J. J., and Power, M. C. (2010). Anti-inflammatory drugs and risk of Parkinson disease: a meta-analysis. *Neurology* 74, 995–1002. doi: 10.1212/WNL.0b013e3181d5a4a3
- Gao, H. M., and Hong, J. S. (2008). Why neurodegenerative diseases are progressive: uncontrolled inflammation drives disease progression. *Trends Immunol.* 29, 357–365. doi: 10.1016/j.it.2008.05.002
- Gao, X., Chen, H., Schwarzschild, M. A., and Ascherio, A. (2011). Use of ibuprofen and risk of Parkinson disease. *Neurology* 76, 863–869. doi: 10.1212/WNL.0b013e31820f2d79
- George, S., Rey, N. L., Tyson, T., Esquibel, C., Meyerdirk, L., Schulz, E., et al. (2019). Microglia affect alpha-synuclein cell-to-cell transfer in a mouse model of Parkinson's disease. *Mol. Neurodegener.* 14:34. doi: 10.1186/s13024-019-0335-3
- Gerhard, A., Pavese, N., Hotton, G., Turkheimer, F., Es, M., Hammers, A., et al. (2006). In vivo imaging of microglial activation with [<sup>11</sup>C](R)-PK11195 PET in idiopathic Parkinson's disease. *Neurobiol. Dis.* 21, 404–412. doi: 10.1016/j.nbd.2005.08.002
- Ghadery, C., Koshimori, Y., Coakeley, S., Harris, M., Rusjan, P., Kim, J., et al. (2017). Microglial activation in Parkinson's disease using [(18)F]-FEPPA. *J. Neuroinflamm.* 14:8. doi: 10.1186/s12974-016-0778-1
- Ghasemi, F., Bagheri, H., Barreto, G. E., Read, M. I., and Sahebkar, A. (2019). Effects of curcumin on microglial cells. *Neurotox. Res.* 36, 12–26. doi: 10.1007/s12640-019-00030-0
- Ghosh, M., Xu, Y., and Pearce, D. D. (2016). Cyclic AMP is a key regulator of M1 to M2a phenotypic conversion of microglia in the presence of Th2 cytokines. *J. Neuroinflamm.* 13:9. doi: 10.1186/s12974-015-0463-9
- Glass, C. K., Saijo, K., Winner, B., Marchetto, M. C., and Gage, F. H. (2010). Mechanisms underlying inflammation in neurodegeneration. *Cell* 140, 918–934. doi: 10.1016/j.cell.2010.02.016
- Gonzalez, H., Elgueta, D., Montoya, A., and Pacheco, R. (2014). Neuroimmune regulation of microglial activity involved in neuroinflammation and neurodegenerative diseases. *J. Neuroimmunol.* 274, 1–13. doi: 10.1016/j.jneuroim.2014.07.012
- Gordon, R., Albornoz, E. A., Christie, D. C., Langley, M. R., Kumar, V., Mantovani, S., et al. (2018). Inflammasome inhibition prevents alpha-synuclein pathology and dopaminergic neurodegeneration in mice. *Sci. Transl. Med.* 10:eah4066. doi: 10.1126/scitranslmed.aah4066
- Gosselin, D., Skola, D., Coufal, N. G., Holtman, I. R., Schlachetzki, J. C. M., Sajti, E., et al. (2017). An environment-dependent transcriptional network specifies human microglia identity. *Science* 356:eaa3222. doi: 10.1126/science.aal3222
- Grabert, K., Michoel, T., Karavolos, M. H., Clohisy, S., Baillie, J. K., Stevens, M. P., et al. (2016). Microglial brain region-dependent diversity and selective regional sensitivities to aging. *Nat. Neurosci.* 19, 504–516. doi: 10.1038/nn.4222
- Gupta, A., Dhir, A., Kumar, A., and Kulkarni, S. K. (2009). Protective effect of cyclooxygenase (COX)-inhibitors against drug-induced catatonia and MPTP-induced striatal lesions in rats. *Pharmacol. Biochem. Behav.* 94, 219–226. doi: 10.1016/j.pbb.2009.07.018
- Hain, E. G., Sparenberg, M., Rasinska, J., Klein, C., Akyuz, L., and Steiner, B. (2018). Indomethacin promotes survival of new neurons in the adult murine hippocampus accompanied by anti-inflammatory effects following MPTP-induced dopamine depletion. *J. Neuroinflamm.* 15:162. doi: 10.1186/s12974-018-1179-4
- Hamza, T. H., Zabetian, C. P., Tenesa, A., Laederach, A., Montimurro, J., Yearout, D., et al. (2010). Common genetic variation in the HLA region is associated with

- late-onset sporadic Parkinson's disease. *Nat. Genet.* 42, 781–785. doi: 10.1038/ng.642
- Hansen, C., Angot, E., Bergstrom, A. L., Steiner, J. A., Pieri, L., Paul, G., et al. (2011). alpha-Synuclein propagates from mouse brain to grafted dopaminergic neurons and seeds aggregation in cultured human cells. *J. Clin. Invest.* 121, 715–725. doi: 10.1172/jci43366
- Hare, D. J., and Double, K. L. (2016). Iron and dopamine: a toxic couple. *Brain* 139, 1026–1035. doi: 10.1093/brain/aww022
- Harms, A. S., Barnum, C. J., Ruhn, K. A., Varghese, S., Trevino, I., Blesch, A., et al. (2011). Delayed dominant-negative TNF gene therapy halts progressive loss of nigral dopaminergic neurons in a rat model of Parkinson's disease. *Mol. Ther.* 19, 46–52. doi: 10.1038/mt.2010.217
- Harrison, J. K., Jiang, Y., Chen, S., Xia, Y., Maciejewski, D., McNamara, R. K., et al. (1998). Role for neuronally derived fractalkine in mediating interactions between neurons and CX3CR1-expressing microglia. *Proc. Natl. Acad. Sci. U.S.A.* 95, 10896–10901. doi: 10.1073/pnas.95.18.10896
- Healy, S., McMahon, J., Owens, P., and FitzGerald, U. (2016). Significant glial alterations in response to iron loading in a novel organotypic hippocampal slice culture model. *Sci. Rep.* 6:36410. doi: 10.1038/srep36410
- Heng, Y., Zhang, Q. S., Mu, Z., Hu, J. F., Yuan, Y. H., and Chen, N. H. (2016). Ginsenoside Rg1 attenuates motor impairment and neuroinflammation in the MPTP-probenecid-induced parkinsonism mouse model by targeting alpha-synuclein abnormalities in the substantia nigra. *Toxicol. Lett.* 243, 7–21. doi: 10.1016/j.toxlet.2015.12.005
- Hernan, M. A., Logroscino, G., and Garcia Rodriguez, L. A. (2006). Nonsteroidal anti-inflammatory drugs and the incidence of Parkinson disease. *Neurology* 66, 1097–1099. doi: 10.1212/01.wnl.0000204446.82823.28
- Hill-Burns, E. M., Factor, S. A., Zabetian, C. P., Thomson, G., and Payami, H. (2011). Evidence for more than one Parkinson's disease-associated variant within the HLA region. *PLoS One* 6:e27109. doi: 10.1371/journal.pone.0027109
- Hirsch, E. C., and Hunot, S. (2009). Neuroinflammation in Parkinson's disease: a target for neuroprotection? *Lancet Neurol.* 8, 382–397. doi: 10.1016/s1474-4422(09)70062-6
- Hirsch, L., Jette, N., Frolkis, A., Steeves, T., and Pringsheim, T. (2016). The incidence of parkinson's disease: a systematic review and meta-analysis. *Neuroepidemiology* 46, 292–300. doi: 10.1159/000445751
- Ho, M. S. (2019). Microglia in parkinson's disease. *Adv. Exp. Med. Biol.* 1175, 335–353. doi: 10.1007/978-981-13-9913-8\_13
- Holtman, I. R., Raj, D. D., Miller, J. A., Schaafsma, W., Yin, Z., Brouwer, N., et al. (2015). Induction of a common microglia gene expression signature by aging and neurodegenerative conditions: a co-expression meta-analysis. *Acta Neuropathol. Commun.* 3:31. doi: 10.1186/s40478-015-0203-5
- Hossain, M. M., Weig, B., Reuhl, K., Gearing, M., Wu, L. J., and Richardson, J. R. (2018). The anti-parkinsonian drug zonisamide reduces neuroinflammation: role of microglial Nav 1.6. *Exp. Neurol.* 308, 111–119. doi: 10.1016/j.expneurol.2018.07.005
- Houser, M. C., and Tansey, M. G. (2017). The gut-brain axis: is intestinal inflammation a silent driver of Parkinson's disease pathogenesis? *NPJ Parkinsons Dis.* 3:3. doi: 10.1038/s41531-016-0002-0
- Hu, X., and Ivashkiv, L. B. (2009). Cross-regulation of signaling pathways by interferon-gamma: implications for immune responses and autoimmune diseases. *Immunity* 31, 539–550. doi: 10.1016/j.immuni.2009.09.002
- Hughes, C. D., Choi, M. L., Ryten, M., Hopkins, L., Drews, A., Botia, J. A., et al. (2019). Picomolar concentrations of oligomeric alpha-synuclein sensitizes TLR4 to play an initiating role in Parkinson's disease pathogenesis. *Acta Neuropathol.* 137, 103–120. doi: 10.1007/s00401-018-1907-y
- Hunot, S., and Hirsch, E. C. (2003). Neuroinflammatory processes in Parkinson's disease. *Ann. Neurol.* 53, S49–S58. doi: 10.1002/ana.10481
- Iannaccone, S., Cerami, C., Alessio, M., Garibotto, V., Panzacchi, A., Olivieri, S., et al. (2013). In vivo microglia activation in very early dementia with Lewy bodies, comparison with Parkinson's disease. *Parkinsonism Relat. Disord.* 19, 47–52. doi: 10.1016/j.parkreldis.2012.07.002
- Imamura, K., Hishikawa, N., Sawada, M., Nagatsu, T., Yoshida, M., and Hashizume, Y. (2003). Distribution of major histocompatibility complex class II-positive microglia and cytokine profile of Parkinson's disease brains. *Acta Neuropathol.* 106, 518–526. doi: 10.1007/s00401-003-0766-2
- Ingelsson, M. (2016). Alpha-synuclein oligomers-neurotoxic molecules in Parkinson's Disease and other lewy body disorders. *Front. Neurosci.* 10:408. doi: 10.3389/fnins.2016.00408
- Iravani, M. M., Kashefi, K., Mander, P., Rose, S., and Jenner, P. (2002). Involvement of inducible nitric oxide synthase in inflammation-induced dopaminergic neurodegeneration. *Neuroscience* 110, 49–58. doi: 10.1016/s0306-4522(01)00562-0
- Janda, E., Boi, L., and Carta, A. R. (2018). Microglial phagocytosis and its regulation: a therapeutic target in Parkinson's Disease? *Front. Mol. Neurosci.* 11:144. doi: 10.3389/fnmol.2018.00144
- Jang, Y., Koo, J. H., Kwon, I., Kang, E. B., Um, H. S., Soya, H., et al. (2017). Neuroprotective effects of endurance exercise against neuroinflammation in MPTP-induced Parkinson's disease mice. *Brain Res.* 1655, 186–193. doi: 10.1016/j.brainres.2016.10.029
- Javed, H., Azimullah, S., Haque, M. E., and Ojha, S. K. (2016). Cannabinoid type 2 (CB2) receptors activation protects against oxidative stress and neuroinflammation associated dopaminergic neurodegeneration in rotenone model of parkinson's disease. *Front. Neurosci.* 10:321. doi: 10.3389/fnins.2016.00321
- Jiang, H., Li, L. J., Wang, J., and Xie, J. X. (2008). Ghrelin antagonizes MPTP-induced neurotoxicity to the dopaminergic neurons in mouse substantia nigra. *Exp. Neurol.* 212, 532–537. doi: 10.1016/j.expneurol.2008.05.006
- Jiang, T., Hoekstra, J., Heng, X., Kang, W., Ding, J., Liu, J., et al. (2015). P2X7 receptor is critical in alpha-synuclein-mediated microglial NADPH oxidase activation. *Neurobiol. Aging* 36, 2304–2318. doi: 10.1016/j.neurobiolaging.2015.03.015
- Jiang, T., Zhang, Y. D., Chen, Q., Gao, Q., Zhu, X. C., Zhou, J. S., et al. (2016). TREM2 modifies microglial phenotype and provides neuroprotection in P301S tau transgenic mice. *Neuropharmacology* 105, 196–206. doi: 10.1016/j.neuropharm.2016.01.028
- Joers, V., Tansey, M. G., Mulas, G., and Carta, A. R. (2017). Microglial phenotypes in Parkinson's disease and animal models of the disease. *Prog. Neurobiol.* 155, 57–75. doi: 10.1016/j.pneurobio.2016.04.006
- Joniec-Maciejak, I., Ciesielska, A., Wawer, A., Szejder-Pacholek, A., Schwenkgrub, J., Cudna, A., et al. (2014). The influence of AAV2-mediated gene transfer of human IL-10 on neurodegeneration and immune response in a murine model of Parkinson's disease. *Pharmacol. Rep.* 66, 660–669. doi: 10.1016/j.pharep.2014.03.008
- Kaur, D., Yantiri, F., Rajagopalan, S., Kumar, J., Mo, J. Q., Boonplueang, R., et al. (2003). Genetic or pharmacological iron chelation prevents MPTP-induced neurotoxicity in vivo: a novel therapy for Parkinson's disease. *Neuron* 37, 899–909. doi: 10.1016/s0896-6273(03)00126-0
- Kawabori, M., Kacimi, R., Kauppinen, T., Calosing, C., Kim, J. Y., Hsieh, C. L., et al. (2015). Triggering receptor expressed on myeloid cells 2 (TREM2) deficiency attenuates phagocytic activities of microglia and exacerbates ischemic damage in experimental stroke. *J. Neurosci.* 35, 3384–3396. doi: 10.1523/jneurosci.2620-14.2015
- Kawai, T., and Akira, S. (2007). Signaling to NF-kappaB by Toll-like receptors. *Trends Mol. Med.* 13, 460–469. doi: 10.1016/j.molmed.2007.09.002
- Kawai, T., and Akira, S. (2010). The role of pattern-recognition receptors in innate immunity: update on Toll-like receptors. *Nat. Immunol.* 11, 373–384. doi: 10.1038/ni.1863
- Kawai, T., Takeuchi, O., Fujita, T., Inoue, J., Muhlradt, P. F., Sato, S., et al. (2001). Lipopolysaccharide stimulates the MyD88-independent pathway and results in activation of IFN-regulatory factor 3 and the expression of a subset of lipopolysaccharide-inducible genes. *J. Immunol.* 167, 5887–5894. doi: 10.4049/jimmunol.167.10.5887
- Kettenmann, H., Hanisch, U. K., Noda, M., and Verkhratsky, A. (2011). Physiology of microglia. *Physiol. Rev.* 91, 461–553. doi: 10.1152/physrev.00011.2010
- Kierdorf, K., and Prinz, M. (2017). Microglia in steady state. *J. Clin. Invest.* 127, 3201–3209. doi: 10.1172/JCI90602
- Kim, B. W., Koppula, S., Kumar, H., Park, J. Y., Kim, I. W., More, S. V., et al. (2015). alpha-Asarone attenuates microglia-mediated neuroinflammation by inhibiting NF kappa B activation and mitigates MPTP-induced behavioral deficits in a mouse model of Parkinson's disease. *Neuropharmacology* 97, 46–57. doi: 10.1016/j.neuropharm.2015.04.037
- Kim, C., Ho, D. H., Suk, J. E., You, S., Michael, S., Kang, J., et al. (2013). Neuron-released oligomeric alpha-synuclein is an endogenous agonist of TLR2



- for paracrine activation of microglia. *Nat. Commun.* 4:1562. doi: 10.1038/ncomms2534
- Kim, J. S., Ryu, S. Y., Yun, I., Kim, W. J., Lee, K. S., Park, J. W., et al. (2006). 1 $\alpha$ ,25-dihydroxyvitamin D(3) protects dopaminergic neurons in rodent models of Parkinson's disease through inhibition of microglial activation. *J. Clin. Neurol.* 2, 252–257. doi: 10.3988/jcn.2006.2.4.252
- Kinoshita, K. I., Muroi, Y., Unno, T., and Ishii, T. (2017). Rolipram improves facilitation of contextual fear extinction in the 1-methyl-4-phenyl-1,2,3,6-tetrahydropyridine-induced mouse model of Parkinson's disease. *J. Pharmacol. Sci.* 134, 55–58. doi: 10.1016/j.jpshs.2017.04.002
- Knott, C., Stern, G., and Wilkin, G. P. (2000). Inflammatory regulators in Parkinson's disease: iNOS, lipocortin-1, and cyclooxygenases-1 and -2. *Mol. Cell. Neurosci.* 16, 724–739. doi: 10.1006/mcne.2000.0914
- Kobayashi, K., Imagama, S., Ohgomi, T., Hirano, K., Uchimura, K., Sakamoto, K., et al. (2013). Minocycline selectively inhibits M1 polarization of microglia. *Cell Death Dis.* 4:e525. doi: 10.1038/cddis.2013.54
- Konishi, H., and Kiyama, H. (2018). Microglial TREM2/DAP12 signaling: a double-edged sword in neural diseases. *Front. Cell. Neurosci.* 12:206. doi: 10.3389/fncel.2018.00206
- Koo, J. H., Jang, Y. C., Hwang, D. J., Um, H. S., Lee, N. H., Jung, J. H., et al. (2017). Treadmill exercise produces neuroprotective effects in a murine model of Parkinson's disease by regulating the TLR2/MyD88/NF-kappaB signaling pathway. *Neuroscience* 356, 102–113. doi: 10.1016/j.neuroscience.2017.05.016
- Kouli, A., Horne, C. B., and Williams-Gray, C. H. (2019). Toll-like receptors and their therapeutic potential in Parkinson's disease and alpha-synucleinopathies. *Brain Behav. Immun.* 81, 41–51. doi: 10.1016/j.bbi.2019.06.042
- Kumar, A., and Singh, N. (2017). Inhibitor of Phosphodiesterase-4 improves memory deficits, oxidative stress, neuroinflammation and neuropathological alterations in mouse models of dementia of Alzheimer's Type. *Biomed. Pharmacother.* 88, 698–707. doi: 10.1016/j.biopha.2017.01.059
- Kurkowska-Jastrzebska, I., Wronska, A., Kohutnicka, M., Czlonkowska, A., and Czlonkowska, A. (1999). The inflammatory reaction following 1-methyl-4-phenyl-1,2,3, 6-tetrahydropyridine intoxication in mouse. *Exp. Neurol.* 156, 50–61. doi: 10.1006/exnr.1998.6993
- La Vitola, P., Balducci, C., Cerovic, M., Santamaria, G., Brandi, E., Grandi, F., et al. (2018). Alpha-synuclein oligomers impair memory through glial cell activation and via Toll-like receptor 2. *Brain Behav. Immun.* 69, 591–602. doi: 10.1016/j.bbi.2018.02.012
- Lawand, N. B., Saade, N. E., El-Agnaf, O. M., and Safieh-Garabedian, B. (2015). Targeting alpha-synuclein as a therapeutic strategy for Parkinson's disease. *Expert Opin. Ther. Targets* 19, 1351–1360. doi: 10.1517/14728222.2015.1062877
- Lawson, L. J., Perry, V. H., Dri, P., and Gordon, S. (1990). Heterogeneity in the distribution and morphology of microglia in the normal adult mouse brain. *Neuroscience* 39, 151–170. doi: 10.1016/0306-4522(90)90229-w
- Le, W., Rowe, D., Xie, W., Ortiz, I., He, Y., and Appel, S. H. (2001). Microglial activation and dopaminergic cell injury: an in vitro model relevant to Parkinson's disease. *J. Neurosci.* 21, 8447–8455. doi: 10.1523/jneurosci.21-21-08447.2001
- Lee, E. J., Woo, M. S., Moon, P. G., Baek, M. C., Choi, I. Y., Kim, W. K., et al. (2010). Alpha-synuclein activates microglia by inducing the expressions of matrix metalloproteinases and the subsequent activation of protease-activated receptor-1. *J. Immunol.* 185, 615–623. doi: 10.4049/jimmunol.0903480
- Lee, M. K., Stirling, W., Xu, Y., Xu, X., Qui, D., Mandir, A. S., et al. (2002). Human alpha-synuclein-harboring familial Parkinson's disease-linked Ala-53  $\rightarrow$  Thr mutation causes neurodegenerative disease with alpha-synuclein aggregation in transgenic mice. *Proc. Natl. Acad. Sci. U.S.A.* 99, 8968–8973. doi: 10.1073/pnas.132197599
- Lehericy, S., Bardin, E., Poupon, C., Vidailhet, M., and Francois, C. (2014). 7 Tesla magnetic resonance imaging: a closer look at substantia nigra anatomy in Parkinson's disease. *Mov. Disord.* 29, 1574–1581. doi: 10.1002/mds.26043
- L'Episcopo, F., Tirolo, C., Serapide, M. F., Caniglia, S., Testa, N., Leggio, L., et al. (2018). Microglia polarization, gene-environment interactions and wnt/beta-catenin signaling: emerging roles of glia-neuron and glia-stem/neuroprogenitor crosstalk for dopaminergic neurorestoration in aged parkinsonian brain. *Front. Aging Neurosci.* 10:12. doi: 10.3389/fnagi.2018.00012
- Lhermitte, J., Kraus, W. M., and McAlpine, D. (1924). Original Papers: on the occurrence of abnormal deposits of iron in the brain in parkinsonism with special reference to its localisation. *J. Neurol. Psychopathol.* 5, 195–208. doi: 10.1136/jnnp.s1-5.19.195
- Li, J. Y., Englund, E., Holton, J. L., Soulet, D., Hagell, P., Lees, A. J., et al. (2008). Lewy bodies in grafted neurons in subjects with Parkinson's disease suggest host-to-graft disease propagation. *Nat. Med.* 14, 501–503. doi: 10.1038/nm1746
- Lima, L. A. R., Lopes, M. J. P., Costa, R. O., Lima, F. A. V., Neves, K. R. T., Calou, I. B. F., et al. (2018). Vitamin D protects dopaminergic neurons against neuroinflammation and oxidative stress in hemiparkinsonian rats. *J. Neuroinflamm.* 15:249. doi: 10.1186/s12974-018-1266-6
- Lin, S. C., Lo, Y. C., and Wu, H. (2010). Helical assembly in the MyD88-IRAK4-IRAK2 complex in TLR/IL-1R signalling. *Nature* 465, 885–890. doi: 10.1038/nature09121
- Longhena, F., Faustini, G., Spillantini, M. G., and Bellucci, A. (2019). Living in promiscuity: the multiple partners of alpha-synuclein at the synapse in physiology and pathology. *Int. J. Mol. Sci.* 20:E141. doi: 10.3390/ijms20010141
- Lopez Gonzalez, I., Garcia-Esparcia, P., Llorens, F., and Ferrer, I. (2016). Genetic and transcriptomic profiles of inflammation in neurodegenerative diseases: alzheimer, parkinson, creutzfeldt-jakob and tauopathies. *Int. J. Mol. Sci.* 17:206. doi: 10.3390/ijms17020206
- Lv, R., Du, L., Liu, X., Zhou, F., Zhang, Z., and Zhang, L. (2019). Rosmarinic acid attenuates inflammatory responses through inhibiting HMGB1/TLR4/NF-kappaB signaling pathway in a mouse model of Parkinson's disease. *Life Sci.* 223, 158–165. doi: 10.1016/j.lfs.2019.03.030
- Manocha, G. D., Floden, A. M., Puig, K. L., Nagamoto-Combs, K., Scherzer, C. R., and Combs, C. K. (2017). Defining the contribution of neuroinflammation to Parkinson's disease in humanized immune system mice. *Mol. Neurodegener.* 12:17. doi: 10.1186/s13024-017-0158-z
- Mantovani, A., Sica, A., and Locati, M. (2005). Macrophage polarization comes of age. *Immunity* 23, 344–346. doi: 10.1016/j.immuni.2005.10.001
- Maresz, K., Carrier, E. J., Ponomarev, E. D., Hillard, C. J., and Dittel, B. N. (2005). Modulation of the cannabinoid CB2 receptor in microglial cells in response to inflammatory stimuli. *J. Neurochem.* 95, 437–445. doi: 10.1111/j.1471-4159.2005.03380.x
- Marinova-Mutafchieva, L., Sadeghian, M., Broom, L., Davis, J. B., Medhurst, A. D., and Dexter, D. T. (2009). Relationship between microglial activation and dopaminergic neuronal loss in the substantia nigra: a time course study in a 6-hydroxydopamine model of Parkinson's disease. *J. Neurochem.* 110, 966–975. doi: 10.1111/j.1471-4159.2009.06189.x
- Martinez, F. O., and Gordon, S. (2014). The M1 and M2 paradigm of macrophage activation: time for reassessment. *F1000Prime Rep.* 6:13. doi: 10.12703/p6-13
- Martinez, F. O., Gordon, S., Locati, M., and Mantovani, A. (2006). Transcriptional profiling of the human monocyte-to-macrophage differentiation and polarization: new molecules and patterns of gene expression. *J. Immunol.* 177, 7303–7311. doi: 10.4049/jimmunol.177.10.7303
- Matak, P., Matak, A., Moustafa, S., Aryal, D. K., Benner, E. J., Wetsel, W., et al. (2016). Disrupted iron homeostasis causes dopaminergic neurodegeneration in mice. *Proc. Natl. Acad. Sci. U.S.A.* 113, 3428–3435. doi: 10.1073/pnas.1519473113
- McCoy, M. K., Martinez, T. N., Ruhn, K. A., Szymkowski, D. E., Smith, C. G., Botterman, B. R., et al. (2006). Blocking soluble tumor necrosis factor signaling with dominant-negative tumor necrosis factor inhibitor attenuates loss of dopaminergic neurons in models of Parkinson's disease. *J. Neurosci.* 26, 9365–9375. doi: 10.1523/jneurosci.1504-06.2006
- McCoy, M. K., Ruhn, K. A., Martinez, T. N., McAlpine, F. E., Blesch, A., and Tansey, M. G. (2008). Intraneuronal delivery of dominant-negative TNF attenuates neurodegeneration and behavioral deficits in hemiparkinsonian rats. *Mol. Ther.* 16, 1572–1579. doi: 10.1038/mt.2008.146
- McGeer, P. L., Itagaki, S., Boyes, B. E., and McGeer, E. G. (1988). Reactive microglia are positive for HLA-DR in the substantia nigra of Parkinson's and Alzheimer's disease brains. *Neurology* 38, 1285–1291.
- Mecca, C., Giambanco, I., Donato, R., and Arcuri, C. (2018). Microglia and aging: the role of the TREM2-DAP12 and CX3CL1-CX3CR1 axes. *Int. J. Mol. Sci.* 19:E318. doi: 10.3390/ijms19010318
- Mee-Inta, O., Zhao, Z. W., and Kuo, Y. M. (2019). Physical exercise inhibits inflammation and microglial activation. *Cells* 8:E691. doi: 10.3390/cells8070691
- Mehlase, J., Sandig, G., Pantopoulos, K., and Grune, T. (2005). Oxidation-induced ferritin turnover in microglial cells: role of proteasome. *Free Radic. Biol. Med.* 38, 276–285. doi: 10.1016/j.freeradbiomed.2004.10.025

- Meng, F., Guo, Z., Hu, Y., Mai, W., Zhang, Z., Zhang, B., et al. (2019). CD73-derived adenosine controls inflammation and neurodegeneration by modulating dopamine signalling. *Brain* 142, 700–718. doi: 10.1093/brain/awz351
- Michell-Robinson, M. A., Touil, H., Healy, L. M., Owen, D. R., Durafour, B. A., Bar-Or, A., et al. (2015). Roles of microglia in brain development, tissue maintenance and repair. *Brain* 138, 1138–1159. doi: 10.1093/brain/awv066
- Miron, V. E., Boyd, A., Zhao, J. W., Yuen, T. J., Ruckh, J. M., Shadrach, J. L., et al. (2013). M2 microglia and macrophages drive oligodendrocyte differentiation during CNS remyelination. *Nat. Neurosci.* 16, 1211–1218. doi: 10.1038/nn.3469
- Mogi, M., Harada, M., Kondo, T., Riederer, P., Inagaki, H., Minami, M., et al. (1994a). Interleukin-1 beta, interleukin-6, epidermal growth factor and transforming growth factor-alpha are elevated in the brain from parkinsonian patients. *Neurosci. Lett.* 180, 147–150. doi: 10.1016/0304-3940(94)90508-8
- Mogi, M., Harada, M., Riederer, P., Narabayashi, H., Fujita, K., and Nagatsu, T. (1994b). Tumor necrosis factor-alpha (TNF-alpha) increases both in the brain and in the cerebrospinal fluid from parkinsonian patients. *Neurosci. Lett.* 165, 208–210. doi: 10.1016/0304-3940(94)90746-3
- Mogi, M., Harada, M., Narabayashi, H., Inagaki, H., Minami, M., and Nagatsu, T. (1996). Interleukin (IL)-1 beta, IL-2, IL-4, IL-6 and transforming growth factor-alpha levels are elevated in ventricular cerebrospinal fluid in juvenile parkinsonism and Parkinson's disease. *Neurosci. Lett.* 211, 13–16. doi: 10.1016/0304-3940(96)12706-3
- Moon, M., Kim, H. G., Hwang, L., Seo, J. H., Kim, S., Hwang, S., et al. (2009). Neuroprotective effect of ghrelin in the 1-methyl-4-phenyl-1,2,3,6-tetrahydropyridine mouse model of Parkinson's disease by blocking microglial activation. *Neurotox. Res.* 15, 332–347. doi: 10.1007/s12640-009-9037-x
- Morganti, J. M., Riparip, L. K., and Rosi, S. (2016). Call off the Dog(ma): M1/M2 polarization is concurrent following traumatic brain injury. *PLoS One* 11:e0148001. doi: 10.1371/journal.pone.0148001
- Myeku, N., Clelland, C. L., Emrani, S., Kukushkin, N. V., Yu, W. H., Goldberg, A. L., et al. (2016). Tau-driven 26S proteasome impairment and cognitive dysfunction can be prevented early in disease by activating cAMP-PKA signaling. *Nat. Med.* 22, 46–53. doi: 10.1038/nm.4011
- Nagatsu, T., Mogi, M., Ichinose, H., and Togari, A. (2000). Changes in cytokines and neurotrophins in Parkinson's disease. *J. Neural Transm. Suppl.* 2000, 277–290. doi: 10.1007/978-3-7091-6301-6\_19
- Nalls, M. A., Plagnol, V., Hernandez, D. G., Sharma, M., Sheerin, U. M., Saad, M., et al. (2011). Imputation of sequence variants for identification of genetic risks for Parkinson's disease: a meta-analysis of genome-wide association studies. *Lancet* 377, 641–649. doi: 10.1016/S0140-6736(10)62345-8
- Navarrete, F., Garcia-Gutierrez, M. S., Aracil-Fernandez, A., Lanciego, J. L., and Manzanares, J. (2018). Cannabinoid CB1 and CB2 receptors, and monoacylglycerol lipase gene expression alterations in the basal ganglia of patients with parkinson's disease. *Neurotherapeutics* 15, 459–469. doi: 10.1007/s13311-018-0603-x
- Navarro, G., Borroto-Escuela, D., Angelats, E., Etayo, I., Reyes-Resina, I., Pulido-Salgado, M., et al. (2018). Receptor-heteromer mediated regulation of endocannabinoid signaling in activated microglia. Role of CB1 and CB2 receptors and relevance for Alzheimer's disease and levodopa-induced dyskinesia. *Brain Behav. Immun.* 67, 139–151. doi: 10.1016/j.bbi.2017.08.015
- Neumann, H., Kotter, M. R., and Franklin, R. J. (2009). Debris clearance by microglia: an essential link between degeneration and regeneration. *Brain* 132, 288–295. doi: 10.1093/brain/awn109
- Nimmerjahn, A., Kirchhoff, F., and Helmchen, F. (2005). Resting microglial cells are highly dynamic surveillants of brain parenchyma in vivo. *Science* 308, 1314–1318. doi: 10.1126/science.1110647
- Ninds Exploratory Trials in Parkinson Disease (Net-Pd) Fs-Zone Investigators. (2015). Pioglitazone in early Parkinson's disease: a phase 2, multicentre, double-blind, randomised trial. *Lancet Neurol.* 14, 795–803. doi: 10.1016/S1474-4422(15)00144-1
- Ojha, S., Javed, H., Azimullah, S., and Haque, M. E. (2016). beta-Caryophyllene, a phytocannabinoid attenuates oxidative stress, neuroinflammation, glial activation, and salvages dopaminergic neurons in a rat model of Parkinson disease. *Mol. Cell. Biochem.* 418, 59–70. doi: 10.1007/s11010-016-2733-y
- Olanow, C. W., Savolainen, M., Chu, Y., Halliday, G. M., and Kordower, J. H. (2019). Temporal evolution of microglia and alpha-synuclein accumulation following foetal grafting in Parkinson's disease. *Brain* 142, 1690–1700. doi: 10.1093/brain/awz104
- Orihuela, R., McPherson, C. A., and Harry, G. J. (2016). Microglial M1/M2 polarization and metabolic states. *Br. J. Pharmacol.* 173, 649–665. doi: 10.1111/bph.13139
- Ouchi, Y., Yoshikawa, E., Sekine, Y., Futatsubashi, M., Kanno, T., Ogosu, T., et al. (2005). Microglial activation and dopamine terminal loss in early Parkinson's disease. *Ann. Neurol.* 57, 168–175. doi: 10.1002/ana.20338
- Pabon, M. M., Bachstetter, A. D., Hudson, C. E., Gemma, C., and Bickford, P. C. (2011). CX3CL1 reduces neurotoxicity and microglial activation in a rat model of Parkinson's disease. *J. Neuroinflamm.* 8:9. doi: 10.1186/1742-2094-8-9
- Pais, T. F., Figueiredo, C., Peixoto, R., Braz, M. H., and Chatterjee, S. (2008). Necrotic neurons enhance microglial neurotoxicity through induction of glutaminase by a MyD88-dependent pathway. *J. Neuroinflamm.* 5:43. doi: 10.1186/1742-2094-5-43
- Paolicelli, R. C., Bolasco, G., Pagani, F., Maggi, L., Scianni, M., Panzanelli, P., et al. (2011). Synaptic pruning by microglia is necessary for normal brain development. *Science* 333, 1456–1458. doi: 10.1126/science.1202529
- Pietrzak, A., Wierzbicki, M., Wiktorska, M., and Brzezinska-Blaszczak, E. (2011). Surface TLR2 and TLR4 expression on mature rat mast cells can be affected by some bacterial components and proinflammatory cytokines. *Mediators Inflamm.* 2011:427473. doi: 10.1155/2011/427473
- Pifarre, P., Prado, J., Baltrons, M. A., Giral, M., Gabarro, P., Feinstein, D. L., et al. (2011). Sildenafil (Viagra) ameliorates clinical symptoms and neuropathology in a mouse model of multiple sclerosis. *Acta Neuropathol.* 121, 499–508. doi: 10.1007/s00401-010-0795-6
- Pisanu, A., Lecca, D., Mulas, G., Wardas, J., Simbula, G., Spiga, S., et al. (2014). Dynamic changes in pro- and anti-inflammatory cytokines in microglia after PPAR-γ agonist neuroprotective treatment in the MPTP mouse model of progressive Parkinson's disease. *Neurobiol. Dis.* 71, 280–291. doi: 10.1016/j.nbd.2014.08.011
- Pluvinage, J. V., Haney, M. S., Smith, B. A. H., Sun, J., Iram, T., Bonanno, L., et al. (2019). CD22 blockade restores homeostatic microglial phagocytosis in ageing brains. *Nature* 568, 187–192. doi: 10.1038/s41586-019-1088-4
- Poly, T. N., Islam, M. M. R., Yang, H. C., and Li, Y. J. (2019). Non-steroidal anti-inflammatory drugs and risk of Parkinson's disease in the elderly population: a meta-analysis. *Eur. J. Clin. Pharmacol.* 75, 99–108. doi: 10.1007/s00228-018-2561-y
- Porro, C., Panaro, M. A., Lofrumento, D. D., Hasalla, E., and Trotta, T. (2019). The multiple roles of exosomes in Parkinson's disease: an overview. *Immunopharmacol. Immunotoxicol.* 41, 469–476. doi: 10.1080/08923973.2019.1650371
- Prots, I., Grosch, J., Brazdis, R. M., Simmnacher, K., Veber, V., Havlicek, S., et al. (2018). alpha-Synuclein oligomers induce early axonal dysfunction in human iPSC-based models of synucleinopathies. *Proc. Natl. Acad. Sci. U.S.A.* 115, 7813–7818. doi: 10.1073/pnas.1713129115
- Rabal, O., Sanchez-Arias, J. A., Cuadrado-Tejedor, M., de Miguel, I., Perez-Gonzalez, M., Garcia-Barroso, C., et al. (2018). Design, synthesis, biological evaluation and in vivo testing of dual phosphodiesterase 5 (PDE5) and histone deacetylase 6 (HDAC6)-selective inhibitors for the treatment of Alzheimer's disease. *Eur. J. Med. Chem.* 150, 506–524. doi: 10.1016/j.ejmech.2018.03.005
- Ramazani, E., Tayarani-Najaran, Z., and Fereidoni, M. (2019). Celecoxib, indomethacin, and ibuprofen prevent 6-hydroxydopamine-induced PC12 cell death through the inhibition of NFκB and SAPK/JNK pathways. *Iran. J. Basic Med. Sci.* 22, 477–484. doi: 10.22038/ijbms.2019.34011.8091
- Ransohoff, R. M. (2016). A polarizing question: do M1 and M2 microglia exist? *Nat. Neurosci.* 19, 987–991. doi: 10.1038/nn.4338
- Ransohoff, R. M., and Perry, V. H. (2009). Microglial physiology: unique stimuli, specialized responses. *Annu. Rev. Immunol.* 27, 119–145. doi: 10.1146/annurev.immunol.021908.132528
- Rayaprolu, S., Mullen, B., Baker, M., Lynch, T., Finger, E., Seeley, W. W., et al. (2013). TREM2 in neurodegeneration: evidence for association of the p.R47H variant with frontotemporal dementia and Parkinson's disease. *Mol. Neurodegener.* 8:19. doi: 10.1186/1750-1326-8-19
- Rees, K., Stowe, R., Patel, S., Ives, N., Breen, K., Clarke, C. E., et al. (2011). Non-steroidal anti-inflammatory drugs as disease-modifying agents for Parkinson's disease: evidence from observational studies. *Cochrane Database Syst. Rev.* 87:CD008454. doi: 10.1002/1461858.CD008454.pub2

- Ren, M., Guo, Y., Wei, X., Yan, S., Qin, Y., Zhang, X., et al. (2018). TREM2 overexpression attenuates neuroinflammation and protects dopaminergic neurons in experimental models of Parkinson's disease. *Exp. Neurol.* 302, 205–213. doi: 10.1016/j.expneurol.2018.01.016
- Riederer, P., Sofic, E., Rausch, W. D., Schmidt, B., Reynolds, G. P., Jellinger, K., et al. (1989). Transition metals, ferritin, glutathione, and ascorbic acid in parkinsonian brains. *J. Neurochem.* 52, 515–520. doi: 10.1111/j.1471-4159.1989.tb09150.x
- Rothhammer, V., Borucki, D. M., Tjon, E. C., Takenaka, M. C., Chao, C. C., Ardura-Fabregat, A., et al. (2018). Microglial control of astrocytes in response to microbial metabolites. *Nature* 557, 724–728. doi: 10.1038/s41586-018-0119-x
- Ruano, D., Revilla, E., Gavilan, M. P., Vizuete, M. L., Pintado, C., Vitorica, J., et al. (2006). Role of p38 and inducible nitric oxide synthase in the in vivo dopaminergic cells' degeneration induced by inflammatory processes after lipopolysaccharide injection. *Neuroscience* 140, 1157–1168. doi: 10.1016/j.neuroscience.2006.02.073
- Sacino, A. N., Brooks, M., McKinney, A. B., Thomas, M. A., Shaw, G., Golde, T. E., et al. (2014). Brain injection of alpha-synuclein induces multiple proteinopathies, gliosis, and a neuronal injury marker. *J. Neurosci.* 34, 12368–12378. doi: 10.1523/jneurosci.2102-14.2014
- Samii, A., Etminan, M., Wiens, M. O., and Jafari, S. (2009). NSAID use and the risk of Parkinson's disease: systematic review and meta-analysis of observational studies. *Drugs Aging* 26, 769–779. doi: 10.2165/11316780-000000000-00000
- Sasso, V., Bisicchia, E., Latini, L., Ghiglieri, V., Cacace, F., Carola, V., et al. (2016). Repetitive transcranial magnetic stimulation reduces remote apoptotic cell death and inflammation after focal brain injury. *J. Neuroinflamm.* 13:150. doi: 10.1186/s12974-016-0616-5
- Saunders, J. A., Estes, K. A., Kosloski, L. M., Allen, H. E., Dempsey, K. M., Torres-Russotto, D. R., et al. (2012). CD4+ regulatory and effector/memory T cell subsets profile motor dysfunction in Parkinson's disease. *J. Neuroimmune Pharmacol.* 7, 927–938. doi: 10.1007/s11481-012-9402-z
- Schafer, D. P., Lehrman, E. K., Kautzman, A. G., Koyama, R., Mardinly, A. R., Yamasaki, R., et al. (2012). Microglia sculpt postnatal neural circuits in an activity and complement-dependent manner. *Neuron* 74, 691–705. doi: 10.1016/j.neuron.2012.03.026
- Schwenkgrub, J., Joniec-Maciejak, I., Szejder-Pacholek, A., Wawer, A., Ciesielska, A., Bankiewicz, K., et al. (2013). Effect of human interleukin-10 on the expression of nitric oxide synthases in the MPTP-based model of Parkinson's disease. *Pharmacol. Rep.* 65, 44–49. doi: 10.1016/s1734-1140(13)70962-9
- Schwenkgrub, J., Zaremba, M., Joniec-Maciejak, I., Cudna, A., Mirowska-Guzel, D., and Kurkowska-Jastrzebska, I. (2017). The phosphodiesterase inhibitor, ibudilast, attenuates neuroinflammation in the MPTP model of Parkinson's disease. *PLoS One* 12:e0182019. doi: 10.1371/journal.pone.0182019
- Sharma, N., and Nehru, B. (2016). Apocyanin, a microglial NADPH oxidase inhibitor prevents dopaminergic neuronal degeneration in lipopolysaccharide-induced parkinson's disease model. *Mol. Neurobiol.* 53, 3326–3337. doi: 10.1007/s12035-015-9267-2
- Sheridan, G. K., and Murphy, K. J. (2013). Neuron-glia crosstalk in health and disease: fractalkine and CX3CR1 take centre stage. *Open Biol.* 3, 130181. doi: 10.1098/rsob.130181
- Sierra, A., Encinas, J. M., Deudero, J. J., Chancey, J. H., Enikolopov, G., Overstreet-Wadiche, L. S., et al. (2010). Microglia shape adult hippocampal neurogenesis through apoptosis-coupled phagocytosis. *Cell Stem Cell* 7, 483–495. doi: 10.1016/j.stem.2010.08.014
- Skaper, S. D., Facci, L., Zusso, M., and Giusti, P. (2017). Neuroinflammation. Mast cells, and glia: dangerous liaisons. *Neuroscientist* 23, 478–498. doi: 10.1177/1073858416687249
- Skaper, S. D., Facci, L., Zusso, M., and Giusti, P. (2018). An inflammation-centric view of neurological disease: beyond the neuron. *Front. Cell. Neurosci.* 12:72. doi: 10.3389/fncel.2018.00072
- Sofic, E., Riederer, P., Heinsen, H., Beckmann, H., Reynolds, G. P., Hebenstreit, G., et al. (1988). Increased iron (III) and total iron content in post mortem substantia nigra of parkinsonian brain. *J. Neural Transm.* 74, 199–205. doi: 10.1007/bf01244786
- Song, G. J., Nam, Y., Jo, M., Jung, M., Koo, J. Y., Cho, W., et al. (2016). A novel small-molecule agonist of PPAR-gamma potentiates an anti-inflammatory M2 glial phenotype. *Neuropharmacology* 109, 159–169. doi: 10.1016/j.neuropharm.2016.06.009
- Song, G. J., and Suk, K. (2017). Pharmacological modulation of functional phenotypes of microglia in neurodegenerative diseases. *Front. Aging Neurosci.* 9:139. doi: 10.3389/fnagi.2017.00139
- Song, N., Wang, J., Jiang, H., and Xie, J. (2018). Astroglial and microglial contributions to iron metabolism disturbance in Parkinson's disease. *Biochim. Biophys. Acta Mol. Basis Dis.* 1864, 967–973. doi: 10.1016/j.bbdis.2018.01.008
- Stefanova, N., Fellner, L., Reindl, M., Masliah, E., Poewe, W., and Wenning, G. K. (2011). Toll-like receptor 4 promotes alpha-synuclein clearance and survival of nigral dopaminergic neurons. *Am. J. Pathol.* 179, 954–963. doi: 10.1016/j.ajpath.2011.04.013
- Stein, M., Keshav, S., Harris, N., and Gordon, S. (1992). Interleukin 4 potently enhances murine macrophage mannose receptor activity: a marker of alternative immunologic macrophage activation. *J. Exp. Med.* 176, 287–292. doi: 10.1084/jem.176.1.287
- Su, X., Federoff, H. J., and Maguire-Zeiss, K. A. (2009). Mutant alpha-synuclein overexpression mediates early proinflammatory activity. *Neurotox. Res.* 16, 238–254. doi: 10.1007/s12640-009-9053-x
- Su, X., Maguire-Zeiss, K. A., Giuliano, R., Prifti, L., Venkatesh, K., and Federoff, H. J. (2008). Synuclein activates microglia in a model of Parkinson's disease. *Neurobiol. Aging* 29, 1690–1701. doi: 10.1016/j.neurobiolaging.2007.04.006
- Subramaniam, S. R., and Federoff, H. J. (2017). Targeting microglial activation states as a therapeutic avenue in Parkinson's Disease. *Front. Aging Neurosci.* 9:176. doi: 10.3389/fnagi.2017.00176
- Swanson, C. R., Joers, V., Bondarenko, V., Brunner, K., Simmons, H. A., Ziegler, T. E., et al. (2011). The PPAR-gamma agonist pioglitazone modulates inflammation and induces neuroprotection in parkinsonian monkeys. *J. Neuroinflamm.* 8:91. doi: 10.1186/1742-2094-8-91
- Swiatkiewicz, M., Zaremba, M., Joniec, I., Czlonkowski, A., and Kurkowska-Jastrzebska, I. (2013). Potential neuroprotective effect of ibuprofen, insights from the mice model of Parkinson's disease. *Pharmacol. Rep.* 65, 1227–1236. doi: 10.1016/s1734-1140(13)71480-4
- Symons, A., Beinke, S., and Ley, S. C. (2006). MAP kinase kinases and innate immunity. *Trends Immunol.* 27, 40–48. doi: 10.1016/j.it.2005.11.007
- Szalay, G., Martinecz, B., Lenart, N., Kornyei, Z., Orsolits, B., Judak, L., et al. (2016). Microglia protect against brain injury and their selective elimination dysregulates neuronal network activity after stroke. *Nat. Commun.* 7:11499. doi: 10.1038/ncomms11499
- Szulzewsky, F., Pelz, A., Feng, X., Synowitz, M., Markovic, D., Langmann, T., et al. (2015). Glioma-associated microglia/macrophages display an expression profile different from M1 and M2 polarization and highly express Gpnmb and Spp1. *PLoS One* 10:e0116644. doi: 10.1371/journal.pone.0116644
- Takahashi, K., Prinz, M., Stagi, M., Chechneva, O., and Neumann, H. (2007). TREM2-transduced myeloid precursors mediate nervous tissue debris clearance and facilitate recovery in an animal model of multiple sclerosis. *PLoS Med.* 4:e124. doi: 10.1371/journal.pmed.0040124
- Takahashi, K., Rochford, C. D., and Neumann, H. (2005). Clearance of apoptotic neurons without inflammation by microglial triggering receptor expressed on myeloid cells-2. *J. Exp. Med.* 201, 647–657. doi: 10.1084/jem.2004.1611
- Takeda, K., and Akira, S. (2004). TLR signaling pathways. *Semin. Immunol.* 16, 3–9. doi: 10.1016/j.smim.2003.10.003
- Tansey, M. G., and Goldberg, M. S. (2010). Neuroinflammation in Parkinson's disease: its role in neuronal death and implications for therapeutic intervention. *Neurobiol. Dis.* 37, 510–518. doi: 10.1016/j.nbd.2009.11.004
- Taylor, J. M., Main, B. S., and Crack, P. J. (2013). Neuroinflammation and oxidative stress: co-conspirators in the pathology of Parkinson's disease. *Neurochem. Int.* 62, 803–819. doi: 10.1016/j.neuint.2012.12.016
- Theillet, F. X., Binolfi, A., Bekei, B., Martorana, A., Rose, H. M., Stuijver, M., et al. (2016). Structural disorder of monomeric alpha-synuclein persists in mammalian cells. *Nature* 530, 45–50. doi: 10.1038/nature16531
- Theodore, S., Cao, S., McLean, P. J., and Standaert, D. G. (2008). Targeted overexpression of human alpha-synuclein triggers microglial activation and an adaptive immune response in a mouse model of Parkinson disease. *J. Neuropathol. Exp. Neurol.* 67, 1149–1158. doi: 10.1097/NEN.0b013e31818e5e99
- Toschakov, V., Jones, B. W., Perera, P. Y., Thomas, K., Cody, M. J., Zhang, S., et al. (2002). TLR4, but not TLR2, mediates IFN-beta-induced



- STAT1alpha/beta-dependent gene expression in macrophages. *Nat. Immunol.* 3, 392–398. doi: 10.1038/nl774
- Ueno, M., Fujita, Y., Tanaka, T., Nakamura, Y., Kikuta, J., Ishii, M., et al. (2013). Layer V cortical neurons require microglial support for survival during postnatal development. *Nat. Neurosci.* 16, 543–551. doi: 10.1038/nn.3358
- Urrutia, P., Aguirre, P., Esparza, A., Tapia, V., Mena, N. P., Arredondo, M., et al. (2013). Inflammation alters the expression of DMT1, FPN1 and hepcidin, and it causes iron accumulation in central nervous system cells. *J. Neurochem.* 126, 541–549. doi: 10.1111/jnc.12244
- Valera, E., Mante, M., Anderson, S., Rockenstein, E., and Masliah, E. (2015). Lenalidomide reduces microglial activation and behavioral deficits in a transgenic model of Parkinson's disease. *J. Neuroinflamm.* 12:93. doi: 10.1186/s12974-015-0320-x
- Vay, S. U., Flitsch, L. J., Rabenstein, M., Rogall, R., Blaschke, S., Kleinhaus, J., et al. (2018). The plasticity of primary microglia and their multifaceted effects on endogenous neural stem cells in vitro and in vivo. *J. Neuroinflamm.* 15:226. doi: 10.1186/s12974-018-1261-y
- Verma, R., and Kim, J. Y. (2016). 1,25-Dihydroxyvitamin D3 Facilitates M2 Polarization and Upregulates TLR10 Expression on Human Microglial Cells. *Neuroimmunomodulation* 23, 75–80. doi: 10.1159/000444300
- Wahner, A. D., Bronstein, J. M., Bordelon, Y. M., and Ritz, B. (2007). Nonsteroidal anti-inflammatory drugs may protect against Parkinson disease. *Neurology* 69, 1836–1842. doi: 10.1212/01.wnl.0000279519.99344.ad
- Wake, H., Moorhouse, A. J., Jinno, S., Kohsaka, S., and Nabekura, J. (2009). Resting microglia directly monitor the functional state of synapses in vivo and determine the fate of ischemic terminals. *J. Neurosci.* 29, 3974–3980. doi: 10.1523/jneurosci.4363-08.2009
- Wakselman, S., Bechade, C., Roumier, A., Bernard, D., Triller, A., and Bessis, A. (2008). Developmental neuronal death in hippocampus requires the microglial CD11b integrin and DAP12 immunoreceptor. *J. Neurosci.* 28, 8138–8143. doi: 10.1523/jneurosci.1006-08.2008
- Wang, C., Fan, G., Xu, K., and Wang, S. (2013). Quantitative assessment of iron deposition in the midbrain using 3D-enhanced T2 star weighted angiography (ESWAN): a preliminary cross-sectional study of 20 Parkinson's disease patients. *Magn. Reson. Imaging* 31, 1068–1073. doi: 10.1016/j.mri.2013.04.015
- Wang, J., Song, N., Jiang, H., Wang, J., and Xie, J. (2013). Pro-inflammatory cytokines modulate iron regulatory protein 1 expression and iron transportation through reactive oxygen/nitrogen species production in ventral mesencephalic neurons. *Biochim. Biophys. Acta* 1832, 618–625. doi: 10.1016/j.bbdis.2013.01.021
- Wang, Q., Chu, C. H., Oyarzabal, E., Jiang, L., Chen, S. H., Wilson, B., et al. (2014). Subpicomolar diphenyleneiodonium inhibits microglial NADPH oxidase with high specificity and shows great potential as a therapeutic agent for neurodegenerative diseases. *Glia* 62, 2034–2043. doi: 10.1002/glia.22724
- Wang, S., Chu, C. H., Stewart, T., Ginghina, C., Wang, Y., Nie, H., et al. (2015a). alpha-Synuclein, a chemoattractant, directs microglial migration via H2O2-dependent Lyn phosphorylation. *Proc. Natl. Acad. Sci. U.S.A.* 112, E1926–E1935. doi: 10.1073/pnas.1417883112
- Wang, S., Jing, H., Yang, H., Liu, Z., Guo, H., Chai, L., et al. (2015b). Tanshinone I selectively suppresses pro-inflammatory genes expression in activated microglia and prevents nigrostriatal dopaminergic neurodegeneration in a mouse model of Parkinson's disease. *J. Ethnopharmacol.* 164, 247–255. doi: 10.1016/j.jep.2015.01.042
- Wang, Q., Liu, Y., and Zhou, J. (2015c). Neuroinflammation in Parkinson's disease and its potential as therapeutic target. *Transl. Neurodegener.* 4:19. doi: 10.1186/s40035-015-0042-0
- Wang, Q., Qian, L., Chen, S. H., Chu, C. H., Wilson, B., Oyarzabal, E., et al. (2015d). Post-treatment with an ultra-low dose of NADPH oxidase inhibitor diphenyleneiodonium attenuates disease progression in multiple Parkinson's disease models. *Brain* 138, 1247–1262. doi: 10.1093/brain/awv034
- Wang, X. J., Zhang, S., Yan, Z. Q., Zhao, Y. X., Zhou, H. Y., Wang, Y., et al. (2011). Impaired CD200-CD200R-mediated microglia silencing enhances midbrain dopaminergic neurodegeneration: roles of aging, superoxide, NADPH oxidase, and p38 MAPK. *Free Radic. Biol. Med.* 50, 1094–1106. doi: 10.1016/j.freeradbiomed.2011.01.032
- Ward, R. J., Zucca, F. A., Duyn, J. H., Crichton, R. R., and Zecca, L. (2014). The role of iron in brain ageing and neurodegenerative disorders. *Lancet Neurol.* 13, 1045–1060. doi: 10.1016/s1474-4422(14)70117-6
- Whitton, P. S. (2007). Inflammation as a causative factor in the aetiology of Parkinson's disease. *Br. J. Pharmacol.* 150, 963–976. doi: 10.1038/sj.bjp.0707167
- Wolf, S. A., Boddeke, H. W., and Kettenmann, H. (2017). Microglia in physiology and disease. *Annu. Rev. Physiol.* 79, 619–643. doi: 10.1146/annurev-physiol-022516-034406
- Wu, D. C., Jackson-Lewis, V., Vila, M., Tieu, K., Teismann, P., Vadseth, C., et al. (2002). Blockade of microglial activation is neuroprotective in the 1-methyl-4-phenyl-1,2,3,6-tetrahydropyridine mouse model of Parkinson disease. *J. Neurosci.* 22, 1763–1771. doi: 10.1523/jneurosci.22-05-01763.2002
- Xia, Y., Zhang, G., Han, C., Ma, K., Guo, X., Wan, F., et al. (2019). Microglia as modulators of exosomal alpha-synuclein transmission. *Cell Death Dis.* 10:174. doi: 10.1038/s41419-019-1404-9
- Xu, Y., Zhu, N., Xu, W., Ye, H., Liu, K., Wu, F., et al. (2018). Inhibition of phosphodiesterase-4 reverses abeta-induced memory impairment by regulation of HPA axis related cAMP signaling. *Front. Aging Neurosci.* 10:204. doi: 10.3389/fnagi.2018.00204
- Yang, W., Chen, Y. H., Liu, H., and Qu, H. D. (2015). Neuroprotective effects of piperine on the 1-methyl-4-phenyl-1,2,3,6-tetrahydropyridine-induced Parkinson's disease mouse model. *Int. J. Mol. Med.* 36, 1369–1376. doi: 10.3892/ijmm.2015.2356
- Yao, K., and Zhao, Y. F. (2018). Aging modulates microglia phenotypes in neuroinflammation of MPTP-PD mice. *Exp. Gerontol.* 111, 86–93. doi: 10.1016/j.exger.2018.07.010
- Zecca, L., Berg, D., Arzberger, T., Ruprecht, P., Rausch, W. D., Musicco, M., et al. (2005). In vivo detection of iron and neuromelanin by transcranial sonography: a new approach for early detection of substantia nigra damage. *Mov. Disord.* 20, 1278–1285. doi: 10.1002/mds.20550
- Zeng, K. W., Zhao, M. B., Ma, Z. Z., Jiang, Y., and Tu, P. F. (2012). Protosappanin A inhibits oxidative and nitritative stress via interfering the interaction of transmembrane protein CD14 with Toll-like receptor-4 in lipopolysaccharide-induced BV-2 microglia. *Int. Immunopharmacol.* 14, 558–569. doi: 10.1016/j.intimp.2012.09.004
- Zhang, F., Shi, J. S., Zhou, H., Wilson, B., Hong, J. S., and Gao, H. M. (2010). Resveratrol protects dopamine neurons against lipopolysaccharide-induced neurotoxicity through its anti-inflammatory actions. *Mol. Pharmacol.* 78, 466–477. doi: 10.1124/mol.110.064535
- Zhang, J., Zhang, Y., Wang, J., Cai, P., Luo, C., Qian, Z., et al. (2010). Characterizing iron deposition in Parkinson's disease using susceptibility-weighted imaging: an in vivo MR study. *Brain Res.* 1330, 124–130. doi: 10.1016/j.brainres.2010.03.036
- Zhang, Q. S., Heng, Y., Yuan, Y. H., and Chen, N. H. (2017). Pathological alpha-synuclein exacerbates the progression of Parkinson's disease through microglial activation. *Toxicol. Lett.* 265, 30–37. doi: 10.1016/j.toxlet.2016.11.002
- Zhang, S., Wang, X. J., Tian, L. P., Pan, J., Lu, G. Q., Zhang, Y. J., et al. (2011). CD200-CD200R dysfunction exacerbates microglial activation and dopaminergic neurodegeneration in a rat model of Parkinson's disease. *J. Neuroinflamm.* 8:154. doi: 10.1186/1742-2094-8-154
- Zhang, W., Wang, T., Pei, Z., Miller, D. S., Wu, X., Block, M. L., et al. (2005). Aggregated alpha-synuclein activates microglia: a process leading to disease progression in Parkinson's disease. *FASEB J.* 19, 533–542. doi: 10.1096/fj.04-2751com
- Zhang, X., Dong, H., Li, N., Zhang, S., Sun, J., Zhang, S., et al. (2016). Activated brain mast cells contribute to postoperative cognitive dysfunction by evoking microglia activation and neuronal apoptosis. *J. Neuroinflamm.* 13:127. doi: 10.1186/s12974-016-0592-9
- Zhang, Y., Feng, S., Nie, K., Li, Y., Gao, Y., Gan, R., et al. (2018). TREM2 modulates microglia phenotypes in the neuroinflammation of Parkinson's disease. *Biochem. Biophys. Res. Commun.* 499, 797–802. doi: 10.1016/j.bbrc.2018.03.226
- Zhao, S., Yang, J., Wang, L., Peng, S., Yin, J., Jia, L., et al. (2016). NF-kappaB upregulates type 5 phosphodiesterase in N9 microglial cells: inhibition by sildenafil and yonkenafil. *Mol. Neurobiol.* 53, 2647–2658. doi: 10.1007/s12035-015-9293-0
- Zhou, P., Homberg, J. R., Fang, Q., Wang, J., Li, W., Meng, X., et al. (2019). Histamine-4 receptor antagonist JNJ777120 inhibits pro-inflammatory microglia and prevents the progression of Parkinson-like pathology and behaviour in a rat model. *Brain Behav. Immun.* 76, 61–73. doi: 10.1016/j.bbi.2018.11.006



- Zhou, T. T., Zu, G., Wang, X., Zhang, X. G., Li, S., Liang, Z. H., et al. (2015). Immunomodulatory and neuroprotective effects of ginsenoside Rg1 in the MPTP(1-methyl-4-phenyl-1,2,3,6-tetrahydropyridine) -induced mouse model of Parkinson's disease. *Int. Immunopharmacol.* 29, 334–343. doi: 10.1016/j.intimp.2015.10.032
- Zhu, Y. L., Sun, M. F., Jia, X. B., Cheng, K., Xu, Y. D., Zhou, Z. L., et al. (2019). Neuroprotective effects of astilbin on MPTP-induced Parkinson's disease mice: glial reaction, alpha-synuclein expression and oxidative stress. *Int. Immunopharmacol.* 66, 19–27. doi: 10.1016/j.intimp.2018.11.004

**Conflict of Interest:** The authors declare that the research was conducted in the absence of any commercial or financial relationships that could be construed as a potential conflict of interest.

Copyright © 2019 Liu, Wang, Liu and Zhang. This is an open-access article distributed under the terms of the Creative Commons Attribution License (CC BY). The use, distribution or reproduction in other forums is permitted, provided the original author(s) and the copyright owner(s) are credited and that the original publication in this journal is cited, in accordance with accepted academic practice. No use, distribution or reproduction is permitted which does not comply with these terms.



# The Rules of Engagement: Do Microglia Seal the Fate in the Inverse Relation of Glioma and Alzheimer's Disease?

**Mathilde Cheray<sup>1</sup>, Vassilis Stratoulis<sup>1,2</sup>, Bertrand Joseph<sup>1</sup> and Kathleen Grabert<sup>1\*</sup>**

<sup>1</sup> Toxicology Unit, Institute of Environmental Medicine, Karolinska Institutet, Stockholm, Sweden, <sup>2</sup> Neuroscience Center, Helsinki Institute of Life Science, University of Helsinki, Helsinki, Finland

## OPEN ACCESS

### Edited by:

Rocio Martínez De Pablos,  
University of Seville, Spain

### Reviewed by:

Manuel Sarmiento Soto,  
University of Seville, Spain

Barbara Monti,  
University of Bologna, Italy

### \*Correspondence:

Kathleen Grabert  
kathleen.grabert@ki.se

### Specialty section:

This article was submitted to  
Non-Neuronal Cells,  
a section of the journal  
Frontiers in Cellular Neuroscience

**Received:** 02 October 2019

**Accepted:** 07 November 2019

**Published:** 20 November 2019

### Citation:

Cheray M, Stratoulis V, Joseph B  
and Grabert K (2019) The Rules  
of Engagement: Do Microglia Seal  
the Fate in the Inverse Relation  
of Glioma and Alzheimer's Disease?  
*Front. Cell. Neurosci.* 13:522.  
doi: 10.3389/fncel.2019.00522

Microglia, the immune cells of the brain, play a major role in the maintenance of brain homeostasis and constantly screen the brain environment to detect any infection or damage. Once activated by a stimulus, microglial cells initiate an immune response followed by the resolution of brain inflammation. A failure or deviation in the housekeeping function of these guardian cells can lead to multiple diseases, including brain cancer and neurodegenerative diseases such as Alzheimer's disease (AD). A small number of studies have investigated the causal relation of both diseases, thereby revealing an inverse relationship where cancer patients have a reduced risk to develop AD and *vice versa*. In this review, we aim to shed light on the role of microglia in the fate to develop specifically glioma as one type of cancer or AD. We will examine the common and/or opposing genetic predisposition as well as associated pathways of these diseases to unravel a possible involvement of microglia in the occurrence of either disease. Lastly, a set of guidelines will be proposed for future research and diagnostics to clarify and improve the knowledge on the role of microglia in the decision toward one pathology or another.

**Keywords:** disease-associated microglia, glioma, Alzheimer's disease, inverse correlation, risk genes

## INTRODUCTION

The central nervous system (CNS) can be affected at any stage in life by numerous neurological disorders and neurodegenerative diseases. Microglia, as key innate immune cells of the CNS, are the first responders and able to recognize an abundance of factors that could compromise the CNS. For the protection of the brain, microglia can trigger a vigorous immune and inflammatory response and therefore puts them at the center of neurological conditions (Biber et al., 2007; Wake et al., 2009; Chen and Trapp, 2016). The responsiveness of microglia in various diseases has been studied in great detail. Collectively, these studies revealed the high plasticity of microglia and associated regulative processes evident by the acquisition of regionally distinct spatio-temporal phenotypes throughout life as adaptation to their local environment (Shemer et al., 2015; Grabert et al., 2016; Ayata et al., 2018; Cheray and Joseph, 2018; Hammond et al., 2019; Masuda et al., 2019; Stratoulis et al., 2019). Overall, microglia phenotype is influenced by a variety of factors including ontogeny (Ginhoux et al., 2010; Kierdorf et al., 2013; Matcovitch-Natan et al., 2016), sex (Guneykaya et al., 2018; Villa et al., 2018; Hammond et al., 2019), location (de Haas et al., 2008; Grabert et al., 2016;

Masuda et al., 2019), disease (Bisht et al., 2016; Keren-Shaul et al., 2017), and age (Grabert et al., 2016; Galatro et al., 2017). Aging is a natural, yet highly complex process, in which every part of an organism gradually declines. It is a devious and multi-layered progression affecting both the gene and protein level (e.g., DNA replication errors, epigenetic changes, protein misfolding) as well as cellular biochemistry and bioenergetics, which overall leads to an impairment of tissue homeostasis and function (López-Otín et al., 2013). Glioma and AD share aging as a common risk factor. In light of microglial plasticity, it is highly interesting that a number of studies suggest an inverse correlation between AD and cancer in general implying microglia may be set or contribute to an environment, which does not allow to change direction. Considering the vast advances made in microglia biology in glioma and AD, very little is known about the involvement of these immune sentinels to regulate or contribute to this intriguing relation of developing one yet being protected from acquiring the other pathology.

In this short review, we will depict the findings of the role and functionality of microglia in primary brain tumors and AD. Furthermore, we will provide a brief overview of longitudinal studies describing the inverse relation of both diseases. We then endeavor to discuss and elucidate in microglia reported risk genes and associate pathways to establish a link and/or cause in the fate toward either pathology.

## MICROGLIA IN GLIOMA

Glioma, the most frequent of primary CNS tumors in adults, are divided into subtypes by the World Health Organization (WHO). While the low grade astrocytoma (grade I or II) are treatable when diagnosed early, high-grade glioma like Glioblastoma (grade IV) have a median survival limited to ~15 months (Stupp et al., 2005). To date, it remains unclear how or why this type of cancer is initiated. The classification of different grades of glioma has allowed a better understanding on the different genetic actors involved in the progression of the disease. The mutation status of the isocitrate dehydrogenase (*IDH*) gene and the amplification of platelet-derived growth factor receptor (*PDGFR*) and epidermal growth factor receptor (*EGFR*) is of importance in the diagnosis and prognosis of glioma (Verhaak et al., 2010; Leu et al., 2013; The Cancer Genome Atlas Research Network, 2015). Additionally, the status of the deletion 1p/19q will differentiate grade I from grade II tumors (Leeper et al., 2015). New tumor microenvironment-derived subtypes of GBM (Wang et al., 2017) and new markers related to epigenetic changes, such as the promoter methylation status of the DNA repair enzyme, O<sup>6</sup>-methylguanine-DNA-methyltransferase (*MGMT*), have been added to the pool of known markers of the glioma progression (Reifenberger et al., 2016). These constant advancements are helpful tools for the diagnosis of the disease but the treatment efficiency and options remain limited. Due to the existence of many different subtypes, we focused on the GBM subtype and summarized the features of the disease in **Figure 1**.



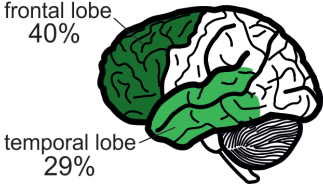
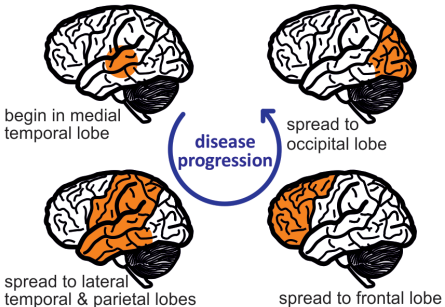


In the last decade, research has intensified on deciphering the complexity of this devastating disease, yet there is no cure

for GBM. The current treatment for glioma is a combination of chemotherapy using Temozolomide and irradiation after resection of the tumor. Despite this radical procedure the average survival increases by 3 months only (Stupp et al., 2005). The detrimental prognosis of glioma is due to the high aggressiveness of the disease where recurrence of the tumor after its resection commonly occurs. Gliomas can use their environment to grow and invade very quickly the healthy brain. Recent findings demonstrate the ability of glioma cells to seize control by the incorporation into the neuronal network of the brain (Venkatesh et al., 2019). Peripheral microglia are attracted and recruited inside the tumor core by the secreted factors released from the tumor cells like CCL2, CSF1, or EGF (Nolte et al., 1997; Zhang et al., 2012; Pyonteck et al., 2013; Sielska et al., 2013). These tumoral environment enrolled microglia will turn into pro-tumoral cells displaying an opposing function to their protective brain homeostatic role. This is evident by the secretion of factors involved in extracellular matrix degradation like MMPs or in angiogenesis like VEGF, EGF, or IL1B (Tsai et al., 1995; Lafuente et al., 1999; Markovic et al., 2009), which are needed for tumor growth and the invasion into the healthy tissue.

Even though the study of glioma-associated microglia is challenging due to the lack of specific microglia markers and the infiltration of peripheral myeloid cells, a few human and mouse studies have defined up-regulated markers linked with microglia/macrophages in the glioma context. Both, CD163 and CD204, identify anti-inflammatory glioma-associated microglia/macrophages (or GAMs), which are present in higher glioma grade and consequently leading to worse survival (Komohara et al., 2008). A recent gene expression meta-analysis on two different glioma mouse models by Haage et al. (2019) distinguished microglia from macrophages in the healthy brain and under glioma conditions. Using publicly available mouse datasets, the authors identified in line with other studies (Hickman et al., 2013; Butovsky et al., 2014; Bennett et al., 2016) *P2ry12*, *Tmem119*, *Slc2a5*, and *Fcrls* as a set of genes specific to microglia that will help to differentiate these from macrophages as has been validated in RCAS and GL261 glioma mouse models (Haage et al., 2019). This study confirmed previous data obtained by Bowman et al. (2016) where, using lineage tracing mouse models, they observe that macrophages and microglia would acquire specific transcriptional networks through a tumor-mediated education.

## MICROGLIA IN AD

Alzheimer's disease is the most common neurodegenerative disease with a higher prevalence in women (**Figure 1**) and clinically defined by the gradual decline in memory and other cognitive functions. Regionally, AD begins in the medial temporal lobes and progresses in a caudal-rostral manner to the frontal lobe (**Figure 1**). Pathologically, it is characterized by neuroinflammation, extensive neuronal loss, and the progressive accumulation and deposition of insoluble amyloid  $\beta$  (A $\beta$ ) plaques in the brain. Plaques have long been considered as a causal effect to AD initiation, yet this hypothesis is under debate

	<b>Glioblastoma</b> 		<b>Alzheimer's Disease</b> 	
<b>Prevalence</b>	~2-3 per 100,000 individuals		~700 per 100,000 individuals	
<b>Gender</b>	♀ ~40%	~60% ♂	♀ ~66%	~33% ♂
<b>Age at diagnosis</b>	64 years (median)		>65 years	
<b>Survival rate</b>	~15 months		~8.3 years	
<b>Brain location</b>				
<b>Risk genes</b>	<i>ATRX</i> , <i>IDH</i> statuses, <i>MGMT</i> methylation <i>PDGFR/EGFR</i> amplification <i>TERT</i> promoter mutation, <i>PTEN</i> mutation		<i>TREM2</i> , <i>CD33</i> , <i>INPP5D</i> , <i>HLA-DQA1</i> , <i>MS4A4</i> , <i>CASS1</i> , <i>SORL1</i> , <i>SCIMP</i> , <i>SPPL2A</i> , <i>APOC1</i> , <i>ATXN7L</i>	
<b>Microglial component</b>	 <ul style="list-style-type: none"> <li>° microglia constitute large proportion of tumor mass</li> <li>° microglia support expansion and invasion of glioma cells</li> </ul>		 <ul style="list-style-type: none"> <li>° microglia concentrated around amyloid plaques</li> <li>° AD risk genes highly expressed by microglia</li> </ul>	

**FIGURE 1** | Comparison of distinct features for Glioblastoma and AD reveals contrasting pathologies and involvement of microglia.

(De Strooper and Karran, 2016). The amyloid hypothesis was fueled by the identification of a dominant inherited genomic alteration in three genes resulting in imbalanced processing and subsequent aggregation of A $\beta$ . Mutations in *APP*, *PSEN2*, and *PSEN2* as well as the triplication of the *APP* gene contribute to 5–10% of early onset familial forms of AD. However, familial early onset AD is extremely rare and maybe an atypical form of the disease, representing 1–2% of all cases (Campion et al., 1999).

Aging and genetic components are the two main risk factors for AD with the vast majority of patients displaying AD symptoms from 65 years of age with an average survival time of 8.3 years from diagnosis (Figure 1; Alzheimer's Association, 2019). Although this late onset AD (LOAD) involves a strong genetic predisposition, no single model can explain the mode

of disease transmission. To date, more than 30 gene loci have been implicated in LOAD with the *APOE* gene being the major risk factor (Corder et al., 1993). Several other low-risk loci have been implicated in LOAD including *TREM2*, *CLU*, *PICALM*, *CR1*, *BIN1*, *MS4A* gene cluster, *CD2AP*, *CD33*, *EPHA1*, and *ABCA7* (Harold et al., 2009; Lambert et al., 2009; Hollingworth et al., 2011; Naj et al., 2011; Kunkle et al., 2019). Risk variants of AD that are associated with microglia of the aged brain (Figure 1) are *TREM2*, *CD33*, *INPP5D*, *HLA-DQA1*, *MS4A4A*, *CASS1*, *SORL1*, *SCIMP*, *SPPL2A*, *APOC1*, and *ATXN7L* (Olah et al., 2018), which makes microglia a central player in recent AD research. Although it is currently not clear how microglia contribute to the disease, various studies point toward inefficient microglial phagocytosis of A $\beta$  plaques and lipid processing



(Shi and Holtzman, 2018) as at least one of the main contributors. Microglia are associated with plaques in murine AD models, as well as in AD patients. Current understanding of the role of these plaque-associated microglia indicates that they form a barrier surrounding amyloid deposits, limiting their outward expansion (Yuan et al., 2018).

## SUPPORTING EVIDENCE FOR THE INVERSE RELATION BETWEEN AD AND CANCER

Almost three decades ago the first two reports emerged on a negative association regarding the occurrence of cancer of various tissue origin and AD in the same individual (Tirumalasetti et al., 1991; DeSouky, 1992). Both letters state that patients diagnosed with AD did not have cancer or undergone cancer treatment at the time of the investigation. *Vice versa*, cancer patients are less likely to develop AD. Since then a small number of longitudinal studies were conducted all of which reinforce these observations (Yamada et al., 1999; Roe et al., 2005, 2010; Driver et al., 2012; Musicco et al., 2013; Ou et al., 2013). Two independent lines of research revealed that patients with a history of cancer had a reduced risk of developing AD by 33–40%, while dementia patients demonstrated a reduced risk of 56–70% for future cancer (Roe et al., 2010; Driver et al., 2012). Additionally, the quantity of cancer (> 1) has shown to lower the chances of AD (Nudelman et al., 2014). Most interestingly, this inverse relationship was greatly affected by the type of dementia. While reportedly vascular dementia demonstrated no significant association to cancer, the likelihood to develop cancer was the lowest in patients with pure or probable AD (Roe et al., 2010; Driver et al., 2012). One of the common risk factors for both diseases is age, which has been taken into consideration by two independent studies. The research conducted in Taiwan reported that especially female patients diagnosed with AD between 60 and 79 years of age had a reduced risk for cancer (Ou et al., 2013). Musicco et al. (2013) revealed a greater decrease on cancer risk in AD patients of both genders from 65 years onward, which is in line with the average begin of diagnosis of AD (Alzheimer's Association, 2019). In contrast, this study comprised of an Italian cohort suggests that the risk remained low with increasing age to 85+ years (Musicco et al., 2013). The age-related observation in patients with a cancer history exhibiting a smaller likelihood to develop AD was made in the same study. Despite the knowledge that the type of dementia can play a role in the described effect here, nearly all studies applied data of cancer overall and largely not distinguishing between different types of cancer. This is due to the high variability in the prevalence of various cancers. Our interest lies in the relationship between AD and glioma and more specifically the role of microglia in this association. The current challenge is the collection of sufficient and significant information on the relationship between glioma and AD considering the low incidence rate of primary brain tumors such as GBM (~2–3 in 100,000).

## MICROGLIA ASSOCIATED GENES AND PATHWAYS AS POSSIBLE PLAYERS IN DISEASE FATE

The underlying mechanism and/or genetic predisposition that support the pathology of one but not the other disease has been speculated (Behrens et al., 2009; Liu T. et al., 2013; Snyder et al., 2017), yet the question what initiates the fate toward either condition remains. What came first? Glioma or AD and what specific role could microglia play in this correlation? In the absence of disease, age-related changes of the microglia transcriptome are apparent as early as middle-age and regionally distinct. Particularly, changes in sensing and engaging with their local environment correlate with the regional susceptibility to age-related neurodegenerative diseases (Grabert et al., 2016). While AD is diagnosed for the majority of cases from 65 years of age (Alzheimer's Association, 2019), the development of the disease and early markers (e.g., CSF, A $\beta$ ) has its beginnings decades before (Jack and Holtzman, 2013; Selkoe and Hardy, 2016). Thus, as AD progresses over years prior to the clinical diagnosis the local environment may be pushed in one direction and thereby restrain the development of glioma. In contrast, the prevalence of glioma increases drastically at the age of 45 years (Ferris et al., 2017). Cells (e.g., microglia) of cancer survivors may have acquired a distinct phenotype throughout the disease and treatment which prevents the development of AD. Here we describe a small number of selected genes and pathway related to microglia in either disease, which we think could be of interest for future investigations and application.

TREM2 is a cell surface receptor highly expressed in microglia. It recognizes multiple components including apoptotic cells, apolipoproteins (e.g., APOE and CLU), A $\beta$  oligomers (Zhao et al., 2018), and endogenous ligands such as galectin-3 (Boza-Serrano et al., 2019). Activation of TREM2 leads to the sequestration of DAP12 leading to microglial proliferation, survival, and phagocytosis (reviewed by Shi and Holtzman, 2018). Notably, APOE, CLU, and DAP12 are identified as AD risk genes (Figure 1). The role of TREM2 in AD has been the subject of intense research. TREM2 expression is upregulated in microglia with the progression of the disease, when microglia feature an enhanced phagocytotic profile (Keren-Shaul et al., 2017). TREM2-deficient microglia show reduced A $\beta$  uptake *in vitro* (Yeh et al., 2016), *in vivo* (Wang Y. et al., 2016; Yuan et al., 2018), as well as reduced aggregation and proliferation around plaques (Jay et al., 2015; Wang et al., 2015). On the other hand, a recent study reported that TREM2 is significantly upregulated in glioma tissue and is associated with glioma progression (Wang X.-Q. et al., 2016). Further studies to elucidate the role of TREM2 in AD and glioma and its relation to microglia are needed.

APOE is a lipid carrier regulating lipid homeostasis and also acts as a ligand for TREM2, regulating the TREM2-mediated microglia phagocytosis (Yeh et al., 2016). There are three common human APOE alleles,  $\epsilon$ 2,  $\epsilon$ 3, and  $\epsilon$ 4, which differ by two amino acids. APOE allele  $\epsilon$ 4 is the major known genetic risk factor for AD; it is estimated that 40% of people diagnosed with

AD have this allele (Liu C.-C. et al., 2013). In contrast, APOE  $\epsilon$ 3 appears not to have a correlation with AD, while APOE  $\epsilon$ 2 has been shown to infer a protective role (Yeh et al., 2016). If APOE should have a role in glioma, it has not yet been revealed.

Neuropilin-1 (or NRP1), a transmembrane receptor expressed by various cells in the body, plays a role in brain tumor progression through its expression in microglia. Indeed, Miyauchi et al. (2016, 2018) demonstrated that the deletion of NRP1 in microglia leads to the reduction of glioma progression *in vivo* and its expression in microglial cells is correlated with poor prognosis in high grade gliomas (Caponegro et al., 2018). The function of NRP1 in AD is poorly studied with only one study hinting toward NRP1 as potential marker of inflammatory microglia in AD based on the proteomics analysis of microglial plasma membranes after treatment with a synthetic A $\beta$  peptide (Correani et al., 2017).

Our group uncovered the non-apoptotic role of Caspase-3 (CASP3) in the phenotype polarization of microglia. The stimulation of microglia cells by inflammogens will lead to the activation of CASP3 without cell death induction *in vitro* or *in vivo*. In turn, active CASP3 promotes, through a PKC $\delta$ -dependent pathway, the pro-inflammatory activation of microglia. This microglial CASP3 activation has been observed in the frontal cortex of AD patients which confirms a role for CASP3 in AD (Burguillos et al., 2011). In contrast, the activation of microglia into a pro-tumoral phenotype under glioma conditions is associated with a decrease of the basal level of CASP3 in microglia by the glioma cells (Shen et al., 2016). These opposite roles of CASP3 in the different microglial phenotypes acquisition between AD and glioma could be an explanation of the inverse correlation of the two pathologies and the role microglia could play in the fate of the brain (for review see Shen et al., 2017, 2018).

A few studies have highlighted the phosphoinositide 3 kinase – Akt – mammalian target of rapamycin (PI3k-Akt-mTor, PAM) pathway (Liu T. et al., 2013; Majd et al., 2019) as a possible common mechanism that may be the link in the inverse relation between AD and cancer in general. Thus, proteins upstream or downstream of this pathway could exert influence. Interestingly, some of the example genes described here can partly be linked with PAM underlining a potentially critical role in the decision process for either disease. In case of TREM2, upon ligand binding (e.g., APOE) and interacting with DAP12 as adapter protein the PI3K cascade is activated leading to cellular proliferation, survival, and phagocytosis (Konishi and Kiyama, 2018). With regards to AD, this mechanism is thought to support highly energetic microglia in order to cluster around A $\beta$  plaques (Zhou et al., 2018). Yet it could be identified that the microglial cells of AD patients with a confirmed deficiency in TREM2 trigger the enhancement of mTOR-regulated autophagy for survival (Ulland et al., 2018).

In conclusion, these few examples demonstrate the current lack of information in the interplay of microglia-associated genes and pathways toward either pathology. Less than a handful of genes are well described to be active in AD (e.g., CASP3) but decrease in glioma; or upregulated in glioma and being a risk variant in AD leading to gene deficiency (e.g., TREM2).

Yet, some genes could be both up- or downregulated in either disease due to the effect of aging. CLEC7A (C-type lectin domain containing 7a, also known as DECTIN-1) is one example. This anti-microbial pattern recognition receptor (Goodridge et al., 2011) is increasingly expressed by microglia with age (Holtman et al., 2015; Raj et al., 2017). Moreover, the expression of *Clec7a* in mouse models of neurodegeneration (e.g., multiple sclerosis, amyotrophic lateral sclerosis, AD) (Olah et al., 2012; Keren-Shaul et al., 2017; Krasemann et al., 2018) and glioma (Szulzewsky et al., 2015) was upregulated and has recently included as a marker for disease-associated microglia (DAM) (Keren-Shaul et al., 2017). Thus, it is necessary to extend the scope of future research for which we provide a number of suggestions in the subsequent section.

## PROPOSED GUIDELINES FOR FUTURE RESEARCH AND DIAGNOSTICS

To uncover and understand the microglial and mechanistic contribution to the inverse relation of AD and glioma, future research faces a number of challenges, which once overcome can lead to new tools in diagnostics and ultimately alternative treatment opportunities. In **Figure 2**, we summarized our suggestions for future studies in a form of potential guidelines that could be followed either in research investigations or in a clinical setting.

The majority of longitudinal studies examined the relation between cancer and AD on a broad scale largely unable to concentrate on the association of AD with a distinct type of cancer. Certainly, the analysis into the relation of glioma with AD will take a considerable number of years due to the low frequency occurrence of glioma. A large-scale study stretching over a significant period of time would further allow the distinction between men and women (**Figure 2**) as has been reported that women are more likely to develop AD than cancer, while this is the opposite for men. Moreover, the evidence regarding the differences of microglia based on gender is increasing (Guneykaya et al., 2018; Villa et al., 2018) underlining the importance of distinction. One issue of previous and possibly future studies will be the misdiagnosis of glioma for AD and *vice versa* (**Figure 2**) as initial pathology with the performance of minimal test to establish correct diagnosis as likely reason. Furthermore, once a patient is diagnosed with either disease no additional examination is being performed to exclude the possibility of the other. Thus, either disease may remain undetected and therefore is not being reported (**Figure 2**). Future work, although laborious and costly, would profoundly benefit from extended examination to underline present findings. Simple tools such as diagnostic marker would facilitate this procedure.

The use of microglial markers that are expressed in one pathology and not the other will be of great benefit for the diagnosis at early stages of the diseases. As mentioned previously, a marker like Caspase-3 or disease-associated risk alleles, which are expressed differentially in microglia based on the disease context would be a highly valuable tool to add in the first steps of

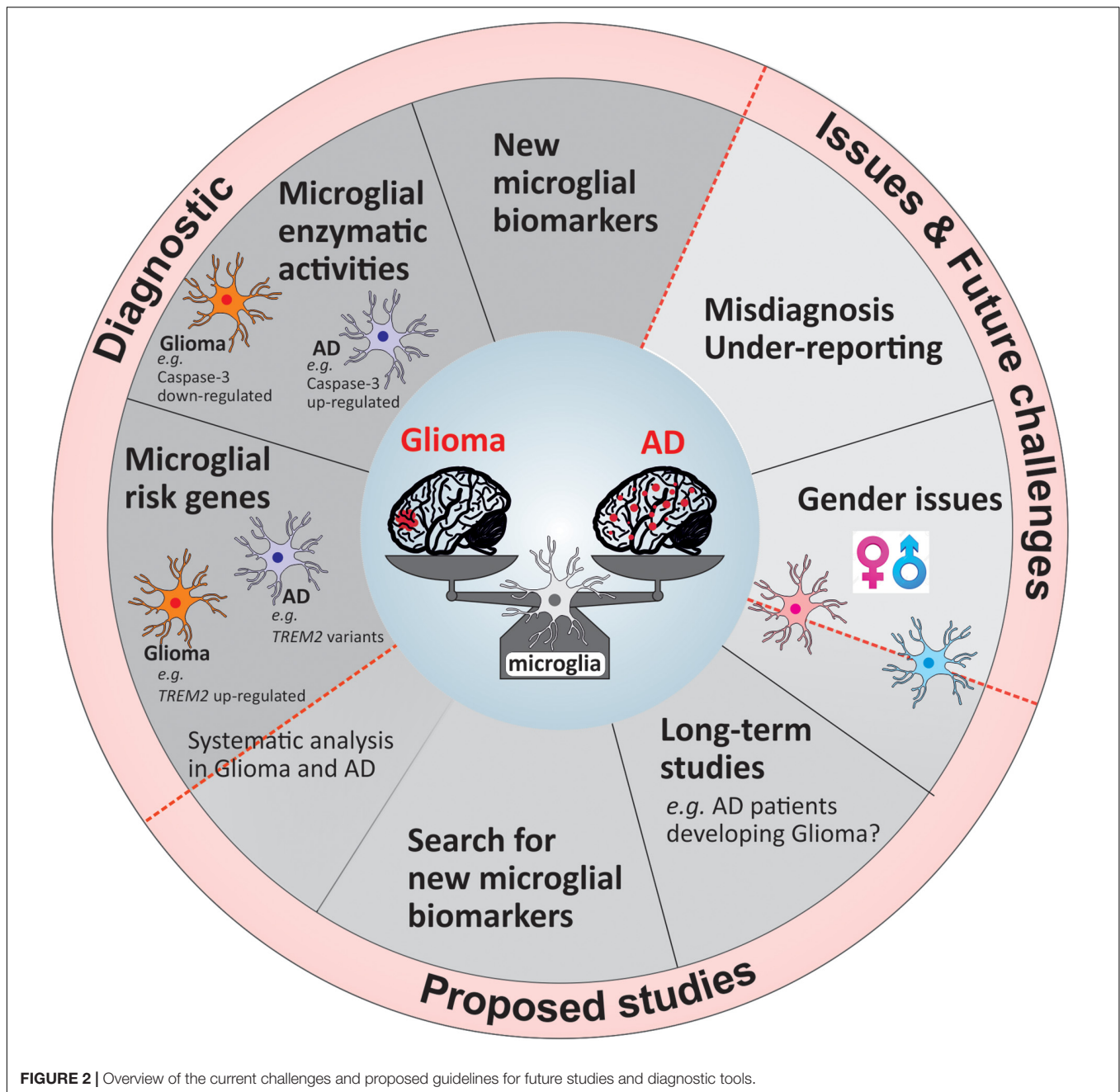


**FIGURE 2 |** Overview of the current challenges and proposed guidelines for future studies and diagnostic tools.

the patients' clinical investigation. The challenge to identify genes or proteins that could be applied in the clinical setting is due to the high percentage of studies focusing on few of many microglia-associated risk genes in AD in great detail (e.g., TREM2, APOE). Simultaneously, identified AD risk genes are not or weakly studied in a different disease setting such as glioma. Considering the remarkable inverse relationship of these pathologies it could be worth to investigate distinct risk genes greatly associated with one disease regarding their nature in the other. There is an obvious need to identify other potential microglial targets useful for diagnostics which could be done by developing a larger scale study including AD and glioma patients.

In summary, there is very little knowledge and evidence how microglia may contribute toward the fate of these two opposing pathologies. More than a decade ago, Schwartz et al. (2006) reviewed the idea whether stimulated microglia may be set for a distinct phenotype or if there is the possibility to reverse an induced functional phenotype. It was concluded that based on the type of the primary and secondary trigger, microglia are capable either to reverse or exaggerate their commitment. It is then possible to consider that once activated in a specific disease context, microglia would maintain this acquired disease phenotype (e.g., AD) and could be unable to go back to another state, excluding the apparition of another disease such as glioma.



## AUTHOR CONTRIBUTIONS

MC, VS, BJ, and KG planned and wrote the manuscript.

## FUNDING

This work has been supported by grants from the Swedish Research Council, the Swedish Cancer Foundation, the Swedish

Society, the Swedish Brain Foundation, the Åke Wibergs Foundation, and The Wenner-Gren Foundation.

## ACKNOWLEDGMENTS

We apologize to authors whose primary references could not be cited owing to space limitations.

## REFERENCES

- Alzheimer's Association (2019). 2019 Alzheimer's disease facts and figures. *Alzheimers Dement.* 15, 321–387. doi: 10.1016/j.jalz.2019.01.010
- Ayata, P., Badimon, A., Strasburger, H. J., Duff, M. K., Montgomery, S. E., Loh, Y.-H. E., et al. (2018). Epigenetic regulation of brain region-specific microglia clearance activity. *Nat. Neurosci.* 21, 1049–1060. doi: 10.1038/s41593-018-0192-3
- Behrens, M. I., Lendon, C., and Roe, C. M. (2009). A common biological mechanism in cancer and Alzheimer's disease? *Curr. Alzheimer Res.* 6, 196–204. doi: 10.2174/156720509788486608
- Bennett, M. L., Bennett, F. C., Liddel, S. A., Ajami, B., Zamanian, J. L., Fernhoff, N. B., et al. (2016). New tools for studying microglia in the mouse and human CNS. *Proc. Natl. Acad. Sci. U.S.A.* 113, 1738–1746. doi: 10.1073/pnas.1525528113
- Biber, K., Neumann, H., Inoue, K., and Boddeke, H. W. G. M. (2007). Neuronal "On" and "Off" signals control microglia. *Trends Neurosci.* 30, 596–602. doi: 10.1016/j.tins.2007.08.007
- Bisht, K., Sharma, K. P., Lecours, C., Gabriela Sánchez, M., El Hajj, H., Milior, G., et al. (2016). Dark microglia: a new phenotype predominantly associated with pathological states. *Glia* 64, 826–839. doi: 10.1002/glia.22966
- Bowman, R. L., Klemm, F., Akkari, L., Pyonteck, S. M., Sevenich, L., Quail, D. F., et al. (2016). Macrophage Ontogeny Underlies Differences in Tumor-Specific Education in Brain Malignancies. *Cell Rep.* 17, 2445–2459. doi: 10.1016/j.celrep.2016.10.052
- Boza-Serrano, A., Ruiz, R., Sanchez-Varo, R., García-Revilla, J., Yang, Y., Jimenez-Ferrer, I., et al. (2019). Galectin-3, a novel endogenous TREM2 ligand, detrimentally regulates inflammatory response in Alzheimer's disease. *Acta Neuropathol.* 138, 251–273. doi: 10.1007/s00401-019-02013-z
- Burguillos, M. A., Deierborg, T., Kavanagh, E., Persson, A., Hajji, N., Garcia-Quintanilla, A., et al. (2011). Caspase signalling controls microglia activation and neurotoxicity. *Nature* 472, 319–324. doi: 10.1038/nature09788
- Butovsky, O., Jedrychowski, M. P., Moore, C. S., Cialic, R., Lanser, A. J., Gabriely, G., et al. (2014). Identification of a unique TGF- $\beta$ -dependent molecular and functional signature in microglia. *Nat. Neurosci.* 17, 131–143. doi: 10.1038/nn.3599
- Campion, D., Dumanchin, C., Hannequin, D., Dubois, B., Belliard, S., Puel, M., et al. (1999). Early-onset autosomal dominant Alzheimer disease: prevalence, genetic heterogeneity, and mutation spectrum. *Am. J. Hum. Genet.* 65, 664–670. doi: 10.1086/302553
- Caponegro, M. D., Moffitt, R. A., and Tsirka, S. E. (2018). Expression of neuropilin-1 is linked to glioma associated microglia and macrophages and correlates with unfavorable prognosis in high grade gliomas. *Oncotarget* 9, 35655–35665. doi: 10.18632/oncotarget.26273
- Chen, Z., and Trapp, B. D. (2016). Microglia and neuroprotection. *J. Neurochem.* 136, 10–17. doi: 10.1111/jnc.13062
- Cheray, M., and Joseph, B. (2018). Epigenetics Control Microglia Plasticity. *Front. Cell. Neurosci.* 12:243. doi: 10.3389/fncel.2018.00243
- Corder, E. H., Saunders, A. M., Strittmatter, W. J., Schmechel, D. E., Gaskell, P. C., Small, G. W., et al. (1993). Gene dose of apolipoprotein E type 4 allele and the risk of Alzheimer's disease in late onset families. *Science* 261, 921–923. doi: 10.1126/science.8346443
- Correani, V., Di Francesco, L., Mignogna, G., Fabrizi, C., Leone, S., Giorgi, A., et al. (2017). Plasma membrane protein profiling in beta-amyloid-treated microglia cell line. *Proteomics* 17:1600439. doi: 10.1002/pmic.201600439
- de Haas, A. H., Boddeke, H. W., and Biber, K. (2008). Region-specific expression of immunoregulatory proteins on microglia in the healthy CNS. *Glia* 56, 888–894. doi: 10.1002/glia.20663
- De Strooper, B., and Karran, E. (2016). The cellular phase of Alzheimer's Disease. *Cell* 164, 603–615. doi: 10.1016/j.cell.2015.12.056
- DeSouky, A. L. (1992). The relationship between cancer and Alzheimer's disease. *J. Am. Geriatr. Soc.* 40:1075.
- Driver, J. A., Beiser, A., Au, R., Kreger, B. E., Splansky, G. L., Kurth, T., et al. (2012). Inverse association between cancer and Alzheimer's disease: results from the framingham heart study. *BMJ* 344:e1442. doi: 10.1136/bmj.e1442
- Ferris, S. P., Hofmann, J. W., Solomon, D. A., and Perry, A. (2017). Characterization of gliomas: from morphology to molecules. *Virchows Arch.* 471, 257–269. doi: 10.1007/s00428-017-2181-4
- Galatro, T. F., Holtman, I. R., Lerario, A. M., Vainchtein, I. D., Brouwer, N., Sola, P. R., et al. (2017). Transcriptomic analysis of purified human cortical microglia reveals age-associated changes. *Nat. Neurosci.* 20, 1162–1171. doi: 10.1038/nn.4597
- Ginhoux, F., Greter, M., Leboeuf, M., Nandi, S., See, P., Gokhan, S., et al. (2010). Fate mapping analysis reveals that adult microglia derive from primitive macrophages. *Science* 330, 841–845. doi: 10.1126/science.1194637
- Goodridge, H. S., Reyes, C. N., Becker, C. A., Katsumoto, T. R., Ma, J., Wolf, A. J., et al. (2011). Activation of the innate immune receptor Dectin-1 upon formation of a phagocytic synapse. *Nature* 472, 471–475. doi: 10.1038/nature10071
- Grabert, K., Michoel, T., Karavolos, M. H., Clohisey, S., Baillie, J. K., Stevens, M. P., et al. (2016). Microglial brain region-dependent diversity and selective regional sensitivities to aging. *Nat. Neurosci.* 19, 504–516. doi: 10.1038/nn.4222
- Guneykaya, D., Ivanov, A., Hernandez, D. P., Haage, V., Wojtas, B., Meyer, N., et al. (2018). Transcriptional and translational differences of microglia from male and female brains. *Cell Rep.* 24, 2773.e6–2783.e6. doi: 10.1016/j.celrep.2018.08.001
- Haage, V., Semtner, M., Vidal, R. O., Hernandez, D. P., Pong, W. W., Chen, Z., et al. (2019). Comprehensive gene expression meta-analysis identifies signature genes that distinguish microglia from peripheral monocytes/macrophages in health and glioma. *Acta Neuropathol. Commun.* 7:20. doi: 10.1186/s40478-019-0665-y
- Hammond, T. R., Dufort, C., Dissing-Olesen, L., Giera, S., Young, A., Wysoker, A., et al. (2019). Single-Cell RNA Sequencing of Microglia throughout the Mouse Lifespan and in the Injured Brain Reveals Complex Cell-State Changes. *Immunity* 50, 253.e6–271.e6. doi: 10.1016/j.immuni.2018.11.004
- Harold, D., Abraham, R., Hollingworth, P., Sims, R., Gerrish, A., Hamshere, M. L., et al. (2009). Genome-wide association study identifies variants at CLU and PICALM associated with Alzheimer's disease. *Nat. Genet.* 41, 1088–1093.
- Hickman, S. E., Kingery, N. D., Ohsumi, T. K., Borowsky, M. L., Wang, L., Means, T. K., et al. (2013). The microglial sensome revealed by direct RNA sequencing. *Nat. Neurosci.* 16, 1896–1905. doi: 10.1038/nn.3554
- Hollingworth, P., Harold, D., Sims, R., Gerrish, A., Lambert, J.-C., Carrasquillo, M. M., et al. (2011). Common variants at ABCA7, MS4A6A/MS4A4E, EPHA1, CD33 and CD2AP are associated with Alzheimer's disease. *Nat. Genet.* 43, 429–435. doi: 10.1038/ng.803
- Holtman, I. R., Raj, D. D., Miller, J. A., Schaafsma, W., Yin, Z., Brouwer, N., et al. (2015). Induction of a common microglia gene expression signature by aging and neurodegenerative conditions: a co-expression meta-analysis. *Acta Neuropathol. Commun.* 3:31. doi: 10.1186/s40478-015-0203-5



- Jack, C. R., and Holtzman, D. M. (2013). Biomarker modeling of Alzheimer's Disease. *Neuron* 80, 1347–1358.
- Jay, T. R., Miller, C. M., Cheng, P. J., Graham, L. C., Bemiller, S., Broihier, M. L., et al. (2015). TREM2 deficiency eliminates TREM2+ inflammatory macrophages and ameliorates pathology in Alzheimer's disease mouse models. *J. Exp. Med.* 212, 287–295. doi: 10.1084/jem.20142322
- Keren-Shaul, H., Spinrad, A., Weiner, A., Matcovitch-Natan, O., Dvir-Szternfeld, R., Ulland, T. K., et al. (2017). A unique microglia type associated with restricting development of Alzheimer's Disease. *Cell* 169, 1276–1290. doi: 10.1016/j.cell.2017.05.018
- Kierdorf, K., Erny, D., Goldmann, T., Sander, V., Schulz, C., Perdiguero, E. G., et al. (2013). Microglia emerge from erythromyeloid precursors via Pu.1- and Irf8-dependent pathways. *Nat. Neurosci.* 16:273. doi: 10.1038/nn.3318
- Komohara, Y., Ohnishi, K., Kurasu, J., and Takeya, M. (2008). Possible involvement of the M2 anti-inflammatory macrophage phenotype in growth of human gliomas. *J. Pathol.* 216, 15–24. doi: 10.1002/path.2370
- Konishi, H., and Kiyama, H. (2018). Microglial TREM2/DAP12 signaling: a double-edged sword in neural diseases. *Front. Cell. Neurosci.* 12:206. doi: 10.3389/fncel.2018.00206
- Krasemann, S., Madore, C., Cialic, R., Baufeld, C., Calcagno, N., El Fatimy, R., et al. (2018). The TREM2-APOE pathway drives the transcriptional phenotype of dysfunctional microglia in neurodegenerative diseases. *Immunity* 47, 566.e9–581.e9. doi: 10.1016/j.immuni.2017.08.008
- Kunkle, B. W., Grenier-Boley, B., Sims, R., Bis, J. C., Damotte, V., Naj, A. C., et al. (2019). Genetic meta-analysis of diagnosed Alzheimer's disease identifies new risk loci and implicates A $\beta$ , tau, immunity and lipid processing. *Nat. Genet.* 51, 414–430.
- Lafuente, J. V., Adán, B., Alkiza, K., Garibi, J. M., Rossi, M., and Cruz-Sánchez, F. F. (1999). Expression of vascular endothelial growth factor (VEGF) and platelet-derived growth factor receptor-beta (PDGFR-beta) in human gliomas. *J. Mol. Neurosci.* 13, 177–185.
- Lambert, J.-C., Heath, S., Even, G., Campion, D., Sleegers, K., Hiltunen, M., et al. (2009). Genome-wide association study identifies variants at CLU and CR1 associated with Alzheimer's disease. *Nat. Genet.* 41, 1094–1099. doi: 10.1038/ng.439
- Leeper, H. E., Caron, A. A., Decker, P. A., Jenkins, R. B., Lachance, D. H., and Giannini, C. (2015). IDH mutation, 1p19q codeletion and ATRX loss in WHO grade II gliomas. *Oncotarget* 6, 30295–30305. doi: 10.18632/oncotarget.4497
- Leu, S., von Felten, S., Frank, S., Vassella, E., Vajtai, I., Taylor, E., et al. (2013). IDH/MGMT-driven molecular classification of low-grade glioma is a strong predictor for long-term survival. *Neuro Oncol.* 15, 469–479. doi: 10.1093/neuonc/nos317
- Liu, C.-C., Kanekiyo, T., Xu, H., and Bu, G. (2013). Apolipoprotein E and Alzheimer disease: risk, mechanisms and therapy. *Nat. Rev. Neurol.* 9, 106–118. doi: 10.1038/nrneurol.2012.263
- Liu, T., Ren, D., Zhu, X., Yin, Z., Jin, G., Zhao, Z., et al. (2013). Transcriptional signaling pathways inversely regulated in Alzheimer's disease and glioblastoma multiform. *Sci. Rep.* 3:3467. doi: 10.1038/srep03467
- López-Otín, C., Blasco, M. A., Partridge, L., Serrano, M., and Kroemer, G. (2013). The hallmarks of aging. *Cell* 153, 1194–1217. doi: 10.1016/j.cell.2013.05.039
- Majd, S., Power, J., and Majd, Z. (2019). Alzheimer's disease and cancer: when two monsters cannot be together. *Front. Neurosci.* 13:155. doi: 10.3389/fnins.2019.00155
- Markovic, D. S., Vinnakota, K., Chirasani, S., Synowitz, M., Raguet, H., Stock, K., et al. (2009). Gliomas induce and exploit microglial MT1-MMP expression for tumor expansion. *Proc. Natl. Acad. Sci. U.S.A.* 106, 12530–12535. doi: 10.1073/pnas.0804273106
- Masuda, T., Sankowski, R., Staszewski, O., Böttcher, C., Amann, L., Scheiwe, C., et al. (2019). Spatial and temporal heterogeneity of mouse and human microglia at single-cell resolution. *Nature* 566, 388–392. doi: 10.1038/s41586-019-0924-x
- Matcovitch-Natan, O., Winter, D. R., Giladi, A., Vargas Aguilar, S., Spinrad, A., Sarrazin, S., et al. (2016). Microglia development follows a stepwise program to regulate brain homeostasis. *Science* 353:aad8670. doi: 10.1126/science.aad8670
- Miyauchi, J. T., Caponegro, M. D., Chen, D., Choi, M. K., Li, M., and Tsirka, S. E. (2018). Deletion of neuropilin 1 from microglia or bone marrow-derived macrophages slows glioma progression. *Cancer Res.* 78, 685–694. doi: 10.1158/0008-5472.CAN-17-1435
- Miyauchi, J. T., Chen, D., Choi, M., Nissen, J. C., Shroyer, K. R., Djordjevic, S., et al. (2016). Ablation of neuropilin 1 from glioma-associated microglia and macrophages slows tumor progression. *Oncotarget* 7, 9801–9814. doi: 10.18632/oncotarget.6877
- Musico, M., Adorni, F., Di Santo, S., Prinelli, F., Pettenati, C., Caltagirone, C., et al. (2013). Inverse occurrence of cancer and Alzheimer disease. *Neurology* 81, 322–328. doi: 10.1212/wnl.0b013e31829c5ec1
- Naj, A. C., Jun, G., Beecham, G. W., Wang, L.-S., Vardarajan, B. N., Buross, J., et al. (2011). Common variants at MS4A4/MS4A6E, CD2AP, CD33 and EPHA1 are associated with late-onset Alzheimer's disease. *Nat. Genet.* 43, 436–441. doi: 10.1038/ng.801
- Nolte, C., Kirchhoff, F., and Kettenmann, H. (1997). Epidermal growth factor is a motility factor for microglial cells in vitro: evidence for EGF receptor expression. *Eur. J. Neurosci.* 9, 1690–1698. doi: 10.1111/j.1460-9568.1997.tb01526.x
- Nudelman, K. N. H., Risacher, S. L., West, J. D., McDonald, B. C., Gao, S., and Saykin, A. J. (2014). Association of cancer history with Alzheimer's disease onset and structural brain changes. *Front. Physiol.* 5:423. doi: 10.3389/fphys.2014.00423
- Olah, M., Amor, S., Brouwer, N., Vinet, J., Eggen, B., Biber, K., et al. (2012). Identification of a microglia phenotype supportive of remyelination. *Glia* 60, 306–321. doi: 10.1002/glia.21266
- Olah, M., Patrick, E., Villani, A.-C., Xu, J., White, C. C., Ryan, K. J., et al. (2018). A transcriptomic atlas of aged human microglia. *Nat. Commun.* 9:539. doi: 10.1038/s41467-018-02926-5
- Ou, S.-M., Lee, Y.-J., Hu, Y.-W., Liu, C.-J., Chen, T.-J., Fuh, J.-L., et al. (2013). Does Alzheimer's disease protect against cancers? A nationwide population-based study. *Neuroepidemiology* 40, 42–49. doi: 10.1159/000341411
- Pyonteck, S. M., Akkari, L., Schuhmacher, A. J., Bowman, R. L., Sevenich, L., Quail, D. F., et al. (2013). CSF-1R inhibition alters macrophage polarization and blocks glioma progression. *Nat. Med.* 19, 1264–1272. doi: 10.1038/nm.3337
- Raj, D., Yin, Z., Breur, M., Doorduyn, J., Holtman, I. R., Olah, M., et al. (2017). Increased white matter inflammation in aging- and Alzheimer's disease brain. *Front. Mol. Neurosci.* 10:206.
- Reifenberger, G., Wirsching, H.-G., Knobbe-Thomsen, C. B., and Weller, M. (2016). Advances in the molecular genetics of gliomas — implications for classification and therapy. *Nat. Rev. Clin. Oncol.* 14, 434–452. doi: 10.1038/nrclinonc.2016.204
- Roe, C. M., Behrens, M. I., Xiong, C., Miller, J. P., and Morris, J. C. (2005). Alzheimer disease and cancer. *Neurology* 64, 895–898.
- Roe, C. M., Fitzpatrick, A. L., Xiong, C., Sieh, W., Kuller, L., Miller, J. P., et al. (2010). Cancer linked to Alzheimer disease but not vascular dementia. *Neurology* 74, 106–112.
- Schwartz, M., Butovsky, O., Brück, W., and Hanisch, U.-K. (2006). Microglial phenotype: is the commitment reversible? *Trends Neurosci.* 29, 68–74. doi: 10.1016/j.tins.2005.12.005
- Selkoe, D. J., and Hardy, J. (2016). The amyloid hypothesis of Alzheimer's disease at 25 years. *EMBO Mol. Med.* 8, 595–608.
- Shemer, A., Erny, D., Jung, S., and Prinz, M. (2015). Microglia plasticity during health and disease: an immunological perspective. *Trends Immunol.* 36, 614–624. doi: 10.1016/j.it.2015.08.003
- Shen, X., Burguillos, M. A., and Joseph, B. (2017). Guilt by association, caspase-3 regulates microglia polarization. *Cell Cycle* 16, 306–307. doi: 10.1080/15384101.2016.1254979
- Shen, X., Burguillos, M. A., Osman, A. M., Frijhoff, J., Carrillo-Jiménez, A., Kanatani, S., et al. (2016). Glioma-induced inhibition of caspase-3 in microglia promotes a tumor-supportive phenotype. *Nat. Immunol.* 17:1282. doi: 10.1038/ni.3545
- Shen, X., Venero, J. L., Joseph, B., and Burguillos, M. A. (2018). Caspases orchestrate microglia instrumental functions. *Prog. Neurobiol.* 171, 50–71. doi: 10.1016/j.pneurobio.2018.09.007
- Shi, Y., and Holtzman, D. M. (2018). Interplay between innate immunity and Alzheimer disease: APOE and TREM2 in the spotlight. *Nat. Rev. Immunol.* 18, 759–772. doi: 10.1038/s41577-018-0051-1
- Sielska, M., Przanowski, P., Wylot, B., Gabrusiewicz, K., Maleszewska, M., Kijewska, M., et al. (2013). Distinct roles of CSF family cytokines in macrophage infiltration and activation in glioma progression and injury response. *J. Pathol.* 230, 310–321. doi: 10.1002/path.4192

- Snyder, H. M., Ahles, T., Calderwood, S., Carrillo, M. C., Chen, H., Chang, C.-C. H., et al. (2017). Exploring the nexus of Alzheimer's disease and related dementias with cancer and cancer therapies: a convening of the Alzheimer's association & Alzheimer's drug discovery foundation. *Alzheimers Dement.* 13, 267–273. doi: 10.1016/j.jalz.2016.11.002
- Stratoulis, V., Venero, J. L., Tremblay, M. -È, and Joseph, B. (2019). Microglial subtypes: diversity within the microglial community. *EMBO J.* 38:e101997. doi: 10.15252/embj.2019101997
- Stupp, R., Mason, W. P., van den Bent, M. J., Weller, M., Fisher, B., Taphoorn, M. J. B., et al. (2005). Radiotherapy plus concomitant and adjuvant temozolomide for glioblastoma. *N. Engl. J. Med.* 352, 987–996.
- Szulzewsky, F., Pelz, A., Feng, X., Synowitz, M., Markovic, D., Langmann, T., et al. (2015). Glioma-associated microglia/macrophages display an expression profile different from M1 and M2 polarization and highly express Gpnmb and Spp1. *PLoS One* 10:e0116644. doi: 10.1371/journal.pone.0116644
- The Cancer Genome Atlas Research Network (2015). Comprehensive, integrative genomic analysis of diffuse lower-grade gliomas. *N. Engl. J. Med.* 372, 2481–2498. doi: 10.1056/NEJMoa1402121
- Tirumalasetti, F., Han, L., and Birkett, D. P. (1991). The relationship between cancer and Alzheimer's disease. *J. Am. Geriatr. Soc.* 39:840.
- Tsai, J. C., Goldman, C. K., and Gillespie, G. Y. (1995). Vascular endothelial growth factor in human glioma cell lines: induced secretion by EGF, PDGF-BB, and bFGF. *J. Neurosurg.* 82, 864–873. doi: 10.3171/jns.1995.82.5.0864
- Ulland, T. K., Song, W. M., Huang, S. C.-C., Ulrich, J. D., Sergushichev, A., Beatty, W. L., et al. (2018). TREM2 Maintains Microglial Metabolic Fitness in Alzheimer's Disease. *Cell* 170, 649.e13–663.e13. doi: 10.1016/j.cell.2017.07.023
- Venkatesh, H. S., Morishita, W., Geraghty, A. C., Silverbush, D., Gillespie, S. M., Arzt, M., et al. (2019). Electrical and synaptic integration of glioma into neural circuits. *Nature* 573, 539–545. doi: 10.1038/s41586-019-1563-y
- Verhaak, R. G. W., Hoadley, K. A., Purdom, E., Wang, V., Qi, Y., Wilkerson, M. D., et al. (2010). Integrated genomic analysis identifies clinically relevant subtypes of glioblastoma characterized by abnormalities in PDGFRA, IDH1, EGFR, and NF1. *Cancer Cell* 17, 98–110. doi: 10.1016/j.ccr.2009.12.020
- Villa, A., Gelosa, P., Castiglioni, L., Cimino, M., Rizzi, N., Pepe, G., et al. (2018). Sex-specific features of microglia from adult mice. *Cell Rep.* 23, 3501–3511. doi: 10.1016/j.celrep.2018.05.048
- Wake, H., Moorhouse, A. J., Jinno, S., Kohsaka, S., and Nabekura, J. (2009). Resting microglia directly monitor the functional state of synapses in vivo and determine the fate of ischemic terminals. *J. Neurosci.* 29, 3974–3980. doi: 10.1523/JNEUROSCI.4363-08.2009
- Wang, Q., Hu, B., Hu, X., Kim, H., Squatrito, M., Scarpacci, L., et al. (2017). Tumor Evolution of Glioma-Intrinsic Gene Expression Subtypes Associates with Immunological Changes in the Microenvironment. *Cancer Cell* 32, 42.e6–56.e6.
- Wang, X.-Q., Tao, B.-B., Li, B., Wang, X.-H., Zhang, W.-C., Wan, L., et al. (2016). Overexpression of TREM2 enhances glioma cell proliferation and invasion: a therapeutic target in human glioma. *Oncotarget* 7, 2354–2366. doi: 10.18632/oncotarget.6221
- Wang, Y., Ulland, T. K., Ulrich, J. D., Song, W., Tzaferis, J. A., Hole, J. T., et al. (2016). TREM2-mediated early microglial response limits diffusion and toxicity of amyloid plaques. *J. Exp. Med.* 213, 667–675. doi: 10.1084/jem.2015.1948
- Wang, Y., Cella, M., Mallinson, K., Ulrich, J. D., Young, K. L., Robinette, M. L., et al. (2015). TREM2 lipid sensing sustains the microglial response in an Alzheimer's disease model. *Cell* 160, 1061–1071. doi: 10.1016/j.cell.2015.01.049
- Yamada, M., Sasaki, H., Mimori, Y., Kasagi, F., Sudoh, S., Ikeda, J., et al. (1999). Prevalence and risks of dementia in the Japanese population: RERF's adult health study Hiroshima subjects. *J. Am. Geriatr. Soc.* 47, 189–195. doi: 10.1111/j.1532-5415.1999.tb04577.x
- Yeh, F. L., Wang, Y., Tom, I., Gonzalez, L. C., and Sheng, M. (2016). TREM2 binds to apolipoproteins, including APOE and CLU/APOJ, and thereby facilitates uptake of amyloid-beta by microglia. *Neuron* 91, 328–340. doi: 10.1016/j.neuron.2016.06.015
- Yuan, P., Condello, C., Keene, C. D., Wang, Y., Bird, T. D., Paul, S. M., et al. (2018). TREM2 haploinsufficiency in mice and humans impairs the microglia barrier function leading to decreased amyloid compaction and severe axonal dystrophy. *Neuron* 90, 724–739. doi: 10.1016/j.neuron.2016.05.003
- Zhang, J., Sarkar, S., Cua, R., Zhou, Y., Hader, W., and Yong, V. W. (2012). A dialog between glioma and microglia that promotes tumor invasiveness through the CCL2/CCR2/interleukin-6 axis. *Carcinogenesis* 33, 312–319. doi: 10.1093/carcin/bgr289
- Zhao, Y., Wu, X., Li, X., Jiang, L.-L., Gui, X., Liu, Y., et al. (2018). TREM2 Is a receptor for  $\beta$ -amyloid that mediates microglial function. *Neuron* 97, 1023.e7–1031.e7. doi: 10.1016/j.neuron.2018.01.031
- Zhou, Y., Ulland, T. K., and Colonna, M. (2018). TREM2-Dependent Effects on Microglia in Alzheimer's Disease. *Front. Aging Neurosci.* 10:202. doi: 10.3389/fnagi.2018.00202

**Conflict of Interest:** The authors declare that the research was conducted in the absence of any commercial or financial relationships that could be construed as a potential conflict of interest.

Copyright © 2019 Cheray, Stratoulis, Joseph and Grabert. This is an open-access article distributed under the terms of the Creative Commons Attribution License (CC BY). The use, distribution or reproduction in other forums is permitted, provided the original author(s) and the copyright owner(s) are credited and that the original publication in this journal is cited, in accordance with accepted academic practice. No use, distribution or reproduction is permitted which does not comply with these terms.



# Increased Inflammation and Unchanged Density of Synaptic Vesicle Glycoprotein 2A (SV2A) in the Postmortem Frontal Cortex of Alzheimer's Disease Patients

Athanasios Metaxas<sup>1\*</sup>, Camilla Thygesen<sup>1</sup>, Sanne R. R. Briting<sup>1</sup>, Anne M. Landau<sup>2,3</sup>, Sultan Darvesh<sup>4,5</sup> and Bente Finsen<sup>1</sup>

<sup>1</sup> Department of Neurobiology Research, Institute of Molecular Medicine, University of Southern Denmark, Odense, Denmark, <sup>2</sup> Translational Neuropsychiatry Unit, Aarhus University, Aarhus, Denmark, <sup>3</sup> Department of Nuclear Medicine and PET-Center, Aarhus University, Aarhus, Denmark, <sup>4</sup> Department of Medical Neuroscience, Dalhousie University, Halifax, NS, Canada, <sup>5</sup> Department of Medicine, Neurology, and Geriatric Medicine, Dalhousie University, Halifax, NS, Canada

## OPEN ACCESS

### Edited by:

Victoria Campos-Peña,  
National Institute of Neurology  
and Neurosurgery (INNN), Mexico

### Reviewed by:

Rodrigo A. Cunha,  
University of Coimbra, Portugal  
Alberto Serrano-Pozo,  
Harvard Medical School,  
United States

### \*Correspondence:

Athanasios Metaxas  
ametaxas@health.sdu.dk

### Specialty section:

This article was submitted to  
Cellular Neuropathology,  
a section of the journal  
Frontiers in Cellular Neuroscience

**Received:** 27 September 2019

**Accepted:** 20 November 2019

**Published:** 05 December 2019

### Citation:

Metaxas A, Thygesen C, Briting SRR, Landau AM, Darvesh S and Finsen B (2019) Increased Inflammation and Unchanged Density of Synaptic Vesicle Glycoprotein 2A (SV2A) in the Postmortem Frontal Cortex of Alzheimer's Disease Patients.  
*Front. Cell. Neurosci.* 13:538.  
doi: 10.3389/fncel.2019.00538

Sections from the middle frontal gyrus (Brodmann area 46) of autopsy-confirmed Alzheimer's disease (AD) patients and non-demented subjects were examined for the prevalence of hallmark AD pathology, including amyloid- $\beta$  (A $\beta$ ) plaques, phosphorylated tau (pTau) tangles, neuroinflammation and synaptic loss ( $n = 7$  subjects/group). Dense-core deposits of A $\beta$  were present in all AD patients (7/7) and some non-demented subjects (3/7), as evidenced by 6E10 immunohistochemistry. Levels of A $\beta$  immunoreactivity were higher in AD vs. non-AD cases. For pTau, AT8-positive neurofibrillary tangles and threads were exclusively observed in AD patient tissue. Levels of [<sup>3</sup>H]PK11195 binding to the translocator protein (TSPO), a marker of inflammatory processes, were elevated in the gray matter of AD patients compared to non-demented subjects. Levels of [<sup>3</sup>H]UCB-J binding to synaptic vesicle glycoprotein 2A (SV2A), a marker of synaptic density, were not different between groups. In AD patients, pTau immunoreactivity was positively correlated with [<sup>3</sup>H]PK11195, and negatively correlated with [<sup>3</sup>H]UCB-J binding levels. No correlation was observed between A $\beta$  immunoreactivity and markers of neuroinflammation or synaptic density. These data demonstrate a close interplay between tau pathology, inflammation and SV2A density in AD, and provide useful information on the ability of neuroimaging biomarkers to diagnose AD dementia.

**Keywords:** neuroinflammation, translocator protein, [<sup>3</sup>H]PK11195, synapses, synaptic vesicle glycoprotein 2A, [<sup>3</sup>H]UCB-J, amyloid, tau

## INTRODUCTION

Despite considerable advances in biological fluid and brain imaging biomarkers, autopsy remains the most reliable means of obtaining a definitive diagnosis of dementia due to Alzheimer's disease (AD). The diagnosis is based on the microscopic identification of hallmark AD pathology in the brain, most notably the deposition of amyloid-beta (A $\beta$ ) peptides into plaques, the accumulation of

hyperphosphorylated tau (pTau) protein into neurofibrillary tangles and neurodegeneration (Jack et al., 2018). In addition, a brain-specific form of low-grade, chronic inflammation is known to accompany the progression of AD (Heneka et al., 2015).

It is now recognized that symptomatic AD is preceded by a long preclinical phase, which is characterized by the insidious accumulation of AD neuropathologic lesions. Biomarker studies in subjects with normal cognition indicate that the accumulation of A $\beta$  may precede the onset of memory decline by at least a decade (Jansen et al., 2018). Moreover, autopsy studies demonstrate that aggregated A $\beta$  and pTau can be detected in certain brain areas of cognitively intact individuals by the third to fourth decades of life (Braak and Braak, 1997; Braak et al., 2011). As the pathognomonic lesions of AD are present in a significant proportion of individuals with normal cognition, dissociating AD from physiological brain aging represents a major challenge in the dementia research field. Of note, the assumption that A $\beta$  and pTau biomarker-positive subjects are on a path to developing dementia remains a point of contention (Nelson et al., 2011; Franceschi et al., 2018).

In the present study, markers of neuroinflammation and synaptic density were evaluated for their ability to distinguish between autopsy-confirmed AD patients and non-AD subjects. Levels of the translocator protein (TSPO) and synaptic vesicle glycoprotein 2A (SV2A) were measured by autoradiography in sections from the middle frontal gyrus (Brodmann area 46) of AD patients and non-demented subjects. The middle frontal gyrus was chosen for examination based on its susceptibility to both age- and AD-related atrophy (Bakkour et al., 2013),

and because of its enhanced vulnerability to A $\beta$  deposition in both cognitively impaired and healthy individuals (Rodrigue et al., 2009). Our results show that there is increased inflammation in Brodmann area 46 in AD, while SV2A levels remain unchanged. These data provide useful insights into the molecular neuropathology of AD and can inform the debate over the ability of imaging biomarkers to confirm a clinical AD diagnosis.

## MATERIALS AND METHODS

### Ethics Statement

The study was carried out in accordance with the recommendations of the Danish Biomedical Research Ethical Committee for the Region of Southern Denmark (Project Id. S-20160036) and the Nova Scotia Health Authority Research Ethics Board in Halifax, NS, Canada. Written, informed consent forms were obtained for all subjects, in accordance with the Declaration of Helsinki. Samples were transported to the University of Southern Denmark from the Maritime Brain Tissue Bank, Department of Medical Neuroscience, Faculty of Medicine, Dalhousie University, Halifax, Canada.

### Subjects and Tissue Sectioning

Snap-frozen samples from the middle frontal gyrus of autopsy-confirmed AD patients and non-demented subjects were used ( $n = 7/\text{group}$ ; **Table 1**). The groups were matched for sex (3 females, 4 males) and age (median: AD = 79 years, range:

**TABLE 1** | Subject characteristics.

No	Age range (years)	Brain weight (g)	PMI (h)	CERAD	Braak	Cause of death	Co-morbidities	Study group
1	61–65	1100	24	Frequent (C3)	VI	N/A	N/A	AD
2	76–80	1250	9.5	Moderate (C2)	VI	Pneumonia, Dehydration	Type-2 diabetes, HTN	AD
3	81–85	950	9	Frequent (C3)	V	Inanition	None	AD
4	91–95	1149	64	Frequent (C3)	VI	N/A	None	AD
5	76–80	1200	9	Frequent (C3)	IV	N/A	Emphysema, hyperthyroidism	AD
6	71–75	1151	6.5	Frequent (C3)	VI	Sepsis	Cardiovascular (atherosclerosis)	AD
7	81–85	1293	17.5	Moderate-Frequent (C2-3)	V	N/A	Giant cell arteritis	AD
8	46–50	1275	N/A	None (C0)	0	N/A	None	Non-AD
9	81–85	1210	5.5	Sparse (C1)	0	Surgery complications	Type-2 diabetes, HTN, cardiovascular (atrial fibrillation)	Non-AD
10	81–85	1235	N/A	Moderate (C2)	II	Cancer (breast)	None	Non-AD
11	71–75	1350	36	Sparse (C1)	0	Pancreatitis	None	Non-AD
12	86–90	1300	24	Sparse (C1)	0	Cancer (abdominal)	None	Non-AD
13	46–50	1410	N/A	None (C0)	0	Myocardial infarction	Type-1 diabetes, HTN	Non-AD
14	71–75	1451	68.5	Sparse-moderate (C1-2)	I–II	Pulmonary embolism	None	Non-AD

PMI, post-mortem interval; N/A, information not available; HTN, hypertension.



64–92; non-AD = 73 years, range: 47–86;  $U = 19.5$ ,  $P = 0.56$ ). Brain weight at time of removal was lower for AD, compared to non-demented subjects (median: AD = 1151 g, range: 950–1293; non-AD = 1300 g, range: 1210–1451;  $U = 5.0$ ,  $P = 0.01$ ). Histopathological examination of the brain was performed for all subjects.

Consecutive, 20  $\mu\text{m}$ -thick sections were collected at  $-20^\circ\text{C}$  using a Leica CM3050S cryostat (Leica Biosystems). The sections were mounted onto Superfrost<sup>TM</sup> Plus slides and kept at  $-80^\circ\text{C}$  until use.

## A $\beta$ and pTau Immunohistochemistry

Frozen sections were fixed in 4% paraformaldehyde overnight and processed for A $\beta$  and pTau immunohistochemistry using standard protocols (Metaxas et al., 2018). Biotinylated mouse primary antibodies against human A $\beta$  (clone 6E10, 2  $\mu\text{g}/\text{mL}$ ; 803008, BioLegend<sup>®</sup>) and pTau (clone AT8, 0.2  $\mu\text{g}/\text{mL}$ ; MN1020B, Thermo Fisher Scientific) were diluted in Tris-buffered saline (TBS; pH 7.4), containing 10% fetal bovine serum. Sections were incubated with primary antibodies at  $-4^\circ\text{C}$  overnight, followed by washing and incubation for 2 h at room temperature with HRP-Streptavidin (1:200; RPN1231V, GE Healthcare). The slides were developed in TBS (pH 7.4), containing 3,3'-diaminobenzidine (DAB; 0.05%) and  $\text{H}_2\text{O}_2$  (0.01%). Biotin-labeled mouse IgG1 (MG115, Thermo Fisher Scientific), diluted to the same concentration as the primary antibodies, was used for isotype control. The sections were dehydrated in ascending concentration of ethanol, cleared in xylene and cover-slipped with PERTEX<sup>®</sup> (Histolab Products AB). Digital images were obtained under the 4x objective of an Olympus DP80 Dual Monochrome CCD camera, mounted on a motorized BX63 Olympus microscope. For analysis, the images were converted to 8-bit and manually thresholded in ImageJ (version 1.51; National Institutes of Health, MD, United States). The particle analysis plugin was used to measure the percentage of immunoreactive area relative to total image area (% area fraction).

## TSPO and SV2A Autoradiography

Sections were thawed to room temperature and prewashed in 50 mM Tris-HCl buffer (pH 7.4), containing 150 mM NaCl, 5 mM KCl, 1.5 mM  $\text{MgCl}_2$ , and 1.5 mM  $\text{CaCl}_2$  (assay buffer;  $2 \times 10$  min). For TSPO, the sections were incubated for 2 h in assay buffer, containing 3 nM [ $^3\text{H}$ ]PK11195 (specific activity 82.7 Ci/mmol; NET885, PerkinElmer). To determine non-specific binding (NSB), adjacent sections were incubated with 3 nM [ $^3\text{H}$ ]PK11195 in the presence of 10  $\mu\text{M}$  unlabeled PK11195 (C0424; Sigma-Aldrich). Incubations were terminated by three 1-min washes into ice-cold 50 mM Tris-HCl buffer (pH 7.4), followed by a rapid rinse in ice-cold deionized  $\text{H}_2\text{O}$  ( $\text{dH}_2\text{O}$ ). The sections were rapidly dried and laid down to Carestream<sup>®</sup> Kodak<sup>®</sup> BioMax MR film for 4 weeks. To allow quantification,  $^3\text{H}$  microscales of known radioactive concentration were also exposed to film (American Radiolabeled Chemicals, Inc). The films were developed with KODAK substitute D-19 developer (TED PELLA, Inc), washed in  $\text{dH}_2\text{O}$ , and fixed in Carestream<sup>®</sup> autoradiography GBX fixer. Images were digitized using a white

sample tray and the Coomassie Blue settings on a ChemiDoc<sup>TM</sup> MP imaging system (BIO-RAD). Values of specific binding were derived after subtraction of non-specific from total binding images, using ImageJ software.

For SV2A, sections were incubated for 2 h in assay buffer, containing 1 nM [ $^3\text{H}$ ]UCB-J (specific activity 82.0 Ci/mmol; NT1099, NOVANDI Chemistry AB). NSB was determined in the presence of 500  $\mu\text{M}$  Levetiracetam (TOCRIS). The films were developed after 5 weeks of exposure using a PROTEC OPTIMAX 2010 automatic film processor. All remaining procedures were as described for TSPO autoradiography.

## Statistical Analysis

Data were analyzed with GraphPad Prism (v. 8.2.0; GraphPad Software), using non-parametric statistics. Age, brain weight, 6E10- and AT8-positive area fractions, [ $^3\text{H}$ ]UCB-J and [ $^3\text{H}$ ]PK11195 binding levels, were compared between AD and non-AD subjects by unpaired, two-tailed Mann-Whitney  $U$  tests. Spearman's correlation was used to examine the association between radioligand binding levels and 6E10- or AT8-positive area fractions in the gray matter of AD patients. In all cases, the significance level was set at 5%. Results are presented as the median and interquartile range of  $n = 7$  subjects/group.

## RESULTS

### Prevalence of A $\beta$ and pTau Pathology

Representative photomicrographs of A $\beta$  and pTau immunostainings are shown in **Figure 1**. Dense-core plaques were present in all AD cases and in 3 out of 7 non-demented individuals (No. 10, 12, 14; **Figure 1A**). Variable levels of diffuse, ill-contoured deposits were present in all subjects. There was no association between age at death and 6E10 immunoreactivity (Spearman  $r = -0.07$ ,  $P = 0.82$ ). The 6E10-positive area fraction was higher in AD patients compared to non-AD subjects ( $U = 7.0$ ,  $P < 0.05$ ). For pTau, AT8-immunoreactive tangles and threads were exclusively observed in material from AD patients ( $U = 6.5$ ,  $P < 0.05$ ; **Figure 1B**). There was no significant association between age at death and the percent area occupied by AT8 immunoreactivity (Spearman  $r = -0.57$ ,  $P = 0.20$ ).

### Increased [ $^3\text{H}$ ]PK11195 Binding Levels in AD

Representative autoradiograms of [ $^3\text{H}$ ]PK11195 binding sites are shown in **Figure 2A**. Specific binding amounted to 63% of total binding levels and was primarily observed in the gray matter. There were increased [ $^3\text{H}$ ]PK11195 binding levels in the gray matter of AD patients compared to non-demented subjects ( $U = 5.0$ ,  $P = 0.01$ ; **Figure 2B**). No between-group differences were observed in the white matter ( $U = 19.0$ ,  $P = 0.52$ ). In the gray matter, [ $^3\text{H}$ ]PK11195 binding density was positively correlated with AT8 immunoreactivity (Spearman  $r = 0.89$ ;  $P = 0.01$ ; **Figure 2C**). There was no correlation between levels of [ $^3\text{H}$ ]PK11195 binding and the A $\beta$ -immunoreactive area fraction (Spearman  $r = -0.28$ ;  $P = 0.33$ ).

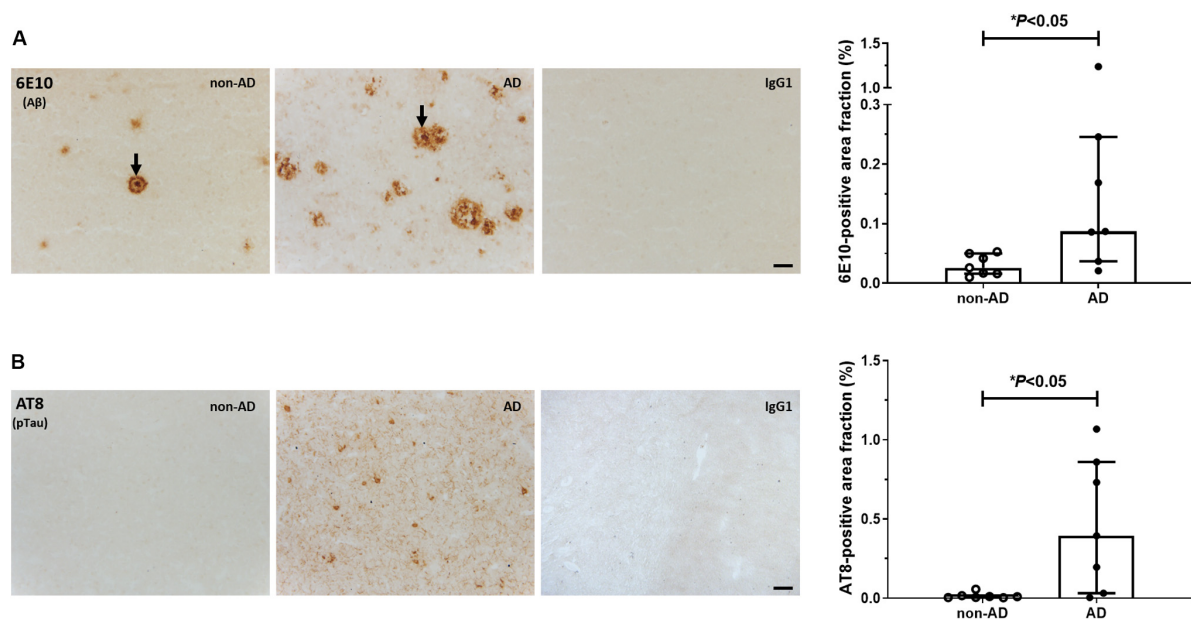


**FIGURE 1 |** Immunohistochemical analysis of Aβ and pTau. Representative photomicrographs and quantification of 6E10-positive Aβ plaques (**A**) and AT8-positive pTau lesions (**B**) in the middle frontal gyrus of non-demented subjects and AD patients. Arrows in (**A**) point to dense-core plaques. No signal was observed in the IgG1 isotype controls. Levels of Aβ and pTau immunoreactivity were higher in AD vs. non-AD subjects (\* $P < 0.05$ , Mann-Whitney  $U$  tests, two-tailed). Results are presented as the median and interquartile range of  $n = 7$  subjects/group. Scale bars: 50  $\mu\text{m}$ .

## Unaltered [ $^3\text{H}$ ]UCB-J Binding Levels in AD

Representative autoradiograms of [ $^3\text{H}$ ]UCB-J binding sites are shown in **Figure 3A**. Specific binding amounted to 81% of total binding levels and was exclusively observed in the gray matter. There were no differences in [ $^3\text{H}$ ]UCB-J binding levels between AD and non-demented subjects ( $U = 23.0$ ,  $P = 0.87$ ; **Figure 3B**). In AD patients, [ $^3\text{H}$ ]UCB-J binding density was negatively correlated with both AT8 immunoreactivity (Spearman  $r = -0.89$ ;  $P = 0.01$ ; **Figure 3C**) and [ $^3\text{H}$ ]PK11195 binding levels (Spearman  $r = -0.78$ ;  $P < 0.05$ ; **Figure 3D**). No correlation was observed between [ $^3\text{H}$ ]UCB-J binding and the Aβ-immunoreactive area fraction (Spearman  $r = -0.00$ ;  $P = 0.99$ ).

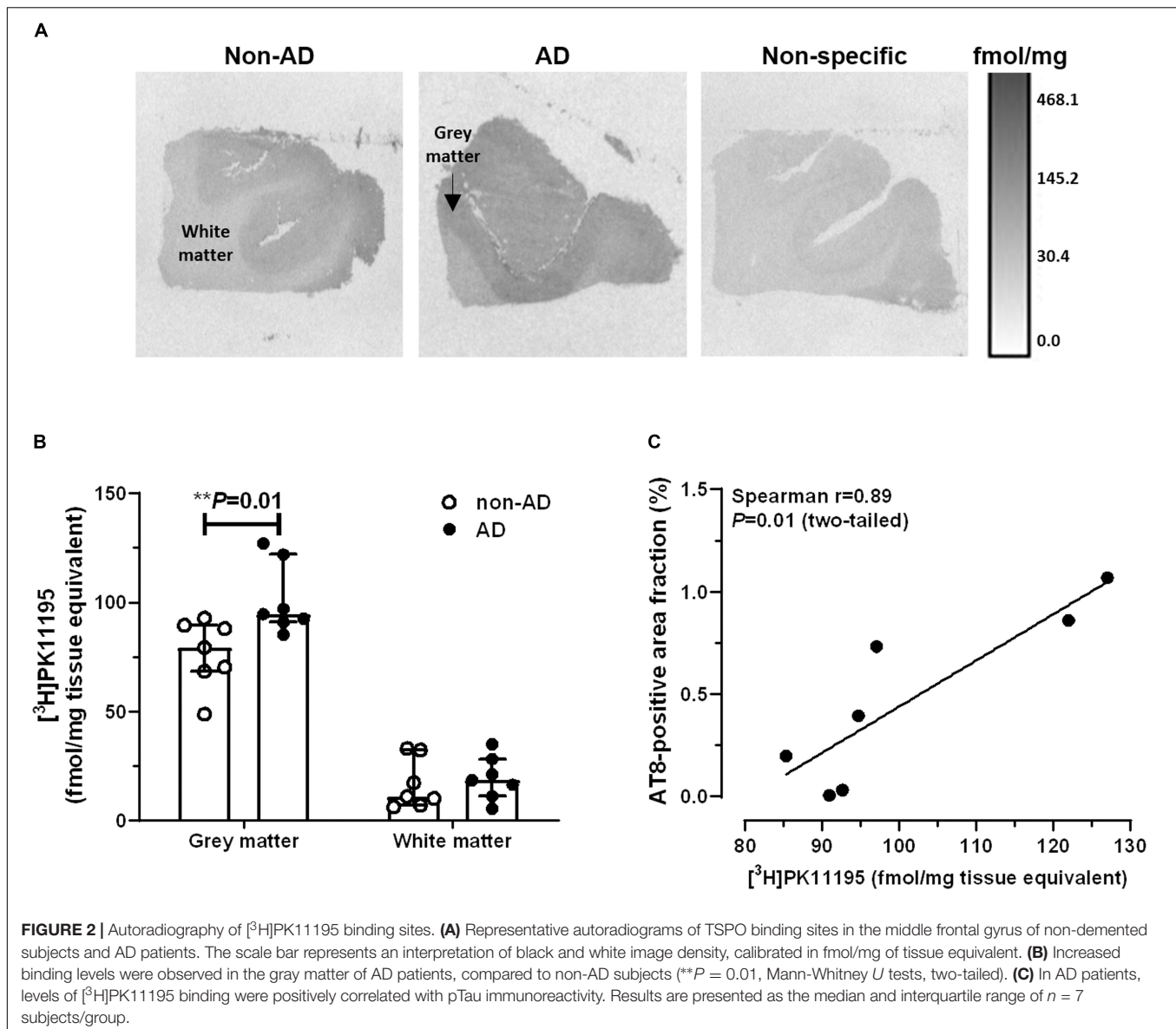
## DISCUSSION

We have compared levels of the presynaptic marker [ $^3\text{H}$ ]UCB-J and the inflammation marker [ $^3\text{H}$ ]PK11195 between autopsy-confirmed AD patients and non-demented subjects in the middle frontal gyrus, a region that is vulnerable to Aβ deposition and atrophy in cognitively intact individuals (Oh et al., 2011; Fjell et al., 2014). While binding levels of [ $^3\text{H}$ ]UCB-J correlated with pTau load and [ $^3\text{H}$ ]PK11195 in AD patients, there was no difference in SV2A density between groups. In addition to Aβ and pTau, increased levels of the inflammatory marker TSPO were observed in AD patients vs. non-AD subjects.

Biomarker studies highlight the early involvement of amyloid in the pathologic changes of AD. In longitudinal investigations

(Sutphen et al., 2015), the concentration of soluble Aβ42 is decreased in the cerebrospinal fluid (CSF) of cognitively intact subjects, starting in the early middle-age (45–54 years). The reduction is associated with the aggregation and subsequent deposition of Aβ42 into cerebral plaques (Vlassenko et al., 2016). Positron emission tomography (PET) studies show that up to 35% of elderly individuals with normal scores in cognitive tests have fibrillar Aβ plaques in the brain (Villemagne et al., 2018). Thus, amyloid positivity is not only required for a definitive diagnosis of AD, but is also important for identifying asymptomatic individuals with neuropathologic evidence of AD (Jack et al., 2018). In our small cohort of non-demented cases, dense-core plaques were observed in 3 out of 7 subjects, a proportion that is within the range of amyloid positivity reported by PET studies. Diffuse Aβ deposits, however, were detected in all cases, irrespective of dementia state. Although the pathological (Abner et al., 2018) and practical (Ikonovic et al., 2018) significance of diffuse Aβ is being investigated, these observations imply that the prevalence of amyloid positivity among people without dementia may be higher than what is currently being detected by imaging biomarkers. Similarly, tau imaging agents are unlikely to detect AT8-positive pretangle material, which is present in all individuals by the 5th decade of life, primarily in subcortical regions (Braak et al., 2011). Determining how these pervasive neuropathologic changes culminate to dementia in the AD continuum will require longitudinal studies and the earliest detection of disease-relevant biomarkers.

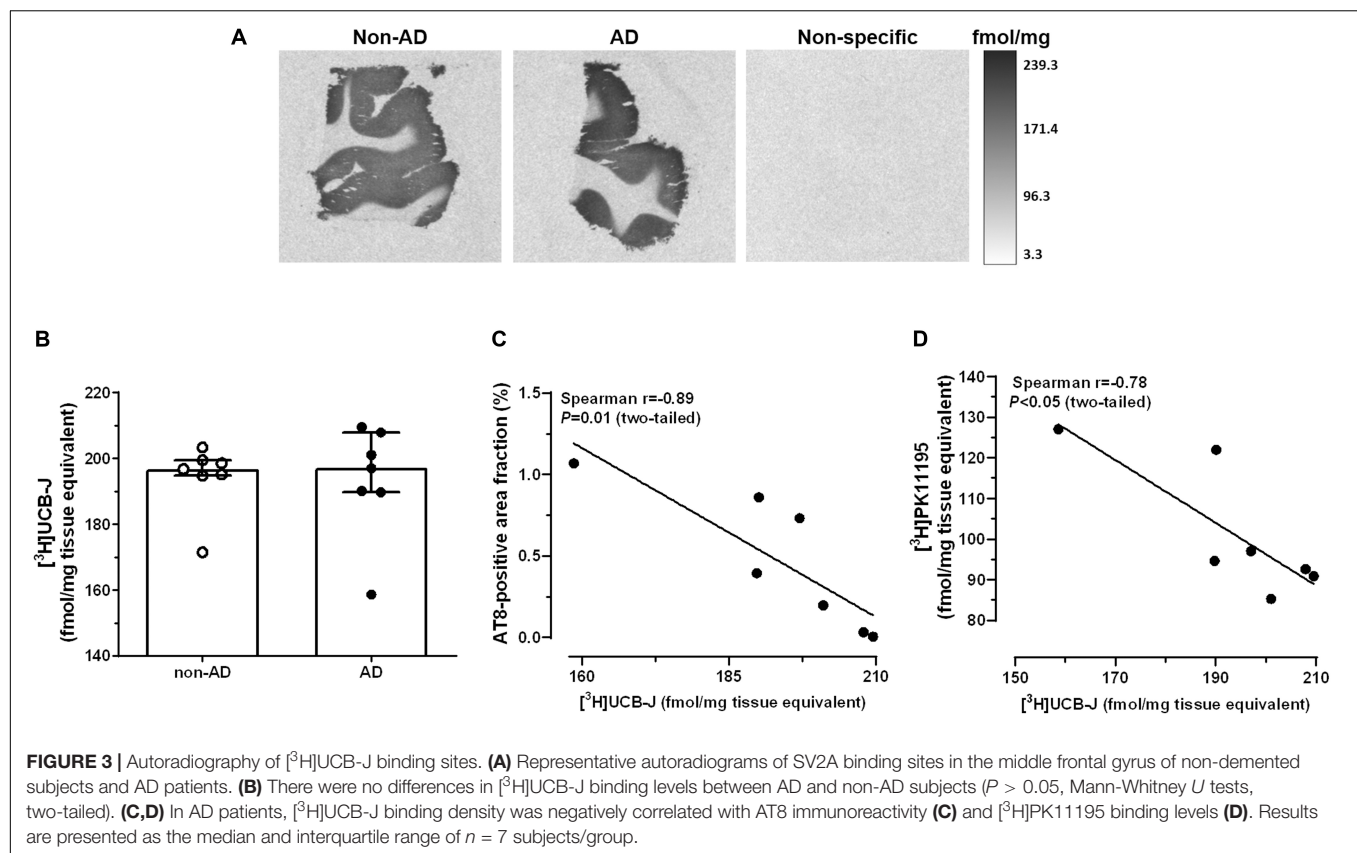
Levels of TSPO are low in the neuropil under physiological conditions, but increase in response to acute or chronic injury, rendering TSPO a key biomarker of inflammatory processes



in the brain. Although not a universal finding (Xu et al., 2019), most autoradiography studies indicate that the binding of [ $^3\text{H}$ ]PK11195 is elevated in the postmortem frontal cortex of AD patients compared to non-AD subjects (Diorio et al., 1991; Venet et al., 2009). Increased uptake of [ $^{11}\text{C}$ ]PK11195 in the AD brain has been also reported by several imaging studies (reviewed in Edison et al., 2018). The increased TSPO signal may reflect both pro- and anti-inflammatory processes, depending on age (Schuitemaker et al., 2012), AD stage (Fan et al., 2017) and the dynamic roles that TSPO-expressing glia play in the course of disease (Guilarte, 2019). In the present study, [ $^3\text{H}$ ]PK11195 binding levels were associated with increased pTau load and reduced SV2A density in the AD group, indicating that the elevated TSPO signal is likely representative of a pro-inflammatory environment. Our observations are in line with studies showing that microgliosis and astrocytosis correlate

positively with the burden of neurofibrillary tangles in the AD brain (Serrano-Pozo et al., 2011). They are further consistent with longitudinal PET studies, showing that TSPO levels correlate positively with tau aggregation (Dani et al., 2018), and negatively with synaptic function in AD (Fan et al., 2015). These findings imply that reducing inflammation could play a beneficial role in attenuating tau pathology and synaptic dysfunction in AD. It should be mentioned that a positive correlation between TSPO and pTau immunoreactivity was not observed in the postmortem temporal cortex of AD patients (Gui et al., 2019), suggesting that the interplay between inflammation and tau pathology may occur in a region-specific manner.

In agreement with results from SV2A imaging studies in AD patients (Chen et al., 2018) and models of AD (Toyonaga et al., 2019), we observed no differences in the neocortical binding levels of [ $^3\text{H}$ ]UCB-J between AD and non-AD subjects. As AD



is a neurodegenerative disorder, several mechanisms have been put forward to explain the apparent preservation of neocortical presynaptic elements in [<sup>11</sup>C]UCB-J PET studies. These include compensatory mechanisms, which can maintain the numbers of synaptic vesicles in the frontal cortex of AD patients (Scheff and Price, 2006), as well as mechanisms that may obscure the extent of SV2A loss in the plaque-rich AD neocortex (Snow et al., 1996). In addition, while SV2A is equally expressed by excitatory and inhibitory synapses (Gronborg et al., 2010), evidence suggests that there is preferential loss of glutamatergic rather than GABAergic nerve terminals in AD (Kirvell et al., 2006; Govindpani et al., 2017). This asymmetric loss may reduce the ability of [<sup>11</sup>C]UCB-J to detect decreases in SV2A density. Of note, SV2A-targeting drugs have been shown to preferentially disrupt GABAergic neurotransmission in epilepsy studies (Ohno and Tokudome, 2017). Additional explanations for the unchanged levels of SV2A density in this study include the presence of SV2A protein in mitochondria (Stockburger et al., 2016), which may mask reductions in SV2A levels in synaptic vesicles, and the fact that not all presynaptic proteins are equally reduced in AD (Poirel et al., 2018). For example, “general” markers of the presynaptic compartment, such as synaptophysin, are relatively spared compared to neurotransmitter-specific markers, even at the late AD stages. Moreover, synapses in Brodmann area 46 are known to be particularly susceptible to the effects of aging. Electron microscopy studies indicate that aging reduces the density of synapses in the primate

prefrontal cortex by at least 30% (Morrison and Baxter, 2012). This extensive physiological reduction may explain why meta-analysis reveals limited decrease of synapse numbers in the postmortem frontal cortex of AD patients compared to age-matched, non-AD subjects (de Wilde et al., 2016). Despite comparable [<sup>3</sup>H]UCB-J binding levels between AD and non-AD cases in our study, the observation that SV2A density was inversely correlated with increases in tau phosphorylation and neuroinflammation, indicates that SV2A levels are regulated by AD-associated processes.

## CONCLUSION

In conclusion, we have examined markers of neuroinflammation and synapses in the middle frontal gyrus of autopsy-confirmed AD patients and non-demented subjects. Our small exploratory study provides evidence of tight associations between inflammation levels, tau pathology, and SV2A density in AD. Studies with larger sample sizes, including more brain regions, are warranted.

## DATA AVAILABILITY STATEMENT

The raw data supporting the conclusions of this article will be made available by the authors, without undue reservation, to any qualified researcher.



## ETHICS STATEMENT

The study was carried out in accordance with the recommendations of the Danish Biomedical Research Ethical Committee for the Region of Southern Denmark (Project Id. S-20160036) and the Nova Scotia Health Authority Research Ethics Board in Halifax, NS, Canada. Written, informed consent forms were obtained for all subjects, in accordance with the Declaration of Helsinki. Samples were transported to the University of Southern Denmark from the Maritime Brain Tissue Bank, Department of Medical Neuroscience, Faculty of Medicine, Dalhousie University, Halifax, Canada.

## AUTHOR CONTRIBUTIONS

AM wrote the manuscript and performed the SV2A autoradiography and data analysis. CT performed the immunohistochemistry experiments. SB performed the tissue

sectioning and TSPO autoradiography. AL and SD provided the reagents and tissue. BF supervised the project. All authors made substantial contributions to study design, participated in drafting and critically reviewing the manuscript, and approved its final version.

## FUNDING

This study was supported by the University of Southern Denmark (SDU2020; CoPING AD: Collaborative Project on the Interaction between Neurons and Glia in AD).

## ACKNOWLEDGMENTS

We thank Andrew Reid, senior technician and manager of the Maritime Brain Tissue Bank, for organizing the transportation of human tissue.

## REFERENCES

- Abner, E. L., Neltner, J. H., Jicha, G. A., Patel, E., Anderson, S. L., Wilcock, D. M., et al. (2018). Diffuse amyloid-beta plaques, neurofibrillary tangles, and the impact of apoe in elderly persons' brains lacking neuritic amyloid plaques. *J. Alzheimers Dis.* 64, 1307–1324. doi: 10.3233/JAD-180514
- Bakkour, A., Morris, J. C., Wolk, D. A., and Dickerson, B. C. (2013). The effects of aging and Alzheimer's disease on cerebral cortical anatomy: specificity and differential relationships with cognition. *Neuroimage* 76, 332–344. doi: 10.1016/j.neuroimage.2013.02.059
- Braak, H., and Braak, E. (1997). Frequency of stages of Alzheimer-related lesions in different age categories. *Neurobiol. Aging* 18, 351–357. doi: 10.1016/s0197-4580(97)00056-0
- Braak, H., Thal, D. R., Ghebremedhin, E., and Del Tredici, K. (2011). Stages of the pathologic process in Alzheimer disease: age categories from 1 to 100 years. *J. Neuropathol. Exp. Neurol.* 70, 960–969. doi: 10.1097/NEN.0b013e318232a379
- Chen, M. K., Mecca, A. P., Naganawa, M., Finnema, S. J., Toyonaga, T., Lin, S. F., et al. (2018). Assessing synaptic density in alzheimer disease with synaptic vesicle glycoprotein 2a positron emission tomographic imaging. *JAMA Neurol.* 75, 1215–1224. doi: 10.1001/jamaneurol.2018.1836
- Dani, M., Wood, M., Mizoguchi, R., Fan, Z., Walker, Z., Morgan, R., et al. (2018). Microglial activation correlates in vivo with both tau and amyloid in Alzheimer's disease. *Brain* 141, 2740–2754. doi: 10.1093/brain/awy188
- de Wilde, M. C., Overk, C. R., Sijben, J. W., and Masliah, E. (2016). Meta-analysis of synaptic pathology in Alzheimer's disease reveals selective molecular vesicular machinery vulnerability. *Alzheimers Dement.* 12, 633–644. doi: 10.1016/j.jalz.2015.12.005
- Diorio, D., Welner, S. A., Butterworth, R. F., Meaney, M. J., and Suranyi-Cadotte, B. E. (1991). Peripheral benzodiazepine binding sites in alzheimer's disease frontal and temporal cortex. *Neurobiol. Aging* 12, 255–258. doi: 10.1016/0197-4580(91)90106-t
- Edison, P., Donat, C. K., and Sastre, M. (2018). In vivo imaging of glial activation in alzheimer's disease. *Front. Neurol.* 9:625. doi: 10.3389/fneur.2018.00625
- Fan, Z., Brooks, D. J., Okello, A., and Edison, P. (2017). An early and late peak in microglial activation in Alzheimer's disease trajectory. *Brain* 140, 792–803. doi: 10.1093/brain/aww349
- Fan, Z., Okello, A. A., Brooks, D. J., and Edison, P. (2015). Longitudinal influence of microglial activation and amyloid on neuronal function in Alzheimer's disease. *Brain* 138, 3685–3698. doi: 10.1093/brain/awv288
- Fjell, A. M., McEvoy, L., Holland, D., Dale, A. M., Walhovd, K. B., Alzheimer's Disease, et al. (2014). What is normal in normal aging? effects of aging, amyloid and alzheimer's disease on the cerebral cortex and the hippocampus. *Prog. Neurobiol.* 117, 20–40. doi: 10.1016/j.pneurobio.2014.02.004
- Franceschi, C., Garagnani, P., Morsiani, C., Conte, M., Santoro, A., Grignolio, A., et al. (2018). The continuum of aging and age-related diseases: common mechanisms but different rates. *Front. Med.* 5:61. doi: 10.3389/fmed.2018.00061
- Govindpani, K., Calvo-Flores Guzman, B., Vinnakota, C., Waldvogel, H. J., Faull, R. L., and Kwakowsky, A. (2017). Towards a better understanding of gabaergic remodeling in alzheimer's disease. *Int. J. Mol. Sci.* 18:E1813. doi: 10.3390/ijms18081813
- Gronborg, M., Pavlos, N. J., Brunk, I., Chua, J. J., Munster-Wandowski, A., Riedel, D., et al. (2010). Quantitative comparison of glutamatergic and GABAergic synaptic vesicles unveils selectivity for few proteins including MAL2, a novel synaptic vesicle protein. *J. Neurosci.* 30, 2–12. doi: 10.1523/JNEUROSCI.4074-09.2010
- Gui, Y., Marks, J. D., Das, S., Hyman, B. T., and Serrano-Pozo, A. (2019). Characterization of the 18 kDa translocator protein (TSPO) expression in post-mortem normal and alzheimer's disease brains. *Brain Pathol.* [Epub ahead of print].
- Guilarte, T. R. (2019). TSPO in diverse CNS pathologies and psychiatric disease: a critical review and a way forward. *Pharmacol. Ther.* 194, 44–58. doi: 10.1016/j.pharmthera.2018.09.003
- Heneka, M. T., Carson, M. J., El Khoury, J., Landreth, G. E., Brosseron, F., Feinstein, D. L., et al. (2015). Neuroinflammation in alzheimer's disease. *Lancet Neurol.* 14, 388–405. doi: 10.1016/S1474-4422(15)70016-70015
- Ikonomic, M. D., Fantoni, E. R., Farrar, G., and Salloway, S. (2018). Infrequent false positive [(18)F]flutemetamol PET signal is resolved by combined histological assessment of neuritic and diffuse plaques. *Alzheimers Res. Ther.* 10:60. doi: 10.1186/s13195-018-0387-386
- Jack, C. R. Jr., Bennett, D. A., Blennow, K., Carrillo, M. C., Dunn, B., Haeberlein, S. B., et al. (2018). NIA-AA research framework: toward a biological definition of alzheimer's disease. *Alzheimers Dement.* 14, 535–562. doi: 10.1016/j.jalz.2018.02.018
- Jansen, W. J., Ossenkoppele, R., Tijms, B. M., Fagan, A. M., Hansson, O., Klunk, W. E., et al. (2018). Association of cerebral amyloid-beta aggregation with cognitive functioning in persons without dementia. *JAMA Psychiatry* 75, 84–95. doi: 10.1001/jamapsychiatry.2017.3391
- Kirvell, S. L., Esiri, M., and Francis, P. T. (2006). Down-regulation of vesicular glutamate transporters precedes cell loss and pathology in alzheimer's disease. *J. Neurochem.* 98, 939–950. doi: 10.1111/j.1471-4159.2006.03935.x
- Metaxas, A., Vaitheeswaran, R., Jensen, K. T., Thygesen, C., Ilkjaer, L., Darvesh, S., et al. (2018). Reduced serotonin transporter levels and inflammation in the midbrain raphe of 12 month old appsw/psen1d9 mice. *Curr. Alzheimer Res.* 15, 420–428. doi: 10.2174/1567205014666171004113537

- Morrison, J. H., and Baxter, M. G. (2012). The ageing cortical synapse: hallmarks and implications for cognitive decline. *Nat. Rev. Neurosci.* 13, 240–250. doi: 10.1038/nrn3200
- Nelson, P. T., Head, E., Schmitt, F. A., Davis, P. R., Neltner, J. H., Jicha, G. A., et al. (2011). Alzheimer's disease is not "brain aging": neuropathological, genetic, and epidemiological human studies. *Acta Neuropathol.* 121, 571–587. doi: 10.1007/s00401-011-0826-y
- Oh, H., Mormino, E. C., Madison, C., Hayenga, A., Smiljic, A., and Jagust, W. J. (2011). beta-amyloid affects frontal and posterior brain networks in normal aging. *Neuroimage* 54, 1887–1895. doi: 10.1016/j.neuroimage.2010.10.027
- Ohno, Y., and Tokudome, K. (2017). Therapeutic role of synaptic vesicle glycoprotein 2a (sv2a) in modulating epileptogenesis. *CNS Neurol. Disord. Drug. Targets* 16, 463–471. doi: 10.2174/1871527316666170404115027
- Poirel, O., Mella, S., Videau, C., Ramet, L., Davoli, M. A., Herzog, E., et al. (2018). Moderate decline in select synaptic markers in the prefrontal cortex (BA9) of patients with alzheimer's disease at various cognitive stages. *Sci. Rep.* 8:938. doi: 10.1038/s41598-018-19154-y
- Rodrigue, K. M., Kennedy, K. M., and Park, D. C. (2009). Beta-amyloid deposition and the aging brain. *Neuropsychol. Rev.* 19, 436–450. doi: 10.1007/s11065-009-9118-x
- Scheff, S. W., and Price, D. A. (2006). Alzheimer's disease-related alterations in synaptic density: neocortex and hippocampus. *J. Alzheimers Dis.* 101–115. doi: 10.3233/jad-2006-9s312
- Schuitmaker, A., van der Doef, T. F., Boellaard, R., van der Flier, W. M., Yaqub, M., Windhorst, A. D., et al. (2012). Microglial activation in healthy aging. *Neurobiol. Aging* 33, 1067–1072. doi: 10.1016/j.neurobiolaging.2010.09.016
- Serrano-Pozo, A., Mielke, M. L., Gomez-Isla, T., Betensky, R. A., Growdon, J. H., Frosch, M. P., et al. (2011). Reactive glia not only associates with plaques but also parallels tangles in alzheimer's disease. *Am. J. Pathol.* 179, 1373–1384. doi: 10.1016/j.ajpath.2011.05.047
- Snow, A. D., Nochlin, D., Sekiguchi, R., and Carlson, S. S. (1996). Identification in immunolocalization of a new class of proteoglycan (keratan sulfate) to the neuritic plaques of alzheimer's disease. *Exp. Neurol.* 138, 305–317. doi: 10.1006/exnr.1996.0069
- Stockburger, C., Miano, D., Baeumlisberger, M., Pallas, T., Arrey, T. N., Karas, M., et al. (2016). A mitochondrial role of sv2a protein in aging and alzheimer's disease: studies with levetiracetam. *J. Alzheimers Dis.* 50, 201–215. doi: 10.3233/JAD-150687
- Sutphen, C. L., Jasielec, M. S., Shah, A. R., Macy, E. M., Xiong, C., Vlassenko, A. G., et al. (2015). Longitudinal cerebrospinal fluid biomarker changes in preclinical alzheimer disease during middle age. *JAMA Neurol.* 72, 1029–1042. doi: 10.1001/jamaneurol.2015.1285
- Toyonaga, T., Smith, L. M., Finnema, S. J., Gallezot, J. D., Naganawa, M., Bini, J., et al. (2019). In vivo synaptic density imaging with (11)c-ucb-j detects treatment effects of saracatinib (azd0530) in a mouse model of alzheimer's disease. *J. Nucl. Med.* [Epub ahead of print].
- Venetti, S., Lopresti, B. J., Wang, G., Hamilton, R. L., Mathis, C. A., Klunk, W. E., et al. (2009). PK11195 labels activated microglia in alzheimer's disease and in vivo in a mouse model using pet. *Neurobiol. Aging* 30, 1217–1226. doi: 10.1016/j.neurobiolaging.2007.11.005
- Villemagne, V. L., Dore, V., Burnham, S. C., Masters, C. L., and Rowe, C. C. (2018). Imaging tau and amyloid-beta proteinopathies in alzheimer disease and other conditions. *Nat. Rev. Neurol.* 14, 225–236. doi: 10.1038/nrneurol.2018.9
- Vlassenko, A. G., McCue, L., Jasielec, M. S., Su, Y., Gordon, B. A., Xiong, C., et al. (2016). Imaging and cerebrospinal fluid biomarkers in early preclinical alzheimer disease. *Ann. Neurol.* 80, 379–387. doi: 10.1002/ana.24719
- Xu, J., Sun, J., Perrin, R. J., Mach, R. H., Bales, K. R., Morris, J. C., et al. (2019). Translocator protein in late stage alzheimer's disease and dementia with lewy bodies brains. *Ann. Clin. Transl. Neurol.* 6, 1423–1434. doi: 10.1002/acn3.50837

**Conflict of Interest:** The authors declare that the research was conducted in the absence of any commercial or financial relationships that could be construed as a potential conflict of interest.

Copyright © 2019 Metaxas, Thygesen, Briting, Landau, Darvesh and Finsen. This is an open-access article distributed under the terms of the Creative Commons Attribution License (CC BY). The use, distribution or reproduction in other forums is permitted, provided the original author(s) and the copyright owner(s) are credited and that the original publication in this journal is cited, in accordance with accepted academic practice. No use, distribution or reproduction is permitted which does not comply with these terms.



# Neuroprotective Effect of AM404 Against NMDA-Induced Hippocampal Excitotoxicity

Soraya Wilke Saliba<sup>1</sup>, Tiziana Bonifacino<sup>2</sup>, Tsvetan Serchov<sup>3</sup>, Giambattista Bonanno<sup>2,4</sup>, Antônio Carlos Pinheiro de Oliveira<sup>5</sup> and Bernd L. Fiebich<sup>1\*</sup>

<sup>1</sup>Neuroimmunology and Neurochemistry Research Group, Department of Psychiatry and Psychotherapy, Medical Center—University of Freiburg, Faculty of Medicine, University of Freiburg, Freiburg, Germany, <sup>2</sup>Unit of Pharmacology and Toxicology and Center of Excellence for Biomedical Research, Department of Pharmacy, School of Medical and Pharmaceutical Sciences, University of Genoa, Genoa, Italy, <sup>3</sup>Laboratory of Stereotaxy and Interventional Neuroscience, Department of Stereotactic and Functional Neurosurgery, Medical Center—University of Freiburg, Faculty of Medicine, University of Freiburg, Freiburg, Germany, <sup>4</sup>Istituto di Ricovero e Cura a Carattere Scientifico (IRCCS), Ospedale Policlinico San Martino, Genoa, Italy, <sup>5</sup>Department of Pharmacology, Universidade Federal de Minas Gerais, Belo Horizonte, Brazil

## OPEN ACCESS

### Edited by:

Rocío Martínez De Pablos,  
University of Seville, Spain

### Reviewed by:

Elisa Landucci,  
University of Florence, Italy  
Carla Ines Tasca,  
Federal University of Santa Catarina,  
Brazil

### \*Correspondence:

Bernd L. Fiebich  
bernd.fiebich@uniklinik-freiburg.de

**Received:** 26 September 2019

**Accepted:** 06 December 2019

**Published:** 20 December 2019

### Citation:

Saliba SW, Bonifacino T, Serchov T, Bonanno G, de Oliveira ACP and Fiebich BL (2019) Neuroprotective Effect of AM404 Against NMDA-Induced Hippocampal Excitotoxicity. *Front. Cell. Neurosci.* 13:566. doi: 10.3389/fncel.2019.00566

Different studies have demonstrated that inflammation and alterations in glutamate neurotransmission are two events contributing to the pathophysiology of neurodegenerative or neurological disorders. There are evidences that N-arachidonoylphenolamine (AM404), a cannabinoid system modulator and paracetamol metabolite, modulates inflammation and exerts neuroprotective effects on Huntington's (HD) and Parkinson's diseases (PD), and ischemia. However, the effects of AM404 on the production of inflammatory mediators and excitotoxicity in brain tissue stimulated with N-methyl-D-aspartic acid (NMDA) are not elucidated. In this present study, we investigated the effects of AM404 on the production of inflammatory mediators and neuronal cell death induced by NMDA in organotypic hippocampal slices cultures (OHSC) using qPCR, western blot (WB), and immunohistochemistry. Moreover, to comprehend the mechanism of excitotoxicity, we evaluated the effects of AM404 on glutamate release in hippocampal synaptosomes and the NMDA-induced calcium responses in acute hippocampal slices. Our results showed that AM404 led to a significant decrease in cell death induced by NMDA, through a mechanism possibly involving the reduction of glutamate release and the calcium ions responses. Furthermore, it decreased the expression of the interleukin (IL)-1 $\beta$ . This study provides new significant insights about the anti-inflammatory and neuroprotection effects of AM404 on NMDA-induced excitotoxicity. To understand the effects of AM404 in these processes might contribute to the therapeutic potential of AM404 in diseases with involvement of neuroinflammation and neurodegeneration and might lead to a possible future treatment of neurodegenerative diseases.

**Keywords:** AM404, hippocampus, neuroinflammation, excitotoxicity, LPS, NMDA, cannabinoid receptor, vanilloid receptor

## INTRODUCTION

The role of excitotoxicity in the etiology or progression of several human neurodegenerative disorders such as Alzheimer's (AD), Parkinson's (PD) and Huntington's (HD) diseases, epilepsy or amyotrophic lateral sclerosis (ALS) has been proposed (Palop et al., 2006; Dong et al., 2009). Excitotoxicity is a pathologic process characterized by the increase of calcium ions influx through mainly N-methyl-D-aspartic acid (NMDA) receptors that result in both, an increase of glutamate release and activation of many enzymes culminating in neuronal cell death (Choi, 1988; Waxman and Lynch, 2005). A promising target for the therapeutic intervention of several progressive neurodegenerative diseases is the modulation of the endocannabinoid system (Scotter et al., 2010). Some studies have suggested that the endocannabinoid system plays a protective role against excitotoxic damage (Marsicano et al., 2003; Mechoulam, 2003; Veldhuis et al., 2003), mostly *via* cannabinoid CB1 receptor inhibiting N-type  $\text{Ca}^{2+}$  channels activity and consequently reduces glutamatergic transmission (Shen et al., 1996; L  v  n  s et al., 1998; van der Stelt et al., 2002). The CB1 receptor is the most abundant G protein-coupled receptor in the brain (Howlett et al., 1990, 2010) and it is expressed on glutamatergic and GABAergic neurons in brain regions such as the hippocampus, cortex, and basal ganglia (Tsou et al., 1998; Mackie, 2005). Besides CB1 and CB2 receptors, cannabinoid agonists also activate transient receptor potential vanilloid type 1 (TRPV1; Smart et al., 2000; Ross, 2003). TRPV1 is a non-selective cation channel and similarly expressed in numerous regions in the brain, including cortex, hippocampus, and corpus callosum (T  th et al., 2005).

N-arachidonoylphenolamine (AM404), a paracetamol metabolite, blocks the anandamide membrane transporter (AMT; Beltramo et al., 1997; Giuffrida et al., 2000) and is an agonist of TRPV1 (De Petrocellis et al., 2000; Zygmunt et al., 2000) and CB1 receptors (Khanolkar et al., 1996; Beltramo et al., 2000; Mitchell et al., 2007). The neuroprotective effects of AM404 on some neurodegenerative models through the activation of the CB1 or/and TRPV1 receptors has been demonstrated. In a rat model of HD induced by the injection of 3-nitropropionic acid, AM404 was able to attenuate the hyperkinetic signs and recover neurochemical (GABA and dopamine) deficits (Lastres-Becker et al., 2002) *via* TRPV1 receptor (Lastres-Becker et al., 2003). However, on an ischemia-induced neuronal injury, AM404 protected CA1 layer neurons of the hippocampus through CB1 and opioid receptors but not involving TRPV1, and prevented ischemia-induced memory impairment (Zani et al., 2007).

AM404 ameliorates parkinsonian effects induced by 6-hydroxydopamine in rats (Fernandez-Espejo et al., 2004) and recovered the dopamine depletion and tyrosine hydroxylase deficit, probably by an antioxidant effect (Garc  a-Arencibia et al., 2007). In this model of 6-OHDA, enhanced glutamatergic transmission after DA depletion has been shown and AM404 was able to reduce the frequency of glutamatergic spontaneous activity and SR141716 (CB1 antagonist) but not capsazepine (TRPV1 antagonist) blocked this effect (Gubellini et al., 2002).

Moreover, AM404 has been described to attenuate seizures from epilepsy models using pentylenetetrazole (PTZ; Manna and Umathe, 2012) or kainic acid (Shubina et al., 2015, 2017). Manna and Umathe (2012) further demonstrated that in an epilepsy model using PTZ, the protective effects of AM404 involved CB1 but not TRPV1 receptors.

The effects of AM404 on the excitotoxicity and production of inflammatory mediators in brain tissue stimulated with NMDA are not elucidated. Thus, in this current study, we evaluated if AM404 is able to prevent NMDA-induced excitotoxicity and inflammation by evaluating cell death and inflammatory parameters in organotypic hippocampal slices cultures (OHSC), glutamate release in synaptosomes, and intracellular calcium responses in acute hippocampal slices stimulated with NMDA.

## MATERIALS AND METHODS

### Ethics Statement

The experiments were performed using neonatal female and male C57BL/6 wild-type (WT). Neonatal mice pups were obtained from Center for experimental models and transgenic services (CEMT, Freiburg) and used in accordance with the German animal welfare law for the use of experimental animals (approved protocol No. X-13/06A by the Regierungspr  sidium Freiburg).

### Drugs

AM404 (Alomone Labs) was dissolved in the physiological medium for the synaptosome experiment and in DMSO for the other experiments (Merck KGaA, Darmstadt, Germany). NMDA was resuspended in Dulbecco's phosphate-buffered saline (DPBS; Gibco<sup>  </sup> by Life Technologies, Germany) as 100 mM stock, and was used at a final concentration of 10–50  $\mu\text{M}$  in the OHSC. Lipopolysaccharide (LPS) from *Salmonella typhimurium* was resuspended in DPBS as 5 mg/ml stock and was used at a final concentration of 10 ng/ml or 100 ng/ml. Solvent concentrations in the culture media were maintained at 0.1%.

### Preparation of Organotypic Hippocampal Slice Cultures (OHSC)

As previously described (Saliba et al., 2017a), OHSCs were prepared from 2 to 3 days old C57BL/6 WT mice. Animals were decapitated, the hippocampi were dissected and placed in a chopper for the preparation of the slices with a thickness of 350  $\mu\text{M}$ . The integral slices were selected and transferred to a 0.4  $\mu\text{M}$  culture plate inserts (Millipore). The inserts were placed in a 6-well culture plate containing 1 ml of OHSC medium [0.5 $\times$  minimum essential medium (MEM) containing Earl's salts, 25% horse serum, 25% basal medium (BME) without glutamate and containing Earl's salts, 2 mM glutamax, and 0.35% glucose]. Then, the plate was incubated at 35  C in a humidified atmosphere with 5%  $\text{CO}_2$  and the culture medium was changed after the first day of preparation following every 2 days.



## Quantification of Neuronal Cell Death in OHSC

After 7 days in culture, OHSCs were pre-treated with AM404 (10, 25, or 50  $\mu\text{M}$ ) for 30 min and NMDA (25  $\mu\text{M}$ ) was added for additional 4 h. The slices were then washed with 37°C DPBS and the media replaced with NMDA-free medium containing 5  $\mu\text{g/ml}$  propidium iodide (PI, Sigma), and incubated for 24 h. Thereafter, OHSCs were washed with cold DPBS followed by 4% PFA incubation for 1 h. After fixation, the slices were washed with DPBS and incubated with 5% normal goat serum (NGS) in PBS containing 0.3% Triton X-100 (PBS<sup>+</sup>) for at least 2 h. Then, slices were incubated overnight with an anti-mouse-NeuN-488 (1:1,000) in 1% NGS/PBS<sup>+</sup> at 4°C. Analyses of the slices were done by confocal imaging using a Zeiss microscope (Zeiss, Oberkochen, Germany) from Life Imaging Center (LIC, Center for Biological Systems Analysis, Freiburg, Germany). Quantification of fluorescence intensity was done using ImageJ software.

## Synaptosome Purification

Synaptosomes were prepared from C57BL/6 WT mouse hippocampus as described (Raiteri et al., 2008). The tissue was homogenized in 0.32 M sucrose, buffered at pH 7.4. The homogenate was centrifuged (5 min,  $1,000\times g$  at 4°C) and the supernatant again centrifuged at  $12,000\times g$  for 10 min. The pellet was resuspended in Tris-buffered 0.32 M sucrose, layered on a discontinuous Percoll<sup>®</sup> gradient (2, 6, 10, and 20% v/v in Tris-buffered 0.32 M sucrose), and centrifuged at  $33,500\times g$  for 5 min. The layer between 10 and 20% Percoll<sup>®</sup> was collected, washed and centrifuged at  $20,000\times g$  for 15 min. The pellet was resuspended in physiological medium having the following composition (mM): NaCl, 140; KCl, 3; MgSO<sub>4</sub>, 1.2; NaH<sub>2</sub>PO<sub>4</sub>, 1.2; NaHCO<sub>3</sub>, 5; CaCl<sub>2</sub>, HEPES, 10; glucose, 10; pH 7.4.

## Release Experiments

Synaptosomes were incubated (15 min, 37°C) with 0.05  $\mu\text{M}$  [<sup>3</sup>H]D-Aspartate ([<sup>3</sup>H]D-Asp), a non-metabolizable analog of Glu which labels the intra-terminal releasable pools of the excitatory amino acid (Fleck et al., 2001; Raiteri et al., 2007). Aliquots were distributed on microporous filters placed at the bottom of a set of 24 parallel superfusion chambers maintained at 37°C (Superfusion System, Ugo Basile, Comerio, Varese, Italy) and superfused as described (Milanese et al., 2010). Superfusion was started with a physiological medium at a rate of 0.5 ml/min and continued for 51 min. After 36 min of superfusion, to equilibrate the system, six samples ( $t = 33\text{--}36$ ;  $t = 36\text{--}39$ ;  $t = 39\text{--}42$ ;  $t = 42\text{--}45$ ;  $t = 45\text{--}48$ ;  $t = 48\text{--}51$ ) were collected. NMDA (30  $\mu\text{M}$ ) plus glycine (1  $\mu\text{M}$ ) was added at  $t = 39$  min; and AM404 (0.1, 1 or 50  $\mu\text{M}$ ) at  $t = 30$  and maintained until the end of the experiment. Then, samples were collected and superfused synaptosomes were counted for radioactivity. Tritium released in each sample was calculated as fractional rate  $\times 100$  (percentage of the total synaptosomal neurotransmitter content at the beginning of the respective collection period). Drug effects were evaluated by calculating the ratio between the efflux in the fourth sample collected (in which the maximum effect of NMDA was generally reached) and the efflux of the

second sample collected (basal efflux). This ratio was compared to the corresponding ratio obtained under control conditions. Appropriate ratios in each experiment were compared to evaluate the AM404 effect.

## Calcium Imaging

Acute brain slices of C57BL/6 WT mice were prepared as described (Dawitz et al., 2011; Holz et al., 2019). In brief, 6 days old animals were decapitated and the forebrain was removed and replaced in carbogenated (5% CO<sub>2</sub> and 95% O<sub>2</sub>) ice-cold artificial cerebrospinal fluid (ACSF; 125 mM NaCl, 25 mM NaHCO<sub>3</sub>, 27 mM Glucose, 2.5 mM KCl, 1.25 mM NaH<sub>2</sub>PO<sub>4</sub>, 1 mM MgCl<sub>2</sub> and 2 mM CaCl<sub>2</sub>). Four to six coronal slices (300  $\mu\text{m}$  thickness) containing the hippocampus area were cut by using a vibratome (DTK-1000, Dosaka, Japan). The slices were collected and recovered at room temperature (RT) for 30 min in carbogenated ACSF. In a chamber containing 1 ml of carbogenated ACSF, the hemispheres were separated and incubated with 50 mM Fura-2 acetoxymethyl ester (Invitrogen) in the presence of 0.1% pluronic acid (Invitrogen), for 20–30 min at 35°C protected from the light. After incubation, the slices were rinsed in carbogenated ACSF and incubated with 50  $\mu\text{M}$  AM404 for 30 min. One slice was placed in the imaging chamber and fixed with a metal harp superfused with carbogenated ACSF containing 1.5 mM MgCl<sub>2</sub> and 1.6 mM CaCl<sub>2</sub>. The fluorescence imaging was taken at the light microscope (Axioskop FS2, Zeiss; 40 $\times$  water immersion objective, Olympus Optical, Tokyo, Japan) using the TILLvisION program. Single Fura-2-fluorescent neurons were selected as regions of interest and the baseline fluorescence signal ( $F_0$ ) was recorded for at least 30 s before NMDA. The changes on the fluorescence signals ( $\Delta F$ ) were calculated with the formula ( $F - F_0 / F_0$ ) where  $F$  is fluorescence intensity and  $F_0$  is baseline fluorescence intensity. The area under the curve was determined for 90 s after NMDA.

## qPCR Analysis

After 7 days in culture, OHSCs were pre-treated with AM404 (10, 25 or 50  $\mu\text{M}$ ) for 30 min and NMDA (25  $\mu\text{M}$ ) was added for an additional 4 h. Thereafter, OHSCs were washed with cold DPBS followed the mRNA isolation was performed using the GeneMATRIX Universal RNA Purification Kit from Roboklon, according to the manufacturer's protocol. After the isolation, 500 ng RNA were mixed with 2  $\mu\text{g}$  of random hexamer oligonucleotides in a 30  $\mu\text{l}$  total reaction volume and denatured at 70°C (10 min). The synthesized cDNA was used for the real-time PCR amplification that was carried out using the CFX96 real-time PCR detection system (Bio-Rad Laboratories GmbH, Munich, Germany). The primers (table below) were designed by using Universal Probe Library Assay Design Center.

## Western Blot (WB)

After 7 days in culture, OHSCs were pre-treated with AM404 (10, 25 or 50  $\mu\text{M}$ ) for 30 min and NMDA (25  $\mu\text{M}$ ) was added for an additional 4 h. The slices were then washed with 37°C DPBS and the media replaced with NMDA-free medium and incubated for 24 h. Thereafter, OHSCs were washed with

Gene	Forward primer (5'–3')	Reverse primer (5'–3')
CD11b	TACCGTCTACTACCCATCTGGC	TTGGTGAGCGGGTTCTGG
CSF1R	CGAGGGAGACTCCAGCTACA	GACTGGAGAAGCCACTGTCC
GAPDH	TGGGAAGCTGGTCATCAAC	GCATCACCCCATTTGATGTT
GFAP	GGAGGTGGAGAGGGACAAC	GTTTCATCTTGGAGCTTCTGC
Iba-1	CAGGGATTTGCAGGGAGGAAA	AGTTTGGACGCGAGATCCTC
IL-1β	TGTGATGAAAGACGGCACAC	CTTCTTCTTTGGGTATTGTTTG
IL-6	CCTGGAGTTTGTGAAGAACAAC	GGAAGTTGGGGTAGGAAGGA
iNOS	CTTTGCCACGGACGAGAC	TCATTGACTCTGAGGGCTGAC
mPGES-1	GCACACTGCTGGTCATCAAG	ACGTTTCAACGCGCTCCTC
TNFα	CCCACGTCGTAGCAAACCA	CCATTGGCCAGGAGGGCGTTG

cold DPBS and lysed in the lysis buffer (42 mM Tris-HCl, 1.3% sodium dodecyl sulfate, 6.5% glycerin, 100 μM sodium orthovanadate, and 2% phosphatase and protease inhibitors; Saliba et al., 2017a). The protein concentration of the samples was measured using the bicinchoninic acid (BCA) protein assay kit (Thermo Fisher Scientific, Bonn, Germany) according to the manufacturer's instructions. For western blot (WB), 10–20 μg of total protein from each sample were subjected to sodium dodecyl sulfate-polyacrylamide gel electrophoresis (SDS-PAGE) under reducing conditions. Afterward, proteins were transferred onto polyvinylidene fluoride (PVDF) membranes

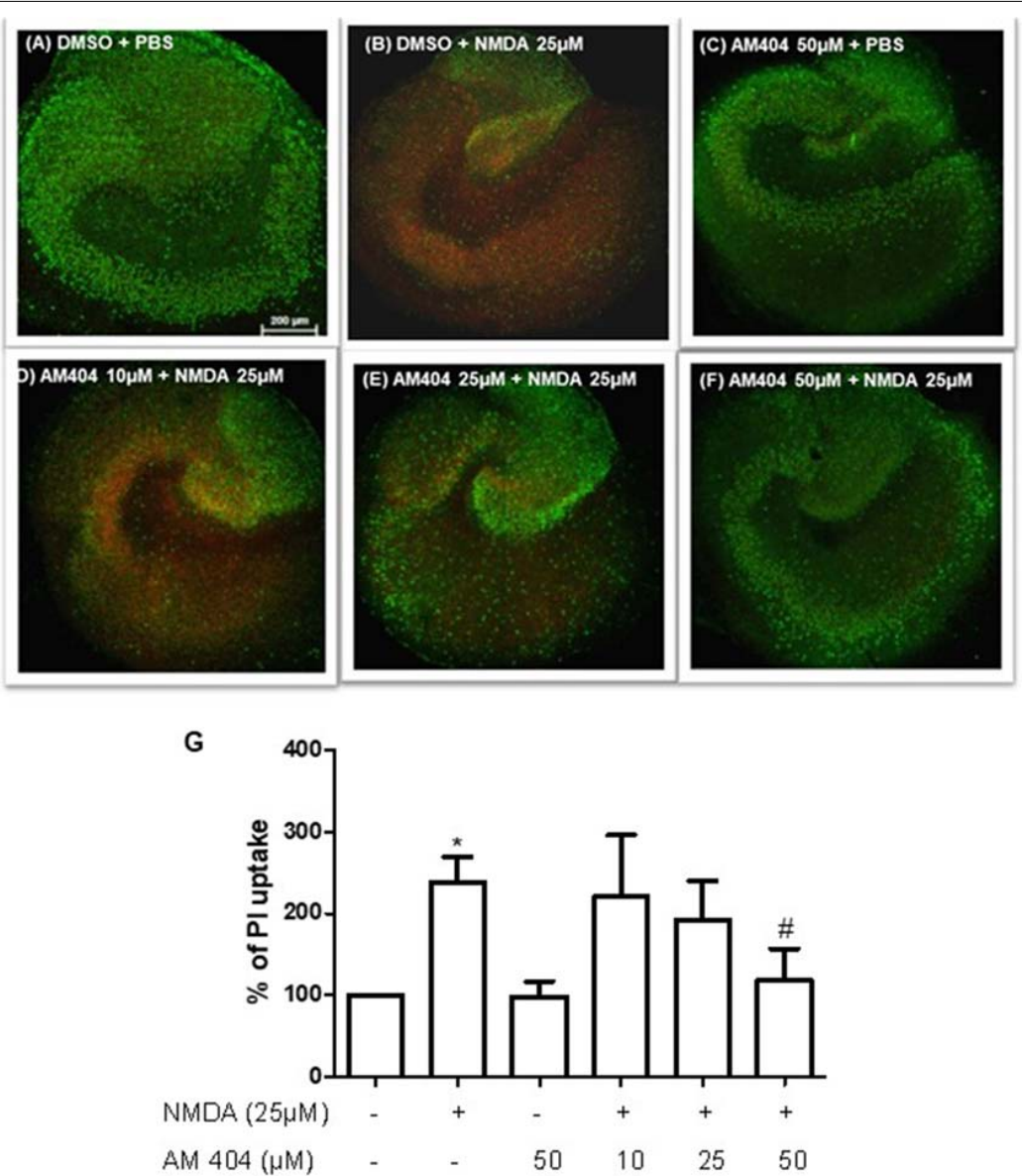


**FIGURE 1 |** Effects of N-arachidonoylphenolamine (AM404) on excitotoxicity in mouse hippocampal slices cultures [*n* = 3 organotypic hippocampal slices cultures (OHSCs)/group]. **(A–F)** Representative confocal images of the immunostaining with propidium iodide (PI; red) and with the neuronal nuclear marker NeuN (green). **(G)** Quantitative analysis of the PI fluorescence. The results are expressed as mean ± SEM. \**p* < 0.05 with respect to negative control and #*p* < 0.05 compared with N-methyl-D-aspartic acid [NMDA; 25 μM; one-way analysis of variance (ANOVA), Newman–Keuls test].

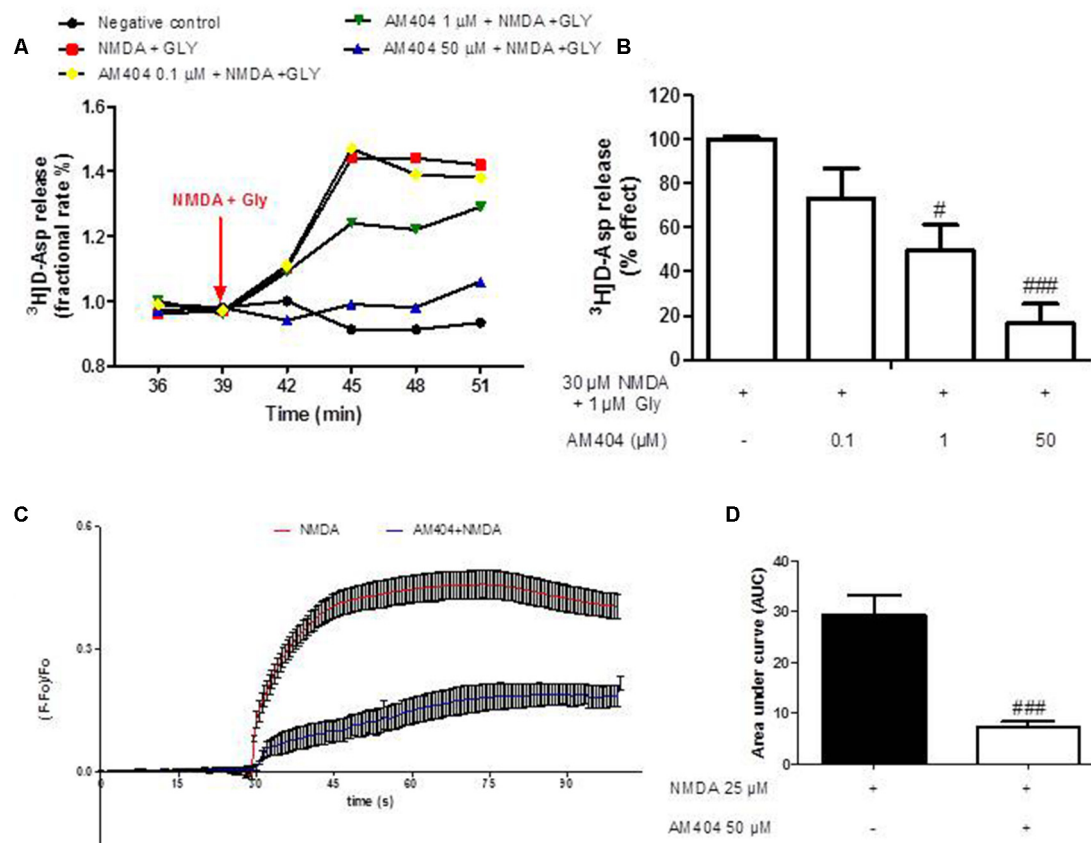


**FIGURE 2 |** Effects of AM404 on [ $^3\text{H}$ ]D-Asp release in hippocampal synaptosomes and intracellular  $\text{Ca}^{2+}$  responses. **(A)** Time course of [ $^3\text{H}$ ]D-Asp release induced by NMDA plus Gly and effects of AM404 in hippocampal synaptosomes. Results are expressed as fractional rate percent. **(B)** AM404 inhibition of the NMDA plus Glycine-evoked [ $^3\text{H}$ ]D-Asp release in hippocampal synaptosomes. **(C)** Data of calcium imaging expressed as fluorescence intensity ( $\Delta F/F_0$  baseline) vs. time. **(D)** Data of calcium imaging calculated the area under the curve (AUC). Data are means  $\pm$  SEM of three independent experiments.  $^{\#}p < 0.05$  and  $^{###}p < 0.001$  compared to NMDA (one-way ANOVA followed by Bonferroni *post hoc* tests for [ $^3\text{H}$ ]D-Asp release and unpaired *t*-test of three independent experiments for calcium imaging).

(Merck Millipore, Darmstadt, Germany) by semi-dry blotting. After blocking with Roti-Block (Roth, Karlsruhe, Germany), membranes were incubated overnight with primary antibodies: goat anti-COX-2 (1:500; Santa Cruz Biotechnology, Heidelberg, Germany), and rabbit anti-actin (1:5,000; Sigma Aldrich). The proteins were detected with horseradish peroxidase-coupled rabbit anti-goat IgG (Santa Cruz, 1:100,000 dilution) and goat anti-rabbit IgG (GE Healthcare, 1:25,000 dilution) using enhanced chemiluminescence (ECL) reagents (GE Healthcare, Freiburg, Germany). Densitometric analysis was performed using ImageJ software (NIH, Bethesda, MD, USA), and  $\beta$ -actin control was used to confirm equal sample loading and normalization of the data.

## Data Analysis

The results were presented as mean  $\pm$  SEM. Data were analyzed using one-way analysis of variance (ANOVA) followed by Newman-Keuls post-test. The level of statistical significance was considered as  $^*p < 0.05$ ,  $^{**}p < 0.01$ ,  $^{***}p < 0.001$ . Graph Pad Prism (Graph Pad Software, San Diego, CA, USA) was used for performing all statistical analysis.

Data for synaptosomes are expressed as mean  $\pm$  SEM and  $p$ -value  $< 0.05$  was considered significant. Multiple comparisons were performed using the ANOVA followed by Bonferroni *post hoc* test. Analyses were performed by SigmaStat (Systat Software, Inc., San Jose, CA, USA) software.

Data for calcium imaging were expressed as fluorescence intensity ( $\Delta F/F_0$  baseline) vs. time and calculated the area under the curve (AUC). To compare the groups, unpaired *t*-test was evaluated using Graph Pad Prism (Graph Pad Software, San Diego, CA, USA).

## RESULTS

### AM404 Prevented the NMDA-Induced Neuronal Toxicity in OHSC

We studied whether AM404 has a neuroprotective effect on excitotoxicity induced by NMDA in OHSC. As shown in **Figure 1B**, the intensity of PI uptake was increased in OHSC after NMDA (25  $\mu\text{M}$ ) stimulation compared with negative control (**Figure 1A**). Incubation of OHSC with 10 or 25  $\mu\text{M}$  of AM404 did not alter the intensity of PI uptake (**Figures 1D,E,G**).



However, pre-treatment with 50  $\mu$ M of AM404 (Figures 1E,G) potently prevented the increase of PI uptake levels and thus excitotoxicity induced by NMDA back to basal levels (Figures 1A,C).

### AM404 Reduced [ $^3$ H]D-Asp Release in Hippocampal Synaptosomes and the NMDA-Induced Calcium Responses in Acute Hippocampal Brain Slices

In order to investigate whether AM404 might modulate glutamate release and calcium responses contributing to its neuroprotective effect, we evaluated the effect of AM404 on [ $^3$ H]D-Asp release induced by NMDA plus glycine (Gly) in hippocampal synaptosomes and calcium imaging in OHSC. As shown in Figure 2A, NMDA (30  $\mu$ M) plus Gly (1  $\mu$ M) increased [ $^3$ H]D-Asp release and this effect reached the maximal value starting from  $t = 45$  min of superfusion. AM404 (0.1, 1 and 50  $\mu$ M) strongly and concentration-dependently reduced NMDA plus Gly-evoked-[ $^3$ H]D-Asp release by about 30%, 51%, and 87%, respectively (Figure 2B). In addition, NMDA increased the calcium ions responses, which was prevented by AM404 (50  $\mu$ M; Figures 2C,D).

### AM404 Prevented NMDA-Induced Increase of IL-1 $\beta$ Expression but Did Not Affect the NMDA Mediated Expression of IL-6, TNF $\alpha$ , mPGES-1, and iNOS

The excitotoxicity process is directly correlated with inflammation. To confirm this, we first evaluated the effects of different concentrations of NMDA on the expression of inflammatory mediators in OHSC. As shown in Supplementary Figure S1, NMDA (25  $\mu$ M) increased all inflammatory parameters tested. To investigate the effects of AM404 on inflammation induced by excitotoxicity, we stimulated the slices with 25  $\mu$ M of NMDA for 4 h. LPS (10 ng/ml) was used as a positive control. As expected, LPS and NMDA statistically increased inflammatory mediators (Figures 3A–E). The pre-treatment with AM404 statistically prevented NMDA-induced IL-1 $\beta$  expression (Figure 3A) and tended towards a decrease of COX-2 protein (Figure 3F). AM404 did not affect the levels of the other cytokines, mPGES-1, and iNOS.

### AM404 Did Not Alter the mRNA Expression of Microglia and Astrocytes Markers

The main source for neuroinflammatory mediators are immune cells. Thus, we next investigated the effect of AM404 to modulate the activation of microglia and astrocytes. As demonstrated in Figure 4, NMDA statistically increased the expression of microglia (Figures 4A–C) and astrocyte markers (Figure 4D). However, the pre-treatment with AM404 did not alter these effects.

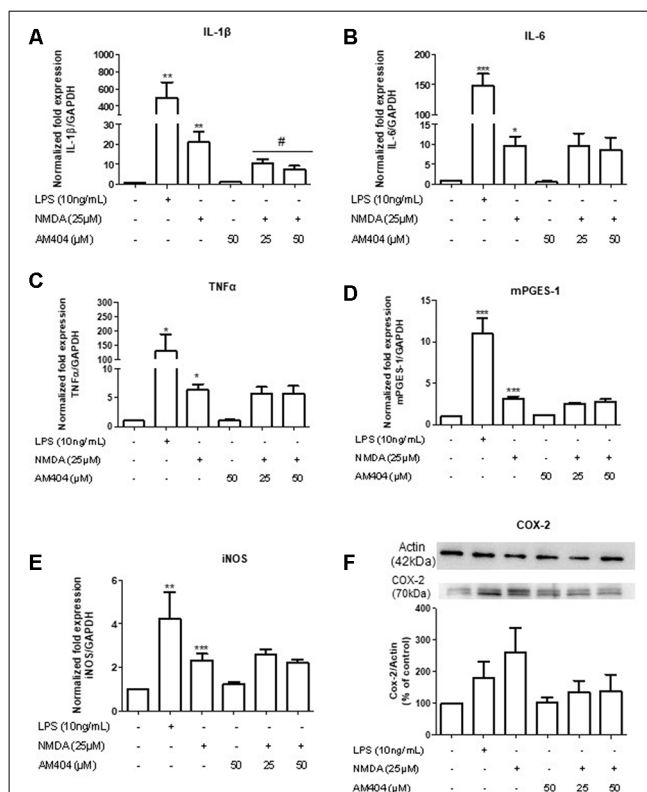


**FIGURE 3 |** Effects of AM404 on NMDA-induced inflammatory mediators in organotypic hippocampal slices cultures (OHSC). OHSCs were pre-treated with two concentrations of AM404 (25 or 50  $\mu$ M) for 30 min before stimulating with 10 ng/ml LPS or 25  $\mu$ M NMDA. After 4 h, interleukin (IL)-1 $\beta$  (A), IL-6 (B), TNF $\alpha$  (C), mPGES-1 (D), and iNOS (E) were measured by PCR. After 24 h, COX-2 (F) was evaluated by western blot (WB). Data are expressed as mean  $\pm$  SEM of at least three OHSCs/group. \* $p < 0.05$ , \*\* $p < 0.01$  and \*\*\* $p < 0.001$  with respect to negative control and # $p < 0.05$  in comparison to 25  $\mu$ M NMDA (one-way ANOVA followed by the Newman-Keuls post-test).

## DISCUSSION

In this study, we have demonstrated that NMDA increased cell death in OHSC and AM404 prevented this effect in a concentration-dependent manner through a mechanism possibly involving the decrease of glutamate release in hippocampal synaptosomes and intracellular calcium responses in hippocampal slices. The cannabinoid modulator/paracetamol metabolite also reduced the production of IL-1 $\beta$ , an important mediator associated with neurodegenerative and neuroinflammatory conditions.

In accordance with our results, some studies have shown neuroprotective effects of AM404 on different models. AM404 has been found to protect against neuronal death in an animal model of ischemia (Zani et al., 2007) and epilepsy (Shubina et al., 2017). Huang et al. (2019) demonstrated the treatment with AM404 significantly induced neuroprotection in hippocampal neuronal culture. Moreover, the combination of AM404 and AM374 (Fatty acid amide hydrolase, FAAH, inhibitor) protected against excitotoxicity induced by AMPA (Karanian et al., 2005).



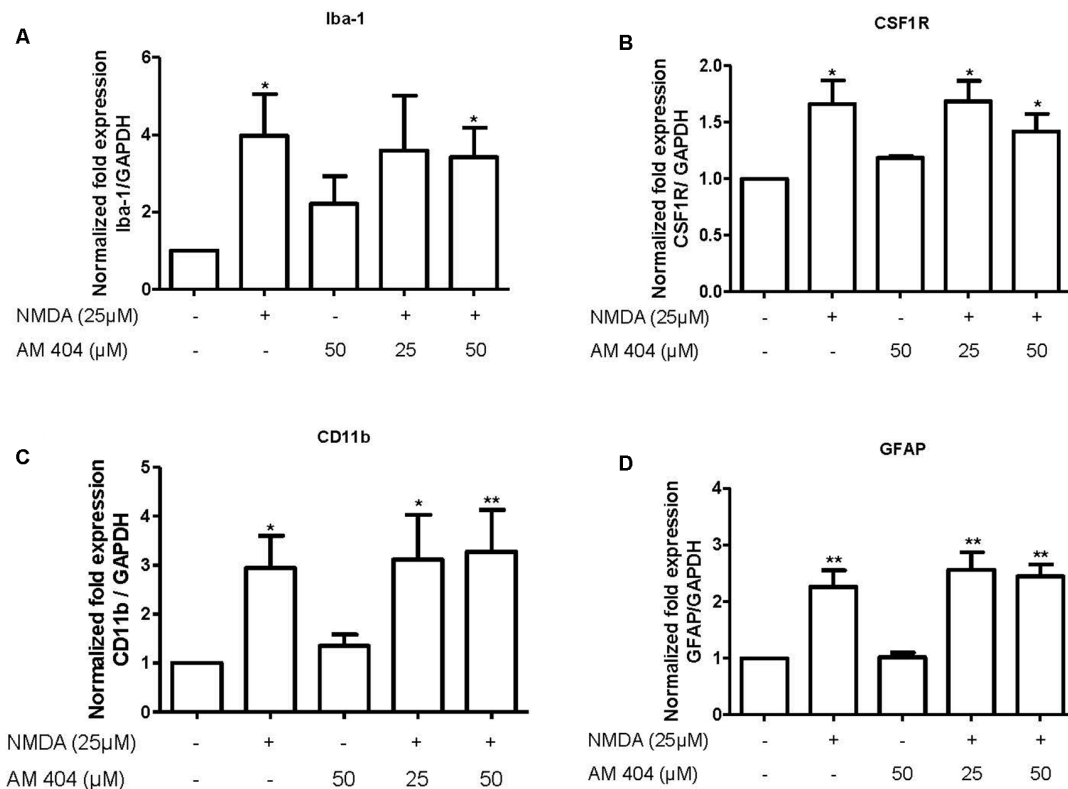


**FIGURE 4 |** Effect of AM404 on microglia and astrocyte after 25  $\mu$ M NMDA in OHSC. The OHSCs were pre-treated with two concentrations of AM404 (25 or 50  $\mu$ M) for 30 min before stimulating with 25  $\mu$ M NMDA. After 4 h, microglia markers, Iba-1 (**A**), CSF1R (**B**) and CD11b (**C**), an astrocyte marker, GFAP (**D**) were measured by qPCR. Data are expressed as mean  $\pm$  SEM of at least three OHSCs/group. \* $p < 0.05$ , \*\* $p < 0.01$  with respect to negative control (one-way ANOVA followed by the Newman-Keuls post-test).

The effects of AM404 on calcium entry have been demonstrated contradictory, depending on the cell type used. AM404 decreased calcium influx in hippocampal neurons (Hampson et al., 2011; Naziğlu et al., 2019). Moreover, AM404 directly inhibited the function of L-type voltage-dependent  $\text{Ca}^{2+}$  channels in rat myotubes (Alptekin et al., 2010) and weakly inhibited Cav3.2 T-type calcium channel in mouse supraspinal (Kerckhove et al., 2014). In contrast, it has been described that AM404 increased the influx of intracellular calcium in a concentration-dependent manner in human MG63 osteosarcoma cells (Chang et al., 2008).

The activation of NMDA receptors increased cytokines which contribute to neurodegeneration (Kaindl et al., 2008). Thus, we evaluated the effects of NMDA receptor activation on the production of inflammatory mediators in OHSCs. We first verified that mRNA expression of some inflammatory parameters (IL-1 $\beta$ , IL-6, TNF $\alpha$ , mPGES-1, iNOS, and COX-2) is induced by NMDA and we show here that the pre-treatment of AM404 prevented the increase on IL-1 $\beta$  expression and had the tendency to decrease COX-2 protein levels induced by NMDA. So far, we are not able to explain why AM404 is only able to reduce IL-1 $\beta$  levels. Possible mechanism might be, that AM404 targets specific signaling pathways involved in IL-1 $\beta$  expression or

affects the stability of IL-1 $\beta$  mRNA but not of the other genes investigated.

The direct correlation between IL-1 $\beta$  and excitotoxicity has been described (Fogal and Hewett, 2008) and its involvement in neurodegeneration has been observed in different neurological disorders such as epilepsy (Vezzani and Baram, 2007) and multiple sclerosis (Rossi et al., 2014). IL-1 $\beta$  enhanced NMDA receptor-mediated intracellular calcium and neuronal death (Viviani et al., 2003) and the increase in IL-1 $\beta$  signaling enhanced glutamate-mediated synaptic excitability and neurotoxicity (Rossi et al., 2012). Moreover, an interaction between IL-1 $\beta$  and the endocannabinoid system has been described, based on the evidences that IL-1 $\beta$  increased the frequency of spontaneous excitatory postsynaptic currents (sEPSCs) through TRPV1 channels (Musumeci et al., 2011; Rossi et al., 2012) and that it blocked the capability of CB1 receptors in the control of glutamate transmission (De Chiara et al., 2013). Furthermore, IL-1 $\beta$  plays a crucial role in the induction of COX-2, 1 and PGE2 (Fiebich et al., 2000). Non-steroidal anti-inflammatory drugs (NSAIDs) inhibiting COX-activity, were able to decrease the inflammatory effects of IL-1 $\beta$  in the brain (Favrais et al., 2007). We show here a tendency of decreased COX-2 levels by AM404, whereas mPGES-1 expression was not affected. In our previous study, corroborating with our findings, we demonstrated that

AM404 slightly decreased the levels of LPS-induced COX-2 protein but not of LPS-induced mPGES-1 (Saliba et al., 2017a).

The production of inflammatory mediators is mainly modulated by the neuroimmune cells, microglia, and astrocytes. IL-1 $\beta$  expression in microglia and astrocytes were increased in the cortex and striatum of rats after NMDA-induced excitotoxicity (Pearson et al., 1999). Subsequently, we verified the expression of cellular markers of microglia and astrocytes after NMDA stimulation and pre-treatment with AM404. NMDA stimulation statistically increased the expression of both markers, but AM404 did not alter these effects. In one of our previous studies using a mouse model of quinolinic acid (QA)-induced excitotoxicity pre-treated with rapamycin, we also observed no correlation between the alterations on cytokine expression and the activation of microglia or astrocytes (Saliba et al., 2017b).

Undoubtedly, further studies are still necessary to understand the role of AM404 during excitotoxic events and, additionally, to understand if the effects observed involve the activation of TRPV1 and CB1 receptors.

## CONCLUSIONS

In conclusion, we provide direct evidence that AM404 modulates the two major processes involved in neurodegenerative diseases, excitotoxicity and neuroinflammation, by decreasing pro-inflammatory mediators, reducing glutamate release, and calcium ions responses.

To understand the effects of AM404 in these processes might contribute to the therapeutic potential of AM404 in diseases with involvement of neuroinflammation and neurodegeneration and might lead to a possible future treatment of neurodegenerative diseases. However, further pre-clinical and clinical experiments in humans are necessary to evaluate other pharmacological parameters and safety of AM404 for further drug development.

## DATA AVAILABILITY STATEMENT

All datasets generated for this study are included in the article/**Supplementary Material**.

## ETHICS STATEMENT

The animal study was reviewed and approved by Regierungspräsidium Freiburg (protocol No. X-13/06A),

and carried out in accordance with the German animal welfare law for the use of experimental animals.

## AUTHOR CONTRIBUTIONS

SS, TB, TS, AO, and BF participated in the research design. The experiments were performed by SS, TB, and TS. Data were analyzed by SS and TB. SS, TB, TS, GB, AO, and BF wrote or contributed to the writing of the manuscript. In addition, SS, TB, TS, GB, AO, and BF reviewed the data and discussed the manuscript. All authors have read and approved the final version of the manuscript.

## FUNDING

SS received a fellowship from CNPq/CSF (Brasília/Brazil) and DAAD (Germany). TS was funded by a grant from the German Research Council (SE 2666/2-1) and a grant from the Forschungskommission of the Medical Faculty of University of Freiburg (SER1149/17). The article processing charge was funded by the University of Freiburg Library in the funding program “Open Access Publishing”.

## ACKNOWLEDGMENTS

SS acknowledges CNPq/CSF (Brasília/Brazil) and DAAD (Germany) for financial support. AO acknowledges CNPq for the research productivity fellowship. TS acknowledges the German Research Council and Forschungskommission of the Medical Faculty of the University of Freiburg. We thank the University of Freiburg Library for their support *via* the funding program “Open Access Publishing”.

## SUPPLEMENTARY MATERIAL

The Supplementary Material for this article can be found online at: <https://www.frontiersin.org/articles/10.3389/fncel.2019.00566/full#supplementary-material>.

**FIGURE S1** | Effects of NMDA on levels of inflammatory mediators in OHSC. The OHSCs were stimulated with LPS or NMDA (10–50  $\mu$ M). After 4 h, IL-1 $\beta$  (**A**), IL-6 (**B**), TNF $\alpha$  (**C**), mPGES-1 (**D**), and iNOS (**E**) were measured by qPCR. After 24 h, COX-2 (**F**) was evaluated by western blot. Data are expressed as mean  $\pm$  SEM of at least three OHSCs/group. \* $p$  < 0.05, \*\* $p$  < 0.01 and \*\*\* $p$  < 0.001 with respect to negative control (one-way ANOVA followed by the Newman–Keuls post-test).

## REFERENCES

- Alptekin, A., Galadari, S., Shuba, Y., Petroianu, G., and Oz, M. (2010). The effects of anandamide transport inhibitor AM404 on voltage-dependent calcium channels. *Eur. J. Pharmacol.* 634, 10–15. doi: 10.1016/j.ejphar.2010.02.013
- Beltramo, M., de Fonseca, F. R., Navarro, M., Calignano, A., Gorriti, M. A., Grammatikopoulos, G., et al. (2000). Reversal of dopamine D<sub>2</sub> receptor responses by an anandamide transport inhibitor. *J. Neurosci.* 20, 3401–3407. doi: 10.1523/JNEUROSCI.20-14-j0002.2000
- Beltramo, M., Stella, N., Calignano, A., Lin, S. Y., Makriyannis, A., and Piomelli, D. (1997). Functional role of high-affinity anandamide transport, as revealed by selective inhibition. *Science* 277, 1094–1097. doi: 10.1126/science.277.5329.1094
- Chang, H.-T., Huang, C.-C., Cheng, H.-H., Wang, J.-L., Lin, K.-L., Hsu, P.-T., et al. (2008). Mechanisms of AM404-induced [Ca<sup>2+</sup>]<sub>i</sub> rise and death in human osteosarcoma cells. *Toxicol. Lett.* 179, 53–58. doi: 10.1016/j.toxlet.2008.04.002
- Choi, D. (1988). Glutamate neurotoxicity and diseases of the nervous system. *Neuron* 1, 623–634. doi: 10.1016/0896-6273(88)90162-6
- Dawitz, J., Kroon, T., Hjorth, J. J. J., and Meredith, R. M. (2011). Functional calcium imaging in developing cortical networks. *J. Vis. Exp.* 56:e3550. doi: 10.3791/3550
- De Chiara, V., Motta, C., Rossi, S., Studer, V., Barbieri, F., Lauro, D., et al. (2013). Interleukin-1 $\beta$  alters the sensitivity of cannabinoid CB1 receptors controlling glutamate transmission in the striatum. *Neuroscience* 250, 232–239. doi: 10.1016/j.neuroscience.2013.06.069

- De Petrocellis, L., Bisogno, T., Davis, J. B., Pertwee, R. G., and Di Marzo, V. (2000). Overlap between the ligand recognition properties of the anandamide transporter and the VR1 vanilloid receptor: inhibitors of anandamide uptake with negligible capsaicin-like activity. *FEBS Lett.* 483, 52–56. doi: 10.1016/S0014-5793(00)02082-2
- Dong, X., Wang, Y., and Qin, Z. (2009). Molecular mechanisms of excitotoxicity and their relevance to pathogenesis of neurodegenerative diseases. *Acta Pharmacol. Sin.* 30, 379–387. doi: 10.1038/aps.2009.24
- Favrais, G., Schwendimann, L., Gressens, P., and Lelièvre, V. (2007). Cyclooxygenase-2 mediates the sensitizing effects of systemic IL-1 $\beta$  on excitotoxic brain lesions in newborn mice. *Neurobiol. Dis.* 25, 496–505. doi: 10.1016/j.nbd.2006.10.012
- Fernandez-Espejo, E., Caraballo, I., Rodriguez de Fonseca, F., Ferrer, B., El Banoua, F., Flores, J. A., et al. (2004). Experimental parkinsonism alters anandamide precursor synthesis and functional deficits are improved by AM404: a modulator of endocannabinoid function. *Neuropsychopharmacology* 29, 1134–1142. doi: 10.1038/sj.npp.1300407
- Fiebich, B. L., Mueksch, B., Boehringer, M., and Hüll, M. (2000). Interleukin-1 $\beta$  induces cyclooxygenase-2 and prostaglandin E<sub>2</sub> synthesis in human neuroblastoma cells: involvement of p38 mitogen-activated protein kinase and nuclear factor- $\kappa$ B. *J. Neurochem.* 75, 2020–2028. doi: 10.1046/j.1471-4159.2000.0752020.x
- Fleck, M. W., Barriónuevo, G., and Palmer, A. M. (2001). Synaptosomal and vesicular accumulation of L-glutamate, L-aspartate and D-aspartate. *Neurochem. Int.* 39, 217–225. doi: 10.1016/S0197-0186(01)00018-3
- Fogal, B., and Hewett, S. J. (2008). Interleukin-1 $\beta$ : a bridge between inflammation and excitotoxicity? *J. Neurochem.* 106, 1–23. doi: 10.1111/j.1471-4159.2008.05315.x
- García-Arencibia, M., González, S., de Lago, E., Ramos, J. A., Mechoulam, R., and Fernández-Ruiz, J. (2007). Evaluation of the neuroprotective effect of cannabinoids in a rat model of Parkinson's disease: importance of antioxidant and cannabinoid receptor-independent properties. *Brain Res.* 1134, 162–170. doi: 10.1016/j.brainres.2006.11.063
- Giuffrida, A., Rodriguez de Fonseca, F., Nava, F., Loubet-Lescoulié, P., and Piomelli, D. (2000). Elevated circulating levels of anandamide after administration of the transport inhibitor, AM404. *Eur. J. Pharmacol.* 408, 161–168. doi: 10.1016/S0014-2999(00)00786-x
- Gubellini, P., Picconi, B., Bari, M., Battista, N., Calabresi, P., Centonze, D., et al. (2002). Experimental parkinsonism alters endocannabinoid degradation: implications for striatal glutamatergic transmission. *J. Neurosci.* 22, 6900–6907. doi: 10.1523/JNEUROSCI.22-16-06900.2002
- Hampson, R. E., Miller, F., Palchik, G., and Deadwyler, S. A. (2011). Cannabinoid receptor activation modifies NMDA receptor mediated release of intracellular calcium: implications for endocannabinoid control of hippocampal neural plasticity. *Neuropharmacology* 60, 944–952. doi: 10.1016/j.neuropharm.2011.01.039
- Holz, A., Mülsch, F., Schwarz, M. K., Hollmann, M., Döbrössy, M. D., Coenen, V. A., et al. (2019). Enhanced mGlu5 signaling in excitatory neurons promotes rapid antidepressant effects via AMPA receptor activation. *Neuron* 104, 338.e7–352.e7. doi: 10.1016/j.neuron.2019.07.011
- Howlett, A. C., Bidaut-Russell, M., Devane, W. A., Melvin, L. S., Johnson, M. R., and Herkenham, M. (1990). The cannabinoid receptor: biochemical, anatomical and behavioral characterization. *Trends Neurosci.* 13, 420–423. doi: 10.1016/0166-2236(90)90124-s
- Howlett, A. C., Blume, L. C., and Dalton, G. D. (2010). CB(1) cannabinoid receptors and their associated proteins. *Curr. Med. Chem.* 17, 1382–1393. doi: 10.2174/092986710790980023
- Huang, H. J., Chen, S. L., Huang, H. Y., Sun, Y. C., Lee, G. C., Lee-Chen, G. J., et al. (2019). Chronic low dose of AM404 ameliorates the cognitive impairment and pathological features in hyperglycemic 3xTg-AD mice. *Psychopharmacology* 236, 763–773. doi: 10.1007/s00213-018-5108-0
- Kaindl, A., Degos, V., Peineau, S., Gouadon, E., Loron, G., Lombet, A., et al. (2008). Microglia express functional NMDA receptors: a novel finding and a promise for innovative treatment of excitotoxic and inflammatory brain disease. *Neuropediatrics* 39:V23. doi: 10.1055/s-0029-1215736
- Karanian, D. A., Brown, Q. B., Makriyannis, A., Kosten, T. A., and Bahr, B. A. (2005). Dual modulation of endocannabinoid transport and fatty acid amide hydrolase protects against excitotoxicity. *J. Neurosci.* 25, 7813–7820. doi: 10.1523/JNEUROSCI.2347-05.2005
- Kerckhove, N., Mallet, C., François, A., Boudes, M., Chemin, J., Voets, T., et al. (2014). Cav3.2 calcium channels: the key protagonist in the supraspinal effect of paracetamol. *Pain* 155, 764–772. doi: 10.1016/j.pain.2014.01.015
- Khanolkar, A. D., Abadji, V., Lin, S., Hill, W. A. G., Taha, G., Abouzid, K., et al. (1996). Head group analogs of arachidonyl ethanolamide, the endogenous cannabinoid ligand. *J. Med. Chem.* 39, 4515–4519. doi: 10.1021/jm960152y
- Lastres-Becker, I., de Miguel, R., De Petrocellis, L., Makriyannis, A., Di Marzo, V., and Fernández-Ruiz, J. (2003). Compounds acting at the endocannabinoid and/or endovanilloid systems reduce hyperkinesia in a rat model of Huntington's disease. *J. Neurochem.* 84, 1097–1109. doi: 10.1046/j.1471-4159.2003.01595.x
- Lastres-Becker, I., Hansen, H. H., Berrendero, F., De Miguel, R., Pérez-Rosado, A., Manzanares, J., et al. (2002). Alleviation of motor hyperactivity and neurochemical deficits by endocannabinoid uptake inhibition in a rat model of Huntington's disease: cannabinoid therapy in Huntington's disease. *Synapse* 44, 23–35. doi: 10.1002/syn.10054
- Lévenès, C., Daniel, H., Soubrié, P., and Crépel, F. (1998). Cannabinoids decrease excitatory synaptic transmission and impair long-term depression in rat cerebellar Purkinje cells. *J. Physiol.* 510, 867–879. doi: 10.1111/j.1469-7793.1998.867bj.x
- Mackie, K. (2005). "Distribution of cannabinoid receptors in the central and peripheral nervous system," in *Cannabinoids. Handbook of Experimental Pharmacology*, ed. R. G. Pertwee (Berlin/Heidelberg: Springer-Verlag), 299–325.
- Manna, S. S. S., and Umathe, S. N. (2012). Involvement of transient receptor potential vanilloid type 1 channels in the pro-convulsant effect of anandamide in pentylenetetrazole-induced seizures. *Epilepsy Res.* 100, 113–124. doi: 10.1016/j.eplepsyres.2012.02.003
- Marsicano, G., Goodenough, S., Monory, K., Hermann, H., Eder, M., Cannich, A., et al. (2003). CB1 cannabinoid receptors and on-demand defense against excitotoxicity. *Science* 302, 84–88. doi: 10.1126/science.1088208
- Mechoulam, R. (2003). Neuroscience: stout guards of the central nervous system. *Science* 302, 65–67. doi: 10.1126/science.1091256
- Milanesi, M., Zappettini, S., Jacchetti, E., Bonifacino, T., Cervetto, C., Usai, C., et al. (2010). *In vitro* activation of GAT1 transporters expressed in spinal cord gliosomes stimulates glutamate release that is abnormally elevated in the SOD1/G93A(+) mouse model of amyotrophic lateral sclerosis. *J. Neurochem.* 113, 489–501. doi: 10.1111/j.1471-4159.2010.06628.x
- Mitchell, V. A., Greenwood, R., Jayamanne, A., and Vaughan, C. W. (2007). Actions of the endocannabinoid transport inhibitor AM404 in neuropathic and inflammatory pain models. *Clin. Exp. Pharmacol. Physiol.* 34, 1186–1190. doi: 10.1111/j.1440-1681.2007.04692.x
- Musumeci, G., Grasselli, G., Rossi, S., De Chiara, V., Musella, A., Motta, C., et al. (2011). Transient receptor potential vanilloid 1 channels modulate the synaptic effects of TNF- $\alpha$  and of IL-1 $\beta$  in experimental autoimmune encephalomyelitis. *Neurobiol. Dis.* 43, 669–677. doi: 10.1016/j.nbd.2011.05.018
- Nazıglı, M., Taner, A. N., Balbay, E., and Çiğ, B. (2019). Inhibitions of anandamide transport and FAAH synthesis decrease apoptosis and oxidative stress through inhibition of TRPV1 channel in an *in vitro* seizure model. *Mol. Cell. Biochem.* 453, 143–155. doi: 10.1007/s11010-018-3439-0
- Palop, J. J., Chin, J., and Mucke, L. (2006). A network dysfunction perspective on neurodegenerative diseases. *Nature* 443, 768–773. doi: 10.1038/nature05289
- Pearson, V. L., Rothwell, N. J., and Toulmond, S. (1999). Excitotoxic brain damage in the rat induces interleukin-1 $\beta$  protein in microglia and astrocytes: correlation with the progression of cell death. *Glia* 25, 311–323. doi: 10.1002/(sici)1098-1136(19990215)25:4<311::aid-glia1>3.3.co;2-5
- Raiteri, L., Stigliani, S., Usai, C., Diaspro, A., Paluzzi, S., Milanesi, M., et al. (2008). Functional expression of release-regulating glycine transporters GLYT1 on GABAergic neurons and GLYT2 on astrocytes in mouse spinal cord. *Neurochem. Int.* 52, 103–112. doi: 10.1016/j.neuint.2007.04.027
- Raiteri, L., Zappettini, S., Milanesi, M., Fedele, E., Raiteri, M., and Bonanno, G. (2007). Mechanisms of glutamate release elicited in rat cerebrocortical nerve endings by 'pathologically' elevated extracellular K<sup>+</sup> concentrations. *J. Neurochem.* 103, 952–961. doi: 10.1111/j.1471-4159.2007.04784.x

- Ross, R. A. (2003). Anandamide and vanilloid TRPV1 receptors. *Br. J. Pharmacol.* 140, 790–801. doi: 10.1038/sj.bjp.0705467
- Rossi, S., Furlan, R., De Chiara, V., Motta, C., Studer, V., Mori, F., et al. (2012). Interleukin-1 $\beta$  causes synaptic hyperexcitability in multiple sclerosis. *Ann. Neurol.* 71, 76–83. doi: 10.1002/ana.22512
- Rossi, S., Motta, C., Studer, V., Macchiareulo, G., Volpe, E., Barbieri, F., et al. (2014). Interleukin-1 $\beta$  causes excitotoxic neurodegeneration and multiple sclerosis disease progression by activating the apoptotic protein p53. *Mol. Neurodegener.* 9:56. doi: 10.1186/1750-1326-9-56
- Saliba, S. W., Marcotequi, A. R., Fortwängler, E., Ditrich, J., Perazzo, J. C., Muñoz, E., et al. (2017a). AM404, paracetamol metabolite, prevents prostaglandin synthesis in activated microglia by inhibiting COX activity. *J. Neuroinflammation* 14:246. doi: 10.1186/s12974-017-1014-3
- Saliba, S. W., Vieira, E. L. M., de Santos, R. P. M., Candelario-Jalil, E., Fiebich, B. L., Vieira, L. B., et al. (2017b). Neuroprotective effects of intrastriatal injection of rapamycin in a mouse model of excitotoxicity induced by quinolinic acid. *J. Neuroinflammation* 14:25. doi: 10.1186/s12974-017-0793-x
- Scotter, E. L., Abood, M. E., and Glass, M. (2010). The endocannabinoid system as a target for the treatment of neurodegenerative disease: Endocannabinoids in neurodegenerative disease. *Br. J. Pharmacol.* 160, 480–498. doi: 10.1111/j.1476-5381.2010.00735.x
- Shen, M., Piser, T. M., Seybold, V. S., and Thayer, S. A. (1996). Cannabinoid receptor agonists inhibit glutamatergic synaptic transmission in rat hippocampal cultures. *J. Neurosci.* 16, 4322–4334. doi: 10.1523/JNEUROSCI.16-14-04322.1996
- Shubina, L., Aliev, R., and Kitchigina, V. (2015). Attenuation of kainic acid-induced status epilepticus by inhibition of endocannabinoid transport and degradation in guinea pigs. *Epilepsy Res.* 111, 33–44. doi: 10.1016/j.epilepsyres.2015.01.003
- Shubina, L., Aliev, R., and Kitchigina, V. (2017). Endocannabinoid-dependent protection against kainic acid-induced long-term alteration of brain oscillations in guinea pigs. *Brain Res.* 1661, 1–14. doi: 10.1016/j.brainres.2017.02.003
- Smart, D., Gunthorpe, M. J., Jerman, J. C., Nasir, S., Gray, J., Muir, A. I., et al. (2000). The endogenous lipid anandamide is a full agonist at the human vanilloid receptor (hVR1). *Br. J. Pharmacol.* 129, 227–230. doi: 10.1038/sj.bjp.0703050
- Tóth, A., Boczán, J., Kedei, N., Lizanecz, E., Bagi, Z., Papp, Z., et al. (2005). Expression and distribution of vanilloid receptor 1 (TRPV1) in the adult rat brain. *Mol. Brain Res.* 135, 162–168. doi: 10.1016/j.molbrainres.2004.12.003
- Tsou, K., Brown, S., Sañudo-Peña, M. C., Mackie, K., and Walker, J. M. (1998). Immunohistochemical distribution of cannabinoid CB1 receptors in the rat central nervous system. *Neuroscience* 83, 393–411. doi: 10.1016/s0306-4522(97)00436-3
- van der Stelt, M., Veldhuis, W. B., Maccarrone, M., Bär, P. R., Nicolay, K., Veldink, G. A., et al. (2002). Acute neuronal injury, excitotoxicity, and the endocannabinoid system. *Mol. Neurobiol.* 26, 317–346. doi: 10.1385/mn:26:2-3:317
- Veldhuis, W. B., van der Stelt, M., Wadman, M. W., van Zadelhoff, G., Maccarrone, M., Fezza, F., et al. (2003). Neuroprotection by the endogenous cannabinoid anandamide and arvanil against *in vivo* excitotoxicity in the rat: role of vanilloid receptors and lipoxygenases. *J. Neurosci.* 23, 4127–4133. doi: 10.1523/JNEUROSCI.23-10-04127.2003
- Vezzani, A., and Baram, T. Z. (2007). New roles for interleukin-1  $\beta$  in the mechanisms of epilepsy. *Epilepsy Curr.* 7, 45–50. doi: 10.1111/j.1535-7511.2007.00165.x
- Viviani, B., Bartsaghi, S., Gardoni, F., Vezzani, A., Behrens, M. M., Bartfai, T., et al. (2003). Interleukin-1 $\beta$  enhances NMDA receptor-mediated intracellular calcium increase through activation of the Src family of kinases. *J. Neurosci.* 23, 8692–8700. doi: 10.1523/JNEUROSCI.23-25-08692.2003
- Waxman, E. A., and Lynch, D. R. (2005). N-methyl-D-aspartate receptor subtypes: multiple roles in excitotoxicity and neurological disease. *Neuroscientist* 11, 37–49. doi: 10.1177/1073858404269012
- Zani, A., Braid, D., Capurro, V., and Sala, M. (2007).  $\Delta$ 9-tetrahydrocannabinol (THC) and AM 404 protect against cerebral ischemia in gerbils through a mechanism involving cannabinoid and opioid receptors. *Br. J. Pharmacol.* 152, 1301–1311. doi: 10.1038/sj.bjp.0707514
- Zygmunt, P. M., Chuang, H., Movahed, P., Julius, D., and Högestätt, E. D. (2000). The anandamide transport inhibitor AM404 activates vanilloid receptors. *Eur. J. Pharmacol.* 396, 39–42. doi: 10.1016/s0014-2999(00)00207-7

**Conflict of Interest:** The authors declare that the research was conducted in the absence of any commercial or financial relationships that could be construed as a potential conflict of interest.

Copyright © 2019 Saliba, Bonifacino, Serchov, Bonanno, de Oliveira and Fiebich. This is an open-access article distributed under the terms of the Creative Commons Attribution License (CC BY). The use, distribution or reproduction in other forums is permitted, provided the original author(s) and the copyright owner(s) are credited and that the original publication in this journal is cited, in accordance with accepted academic practice. No use, distribution or reproduction is permitted which does not comply with these terms.





# Early Neurotoxic Effects of Inorganic Arsenic Modulate Cortical GSH Levels Associated With the Activation of the Nrf2 and NF $\kappa$ B Pathways, Expression of Amino Acid Transporters and NMDA Receptors and the Production of Hydrogen Sulfide

Daniela Silva-Adaya<sup>1,2</sup>, Lucio Antonio Ramos-Chávez<sup>3</sup>, Pavel Petrosyan<sup>1</sup>, Wendy Leslie González-Alfonso<sup>1</sup>, Alegna Pérez-Acosta<sup>1</sup> and Maria E. Gonsébat<sup>1\*</sup>

<sup>1</sup>Departamento de Medicina Genómica, Instituto de Investigaciones Biomédicas, Universidad Nacional Autónoma de México, México, Mexico, <sup>2</sup>Laboratorio Experimental de Enfermedades Neurodegenerativas, Instituto Nacional de Neurología y Neurocirugía, México, Mexico, <sup>3</sup>Departamento de Neuroquímica, Subdirección de Investigaciones Clínicas, Instituto Nacional de Psiquiatría Ramón de la Fuente, Ciudad de México, México, Mexico

## OPEN ACCESS

### Edited by:

Rocío Martínez De Pablos,  
University of Seville, Spain

### Reviewed by:

Fawaz Alasmari,  
King Saud University, Saudi Arabia  
Koji Aoyama,  
Teikyo University, Japan

### \*Correspondence:

Maria E. Gonsébat  
margen@unam.mx

**Received:** 01 November 2019

**Accepted:** 21 January 2020

**Published:** 25 February 2020

### Citation:

Silva-Adaya D, Ramos-Chávez LA, Petrosyan P, González-Alfonso WL, Pérez-Acosta A and Gonsébat ME (2020) Early Neurotoxic Effects of Inorganic Arsenic Modulate Cortical GSH Levels Associated With the Activation of the Nrf2 and NF $\kappa$ B Pathways, Expression of Amino Acid Transporters and NMDA Receptors and the Production of Hydrogen Sulfide. *Front. Cell. Neurosci.* 14:17. doi: 10.3389/fncel.2020.00017

Exposure to toxic metals and metalloids is an important cause of preventable diseases worldwide. Inorganic arsenic (iAs) affects several organs and tissues, causing neurobehavioral alterations in the central nervous system (CNS) that might lead to neurodegeneration. In this work, we wanted to explore the time- and dose-related changes on glutathione (GSH) levels in several regions of the CNS, such as the cortex, striatum, hippocampus, and cerebellum, to identify the initial cellular changes associated to GSH depletion due to iAs exposure. Mice received a single intraperitoneal injection containing 5 or 14 mg/kg sodium arsenite. Animals were killed at 2, 6, and 24 h. Significant depletion of GSH levels was observed in the cortex at 2 and 6 h, while on the striatum, hippocampus, or cerebellum regions, no significant changes were observed. GSH depletion in the cortex was associated with the activation of the nuclear factor erythroid 2-related factor 2 (Nrf2) and nuclear factor kappa B (NF $\kappa$ B) pathways, which led to the upregulation of xCT, excitatory amino acid carrier 1 (EAAC1), glutamate/aspartate transporter (GLAST), and glial glutamate transporter 1 (GLT-1), and the activation of the transsulfuration pathways, which led to the overproduction of H<sub>2</sub>S in the cortex and increased levels of GSH in the cortex and cerebellum at 24 h. In the cortex, the *N*-methyl-D-aspartate (NMDA) receptor subunits NR2A and NR2B were also altered at 24 h. These early effects were not homogeneous among different brain regions and indicate early neurotoxic alterations in the cortex and cerebellum.

**Keywords:** arsenic, GSH, Nrf2, NF $\kappa$ B, CNS cysteine/glutamate transporters, H<sub>2</sub>S

## INTRODUCTION

Improvements in the quality of life of humans is reflected in the increase in our life span; however, environmental pollution continues to be the largest cause of disease and premature death worldwide (Landrigan et al., 2018). The overexploitation of water resources exposes a continuously increasing number of people to toxic elements such as pesticides, nitrites, and metals (Kurwadkar, 2017). Arsenic is an element widely distributed on earth in soil and minerals that, naturally or due to anthropogenic activities, might enter the air, water, or food. Today, human exposure to this toxic element occurs mainly through drinking water or food and represents a worldwide problem affecting over 200 million people. Cardiovascular, endocrine, immune, and neurotoxic effects and several types of cancer have been associated with inorganic arsenic (iAs) exposure (Hong et al., 2014).

Acute neurotoxic effects after oral doses include mild to severe encephalopathy, depending on the dose. Symptoms include confusion, hallucinations, reduced memory, and emotional lability (exaggerated changes in mood or affect; Garza-Lombó et al., 2018a,b, 2019). On the other hand, chronic exposure to iAs is associated with the development of peripheral neuropathies (Garza-Lombó et al., 2019). Furthermore, in children exposed to iAs concentrations ranging from 5 to 50 ppb in drinking water, neurobehavioral alterations such as impaired cognitive functions, verbal abilities, and long-term memory, and decreased motor skills have been reported (Calderón et al., 2001; Parvez et al., 2011). However, it is not clear when the initial effects are observed in the central nervous system (CNS; Garza-Lombó et al., 2019).

iAs crosses the blood-brain barrier and accumulates in different brain regions where it is methylated by  $As^{3+}$  methyltransferase, a process that requires thioredoxin or glutathione (GSH) as a reductive agent and S-adenosyl methionine (SAM) as the methyl donor (Thomas et al., 2004; Sánchez-Peña et al., 2010). The SAM pathway and GSH production are linked through the transsulfuration pathway (Rodríguez et al., 2005). In addition, regions with higher energy demand, such as the cortex and CA3/CA4 regions of the hippocampus or cerebellum, show the highest GSH levels and thioredoxin immunoreactivity (Sánchez-Peña et al., 2010).

Owing to its high oxygen consumption and low levels of antioxidant enzymes, the brain is vulnerable to the harmful effects of reactive oxygen species (ROS). GSH is the most important endogenous antioxidant in the CNS and plays an important role in the maintenance of the intracellular redox balance and the detoxification of xenobiotics (Gu et al., 2015), being also considered a cysteine and glutamate reservoir in the brain. Intracellular GSH synthesis requires the availability of its precursor amino acids: L-cysteine (L-cys), L-glutamate (L-glu), and L-glycine (L-gly; Robert et al., 2014). Cysteine is the limiting amino acid for GSH; thus, it is continuously imported or synthesized, depending on the cell type. For example, cystine (the oxidized form of cysteine) is taken up into glial cells by the antiporter system xc<sup>-</sup> (Xc<sup>-</sup>), which is a Na<sup>+</sup>-independent, Cl<sup>-</sup>-dependent cystine/glutamate exchanger

composed of the catalytic subunit xCT and the structural heavy chain 4F2 cell surface antigen (4F2hc). In the brain, the Xc<sup>-</sup> system is predominately expressed in astrocytes (Bannai, 1986; Robert et al., 2014). On the other hand, a member of the family of excitatory amino acid transporters (EAAT), mainly EAAT3 [excitatory amino acid carrier 1 (EAAC1) in mouse], is an important importer of L-cys in neurons that is present at much lower levels than glutamate or glycine (Aoyama et al., 2012). Therefore, EAAT3/EAAC1 supplies the rate-limiting substrate for GSH synthesis in neurons, while other members of this family, such as EAAT1 or glutamate/aspartate transporter (GLAST) and EAAT2 or glial glutamate transporter 1 (GLT-1), are expressed in glia and participate in the uptake of L-glu (Valdovinos-Flores and Gensebatt, 2012). Aoyama et al. (2006) reported that EAAC1-knockout mice have decreased neuronal GSH and increased neuronal oxidative stress. These effects were reversed when the animals received the membrane-permeable L-cys precursor *N*-acetylcysteine (Aoyama et al., 2006). We have observed that gestational exposure to iAs through drinking water induced the upregulation of xCT, which was associated with increased levels of GSH in the cortex and hippocampus (Ramos-Chávez et al., 2015; Nelson-Mora et al., 2018). In addition, the overexpression of xCT leads to increased extracellular glutamate and to the downregulation of both *N*-methyl-D-aspartate (NMDA) and  $\alpha$ -amino-3-hydroxy-5-methyl-4-isoxazolepropionic acid (AMPA) ionotropic glutamate receptors, with significant negative effects on learning and memory (Ramos-Chávez et al., 2015; Nelson-Mora et al., 2018).

The L-cys required for GSH synthesis in astrocytes can also be generated from methionine through the transsulfuration pathway by the action of cystathionine- $\beta$ -synthase (CBS) and cystathionine- $\gamma$ -lyase (CSE; McBean, 2017). In this respect, Coppin et al. (2008) reported CBS upregulation in transformed cultured cells after protracted exposure to iAs that led to increased GSH levels. Moreover, CBS, CSE, and 3-mercaptopyruvate sulfurtransferase (Chen et al., 2004; Singh et al., 2009) are producers of endogenous hydrogen sulfur (H<sub>2</sub>S), a neuromodulator present in the brain that, in excess, could have detrimental effects. CBS is predominantly expressed in the brain and has been associated with the modulation of NMDA receptor (NMDAR)-mediated responses (Huang and Moore, 2015).

Here, we wanted to investigate the early time- and dose-related changes on GSH levels in several regions of the CNS such as the cortex, striatum, hippocampus, and cerebellum, identifying initial cellular changes associated to GSH depletion due to iAs exposure.

## MATERIALS AND METHODS

### Chemicals and Antibodies

All chemicals were purchased from Sigma-Aldrich (St. Louis, MO, USA) unless otherwise indicated. For Western blots, primary rabbit antibodies against xCT, EAAC1, GLAST, GLT-1, and CBS (Abcam Cat# ab37185, RRID:AB\_778944; Abcam Cat# ab124802, RRID:AB\_10974334; Abcam Cat# ab416, RRID:AB\_304334; Abcam Cat# ab41621, RRID:AB\_941782;

Abcam Cat# ab135626, RRID:AB\_2814659, respectively) were obtained from Abcam (Cambridge, MA, USA). Primary anti-NR2A and anti-NR2B (Millipore Cat# AB1555P, RRID:AB\_90770; Millipore Cat# AB1557P, RRID:AB\_90772, respectively) antibodies were purchased from Millipore, Bedford, MA, USA. Primary anti-L-type amino acid transporter 1 (anti-LAT1; Santa Cruz Biotechnology Cat# sc-34554, RRID:AB\_2270583) antibodies were obtained from Santa Cruz Biotechnology (Santa Cruz, CA, USA). Rabbit antimouse  $\beta$ -tubulin (Sigma-Aldrich Cat# T4026, RRID:AB\_477577) was purchased from Sigma-Aldrich.

## Animals and Treatment

Five- to six-week-old male CD-1 mice were obtained from the Animal Care Facility at the Instituto de Investigaciones Biomédicas, UNAM and were maintained at 23–25°C under a 12-h light/dark cycle and relative humidity of 50–60%. Animals had free access to standard food (Harlan 2018S Diet; Harlan, Indianapolis, IN, USA) and water.

Animals were divided into different working groups. To study the acute response, they received an intraperitoneal (i.p.) injection (100  $\mu$ l) containing 0, 5, or 14 mg of sodium arsenite per kilogram of body weight. Controls received an i.p. injection of 100  $\mu$ l of isotonic saline solution. Animals were killed at 2, 6, and 24 h after i.p. injection. A semichronic treatment group to compare the acute response was designed. In this group, the animals received i.p. injections containing 0, 2.5, and 5 mg of sodium arsenite per kilogram of body weight per day for 9 days. Sodium arsenite solutions were prepared daily and dissolved in injectable water.

Animals were killed by cervical dislocation, followed by decapitation. Different brain regions were dissected for immunoblotting determination. To determine GSH and/or to generate the membrane-enriched integral protein fractions and to measure H<sub>2</sub>S, tissue samples were immediately homogenized in their respective buffers and kept frozen at –80°C until analysis.

The experiments were performed following the guidelines stated in the “Principles of Laboratory Animal Care” (NIH publication #85-23, revised 1985) and “Especificaciones técnicas para la producción, cuidado y uso de los animales de laboratorio (Clave NOM-062-ZOO-1999)” of the “Norma Oficial Mexicana de la Secretaría de Agricultura, Ganadería, Desarrollo Rural, Pesca y Alimentación (SAGARPA)” (published in August 2001).

## GSH Level Determination

The levels of reduced GSH were measured in the cortex, hippocampus, striatum, and cerebellum using a microplate-adapted fluorometric o-phthalaldehyde (OPA) method (Ramos-Chávez et al., 2015). The method is based on the GSH reaction with o-phthalaldehyde (OPA) to form a highly stable and fluorescent isoindole derivative. Briefly, wet tissue was homogenized in 10 volumes of ice-cold buffer (154 mM KCl, 5 mM diethylenetriaminepentaacetic acid, and 0.1 M potassium phosphate buffer, pH 6.8). Immediately thereafter, equal volumes of cold acid buffer [40 mM HCl, 10 mM DTPA, 20 mM ascorbic acid, and 10% trichloroacetic acid (TCA)] were added

to one volume of homogenate. Two microliters of supernatant was used for GSH determination. Fluorescence was determined with 365 nm excitation and 430 nm emission filters in a DTX 800/880 Multimode Detector (Beckman Coulter, Fullerton, CA, USA).

## Western Blotting

Western blot assays for CBS determination were performed as follows. Total tissue was homogenized in ice-cold lysis buffer [50 mM Tris-HCl, 150 mM NaCl, 2 mM EDTA, 1 mM ethylene glycol tetraacetic acid (EGTA), 2.5 mM sodium pyrophosphate, 1 mM glycerol-2-phosphate, 1 mM sodium orthovanadate, 1% Triton X-100, 1 mM dithiothreitol (DTT), 1 mM phenylmethylsulfonyl fluoride (PMSF), and inhibitor protease cocktail], containing protease inhibitor cocktail. The homogenates were centrifuged at 15,000  $\times$  g for 15 min at 4°C. Membrane-enriched integral protein fractions were obtained from frozen tissue samples as described by Schindler et al. (2006) for the Western blot analysis of xCT, EAAC1, LAT1, GLAST, GLT-1, NR2A, and NR2B. Frozen tissues were homogenized in 20 volumes of CLB buffer containing 10 mM HEPES, 10 mM NaCl, 1 mM KH<sub>2</sub>PO<sub>4</sub>, 5 mM NaHCO<sub>3</sub>, 5 mM EDTA, 1 mM CaCl<sub>2</sub>, 0.5 mM MgCl<sub>2</sub>, 1 mM PMSF, and inhibitor protease cocktail. The homogenates were centrifuged at 6,300  $\times$  g for 15 min at 4°C. The supernatants were recovered and centrifuged at 100,000  $\times$  g for 30 min at 4°C. The pellets were finally suspended in 150  $\mu$ l of 40 mM Tris-HCl at pH 9.5, 8 M urea, and 4% (w/v) Triton X-100. Protein concentrations were quantified using a Pierce BCA protein assay kit (Thermo Scientific, Rockford, IL, USA).

The samples (20–40  $\mu$ g of protein per well) were subjected to sodium dodecyl sulfate polyacrylamide gel electrophoresis (SDS-PAGE) and transferred onto nitrocellulose membranes (Bio-Rad Laboratories, Germany). The membranes were blocked with Tris-buffered saline (TBS) containing 5% Blotto and 0.1% Tween-20 and incubated overnight at 4°C with the appropriate primary antibodies (CBS, 1:1,000; xCT, 1:2,000; EAAC1, 1:2,000; LAT1, 1:1,000; GLAST, 1:2,000; GLT-1, 1:2,000). The blots were probed with mouse anti- $\beta$ -tubulin (1:5,000) after stripping, which was used as a loading control. The protein bands were visualized with appropriate horseradish peroxidase (HRP)-linked secondary antibodies using the ECL Prime Western Blotting Detection Reagent (GE Healthcare Bio-Sciences, Pittsburgh, PA, USA). Images were captured, and densitometric analysis was performed with ImageJ software version 1.46r software (US National Institutes of Health, Bethesda, MD, USA).

## Quantitative RT-PCR Analysis of *nfe2l2* and *ikkb*

Total RNA from the cortex of mice was isolated using TRIzol (Invitrogen, Carlsbad, CA, USA). The RNA integrity of the samples was assessed by electrophoresis in 1% agarose gels. The absorbance indices  $A_{260/280}$  and  $A_{260/230}$  were used to assess the purity of the isolated RNA. RNA concentrations were determined by measuring the absorbance at 260 nm. One microgram of total RNA from successful individual samples

was reverse transcribed to complementary DNA (cDNA) at 37°C using Moloney murine leukemia virus (M-MLV) reverse transcriptase and oligo(dT)15 primer (Promega, Madison, WI, USA). For quantitative PCR analysis, the cDNA of individual samples was diluted to 20 ng of input total RNA in a reaction mixture containing 0.5  $\mu$ M of each respective forward and reverse primer and 1 $\times$  KAPA SYBR FAST Universal Mix (Kapa Biosystems, Cape Town, South Africa). A Rotor-Gene Q PCR cyclor (Qiagen GmbH, Hilden, Germany) was used to quantify PCR products. The PCR conditions were an initial heating at 94°C for 3 min, followed by 40 cycles of 94°C for 1 s, 63°C for 10 s, and 72°C for 12 s. Finally, melting curves were generated from 73 to 93°C for each PCR run. Succinate dehydrogenase (*SDHA*) was used as the reference gene. The mean amplification efficiency calculated in each PCR run for *nfe2l2*, *ikkb $\alpha$* , and *SDHA* from fivefold dilution curves was  $1.017 \pm 0.035$  (standard deviation), with  $R^2$  being  $0.993 \pm 0.005$  (all above 0.982). The primers used were as follows: 5'-caccagtggatccgcagcta-3' and 5'-tatccagggaagcgactca-3' for *nfe2l2* (Valdovinos-Flores et al., 2019); 5'-aaatctccagatgtaccgagag-3' and 5'-ataatgtcagacgtggcctccaa-3' for *ikkb $\alpha$*  (Valdovinos-Flores and Gensebatt, 2013); and 5'-caaagtctggagaagaatcggt-3' and 5'-catcgacttctgcatgttaggc-3' for *SDHA*. The results were analyzed using the  $2^{-\Delta\Delta CT}$  method (Livak and Schmittgen, 2001) and expressed as the mean normalized *nrf2* and *ikkb $\alpha$*  values  $\pm$  SD.

## Measurement of Hydrogen Sulfide Production

We followed the protocol described by Hine and Mitchell (2017) with some adaptations. Briefly,  $\sim$ 100 mg of frozen cortex or liver samples was homogenized in 250  $\mu$ l of ice-cold lysis buffer (25 mM Tris Base, 1 mM DTT, 5% glycerol, 1% Triton) after homogenization. The samples were placed at 37°C for 5–10 min and frozen again in dry ice for 2–3 min. The freeze–thaw cycle was repeated three times. Supernatants ( $\sim$ 200  $\mu$ l) were removed after the homogenates were centrifuged at  $5,000\times g$  for 5 min at 4°C. Protein concentration was determined using the Pierce BCA Protein Assay kit (Thermo Fisher Scientific, Rockford, IL, USA). Filter papers were soaked in 20 mM lead (II) acetate trihydrate for 20 min and subsequently dried in an oven set at 110°C for 30 min. The assay was run in a 96-well plate with 150  $\mu$ l of the L-cysteine [100 mM in phosphate-buffered solution (PBS)] and pyridoxal 5'-phosphate (PLP; 10 mM in PBS) working solutions and 0–500  $\mu$ g of sample protein. Liver samples from untreated animals were used as positive controls. The dry lead acetate-embedded filter paper was placed directly over the 96-well plate and incubated at 37°C for 6 h for liver homogenates and 16 h (overnight) for cortex homogenates. The images were scanned, and densitometric analysis was performed with ImageJ software version 1.46r software (US National Institutes of Health, Bethesda, MD, USA).

## Data Analysis

The data are expressed as the mean  $\pm$  standard error. The number of animals tested is indicated in each case. One- and two-way analysis of variance (ANOVA) were used to

assess statistical significance followed by Tukey's *post hoc* test, as indicated in the corresponding figures. A  $P < 0.05$  was considered statistically significant in all cases.

## RESULTS

### GSH Levels in the Cortex, Striatum, and Cerebellum Are Affected by iAs

Mice with prolonged exposure to iAs show increased levels of GSH (Ramos-Chávez et al., 2015). Here, significantly decreased levels of GSH were observed in the brain cortex region at 2 and 6 h for both doses of iAs and at 24 h in the animals treated with the highest dose (Figures 1A–C), while animals treated with 5 mg/kg showed upregulated GSH synthesis at 24 h (Figure 1C) in both the cortex, striatum, and cerebellum, suggesting that GSH was actively synthesized in these regions at that time. Animals treated with the highest dose also showed increased levels of GSH in the cerebellum at 24 h (Figure 1C). We measured the levels of GSH in the cortex of animals that received iAs for 9 days and observed a similar dose-related increase in the GSH levels in the cortex (Figure 1D). In the cerebellum, the increase in GSH levels at 9 days was higher than that observed at 2 and 6 h, respectively.

### Expression of xCT and EAAC1 in the Cortex Is Related to GSH Synthesis and to GLT-1 and GLAST Upregulation

At the times tested, the cortex was the brain region where significant changes in protein expression were observed. No changes in the expression of LAT1, EAAC1, or xCT were observed at 2 and 6 h after treatment (Figures 2A–C). However, at 24 h, enhanced expression of EAAC1 and xCT was observed in the 5 and 14 mg/kg iAs-treated groups, respectively (Figures 2A,B). The upregulation of EAAC1 expression was maintained in the 9-day 5 mg/kg (Figure 2A) semichronic iAs treatment group, while xCT expression in both chronic treatment groups decreased (Figure 2B).

The modulation of EAAC1 expression in both the 5 mg/kg group 24 h after injection and in the 9-day 5 mg/kg chronic iAs treatment group was directly related to the modulation of GSH levels (Figures 1, 2A), suggesting the importance of cystine uptake by EAAC1 into the cells to synthesize GSH, mainly in neurons.

No changes in the expression of GLT-1 and GLAST were observed at 2 or 6 h or in the 9-day treatment group (Figures 2D,E). However, enhanced expression of GLT-1 and GLAST (Figures 2D,E) was associated with xCT and EAAC1 upregulation at 24 h in 5 mg/kg iAs-treated animals (Figures 2A,B).

### Modulation of NR2A and NR2B Expression

Chronic exposure to iAs was associated with increased extracellular glutamate and the negative modulation of the expression and activity of the NMDAR subunits NR2A and NR2B (Luo et al., 2009, 2012; Ramos-Chávez et al., 2015; Nelson-Mora et al., 2018). In the cortex, NMDAR acts as a detector for activity-dependent plasticity and associative learning (Hasan et al., 2013). We decided to evaluate the expression of



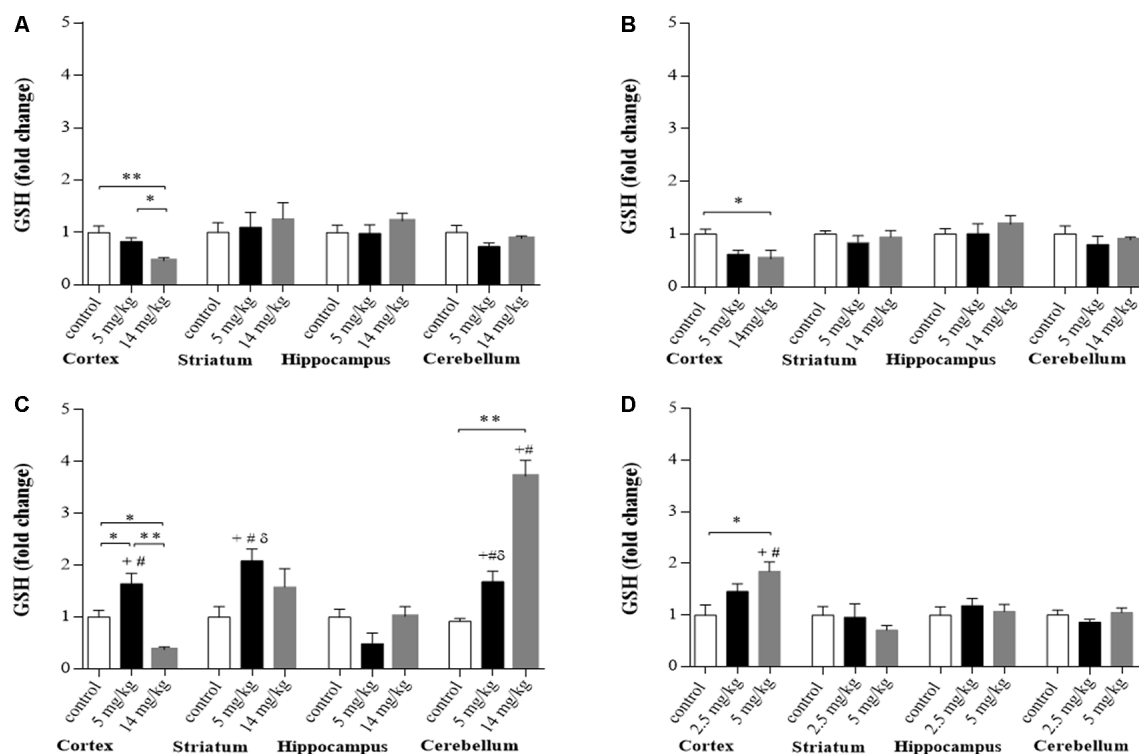


**FIGURE 1 |** Glutathione (GSH) levels in different brain regions of mice treated i.p. with 0 (controls), 2.5, 5, or 14 mg/kg NaAsO<sub>2</sub>. Normalized levels of GSH ratios in animals treated with 5 and 14 mg/kg at 2 h (A), 6 h (B), and 24 h (C) and animals treated with 0, 2.5, or 5 mg/kg for 9 days (D). Data in graphs represent the mean  $\pm$  SE,  $n = 6$ . The data were analyzed using one and two-way analysis of variance (ANOVA) with Tukey's *post hoc* analysis. Different superscript symbols above each column indicate statistically significant differences; \* $P \leq 0.05$  and \*\* $P \leq 0.01$  for dose-related differences; plus symbol denotes differences from the 2 h group, number symbol denotes differences from the 6 h and delta symbol denotes differences from 9-day treatment. Significance was accepted at  $P \leq 0.05$ .

these subunits at 24 h because the expression of GLT-1 and GLAST transporters was enhanced at this timepoint. NR2A subunit expression was increased, while NR2B subunit levels were decreased (Figure 3) only in those animals receiving the highest dose (14 mg/kg group).

## CBS Protein Expression

CBS is the dominant enzyme of the transsulfuration pathway in astrocytes, which provides cysteine for GSH synthesis (Lee et al., 2009; McBean, 2012; Niu et al., 2015). In addition, Coppin et al. (2008) showed that iAs induces GSH synthesis and the transcription of CBS in cultured human cells. In our model, CBS protein levels (Figure 4) were not upregulated in the cortex at any of the times explored, even though GSH levels increased at 24 h in this region (Figure 1).

## Increased Transcription of *nfe2l2* and *ikkb* at 6 h Suggests Nrf2 and NF $\kappa$ B Activation Is Associated with Diminished GSH Pools and Upregulated Amino Acid Transporters

Putative nuclear factor erythroid 2-related factor 2 (Nrf2) and nuclear factor kappa B (NF $\kappa$ B) binding sites have been reported for xCT, LAT, GLT-1, and GLAST (Valdovinos-Flores and

Gonsebatt, 2012; Martinez-Lozada et al., 2016). In addition, there is evidence that NF $\kappa$ B inhibitors diminish the expression of EAAC1 in rats (Tai et al., 2008). Nrf2 and NF $\kappa$ B upregulate the transcription of the *nfe2l2* and *ikkb* genes, respectively (Valdovinos-Flores and Gonsebatt, 2013; Tonelli et al., 2018) and are considered redox-sensitive switches that activate cellular responses to oxidative stress (Moldogazieva et al., 2018). To investigate whether the activation of these transcription factors was associated with increased amino acid transporter expression and increased GSH levels at 24 h, we measured the transcription of the *nfe2l2* and *ikkb* genes by quantitative reverse transcription PCR (RT-PCR) at 2, 6 and 24 h in the cortex region. A significant increase in the levels of *ikkb* messenger RNA (mRNA) was observed at 6 h, while only *nfe2l2* mRNA was significantly increased by the 5 mg/kg dose at this time. At 24 h, the transcription of both genes returned to control levels or below control levels (Figures 5A,B), suggesting the participation of both transcription factors in this acute response to iAs.

## H<sub>2</sub>S Production

Cortex homogenates were assayed for H<sub>2</sub>S production at 24 h, since CBS was not upregulated at this time. H<sub>2</sub>S production

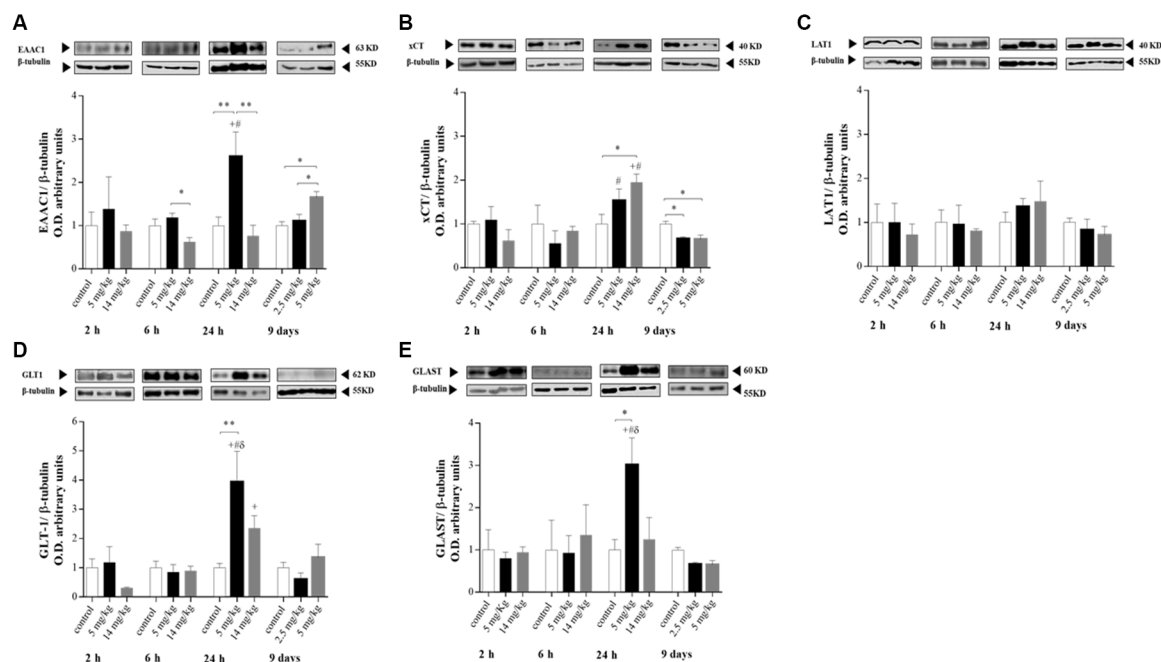


**FIGURE 2 |** Protein levels of the amino acid transporters excitatory amino acid transporter 3 (EAAC3; **A**), xCT (**B**), L-type amino acid transporter 1 (LAT1; **C**), glial glutamate transporter 1 (GLT-1; **D**), and glutamate/aspartate transporter (GLAST; **E**) in the cortex of mice treated with 0, 2.5, 5, or 14 mg/kg NaAsO<sub>2</sub>. Changes in the protein levels in the enriched membrane fraction were evaluated by Western blot analysis at 2, 6, 24 h and 9 days after the last NaAsO<sub>2</sub> administration. Bars represent the densitometric analysis of the protein bands normalized to β-tubulin, mean ± SE,  $n = 6$ . The data were analyzed using one and two-way ANOVA with Tukey's *post hoc* analysis. Different superscript symbols above each column indicate statistically significant differences; \* $P \leq 0.05$ , \*\* $P \leq 0.01$  for dose-related differences; plus symbol denotes differences from the 2 h group, number symbol denotes differences from the 6 h group, and delta symbol denotes differences from 9 days group. Significance was accepted at  $P \leq 0.05$ .

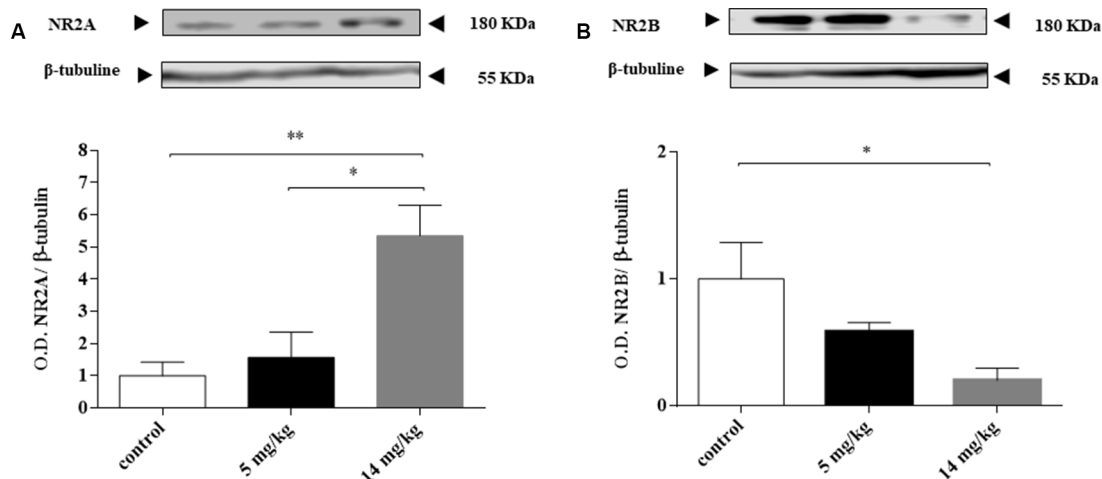
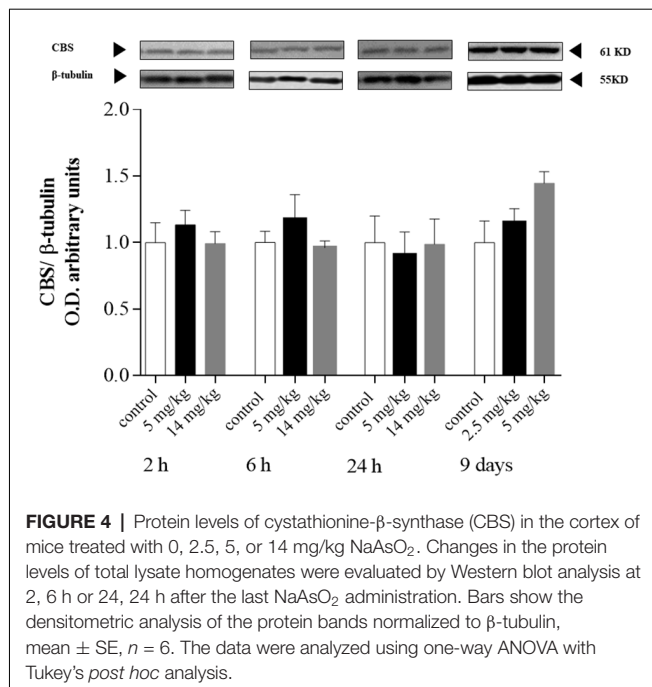


**FIGURE 3 |** Inorganic arsenic (iAs) effect on the protein levels of the *N*-methyl-D-aspartate receptor (NMDAR) subunits NR2A (**A**) and NR2B (**B**) in the cortex of mice treated with 0, 5, or 14 mg/kg NaAsO<sub>2</sub>. Changes in the protein levels in the enriched membrane fraction were evaluated by Western blot analysis 24 h after the last NaAsO<sub>2</sub> administration. Bars show the densitometric analysis of the protein bands normalized to β-tubulin, mean ± SE,  $n = 6$ . The data were analyzed using one-way ANOVA with Tukey's *post hoc* analysis. Different superscript symbols above each column indicate statistically significant differences; \* $P \leq 0.05$ , \*\* $P \leq 0.01$ .

has been directly related to the activity of CBS in the brain, providing L-cys for GSH synthesis *via* transsulfuration from methionine sources (Kandil et al., 2010). IAs-treated animals

(5 and 14 mg/kg) showed a significantly higher production of the neuromodulator than did the control animals (**Figure 6**), suggesting that enhanced CBS (and or CSE) enzymatic activity



is associated with the increased GSH synthesis observed in the 5-mg/kg treated animals.

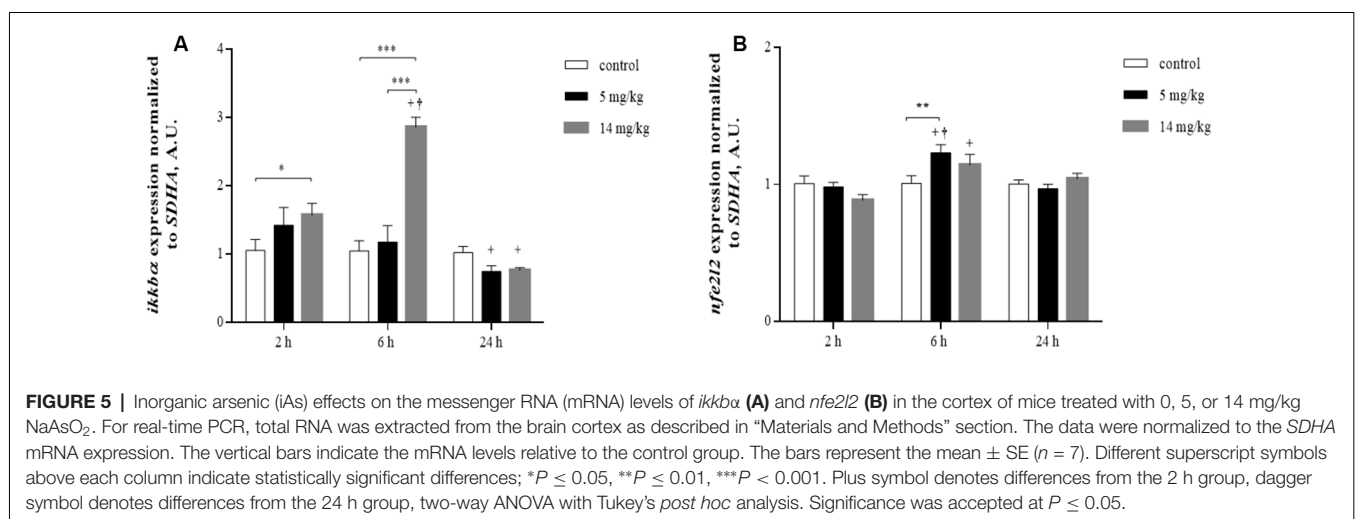
## DISCUSSION

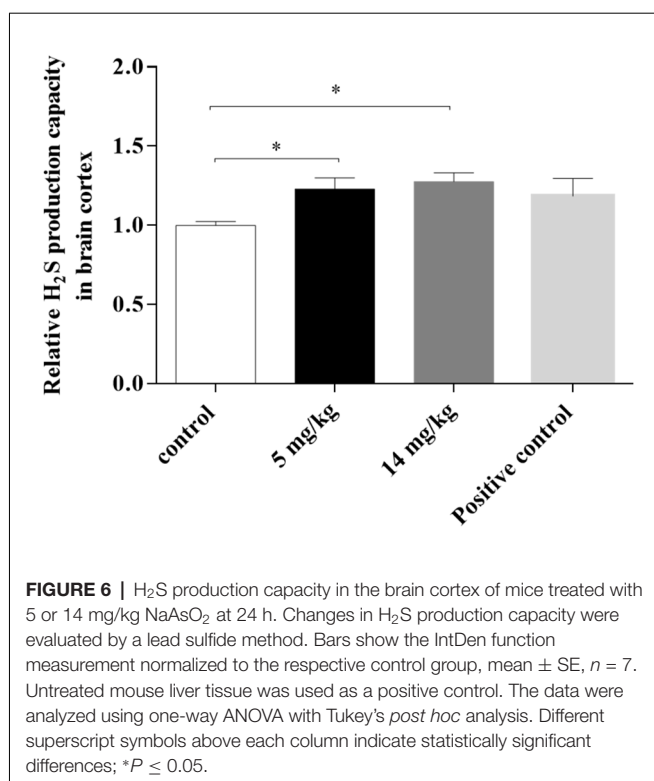
In this acute exposure study, we observed that iAs exposure altered GSH levels and the disposition of key amino acids and their transporters in the cortex and cerebellum. At 24 h, a redox response, probably activated by Nrf2 and NFκB (Figure 5), was observed mainly in the cortex region with increased GSH levels that were associated with the increased production of H<sub>2</sub>S and the upregulation of xCT, GLT-1, GLAST, and EAAC1. In addition, the expression of NMDA subunits was altered at the highest dose employed.

Sato et al. (2001) reported a putative NFκB binding site in the 5'-flanking region of the xCT gene. In addition, NFκB binding sites have been reported for GLT-1 and GLAST (Martinez-Lozada et al., 2016; Pajarillo et al., 2019), and NFκB inhibitors diminished EAAC1 expression (Tai et al., 2008). Evidence shows that both transcription factors are key molecules in redox signal transduction pathways (Valdovinos-Flores and Gonsbatt, 2012; Moldogazieva et al., 2018).

The effects of iAs could be observed as early as 2 and 6 h when GSH levels were diminished significantly, mainly in the cortex region (Figure 1A), which could activate the redox response observed at 6 h by the activation of Nrf2 and NFκB (Figure 5). Valdovinos-Flores and Gonsbatt (2013) observed significant transcription of *ngfb* at 2 h after a 14-mg/kg iAs i.p. injection, which was associated with the activation of the TrkA/Akt/NFκB signaling pathway in the liver but not in the striatum of mice (Valdovinos-Flores et al., 2019). However, systemic activation of this pathway could induce GSH synthesis in other brain regions such as the cortex and cerebellum at 24 h and 9 days (Figures 1C,D). Increased levels of GSH were observed in mouse brain homogenates (Limón-Pacheco et al., 2007) and in the cerebellum at 2 h after the administration of L-buthionine-S-R-sulfoximine (BSO), a systemic inhibitor of GSH synthesis, which diminished GSH levels in the liver and kidneys (Limón-Pacheco et al., 2007; Valdovinos-Flores and Gonsbatt, 2013; Garza-Lombó et al., 2018b).

CD1 mice that received iAs for 9 days showed GSH reductase inhibition in the liver and brain at 10 mg/kg (Rodríguez et al., 2005). This enzyme is key for the reduction in oxidized GSH. Thus, we used lower doses to compare the early effects on GSH and amino acid transporters with those observed after a prolonged exposure. Similar to what has been observed in mice exposed during gestation, the augmentation of GSH levels in the brain was directly related to the expression of amino acid transporters involved in the import of cystine/cysteine for GSH synthesis, such as xCT in astrocytes and EAAC1 in neurons (Figures 1A–D, 2A,B; Ramos-Chávez et al., 2015; Nelson-Mora et al., 2018). However, the upregulation of EAAC1 was





maintained only in the group of mice that received the higher dose of iAs for 9 days (5 mg/kg), which was positively associated with increased levels of GSH in that region (**Figures 1D, 2A**). These observations suggest that the participation of EACC1 might be crucial for maintaining GSH homeostasis after iAs exposure. In this respect, De Bundel et al. (2011) demonstrated that xCT knockout mice do not have a lower hippocampal GSH content or increased oxidative stress. In contrast, mice lacking EAAC1 (Aoyama et al., 2006) have decreased neuronal GSH contents, accompanied by increased neuronal oxidative stress markers and severe spatial reference memory deficits with aging. The L-cys for GSH synthesis in this case, could also be provided by the transsulfuration pathway, although we did not test for the production of H<sub>2</sub>S at this time point.

GLT-1 and GLAST expression was only increased in the cortex at 24 h, at the same time as xCT upregulation. The transporters GLT-1 and GLAST are considered the primary astrocyte regulators that mediate extracellular glutamate clearance in the CNS (Amara and Fontana, 2002). The promoter regions of both GLT-1 and GLAST contain multiple NFκB binding sites (Pajarillo et al., 2019), while for xCT, Nrf2 and NFκB binding sites have been proposed (Valdovinos-Flores and Gonshebbat, 2013). Thus, both the export (xCT) and uptake (GLT-1 and GLAST) of glutamate could be modulated by these transcription factors, which would diminish extracellular glutamate release by the upregulation of xCT at this same time (**Figures 2D,E**). Previously, we observed that the gestational and chronic exposure of mice to iAs resulted in increased glutamate levels in the hippocampus associated with the upregulation of

xCT and the downregulation of GLT1 and GLAST (Ramos-Chávez et al., 2015; Nelson-Mora et al., 2018).

With respect to altered glutamate receptor subunit expression (**Figure 3**), mechanistic studies in rodent models chronically exposed to iAs (Huo et al., 2014; Ramos-Chávez et al., 2015) showed that the negative modulation of the NMDAR subunits NR2A and NR2B was associated with the upregulation of xCT. In our case, the altered expression of NMDA subunits (**Figure 3**) agrees with the upregulation of xCT at 24 h, suggesting that the increased extracellular glutamate exported by the increased xCT could downregulate the NR2B subunit, similar to what was observed in the hippocampus of mice exposed during gestation (Ramos-Chávez et al., 2015). The AMPA receptor subunits GLUA1 and 2 were also tested, but we did not observe changes (data not shown). A similar observation was made by Nelson-Mora et al. (2018) when AMPA modulation was reported at the hippocampus but not in the cortex of mice gestationally exposed to iAs.

The cysteine required for GSH synthesis and iAs metabolism (Garza-Lombó et al., 2019) can be provided through the transsulfuration pathway, which links the SAM pathway and GSH production, both main factors involved in iAs methylation. Coppin et al. (2008) showed that the adaptation of RWPE-1 cells to arsenic includes increased mRNA expression of CBS and GSH production genes, which results in a fivefold increase in GSH. In addition, the presence of CBS polymorphisms in human populations might influence arsenic metabolism (Porter et al., 2010). Here, we did not observe changes in the expression of CBS protein (**Figure 4**) and mRNA in the cortex at 24 h (data not shown), but we observed increased H<sub>2</sub>S production (**Figure 6**) in cortex and liver homogenates (see **Supplementary Figures S1, S2**), suggesting that the activity of the transsulfuration pathway was increased. Since both CBS and CSE are modulated by NFκB (Huang and Moore, 2015), it is possible that the increased production of H<sub>2</sub>S could also be due to CSE.

In addition, H<sub>2</sub>S is a gasotransmitter that can pass through cell membranes, modulating cellular targets at physiological levels by S-sulfhydration (Wang et al., 2014). The increased generation of H<sub>2</sub>S at 24 h might also participate in the modulation of GLT-1 expression observed at this time, increasing the uptake of glutamate interchanged by the input of cystine during xCT overexpression (Lu et al., 2008; Nelson-Mora et al., 2018). It has been reported that H<sub>2</sub>S activates K<sub>ATP</sub> channels by the S-sulfhydration of the Cys6 and Cys26 residues of the rvSUR1 subunit of the K<sub>ATP</sub> channel complex (Jiang et al., 2010). The upregulation of GLT-1 could also be due to the activation of K<sub>ATP</sub> channels by H<sub>2</sub>S since Sun et al. (2008) reported that K<sub>ATP</sub> activators in astrocytes can upregulate glutamate transporters. It has been suggested that, at physiological levels, H<sub>2</sub>S can exert neuroprotective effects, whereas high concentrations of H<sub>2</sub>S may cause neurotoxicity in part by enhancing NMDAR-mediated calcium overload. In our case, we observed an upregulation of NR2A and downregulation of NR2B subunit expression but did not measure NMDA activity, although mice chronically exposed to iAs showed impaired long-term potentiation (LTP) induction in the hippocampus (Nelson-Mora et al., 2018).



Exposure to hazardous environmental metalloids such as iAs throughout our lifetime is almost unavoidable because not only drinking water but also many types of foods might be contaminated with different levels of iAs. Few studies have explored the acute effects of iAs exposure, which are important to elucidate since the early effects were not homogeneous among different brain regions and because iAs exposure compromised antioxidant levels and important amino acid disposition such as glutamate, cysteine, and methionine. The impact of these changes in the CNS might contribute to premature aging and/or to earlier neurodegenerative manifestations. Our results can help in the development of adequate preventive strategies, such as appropriate diets and the development of effective agonists.

## DATA AVAILABILITY STATEMENT

All datasets generated for this study are included in the article/**supplementary material**.

## ETHICS STATEMENT

The animal study was reviewed and approved by Institute of Biomedical Research CICUAL committee.

## AUTHOR CONTRIBUTIONS

DS-A designed the study, performed the experiments, and prepared the manuscript draft. PP helped with the RT-PCR

study and LR-C helped with the Western blot analysis. WG-A and AP-A performed the hydrogen sulfur determination and contributed in the discussion. MG designed the study, applied for approval from the Research Ethics Board, and reviewed the manuscript draft.

## FUNDING

This research was funded by Programa Salud y Ambiente and Posgrado de Ciencias Biológicas, UNAM.

## ACKNOWLEDGMENTS

We thank Renato León for his technical support in animal handling, Patricia De la Torre for amplicon sequencing and Unidad de Modelos Biológicos, Instituto de Investigaciones Biomédicas, UNAM for supplying the animals. DS-A wants to thank the Posgrado en Ciencias Biológicas, UNAM for its support. This study was performed in partial fulfillment of the requirements for the Ph.D. degree in the Posgrado en Ciencias Biológicas at the Universidad Nacional Autónoma de México.

## SUPPLEMENTARY MATERIAL

The Supplementary Material for this article can be found online at: <https://www.frontiersin.org/articles/10.3389/fncel.2020.00017/full#supplementary-material>.

## REFERENCES

- Amara, S. G., and Fontana, A. C. (2002). Excitatory amino acid transporters: keeping up with glutamate. *Neurochem. Int.* 41, 313–318. doi: 10.1016/s0197-0186(02)00018-9
- Aoyama, K., Suh, S. W., Hamby, A. M., Liu, J., Chan, W. Y., Chen, Y., et al. (2006). Neuronal glutathione deficiency and age-dependent neurodegeneration in the EAAC1 deficient mouse. *Nat. Neurosci.* 9, 119–126. doi: 10.1038/nn1609
- Aoyama, K., Watabe, M., and Nakaki, T. (2012). Modulation of neuronal glutathione synthesis by EAAC1 and its interacting protein GTRAP3–18. *Amino Acids* 42, 163–169. doi: 10.1007/s00726-011-0861-y
- Bannai, S. (1986). Exchange of cystine and glutamate across plasma membrane of human fibroblasts. *J. Biol. Chem.* 261, 2256–2263.
- Calderón, J., Navarro, M. E., Jimenez-Capdeville, M. E., Santos-Diaz, M. A., Golden, A., Rodriguez-Leyva, I., et al. (2001). Exposure to arsenic and lead and neuropsychological development in Mexican children. *Environ. Res.* 85, 69–76. doi: 10.1006/enrs.2000.4106
- Chen, X., Jhee, K. H., and Kruger, W. D. (2004). Production of the neuromodulator H2S by cystathionine beta-synthase via the condensation of cysteine and homocysteine. *J. Biol. Chem.* 279, 52082–52086. doi: 10.1074/jbc.c400481200
- Coppin, J. F., Qu, W., and Waalkes, M. P. (2008). Interplay between cellular methyl metabolism and adaptive efflux during oncogenic transformation from chronic arsenic exposure in human cells. *J. Biol. Chem.* 283, 19342–19350. doi: 10.1074/jbc.m802942200
- De Bundel, D., Schallier, A., Loyens, E., Fernando, R., Miyashita, H., Van Liefferinge, J., et al. (2011). Loss of system x(c)- does not induce oxidative stress but decreases extracellular glutamate in hippocampus and influences spatial working memory and limbic seizure susceptibility. *J. Neurosci.* 31, 5792–5803. doi: 10.1523/jneurosci.5465-10.2011
- Garza-Lombó, C., Pappa, A., Panayiotidis, M. I., Gonshebbat, M. E., and Franco, R. (2019). Arsenic-induced neurotoxicity: a mechanistic appraisal. *J. Biol. Inorg. Chem.* 24, 1305–1316. doi: 10.1007/s00775-019-01740-8
- Garza-Lombó, C., Petrosyan, P., Tapia-Rodriguez, M., Valdovinos-Flores, C., and Gonshebbat, M. E. (2018a). Systemic L-buthionine-S-R-sulfoximine administration modulates glutathione homeostasis via NGF/TrkA and mTOR signaling in the cerebellum. *Neurochem. Int.* 121, 8–18. doi: 10.1016/j.neuint.2018.10.007
- Garza-Lombó, C., Posadas, Y., Quintanar, L., Gonshebbat, M. E., and Franco, R. (2018b). Neurotoxicity linked to dysfunctional metal ion homeostasis and xenobiotic metal exposure: redox signaling and oxidative stress. *Antioxid. Redox Signal.* 28, 1669–1703. doi: 10.1089/ars.2017.7272
- Gu, F., Chauhan, V., and Chauhan, A. (2015). Glutathione redox imbalance in brain disorders. *Curr. Opin. Clin. Nutr. Metab. Care* 18, 89–95. doi: 10.1097/mco.0000000000000134
- Hasan, M. T., Hernandez-Gonzalez, S., Dogbevia, G., Trevino, M., Bertocchi, I., Gruart, A., et al. (2013). Role of motor cortex NMDA receptors in learning-dependent synaptic plasticity of behaving mice. *Nat. Commun.* 4:2258. doi: 10.1038/ncomms3258
- Hine, C., and Mitchell, J. R. (2017). Endpoint or kinetic measurement of hydrogen sulfide production capacity in tissue extracts. *Bio Protoc.* 7:e2382. doi: 10.21769/BioProtoc.2382
- Hong, Y. S., Song, K. H., and Chung, J. Y. (2014). Health effects of chronic arsenic exposure. *J. Prev. Med. Public Health* 47, 245–252. doi: 10.3961/jpmph.14.035
- Huang, C. W., and Moore, P. K. (2015). H2S synthesizing enzymes: biochemistry and molecular aspects. *Handb. Exp. Pharmacol.* 230, 3–25. doi: 10.1007/978-3-319-18144-8\_1
- Huo, T., Zhang, Y., Li, W., Yang, H., Jiang, H., and Sun, G. (2014). Effect of realgar on extracellular amino acid neurotransmitters in hippocampal CA1 region determined by online microdialysis-dansyl chloride derivatization-high-performance liquid chromatography and fluorescence detection. *Biomed. Chromatogr.* 28, 1254–1262. doi: 10.1002/bmc.3154
- Jiang, B., Tang, G., Cao, K., Wu, L., and Wang, R. (2010). Molecular mechanism for H(2)S-induced activation of K(ATP) channels. *Antioxid. Redox Signal.* 12, 1167–1178. doi: 10.1089/ars.2009.2894

- Kandil, S., Brennan, L., and McBean, G. J. (2010). Glutathione depletion causes a JNK and p38MAPK-mediated increase in expression of cystathionine-gamma-lyase and upregulation of the transsulfuration pathway in C6 glioma cells. *Neurochem. Int.* 56, 611–619. doi: 10.1016/j.neuint.2010.01.004
- Kurwadkar, S. (2017). Groundwater pollution and vulnerability assessment. *Water Environ. Res.* 89, 1561–1579. doi: 10.2175/106143017X15023776270584
- Landrigan, P. J., Fuller, R., Acosta, N. J. R., Adeyi, O., Arnold, R., Basu, N. N., et al. (2018). The lancet commission on pollution and health. *Lancet* 391, 462–512. doi: 10.1016/S0140-6736(17)32345-0
- Lee, M., Schwab, C., Yu, S., McGeer, E., and McGeer, P. L. (2009). Astrocytes produce the antiinflammatory and neuroprotective agent hydrogen sulfide. *Neurobiol. Aging* 30, 1523–1534. doi: 10.1016/j.neurobiolaging.2009.06.001
- Limón-Pacheco, J. H., Hernandez, N. A., Fanjul-Moles, M. L., and Gonshebbat, M. E. (2007). Glutathione depletion activates mitogen-activated protein kinase (MAPK) pathways that display organ-specific responses and brain protection in mice. *Free Radic. Biol. Med.* 43, 1335–1347. doi: 10.1016/j.freeradbiomed.2007.06.028
- Livak, K. J., and Schmittgen, T. D. (2001). Analysis of relative gene expression data using real-time quantitative PCR and the 2<sup>-delta delta C(T)</sup> method. *Methods* 25, 402–408. doi: 10.1006/meth.2001.1262
- Lu, M., Hu, L. F., Hu, G., and Bian, J. S. (2008). Hydrogen sulfide protects astrocytes against H<sub>2</sub>O<sub>2</sub>-induced neural injury via enhancing glutamate uptake. *Free Radic. Biol. Med.* 45, 1705–1713. doi: 10.1016/j.freeradbiomed.2008.09.014
- Luo, J. H., Qiu, Z. Q., Shu, W. Q., Zhang, Y. Y., Zhang, L., and Chen, J. A. (2009). Effects of arsenic exposure from drinking water on spatial memory, ultra-structures and NMDAR gene expression of hippocampus in rats. *Toxicol. Lett.* 184, 121–125. doi: 10.1016/j.toxlet.2008.10.029
- Luo, J. H., Qiu, Z. Q., Zhang, L., and Shu, W. Q. (2012). Arsenite exposure altered the expression of NMDA receptor and postsynaptic signaling proteins in rat hippocampus. *Toxicol. Lett.* 211, 39–44. doi: 10.1016/j.toxlet.2012.02.021
- Martinez-Lozada, Z., Guillem, A. M., and Robinson, M. B. (2016). Transcriptional regulation of glutamate transporters: from extracellular signals to transcription factors. *Adv. Pharmacol.* 76, 103–145. doi: 10.1016/bs.apha.2016.01.004
- McBean, G. J. (2012). The transsulfuration pathway: a source of cysteine for glutathione in astrocytes. *Amino Acids* 42, 199–205. doi: 10.1007/s00726-011-0864-8
- McBean, G. J. (2017). Cysteine, glutathione and thiol redox balance in astrocytes. *Antioxidants* 6:E62. doi: 10.3390/antiox6030062
- Moldogazieva, N. T., Mokhosoev, I. M., Feldman, N. B., and Lutsenko, S. V. (2018). ROS and RNS signalling: adaptive redox switches through oxidative/nitrosative protein modifications. *Free Radic. Res.* 52, 507–543. doi: 10.1080/10715762.2018.1457217
- Nelson-Mora, J., Escobar, M. L., Rodriguez-Duran, L., Massieu, L., Montiel, T., Rodriguez, V. M., et al. (2018). Gestational exposure to inorganic arsenic (iAs<sup>3+</sup>) alters glutamate disposition in the mouse hippocampus and ionotropic glutamate receptor expression leading to memory impairment. *Arch. Toxicol.* 92, 1037–1048. doi: 10.1007/s00204-017-2111-x
- Niu, W. N., Yadav, P. K., Adamec, J., and Banerjee, R. (2015). S-glutathionylation enhances human cystathionine beta-synthase activity under oxidative stress conditions. *Antioxid. Redox Signal.* 22, 350–361. doi: 10.1089/ars.2014.5891
- Pajarillo, E., Rizor, A., Lee, J., Aschner, M., and Lee, E. (2019). The role of astrocytic glutamate transporters GLT-1 and GLAST in neurological disorders: potential targets for neurotherapeutics. *Neuropharmacology* 161:107559. doi: 10.1016/j.neuropharm.2019.03.002
- Parvez, F., Wasserman, G. A., Factor-Litvak, P., Liu, X., Slavkovich, V., Siddique, A. B., et al. (2011). Arsenic exposure and motor function among children in Bangladesh. *Environ. Health Perspect.* 119, 1665–1670. doi: 10.1289/ehp.1103548
- Porter, K. E., Basu, A., Hubbard, A. E., Bates, M. N., Kalman, D., Rey, O., et al. (2010). Association of genetic variation in cystathionine-beta-synthase and arsenic metabolism. *Environ. Res.* 110, 580–587. doi: 10.1016/j.envres.2010.05.001
- Ramos-Chávez, L. A., Rendon-Lopez, C. R., Zepeda, A., Silva-Adaya, D., Del Razo, L. M., and Gonshebbat, M. E. (2015). Neurological effects of inorganic arsenic exposure: altered cysteine/glutamate transport, NMDA expression and spatial memory impairment. *Front. Cell. Neurosci.* 9:21. doi: 10.3389/fncel.2015.00021
- Robert, S. M., Ogunrinu-Babarinde, T., Holt, K. T., and Sontheimer, H. (2014). Role of glutamate transporters in redox homeostasis of the brain. *Neurochem. Int.* 73, 181–191. doi: 10.1016/j.neuint.2014.01.001
- Rodríguez, V. M., Del Razo, L. M., Limon-Pacheco, J. H., Giordano, M., Sanchez-Pena, L. C., Uribe-Querol, E., et al. (2005). Glutathione reductase inhibition and methylated arsenic distribution in Cd1 mice brain and liver. *Toxicol. Sci.* 84, 157–166. doi: 10.1093/toxsci/kfi057
- Sánchez-Peña, L. C., Petrosyan, P., Morales, M., Gonzalez, N. B., Gutierrez-Ospina, G., Del Razo, L. M., et al. (2010). Arsenic species, AS3MT amount and AS3MT gene expression in different brain regions of mouse exposed to arsenite. *Environ. Res.* 110, 428–434. doi: 10.1016/j.envres.2010.01.007
- Sato, H., Kuriyama-Matsumura, K., Hashimoto, T., Sasaki, H., Wang, H., Ishii, T., et al. (2001). Effect of oxygen on induction of the cystine transporter by bacterial lipopolysaccharide in mouse peritoneal macrophages. *J. Biol. Chem.* 276, 10407–10412. doi: 10.1074/jbc.m007216200
- Schindler, J., Jung, S., Niedner-Schatteburg, G., Friauf, E., and Nothwang, H. G. (2006). Enrichment of integral membrane proteins from small amounts of brain tissue. *J. Neural Transm.* 113, 995–1013. doi: 10.1007/s00702-006-0508-4
- Singh, S., Padovani, D., Leslie, R. A., Chiku, T., and Banerjee, R. (2009). Relative contributions of cystathionine beta-synthase and gamma-cystathionase to H<sub>2</sub>S biogenesis via alternative trans-sulfuration reactions. *J. Biol. Chem.* 284, 22457–22466. doi: 10.1074/jbc.m109.010868
- Sun, X. L., Zeng, X. N., Zhou, F., Dai, C. P., Ding, J. H., and Hu, G. (2008). KATP channel openers facilitate glutamate uptake by GluTs in rat primary cultured astrocytes. *Neuropsychopharmacology* 33, 1336–1342. doi: 10.1038/sj.npp.1301501
- Tai, Y. H., Tsai, R. Y., Wang, Y. H., Cherng, C. H., Tao, P. L., Liu, T. M., et al. (2008). Amitriptyline induces nuclear transcription factor-kappaB-dependent glutamate transporter upregulation in chronic morphine-infused rats. *Neuroscience* 153, 823–831. doi: 10.1016/j.neuroscience.2008.02.055
- Thomas, D. J., Waters, S. B., and Styblo, M. (2004). Elucidating the pathway for arsenic methylation. *Toxicol. Appl. Pharmacol.* 198, 319–326. doi: 10.1016/j.taap.2003.10.020
- Tonelli, C., Chio, I. I. C., and Tuveson, D. A. (2018). Transcriptional regulation by Nrf2. *Antioxid. Redox Signal.* 29, 1727–1745. doi: 10.1089/ars.2017.7342
- Valdovinos-Flores, C., and Gonshebbat, M. E. (2012). The role of amino acid transporters in GSH synthesis in the blood-brain barrier and central nervous system. *Neurochem. Int.* 61, 405–414. doi: 10.1016/j.neuint.2012.05.019
- Valdovinos-Flores, C., and Gonshebbat, M. E. (2013). Nerve growth factor exhibits an antioxidant and an autocrine activity in mouse liver that is modulated by buthionine sulfoximine, arsenic and acetaminophen. *Free Radic. Res.* 47, 404–412. doi: 10.3109/10715762.2013.783210
- Valdovinos-Flores, C., Limon-Pacheco, J. H., Leon-Rodriguez, R., Petrosyan, P., Garza-Lombo, C., and Gonshebbat, M. E. (2019). Systemic L-buthionine -S-R-sulfoximine treatment increases plasma NGF and upregulates L-cys/L-cys2 transporter and gamma-glutamylcysteine ligase mRNAs through the NGF/TrkA/Akt/Nrf2 pathway in the striatum. *Front. Cell. Neurosci.* 13:325. doi: 10.3389/fncel.2019.00325
- Wang, J. F., Li, Y., Song, J. N., and Pang, H. G. (2014). Role of hydrogen sulfide in secondary neuronal injury. *Neurochem. Int.* 64, 37–47. doi: 10.1016/j.neuint.2013.11.002

**Conflict of Interest:** The authors declare that the research was conducted in the absence of any commercial or financial relationships that could be construed as a potential conflict of interest.

Copyright © 2020 Silva-Adaya, Ramos-Chávez, Petrosyan, González-Alfonso, Pérez-Acosta and Gonshebbat. This is an open-access article distributed under the terms of the Creative Commons Attribution License (CC BY). The use, distribution or reproduction in other forums is permitted, provided the original author(s) and the copyright owner(s) are credited and that the original publication in this journal is cited, in accordance with accepted academic practice. No use, distribution or reproduction is permitted which does not comply with these terms.



# Application of Iron Oxide Nanoparticles in the Diagnosis and Treatment of Neurodegenerative Diseases With Emphasis on Alzheimer's Disease

Shen Luo<sup>1,2†</sup>, Chi Ma<sup>3†</sup>, Ming-Qin Zhu<sup>1</sup>, Wei-Na Ju<sup>1</sup>, Yu Yang<sup>1\*</sup> and Xu Wang<sup>1\*</sup>

<sup>1</sup>Department of Neurology and Neuroscience Center, The First Hospital of Jilin University, Changchun, China, <sup>2</sup>Department of Critical Care Medicine, The First Affiliated Hospital, Sun Yat-sen University, Guangzhou, China, <sup>3</sup>Department of Neurosurgery, The First Hospital of Jilin University, Changchun, China

## OPEN ACCESS

### Edited by:

Rocío Martínez De Pablos,  
University of Seville, Spain

### Reviewed by:

Rachid El Fatimy,  
Harvard Medical School,  
United States  
Lucia Martín Banderas,  
Universidad de Sevilla, Spain

### \*Correspondence:

Xu Wang  
sunny.uu@163.com  
Yu Yang  
m15754306093@163.com

<sup>†</sup>These authors have contributed  
equally to this work

**Received:** 31 August 2019

**Accepted:** 24 January 2020

**Published:** 28 February 2020

### Citation:

Luo S, Ma C, Zhu M-Q, Ju W-N,  
Yang Y and Wang X  
(2020) Application of Iron Oxide  
Nanoparticles in the Diagnosis and  
Treatment of Neurodegenerative  
Diseases With Emphasis on  
Alzheimer's Disease.  
*Front. Cell. Neurosci.* 14:21.  
doi: 10.3389/fncel.2020.00021

Neurodegenerative diseases are characterized by chronic progressive degeneration of the structure and function of the nervous system, which brings an enormous burden on patients, their families, and society. It is difficult to make early diagnosis, resulting from the insidious onset and progressive development of neurodegenerative diseases. The drugs on the market cannot cross the blood–brain barrier (BBB) effectively, which leads to unfavorable prognosis and less effective treatments. Therefore, there is an urgent demand to develop a novel detection method and therapeutic strategies. Recently, nanomedicine has aroused considerable attention for diagnosis and therapy of central nervous system (CNS) diseases. Nanoparticles integrate targeting, imaging, and therapy in one system and facilitate the entry of drug molecules across the blood–brain barrier, offering new hope to patients. In this review, we summarize the application of iron oxide nanoparticles (IONPs) in the diagnosis and treatment of neurodegenerative disease, including Alzheimer's disease (AD), Parkinson's disease (PD), and amyotrophic lateral sclerosis (ALS). We focus on IONPs as magnetic resonance imaging (MRI) contrast agents (CAs) and drug carriers in AD. What most neurodegenerative diseases have in common is that hall marker lesions are represented by protein aggregates (Soto and Pritzkow, 2018). These diseases are of unknown etiology and unfavorable prognosis, and the treatments toward them are less effective (Soto and Pritzkow, 2018). Such diseases usually develop in aged people, and early clinical manifestations are atypical, resulting in difficulty in early diagnosis. Recently, nanomedicine has aroused considerable attention for therapy and diagnosis of CNS diseases because it integrates targeting, imaging, and therapy in one system (Gupta et al., 2019). In this review article, we first introduce the neurodegenerative diseases and commonly

**Abbreviations:** A $\beta$ , amyloid  $\beta$ ; AD, Alzheimer's disease; ALS, amyotrophic lateral sclerosis; BBB, blood–brain barrier; CA, contrast agent; CNS, central nervous system; CSF, cerebrospinal fluid; IONP, iron oxide nanoparticle; MNP, magnetic nanoparticle; MRI, magnetic resonance imaging; PET, positron emission tomography; PD, Parkinson's disease; USPIO, ultrasmall superparamagnetic iron oxide; SPIO, superparamagnetic iron oxide; SPION, superparamagnetic iron oxide nanoparticle.

used MRI CAs. Then we review the application of IONPs in the diagnosis and treatment of neurodegenerative diseases with the purpose of assisting early theranostics (therapy and diagnosis).

**Keywords:** iron oxide nanoparticle, magnetic resonance imaging, Alzheimer's disease, amyloid- $\beta$ , neurodegeneration

## INTRODUCTION

### Introduction of Neurodegenerative Diseases

#### Introduction of Alzheimer Disease (AD)

The main characteristic of Alzheimer's disease (AD) is the progressive deterioration of cognitive function, most commonly the loss of memory, increasingly influencing patients' activity of daily living and leading to loss of independency (Tiwari et al., 2019). The hallmark histological abnormalities of AD comprise of the extracellular aggregation of amyloid plaques and fibrillar aggregates of the microtubule associated with tau protein (Tiwari et al., 2019). The deposition of amyloid plaque, which is caused by the mounting production, accumulation, and aggregation of the amyloid- $\beta$  (A $\beta$ ), is the primary histopathological characteristic of AD (Tiwari et al., 2019). The most widely accepted AD etiology is the amyloid cascade hypothesis (Barage and Sonawane, 2015). The incorrect process of the A $\beta$  protein precursor (A $\beta$ PP) by  $\gamma$ -secretase, which gives rise to the pathological 40–42 amino acid long cleaved peptide, known as A $\beta$ , is fundamental to this hypothesis (Chen and Mobley, 2019; Tiwari et al., 2019). The excess of A $\beta$  finally results in the aggregated fibrils of plaques and neurotoxic oligomers (Chen and Mobley, 2019).

Currently for AD, the early diagnosis could provide treatment opportunities to high-risk groups, and the way to cure diseases under development seems to be proven effective only at the very early stages of the initiated amyloid deposition (Frisoni et al., 2017). For patients in the earlier stage of AD, the correct diagnosis and treatment would enable to delay cognitive impairment and irreversible neuronal damage (Frisoni et al., 2017). Therefore, there is a rising demand to develop reliable early detective tools for AD.

#### Introduction of Parkinson's Disease (PD) and Other Neurodegenerative Diseases

Parkinson's disease (PD) is the second most common neurodegenerative disease in the whole world (Balestrino and Schapira, 2019). PD mainly affects the locomotor system by degenerating the neuron, finally leading to severe disability (Balestrino and Schapira, 2019). The clinical criteria for diagnosis of PD depend mainly on the observation of movement disorders such as cogwheel rigidity, bradykinesia, resting tremor, etc. (Balestrino and Schapira, 2019). In the dopaminergic neurons, phosphor- $\alpha$ -synuclein molecules can aggregate with one another easily to form Lewy body, and these degenerative dopaminergic neurons lose the function of expressing dopamine, finally leading to the damage of the motor cortex and movement disorders (Ikenaka et al., 2019). Thus, for PD,  $\alpha$ -synuclein is the most acknowledged biomarker (Ikenaka et al., 2019). If the quantity

of degenerative dopaminergic neurons in the basal ganglia is over 50%, the clinical features of PD can gradually present. The clinical symptoms of PD might overlap with other movement disorders such as progressive supranuclear palsy (PSP) and multiple system atrophy (MSA; Giagkou and Stamelou, 2018). Therefore, going by clinical manifestations only, early PD diagnosis is difficult and prone to misdiagnosis.

Another neurodegenerative disease, amyotrophic lateral sclerosis (ALS), is an adult-onset neurodegenerative disorder. The major pathological manifestations of ALS are progressive loss of upper motor neurons of the corticospinal tract, lower motor neurons of ventral roots of the spinal cord, and brainstem nuclei (Gagliardi et al., 2019).

For the moment, despite the fact that many kinds of treatment appeared, no treatment has been shown to be effective for neurodegenerative diseases. Mesenchymal stem cell (MSC) therapy is regarded as one of the most prospective approaches for the treatment of neurodegenerative diseases, including PD and ALS (Baloh et al., 2018; Staff et al., 2019). In addition to MSC, neural stem cells (NSCs) could turn to be an optimal selection to replace specific lost neurons *in vitro* and *in vivo* (Sugaya and Vaidya, 2018).

### Common Auxiliary Examination Methods for Neurodegenerative Diseases

#### Autopsy

Currently for AD, there is no other confirmed diagnostic method except autopsy (Pillai et al., 2018). Although researchers use plenty of neuropsychological tests to make the clinical diagnosis, the diagnosis process could be affected by many other factors. So the definitive diagnosis still depends on autopsy with histological and pathological findings of sufficient numbers of plaques (Tiwari et al., 2019). But this method is an invasive test and is not usually accepted by patients.

#### Laboratory Inspection

Cerebrospinal fluid (CSF) is usually collected through the lumbar puncture, which is invasive and uncomfortable. The reduction of CSF A $\beta$ 42 and the elevation of CSF tau are the biomarkers of AD. But the elevated CSF tau is just a biomarker of neuronal injury, not specific to AD (Olsson et al., 2016).

Compared to CSF, blood sample is much easier to obtain in clinics (Yang et al., 2016). For PD,  $\alpha$ -synuclein can be expressed in the peripheral blood system at very low amounts, but it is not applicable for clinical use due to the poor low-detection limit of blood test (Yang et al., 2016).

Nanotechnology can play an important role in increasing the sensitivity of detection of biomarkers (Gupta et al., 2019). Applications of the magnetic nanoparticles (MNPs) detecting



biomarkers for AD and PD are mentioned later in the section The Application of Iron Oxide Nanoparticles (IONPs) in Neurodegenerative Diseases.

### Positron Emission Tomography (PET)

On positron emission tomography (PET), one of the biomarkers of AD-related synaptic dysfunction is the decreased fluorodeoxyglucose  $^{18}\text{F}$  (FDG) uptake, which indicates temporoparietal hypometabolism (Chandra et al., 2019). Thus, currently PET is being used to image the amyloid deposition in AD, mild cognitive impairment (MCI), and normal aged controls in human (Chandra et al., 2019). However, in terms of PET, the visualization of individual plaques may be limited by the low spatial resolution for it is not clear enough to detect the earliest stage of amyloid deposition (Wadghiri et al., 2013).

### Magnetic Resonance Imaging (MRI)

Compared with PET, magnetic resonance imaging (MRI) has a much higher spatial resolution especially for soft tissue and does not require radiotracer injection (Wadghiri et al., 2013). And the instrumentation operating at 1.5–3 T is widely used for patient and animal imaging (Wadghiri et al., 2013). MRI can be used not only for imaging A $\beta$  aggregation in the murine brain but also for monitoring other AD-related morphological and functional alterations (Rotman et al., 2011).

Chamberlain et al. (2009) reported that the susceptibility-weighted imaging (SWI) method can provide high plaque contrast for *ex vivo* plaque imaging, which increases the sharpness of the image in about 1 h 30 min. But *in vivo*, the SWI method has been found impractical due to the magnetic susceptibility artifact from the surface vessels and the air-to-skull interface (Chamberlain et al., 2011).

### Others

Genetic sequence analysis might be a method for diagnosis of early-stage PD, whereas only about 10% of PD patients are hereditary (Yang et al., 2016).

## Commonly Used MRI Contrast Agents (CAs)

### Introduction of MRI CAs

The contrast agents (CAs) in MRI can enhance the image contrast of the tissue/regions where they are delivered by shortening the water protons spin–lattice T1 and/or spin–spin T2 relaxation times (Busquets et al., 2014). Therefore, the image is CA affection to the relaxivity of the adjacent water protons through the dipolar interaction predominantly, rather than the CA compound itself (Busquets et al., 2014).

Traditionally, there are two different categories for MRI CAs taking effect in T1 and T2, respectively. T1 CAs can increase the T1 relaxation time, resulting in high signal in T1-weighted images. T2 CAs could reduce the T2 relaxation time, which reduces both T2 and T2\* signals and gives rise to dark contrast in T2-weighted images (De et al., 2011). MRI CAs are also divided into “positive” CAs, which are in the majority, and “negative” CAs. In brief, “positive” CAs are the contrasts made by a gadolinium-based compound (paramagnetic CAs) administration, which enhances the MRI

intensity of the signal. “Negative” CAs mean iron oxide based on superparamagnetic CAs. Superparamagnetic CAs can commonly decrease the MRI signal of the regions where they are delivered (Busquets et al., 2014).

### Commonly Used MRI CAs

Currently, the most widely used MRI CAs are gadolinium ( $\text{Gd}^{3+}$ ) chelates (Marasini et al., 2020). By using high-field MRI,  $\text{Gd}^{3+}$  chelates can demonstrate the A $\beta$  plaque imaging both *ex vivo* and *in vivo* (Sillerud et al., 2013). Due to the long electron spin-lattice relaxation time and abundant unpaired electrons (seven) per  $\text{Gd}^{3+}$  ion has, the relaxation rate of water hydrogen can be increased significantly. However, ionic gadolinium complexes can leak toxic  $\text{Gd}^{3+}$  ions with short half-life and it has been reported that  $\text{Gd}^{3+}$  chelates can lead to renal insufficiency (Rashid et al., 2016; Marasini et al., 2020). Fluorinated small molecules that bind to amyloid plaques can be detected by  $^{19}\text{F}$  MRI (Jirak et al., 2019). But for their low *in vivo* concentrations, this method might be difficult to be applied to human clinical medicine (Sillerud et al., 2013). Besides, gold nanoparticles (Au NPs) present a significant MRI signal change during A $\beta$  self-aggregation, but the intrinsic cytotoxicity caused by Co in preparing the NPs remains to be thoroughly evaluated (Brambilla et al., 2011).

Among all these MRI CAs, pure iron oxides such as magnetite ( $\text{Fe}_3\text{O}_4$ ) and maghemite ( $\gamma\text{-Fe}_2\text{O}_3$ ) are the most common biocompatible magnetic nanomaterials (Ling and Hyeon, 2013). Iron oxides are benign, nontoxic, and tolerated biologically, and they can be injected into the human body and incorporated into human natural processes of metabolism, serving as MRI CAs or drug delivery system (Ling and Hyeon, 2013). Currently, some IONP-based MRI CAs have already been used in clinical trials. Apart from the benefits mentioned above, IONPs offer many important biomedical applications, such as cell tracking, protein separation, and hyperthermia (Ling and Hyeon, 2013).

IONPs usually accumulate in liver and spleen. They can be eliminated by liver, spleen, and kidney (Arami et al., 2015). The potential toxic effects of free iron ions released from IONPs can be blocked by maintaining iron homeostasis. Excess iron ions can combine with ferritin to maintain the iron store, which is involved in many biological processes, including hemoglobin synthesis (Arami et al., 2015). One study has showed that the release of iron ions from IONPs may result in iron accumulation, oxidative stress, and protein aggregation, which are toxic to the neural cell. However, the toxicity levels of IONPs are determined by their properties, including the size, concentration, surface charge, and the type of coating and functional groups (Yarjanli et al., 2017).

Besides, colloidal IONPs such as ultrasmall superparamagnetic iron oxide (USPIO) and superparamagnetic iron oxide (SPIO) have already been used as MRI CAs in targeting drug delivery (Busquets et al., 2014; Dulińska-Litewka et al., 2019). Superparamagnetic iron oxide nanoparticles (SPIONs), with the iron oxide core and magnetic coating, have fundamental features such as high saturation magnetic moment, relatively stable chemical properties, and minimized potential

toxicity (Busquets et al., 2014; Dulińska-Litewka et al., 2019). They can improve the MRI sensitivity by serving as *in vivo* or *in vitro* CAs and thus have potential biomedical applications for MRI CAs (Busquets et al., 2014; Dulińska-Litewka et al., 2019). The commonly used MRI CAs are briefly summarized in Table 1.

## The Carrier

### The Introduction of the Blood–Brain Barrier

The blood–brain barrier (BBB) is mainly formed by neuronal pericytes, perivascular astrocytes, and brain capillary endothelial cells (BCECs). The infrastructure that each BCEC tightly connects with all their neighboring cells can firmly constitute a physical, chemical, and immunological barrier, and thus can keep the central nervous system (CNS) separate from peripheral blood circulation (Teleanu et al., 2019). The BBB permits only a few percent of potential CNS drugs into the CNS (Teleanu et al., 2019). Take MNPs for example; atomic force microscopy demonstrated that when MNPs cross the BBB, they can be internalized by endothelial cells (Kong et al., 2012). The BBB is responsible for the accurate internal regulation of the CNS; thus, any damage of the BBB can be related to systemic inflammatory or immune dysfunction, which further leads to the initiation of several neurodegenerative pathways (Teleanu et al., 2019).

In general, there are two ways of carrying drugs: (1) directly immobilized on the MNPs surface; and (2) tethered *via* polyethylene glycol (PEG) coating or other organic/inorganic polymer layer. The problem is that the free drugs can be eliminated by metabolism (enzymatic mainly) easily before they reach the target (Ding et al., 2014).

There has been a study examining the biodistribution of IONPs using lysophosphatidic acid (LPA) to help the entry to the brain. IONPs without LPA coating were mainly deposited

in liver and spleen, with a plasma half-life of 6 min. The accumulation amount of IONPs with LPA coating in the brain and spleen increased approximately 4-fold compared with the control. Mice treated with LPA and IONP showed no sign of peripheral immune cell passing through the BBB and minimal activation of microglia and astrocytes, indicating a safe and effective strategy for IONP delivery to the brain (Sun et al., 2016).

CAs or therapeutic drugs can be delivered from the olfactory mucosa to the brain by neuronal cells through the olfactory pathway, which consists of olfactory epithelium in nasal cavity, lamina propria, and olfactory bulb in the CNS (Khan et al., 2017). Since the nasal passage is the only direct connection between the external environment and the brain, it provides an applicable method for CAs or therapeutic drugs to enter the brain by bypassing the BBB rather than to cross it (Salama et al., 2017). Thus, the olfactory pathway is more efficient for reducing hepatic/renal clearance and the systemic exposure (Akilo et al., 2016; Khan et al., 2017).

### The Function of the Carrier

For the carriers whose sizes fall within the range from 120 to 200 nm, they can pass the trap of the reticuloendothelial system (RES) easily and cannot be detected by the cells of liver and spleen. This can prolong the time that the carriers remain in contact with the BBB, thus increasing the odds for the drug to be absorbed by the CNS ultimately (Sachdeva et al., 2015). Carriers such as MNPs can be encapsulated in liposomes while carrying potential therapeutic molecules such as cDNA, siRNA, and polypeptides, which serves as the drug delivery system (Thomsen et al., 2015).

Of all the drug delivery strategies, SPIONs comprising of maghemite ( $\text{Fe}_2\text{O}_3$ ) and magnetite ( $\text{Fe}_3\text{O}_4$ ) prove their advantage in targeted drug delivery systems (Anwar et al., 2014). The characteristics of both CAs and the delivery system make

**TABLE 1 |** Commonly used magnetic resonance imaging (MRI) contrast agents.

	Service conditions	Advantages	Disadvantages
Gadolinium chelate commercial available products: Magnevist® (Gd-DTPA), Dotarem® (Gd-DOTA), Prohance® (Gd-HP-DO3A), Primovist®, Eovist® (Gd-EOB-DTPA), etc.	High-field MRI	Increase the relaxation rate of water hydrogen significantly	Leak toxic $\text{Gd}^{3+}$ ions; lead to renal insufficiency (Rashid et al., 2016; Marasini et al., 2020)
Fluorinated small molecules	$^{19}\text{F}$ MRI	The sensitivity of magnetic resonance of $^{19}\text{F}$ is relatively high; endogenous $^{19}\text{F}$ -derived background noise should be very low; $^{19}\text{F}$ can be found abundantly, result in low manufacturing cost.	Low <i>in vivo</i> concentrations (Sillerud et al., 2013; Jirak et al., 2019)
Gold nanoparticles (Au NPs)	Regular MRI	Present a significant MRI signals change	Intrinsic cytotoxicity (Brambilla et al., 2011)
Pure iron oxides $\gamma\text{-Fe}_2\text{O}_3$ and $\text{Fe}_3\text{O}_4$	MRI	Benign, nontoxic, tolerated biologically	Naked iron oxide nanocrystals can cause damage to <i>in vitro</i> cytotoxicity (Ling and Hyeon, 2013)
Colloidal iron oxide nanoparticles SPIOs USPIOs Commercial available products: Feridex® (Ferumoxides), Resovist® (Ferucarbotran)	MRI	High saturation magnetic moment, relatively stable chemical properties, minimized potential toxicity	The use of organic solvents in the synthetic schemes result in the hydrophobic of SPIONs (Busquets et al., 2014; Dulińska-Litewka et al., 2019)

SPIOs the optimal choice for targeting drug delivery systems (Anwar et al., 2014; Dulińska-Litewka et al., 2019).

## THE APPLICATION OF IRON OXIDE NANOPARTICLES IN NEURODEGENERATIVE DISEASES

In this section, we simply summarized the application of iron nanoparticles in diagnosis and treatment in neurodegenerative disease, including AD, PD, and ALS. The following parts related to AD are summarized in **Figure 1**.

### Detecting Iron Deposit in Amyloid Plaques by MRI

The deposition of A $\beta$  is one of the primary histopathological characteristics of AD (Tiwari et al., 2019). With the relatively large size and being located intercellularly, A $\beta$  can be regarded as an ideal imaging biomarker (Zhang et al., 2015). The A $\beta$  deposition is earlier than clinical manifestations

and increases gradually with the progress of the disease (Tiwari et al., 2019).

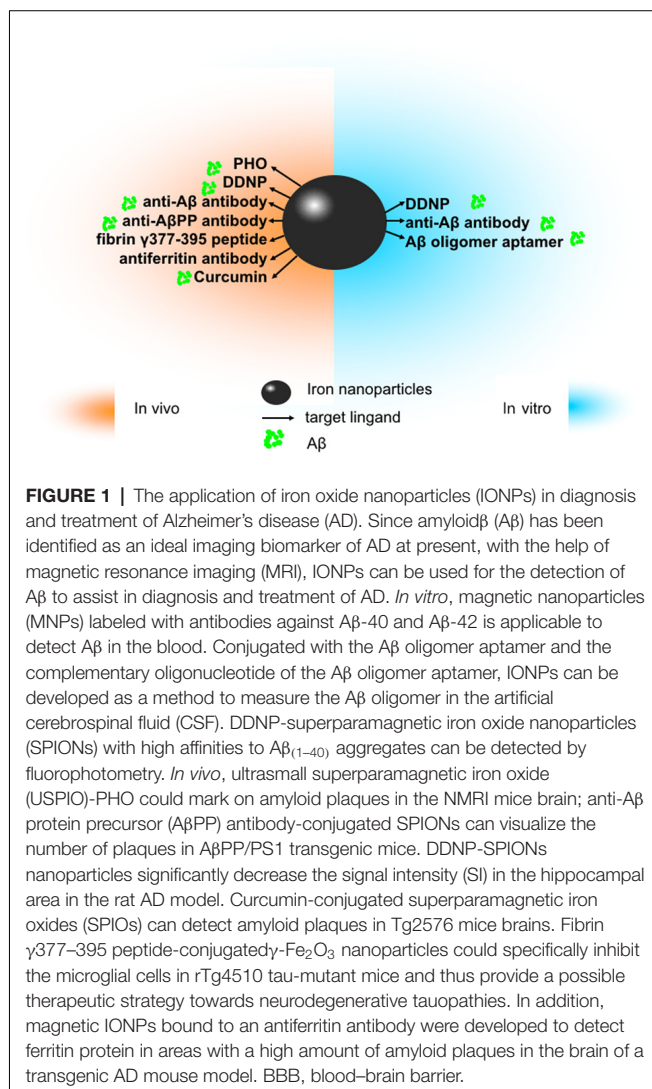
It has been reported that because of the limited brain uptake after the intravenous injection, the styrylbenzenes and the pathological staining dye analogs, such as X-34, ISB, IMSB, Congo Red, and Chrysamine G, are not suitable for the imaging of the A $\beta$  plaque (Zhou et al., 2014). Since there are iron deposits in the amyloid plaques, in T2- and T2\*-weighted MR images, the plaques showed a hypointense signal (Chamberlain et al., 2009). Thus, with the help of specific MRI sequences, the detection of amyloid plaques can use not the CAs but the iron content (Ansiaux et al., 2015). Since the detection of iron relies on the nature properties of the amyloid plaques and the stage of the disease (larger plaques contain higher amounts of iron, which makes the detection easier), it normally requires greater than 7-T magnetic field and several hours as acquisition time (Ansiaux et al., 2015). In AD transgenic mice, the levels of iron were high in thalamic plaques and low in cortical/hippocampal plaques, and by using different MRI sequences, the visibility of plaques in the cortex/hippocampus was different from those in the thalamus (Wengenack et al., 2011). The results showed that by T(2)SE, all plaques were detectable equally, but by T(2)\*GE pulse sequences, only thalamic plaques were detected reliably (Wengenack et al., 2011). Human AD plaques are similar to cortical/hippocampal plaques of AD mice, and MRI methods that are less dependent on iron magnetic susceptibility effect might be suitable for imaging the human AD plaque (Wengenack et al., 2011). Studies have shown that CAs can conduce to A $\beta$  plaques detecting under the condition of high field MRI both *in vitro* and *in vivo* (Yang et al., 2011a; Petiet et al., 2012).

### Iron Oxide Nanoparticles in the Diagnosis of AD *in vitro*

The effective treatments for AD depend on the detection and quantitation of soluble AD biomarkers as early diagnosis, mainly by measuring the total tau protein and A $\beta$  concentrations in CSF or plasma and detecting a suspected pathogenic biomarker. But being affected by low concentrations and other factors, these two strategies may lead to inconclusive imprecise results (Brambilla et al., 2011).

It has been reported that magnetic reagents that consist of MNPs magnetically labeled with antibodies against A $\beta$ -40 and A $\beta$ -42 can be applied to detect A $\beta$  in the blood (Yang et al., 2011a). By applying the immunomagnetic reduction (IMR) assay, the concentration can be detected, which is lower than 10 pg/ml at A $\beta$ -40 and 20 pg/ml at A $\beta$ -42 and, furthermore, with high specificity (Yang et al., 2011a). Skaat et al. (2013) reported that the fixation of the aA $\beta$ mAb clone BAM10 to near-infrared fluorescent maghemite nanoparticles enables to detect A $\beta$ <sub>40</sub> fibrils specifically *ex vivo* by both fluorescence and MRI.

1,1-Dicyano-2-[6-(dimethylamino)naphthalene-2-yl]propene (DDNP) carboxyl derivative-modified SPIONs (DDNP-SPIONs), synthesized by Zhou et al. (2014) have shown high binding affinities toward A $\beta$ <sub>(1-40)</sub> aggregates by the investigation of fluorophotometry *in vitro* trials. Because of





benefits such as versatile surface chemistry, relatively small size, and monodisperse size distribution, DDNP-SPIONs would provide opportunity for the molecular diagnosis of AD (Zhou et al., 2014).

With BaYF5:Yb, Er nanoparticles (UCNPs) as upconversion fluorescence labels, Fe<sub>3</sub>O<sub>4</sub> MNPs as the recognition and concentration elements conjugated with the A $\beta$  oligomer aptamer and the complementary oligonucleotide of the A $\beta$  oligomer aptamer, respectively (Jiang et al., 2017). The developed method measured A $\beta$  oligomer in artificial CSF successfully (Jiang et al., 2017).

With corresponding antibodies conjugated as targeting ligands, magnetic IONPs coated by antibiofouling polymer polyethylene glycol-block-allyl glycidyl ether (PEG-b-AGE) could capture A $\beta$ <sub>40</sub> and A $\beta$ <sub>42</sub> peptides and tau protein in CSF- and serum-mimicking samples, with high specificity (>90%) and sensitivity (>95%; Li et al., 2019). And the antibody-conjugated IONPs also detected A $\beta$ s and tau protein from the human whole blood samples, with significantly higher sensitivities than those of antibody-conjugated Dynabeads (Li et al., 2019).

## Iron Oxide Nanoparticles in the Diagnosis of AD *in vivo*

It is reported that in AD transgenic mice, a gadolinium-loaded molecular probe can cross the BBB and specifically bind to the A $\beta$  plaques after intravenous injection, and gained more than ninefold enhancement in the cortex and the hippocampus by using 7-T MRI (Poduslo et al., 2002). But as set forth, ionic gadolinium complexes can leak toxic Gd<sup>3+</sup> ions with short half-life, and the Gd<sup>3+</sup> chelates can lead to renal insufficiency.

Another research suggested that after introducing several magnetic CAs in AD transgenic mice to detect amyloid plaques, the USPIOs were able to commendably identify transgenic mice to the wild type by detecting amyloid plaques T2\*-weighted in MRI (Yang et al., 2011b). Ansciaux et al. (2015) reported that a USPIO-PHO (USPIO coupled to peptide C-IPLPFYN-C) could cross the BBB of NMRI mice by intravenous injection and accumulates in the brain for 90 min, with high affinity (nanomolar binding affinity) and low toxicity. The half-life of USPIO-PHO was about 3 h. These MRI and histochemistry studies showed that USPIO-PHO had the potential to label amyloid plaques in the brain (Ansciaux et al., 2015). Sillerud et al. (2013) synthesized an anti-A $\beta$ PP antibody-conjugated SPION, which can cross the BBB and act as an *in vivo* CA for MRI of A $\beta$  plaques in AD. By MRI, the number of plaques visible per brain was about twice in A $\beta$ PP/PS1 transgenic mice than that in control AD mice (Sillerud et al., 2013). DDNP-SPION nanoparticles were further tested by intrahippocampal injection of A $\beta$ <sub>1-40</sub> in a rat AD model (Zhang et al., 2015). After intravenous injection of DDNP-SPIONs in AD rats and testing by coronal T2\*-weighted images, the signal intensity (SI) detected in the hippocampal area was decreased significantly, which indicated the binding of DDNP-SPIONs to the A $\beta$  plaques (Zhang et al., 2015). Curcumin is a natural compound that can bind to amyloid plaques specifically (Cheng et al., 2015). Cheng et al. (2015) injected curcumin-conjugated SPIOs to Tg2576 mouse and nontransgenic mice;

amyloid plaques were detectable in Tg2576 mice brains by *ex vivo* T2\*-weighted MRI, but no plaques were found in the control group.

Growing evidence shows that vascular remodeling might be an important factor in the pathophysiologic mechanisms of AD (Klohs et al., 2012). Based on this, Klohs et al. (2012) used contrast-enhanced magnetic resonance microangiography (CE- $\mu$ MRA) in wild-type control mice and arcA $\beta$  mice to estimate the density of the cortical microvasculature before and after the administration of SPIONs. CE- $\mu$ MRA can be available for visualizing the cerebral arteries and veins whose diameter is less than 60  $\mu$ m, the nominal pixel resolution (Klohs et al., 2012). The authors take the attitude that the deposition of A $\beta$  and fibrin results in impaired perfusion and vascular occlusion, which may finally contribute to the density reduction of transcortical vessels (Klohs et al., 2012).

In addition to the experiments on animals mentioned above, medical researchers may consider using a new and broader approach, including T1 $\rho$ -weighting, macroscopic T2 mapping, SE imaging, FSE imaging, and gradient-echo (GRE) imaging, to detect the plaque in human clinical trials (Chamberlain et al., 2009).

By *ex vivo* MRI (11.7 T), anti-amyloid targeted superparamagnetic IONPs were capable of detecting deposition of amyloid  $\beta$  plaques and neuroinflammation activation by microglia in 3X AD transgenic mice (Tafoya et al., 2017).

Based on magnetic resonance molecular imaging (MRMI), ultrasmall particles of iron oxide (USPIO) functionalized with a disulfide constrained cyclic heptapeptide (PHO) was able to target A $\beta$  plaques and cross the BBB in AD transgenic mice (André et al., 2017). The colocalization of USPIO-PHO with amyloid plaques on brain sections was demonstrated by immunohistochemistry and immunofluorescent experiment (André et al., 2017). Moreover, the amount of amyloid plaques detected by USPIO-PHO was in good correlation with that of plaques detected with anti-amyloid  $\beta$  antibody and Perls'-DAB staining (André et al., 2017).

In a recent study, magnetic IONPs bound to an antiferritin antibody were developed to detect ferritin protein in areas with a high amount of amyloid plaques, in particular the subiculum in the hippocampal area, in the brain of a transgenic mouse model with five familial AD mutations (Fernández et al., 2018). Functionalized IONPs were capable of recognizing and combining specifically to the ferritin protein accumulated in the subiculum area of the AD transgenic mice (Fernández et al., 2018).

## Application of Iron Oxide Nanoparticles in the Treatment of AD

For AD, drug therapy can improve the symptoms but cannot prevent the development of the disease (Busquets et al., 2014). For patients whose disease course beyond an average of 6 months, the benefits of drug therapy are not sustained (Corbett et al., 2012). The drug distribution spreading across the whole brain may decrease the amount of drug reaching the target, thus reducing the effectiveness of the therapeutic. Therefore, a delivery system must be developed to ensure that the drug



reaches the exact lesion site. Major efforts have been directed toward developing molecules with high affinity for A $\beta$ , which can reduce the A $\beta$  level in the brain (Brambilla et al., 2011).

It is reported that prominent microglial activation precedes tangle formation, and elimination of tau-induced microglial activation could delay the progression of neurodegenerative tauopathies (Yoshiyama et al., 2007). Adams et al. (2007) conjugated fibrin  $\gamma$ 377–395 peptide [one fibrin-derived peptide that can inhibit microglial activity *in vivo* specifically to iron oxide ( $\gamma$ -Fe $_2$ O $_3$ ) nanoparticles with diameters  $21 \pm 3.5$  nm] in order to counteract the short half-life of the peptide. The study showed that, compared to the free peptide of the same concentration,  $\gamma$ -Fe $_2$ O $_3$  nanoparticles could specifically inhibit the microglial cells in rTg4510 tau-mutant mice, supporting the fact that the nanoparticles can be used for the delivery of substances to the brain and for providing a possible therapeutic strategy to neurodegenerative tauopathies (Glat et al., 2013).

Kouyoumdjian et al. (2013) reported a biomimetic path using glyconanoparticles-SPIO to detect A $\beta$ . The superparamagnetic nature enabled the detection of A $\beta$  both *in vitro* and in mouse brains by MRI. The glyconanoparticles not only can reduce A $\beta$  mediated cytotoxicity damage to cells greatly but also can highlight the detection and imaging potential of A $\beta$  (Kouyoumdjian et al., 2013).

There are studies describing the effect of magnetic nanoparticulate on A $\beta$  fibrillation. Depending on the size and the surface area, a dual effect on the A $\beta$  fibrillation kinetics was observed, with lower concentrations of SPIONs decreasing the rate of A $\beta$  fibrillation, while higher concentrations enhanced the rate in the aqueous solution (Mahmoudi et al., 2013). Consistent with the previous study, Mirsadeghi et al. (2016) showed that lower concentrations of SPIONs coated by PEG-NH $_2$  inhibited the process of A $\beta$  fibrillation under magnetic field, whereas high concentrations accelerated the process. Furthermore, the coating charge also exerts a considerable effect on the A $\beta$  fibrillation process. In comparison with the negatively charged or uncharged SPIONs, lower concentrations of SPIONs with positive coating charge promoted the fibrillation (Mirsadeghi et al., 2016). By applying thioflavin-T fluorescence emission, the effect of SPIONs with different electric charges on both  $\beta$ -amyloid and  $\alpha$ -synuclein fibrillation process was investigated. The negatively charged nanoparticles encoded to -COOH by dextran-coating decreased the binding level of thioflavin-T particles to  $\beta$ -sheets (Javdani et al., 2019).

Combining nerve growth factor (NGF) and quercetin with superparamagnetic IONPs promoted neurite outgrowth and increased the complexity of the neuronal branching trees in PC12 cells, as potential therapeutics for neurodegenerative diseases (Katebi et al., 2019).

Sonawane et al. (2019) screened out one kind of protein-capped (PC) metal nanoparticles that inhibit Tau aggregation *in vitro* for the first time. They proved that because of the increased reactive oxygen species production and the resulting oxidative stress, the uncapped CdS nanoparticles make themselves toxic to HeLa cells and bacteria, but by capping, these CdS can obtain an entirely different property and become more biocompatible; thus, the biosynthetic PC metal nanoparticles,

particularly iron oxide, will not influence the viability of neuroblastoma cells (Sonawane et al., 2019).

## Application of Iron Oxide Nanoparticles in the Diagnosis of PD

Yang et al. (2016) invented a reagent for IMR consisting of antibodies against  $\alpha$ -synuclein functionalized with MNPs. By using an ultrasensitive immunoassay utilizing IMR, the  $\alpha$ -synuclein detection dynamic range is from 0.3 fg/ml to 310 pg/ml in plasma (Yang et al., 2016). The nanoparticles can differentiate PD patients, PDD (PD dementia) patients, and healthy subjects depending on the significantly different concentration of plasma  $\alpha$ -synuclein (Yang et al., 2016).

Studies have conjugated multimodal IONPs to Rhodamine-B (MION-Rh), and then labeled with MSCs from umbilical cord blood (UC-MSC; Sibov et al., 2014). Labeled cells were infused into the striatum of PD adult male rats, and 15 days later by T2 MRI, the cells were observed migrating along the medial forebrain bundle to the substantia nigra as hypointense spots (Sibov et al., 2014).

## Application of Iron Oxide Nanoparticles in the Treatment of PD

Gene therapy, which targets the expression of  $\alpha$ -synuclein in neurons, is of great concern, and shRNA (short hairpin RNA) has been identified as a promising treatment of PD (Niu et al., 2017). Therefore, researchers coated magnetic Fe $_3$ O $_4$  nanoparticles with oleic acid molecules as a nanocarrier and absorbed shRNA. They demonstrated that these superparamagnetic nanoparticles can reduce the expression of  $\alpha$ -synuclein and thus can prevent the toxic effects on the cell and suppress apoptosis by  $\alpha$ -synuclein (Niu et al., 2017).

Salama et al. (2017) isolated MSCs from C57BL/6 mice, incubated MSCs with micrometer-sized iron oxide (referred to as MPIOs) particles, and finally administrated them in a PD mouse model by the way of the intranasal (IN) route. In the experiment, MPIO-labeled MSCs were used as stem cell tracking stained with Prussian blue (Salama et al., 2017). The following histopathological evaluation by positive Prussian blue staining revealed the successful delivery of MSCs (Salama et al., 2017). The neurobehavioral assessment was improved following MSC administration (Salama et al., 2017).

Studies have confirmed that after receiving human ventral mesencephalic NSC (hVM1) grafts, parkinsonian animals showed an amelioration in resting tremor and cognitive performance (Kouyoumdjian et al., 2013). Based on this, Ramos-Gómez et al. (2015) believed that hVM1 cells and their derivatives represented a helpful method for cell therapies focused on neurodegenerative diseases, PD in particular. In the study, they found that MNPs of different sizes (with a diameter of 50 and 100 nm) were labeled with hVM cells nearly 100% in defect of any transfection agents (Ramos-Gómez et al., 2015). After transplanting MNP-labeled hVM cells into the striatum of the PD rat model, MNPs were distributed evenly throughout the transplant region detected by histological analysis (Ramos-Gómez et al., 2015). The researchers used MNPs to label hNSCs (human NSCs) and injected them into hemiparkinsonian rats

in order to follow stem cell fate over time to verify the efficient application of stem cells after transplantation (Ramos-Gómez et al., 2015). The result shows that by the use of MRI, the MNP-labeled hNSCs grafted into hemiparkinsonian rats can be successfully visualized up to 5 months after transplantation at different time points (Ramos-Gómez et al., 2015).

A recent study has demonstrated that dextran-coated IONPs (Dex-IO NPs) can improve the therapeutic effects of human MSCs in a mouse model of PD (Chung et al., 2018). The loss of dopaminergic neurons was decreased and the migration capacity and the differentiation of human MSCs to dopaminergic neurons were enhanced (Chung et al., 2018). Therefore, Dex-IO NPs can be considered as a promising carrier for MSC therapy for PD.

## Application of Iron Oxide Nanoparticles in the Diagnosis of ALS

Evans et al. (2014) suggested that T2-weighted MRI offered a strong biomarker potential in superoxide dismutase (SOD1) G93A transgenic ALS mouse model. They put VCAM-1 (vascular cell adhesion molecule 1, one cellular adhesion molecule that can upregulate during endothelial activation) together with MPIO (microparticles of iron oxide; Evans et al., 2014). However, they concluded that VCAM-MPIO as a biomarker in SOD1 ALS is useless (Evans et al., 2014).

## Application of Iron Oxide Nanoparticles in the Treatment of ALS

The therapeutic efficacy of SkmSCs (subpopulation of human skeletal muscle-derived stem cells) with MSC-like features was evaluated after intracerebroventricular injection to the Wr mouse (Wobbler mouse, the most typical model of spontaneous motor neuron degeneration) by Canzi et al. (2012). The research team confirmed that MRI can visualize stem cells and follow their migration after transplantation in the CNS of rodents (Canzi et al., 2012). Bigini et al. (2012) traced amniotic fluid cells (hAFCs) in a chronic neurodegenerative/inflammatory environment in a similar approach; after SPION loaded hAFC administration, the signal in the ventricles of the brain became hypointense in both healthy and Wr mice. All the abovementioned indicate that SPION can be a tracer to monitor the efficacy of stem cell therapy for ALS.

## SUMMARY

For neurodegenerative diseases such as AD, PD, and ALS, the early diagnosis toward these diseases is difficult. In order to improve the symptoms by drug therapy based on the diagnosis at the early stage of the disease, MRI CAs, especially SPIO and USPIO, have already been developed in

imaging and targeting drug delivery. Despite the fact that regulatory bodies have already approved some SPIO agents for many years, the clinical application of these agents has been proven a difficult journey (Wáng and Idée, 2017). For instance, by the end of 2015, only five types of SPIO had been designed and applied in clinical settings as magnetic resonance CAs (Yang et al., 2016). Of these, one is available only in a few countries; the other four have already been terminated in the follow-up study or even pulled out of the market (Yang et al., 2016). The mandatory requirements of nanoparticles should be improved, including biocompatibility, biodegradability, biodistribution, stability under physiological conditions, accurate pharmacokinetics, and minimal side effects. Designing nanoparticles to pass through the BBB is even more challenging and complex than conventional drug delivery. Major efforts should be made to improve targeted drug release and therapeutic efficacy, and to increase sensitivity and specificity of noninvasive imaging. And the olfactory pathway provides a noninvasive route for nanoparticles to enter the CNS. Even if the noninvasive imaging examination method cannot be applied to the human body temporarily, they can be used to the mouse model to explore new diagnostic and therapeutic methods for neurodegenerative diseases. It is not too far off before IONPs hold promise for the development of early diagnosis and the accomplishment of the aim of personalized therapy toward neurodegenerative diseases.

## AUTHOR CONTRIBUTIONS

SL, CM, M-QZ, and W-NJ searched the literature and drafted the manuscript. XW and YY critically revised the manuscript. All authors listed have made a substantial, direct, and intellectual contribution to the work, and approved it for publication.

## FUNDING

This study was supported by grants from the National Natural Science Foundation of China (Grant No. 81901083), Norman Bethune Program of Jilin University (Grant No. 2015335), the Key National Research Projects on Prevention and Control of Major Chronic Non-communicable Disease (2018YFC1312300), as well as from Fund of Science and Technology Development Project of Jilin Province (20180414041GH) and Jilin Health Technology Innovation Project (2019J003).

## ACKNOWLEDGMENTS

We would like to thank Editage for English language editing.

## REFERENCES

- Adams, R. A., Bauer, J., Flick, M. J., Sikorski, S. L., Nuriel, T., Lassmann, H., et al. (2007). The fibrin-derived gamma377–395 peptide inhibits microglia activation and suppresses relapsing paralysis in central nervous system autoimmune disease. *J. Exp. Med.* 204, 571–582. doi: 10.1084/jem.20061931
- Akilo, O. D., Choonara, Y. E., Strydom, A. M., du Toit, L. C., Kumar, P., Modi, G., et al. (2016). AN *in vitro* evaluation of a carmustine-loaded Nano-co-Plex for potential magnetic-targeted intranasal delivery to the brain. *Int. J. Pharm.* 500, 196–209. doi: 10.1016/j.ijpharm.2016.01.043
- André, S., Ansciaux, E., Saidi, E., Larbanoix, L., Stanicki, D., Nonclercq, D., et al. (2017). Validation by magnetic resonance imaging of the diagnostic potential of a heptapeptide-functionalized imaging probe targeted to amyloid-beta

- and able to cross the blood-brain barrier. *J. Alzheimers Dis.* 60, 1547–1565. doi: 10.3233/jad-170563
- Ansciaux, E., Burtet, C., Laurent, S., Crombez, D., Nonclercq, D., Vander Elst, L., et al. (2015). *In vitro* and *in vivo* characterization of several functionalized ultrasmall particles of iron oxide, vectorized against amyloid plaques and potentially able to cross the blood-brain barrier: toward earlier diagnosis of Alzheimer's disease by molecular imaging. *Contrast Media Mol. Imaging* 10, 211–224. doi: 10.1002/cmmi.1626
- Anwar, M., Asfer, M., Prajapati, A. P., Mohapatra, S., Akhter, S., Ali, A., et al. (2014). Synthesis and *in vitro* localization study of curcumin-loaded SPIONs in a micro capillary for simulating a targeted drug delivery system. *Int. J. Pharm.* 468, 158–164. doi: 10.1016/j.ijpharm.2014.04.038
- Arami, H., Khandhar, A., Liggitt, D., and Krishnan, K. M. (2015). *In vivo* delivery, pharmacokinetics, biodistribution and toxicity of iron oxide nanoparticles. *Chem. Soc. Rev.* 44, 8576–8607. doi: 10.1039/c5cs00541h
- Balestrino, R., and Schapira, A. H. V. (2019). Parkinson disease. *Eur. J. Neurol.* doi: 10.1111/ene.14108 [Epub ahead of print].
- Baloh, R. H., Glass, J. D., and Svendsen, C. N. (2018). Stem cell transplantation for amyotrophic lateral sclerosis. *Curr. Opin. Neurol.* 31, 655–661. doi: 10.1097/WCO.0000000000000598
- Barage, S. H., and Sonawane, K. D. (2015). Amyloid cascade hypothesis: pathogenesis and therapeutic strategies in Alzheimer's disease. *Neuropeptides* 52, 1–18. doi: 10.1016/j.npep.2015.06.008
- Bigini, P., Diana, V., Barbera, S., Fumagalli, E., Micotti, E., Sitia, L., et al. (2012). Longitudinal tracking of human fetal cells labeled with super paramagnetic iron oxide nanoparticles in the brain of mice with motor neuron disease. *PLoS One* 7:e32326. doi: 10.1371/journal.pone.0032326
- Brambilla, D., Le Droumaguet, B., Nicolas, J., Hashemi, S. H., Wu, L. P., Moghimi, S. M., et al. (2011). Nanotechnologies for Alzheimer's disease: diagnosis, therapy, and safety issues. *Nanomedicine* 7, 521–540. doi: 10.1016/j.nano.2011.03.008
- Busquets, M. A., Sabate, R., and Estelrich, J. (2014). Potential applications of magnetic particles to detect and treat Alzheimer's disease. *Nanoscale Res. Lett.* 9:538. doi: 10.1186/1556-276x-9-538
- Canzi, L., Castellana, V., Navone, S., Nava, S., Dossena, M., Zucca, I., et al. (2012). Human skeletal muscle stem cell antiinflammatory activity ameliorates clinical outcome in amyotrophic lateral sclerosis models. *Mol. Med.* 18, 401–411. doi: 10.2119/molmed.2011.00123
- Chamberlain, R., Reyes, D., Curran, G. L., Marjanska, M., Wengenack, T. M., Poduslo, J. F., et al. (2009). Comparison of amyloid plaque contrast generated by T2-weighted, T2\*-weighted, and susceptibility-weighted imaging methods in transgenic mouse models of Alzheimer's disease. *Magn. Reson. Med.* 61, 1158–1164. doi: 10.1002/mrm.21951
- Chamberlain, R., Wengenack, T. M., Poduslo, J. F., Garwood, M., and Jack, C. R. Jr. (2011). Magnetic resonance imaging of amyloid plaques in transgenic mouse models of Alzheimer's disease. *Curr. Med. Imaging Rev.* 7, 3–7. doi: 10.2174/157340511794653522
- Chandra, A., Valkimadi, P. E., Pagano, G., Cousins, O., Dervenoulas, G., and Politis, M. (2019). Applications of amyloid, tau, and neuroinflammation PET imaging to Alzheimer's disease and mild cognitive impairment. *Hum. Brain Mapp.* 40, 5424–5442. doi: 10.1002/hbm.24782
- Chen, X. Q., and Mobley, W. C. (2019). Alzheimer disease pathogenesis: insights from molecular and cellular biology studies of oligomeric A $\beta$  and tau species. *Front. Neurosci.* 13:659. doi: 10.3389/fnins.2019.00659
- Cheng, K. K., Chan, P. S., Fan, S., Kwan, S. M., Yeung, K. L., Wang, Y. X., et al. (2015). Curcumin-conjugated magnetic nanoparticles for detecting amyloid plaques in Alzheimer's disease mice using magnetic resonance imaging (MRI). *Biomaterials* 44, 155–172. doi: 10.1016/j.biomaterials.2014.12.005
- Chung, T. H., Hsu, S. C., Wu, S. H., Hsiao, J. K., Lin, C. P., Yao, M., et al. (2018). Dextran-coated iron oxide nanoparticle-improved therapeutic effects of human mesenchymal stem cells in a mouse model of Parkinson's disease. *Nanoscale* 10, 2998–3007. doi: 10.1039/c7nr06976f
- Corbett, A., Smith, J., and Ballard, C. (2012). New and emerging treatments for Alzheimer's disease. *Expert Rev. Neurother.* 12, 535–543. doi: 10.1586/ern.12.43
- De, M., Chou, S. S., Joshi, H. M., and Dravid, V. P. (2011). Hybrid magnetic nanostructures (MNS) for magnetic resonance imaging applications. *Adv. Drug Deliv. Rev.* 63, 1282–1299. doi: 10.1016/j.addr.2011.07.001
- Ding, H., Sagar, V., Agudelo, M., Pilakka-Kanthikeel, S., Atluri, V. S., Raymond, A., et al. (2014). Enhanced blood-brain barrier transmigration using a novel transferrin embedded fluorescent magneto-liposome nanoformulation. *Nanotechnology* 25:055101. doi: 10.1088/0957-4484/25/5/055101
- Dulińska-Litewka, J., Łazarczyk, A., Hałubiec, P., Szafranski, O., Karnas, K., and Karewicz, A. (2019). Superparamagnetic iron oxide nanoparticles—current and prospective medical applications. *Materials (Basel)* 12:E617. doi: 10.3390/ma12040617
- Evans, M. C., Serres, S., Khrapitchev, A. A., Stolp, H. B., Anthony, D. C., Talbot, K., et al. (2014). T(2)-weighted MRI detects presymptomatic pathology in the SOD1 mouse model of ALS. *J. Cereb. Blood Flow Metab.* 34, 785–793. doi: 10.1038/jcbfm.2014.19
- Fernández, T., Martínez-Serrano, A., Cussó, L., Desco, M., and Ramos-Gómez, M. (2018). Functionalization and characterization of magnetic nanoparticles for the detection of ferritin accumulation in Alzheimer's disease. *ACS Chem. Neurosci.* 9, 912–924. doi: 10.1021/acscchemneuro.7b00260
- Frisoni, G. B., Boccardi, M., Barkhof, F., Blennow, K., Cappa, S., Chiotis, K., et al. (2017). Strategic roadmap for an early diagnosis of Alzheimer's disease based on biomarkers. *Lancet Neurol.* 16, 661–676. doi: 10.1016/S1474-4422(17)30159-X
- Gagliardi, D., Meneri, M., Saccomanno, D., Bresolin, N., Comi, G. P., and Corti, S. (2019). Diagnostic and prognostic role of blood and cerebrospinal fluid and blood neurofilaments in amyotrophic lateral sclerosis: a review of the literature. *Int. J. Mol. Sci.* 20:E4152. doi: 10.3390/ijms20174152
- Giagkou, N., and Stamelou, M. (2018). Therapeutic management of the overlapping syndromes of atypical Parkinsonism. *CNS Drugs* 32, 827–837. doi: 10.1007/s40263-018-0551-3
- Glat, M., Skaat, H., Menkes-Caspi, N., Margel, S., and Stern, E. A. (2013). Age-dependent effects of microglial inhibition *in vivo* on Alzheimer's disease neuropathology using bioactive-conjugated iron oxide nanoparticles. *J. Nanobiotechnology* 11:32. doi: 10.1186/1477-3155-11-32
- Gupta, J., Fatima, M. T., Islam, Z., Khan, R. H., Uversky, V. N., and Salahuddin, P. (2019). Nanoparticle formulations in the diagnosis and therapy of Alzheimer's disease. *Int. J. Biol. Macromol.* 130, 515–526. doi: 10.1016/j.ijbiomac.2019.02.156
- Ikenaka, K., Suzuki, M., Mochizuki, H., and Nagai, Y. (2019). Lipids as trans-acting effectors for alpha-synuclein in the pathogenesis of Parkinson's disease. *Front. Neurosci.* 13:693. doi: 10.3389/fnins.2019.00693
- Javdani, N., Rahpeyma, S. S., Ghasemi, Y., and Raheb, J. (2019). Effect of superparamagnetic nanoparticles coated with various electric charges on  $\alpha$ -synuclein and  $\beta$ -amyloid proteins fibrillation process. *Int. J. Nanomedicine* 14, 799–808. doi: 10.2147/ijn.s190354
- Jiang, L. F., Chen, B. C., Chen, B., Li, X. J., Liao, H. L., Huang, H. M., et al. (2017). Detection of A $\beta$  oligomers based on magnetic-field-assisted separation of aptamer-functionalized Fe $_3$ O $_4$  magnetic nanoparticles and BaYF $_5$ :Yb,Er nanoparticles as upconversion fluorescence labels. *Talanta* 170, 350–357. doi: 10.1016/j.talanta.2017.04.021
- Jirak, D., Galisova, A., Kolouchova, K., Babuka, D., and Hruby, M. (2019). Fluorine polymer probes for magnetic resonance imaging: quo vadis? *MAGMA* 32, 173–185. doi: 10.1007/s10334-018-0724-6
- Katebi, S., Esmaili, A., Ghaedi, K., and Zarrabi, A. (2019). Superparamagnetic iron oxide nanoparticles combined with NGF and quercetin promote neuronal branching morphogenesis of PC12 cells. *Int. J. Nanomedicine* 14, 2157–2169. doi: 10.2147/ijn.s191878
- Khan, A. R., Liu, M., Khan, M. W., and Zhai, G. (2017). Progress in brain targeting drug delivery system by nasal route. *J. Control Release* 268, 364–389. doi: 10.1016/j.jconrel.2017.09.001
- Klohs, J., Balthes, C., Prinz-Kranz, F., Ratering, D., Nitsch, R. M., Knuesel, I., et al. (2012). Contrast-enhanced magnetic resonance microangiography reveals remodeling of the cerebral microvasculature in transgenic ArcA $\beta$  mice. *J. Neurosci.* 32, 1705–1713. doi: 10.1523/jneurosci.5626-11.2012
- Kong, S. D., Lee, J., Ramachandran, S., Eliceiri, B. P., Shubayev, V. I., Lal, R., et al. (2012). Magnetic targeting of nanoparticles across the intact blood-



- brain barrier. *J. Control Release* 164, 49–57. doi: 10.1016/j.jconrel.2012.09.021
- Kouyoumdjian, H., Zhu, D. C., El-Dakdouki, M. H., Lorenz, K., Chen, J., Li, W., et al. (2013). Glyconanoparticle aided detection of  $\beta$ -amyloid by magnetic resonance imaging and attenuation of  $\beta$ -amyloid induced cytotoxicity. *ACS Chem. Neurosci.* 4, 575–584. doi: 10.1021/cn3002015
- Li, Y., Lim, E., Field, T., Wu, H., and Mao, H. (2019). Improving sensitivity and specificity of amyloid- $\beta$  peptide and tau protein detection with anti-biofouling magnetic nanoparticles for liquid biopsy of Alzheimer's disease. *ACS Biomater. Sci. Eng.* 5, 3595–3605. doi: 10.1021/acsbmaterials.9b00086
- Ling, D., and Hyeon, T. (2013). Chemical design of biocompatible iron oxide nanoparticles for medical applications. *Small* 9, 1450–1466. doi: 10.1002/smll.201202111
- Mahmoudi, M., Quinlan-Pluck, F., Monopoli, M. P., Sheibani, S., Vali, H., Dawson, K. A., et al. (2013). Influence of the physiochemical properties of superparamagnetic iron oxide nanoparticles on amyloid  $\beta$  protein fibrillation in solution. *ACS Chem. Neurosci.* 4, 475–485. doi: 10.1021/cn300196n
- Marasini, R., Thanh Nguyen, T. D., and Aryal, S. (2020). Integration of gadolinium in nanostructure for contrast enhanced-magnetic resonance imaging. *Wiley Interdiscip. Rev. Nanomed. Nanobiotechnol.* 12:e1580. doi: 10.1002/wnan.1580
- Mirsadeghi, S., Shanehsazzadeh, S., Atyabi, F., and Dinarvand, R. (2016). Effect of PEGylated superparamagnetic iron oxide nanoparticles (SPIONs) under magnetic field on amyloid  $\beta$  fibrillation process. *Mater. Sci. Eng. C Mater. Biol. Appl.* 59, 390–397. doi: 10.1016/j.msec.2015.10.026
- Niu, S., Zhang, L. K., Zhang, L., Zhuang, S., Zhan, X., Chen, W. Y., et al. (2017). Inhibition by multifunctional magnetic nanoparticles loaded with  $\alpha$ -synuclein RNAi plasmid in a Parkinson's disease model. *Theranostics* 7, 344–356. doi: 10.7150/thno.16562
- Olsson, B., Lautner, R., Andreasson, U., Ohrfelt, A., Portelius, E., Bjerke, M., et al. (2016). CSF and blood biomarkers for the diagnosis of Alzheimer's disease: a systematic review and meta-analysis. *Lancet Neurol.* 15, 673–684. doi: 10.1016/S1474-4422(16)00070-3
- Petiet, A., Santin, M., Bertrand, A., Wiggins, C. J., Petit, F., Houitte, D., et al. (2012). Gadolinium-staining reveals amyloid plaques in the brain of Alzheimer's transgenic mice. *Neurobiol. Aging* 33, 1533–1544. doi: 10.1016/j.neurobiolaging.2011.03.009
- Pillai, J. A., Appleby, B. S., Safar, J., and Leverenz, J. B. (2018). Rapidly progressive Alzheimer's disease in two distinct autopsy cohorts. *J. Alzheimers Dis.* 64, 973–980. doi: 10.3233/jad-180155
- Podusko, J. F., Wengenack, T. M., Curran, G. L., Wisniewski, T., Sigurdsson, E. M., Macura, S. I., et al. (2002). Molecular targeting of Alzheimer's amyloid plaques for contrast-enhanced magnetic resonance imaging. *Neurobiol. Dis.* 11, 315–329. doi: 10.1006/nbdi.2002.0550
- Ramos-Gómez, M., Seiz, E. G., and Martínez-Serrano, A. (2015). Optimization of the magnetic labeling of human neural stem cells and MRI visualization in the hemiparkinsonian rat brain. *J. Nanobiotechnology* 13:20. doi: 10.1186/s12951-015-0078-4
- Rashid, H. U., Martinez, M. A. U., Jorge, J., de Moraes, P. M., Umar, M. N., Khan, K., et al. (2016). Cyclen-based  $Gd^{3+}$  complexes as MRI contrast agents: relaxivity enhancement and ligand design. *Bioorg. Med. Chem.* 24, 5663–5684. doi: 10.1016/j.bmc.2016.09.069
- Rotman, M., Snoeks, T. J., and van der Weerd, L. (2011). Pre-clinical optical imaging and MRI for drug development in Alzheimer's disease. *Drug Discov. Today Technol.* 8, e117–e125. doi: 10.1016/j.ddtec.2011.11.005
- Sachdeva, A. K., Misra, S., Pal Kaur, I., and Chopra, K. (2015). Neuroprotective potential of sesamol and its loaded solid lipid nanoparticles in ICV-STZ-induced cognitive deficits: behavioral and biochemical evidence. *Eur. J. Pharmacol.* 747, 132–140. doi: 10.1016/j.ejphar.2014.11.014
- Salama, M., Sobh, M., Emam, M., Abdalla, A., Sabry, D., El-Gamal, M., et al. (2017). Effect of intranasal stem cell administration on the nigrostriatal system in a mouse model of Parkinson's disease. *Exp. Ther. Med.* 13, 976–982. doi: 10.3892/etm.2017.4073
- Sibov, T. T., Pavon, L. F., Miyaki, L. A., Mamani, J. B., Nucci, L. P., Alvarim, L. T., et al. (2014). Umbilical cord mesenchymal stem cells labeled with multimodal iron oxide nanoparticles with fluorescent and magnetic properties: application for *in vivo* cell tracking. *Int. J. Nanomedicine* 9, 337–350. doi: 10.2147/ijn.s53299
- Sillerud, L. O., Solberg, N. O., Chamberlain, R., Orlando, R. A., Heidrich, J. E., Brown, D. C., et al. (2013). SPION-enhanced magnetic resonance imaging of Alzheimer's disease plaques in A $\beta$ PP/PS-1 transgenic mouse brain. *J. Alzheimers Dis.* 34, 349–365. doi: 10.3233/jad-121171
- Skaat, H., Corem-Slakmon, E., Grinberg, I., Last, D., Goetz, D., Mardor, Y., et al. (2013). Antibody-conjugated, dual-modal, near-infrared fluorescent iron oxide nanoparticles for anti-amyloidogenic activity and specific detection of amyloid-beta fibrils. *Int. J. Nanomedicine* 8, 4063–4076. doi: 10.2147/ijn.s52833
- Soto, C., and Pritzkow, S. (2018). Protein misfolding, aggregation and conformational strains in neurodegenerative diseases. *Nat. Neurosci.* 21, 1332–1340. doi: 10.1038/s41593-018-0235-9
- Sonawane, S. K., Ahmad, A., and Chinnathambi, S. (2019). Protein-capped metal nanoparticles inhibit tau aggregation in Alzheimer's disease. *ACS Omega* 4, 12833–12840. doi: 10.1021/acsomega.9b01411
- Staff, N. P., Jones, D. T., and Singer, W. (2019). Mesenchymal stromal cell therapies for neurodegenerative diseases. *Mayo Clin. Proc.* 94, 892–905. doi: 10.1016/j.mayocp.2019.01.001
- Sugaya, K., and Vaidya, M. (2018). Stem cell therapies for neurodegenerative diseases. *Adv. Exp. Med. Biol.* 1056, 61–84. doi: 10.1007/978-3-319-74470-4\_5
- Sun, Z., Worden, M., Thliveris, J. A., Hombach-Klonisch, S., Klonisch, T., van Lierop, J., et al. (2016). Biodistribution of negatively charged iron oxide nanoparticles (IONPs) in mice and enhanced brain delivery using lysophosphatidic acid (LPA). *Nanomedicine* 12, 1775–1784. doi: 10.1016/j.nano.2016.04.008
- Tafaya, M. A., Madi, S., and Sillerud, L. O. (2017). Superparamagnetic nanoparticle-enhanced MRI of Alzheimer's disease plaques and activated microglia in 3X transgenic mouse brains: contrast optimization. *J. Magn. Reson. Imaging* 46, 574–588. doi: 10.1002/jmri.25563
- Teleanu, D. M., Negut, I., Grumezescu, V., Grumezescu, A. M., and Teleanu, R. I. (2019). Nanomaterials for drug delivery to the central nervous system. *Nanomaterials (Basel)* 9:E371. doi: 10.3390/nano9030371
- Thomsen, L. B., Thomsen, M. S., and Moos, T. (2015). Targeted drug delivery to the brain using magnetic nanoparticles. *Ther. Deliv* 6, 1145–1155. doi: 10.4155/tde.15.56
- Tiwari, S., Atluri, V., Kaushik, A., Yndart, A., and Nair, M. (2019). Alzheimer's disease: pathogenesis, diagnostics and therapeutics. *Int. J. Nanomedicine* 14, 5541–5554. doi: 10.2147/IJN.S200490
- Wadghiri, Y. Z., Li, J., Wang, J., Hoang, D. M., Sun, Y., Xu, H., et al. (2013). Detection of amyloid plaques targeted by bifunctional USPIO in Alzheimer's disease transgenic mice using magnetic resonance microimaging. *PLoS One* 8:e57097. doi: 10.1371/journal.pone.0057097
- Wáng, Y. X., and Idée, J. M. (2017). A comprehensive literatures update of clinical researches of superparamagnetic resonance iron oxide nanoparticles for magnetic resonance imaging. *Quant. Imaging Med. Surg.* 7, 88–122. doi: 10.21037/qims.2017.02.09
- Wengenack, T. M., Reyes, D. A., Curran, G. L., Borowski, B. J., Lin, J., Preboske, G. M., et al. (2011). Regional differences in MRI detection of amyloid plaques in AD transgenic mouse brain. *NeuroImage* 54, 113–122. doi: 10.1016/j.neuroimage.2010.08.033
- Yang, C. C., Yang, S. Y., Chieh, J. J., Horng, H. E., Hong, C. Y., Yang, H. C., et al. (2011a). Biofunctionalized magnetic nanoparticles for specifically detecting biomarkers of Alzheimer's disease *in vitro*. *ACS Chem. Neurosci.* 2, 500–505. doi: 10.1021/cn200028j
- Yang, J., Wadghiri, Y. Z., Hoang, D. M., Tsui, W., Sun, Y., Chung, E., et al. (2011b). Detection of amyloid plaques targeted by USPIO-A $\beta$ 1–42 in Alzheimer's disease transgenic mice using magnetic resonance microimaging. *NeuroImage* 55, 1600–1609. doi: 10.1016/j.neuroimage.2011.01.023
- Yang, S. Y., Chiu, M. J., Lin, C. H., Horng, H. E., Yang, C. C., Chieh, J. J., et al. (2016). Development of an ultra-high sensitive immunoassay with plasma biomarker for differentiating Parkinson disease dementia from



- Parkinson disease using antibody functionalized magnetic nanoparticles. *J. Nanobiotechnology* 14:41. doi: 10.1186/s12951-016-0198-5
- Yarjanli, Z., Ghaedi, K., Esmaili, A., Rahgozar, S., and Zarrabi, A. (2017). Iron oxide nanoparticles may damage to the neural tissue through iron accumulation, oxidative stress and protein aggregation. *BMC Neurosci.* 18:51. doi: 10.1186/s12868-017-0369-9
- Yoshiyama, Y., Higuchi, M., Zhang, B., Huang, S. M., Iwata, N., Saido, T. C., et al. (2007). Synapse loss and microglial activation precede tangles in a P301S tauopathy mouse model. *Neuron* 53, 337–351. doi: 10.1016/j.neuron.2007.01.010
- Zhang, D., Fa, H. B., Zhou, J. T., Li, S., Diao, X. W., and Yin, W. (2015). The detection of beta-amyloid plaques in an Alzheimer's disease rat model with DDNP-SPIO. *Clin. Radiol.* 70, 74–80. doi: 10.1016/j.crad.2014.09.019
- Zhou, J., Fa, H., Yin, W., Zhang, J., Hou, C., Huo, D., et al. (2014). Synthesis of superparamagnetic iron oxide nanoparticles coated with a DDNP-carboxyl derivative for *in vitro* magnetic resonance imaging of Alzheimer's disease. *Mater. Sci. Eng. C Mater. Biol. Appl.* 37, 348–355. doi: 10.1016/j.msec.2014.01.005
- Conflict of Interest:** The authors declare that the research was conducted in the absence of any commercial or financial relationships that could be construed as a potential conflict of interest.

Copyright © 2020 Luo, Ma, Zhu, Ju, Yang and Wang. This is an open-access article distributed under the terms of the Creative Commons Attribution License (CC BY). The use, distribution or reproduction in other forums is permitted, provided the original author(s) and the copyright owner(s) are credited and that the original publication in this journal is cited, in accordance with accepted academic practice. No use, distribution or reproduction is permitted which does not comply with these terms.



# Proteostasis of $\alpha$ -Synuclein and Its Role in the Pathogenesis of Parkinson's Disease

Deqiang Han<sup>1,2,3</sup>, Wei Zheng<sup>1,2,3</sup>, Xueyao Wang<sup>1,2,3</sup> and Zhiguo Chen<sup>1,2,3\*</sup>

<sup>1</sup>Key Laboratory of Neurodegenerative Diseases, Ministry of Education, Cell Therapy Center, National Clinical Research Center for Geriatric Diseases, Beijing Institute of Geriatrics, Xuanwu Hospital Capital Medical University, Beijing, China, <sup>2</sup>Center of Neural Injury and Repair, Beijing Institute for Brain Disorders, Beijing, China, <sup>3</sup>Center of Parkinson's Disease, Beijing Institute for Brain Disorders, Beijing, China

Aggregation of  $\alpha$ -Synuclein, possibly caused by disturbance of proteostasis, has been identified as a common pathological feature of Parkinson's disease (PD). However, the initiating events of aggregation have not been fully illustrated, and this knowledge may be critical to understanding the disease mechanisms of PD. Proteostasis is essential in maintaining normal cellular metabolic functions, which regulate the synthesis, folding, trafficking, and degradation of proteins. The toxicity of the aggregating proteins is dramatically influenced by its physical and physiological status. Genetic mutations may also affect the metastable phase transition of proteins. In addition, neuroinflammation, as well as lipid metabolism and its interaction with  $\alpha$ -Synuclein, are likely to contribute to the pathogenesis of PD. In this review article, we will highlight recent progress regarding  $\alpha$ -Synuclein proteostasis in the context of PD. We will also discuss how the phase transition status of  $\alpha$ -Synuclein could correlate with different functional consequences in PD.

## OPEN ACCESS

### Edited by:

Karla Guadalupe Carvajal,  
National Institute of Pediatrics  
(Mexico), Mexico

### Reviewed by:

Tatsuro Mutoh,  
Fujita Health University, Japan  
Krishnan Prabhakaran,  
Norfolk State University,  
United States

### \*Correspondence:

Zhiguo Chen  
chenzhiguo@gmail.com

**Received:** 24 September 2019

**Accepted:** 18 February 2020

**Published:** 10 March 2020

### Citation:

Han D, Zheng W, Wang X and  
Chen Z (2020) Proteostasis of  
 $\alpha$ -Synuclein and Its Role in the  
Pathogenesis of Parkinson's Disease.  
*Front. Cell. Neurosci.* 14:45.  
doi: 10.3389/fncel.2020.00045

**Keywords:**  $\alpha$ -synuclein, phase transition, Parkinson's disease, proteostasis, genetic mutations, inflammation

## INTRODUCTION

Parkinson's disease (PD) is a common progressive neurodegenerative disorder that affects 1–3% of the aging population (Pringsheim et al., 2014; Kalia and Lang, 2015). The clinical symptoms of PD include resting tremor, rigidity, bradykinesia and postural instability (Jankovic, 2008). One of the neuropathological hallmarks of PD is reduced dopaminergic neurons in the substantia nigra (SN) pars compacta, which causes striatal dopamine deficiency (Obeso et al., 2010; Poewe et al., 2017; Hyung Ho Yoon and Jeon, 2018). Another pathological feature is intraneuronal inclusions, such as Lewy bodies and Lewy neurites in residual dopaminergic neurons. The major constituent of Lewy body is aggregated  $\alpha$ -Synuclein (Spillantini et al., 1997; Wakabayashi et al., 2013). Abnormally folded proteins may present with different forms, such as small oligomers, aggregates, and complex inclusions; accumulation of misfolded proteins contributes to the progression of neurodegenerative diseases including PD (Hetz and Mollereau, 2014). Proteostasis is essential in maintaining normal cellular metabolic functions that regulate the synthesis, folding, trafficking, and degradation of proteins. The toxicity of the aggregating proteins is dramatically influenced by the physical and physiological status. In addition, genetic mutations may affect the metastable phase transition of proteins. In addition to playing a central role in the neurodegenerative process of PD,  $\alpha$ -Synuclein contributes to the initiation and persistence of inflammatory responses—another important feature of PD. Also detected in Lewy body aggregates in post-mortem brain tissues are lipid vesicles

and membrane fragments (Shahmoradian et al., 2019), suggesting that lipid metabolism may be implicated in PD. In this review, we will highlight recent progress in the research area regarding  $\alpha$ -Synuclein proteostasis and its role in the pathogenesis of PD. We will also discuss how phase transition and posttranslational modification (PTM) of  $\alpha$ -Synuclein may correlate with different functional consequences. Additionally, we will take into account neuroinflammation and lipid metabolism and discuss its interaction with  $\alpha$ -Synuclein in the context of PD (Figure 1).

## **$\alpha$ -SYNUCLEIN PLAYS A CENTRAL ROLE IN THE NEURODEGENERATIVE PROCESS OF PARKINSON'S DISEASE**

### **Homeostasis of $\alpha$ -Synuclein in PD**

$\alpha$ -Synuclein is the major component of intraneuronal protein aggregates in patients with PD and plays a key function in the progression of this disease (Poewe et al., 2017). Intracellular homeostasis of  $\alpha$ -Synuclein is maintained under intrinsic surveillance mechanisms including the ubiquitin-proteasome system (UPS) and lysosomal autophagy system (LAS). LAS seems to be more important than UPS in clearing the oligomeric assemblies. A recent study showed that inclusion formation is dependent on the concentration of  $\alpha$ -Synuclein, whereas clearance of inclusion is mediated by the autophagy pathway, as revealed by quantitative measurement of the formation and clearance of  $\alpha$ -Synuclein inclusions in a yeast model of PD (Perrino et al., 2019). Accumulation of  $\alpha$ -Synuclein is largely associated with the impairment of these degradation systems (Xilouri et al., 2013). In turn, abnormal proteins can directly or indirectly interfere with the UPS mechanisms and further affect the function of related pathways, leading to irreversible changes in neuronal protein homeostasis and degeneration (Cookson, 2009; Sato et al., 2018).

### **Structure Feature of $\alpha$ -Synuclein Underlies the Pathogenesis of PD**

$\alpha$ -Synuclein is normally expressed at high levels in neurons and possibly in oligodendrocytes in the CNS (Asi et al., 2014; Mehra et al., 2019). It is an intrinsically disordered protein that exists in both a soluble and a membrane-bound form in neurons (Mehra et al., 2019). The structure of  $\alpha$ -Synuclein includes three domains. N-terminal region (1–60 Aa) that enables the protein to bind to membranes, contains seven conserved repeat sequences which form an amphipathic  $\alpha$ -helix (Davidson et al., 1998). Non-amyloid component (NAC; 61–95) containing a highly hydrophobic motif that regulates the oligomerization and fibrillogenesis process is necessary for aggregation of  $\alpha$ -Synuclein. The C-terminal tail (96–140) is involved in nuclear localization as well as interactions with other proteins, small molecules, and metals (Eliezer et al., 2001; Ulmer et al., 2005). The pathological gain of neurotoxicity related to  $\alpha$ -Synuclein involves multiple biological processes. Initially, soluble  $\alpha$ -Synuclein monomers form oligomers, then

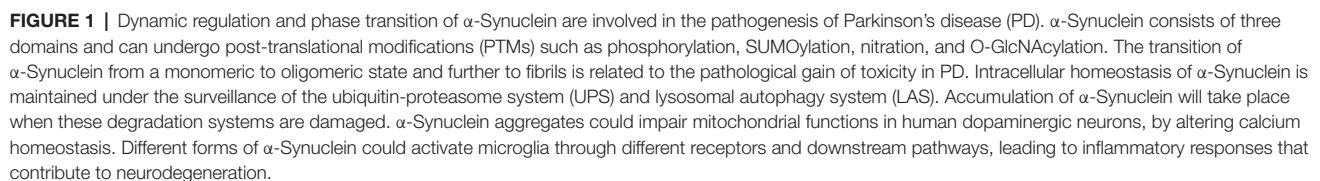
gradually accumulate into insoluble mature fibrils; eventually,  $\alpha$ -Synuclein aggregates into large insoluble fibrils which is more toxic to neurons and can cause cell death and progressive motor impairment (Melki, 2015; Peelaerts et al., 2015; Mor et al., 2016; Karpowicz et al., 2019; Ma et al., 2019). The fibrillar form of  $\alpha$ -Synuclein assemblies is capable of promoting aggregation of monomeric  $\alpha$ -Synuclein *in vitro* and this phenomenon can spread across cells in a prion-like fashion in cell cultures and animal models (Karpowicz et al., 2019; Ma et al., 2019).

### **Phase Transition of $\alpha$ -Synuclein and Its Potential Role in the Pathogenesis of PD**

Phase separation occurs when single-phase complexes divide into a concentrated phase and a diluted phase. Eukaryotic cells use phase transition strategies to facilitate the formation of membraneless intracellular territories (Verdile et al., 2019). Through weak intermolecular interactions, multivalent proteins reach a solubility limit to form liquid condensates (Banani et al., 2017; Shin and Brangwynne, 2017). Several proteins undergoing phase transition include intrinsically disordered regions (IDRs). The IDRs often contain prion-like domains (PLDs) and low complexity domains (LCDs; Hughes et al., 2018; Maharana et al., 2018; Wang et al., 2018). Further, the N-terminal domain of  $\alpha$ -Synuclein that mediates the aggregation process has two LCDs, indicating that  $\alpha$ -Synuclein may, under appropriate conditions, undergo phase separation (Guerrero-Ferreira et al., 2018; Li et al., 2018).

$\alpha$ -Synuclein in monomeric ensembles can exist as distinct conformational phases (Jónsson et al., 2012). Aggregation of abnormally folded proteins is generally considered as a sequential oligomerization process, adding monomers to the already formed nuclei (Serio et al., 2000). The process of aggregation displays an initial lag phase in which precursor clusters assemble spontaneously. To examine such early steps in aggregation, Narayanan et al. (2019) developed a quantitative methodology that employs super-resolution imaging of fixed cells and light-sheet imaging of living cells. They found that mammalian cells have precursor clusters even under normal growth conditions, suggesting that early aggregates behave like condensates.

To further shed light on the early events of aggregation formation of  $\alpha$ -Synuclein, recent studies showed that liquid-liquid phase separation of  $\alpha$ -Synuclein precedes aggregation by using *in vitro* reconstitution and cellular models. Liquid-like droplets of  $\alpha$ -Synuclein generated *in vitro* eventually transition from a liquid to a solid form that contains oligomers and fibrils. Consistently, some aggravation-related factors like low pH, phosphomimetics, and familial PD mutations also promote  $\alpha$ -Synuclein liquid-liquid phase separation and its subsequent maturation. Furthermore, *in vivo* evidence demonstrated that liquid droplets of  $\alpha$ -Synuclein transform into perinuclear aggresomes under oxidative stress. The phase transition of natural unstructured  $\alpha$ -Synuclein and its transformation to an aggregated disease-associated state is closely correlated with the pathogenesis of PD (Ray et al., 2019).



$\alpha$ -Synuclein can be phosphorylated at serine 129; phosphorylation at this position is toxic and can enhance the formation of  $\alpha$ -Synuclein oligomers and accelerate neuronal loss.  $\alpha$ -Synuclein can also be modified by PIAS2 that adds a small ubiquitin-like modifier (SUMO) at lysine residues. However, how SUMOylation may influence the property of  $\alpha$ -Synuclein remains inconclusive and seemingly contradictory results have

Oxidative stress may be another contributor to the pathogenesis of PD. Widespread accumulation of nitrated  $\alpha$ -Synuclein in inclusions have been detected by using antibodies specific to nitrated tyrosine residues of  $\alpha$ -Synuclein (Giasson et al., 2000). Further studies showed that four locations of tyrosine are susceptible to nitration (Y39, Y125, Y133, and Y136; Giasson et al., 2000; Schapira and Jenner, 2011; Bose and Beal, 2016). Abundant evidence suggests that nitration of  $\alpha$ -Synuclein is implicated in the toxicity of aggregates. Nitration of Y-39 speeds up the oligomerization of  $\alpha$ -Synuclein. Interestingly, a mutation of this site to cysteine residue leads to high levels



of fibrillation (Zhou and Freed, 2004; Danielson et al., 2009). Nitrated  $\alpha$ -Synuclein in the form of a monomer or dimer accelerates fibril formation and can seed the fibrillation of unmodified  $\alpha$ -Synuclein. Further study showed that nitration-induced  $\alpha$ -Synuclein oligomerization involves interactions between the N- and C-terminal regions of different  $\alpha$ -Synuclein molecules. Nitration on the N- or C-terminal regions impact the order of oligomerization; for example, only dimers are formed when Y39 is not available for nitration (Burai et al., 2015). Another study showed that nitration of  $\alpha$ -Synuclein can stabilize the formation of lower molecular weight oligomers, resulting in decreased fibril formation (Hodara et al., 2004). In all, nitration may be part of the complicated regulatory mechanisms that control the proteostasis of  $\alpha$ -Synuclein (Burai et al., 2015).

O-GlcNAcylation is a dynamic process, in which GlcNAc is transferred by O-GlcNAc transferase (OGT) from UDP-GlcNAc to the serine and threonine residues, and subsequently removed by O-GlcNAcase (OGA; Hart et al., 2007).  $\alpha$ -Synuclein can be O-GlcNAcylated at nine different positions (Marotta et al., 2015). Proper O-GlcNAcylation of certain proteins prevents their aggregation, and loss of this modification is a contributing factor in the development of neurodegenerative diseases. It has been verified that the O-GlcNAcylation of  $\alpha$ -Synuclein stabilizes the monomeric state of proteins and alters the structure of  $\alpha$ -Synuclein aggregates (Marotta et al., 2015; Zhang et al., 2019). In general, O-GlcNAcylation inhibits the aggregation of  $\alpha$ -Synuclein. Furthermore,  $\alpha$ -Synuclein with three O-GlcNAc modifications can prevent the aggregation of unmodified proteins. O-GlcNAcylation of  $\alpha$ -Synuclein peptide also inhibits the toxicity of extracellular  $\alpha$ -Synuclein fibrils (Levine et al., 2019).

## THE ORDER OF OLIGOMERIZATION AND TOXICITY

The transition of  $\alpha$ -Synuclein from a monomeric to oligomeric state leads to a pathological toxic function in PD.  $\alpha$ -Synuclein as monomers interacts and regulates ATP synthase to augment the efficiency of ATP production under physiological conditions (Ludtmann et al., 2016). In contrast,  $\alpha$ -Synuclein in the state of beta sheet-rich oligomers interacts with mitochondrial proteins such as ATP synthase and disturbs complex I-dependent functions. Interaction with oligomers induces oxidation of the beta subunit of ATP synthase and peroxidation of mitochondrial lipid. These events further augment the likelihood to form permeability transition pore (PTP) which is toxic to cells (Ludtmann et al., 2018).  $\alpha$ -Synuclein fibrils also cause neurotoxicity and cell death by activating nitric oxide synthase (NOS), leading to DNA damage and polymerase-1 (PARP-1) activation. Reciprocally, PAR accelerates the fibrillation of  $\alpha$ -Synuclein (Kam et al., 2018). It seems that different states of  $\alpha$ -Synuclein exert various, even opposing effects in cells. The soluble monomers are harmless, whereas oligomers and fibrils are toxic, although the extent of toxicity may be different. Exactly how the order of oligomerization and change of the

configuration may impact on the toxicity of  $\alpha$ -Synuclein requires further studies.

## PROTEOSTASIS OF $\alpha$ -SYNUCLEIN AND INFLAMMATION CONTRIBUTE TO EARLY PATHOGENESIS OF PARKINSON'S DISEASE

Microglia are the major abundant CNS-specific immune cells that participate in the maintenance of brain homeostasis through mediating inflammation and/or phagocytosis. Chronic microgliosis is considered a pathological feature of PD, and the levels of inflammatory factors secreted by microglia correlate with the progression of PD (Labzin et al., 2018). Different forms of  $\alpha$ -Synuclein exhibit distinct effects in triggering microglial phagocytosis and inflammation. Rather than oligomers of  $\alpha$ -Synuclein which only induce upregulation of IL-1 $\beta$  (Krashia et al., 2019), fibrillar  $\alpha$ -Synuclein is able to elicit strong pro-inflammatory responses in a microglial cell line (Gustot et al., 2015; Hoffmann et al., 2016; Zhou et al., 2016). Fibrillar  $\alpha$ -Synuclein can activate NLRP3 inflammasome which leads to the cleaving of pro-inflammatory cytokines, such as IL-1 $\beta$  and IL-18 (Zhou et al., 2016; Chatterjee et al., 2020; Haque et al., 2020). Also, using a rat model that overexpresses human  $\alpha$ -Synuclein, Krashia et al. found that  $\alpha$ -Synuclein-induced inflammation precedes nigral degeneration, and administration of resolving D1, a potent lipid mediator that can resolve inflammation to promote restoration of tissue homeostasis, prevents neuronal dysfunction and motor deficits (Krashia et al., 2019). Multiple receptors and pathways are responsible for inducing pro-inflammatory responses in microglia in PD (Table 1). Both TLR2 and TLR4, whose expression levels are increased in PD patients and MPTP-administrated models, can be activated by  $\alpha$ -Synuclein to induce sterile inflammation in PD (Kaur et al., 2017; Ferreira and Romero-Ramos, 2018). The oligomer of  $\alpha$ -Synuclein can bind to the P2X7 receptor to activate the PI3K/AKT pathway in BV2 cells, a microglial cell line.  $\alpha$ -Synuclein aggregates can also be internalized in autophagosomes via Fc $\gamma$ R on microglia, which leads to activation of NF- $\kappa$ B pathway (Cao et al., 2012). CD36 is possibly involved in  $\alpha$ -Synuclein-induced microglial activation but the mechanism remains elusive (Ferreira and Romero-Ramos, 2018). Prostaglandin E2 receptor subtype 2 (EP2) on microglia seems to play a critical part in neurotoxicity caused by  $\alpha$ -Synuclein aggregation, based on *in vivo* and *in vitro* evidence (Jin et al., 2007). Aggregated nitrated  $\alpha$ -Synuclein can induce ROS production from microglia, which is inhibited by blockade of potassium channels (Thomas et al., 2007). In turn, activated microglia and inflammation might promote  $\alpha$ -Synuclein misfolding and aggregation. Wang et al. (2016) reported that inflammation-induced caspase 1 activation directly cleaves wild-type  $\alpha$ -Synuclein, and the truncated  $\alpha$ -Synuclein is more prone to aggregation and leads to toxicity in a neuronal PD cellular model. The effect of immune cells and inflammation on the spread of prion-like  $\alpha$ -Synuclein remains largely unexplored. On the one hand, spread of  $\alpha$ -Synuclein is determined by the

**TABLE 1** | Receptors on microglia that are involved in  $\alpha$ -Synuclein-induced responses.

Receptor	$\alpha$ -Synuclein phase	Pro/anti-inflammation	Description	Reference
CD14 and TLR4	Monomer	Pro-inflammation	Mediating phagocytosis of $\alpha$ -Synuclein	Kitchens (2000), Muriel et al. (2002), Stefanova et al. (2011) and Fellner et al. (2013)
TLR1 and TLR2	Oligomer	Pro-inflammation	Relating to $\alpha$ -Synuclein toxicity and inflammation	Klegeris et al. (2008), Wilms et al. (2009), Prabhakaran et al. (2011), Kim et al. (2013) and Daniele et al. (2015)
CD36	Monomer	Pro-inflammation	Mediating oxidative stress	Ferreira and Romero-Ramos (2018)
P2X7R and eATP	Oligomer	Pro-inflammation	Mediating oxidative stress	Jiang et al. (2015)
CD11b/CD18	Oligomer /fibril	Pro-inflammation	Mediating oxidative stress	Wang et al. (2015)
EP2	Oligomer	Pro-inflammation	Regulating $\alpha$ -Synuclein aggregation and associated neurotoxicity	Jin et al. (2007)
Ion transport channel	Nitrated $\alpha$ -Synuclein	Pro-inflammation	Mediating oxidative stress	Thomas et al. (2007)
FcyR	Fibril and IgG	Anti-inflammation	Preventing hyper-activation and inducing SHP-1 activation	Smith and Clatworthy (2010), Choi et al. (2015) and Chauhan et al. (2017)
MHC II	Peptides	Anti-inflammation	Inducing $\alpha$ -Synuclein degradation	Sulzer et al. (2017)

dynamic net sum of seeding, propagation, and phagocytosis of fibrillar  $\alpha$ -Synuclein, and microglia are beneficial in a sense that they can facilitate clearance of  $\alpha$ -Synuclein aggregates and damaged neurons. On the other hand, inflammation-induced reactive species might have a negative influence on the conformation changes of  $\alpha$ -Synuclein; but the detailed mechanisms require further investigation.

## THE ROLE OF LIPID METABOLISM AND ITS INTERACTION WITH $\alpha$ -SYNUCLEIN IN THE PATHOGENESIS OF PD

Accumulating evidence has suggested that lipid metabolism and its interaction with  $\alpha$ -Synuclein are implicated in many aspects of PD pathogenesis. Upon binding of  $\alpha$ -Synuclein to synthetic lipid membranes in an *in vitro* test,  $\alpha$ -Synuclein undergoes a structural transition from random coil to alpha-helical secondary conformation (Davidson et al., 1998).  $\alpha$ -Synuclein binds to small vesicles containing acidic phospholipids preferentially instead of to those with a net neutral charge. The membrane-bound form may have a higher aggregation propensity than the cytosolic form, and membrane-bound  $\alpha$ -Synuclein can generate nuclei which are able to seed the more abundant cytosolic form (Lee et al., 2002). Interaction with the membrane is in agreement with the proposed biological functions of  $\alpha$ -Synuclein, such as regulation of synaptic plasticity. The binding affinity of  $\alpha$ -Synuclein to model membranes is much higher when the membrane is in a fluid phase vs. in a gel phase (Galvagnion et al., 2016). The solubility, but not the fluidity, determine the magnitude by which membrane prompts fibril formation of  $\alpha$ -Synuclein (Galvagnion et al., 2016). This evidences demonstrated that the chemical properties of lipids determine the balance between functional and deleterious interactions of  $\alpha$ -Synuclein with lipid membranes, allowing for a deeper understanding of how this interaction may contribute to neurodegeneration. These data implicate a possible way of involvement of inflammation in aggregate formation since inflammation-induced reactive species can directly alter the property of membranes. Another factor that may influence membrane property is aging. Hallett et al. reported, in the aging brain, an aberrant association between  $\alpha$ -Synuclein and dopamine vesicular membrane, which was concurrent with synaptic destabilization (Hallett et al., 2019). However, overexpression of  $\alpha$ -Synuclein without lipid deregulation does not result in the otherwise observed abnormality, suggesting that the aberrant association is lipid-dependent (Brekke et al., 2018). Lipid trafficking also seems to be involved in PD pathogenesis. Lipids are transported by Rab proteins. Chung et al. (2009) found that Rab3b is more highly expressed in A10 vs. A9 dopaminergic neurons, which could be one reason accountable for the relatively greater vulnerability of A9 neurons compared with A10 neurons; overexpression of Rab3b in A9 neurons in rats confers a protective effect and leads to improved motor functions in a PD model. In another study, overexpression of a different Rab protein, Rab1a, normalizes expression of  $\alpha$ -Synuclein in patient neurons on a genetic background of SNCA triplication, possibly through enhanced

trafficking to lysosomes (Mazzulli et al., 2016). The study points out an interesting approach to cope with the accumulation of  $\alpha$ -Synuclein in PD.

## CROSSTALK BETWEEN $\alpha$ -SYNUCLEIN AND MITOCHONDRIAL DYSFUNCTION

Multiple studies have demonstrated that  $\alpha$ -Synuclein aggregation and mitochondrial dysfunction are both important in the pathogenesis of PD. Accumulating data showed that  $\alpha$ -Synuclein aggregation and mitochondrial defects may have a bidirectional interaction.  $\alpha$ -Synuclein interacts with mitochondria by specifically binding to the TOM20 receptor, inhibiting mitochondrial protein import machinery, and impairing mitochondrial functions (Di Maio et al., 2016).  $\alpha$ -Synuclein aggregation in mitochondria impairs complex I in human dopaminergic neuronal cells, consequently interfering with mitochondrial functions (Devi et al., 2008). Additionally, it was suggested that soluble, prefibrillar  $\alpha$ -Synuclein, but not  $\alpha$ -Synuclein monomers, impairs the retention of  $\text{Ca}^{2+}$  in mitochondria, and induces mitochondrial depolarization and swelling, leading to  $\text{Ca}^{2+}$  dependent mitochondrial dysfunction (Luth et al., 2014). On the other hand, mitochondrial defects result in oligomerization and accumulation of  $\alpha$ -Synuclein, which in turn aggravates the dysfunction of mitochondria. Growing evidence suggests the involvement of  $\alpha$ -Synuclein in the dynamics of mitochondria, such as mitochondrial fission, fusion, and mitophagy. Overexpression of  $\alpha$ -Synuclein in *Caenorhabditis elegans* and cultured cells reduces mitochondrial fusion, resulting in fragmentation of mitochondria (Kamp et al., 2010). And these fusion deficits and mitochondrial fragmentation are rescued by overexpression of PINK1, PARKIN or DJ-1 (Kamp et al., 2010). However, the detailed picture illustrating the interaction between  $\alpha$ -Synuclein accumulation and mitochondrial dysfunction remains obscure and requires further investigation.

## MECHANISMS UNDERLYING THE CONNECTION BETWEEN $\alpha$ -SYNUCLEIN ACCUMULATION AND GENETIC FACTOR-ASSOCIATED PD

The majority of PD are sporadic, and around 5–10% of PD are familial, presenting with monogenic forms of the disease (Rocha et al., 2018). More than 20 PD-related genes have been identified, including SNCA, leucine-rich repeat kinase 2 (LRRK2), glucocerebrosidase (GBA), PINK1, DJ-1 and Parkin (Li et al., 2014; Kalinderi et al., 2016; Balestrino and Schapira, 2018).

Studies showed that accumulation of insoluble  $\alpha$ -Synuclein plays a significant role not only in the neurodegenerative process of sporadic PD but also in familial PD; the interaction between  $\alpha$ -Synuclein and mutant genes contributes to neuronal death, dysfunction, and loss of connectivity (Stojkovska et al., 2018). The genetic mutations are mostly involved in  $\alpha$ -Synuclein

aggregation or clearance pathways, often leading to early-onset PD.

Mutations in the GBA is the single largest risk factor associated with PD (Balestrino and Schapira, 2018). A lot of studies have indicated a key role for  $\alpha$ -Synuclein in the pathogenesis of GBA-PD. GBA encodes lysosomal enzyme GCase that catalyzes the hydrolysis of glucosylceramide (GlcCer), and mutation of this gene normally results in dysfunction of the autophagy-lysosomal pathway (Robak et al., 2017). Since degradation of  $\alpha$ -Synuclein partially depends on autophagy, lysosomal dysfunction caused by GBA mutation could lead to  $\alpha$ -Synuclein accumulation and aggregation (Vogiatzi et al., 2008). Induced pluripotent stem cell (iPSC)-derived neurons from GBA-deficient PD patients show a reduced GCase activity and higher levels of GlcCer as well as  $\alpha$ -Synuclein aggregation due to lysosomal defects (Schöndorf et al., 2014). On the other hand,  $\alpha$ -Synuclein aggregation, in turn, inhibits GCase activity, and the toxic oligomeric form of  $\alpha$ -Synuclein is stabilized by an increased level of GlcCer, the substrate of GCase (Mazzulli et al., 2011). These data demonstrated that  $\alpha$ -Synuclein and GCase may form a bidirectional pathogenic loop, participating in a self-propagating feedback process that eventually leads to neurodegeneration (Mazzulli et al., 2011). In addition, GBA mutations can elevate the level of  $\alpha$ -Synuclein via altered interaction with lipid membranes in addition to lysosomal defects. It was proposed that GlcCer and another glycosphingolipid could induce toxic conversion of  $\alpha$ -Synuclein (Suzuki et al., 2018). Recently, a study revealed that GBA deficiency may impact on the formation of  $\alpha$ -Synuclein tetramers and related multimers (Kim et al., 2018). The major normal structure of  $\alpha$ -Synuclein is a folded tetramer that is resistant to aggregation (Bartels et al., 2011). In comparison with tetramers, the monomer of  $\alpha$ -Synuclein tends to aggregate and transition to insoluble deposits such as Lewy bodies (Bartels et al., 2011). Thus, the authors concluded that the accumulation of GlcCer due to GBA mutation destabilizes  $\alpha$ -Synuclein tetramers and related multimers and increases the level of  $\alpha$ -Synuclein monomers, eventually contributing to  $\alpha$ -Synuclein aggregation and neurodegeneration in PD (Kim et al., 2018). Taken together, these studies highlight the mechanistic connection between GBA deficiency and  $\alpha$ -Synuclein properties, providing unique therapeutic opportunities for reducing neurotoxicity of  $\alpha$ -Synuclein for treatment of PD.

## CONCLUSIONS AND PERSPECTIVES

In this review article, we summarized how phase transition, posttranslational modifications, physical and physiological status of  $\alpha$ -Synuclein, inflammation, lipid metabolism, and genetic mutations may correlate with different functional consequences in PD (Figure 1). Proteostasis of  $\alpha$ -Synuclein, as involved in maintaining normal cellular metabolic functions, plays a key role in the neurodegenerative process. The evolution and transformation of different species of  $\alpha$ -Synuclein significantly affect the pathogenesis of PD.

Further work is required to elucidate the detailed mechanisms that regulate the proteostasis of  $\alpha$ -Synuclein, particularly the initiating events of aggregation. Genetic mutations involved in early-onset familial PD may contribute to the phase transition of  $\alpha$ -Synuclein, especially in the early stage of PD development; and mechanistic insight into this field may help develop novel therapeutic strategies to target  $\alpha$ -Synucleinopathy. iPSC-derived dopaminergic neurons with LRRK2 G2019S mutation present with the accelerated accumulation of  $\alpha$ -Synuclein. Treatment with terazosin, which can activate phosphoglycerate kinase 1 (PGK1) and subsequently increase cellular ATP level, reverses the elevation of  $\alpha$ -Synuclein (Cai et al., 2019). Importantly, a lower frequency and slower progression of PD, and reduced disease-related complications are found in individuals taking the prescribed drug terazosin (Cai et al., 2019). The molecular mechanism remains elusive but one possibility is that ATP has property of a hydrotrope and can inhibit the formation and facilitate the dissolving of aggregates (Patel et al., 2017; Hayes et al., 2018). The study exemplifies that a molecule targeting the phase transition of  $\alpha$ -Synuclein may slow down the progression of PD clinically. With the discovery of more molecules/drugs that target different aspects of  $\alpha$ -Synuclein phase transition and with a better

understanding of the genetic regulation of  $\alpha$ -Synucleinopathy, new interventional opportunities are promised to emerge for treatment of PD.

## AUTHOR CONTRIBUTIONS

DH, WZ, XW, and ZC wrote the manuscript together.

## FUNDING

Grant Sponsors: Stem Cell and Translation National Key Project (2016YFA0101403), National Natural Science Foundation of China (81973351, 81661130160, 81422014, 81561138004), Beijing Municipal Natural Science Foundation (5142005), Beijing Talents Foundation (2017000021223TD03), Support Project of High-level Teachers in Beijing Municipal Universities in the Period of 13th Five-year Plan (CIT and TCD20180333), Beijing Medical System High-Level Talent Award (2015-3-063), Beijing Municipal Health Commission Fund (PXM 2018\_026283\_000002), Beijing One Hundred, Thousand, and Ten Thousand Talents Fund (2018A03), Beijing Municipal Administration of Hospitals Clinical Medicine Development of Special Funding Support (ZYLX201706), and the Royal Society-Newton Advanced Fellowship (NA150482).

## REFERENCES

- Asi, Y. T., Simpson, J. E., Heath, P. R., Wharton, S. B., Lees, A. J., Revesz, T., et al. (2014).  $\alpha$ -synuclein mRNA expression in oligodendrocytes in MSA. *Glia* 62, 964–970. doi: 10.1002/glia.22653
- Balestrino, R., and Schapira, A. H. V. (2018). Glucocerebrosidase and Parkinson disease: molecular, clinical, and therapeutic implications. *Neuroscientist* 24, 540–559. doi: 10.1177/1073858417748875
- Banani, S. F., Lee, H. O., Hyman, A. A., and Rosen, M. K. (2017). Biomolecular condensates: organizers of cellular biochemistry. *Nat. Rev. Mol. Cell Biol.* 18, 285–298. doi: 10.1038/nrm.2017.7
- Bartels, T., Choi, J. G., and Selkoe, D. J. (2011).  $\alpha$ -synuclein occurs physiologically as a helically folded tetramer that resists aggregation. *Nature* 477, 107–110. doi: 10.1038/nature10324
- Bose, A., and Beal, M. F. (2016). Mitochondrial dysfunction in Parkinson's disease. *J. Neurochem.* 139, 216–231. doi: 10.1111/jnc.13731
- Brekke, O. R., Moskites, A., Isacson, O., and Hallett, P. J. (2018). Lipid-dependent deposition of  $\alpha$ -synuclein and Tau on neuronal Secretogranin II-positive vesicular membranes with age. *Sci. Rep.* 8:15207. doi: 10.1038/s41598-018-33474-z
- Burai, R., Ait-Bouziad, N., Chiki, A., and Lashuel, H. A. (2015). Elucidating the role of site-specific nitration of  $\alpha$ -synuclein in the pathogenesis of Parkinson's disease via protein semisynthesis and mutagenesis. *J. Am. Chem. Soc.* 137, 5041–5052. doi: 10.1021/ja5131726
- Cai, R., Zhang, Y., Simmering, J., Schultz, J., Li, Y., Fernandez-Carasa, I., et al. (2019). Enhancing glycolysis attenuates Parkinson's disease progression in models and clinical databases. *J. Clin. Invest.* 129, 4539–4549. doi: 10.1172/jci129987
- Cao, S., Standaert, D. G., and Harms, A. S. (2012). The  $\gamma$  chain subunit of Fc receptors is required for  $\alpha$ -synuclein-induced pro-inflammatory signaling in microglia. *J. Neuroinflammation* 9:259. doi: 10.1186/1742-2094-9-259
- Chatterjee, K., Roy, A., Banerjee, R., Choudhury, S., Mondal, B., Halder, S., et al. (2020). Inflammasome and  $\alpha$ -synuclein in Parkinson's disease: a cross-sectional study. *J. Neuroimmunol.* 338:577089. doi: 10.1016/j.jneuroim.2019.577089
- Chauhan, P., Hu, S., Sheng, W. S., Prasad, S., and Lokensgard, J. R. (2017). Modulation of microglial cell Fc $\gamma$  receptor expression following viral brain infection. *Sci. Rep.* 7:41889. doi: 10.1038/srep41889
- Choi, Y. R., Kang, S. J., Kim, J. M., Lee, S. J., Jou, I., Joe, E. H., et al. (2015). Fc $\gamma$ RIIB mediates the inhibitory effect of aggregated  $\alpha$ -synuclein on microglial phagocytosis. *Neurobiol. Dis.* 83, 90–99. doi: 10.1016/j.nbd.2015.08.025
- Chung, C. Y., Koprich, J. B., Hallett, P. J., and Isacson, O. (2009). Functional enhancement and protection of dopaminergic terminals by RAB3B overexpression. *Proc. Natl. Acad. Sci. U S A* 106, 22474–22479. doi: 10.1073/pnas.0912193106
- Cookson, M. R. (2009).  $\alpha$ -synuclein and neuronal cell death. *Mol. Neurodegener.* 4:9. doi: 10.1186/1750-1326-4-9
- Daniele, S. G., Béraud, D., Davenport, C., Cheng, K., Yin, H., and Maguire-Zeiss, K. A. (2015). Activation of MyD88-dependent TLR1/2 signaling by misfolded  $\alpha$ -synuclein, a protein linked to neurodegenerative disorders. *Sci. Signal.* 8:ra45. doi: 10.1126/scisignal.2005965
- Danielson, S. R., Held, J. M., Schilling, B., Oo, M., Gibson, B. W., and Andersen, J. K. (2009). Preferentially increased nitration of  $\alpha$ -synuclein at tyrosine-39 in a cellular oxidative model of Parkinson's disease. *Anal. Chem.* 81, 7823–7828. doi: 10.1021/ac901176t
- Davidson, W. S., Jonas, A., Clayton, D. F., and George, J. M. (1998). Stabilization of  $\alpha$ -synuclein secondary structure upon binding to synthetic membranes. *J. Biol. Chem.* 273, 9443–9449. doi: 10.1074/jbc.273.16.9443
- Devi, L., Raghavendran, V., Prabhu, B. M., Avadhani, N. G., and Anandatheerthavarada, H. K. (2008). Mitochondrial import and accumulation of  $\alpha$ -synuclein impair complex I in human dopaminergic neuronal cultures and Parkinson disease brain. *J. Biol. Chem.* 283, 9089–9100. doi: 10.1074/jbc.m710012200
- Di Maio, R., Barrett, P. J., Hoffman, E. K., Barrett, C. W., Zharikov, A., Borah, A., et al. (2016).  $\alpha$ -synuclein binds to TOM20 and inhibits mitochondrial protein import in Parkinson's disease. *Sci. Transl. Med.* 8:342ra78. doi: 10.1126/scitranslmed.aaf3634
- Eliezer, D., Kutluay, E., Bussell, R. Jr., and Browne, G. (2001). Conformational properties of  $\alpha$ -synuclein in its free and lipid-associated states. *J. Mol. Biol.* 307, 1061–1073. doi: 10.1006/jmbi.2001.4538
- Fellner, L., Irschick, R., Schanda, K., Reindl, M., Klimaschewski, L., Poewe, W., et al. (2013). Toll-like receptor 4 is required for  $\alpha$ -synuclein dependent activation of microglia and astroglia. *Glia* 61, 349–360. doi: 10.1002/glia.22437
- Ferreira, S. A., and Romero-Ramos, M. (2018). Microglia response during Parkinson's disease:  $\alpha$ -synuclein intervention. *Front. Cell. Neurosci.* 12:247. doi: 10.3389/fncel.2018.00247



- Galvagnion, C., Brown, J. W., Ouberaï, M. M., Flagmeier, P., Vendruscolo, M., Buell, A. K., et al. (2016). Chemical properties of lipids strongly affect the kinetics of the membrane-induced aggregation of  $\alpha$ -synuclein. *Proc. Natl. Acad. Sci. U S A* 113, 7065–7070. doi: 10.1073/pnas.1601899113
- Giasson, B. I., Duda, J. E., Murray, I. V. J., Chen, Q., Souza, J. M., Hurtig, H. I., et al. (2000). Oxidative damage linked to neurodegeneration by selective  $\alpha$ -synuclein nitration in synucleinopathy lesions. *Science* 290, 985–989. doi: 10.1126/science.290.5493.985
- Guerrero-Ferreira, R., Taylor, N. M., Mona, D., Ringler, P., Lauer, M. E., Riek, R., et al. (2018). Cryo-EM structure of  $\alpha$ -synuclein fibrils. *Elife* 7:e36402. doi: 10.7554/eLife.36402
- Gustot, A., Gallea, J. I., Sarroukh, R., Celej, M. S., Ruyschaert, J.-M., and Raussens, V. (2015). Amyloid fibrils are the molecular trigger of inflammation in Parkinson's disease. *Biochem. J.* 471, 323–333. doi: 10.1042/bj20150617
- Haque, M. E., Akther, M., Jakaria, M., Kim, I. S., Azam, S., and Choi, D. K. (2020). Targeting the microglial NLRP3 inflammasome and its role in Parkinson's disease. *Mov. Disord.* 35, 20–33. doi: 10.1002/mds.27874
- Hart, G. W., Housley, M. P., and Slawson, C. (2007). Cycling of O-linked  $\beta$ -N-acetylglucosamine on nucleocytoplasmic proteins. *Nature* 446, 1017–1022. doi: 10.1038/nature05815
- Hallett, P. J., Engelen, S., and Isacson, O. (2019). Lipid and immune abnormalities causing age-dependent neurodegeneration and Parkinson's disease. *J. Neuroinflammation* 16, 153. doi: 10.1186/s12974-019-1532-2
- Hayes, M. H., Peuchen, E. H., Dovichi, N. J., and Weeks, D. L. (2018). Dual roles for ATP in the regulation of phase separated protein aggregates in *Xenopus* oocyte nucleoli. *Elife* 7:e35224. doi: 10.7554/elife.35224
- Hetz, C., and Mollereau, B. (2014). Disturbance of endoplasmic reticulum proteostasis in neurodegenerative diseases. *Nat. Rev. Neurosci.* 15, 233–249. doi: 10.1038/nrn3689
- Hodara, R., Norris, E. H., Giasson, B. I., Mishizen-Eberz, A. J., Lynch, D. R., Lee, V. M.-Y., et al. (2004). Functional consequences of  $\alpha$ -synuclein tyrosine nitration diminished binding to lipid vesicles and increased fibril formation. *J. Biol. Chem.* 279, 47746–47753. doi: 10.1074/jbc.M408906200
- Hoffmann, A., Ettle, B., Bruno, A., Kulinich, A., Hoffmann, A.-C., Von Wittgenstein, J., et al. (2016).  $\alpha$ -synuclein activates BV2 microglia dependent on its aggregation state. *Biochem. Biophys. Res. Commun.* 479, 881–886. doi: 10.1016/j.bbrc.2016.09.109
- Hughes, M. P., Sawaya, M. R., Boyer, D. R., Goldschmidt, L., Rodriguez, J. A., Cascio, D., et al. (2018). Atomic structures of low-complexity protein segments reveal kinked  $\beta$  sheets that assemble networks. *Science* 359, 698–701. doi: 10.1126/science.aan6398
- Hyung Ho Yoon, J. M., and Jeon, S. R. (2018). Optogenetics to restore neural circuit function in Parkinson's disease. *J. Neurorestoratol.* 6, 88–92. doi: 10.26599/JNR.2018.9040007
- Jankovic, J. (2008). Parkinson's disease: clinical features and diagnosis. *J. Neurol. Neurosurg. Psychiatry* 79, 368–376. doi: 10.1136/jnnp.2007.131045
- Jiang, T., Hoekstra, J., Heng, X., Kang, W., Ding, J., Liu, J., et al. (2015). P2X7 receptor is critical in  $\alpha$ -synuclein-mediated microglial NADPH oxidase activation. *Neurobiol. Aging* 36, 2304–2318. doi: 10.1016/j.neurobiolaging.2015.03.015
- Jin, J., Shie, F.-S., Liu, J., Wang, Y., Davis, J., Schantz, A. M., et al. (2007). Prostaglandin E 2 receptor subtype 2 (EP2) regulates microglial activation and associated neurotoxicity induced by aggregated  $\alpha$ -synuclein. *J. Neuroinflammation* 4:2. doi: 10.1186/1742-2094-4-2
- Jónsson, S. A., Mohanty, S., and Irbäck, A. (2012). Distinct phases of free  $\alpha$ -synuclein—a Monte Carlo study. *Proteins* 80, 2169–2177. doi: 10.1002/prot.24107
- Kalia, L. V., and Lang, A. E. (2015). Parkinson's disease. *Lancet* 386, 896–912. doi: 10.1016/S0140-6736(14)61393-3
- Kalinderi, K., Bostantjopoulou, S., and Fidani, L. (2016). The genetic background of Parkinson's disease: current progress and future prospects. *Acta Neurol. Scand.* 134, 314–326. doi: 10.1111/ane.12563
- Kam, T. I., Mao, X., Park, H., Chou, S. C., Karuppagounder, S. S., Umanah, G. E., et al. (2018). Poly(ADP-ribose) drives pathologic  $\alpha$ -synuclein neurodegeneration in Parkinson's disease. *Science* 362:eaat8407. doi: 10.1126/science.aat8407
- Kamp, F., Exner, N., Lutz, A. K., Wender, N., Hegermann, J., Brunner, B., et al. (2010). Inhibition of mitochondrial fusion by  $\alpha$ -synuclein is rescued by PINK1, Parkin and DJ-1. *EMBO J.* 29, 3571–3589. doi: 10.1038/emboj.2010.223
- Karpowicz, R. J. Jr., Trojanowski, J. Q., and Lee, V. M. (2019). Transmission of  $\alpha$ -synuclein seeds in neurodegenerative disease: recent developments. *Lab. Invest.* 99, 971–981. doi: 10.1038/s41374-019-0195-z
- Kaur, K., Gill, J. S., Bansal, P. K., and Deshmukh, R. (2017). Neuroinflammation—A major cause for striatal dopaminergic degeneration in Parkinson's disease. *J. Neurol. Sci.* 381, 308–314. doi: 10.1016/j.jns.2017.08.3251
- Kim, C., Ho, D. H., Suk, J. E., You, S., Michael, S., Kang, J., et al. (2013). Neuron-released oligomeric  $\alpha$ -synuclein is an endogenous agonist of TLR2 for paracrine activation of microglia. *Nat. Commun.* 4:1562. doi: 10.1038/ncomms2534
- Kim, S., Yun, S. P., Lee, S., Umanah, G. E., Bandaru, V. V. R., Yin, X., et al. (2018). GBA1 deficiency negatively affects physiological  $\alpha$ -synuclein tetramers and related multimers. *Proc. Natl. Acad. Sci. U S A* 115, 798–803. doi: 10.1073/pnas.1700465115
- Kitchens, R. L. (2000). Role of CD14 in cellular recognition of bacterial lipopolysaccharides. *Chem. Immunol.* 74, 61–82. doi: 10.1159/000058750
- Klegeris, A., Pelech, S., Giasson, B. I., Maguire, J., Zhang, H., McGeer, E. G., et al. (2008).  $\alpha$ -synuclein activates stress signaling protein kinases in THP-1 cells and microglia. *Neurobiol. Aging* 29, 739–752. doi: 10.1016/j.neurobiolaging.2006.11.013
- Krashia, P., Cordella, A., Nobili, A., La Barbera, L., Federici, M., Leuti, A., et al. (2019). Blunting neuroinflammation with resolvin D1 prevents early pathology in a rat model of Parkinson's disease. *Nat. Commun.* 10:3945. doi: 10.1038/s41467-019-11928-w
- Krumova, P., Meulmeester, E., Garrido, M., Tirard, M., Hsiao, H.-H., Bossis, G., et al. (2011). Sumoylation inhibits  $\alpha$ -synuclein aggregation and toxicity. *J. Cell Biol.* 194, 49–60. doi: 10.1083/jcb.201010117
- Labzin, L. I., Heneka, M. T., and Latz, E. (2018). Innate immunity and neurodegeneration. *Annu. Rev. Med.* 69, 437–449. doi: 10.1146/annurev-med-050715-104343
- Lee, H. J., Choi, C., and Lee, S. J. (2002). Membrane-bound  $\alpha$ -synuclein has a high aggregation propensity and the ability to seed the aggregation of the cytosolic form. *J. Biol. Chem.* 277, 671–678. doi: 10.1074/jbc.M107045200
- Levine, P. M., Galesic, A., Balana, A. T., Mahul-Mellier, A. L., Navarro, M. X., De Leon, C. A., et al. (2019).  $\alpha$ -synuclein O-GlcNAcylation alters aggregation and toxicity, revealing certain residues as potential inhibitors of Parkinson's disease. *Proc. Natl. Acad. Sci. U S A* 116, 1511–1519. doi: 10.1073/pnas.1808845116
- Li, B., Ge, P., Murray, K. A., Sheth, P., Zhang, M., Nair, G., et al. (2018). Cryo-EM of full-length  $\alpha$ -synuclein reveals fibril polymorphs with a common structural kernel. *Nat. Commun.* 9:3609. doi: 10.1038/s41467-018-05971-2
- Li, J. Q., Tan, L., and Yu, J. T. (2014). The role of the LRRK2 gene in Parkinsonism. *Mol. Neurodegener.* 9:47. doi: 10.1186/1750-1326-9-47
- Ludtmann, M. H., Angelova, P. R., Horrocks, M. H., Choi, M. L., Rodrigues, M., Baev, A. Y., et al. (2018).  $\alpha$ -synuclein oligomers interact with ATP synthase and open the permeability transition pore in Parkinson's disease. *Nat. Commun.* 9:2293. doi: 10.1038/s41467-018-04422-2
- Ludtmann, M. H., Angelova, P. R., Ninkina, N. N., Gandhi, S., Buchman, V. L., and Abramov, A. Y. (2016). Monomeric  $\alpha$ -synuclein exerts a physiological role on brain ATP synthase. *J. Neurosci.* 36, 10510–10521. doi: 10.1523/jneurosci.1659-16.2016
- Luth, E. S., Stavrovskaya, I. G., Bartels, T., Kristal, B. S., and Selkoe, D. J. (2014). Soluble, prefibrillar  $\alpha$ -synuclein oligomers promote complex I-dependent,  $\text{Ca}^{2+}$ -induced mitochondrial dysfunction. *J. Biol. Chem.* 289, 21490–21507. doi: 10.1074/jbc.M113.545749
- Ma, J., Gao, J., Wang, J., and Xie, A. (2019). Prion-like mechanisms in Parkinson's disease. *Front. Neurosci.* 13:552. doi: 10.3389/fnins.2019.00552
- Maharana, S., Wang, J., Papadopoulos, D. K., Richter, D., Pozniakovskiy, A., Poser, I., et al. (2018). RNA buffers the phase separation behavior of prion-like RNA binding proteins. *Science* 360, 918–921. doi: 10.1126/science.aar7366
- Marotta, N. P., Lin, Y. H., Lewis, Y. E., Ambrosio, M. R., Zaro, B. W., Roth, M. T., et al. (2015). O-GlcNAc modification blocks the aggregation and toxicity of the protein  $\alpha$ -synuclein associated with Parkinson's disease. *Nat. Chem.* 7, 913–920. doi: 10.1038/nchem.2361

- Mazzulli, J. R., Xu, Y. H., Sun, Y., Knight, A. L., Mclean, P. J., Caldwell, G. A., et al. (2011). Gaucher disease glucocerebrosidase and  $\beta$ -synuclein form a bidirectional pathogenic loop in synucleinopathies. *Cell* 146, 37–52. doi: 10.1016/j.cell.2011.06.001
- Mazzulli, J. R., Zinke, F., Isacson, O., Studer, L., and Krainc, D. (2016).  $\alpha$ -synuclein-induced lysosomal dysfunction occurs through disruptions in protein trafficking in human midbrain synucleinopathy models. *Proc. Natl. Acad. Sci. U S A* 113, 1931–1936. doi: 10.1073/pnas.1520335113
- Mehra, S., Sahay, S., and Maji, S. K. (2019).  $\alpha$ -synuclein misfolding and aggregation: implications in Parkinson's disease pathogenesis. *Biochim. Biophys. Acta Proteins Proteom.* 1867, 890–908. doi: 10.1016/j.bbapap.2019.03.001
- Melki, R. (2015). Role of different  $\alpha$ -synuclein strains in synucleinopathies, similarities with other neurodegenerative diseases. *J. Parkinsons Dis.* 5, 217–227. doi: 10.3233/jpd-150543
- Mor, D. E., Ugras, S. E., Daniels, M. J., and Ischiropoulos, H. (2016). Dynamic structural flexibility of  $\alpha$ -synuclein. *Neurobiol. Dis.* 88, 66–74. doi: 10.1016/j.nbd.2015.12.018
- Muroi, M., Ohnishi, T., and Tanamoto, K. (2002). Regions of the mouse CD14 molecule required for toll-like receptor 2- and 4-mediated activation of NF- $\kappa$ B. *J. Biol. Chem.* 277, 42372–42379. doi: 10.1074/jbc.M205966200
- Narayanan, A., Meriin, A., Andrews, J. O., Spille, J.-H., Sherman, M. Y., and Cisse, I. I. (2019). A first order phase transition mechanism underlies protein aggregation in mammalian cells. *Elife* 8:e39695. doi: 10.7554/eLife.39695
- Obeso, J. A., Rodriguez-Oroz, M. C., Goetz, C. G., Marin, C., Kordower, J. H., Rodriguez, M., et al. (2010). Missing pieces in the Parkinson's disease puzzle. *Nat. Med.* 16, 653–661. doi: 10.1038/nm.2165
- Patel, A., Malinowska, L., Saha, S., Wang, J., Alberti, S., Krishnan, Y., et al. (2017). ATP as a biological hydrotrope. *Science* 356, 753–756. doi: 10.1126/science.aaf6846
- Peelaerts, W., Bousset, L., Van der Perren, A., Moskalyuk, A., Pulizzi, R., Giugliano, M., et al. (2015).  $\alpha$ -synuclein strains cause distinct synucleinopathies after local and systemic administration. *Nature* 522, 340–344. doi: 10.1038/nature14547
- Perrino, G., Wilson, C., Santorelli, M., and Di Bernardo, D. (2019). Quantitative characterization of  $\alpha$ -synuclein aggregation in living cells through automated microfluidics feedback control. *Cell Rep.* 27, 916.e5–927.e5. doi: 10.1016/j.celrep.2019.03.081
- Poewe, W., Seppi, K., Tanner, C. M., Halliday, G. M., Brundin, P., Volkmann, J., et al. (2017). Parkinson disease. *Nat. Rev. Dis. Primers* 3:17013. doi: 10.1038/nrdp.2017.13
- Prabhakaran, K., Chapman, G. D., and Gunasekar, P. G. (2011).  $\alpha$ -Synuclein overexpression enhances manganese-induced neurotoxicity through the NF- $\kappa$ B-mediated pathway. *Toxicol. Mech. Methods* 21, 435–443. doi: 10.3109/15376516.2011.560210
- Pringsheim, T., Jette, N., Frolkis, A., and Steeves, T. D. (2014). The prevalence of Parkinson's disease: a systematic review and meta-analysis. *Mov. Disord.* 29, 1583–1590. doi: 10.1002/mds.25945
- Ray, S., Singh, N., Pandey, S., Kumar, R., Gadhe, L., Datta, D., et al. (2019). Liquid-liquid phase separation and liquid-to-solid transition mediate  $\alpha$ -synuclein amyloid fibril containing hydrogel formation. *bioRxiv* [Preprint]. doi: 10.1101/619858
- Robak, L. A., Jansen, I. E., van Rooij, J., Uitterlinden, A. G., Kraaij, R., Jankovic, J., et al. (2017). Excessive burden of lysosomal storage disorder gene variants in Parkinson's disease. *Brain* 140, 3191–3203. doi: 10.1093/brain/awx285
- Rocha, E. M., De Miranda, B., and Sanders, L. H. (2018).  $\alpha$ -Synuclein: pathology, mitochondrial dysfunction and neuroinflammation in Parkinson's disease. *Neurobiol. Dis.* 109, 249–257. doi: 10.1016/j.nbd.2017.04.004
- Rott, R., Szargel, R., Shani, V., Hamza, H., Savyon, M., Abd Elghani, F., et al. (2017). SUMOylation and ubiquitination reciprocally regulate  $\alpha$ -synuclein degradation and pathological aggregation. *Proc. Natl. Acad. Sci. U S A* 114, 13176–13181. doi: 10.1073/pnas.1704351114
- Sato, S., Uchiyama, T., Fukuda, T., Noda, S., Kondo, H., Saiki, S., et al. (2018). Loss of autophagy in dopaminergic neurons causes Lewy pathology and motor dysfunction in aged mice. *Sci. Rep.* 8:2813. doi: 10.1038/s41598-018-21325-w
- Shapira, A. H., and Jenner, P. (2011). Etiology and pathogenesis of Parkinson's disease. *Mov. Disord.* 26, 1049–1055. doi: 10.1002/mds.23732
- Schöndorf, D. C., Aureli, M., McAllister, F. E., Hindley, C. J., Mayer, F., Schmid, B., et al. (2014). iPSC-derived neurons from GBA1-associated Parkinson's disease patients show autophagic defects and impaired calcium homeostasis. *Nat. Commun.* 5:4028. doi: 10.1038/ncomms5028
- Serio, T. R., Cashikar, A. G., Kowal, A. S., Sawicki, G. J., Moslehi, J. J., Serpell, L., et al. (2000). Nucleated conformational conversion and the replication of conformational information by a prion determinant. *Science* 289, 1317–1321. doi: 10.1126/science.289.5483.1317
- Shahmoradian, S. H., Lewis, A. J., Genoud, C., Hench, J., Moors, T. E., Navarro, P. P., et al. (2019). Lewy pathology in Parkinson's disease consists of crowded organelles and lipid membranes. *Nat. Neurosci.* 22, 1099–1109. doi: 10.1038/s41593-019-0423-2
- Shin, Y., and Brangwynne, C. P. (2017). Liquid phase condensation in cell physiology and disease. *Science* 357:eaf4382. doi: 10.1126/science.aaf4382
- Smith, K. G., and Clatworthy, M. R. (2010). Fc $\gamma$ RIIB in autoimmunity and infection: evolutionary and therapeutic implications. *Nat. Rev. Immunol.* 10, 328–343. doi: 10.1038/nri2762
- Spillantini, M. G., Schmidt, M. L., Lee, V. M.-Y., Trojanowski, J. Q., Jakes, R., and Goedert, M. (1997).  $\alpha$ -Synuclein in lewy bodies. *Nature* 388, 839–840. doi: 10.1038/42166
- Stefanova, N., Fellner, L., Reindl, M., Masliah, E., Poewe, W., and Wenning, G. K. (2011). Toll-like receptor 4 promotes  $\alpha$ -synuclein clearance and survival of nigral dopaminergic neurons. *Am. J. Pathol.* 179, 954–963. doi: 10.1016/j.ajpath.2011.04.013
- Stojkovic, I., Krainc, D., and Mazzulli, J. R. (2018). Molecular mechanisms of  $\alpha$ -synuclein and GBA1 in Parkinson's disease. *Cell Tissue Res.* 373, 51–60. doi: 10.1007/s00441-017-2704-y
- Sulzer, D., Alcalay, R. N., Garretti, F., Cote, L., Kanter, E., Agin-Liebes, J., et al. (2017). T cells from patients with Parkinson's disease recognize  $\alpha$ -synuclein peptides. *Nature* 546, 656–661. doi: 10.1038/nature22815
- Suzuki, M., Sango, K., Wada, K., and Nagai, Y. (2018). Pathological role of lipid interaction with  $\alpha$ -synuclein in Parkinson's disease. *Neurochem. Int.* 119, 97–106. doi: 10.1016/j.neuint.2017.12.014
- Thomas, M. P., Chartrand, K., Reynolds, A., Vitvitsky, V., Banerjee, R., and Gendelman, H. E. (2007). Ion channel blockade attenuates aggregated  $\alpha$  synuclein induction of microglial reactive oxygen species: relevance for the pathogenesis of Parkinson's disease. *J. Neurochem.* 100, 503–519. doi: 10.1111/j.1471-4159.2006.04315.x
- Ulmer, T. S., Bax, A., Cole, N. B., and Nussbaum, R. L. (2005). Structure and dynamics of micelle-bound human  $\alpha$ -synuclein. *J. Biol. Chem.* 280, 9595–9603. doi: 10.1074/jbc.M411805200
- Verdile, V., De Paola, E., and Paronetto, M. P. (2019). Aberrant phase transitions: side effects and novel therapeutic strategies in human disease. *Front. Genet.* 10:173. doi: 10.3389/fgene.2019.00173
- Vogiatzi, T., Xilouri, M., Vekrellis, K., and Stefanis, L. (2008). Wild type  $\alpha$ -synuclein is degraded by chaperone-mediated autophagy and macroautophagy in neuronal cells. *J. Biol. Chem.* 283, 23542–23556. doi: 10.1074/jbc.M801992200
- Wakabayashi, K., Tanji, K., Odagiri, S., Miki, Y., Mori, F., and Takahashi, H. (2013). The Lewy body in Parkinson's disease and related neurodegenerative disorders. *Mol. Neurobiol.* 47, 495–508. doi: 10.1007/s12035-012-8280-y
- Wang, W., Nguyen, L. T., Burlak, C., Chegini, F., Guo, F., Chataway, T., et al. (2016). Caspase-1 causes truncation and aggregation of the Parkinson's disease-associated protein  $\alpha$ -synuclein. *Proc. Natl. Acad. Sci. U S A* 113, 9587–9592. doi: 10.1073/pnas.1610099113
- Wang, M., Tao, X., Jacob, M. D., Bennett, C. A., Ho, J. D., Gonzalgo, M. L., et al. (2018). Stress-induced low complexity RNA activates physiological amyloidogenesis. *Cell Rep.* 24, 1713.e4–1721.e4. doi: 10.1016/j.celrep.2018.07.040
- Wang, Q., Qian, L., Chen, S. H., Chu, C. H., Wilson, B., Oyarzabal, E., et al. (2015). Post-treatment with an ultra-low dose of NADPH oxidase inhibitor diphenyleneiodonium attenuates disease progression in multiple Parkinson's disease models. *Brain* 138, 1247–1262. doi: 10.1093/brain/awv034
- Wilms, H., Rosenstiel, P., Romero-Ramos, M., Arlt, A., Schäfer, H., Seeger, D., et al. (2009). Suppression of MAP kinases inhibits microglial activation and attenuates neuronal cell death induced by  $\alpha$ -synuclein protofibrils.

- Int. J. Immunopathol. Pharmacol.* 22, 897–909. doi: 10.1177/039463200902200405
- Xilouri, M., Brekk, O. R., and Stefanis, L. (2013).  $\alpha$ -synuclein and protein degradation systems: a reciprocal relationship. *Mol. Neurobiol.* 47, 537–551. doi: 10.1007/s12035-012-8341-2
- Zhang, J., Li, X., and Li, J. D. (2019). The roles of post-translational modifications on  $\alpha$ -synuclein in the pathogenesis of Parkinson's diseases. *Front. Neurosci.* 13:381. doi: 10.3389/fnins.2019.00381
- Zhou, W., and Freed, C. R. (2004). Tyrosine-to-cysteine modification of human  $\alpha$ -synuclein enhances protein aggregation and cellular toxicity. *J. Biol. Chem.* 279, 10128–10135. doi: 10.1074/jbc.m307563200
- Zhou, Y., Lu, M., Du, R.-H., Qiao, C., Jiang, C.-Y., Zhang, K.-Z., et al. (2016). MicroRNA-7 targets Nod-like receptor protein 3 inflammasome to modulate neuroinflammation in the pathogenesis of Parkinson's disease. *Mol. Neurodegener.* 11:28. doi: 10.1186/s13024-016-0094-3
- Conflict of Interest:** The authors declare that the research was conducted in the absence of any commercial or financial relationships that could be construed as a potential conflict of interest.
- Copyright © 2020 Han, Zheng, Wang and Chen. This is an open-access article distributed under the terms of the Creative Commons Attribution License (CC BY). The use, distribution or reproduction in other forums is permitted, provided the original author(s) and the copyright owner(s) are credited and that the original publication in this journal is cited, in accordance with accepted academic practice. No use, distribution or reproduction is permitted which does not comply with these terms.



# GSK3 $\beta$ and Tau Protein in Alzheimer's Disease and Epilepsy

Danira Toral-Rios<sup>1</sup>, Pavel S. Pichardo-Rojas<sup>2</sup>, Mario Alonso-Vanegas<sup>3</sup>  
and Victoria Campos-Peña<sup>4\*</sup>

<sup>1</sup>Departamento de Fisiología Biofísica y Neurociencias, Centro de Investigación y de Estudios Avanzados del IPN, Mexico City, Mexico, <sup>2</sup>Facultad de Ciencias de la Salud, Universidad Autónoma de Baja California, Ensenada, Mexico, <sup>3</sup>Centro Internacional de Cirugía de Epilepsia, Instituto Nacional de Neurología y Neurocirugía, HMG, Hospital Coyoacán, Mexico City, Mexico, <sup>4</sup>Laboratorio Experimental de Enfermedades Neurodegenerativas, Instituto Nacional de Neurología y Neurocirugía, Mexico City, Mexico

## OPEN ACCESS

### Edited by:

Rena Li,  
Capital Medical University, China

### Reviewed by:

Aline Stephan,  
Université de Strasbourg, France  
Fengquan Zhou,  
Johns Hopkins University,  
United States

### \*Correspondence:

Victoria Campos-Peña  
neurovcpe@gmail.com

**Received:** 17 July 2019

**Accepted:** 23 January 2020

**Published:** 17 March 2020

### Citation:

Toral-Rios D, Pichardo-Rojas PS,  
Alonso-Vanegas M and  
Campos-Peña V (2020) GSK3 $\beta$  and  
Tau Protein in Alzheimer's Disease  
and Epilepsy.  
Front. Cell. Neurosci. 14:19.  
doi: 10.3389/fncel.2020.00019

Alzheimer's disease (AD) is the most common form of dementia present in older adults; its etiology involves genetic and environmental factors. In recent years, epidemiological studies have shown a correlation between AD and chronic epilepsy since a considerable number of patients with AD may present seizures later on. Although the pathophysiology of seizures in AD is not completely understood, it could represent the result of several molecular mechanisms linked to amyloid beta-peptide (A $\beta$ ) accumulation and the hyperphosphorylation of tau protein, which may induce an imbalance in the release and recapture of excitatory and inhibitory neurotransmitters, structural alterations of the neuronal cytoskeleton, synaptic loss, and neuroinflammation. These changes could favor the recurrent development of hypersynchronous discharges and epileptogenesis, which, in a chronic state, favor the neurodegenerative process and influence the cognitive decline observed in AD. Supporting this correlation, histopathological studies in the brain tissue of temporal lobe epilepsy (TLE) patients have revealed the presence of A $\beta$  deposits and the accumulation of tau protein in the neurofibrillary tangles (NFTs), accompanied by an increase of glycogen synthase kinase-3 beta (GSK3 $\beta$ ) activity that may lead to an imminent alteration in posttranslational modifications of some microtubule-associated proteins (MAPs), mainly tau. The present review is focused on understanding the pathological aspects of GSK3 $\beta$  and tau in the development of TLE and AD.

**Keywords:** tau protein, GSK3 $\beta$ , epilepsy, neurodegeneration, hippocampal sclerosis

## INTRODUCTION

Alzheimer's disease (AD) is characterized by progressive memory loss, behavioral changes, and cognitive decline. Histopathologically, it is defined by the presence of neuritic plaques (NPs) conformed by fibrillar accumulation of amyloid beta-peptide (A $\beta$ ) and neurofibrillary tangles (NFTs) formed by the microtubule-associated protein (MAP) tau. These lesions produce microglial and astrocyte activation, leading to synaptic loss and neuronal death (Meraz-Ríos et al., 2013). It has been proposed that A $\beta$  can interact with Frizzled receptors, impairing the



Wnt/ $\beta$ -catenin signaling pathway conducting to increased activity of the main tau protein kinase, glycogen synthase kinase-3 beta (GSK3 $\beta$ ). Tau hyperphosphorylation promotes the destabilization of cytoskeleton microtubules (MTs), leading to axonal transport abnormalities and neuronal death (Inestrosa and Toledo, 2008). A $\beta$  and tau protein have been linked to excitotoxicity and hyperexcitability (Holth et al., 2013). The relationship of tau and excitability is important in view of the increased incidence of unprovoked seizures observed in AD patients, which may result from alterations in neural circuits and neurodegenerative processes (Pandis and Scarmeas, 2012). In this way, seizures and hyperexcitability of the network could contribute to accelerating the development of cognitive impairment. In addition, the neuronal circuits affected in AD involve brain areas that have been shown to be highly epileptogenic and are strongly related to temporal lobe epilepsy (TLE), the most common type of epilepsy. Histopathological studies in TLE patients have shown the presence of hyperphosphorylated tau protein aggregates (Sen et al., 2007; Thom et al., 2011; Tai et al., 2016). The present review aims at assessing the role of tau and GSK3 $\beta$  proteins in the development of AD and TLE.

## TAU PROTEIN

Tau is a type II MAP, mainly located in axons. It is a heat-stable protein that prevents MT assembly and stabilization in the central nervous system (CNS). Human tau is encoded by the *MAPT* gene located on chromosome 17q21 and consists of 16 exons (Andreadis et al., 1992; Andreadis, 2005; **Figure 1A**). Six different isoforms of the protein are expressed in the adult human brain. Each isoform contains three or four microtubule binding repeats (3R/4R) and the presence or absence of one or two N-terminal inserts (Buée et al., 2000; Martin et al., 2011; **Figure 1B**).

Under normal conditions, tau interacts with motor proteins such as dynein and kinesin, participating in retrograde and anterograde transport (Dixit et al., 2008), in embryonic development, long-term potentiation (LTP; Ahmed et al., 2014), and long-term depression (LTD; Kimura et al., 2014; Regan et al., 2015). Under pathological conditions, it self-assembles into insoluble structures, known as paired helical filaments (PHFs; Goedert, 1999). Two tau posttranslational modifications are present in PHFs: hyperphosphorylation and truncation (Flament et al., 1990; Alonso et al., 1996; Hasegawa et al., 1998).

Hyperphosphorylation prevents tau microtubule binding, resulting in an altered cytoskeletal stability (Evans et al., 2000), a subsequent loss of axonal transport, and other signaling-related functions (Mandelkow et al., 1995); it has also been considered the primary event that triggers the tau pathological aggregation in filaments (Grundke-Iqbal et al., 1986; Wood et al., 1986; Alonso et al., 1996).

## TAU AND EPILEPSY

In recent years, tau protein has been implicated in the disruption of neuronal synchronization and hyperexcitability; in this way,

it could also be linked to epilepsy. Even though the specific pathologic mechanisms are yet to be clarified, there are different reports supporting these claims.

Some models of tau pathology have been shown to induce drastic changes in connectivity and strong uncoupling of the gamma-theta oscillations. However, no signs of epileptiform activity were registered (Ahnaou et al., 2017). Challenging this idea, a transgenic mouse model of human amyloid precursor protein (hAPP) presented an overproduction of A $\beta$  and consequent development of spontaneous seizures. Adding a tau gene knockout to this model revealed that tau reduced levels, prevented N-methyl-D-aspartate receptor (NMDAR) dysfunction, impaired LTP, ameliorated cognitive decline, and reduced epileptiform activity in the hippocampus (Roberson et al., 2007, 2011).

Another interesting study which evaluated the relationship of tau with hyperexcitability is the *Kcna1*<sup>-/-</sup> mouse, a TLE model. These mice have a null allele for the alpha subunit of Kv1.1, a voltage-gated potassium channel that conditions the development of spontaneous seizures in the third week of life. The tau gene knockout in this model reduced the occurrence and frequency of spontaneous seizures and promoted survival, specifically in the CA3 pyramidal region of the hippocampus (Holth et al., 2013). Another similar model demonstrated that A $\beta$ -induced hyperexcitability was associated with a reduction in the levels of Kv4.2, a dendritic potassium channel important in regulating dendritic excitability and synaptic plasticity. Interestingly, enough of both of these phenomena were dramatically reduced in tau knockout mice, suggesting that tau may have a direct role in modulating neuronal excitability (Hall et al., 2015). Similar results were observed in a Tau<sup>-/-</sup> mouse model treated with Pentylentetrazole (PTZ). In this case, it was observed that a reduction in tau expression protects against seizure severity (DeVos et al., 2013). This is interesting considering that it is possible that endogenous tau levels in AD patients may influence the risk of developing seizures.

Although having higher basal levels of tau in the cerebrospinal fluid does not cause seizures in itself, these patients are more likely to develop seizures after an injury, for example, after an ischemic stroke or traumatic brain injury (Camilo and Goldstein, 2004; Kwan, 2010). For this reason, in the future, it could be important to identify high-risk patients through genetic analysis, maybe by identifying polymorphisms in the tau gene (Myers et al., 2007; Kauwe et al., 2008) or levels of tau in the cerebrospinal fluid (Cruchaga et al., 2013), to determine whether, in this population, it may be useful to provide prophylactic antiepileptic therapy.

Hyperphosphorylated tau aggregates and NFTs have been observed in several patients with epilepsy (Sen et al., 2007; Thom et al., 2011; Tai et al., 2016). Moreover, a study on temporal lobe resections in patients with refractory epilepsy demonstrated that the presence of hyperphosphorylated tau and its accumulation in pre-tangles and NFTs seem to correlate with cognitive decline (Tai et al., 2016). Evidence suggests that prolonged or recurrent seizures in epilepsy patients can cause or exacerbate cognitive impairment (Holmes, 2015; Kneynsberg et al., 2017). Pathologic tau has been correlated

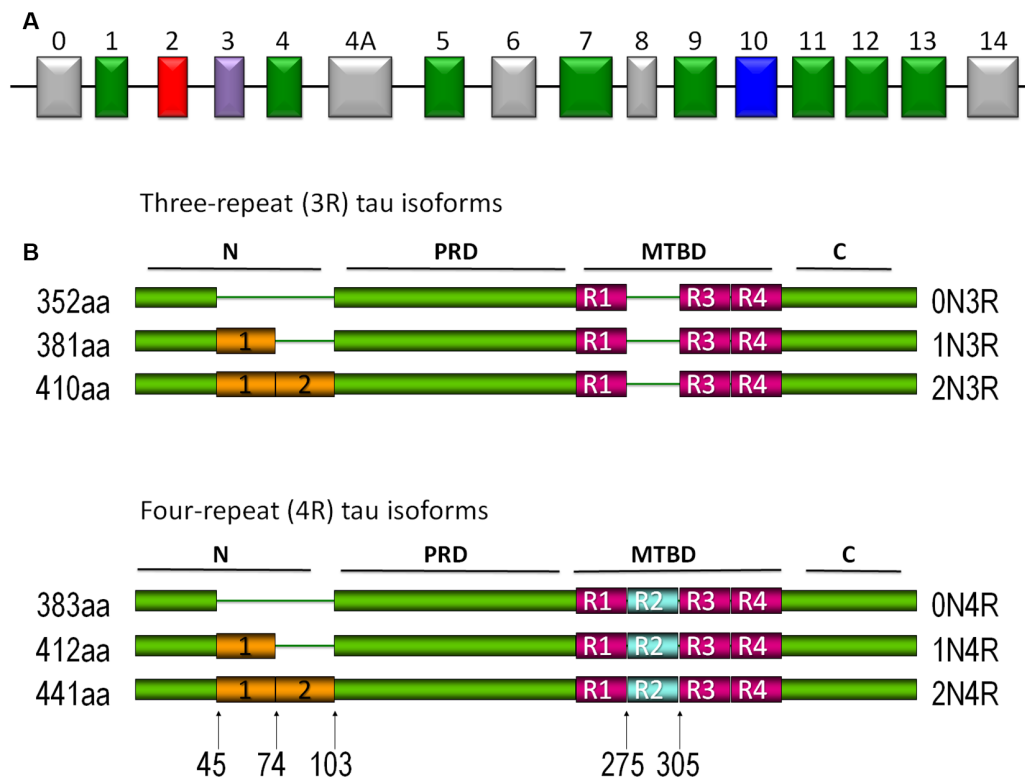


**FIGURE 1 |** Tau protein. **(A)** Tau gene. Exons 2, 3, and 10 are alternatively spliced in the central nervous system (CNS). Exons 9–12 each contain the microtubule-binding domain (MTBD). Exons 4a and 6 have been expressed in isoforms of the peripheral nervous system, whereas exon 8 has not been reported in any isoform. **(B)** Different isoforms of tau protein are expressed in the CNS. The expression of different isoforms is regulated by development. Isoforms with three repeated domains are expressed preferentially in fetal stages, whereas in the adult stages they are characterized by the presence of the six isoforms. The repeated domains that bind to microtubules (MTs) are designated as *R1*, *R2*, *R3*, and *R4*. Another characteristic is the presence or absence (0N) of one (1N) or two (2N) inserts located in the amino terminus of the protein.

with excitotoxicity (Roberson et al., 2007), epilepsy (DeVos et al., 2013), and cognitive impairment, particularly memory (Holmes, 2015). However, to date, the specific mechanisms explaining how hyperphosphorylated tau induces hyperexcitability are an area of active research.

Epileptogenesis is associated with an imbalance between excitatory and inhibitory neurotransmitters. The principal excitatory neurotransmitter dysregulated in epilepsy is glutamate, which favors excitotoxicity by the overstimulation of NMDAR. Furthermore, the activation of NMDAR has been proposed as another mechanism promoting tau phosphorylation. Through this process, tau could regulate NMDAR activation, synaptic plasticity, and neurotoxicity (Mondragón-Rodríguez et al., 2012).

These potential roles of tau opened a new field of study to establish a direct relationship with neuropathology and knowledge of other diseases such as TLE, which courses with seizures linked to imbalances of the hippocampal neuronal networks and neurodegenerative processes. In this way, further research must be done to determine the exact mechanisms of how tau plays a pivotal role in epileptogenesis and, therefore, make potential interventions of diagnostic, therapeutic, and prognostic value.

## GSK3

GSK3 is a proline-directed kinase; there are two isoforms, glycogen synthase kinase-3 alpha (GSK3 $\alpha$ ) and beta (GSK3 $\beta$ ) encoded by chromosomes 19 and 3, respectively. GSK3 $\beta$  is mainly expressed in the CNS, normally located in axons, and is the main kinase that phosphorylates tau protein (Muyllaert et al., 2008). GSK3 $\beta$  could be inactivated through phosphorylation in serine 9 and activated by phosphorylation in tyrosine 216. GSK3 $\beta$  inactivation is regulated by the PI3K/Akt and Wnt/ $\beta$ -catenin pathways. In AD, both are altered and favor an increased activity of GSK3 $\beta$  (Hooper et al., 2008).

Overexpression or overactivity of GSK3 $\beta$  increases tau phosphorylation, allowing it to disassemble from MTs, leading to axonal transport alterations, hippocampal neurodegeneration (Avila et al., 2006; Muyllaert et al., 2008), and learning impairment (Gómez De Barreda et al., 2010). GSK3 is able to phosphorylate tau at 42 sites (Figure 2; Hanger et al., 2009; Martin et al., 2013). Also, GSK3 activity correlates with the amount of NFTs in AD brains (Leroy et al., 2002). Another implication of the kinase in AD is the modulation of the intrinsic pathways of cellular apoptosis which could be favored by the A $\beta$  peptide (Takashima et al., 1996). GSK3 $\beta$  promotes Bax activity,



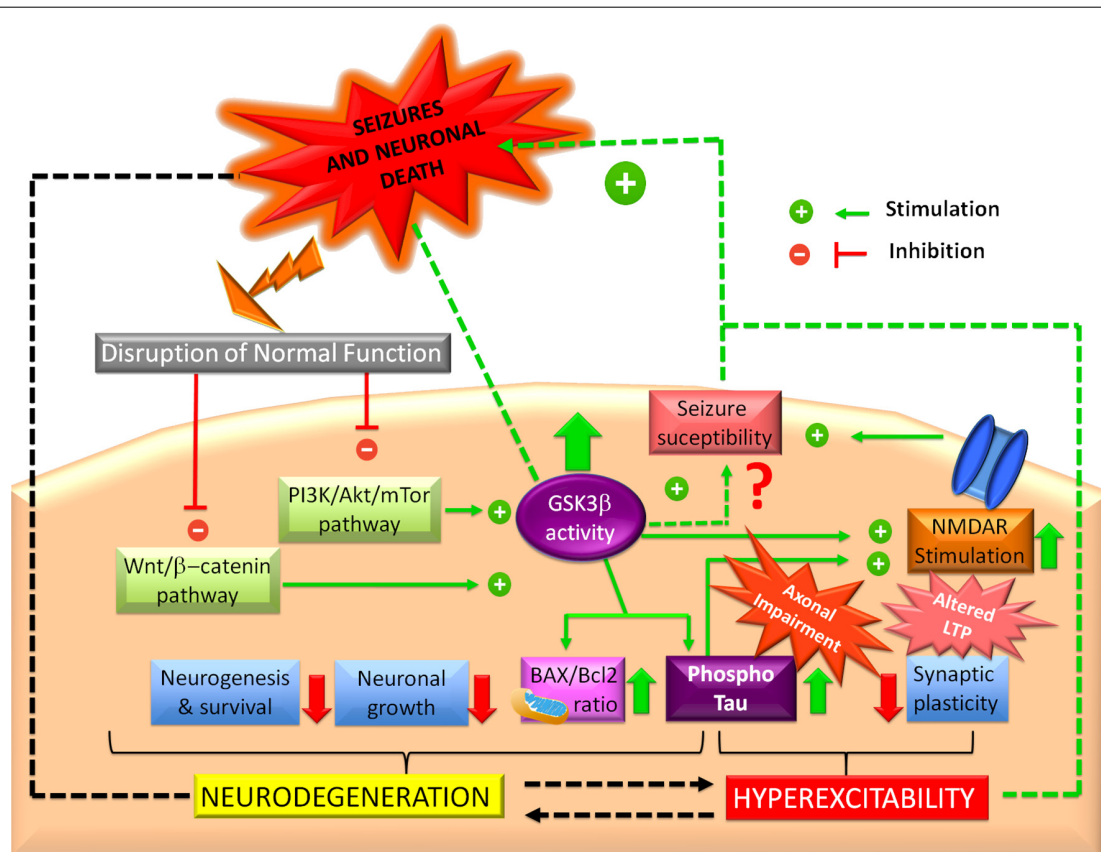


**FIGURE 3 |** Glycogen synthase kinase-3 beta (GSK3 $\beta$  and epilepsy. Impaired PI3K/Akt and Wnt/b-catenin signaling pathways can induce GSK3 $\beta$  increased activity, which could promote *N*-methyl-D-aspartate receptor (NMDAR) overstimulation, leading to hyperexcitability and synaptic plasticity alterations. Probably, this mechanism represents the major link between GSK3 $\beta$  and seizures in the hippocampus, although some studies have proposed that GSK3 $\beta$  increased activity confers protection. In another way, GSK3 $\beta$  could favor tau hyperphosphorylation, promoting axonal transport impairment and hippocampal neuronal death. Hyperphosphorylated tau actively participates in hyperexcitability and neurodegeneration. GSK3 $\beta$  also promotes a mitochondrial pro-apoptotic profile (high BAX/Bcl2 ratio). In this sense, GSK3 $\beta$  also could trigger dysfunctional neurogenesis, which prevents recovery of the synaptic equilibrium of the hippocampus, one neurogenic structure.

probably mediated by the reduced phosphorylation of the GluA1 subunit of the glutamate  $\alpha$ -amino-3-hydroxy-5-methyl-4-isoxazolepropionic acid (AMPA) receptor (Urbanska et al., 2019). This result seems contradictory because of the beneficial effects attributed to GSK3 $\beta$  inhibition, but a recent study exposed that the brain has limited tolerance for the modulation of GSK3 $\beta$  activity on hippocampal damage related to the severity of status epilepticus (Engel et al., 2018).

Another strong hypothesis of GSK3 $\beta$  and its role in epileptogenesis favoring TLE is the close relation with NMDAR and its stimulation, which may induce excitability in the acute stages of the disease (Liu et al., 2017).

All the evidence mentioned above remark on the importance of GSK3 $\beta$  homeostasis in preventing epilepsy. Even though an excitotoxic insult may initially disrupt GSK3 $\beta$ , once this happens, GSK3 $\beta$  actively plays a role in increasing seizure susceptibility (Figure 3). There is no doubt that GSK3 $\beta$  alterations promote the disruption of normal survival signaling pathways and hyperexcitability, which, together, could produce epileptogenesis and neurodegeneration.

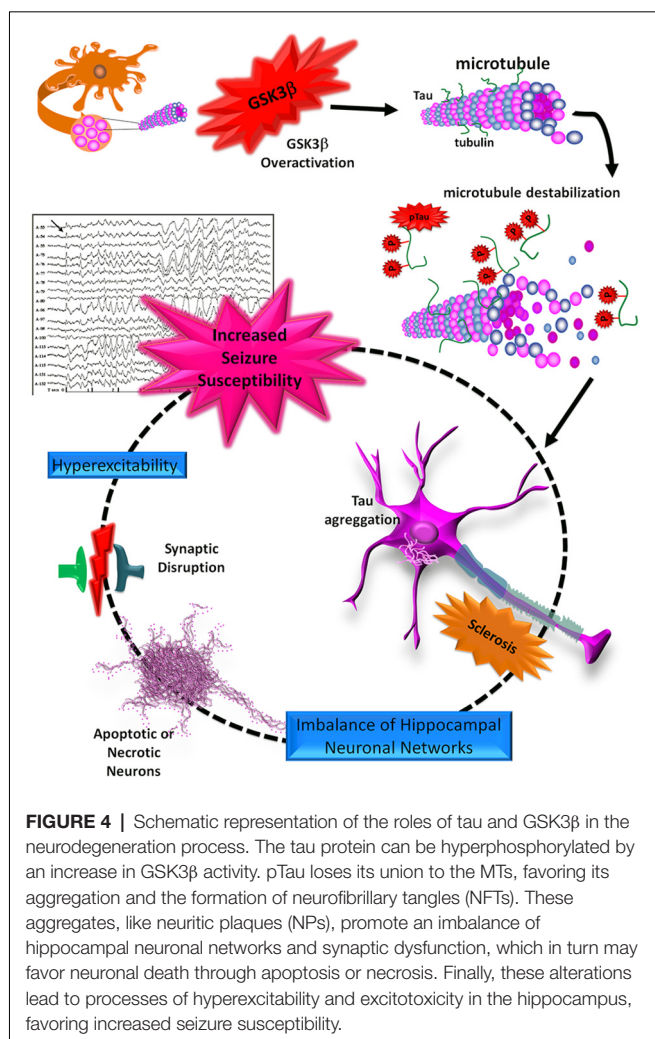
## THERAPEUTICS

As previously mentioned, tau and GSK3 $\beta$  have been associated with several neurological disorders, including AD and TLE; therefore, both represent potential therapeutic targets.

Interestingly, the efficacy of various antiepileptic drugs (AEDs) has been tested in epilepsy experimental models and in AD patients, showing a promising function in cognitive impairment prevention (Sánchez et al., 2018). Since tau hyperphosphorylation is the main mechanism responsible for NFT formation, it has been suggested that inhibiting different tau kinases such as CDK5 and GSK3 $\beta$ , involved in tau hyperphosphorylation, could reduce their aggregation (Xie et al., 2017; Holzer et al., 2018), observed in AD (Morris et al., 2011) and epilepsy (Sen et al., 2007; Thom et al., 2011; Tai et al., 2016).

When AEDs are used in healthy volunteers and different neuropsychological variables are measured, researchers have found that, in general, AEDs like carbamazepine, phenytoin, and valproate have mild cognitive effects (Meador et al., 1995; Martin et al., 2001; Salinsky et al., 2002). In contrast,





when the cognitive effects of oxcarbazepine, gabapentin, and carbamazepine were evaluated in healthy volunteers, the results showed that individuals presented a better performance in the focused attention task and manual writing speed, without any effect on long-term memory (Curran and Java, 1993; Meador et al., 1999). It is worth mentioning that older patients are generally more sensitive to the negative cognitive effects of some AEDs due to the complex interactions among several factors (neuropathologies, genetics, the effects of seizures, psychosocial background, etc.; Kwan and Brodie, 2001).

The efficacy of AEDs in preventing seizures in AD patients has been tested. However, reports regarding their cognitive effects in the elderly are relatively limited, specifically in the elderly with AD. Most of the old AEDs exert negative effects on mood, behavior, and cognitive functions, such as memory (Craig and Tallis, 1994; Meinhold et al., 2005). In contrast, newer AEDs appear to be less harmful and may even produce a slight cognitive benefit, even though some of these newer drugs like topiramate appear to impair language and verbal memory (Fritz et al., 2005). Other various new AEDs like lamotrigine and gabapentin do not impair memory and may have slight beneficial effects on

memory, and even mood (Tekin et al., 1998; Meador et al., 1999). Levetiracetam has demonstrated cognitive benefits, which can be measured in routine clinical practice, particularly in attention and oral fluency (Cumbo and Lorigi, 2010).

The main objective of AED therapy is to improve the patient's quality of life, and even though the main aim is to reduce the quantity of seizures, the current review may provide additional information, which may aid physicians and their patients in making treatment decisions when considering other therapeutic variables like cognition.

The most advanced protein kinase inhibition strategy in the clinic so far has been aimed at GSK3 $\beta$ , leading to the development of novel drugs such as Tideglusib (Hooper et al., 2008; Medina, 2018). Treatment with this thiadiazolidinone (TDZD) compound resulted in decreased amyloid deposition, lower levels of tau phosphorylation, and prevention of memory deficits in a transgenic mouse model (APP<sup>sw</sup>-tau<sup>vlw</sup>; Serenó et al., 2009). Lithium and valproic acid have been used in epilepsy for their anticonvulsant activity and in other psychiatric disorders (Jope and Roh, 2006). Moreover, these inhibitors and TDZD-8, a selective inhibitor of GSK3 $\beta$ , promote the phosphorylation of serine 9, which conducts to GSK3 $\beta$  inactivation (Zhang et al., 2003). The inhibition strategy reduces tau hyperphosphorylation, prevents neuronal death, and inhibits the alteration of neurogenesis processes in the hippocampus in the setting of status epilepticus (Busceti et al., 2007; Bhowmik et al., 2015; Huang et al., 2015; Urbanska et al., 2019). Memantine and ifendropil are NMDAR antagonists and have been demonstrated to conduct to GSK3 $\beta$  inactivation and reduction of tau phosphorylation (Liu et al., 2017). Recently, the use of potent and selective GSK3 $\beta$  inhibitors such as indirubin and BIO-acetoxime showed anticonvulsant properties (Aourz et al., 2019). In this report, PTZ-treated zebrafish larvae were treated with both compounds, which exhibited anticonvulsant activity, with a reduction of epileptiform discharges. In the same way, indirubin and BIO-acetoxime showed anticonvulsant activity in the 6-Hz refractory seizure mouse model (Aourz et al., 2019).

Acetylation is another posttranslational modification that leads to impaired tau function and promotes its pathological aggregation; hence, tau acetylation inhibitors are proposed as a potential therapeutic strategy for AD and other tauopathies (Medina et al., 2016). Salsalate is a nonsteroidal anti-inflammatory drug which inhibits acetyltransferase p300-induced tau acetylation; this drug has been shown to rescue tau-induced memory deficits and prevent hippocampal atrophy in a mouse model of frontotemporal dementia (FTD; Min et al., 2015). Leuco-methylthioninium bis-hydromethanesulfonate (LMTM) is currently in phase III clinical trials and has shown efficacy in inhibiting tau aggregation (Bulic et al., 2013). Passive and active tau immunotherapy is a promising strategy which has been designed for clearing toxic tau species such as monomers, oligomers, prefilaments, granules, fibrils, or insoluble aggregates present in tauopathies and related disorders. The main objectives of immunotherapy are to reduce tau aggregation, prevent neurodegeneration, and improve cognitive functions (Bittar et al., 2018; Medina, 2018; Novak et al., 2018).

Even though all of these therapeutic strategies mainly target AD, it is clear that, in the future, they may well serve for the treatment of other tauopathies, including TLE. Hence, it is important to procure and encourage the potential therapeutic efficacy of tau and GSK3 $\beta$ -based strategies in the future of these diseases.

## CONCLUSIONS

TLE is a common disorder characterized by hippocampal sclerosis and chronic seizures that are frequently resistant to pharmacological treatment and are associated with disabling comorbidities and cognitive decline. Epidemiological studies have shown an increased prevalence of several dementias, including AD, in chronic epilepsy. These pathologies converge in the hyperphosphorylation of tau protein, apparently mediated by an increased activity of GSK3 $\beta$  that can promote apoptosis, aberrant neurogenesis, impaired synaptic plasticity, and hyperexcitability in the hippocampus. These alterations have

been well described in AD, but are not yet completely understood in TLE (Figure 4). For this reason, further studies are necessary to clarify the roles of tau and GSK3 $\beta$  in physiopathology and structural abnormalities and to probe the effectiveness of novel tau immunotherapies. Also, considering that AD and TLE are sporadic and multifactorial diseases, it would be interesting to study different alterations in the GSK3 $\beta$  and the tau (*MAPT*) encoding genes that could represent genetic risk factors for the development of TLE and AD.

## AUTHOR CONTRIBUTIONS

DT-R, PP-R, MA-V, and VC-P drafted the manuscript. All authors read and approved the final manuscript.

## FUNDING

This work was supported by a grant from CONACYT S0008-2016-1, no. 273182.

## REFERENCES

- Ahmed, T., Van Der Jeugd, A., Blum, D., Galas, M. C., D'Hooze, R., Buee, L., et al. (2014). Cognition and hippocampal synaptic plasticity in mice with a homozygous tau deletion. *Neurobiol. Aging* 35, 2474–2478. doi: 10.1016/j.neurobiolaging.2014.05.005
- Ahnaou, A., Moechars, D., Raeymaekers, L., Biernans, R., Manyakov, N. V., Bottelbergs, A., et al. (2017). Emergence of early alterations in network oscillations and functional connectivity in a tau seeding mouse model of Alzheimer's disease pathology. *Sci. Rep.* 7:14189. doi: 10.1038/s41598-017-13839-6
- Alonso, A. C., Grundke-Iqbal, I., and Iqbal, K. (1996). Alzheimer's disease hyperphosphorylated tau sequesters normal tau into tangles of filaments and disassembles microtubules. *Nat. Med.* 2, 783–787. doi: 10.1038/nm0796-783
- Andreadis, A. (2005). Tau gene alternative splicing: expression patterns, regulation and modulation of function in normal brain and neurodegenerative diseases. *Biochim. Biophys. Acta* 1739, 91–103. doi: 10.1016/j.bbdis.2004.08.010
- Andreadis, A., Brown, W. M., and Kosik, K. S. (1992). Structure and novel exons of the human tau gene. *Biochemistry* 31, 10626–10633. doi: 10.1021/bi00158a027
- Aourz, N., Serruys, A. K., Chabwine, J. N., Balegamire, P. B., Afrikanova, T., Edrada-Ebel, R., et al. (2019). Identification of GSK-3 as a potential therapeutic entry point for epilepsy. *ACS Chem. Neurosci.* 10, 1992–2003. doi: 10.1021/acscchemneuro.8b00281
- Avila, J., Santa-María, I., Pérez, M., Hernández, F., and Moreno, F. (2006). Tau phosphorylation, aggregation and cell toxicity. *J. Biomed. Biotechnol.* 2006:74539. doi: 10.1155/jbb/2006/74539
- Bhowmik, M., Khanam, R., Saini, N., and Vohora, D. (2015). Activation of AKT/GSK3 $\beta$  pathway by TDZD-8 attenuates kainic acid induced neurodegeneration but not seizures in mice. *Neurotoxicology* 46, 44–52. doi: 10.1016/j.neuro.2014.11.008
- Bittar, A., Sengupta, U., and Kaye, R. (2018). Prospects for strain-specific immunotherapy in Alzheimer's disease and tauopathies. *NPJ Vaccines* 3:9. doi: 10.1038/s41541-018-0046-8
- Buée, L., Bussiére, T., Buée-Scherrer, V., Delacourte, A., and Hof, P. R. (2000). Tau protein isoforms, phosphorylation and role in neurodegenerative disorders. *Brain Res. Rev.* 33, 95–130. doi: 10.1016/s0165-0173(00)00019-9
- Bulic, B., Pickhardt, M., and Mandelkow, E. (2013). Progress and developments in tau aggregation inhibitors for Alzheimer disease. *J. Med. Chem.* 56, 4135–4155. doi: 10.1021/jm3017317
- Busceti, C. L., Biagioni, F., Aronica, E., Riozzi, B., Storto, M., Battaglia, G., et al. (2007). Induction of the Wnt inhibitor, Dickkopf-1, is associated with neurodegeneration related to temporal lobe epilepsy. *Epilepsia* 48, 694–705. doi: 10.1111/j.1528-1167.2007.01055.x
- Camilo, O., and Goldstein, L. B. (2004). Seizures and epilepsy after ischemic stroke. *Stroke* 35, 1769–1775. doi: 10.1161/01.STR.0000130989.17100.96
- Craig, I., and Tallis, R. (1994). Impact of valproate and phenytoin on cognitive function in elderly patients: results of a single-blind randomized comparative study. *Epilepsia* 35, 381–390. doi: 10.1111/j.1528-1157.1994.tb02448.x
- Crespo-Biel, N., Canudas, A. M., Camins, A., and Pallas, M. (2007). Kainate induces AKT, ERK and cdk5/GSK3 $\beta$  pathway deregulation, phosphorylates tau protein in mouse hippocampus. *Neurochem. Int.* 50, 435–442. doi: 10.1016/j.neuint.2006.10.002
- Cruchaga, C., Kauwe, J. S., Harari, O., Jin, S. C., Cai, Y., Karch, C. M., et al. (2013). GWAS of cerebrospinal fluid tau levels identifies risk variants for Alzheimer's disease. *Neuron* 78, 256–268. doi: 10.1016/j.neuron.2013.02.026
- Cumbo, E., and Ligor, L. D. (2010). Levetiracetam, lamotrigine, and phenobarbital in patients with epileptic seizures and Alzheimer's disease. *Epilepsy Behav.* 17, 461–466. doi: 10.1016/j.yebeh.2010.01.015
- Curran, H. V., and Java, R. (1993). Memory and psychomotor effects of oxcarbazepine in healthy human volunteers. *Eur. J. Clin. Pharmacol.* 44, 529–533. doi: 10.1007/bf02440853
- DeVos, S. L., Goncharoff, D. K., Chen, G., Kebodeaux, C. S., Yamada, K., Stewart, F. R., et al. (2013). Antisense reduction of tau in adult mice protects against seizures. *J. Neurosci.* 33, 12887–12897. doi: 10.1523/jneurosci.2107-13.2013
- Dixit, R., Ross, J. L., Goldman, Y. E., and Holzbaur, E. L. (2008). Differential regulation of dynein and kinesin motor proteins by tau. *Science* 319, 1086–1089. doi: 10.1126/science.1152993
- Engel, T., Gomez-Sintes, R., Alves, M., Jimenez-Mateos, E. M., Fernandez-Nogales, M., Sanz-Rodriguez, A., et al. (2018). Bi-directional genetic modulation of GSK-3 $\beta$  exacerbates hippocampal neuropathology in experimental status epilepticus. *Cell Death Dis.* 9:969. doi: 10.1038/s41419-018-0963-5
- Evans, D. B., Rank, K. B., Bhattacharya, K., Thomsen, D. R., Gurney, M. E., and Sharma, S. K. (2000). Tau phosphorylation at serine 396 and serine 404 by human recombinant tau protein kinase II inhibits tau's ability to promote microtubule assembly. *J. Biol. Chem.* 275, 24977–24983. doi: 10.1074/jbc.m000808200
- Flament, S., Delacourte, A., and Mann, D. M. (1990). Phosphorylation of Tau proteins: a major event during the process of neurofibrillary degeneration. A comparative study between Alzheimer's disease and Down's syndrome. *Brain Res.* 516, 15–19. doi: 10.1016/0006-8993(90)90891-e
- Fritz, N., Glogau, S., Hoffmann, J., Rademacher, M., Elger, C. E., and Helmstaedter, C. (2005). Efficacy and cognitive side effects of tiagabine and topiramate in patients with epilepsy. *Epilepsy Behav.* 6, 373–381. doi: 10.1016/j.yebeh.2005.01.002

- Gangarossa, G., Sakakaki, S., Lory, P., and Valjent, E. (2015). Mouse hippocampal phosphorylation footprint induced by generalized seizures: focus on ERK, mTORC1 and Akt/GSK-3 pathways. *Neuroscience* 311, 474–483. doi: 10.1016/j.neuroscience.2015.10.051
- Goedert, M. (1999). Filamentous nerve cell inclusions in neurodegenerative diseases: tauopathies and  $\alpha$ -synucleinopathies. *Philos. Trans. R. Soc. Lond. B Biol. Sci.* 354, 1101–1118. doi: 10.1098/rstb.1999.0466
- Gómez De Barreda, E., Perez, M., Gomez Ramos, P., De Cristobal, J., Martin-Maestro, P., Moran, A., et al. (2010). Tau-knockout mice show reduced GSK3-induced hippocampal degeneration and learning deficits. *Neurobiol. Dis.* 37, 622–629. doi: 10.1016/j.nbd.2009.11.017
- Grundke-Iqbal, I., Iqbal, K., Quinlan, M., Tung, Y. C., Zaidi, M. S., and Wisniewski, H. M. (1986). Microtubule-associated protein tau. A component of Alzheimer paired helical filaments. *J. Biol. Chem.* 261, 6084–6089.
- Hall, A. M., Throesch, B. T., Buckingham, S. C., Markwardt, S. J., Peng, Y., Wang, Q., et al. (2015). Tau-dependent Kv4.2 depletion and dendritic hyperexcitability in a mouse model of Alzheimer's disease. *J. Neurosci.* 35, 6221–6230. doi: 10.1523/jneurosci.2552-14.2015
- Hanger, D. P., Anderton, B. H., and Noble, W. (2009). Tau phosphorylation: the therapeutic challenge for neurodegenerative disease. *Trends Mol. Med.* 15, 112–119. doi: 10.1016/j.molmed.2009.01.003
- Hasegawa, M., Smith, M. J., and Goedert, M. (1998). Tau proteins with FTDP-17 mutations have a reduced ability to promote microtubule assembly. *FEBS Lett.* 437, 207–210. doi: 10.1016/s0014-5793(98)01217-4
- Holmes, G. L. (2015). Cognitive impairment in epilepsy: the role of network abnormalities. *Epileptic Disord.* 17, 101–116. doi: 10.1684/epd.2015.0739
- Holth, J. K., Bomben, V. C., Reed, J. G., Inoue, T., Younkin, L., Younkin, S. G., et al. (2013). Tau loss attenuates neuronal network hyperexcitability in mouse and *Drosophila* genetic models of epilepsy. *J. Neurosci.* 33, 1651–1659. doi: 10.1523/jneurosci.3191-12.2013
- Holzer, M., Schade, N., Opitz, A., Hilbrich, I., Stieler, J., Vogel, T., et al. (2018). Novel protein kinase inhibitors related to tau pathology modulate tau protein-self interaction using a luciferase complementation assay. *Molecules* 23:E2335. doi: 10.3390/molecules23092335
- Hooper, C., Killick, R., and Lovestone, S. (2008). The GSK3 hypothesis of Alzheimer's disease. *J. Neurochem.* 104, 1433–1439. doi: 10.1111/j.1471-4159.2007.05194.x
- Huang, C., Fu, X. H., Zhou, D., and Li, J. M. (2015). The role of Wnt/ $\beta$ -catenin signaling pathway in disrupted hippocampal neurogenesis of temporal lobe epilepsy: a potential therapeutic target? *Neurochem. Res.* 40, 1319–1332. doi: 10.1007/s11064-015-1614-1
- Inestrosa, N. C., and Toledo, E. M. (2008). The role of Wnt signaling in neuronal dysfunction in Alzheimer's Disease. *Mol. Neurodegener.* 3:9. doi: 10.1186/1750-1326-3-9
- Jope, R. S., and Roh, M. S. (2006). Glycogen synthase kinase-3 (GSK3) in psychiatric diseases and therapeutic interventions. *Curr. Drug Targets* 7, 1421–1434. doi: 10.2174/1389450110607011421
- Kauwe, J. S., Cruchaga, C., Mayo, K., Fenoglio, C., Bertelsen, S., Nowotny, P., et al. (2008). Variation in MAPT is associated with cerebrospinal fluid tau levels in the presence of amyloid- $\beta$  deposition. *Proc. Natl. Acad. Sci. U S A* 105, 8050–8054. doi: 10.1073/pnas.0801227105
- Kimura, T., Whitcomb, D. J., Jo, J., Regan, P., Piers, T., Heo, S., et al. (2014). Microtubule-associated protein tau is essential for long-term depression in the hippocampus. *Philos. Trans. R. Soc. Lond. B Biol. Sci.* 369:20130144. doi: 10.1098/rstb.2013.0144
- Kneynsberg, A., Combs, B., Christensen, K., Morfini, G., and Kanaan, N. M. (2017). Axonal degeneration in tauopathies: disease relevance and underlying mechanisms. *Front. Neurosci.* 11:572. doi: 10.3389/fnins.2017.00572
- Kwan, J. (2010). Stroke: predicting the risk of poststroke epilepsy-why and how? *Nat. Rev. Neurol.* 6, 532–533. doi: 10.1038/nrneurol.2010.140
- Kwan, P., and Brodie, M. J. (2001). Neuropsychological effects of epilepsy and antiepileptic drugs. *Lancet* 357, 216–222. doi: 10.1016/S0140-6736(00)03600-X
- Lee, C. Y., Jaw, T., Tseng, H. C., Chen, I. C., and Liou, H. H. (2012). Lovastatin modulates glycogen synthase kinase-3 $\beta$  pathway and inhibits mossy fiber sprouting after pilocarpine-induced status epilepticus. *PLoS One* 7:e38789. doi: 10.1371/journal.pone.0038789
- Leroy, K., Boutajangout, A., Authélet, M., Woodgett, J. R., Anderton, B. H., and Brion, J. P. (2002). The active form of glycogen synthase kinase-3 $\beta$  is associated with granulovacuolar degeneration in neurons in Alzheimer's disease. *Acta Neuropathol.* 103, 91–99. doi: 10.1007/s004010100435
- Linseman, D. A., Butts, B. D., Precht, T. A., Phelps, R. A., Le, S. S., Laessig, T. A., et al. (2004). Glycogen synthase kinase-3 $\beta$  phosphorylates Bax and promotes its mitochondrial localization during neuronal apoptosis. *J. Neurosci.* 24, 9993–10002. doi: 10.1523/jneurosci.2057-04.2004
- Liu, X., Ou, S., Yin, M., Xu, T., Wang, T., Liu, Y., et al. (2017). N-methyl-D-aspartate receptors mediate epilepsy-induced axonal impairment and tau phosphorylation via activating glycogen synthase kinase-3 $\beta$  and cyclin-dependent kinase 5. *Discov. Med.* 23, 221–234.
- Lohi, H., Ianzano, L., Zhao, X. C., Chan, E. M., Turnbull, J., Scherer, S. W., et al. (2005). Novel glycogen synthase kinase 3 and ubiquitination pathways in progressive myoclonus epilepsy. *Hum. Mol. Genet.* 14, 2727–2736. doi: 10.1093/hmg/ddi306
- Mandelkow, E. M., Biernat, J., Drewes, G., Gustke, N., Trinczek, B., and Mandelkow, E. (1995). Tau domains, phosphorylation, and interactions with microtubules. *Neurobiol. Aging* 16, 355–362; discussion 362–363. doi: 10.1016/0197-4580(95)00025-a
- Martin, L., Latypova, X., and Terro, F. (2011). Post-translational modifications of tau protein: implications for Alzheimer's disease. *Neurochem. Int.* 58, 458–471. doi: 10.1016/j.neuint.2010.12.023
- Martin, L., Latypova, X., Wilson, C. M., Magnaudeix, A., Perrin, M. L., Yardin, C., et al. (2013). Tau protein kinases: involvement in Alzheimer's disease. *Ageing Res. Rev.* 12, 289–309. doi: 10.1016/j.arr.2012.06.003
- Martin, R., Meador, K., Turrentine, L., Faught, E., Sinclair, K., Kuzniecky, R., et al. (2001). Comparative cognitive effects of carbamazepine and gabapentin in healthy senior adults. *Epilepsia* 42, 764–771. doi: 10.1046/j.1528-1157.2001.33300.x
- Meador, K. J., Loring, D. W., Moore, E. E., Thompson, W. O., Nichols, M. E., Oberzan, R. E., et al. (1995). Comparative cognitive effects of phenobarbital, phenytoin, and valproate in healthy adults. *Neurology* 45, 1494–1499. doi: 10.1212/wnl.45.8.1494
- Meador, K. J., Loring, D. W., Ray, P. G., Murro, A. M., King, D. W., Nichols, M. E., et al. (1999). Differential cognitive effects of carbamazepine and gabapentin. *Epilepsia* 40, 1279–1285. doi: 10.1111/j.1528-1157.1999.tb00858.x
- Medina, M. (2018). An overview on the clinical development of tau-based therapeutics. *Int. J. Mol. Sci.* 19:E1160. doi: 10.3390/ijms19041160
- Medina, M., Hernandez, F., and Avila, J. (2016). New features about tau function and dysfunction. *Biomolecules* 6:E21. doi: 10.3390/biom6020021
- Meinhold, J. M., Blake, L. M., Mini, L. J., Welge, J. A., Schwiess, M., and Hughes, A. (2005). Effect of divalproex sodium on behavioural and cognitive problems in elderly dementia. *Drugs Aging* 22, 615–626. doi: 10.2165/00002512-200522070-00007
- Meraz-Ríos, M. A., Toral-Ríos, D., Franco-Bocanegra, D., Villeda-Hernández, J., and Campos-Peña, V. (2013). Inflammatory process in Alzheimer's Disease. *Front. Integr. Neurosci.* 7:59. doi: 10.3389/fnint.2013.00059
- Min, S. W., Chen, X., Tracy, T. E., Li, Y., Zhou, Y., Wang, C., et al. (2015). Critical role of acetylation in tau-mediated neurodegeneration and cognitive deficits. *Nat. Med.* 21, 1154–1162. doi: 10.1038/nm.3951
- Mines, M. A., Beurel, E., and Jope, R. S. (2011). Regulation of cell survival mechanisms in Alzheimer's disease by glycogen synthase kinase-3. *Int. J. Alzheimers Dis.* 2011:861072. doi: 10.4061/2011/861072
- Mondragón-Rodríguez, S., Trillaud-Doppia, E., Dudilot, A., Bourgeois, C., Lauzon, M., Leclerc, N., et al. (2012). Interaction of endogenous tau protein with synaptic proteins is regulated by N-methyl-D-aspartate receptor-dependent tau phosphorylation. *J. Biol. Chem.* 287, 32040–32053. doi: 10.1074/jbc.m112.401240
- Morris, M., Maeda, S., Vossell, K., and Mucke, L. (2011). The many faces of tau. *Neuron* 70, 410–426. doi: 10.1016/j.neuron.2011.04.009
- Muyllaert, D., Kremer, A., Jaworski, T., Borghgraef, P., Devijver, H., Croes, S., et al. (2008). Glycogen synthase kinase-3 $\beta$ , or a link between amyloid and tau pathology? *Genes Brain Behav.* 7, 57–66. doi: 10.1111/j.1601-183x.2007.00376.x
- Myers, A. J., Pittman, A. M., Zhao, A. S., Rohrer, K., Kaleem, M., Marlowe, L., et al. (2007). The MAPT H1c risk haplotype is associated with increased expression of tau and especially of 4 repeat containing transcripts. *Neurobiol. Dis.* 25, 561–570. doi: 10.1016/j.nbd.2006.10.018



- Novak, P., Kontsekova, E., Zilka, N., and Novak, M. (2018). Ten years of tau-targeted immunotherapy: the path walked and the roads ahead. *Front. Neurosci.* 12:798. doi: 10.3389/fnins.2018.00798
- Pandis, D., and Scarmeas, N. (2012). Seizures in Alzheimer disease: clinical and epidemiological data. *Epilepsy Curr.* 12, 184–187. doi: 10.5698/1535-7511-12.5.184
- Peineau, S., Taghibiglou, C., Bradley, C., Wong, T. P., Liu, L., Lu, J., et al. (2007). LTP inhibits LTD in the hippocampus via regulation of GSK3 $\beta$ . *Neuron* 53, 703–717. doi: 10.1016/j.neuron.2007.01.029
- Regan, P., Piers, T., Yi, J. H., Kim, D. H., Huh, S., Park, S. J., et al. (2015). Tau phosphorylation at serine 396 residue is required for hippocampal LTD. *J. Neurosci.* 35, 4804–4812. doi: 10.1523/jneurosci.2842-14.2015
- Roberson, E. D., Halabisky, B., Yoo, J. W., Yao, J., Chin, J., Yan, F., et al. (2011). Amyloid- $\beta$ /Fyn-induced synaptic, network and cognitive impairments depend on tau levels in multiple mouse models of Alzheimer's disease. *J. Neurosci.* 31, 700–711. doi: 10.1523/jneurosci.4152-10.2011
- Roberson, E. D., Searce-Levie, K., Palop, J. J., Yan, F., Cheng, I. H., Wu, T., et al. (2007). Reducing endogenous tau ameliorates amyloid  $\beta$ -induced deficits in an Alzheimer's disease mouse model. *Science* 316, 750–754. doi: 10.1126/science.1141736
- Salcedo-Tello, P., Ortiz-Matamoros, A., and Arias, C. (2011). GSK3 function in the brain during development, neuronal plasticity and neurodegeneration. *Int. J. Alzheimers Dis.* 2011:189728. doi: 10.4061/2011/189728
- Salinsky, M. C., Binder, L. M., Oken, B. S., Storzach, D., Aron, C. R., and Dodrill, C. B. (2002). Effects of gabapentin and carbamazepine on the EEG and cognition in healthy volunteers. *Epilepsia* 43, 482–490. doi: 10.1046/j.1528-1157.2002.22501.x
- Sánchez, M. P., García-Cabrero, A. M., Sanchez-Elexpuru, G., Burgos, D. F., and Serratos, J. M. (2018). Tau-induced pathology in epilepsy and dementia: notions from patients and animal models. *Int. J. Mol. Sci.* 19:E1092. doi: 10.3390/ijms19041092
- Sen, A., Thom, M., Martinian, L., Harding, B., Cross, J. H., Nikolic, M., et al. (2007). Pathological tau tangles localize to focal cortical dysplasia in older patients. *Epilepsia* 48, 1447–1454. doi: 10.1111/j.1528-1167.2007.01107.x
- Serenó, L., Coma, M., Rodríguez, M., Sánchez-Ferrer, P., Sánchez, M. B., Gich, I., et al. (2009). A novel GSK-3 $\beta$  inhibitor reduces Alzheimer's pathology and rescues neuronal loss *in vivo*. *Neurobiol. Dis.* 35, 359–367. doi: 10.1016/j.nbd.2009.05.025
- Tai, X. Y., Koeppe, M., Duncan, J. S., Fox, N., Thompson, P., Baxendale, S., et al. (2016). Hyperphosphorylated tau in patients with refractory epilepsy correlates with cognitive decline: a study of temporal lobe resections. *Brain* 139, 2441–2455. doi: 10.1093/brain/aww187
- Takashima, A., Noguchi, K., Michel, G., Mercken, M., Hoshi, M., Ishiguro, K., et al. (1996). Exposure of rat hippocampal neurons to amyloid  $\beta$  peptide (25–35) induces the inactivation of phosphatidylinositol-3 kinase and the activation of tau protein kinase I/glycogen synthase kinase-3  $\beta$ . *Neurosci. Lett.* 203, 33–36. doi: 10.1016/0304-3940(95)12257-5
- Tan, W. F., Cao, X. Z., Wang, J. K., Lv, H. W., Wu, B. Y., and Ma, H. (2010). Protective effects of lithium treatment for spatial memory deficits induced by tau hyperphosphorylation in splenectomized rats. *Clin. Exp. Pharmacol. Physiol.* 37, 1010–1015. doi: 10.1111/j.1440-1681.2010.05433.x
- Tekin, S., Aykut-Bingol, C., Tanridag, T., and Aktan, S. (1998). Antiglutamatergic therapy in Alzheimer's disease—effects of lamotrigine. Short communication. *J. Neural Transm.* 105, 295–303. doi: 10.1007/s007020050059
- Thom, M., Liu, J. Y., Thompson, P., Phadke, R., Narkiewicz, M., Martinian, L., et al. (2011). Neurofibrillary tangle pathology and Braak staging in chronic epilepsy in relation to traumatic brain injury and hippocampal sclerosis: a post-mortem study. *Brain* 134, 2969–2981. doi: 10.1093/brain/awr209
- Tripathi, P. P., Santorufu, G., Brilli, E., Borrelli, E., and Bozzi, Y. (2010). Kainic acid-induced seizures activate GSK-3 $\beta$  in the hippocampus of D2R $^{-/-}$  mice. *Neuroreport* 21, 846–850. doi: 10.1097/wnr.0b013e32833d5891
- Urbanska, M., Kazmierska-Grebowska, P., Kowalczyk, T., Caban, B., Nader, K., Pijet, B., et al. (2019). GSK3 $\beta$  activity alleviates epileptogenesis and limits GluA1 phosphorylation. *EBioMedicine* 39, 377–387. doi: 10.1016/j.ebiom.2018.11.040
- Wood, J. G., Mirra, S. S., Pollock, N. J., and Binder, L. I. (1986). Neurofibrillary tangles of Alzheimer disease share antigenic determinants with the axonal microtubule-associated protein tau (tau). *Proc. Natl. Acad. Sci. U S A* 83, 4040–4043. doi: 10.1073/pnas.83.11.4040
- Xie, H., Wen, H., Zhang, D., Liu, L., Liu, B., Liu, Q., et al. (2017). Designing of dual inhibitors for GSK-3 $\beta$  and CDK5: virtual screening and *in vitro* biological activities study. *Oncotarget* 8, 18118–18128. doi: 10.18632/oncotarget.15085
- Zhang, F., Phiel, C. J., Spece, L., Gurvich, N., and Klein, P. S. (2003). Inhibitory phosphorylation of glycogen synthase kinase-3 (GSK-3) in response to lithium. Evidence for autoregulation of GSK-3. *J. Biol. Chem.* 278, 33067–33077. doi: 10.1074/jbc.m212635200

**Conflict of Interest:** The authors declare that the research was conducted in the absence of any commercial or financial relationships that could be construed as a potential conflict of interest.

Copyright © 2020 Toral-Rios, Pichardo-Rojas, Alonso-Vanegas and Campos-Peña. This is an open-access article distributed under the terms of the Creative Commons Attribution License (CC BY). The use, distribution or reproduction in other forums is permitted, provided the original author(s) and the copyright owner(s) are credited and that the original publication in this journal is cited, in accordance with accepted academic practice. No use, distribution or reproduction is permitted which does not comply with these terms.





# Methylene Blue Preserves Cytochrome Oxidase Activity and Prevents Neurodegeneration and Memory Impairment in Rats With Chronic Cerebral Hypoperfusion

Allison M. Auchter, Douglas W. Barrett, Marie H. Monfils and F. Gonzalez-Lima\*

Department of Psychology, Institute for Neuroscience, The University of Texas at Austin, Austin, TX, United States

## OPEN ACCESS

### Edited by:

Karla Guadalupe Carvajal,  
National Institute of Pediatrics  
(Mexico), Mexico

### Reviewed by:

Jon Storm-Mathisen,  
University of Oslo, Norway  
Bryan Victor Phillips-Farfan,  
National Institute of Pediatrics  
(Mexico), Mexico

### \*Correspondence:

F. Gonzalez-Lima  
gonzalezlima@utexas.edu

### Specialty section:

This article was submitted to  
Cellular Neuropathology,  
a section of the journal  
Frontiers in Cellular Neuroscience

**Received:** 25 April 2019

**Accepted:** 20 April 2020

**Published:** 20 May 2020

### Citation:

Auchter AM, Barrett DW,  
Monfils MH and Gonzalez-Lima F  
(2020) Methylene Blue Preserves  
Cytochrome Oxidase Activity  
and Prevents Neurodegeneration  
and Memory Impairment in Rats With  
Chronic Cerebral Hypoperfusion.  
Front. Cell. Neurosci. 14:130.  
doi: 10.3389/fncel.2020.00130

Chronic cerebral hypoperfusion in neurocognitive disorders diminishes cytochrome oxidase activity leading to neurodegenerative effects and impairment of learning and memory. Methylene blue at low doses stimulates cytochrome oxidase activity and may thus counteract the adverse effects of cerebral hypoperfusion. However, the effects of methylene blue on cytochrome oxidase activity during chronic cerebral hypoperfusion have not been described before. To test this hypothesis, rats underwent bilateral carotid artery occlusion or sham surgery, received daily 4 mg/kg methylene blue or saline injections, and learned a visual water task. Brain mapping of cytochrome oxidase activity was done by quantitative enzyme histochemistry. Permanent carotid occlusion for 1 month resulted in decreased cytochrome oxidase activity in visual cortex, prefrontal cortex, perirhinal cortex, hippocampus and amygdala, and weaker interregional correlation of cytochrome oxidase activity between these regions. Methylene blue preserved cytochrome oxidase activity in regions affected by carotid occlusion and strengthened their interregional correlations of cytochrome oxidase activity, which prevented neurodegenerative effects and facilitated task-specific learning and memory. Brain-behavior correlations revealed positive correlations between performance and brain regions in which cytochrome oxidase activity was preserved by methylene blue. These results are the first to demonstrate that methylene blue prevents neurodegeneration and memory impairment by preserving cytochrome oxidase activity and interregional correlation of cytochrome oxidase activity in brain regions susceptible to chronic hypoperfusion. This demonstration provides further support for the hypothesis that lower cerebral blood flow results in an Alzheimer's-like syndrome and that stimulating cytochrome oxidase activity with low-dose methylene blue is neuroprotective.

**Keywords:** methylene blue, chronic cerebral hypoperfusion, carotid artery occlusion, cytochrome oxidase, interregional correlations, vascular hypothesis of Alzheimer's dementia

## INTRODUCTION

Aging and dementia involve progressive reduction in cerebral blood flow and energy metabolism that result in cognitive dysfunction (de la Torre, 1999; Farkas and Luiten, 2001). Patients with cerebrovascular disorders and late-onset Alzheimer's disease (AD) show marked cerebral hypoperfusion (de la Torre, 2012). Even normal aging-related reduction in cerebral blood flow results in significant functional pathology when combined with other factors such as cardiovascular disease (Haley et al., 2007) and cerebrovascular ischemia (de la Torre et al., 1997; Cada et al., 2000). Interestingly, in AD patients who have not suffered cerebral infarction, cerebral perfusion is reduced more symmetrically, globally and chronically than in stroke patients (Tachibana et al., 1984), implicating chronic cerebral hypoperfusion in the pathogenesis of AD (de la Torre, 2018).

Permanent bilateral carotid artery occlusion (2-vessel occlusion; 2VO) is a useful model for the reproduction of chronic cerebral hypoperfusion as it occurs in human aging and AD (de la Torre et al., 1992; de la Torre, 1999, 2000; Farkas et al., 2007). Typically, in rats permanent vessel occlusion does not result in reperfusion injury (as a result of instant recovery of perfusion). Additionally, cerebral hypoperfusion is global, damage to nervous tissue is less dramatic, and there are no obvious signs of motor dysfunction or seizures (de la Torre et al., 1992; Farkas et al., 2007). When neurons are starved of glucose and oxygen via chronic cerebral hypoperfusion, the impending result is mitochondrial dysfunction. If mitochondria do not receive enough glucose and oxygen, electrons from the electron transport chain used to drive ATP synthesis are taken up by other molecules, resulting in the formation of damaging reactive oxygen species (Rojas et al., 2012).

We hypothesized that certain properties of low-dose methylene blue (MB) could be neuroprotective under conditions of reduced supply of glucose and oxygen such as in chronic cerebral hypoperfusion (Gonzalez-Lima and Auchter, 2015). Under physiological conditions in nervous tissue, nearly all the electrons donated to the electron transport chain are derived from the transformation of glucose for the generation of the electron donors NADH and FADH (Erecinska and Silver, 1989). However, MB at low doses reaches a redox equilibrium inside mitochondria that allows MB to cycle electrons directly into the electron transport chain (Rojas et al., 2012). In this way, MB could compensate for a reduced supply of glucose to the brain by becoming an alternative source of electrons donated to the electron transport chain. Cytochrome oxidase (CO) is the last enzyme in the electron transport chain that passes the electrons to oxygen as the final electron acceptor (Erecinska and Silver, 1989). However, there is evidence that MB can maintain energy production even under hypoxic conditions (Lee and Urban, 2002) because MB can replace oxygen by accepting electrons from CO at the end of the electron transport chain (Rojas et al., 2012). Therefore, maintaining CO activity by MB's electron cycling could compensate for 2VO reducing both glucose and oxygen.

Neuropathological changes that result from 2VO resemble those of late-onset AD, strengthening its use as an experimental

model (de la Torre, 1999, 2000). Since hippocampal damage is a feature of AD, and the hippocampus is also particularly sensitive to ischemia, the time course of damage to the hippocampus as a result of 2VO surgery has been well characterized. While conspicuous hippocampal damage is not seen during the first week after 2VO (Ohtaki et al., 2006), damage to the CA1 subfield is observed in 6–29% of animals at 2 weeks (Schmidt-Kastner et al., 2001; Farkas et al., 2006), 55% at 4 weeks (Ohtaki et al., 2006), and total hippocampal destruction was observed in 67% of 2VO rats at 8–13 weeks (Farkas et al., 2004; Liu et al., 2006).

2VO also serves as a good model for cognitive aging and dementia because it not only results in global neurological changes, but also results in learning and memory impairment (Cada et al., 2000; de la Torre, 2000). It has been well established that experimental cerebral hypoperfusion compromises spatial learning in rats (Farkas and Luiten, 2001; Liu et al., 2005; Shang et al., 2005). Non-spatial object recognition deficits have also been observed 60 and 90 days following 2VO surgery (Sarti et al., 2002), but we did not observe deficits in odor recognition after 30 days (Auchter et al., 2014).

Methylene blue is a blue dye with neurometabolic enhancing properties at low doses (Rojas et al., 2012). MB crosses the blood-brain barrier and diffuses into the mitochondrial matrix, where at low doses it forms a redox equilibrium with the enzymes of the electron transport chain (Bruchey and Gonzalez-Lima, 2008; Riha et al., 2011). MB enhances mitochondrial respiration, chiefly by increasing the activity of cytochrome oxidase (CO) (Rojas et al., 2012). CO is the terminal enzyme of the electron transport chain and its activity reflects neuronal activity (Wong-Riley, 1989), including neuronal activity of circuits involved in rat water maze tasks (Villarreal et al., 2002; Conejo et al., 2010). MB enhancement of CO activity is coupled with increases in ATP production and oxygen consumption (Riha et al., 2005; Atamna et al., 2008; Bruchey and Gonzalez-Lima, 2008). Through enhanced mitochondrial efficiency, MB also reduces the incidence of reactive oxygen species formation (Salaris et al., 1991) and consequently delays cellular senescence (Atamna et al., 2008).

Methylene blue at low doses has been shown to enhance both spatial (Callaway et al., 2002; Riha et al., 2005; Wrubel et al., 2007) and non-spatial (Gonzalez-Lima and Bruchey, 2004) memories, and such enhancement is also marked by increases in CO activity (Callaway et al., 2002, 2004). In humans, MB enhances various memory tasks and modulates brain functional connectivity (Telch et al., 2014; Rodriguez et al., 2016, 2017; Zoellner et al., 2017). MB has also been shown to be neuroprotective in rodent models of stroke (Salaris et al., 1991; Miclescu et al., 2010; Shen et al., 2013), hypoxia (Huang et al., 2013), Alzheimer's disease (Callaway et al., 2002; Riha et al., 2005), Parkinson's disease (Rojas et al., 2009b; Smith et al., 2017), and mitochondrial optic neuropathy (Zhang et al., 2006; Rojas et al., 2009a). However, MB effects have not been described during chronic cerebral hypoperfusion.

The objectives of this experiment were to describe (1) how 2VO weakens brain regional cytochrome oxidase activity as measured by quantitative enzyme histochemistry, interregional correlation of cytochrome oxidase activity and performance

on a visual discrimination task, (2) how MB strengthens performance and preserves both regional cytochrome oxidase activity and interregional correlation of cytochrome oxidase activity, and (3) how specific changes in brain regional cytochrome oxidase activity are correlated with behavioral performance (Auchter, 2015).

Our hypothesis was that chronic cerebral hypoperfusion results in reduction in regional CO activity in brain regions susceptible to hypoxia and a reduction in interregional correlation of cytochrome oxidase activity between regions involved in visual discrimination learning. Treatment of chronic cerebral hypoperfusion with daily low-dose methylene blue (MB) injections may restore both brain regional activity and interregional correlation of cytochrome oxidase activity, preventing neurodegeneration and memory impairment.

## MATERIALS AND METHODS

### Subjects

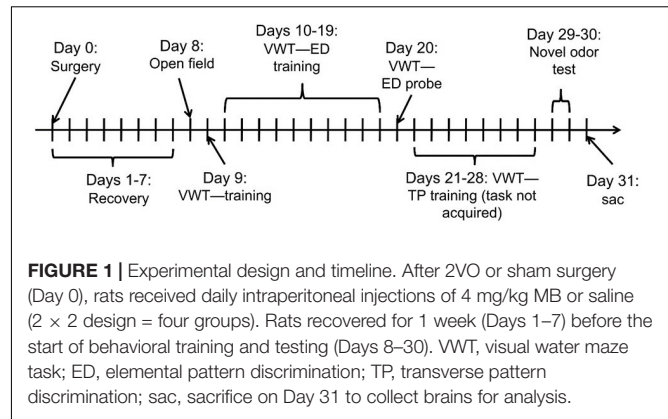
Subjects for this brain analysis were the same subjects used in the behavioral study of Auchter et al. (2014). Subjects were 39 adult male Long-Evans rats weighing approximately 500–600 g at the time of surgery. Two rats died from surgical complications and one rat died of a respiratory infection during visual water task training. Additionally, it was determined upon brain extraction that one subject suffered a hemorrhagic stroke, and thus was excluded from the analysis, making the final  $N = 35$ .

### Ethical and Biosafety Measures

Rats were raised from birth in Association for Assessment and Accreditation of Laboratory Animal Care (AAALAC)-approved facilities under standard laboratory conditions (12 h: 12 h, light: dark cycle) with *ad libitum* access to food and water. All animal care and experimental procedures were approved by the University of Texas at Austin's Institutional Animal Care and Use Committee (IACUC), and followed NIH guidelines as described in the Guide for the Care and Use of Laboratory Animals, 8th edition. All animal research was conducted in the Animal Resources Center at the University of Texas at Austin, an AAALAC-accredited facility which is inspected twice a year by UT's IACUC to ensure compliance with all relevant laws, regulations, and policies regarding animal care and use. Personal protective equipment (PPE) such as lab coats, gloves, and face masks were used for all animal interactions. Cytochrome oxidase histochemistry was performed in the histochemical suite of the PI's lab in the Animal Resources Center, which is inspected and approved twice a year by UT's Environmental Health and Safety department. PPE was used during all stages of the histochemical staining procedure, and all chemical storage and usage complied with NIH guidelines as described in the NIH Chemical Safety Guide (2015).

### Surgical Procedures and Interventions

Auchter et al. (2014) provides detailed explanations of the surgical and behavioral procedures, and the experimental design is shown in **Figure 1**. Briefly, the experiment followed a  $2 \times 2$



experimental design, whereby subjects were randomly assigned to groups which were given either 2VO surgery or a sham control (without vessel occlusion), followed by daily intraperitoneal injections of either 4 mg/kg MB or an equivalent volume of saline.

Before surgery, we anesthetized the rats beginning with 4% isoflurane inhalation, followed by general anesthesia using 1.5–3% during the surgery, with an E-Z Anesthesia Vaporizer (Euthanex Corp., Palmer PA, United States). During the surgery, we made an incision to the midline of the neck, ventral aspect. We exposed the carotid arteries, dissecting them free from the sheath and from the vagal nerve as in de la Torre and Fortin (1991). For the 2VO group, we double-ligated each artery, posterior to the bifurcation of the carotid, with 4-0 silk sutures. For the sham group, we dissected the carotids free from the sheath, but did not proceed with the occlusion. Before closing, we injected each subject subcutaneously with 1 mg/kg of meloxicam (a surgical analgesic), as well as either MB or saline. Those subjects randomly assigned to the MB group were given the first intraperitoneal injection of MB (4 mg/kg body weight; USP methylene blue, Spectrum, New Brunswick, NJ, United States). Those subjects in the saline group received the same volume of physiological saline. We then sutured the incision and moved the subject to a cage for recovery, monitoring them for 30 min closely, before returning the subject to the home cage.

For the following 30 days, each subject in the MB group received one intraperitoneal injection per day of 4 mg/kg MB, dissolved in saline. The saline group received intraperitoneal injections of physiological saline vehicle for 30 days. The injections were timed to occur just after each daily training session, since there is evidence that methylene blue facilitates memory consolidation when given during the memory consolidation phase post-training (Martinez et al., 1978; Callaway et al., 2004). The subjects recovered for 1 week prior to behavioral testing.

### Visual Water Maze Task

Upon recovery from surgery, subjects were trained on the visual water task (VWT), as described in Prusky et al. (2000). The VWT using a water Y-maze is a variant of the Morris water maze, with some additional features. In the visual water Y-maze task, the subject must make a choice to commit to which arm

contains the escape platform. In addition, explicit visual cues are given to the subject on which arm is correct/incorrect. This allows for a more complex experimental design than the standard Morris water maze, one that includes separate sets of “positive” (+ = approach) and “negative” (– = avoidance) visual stimuli. These visual stimuli involve visual patterns that are more similar to the visual discrimination tests given to humans to test cognitive function. In paradigms like the elemental discrimination task we used, these visual cues are progressively added to make the task progressively more difficult, which would not be possible in the standard Morris water maze. It is important for this study to make the maze task progressively more difficult to be able to reveal progressive memory deficits that develop over days after chronic 2VO surgery.

A metal water-filled trapezoid-shaped Y-maze tank, with one end composed of clear Plexiglas, was used for the task as described in Auchter et al. (2014). Stimuli were presented using a computer monitor, which was located on the other side of the transparent wall of the tank. A divider on the midline bisected the tank, extending from the transparent wall. The divider created two arms, with two different patterns visible on the monitor at each end. During each individual trial, a transparent platform was placed at one arm's end. It was completely submerged and invisible to the subject. Each arm was paired with a visual pattern presented on the monitor. Randomization of the arms for each trial and recording of behavioral results were controlled by a computer program (Acumen; CerebralMechanics Inc.). A correct pattern (+) predicted which arm contained the escape platform. An incorrect pattern (–) predicted the arm without the platform.

During the first day of VWT training, the water tank contained an insert, which was placed such that the rat was forced to swim down one arm only (without the option of swimming down the other arm) for 15 trials. The escape platform was consistently placed at the end of the open arm, and the monitor was blank (no pattern was presented). The subject was placed in the tank, and swam around, discovering the platform at the end. After climbing onto the platform, each rat was removed and put into a heated recovery cage. Thus, the subjects were trained to associate swimming and reaching the platform with escape from the water-filled tank. This also allowed the observation of swimming ability, independent of the discrimination tasks to come. All of the subjects successfully learned the location of the platform at the end of the first few trials. By trial number 10, all of the subjects were consistently swimming straight to the escape platform immediately after they were placed in the water.

Visual water task protocols were adapted from those described by Driscoll et al. (2005). In the first variation of the VWT, subjects were trained for 10 days on three elemental pattern discriminations (A+B–, C+D–, and E+F–). Each subject is placed into the water at the opposite end of the water tank, facing the monitor. The subject swims into one of the arms, toward one of the stimuli presented onscreen. If the arm is correct, the subject climbs onto the escape platform. If the arm is incorrect (i.e., the escape platform is not present), a metal divider is used to block that arm for 10 s, then removed. The subject then swims into the correct arm to reach the escape platform. After reaching the platform, the subject is removed from the water

and placed in a cage until the next trial begins. Subjects were trained on 30 trials per day in a stepwise manner: A+B– first, followed by intermixed trials of A+B– and C+D–, followed by intermixed trials of A+B–, C+D–, and E+F–. Every subject reached a criterion of 8/10 correct trials on the A+B– phase within 4 days. After 10 days, a set of 30 probe trials consisted of randomly alternated presentations of each of the three sets of visual stimuli (with 10 trials for each set). In the second variation of the task, subjects were trained on a more difficult transverse pattern discrimination (X+Y–, Y+Z–, and Z+X–).

## Quantitative Cytochrome Oxidase Histochemistry

Cytochrome oxidase brain mapping was conducted by an investigator blind to experimental condition through a well-established method of optical densitometry of brain sections as detailed by Gonzalez-Lima and Cada (1994). Following behavioral procedures, animals were sacrificed, and brains were quickly removed and frozen in isopentane. Coronal brain sections (40  $\mu$ m thick) were obtained and mounted on slides using a cryostat microtome (Microm HM-505E, Heidelberg, Germany). To obtain increasing gradients of CO activity, a frozen brain homogenate paste was sectioned into different tissue thicknesses (10, 20, 40, 60, and 80  $\mu$ m) and mounted on separate slides. CO activity of the homogenate was spectrophotometrically assessed and used to calculate CO values for the different section thicknesses. The brain paste sections were used as calibration standards for each CO staining batch.

Each CO staining batch consisted of representative cryostat sections (40  $\mu$ m thick) from two brain levels mounted on microscope slides for each subject along with two slides with a set of 5 standards each. Each batch was processed for CO histochemistry following the method previously described by Gonzalez-Lima and Jones (1994). Briefly, slides were fixed for 5 min with 1.5% glutaraldehyde, rinsed three times in phosphate buffer with sucrose and preincubated in a solution containing cobalt chloride and DMSO dissolved in Tris buffer. After rinsing sections with phosphate buffer (pH 7.6; 0.1 M), they were incubated at 37°C for 1 h in the dark and with continuous stirring in a solution containing diaminobenzidine, sucrose, cytochrome c and catalase (Sigma-Aldrich, Barcelona, Spain) dissolved in phosphate buffer (pH 7.6; 0.1 M). The slides were then dehydrated in increasing concentrations of ethanol, coverslipped with permount (Merck, Darmstadt, Germany) and allowed to dry for 48 h.

To obtain CO activity values for regions of interest (ROIs), a calibration step tablet (Kodak, density range 0.06–3.05) and CO-stained slides were placed on a high-precision illuminator and digitized using a CCD digital microscope camera (Leica Microsystems DFC450, Wetzlar, Germany). Images were then analyzed using ImageJ software, which allows the creation of a logarithmic calibration curve of optical density units as a function of pixel (gray level) values in each image. Before analysis, images were corrected for slide and light box artifacts using background subtraction. For brain structure analyses, 44 ROIs were located and outlined in each brain hemisphere in each



subject by an experimenter blind to experimental conditions using a rat brain atlas (Paxinos and Watson, 1996; see **Table 1** for a complete list of ROIs and abbreviations). The measurement obtained was an average optical density (OD) value for the outlined ROI. To maximize the accuracy of OD values, this procedure was repeated in three adjacent brain sections for each ROI, and the mean of the three sections in both cerebral hemispheres was used as the overall mean OD value for that ROI. Mean OD values were later converted into mean CO activity units using calibration curves based on tissue standards and spectrophotometrically determined CO activity. This method yielded a linear relationship ( $r > 0.95$ ) between biochemical CO activity measured spectrophotometrically and histochemical CO reactivity measured by optical density.

**Figure 7** shows how the ROI was outlined for CO measures. For regional CO activity measures, when 2VO-induced lesions were present within the ROI, both the affected and surviving tissue were included in the outlined ROI (i.e., the ROI was defined using the brain atlas, not the lesion). The reason for doing this was two-fold. First, it allowed us to index general CO activity in each ROI, taking into account both lesions and compensatory increases in CO in surviving tissue (if such compensatory phenomena existed). Second, since some lesions did not have clearly defined borders, including the entire ROI gave us measures of CO activity that were unbiased by experimenter evaluation of lesioned vs. penumbra vs. healthy tissue.

## Lesion Volume Analysis

An assessment of lesion volume was conducted in a separate analysis. In 2VO subjects that showed lesions ( $n = 6$ ), volumetric analysis was conducted on affected areas. Lesion volumes ( $V$ ) were derived from the lesion area per slice ( $A$ ) and distance between collected sections ( $d$ ), using the formula  $V = \Sigma A \times d$ . The value  $d$  was calculated as  $d = (T) \times (\text{number of designated sections} - 1)$ , where  $T$  is the distance between every designated section (80  $\mu\text{m}$ ). Lesion area per slice was measured by setting a conservative optical density threshold aimed to prevent the inclusion of any white matter and tissue artifacts as affected tissue. This was especially important since we observed lesions in the striatum, which in rats is speckled with white matter tracts. To ensure the threshold was unbiased, for each subject the minimum and maximum threshold values were set to 85% and 98% of the measured mean OD value for white matter (i.e., “more OD” than white matter, but “less OD” than healthy gray matter tissue). A few subjects showed tissue loss where lesions occurred. In these cases, the maximum value for the threshold was set equal to white matter so that regions with missing tissue were still considered in the calculation of lesion area.

## Statistical Analyses

All statistical testing was carried out using the PASW 22 software package (SPSS, Inc., Chicago, IL, United States). All differences were considered statistically significant at the two-tailed  $p < 0.05$  level. Effect sizes were estimated using Cohen's  $d$  (Cohen, 1988). For univariate group comparisons, average CO values for each ROI were used as dependent variables in separate analyses, with surgery and drug treatment as independent variables.

Since subjects went through two iterations of the visual water task (elemental discrimination and transverse pattern discrimination), a composite “VWT performance score” was calculated by averaging the scores from the final probe for each task. Though subjects did not learn the transverse task (as indicated by the inability to reach and 8/10 criteria for pattern discriminations), their performance in the task likely still influenced CO activity. Thus, brain-behavior correlations were conducted using two-tailed bivariate correlations between the VWT performance score and mean CO activity for each ROI.

Interregional correlation of cytochrome oxidase activity was analyzed in two ways. First, two-tailed bivariate correlations were performed between all brain ROIs within each experimental condition. Then, to detect which regional correlations showed significant differences between groups, correlation coefficients were compared using Fisher's  $z$ -transformations, followed by independent samples  $t$ -tests (Vélez-Hernández et al., 2014).

## RESULTS

The results were obtained by comparisons between four groups ( $2 \times 2$  design): sham + saline group, sham + MB group, 2VO + saline group, and 2VO + MB group. Since the experimental design was the same as in Auchter et al. (2014), detailed explanations of behavioral procedures (and behavioral results) can be found there, and an experimental timeline is shown in **Figure 1**.

### Region of Interest (ROI) Analysis

**Table 1** shows mean CO values and standard errors for each ROI in each experimental condition. Only the secondary visual cortex (V2) showed a significant main effect of surgery,  $F(1,31) = 4.491$ ,  $p = 0.047$ , with an effect size (Cohen's  $d$ ) of 0.82, indicating a large effect size, given that  $|d| < 0.2 = \text{small effect}$ ;  $0.2 < |d| < 0.8 = \text{medium effect}$ ;  $|d| > 0.8 = \text{large effect}$  (Cohen, 1988). There were no main effects for drug treatment. Several regions showed significant surgery by drug treatment interactions, including perirhinal cortex,  $F(1,31) = 5.667$ ,  $p = 0.024$ , Cohen's  $d = 0.81$ ; secondary motor cortex,  $F(1,31) = 5.883$ ,  $p = 0.022$ , Cohen's  $d = 0.73$ ; primary visual cortex,  $F(1,31) = 4.606$ ,  $p = 0.045$ , Cohen's  $d = 0.74$ ; basolateral amygdala,  $F(1,31) = 5.350$ ,  $p = 0.028$ , Cohen's  $d = 0.61$ ; medial amygdala,  $F(1,31) = 5.189$ ,  $p = 0.030$ , Cohen's  $d = 0.63$ ; and the anterior portions of the hippocampus, subfields CA1,  $F(1,31) = 4.951$ ,  $p = 0.034$ , Cohen's  $d = 0.48$ ; subfield CA2,  $F(1,31) = 4.650$ ,  $p = 0.039$ , Cohen's  $d = 0.53$ ; and subfield CA3,  $F(1,31) = 4.940$ ,  $p = 0.034$ , Cohen's  $d = 0.53$ . These significant surgery by drug treatment interactions are shown in **Figure 2**.

### Interregional Correlation of Cytochrome Oxidase Activity

To analyze interregional correlation of cytochrome oxidase activity, CO values for each ROI were correlated with each other for each group. Functional heat maps for these correlation matrices are shown in **Figures 3, 4**. Upon visual comparison of these maps, one can qualitatively deduce that MB treatment

**TABLE 1 |** Mean CO activity values ( $\mu\text{mol}/\text{min}/\text{g}$ )  $\pm$  standard errors (SEM) for each ROI and each experimental condition.

ROI	Sham $\pm$ saline SEM	Sham $\pm$ MB SEM	2VO $\pm$ saline SEM	2VO $\pm$ MB SEM
Prelimbic cortex (PLC)	246.43 $\pm$ 9.88	243.80 $\pm$ 13.63	225.09 $\pm$ 16.21	247.76 $\pm$ 9.69
Medial orbital cortex (MO)	245.24 $\pm$ 11.49	239.99 $\pm$ 11.85	221.16 $\pm$ 15.31	248.61 $\pm$ 9.82
Ventral orbital cortex (VO)	254.38 $\pm$ 9.57	248.35 $\pm$ 12.49	235.53 $\pm$ 12.42	254.43 $\pm$ 8.99
Lateral orbital cortex (LO)	251.27 $\pm$ 8.88	249.62 $\pm$ 11.52	233.50 $\pm$ 11.32	252.09 $\pm$ 7.87
Agranular insular cortex (AI)	227.63 $\pm$ 7.31	220.18 $\pm$ 8.90	211.33 $\pm$ 10.82	229.76 $\pm$ 8.69
Infralimbic cortex (IL)	281.87 $\pm$ 9.58	270.41 $\pm$ 14.29	269.97 $\pm$ 15.16	272.44 $\pm$ 5.28
Primary motor cortex (M1)	237.17 $\pm$ 4.92	230.15 $\pm$ 10.02	222.54 $\pm$ 13.23	232.86 $\pm$ 3.74
Secondary motor cortex (M2)	242.28 $\pm$ 6.10	233.62 $\pm$ 10.50	<b>214.49</b> $\pm$ 8.99	243.12 $\pm$ 7.61
Primary somatosensory cortex (S1)	214.27 $\pm$ 13.65	214.25 $\pm$ 7.76	222.05 $\pm$ 11.91	212.94 $\pm$ 7.10
Secondary somatosensory cortex (S2)	226.35 $\pm$ 7.55	218.51 $\pm$ 10.34	210.28 $\pm$ 7.41	230.64 $\pm$ 8.22
Cingulate cortex (Cin)	259.93 $\pm$ 8.32	244.58 $\pm$ 10.16	258.77 $\pm$ 15.84	257.88 $\pm$ 9.85
Perirhinal cortex (PRh)	230.05 $\pm$ 10.87	210.98 $\pm$ 8.89	<b>186.46</b> $\pm$ 14.63	223.64 $\pm$ 10.99
Primary visual cortex (V1)	241.59 $\pm$ 10.36	242.43 $\pm$ 7.87	<b>201.47</b> $\pm$ 12.24	247.19 $\pm$ 9.66
Secondary visual cortex (V2)	249.72 $\pm$ 11.05	249.49 $\pm$ 9.86	<b>206.10</b> $\pm$ 13.52	<b>239.80</b> $\pm$ 7.90
Medial septal nucleus (MS)	203.40 $\pm$ 8.33	197.97 $\pm$ 12.39	202.64 $\pm$ 10.36	197.97 $\pm$ 6.04
Lateral septal nucleus (LS)	272.30 $\pm$ 8.28	262.01 $\pm$ 12.81	273.92 $\pm$ 11.81	268.67 $\pm$ 5.58
Acumbens core (AcbC)	313.40 $\pm$ 9.76	304.24 $\pm$ 10.43	315.15 $\pm$ 17.36	307.88 $\pm$ 7.59
Acumbens shell (AcbS)	241.13 $\pm$ 10.53	223.67 $\pm$ 8.36	233.98 $\pm$ 8.35	224.90 $\pm$ 7.96
Caudate/Putamen (CPu)	198.87 $\pm$ 13.32	199.51 $\pm$ 8.52	191.14 $\pm$ 11.26	191.27 $\pm$ 6.12
Globus pallidus (GP)	115.97 $\pm$ 6.57	108.53 $\pm$ 4.83	115.23 $\pm$ 5.74	112.64 $\pm$ 4.92
Ventral pallidum (VP)	179.11 $\pm$ 5.82	169.26 $\pm$ 6.40	168.38 $\pm$ 8.74	168.31 $\pm$ 4.50
Lateral hypothalamus (LH)	160.75 $\pm$ 9.32	157.53 $\pm$ 9.78	154.51 $\pm$ 5.90	163.81 $\pm$ 8.06
Paraventricular nucleus (PVH)	191.74 $\pm$ 6.94	183.50 $\pm$ 8.14	184.33 $\pm$ 8.43	203.21 $\pm$ 6.86
Medial preoptic area (MPO)	206.22 $\pm$ 6.62	198.81 $\pm$ 7.51	210.35 $\pm$ 10.84	208.42 $\pm$ 5.72
Bed nucleus stria terminalis (BST)	233.80 $\pm$ 7.98	218.64 $\pm$ 9.49	237.61 $\pm$ 14.51	224.12 $\pm$ 6.61
Subthalamic nucleus (Sub)	273.20 $\pm$ 6.04	249.10 $\pm$ 10.74	249.36 $\pm$ 14.37	248.75 $\pm$ 10.91
Medial geniculate nucleus (MGN)	255.28 $\pm$ 8.38	245.48 $\pm$ 5.66	240.78 $\pm$ 12.86	235.70 $\pm$ 5.45
Basomedial amygdala (BMA)	186.21 $\pm$ 7.73	180.59 $\pm$ 10.02	175.09 $\pm$ 4.88	195.70 $\pm$ 9.16
Medial amygdala (MEA)	227.95 $\pm$ 10.39	220.31 $\pm$ 11.47	<b>194.29</b> $\pm$ 9.88	226.00 $\pm$ 9.75
Basolateral amygdala (BLA)	268.46 $\pm$ 14.51	254.36 $\pm$ 14.44	<b>230.77</b> $\pm$ 12.21	266.47 $\pm$ 12.53
Central amygdala (CEA)	223.13 $\pm$ 8.63	219.37 $\pm$ 10.03	206.30 $\pm$ 9.63	234.55 $\pm$ 9.36
Anterior hippocampus CA1 (CA1A)	213.48 $\pm$ 11.42	199.98 $\pm$ 8.20	<b>188.32</b> $\pm$ 18.91	213.97 $\pm$ 13.79
Anterior hippocampus CA2 (CA2A)	224.26 $\pm$ 13.21	203.44 $\pm$ 8.69	<b>195.70</b> $\pm$ 16.03	214.87 $\pm$ 11.19
Anterior hippocampus CA3 (CA3A)	238.88 $\pm$ 15.71	213.68 $\pm$ 10.05	<b>200.94</b> $\pm$ 15.59	216.38 $\pm$ 8.13
Anterior dentate gyrus (DGA)	319.76 $\pm$ 26.01	294.90 $\pm$ 15.21	306.25 $\pm$ 31.40	297.03 $\pm$ 19.93
Posterior hippocampus CA1 (CA1P)	298.13 $\pm$ 13.98	277.27 $\pm$ 12.72	266.56 $\pm$ 14.28	277.08 $\pm$ 13.51
Posterior hippocampus CA2 (CA2P)	275.84 $\pm$ 11.87	249.69 $\pm$ 11.82	236.40 $\pm$ 17.96	248.44 $\pm$ 10.82
Posterior hippocampus CA3 (CA3P)	292.89 $\pm$ 9.91	272.22 $\pm$ 13.02	255.42 $\pm$ 16.45	269.08 $\pm$ 9.99
Posterior dentate gyrus (DGP)	269.60 $\pm$ 15.75	256.92 $\pm$ 10.66	258.72 $\pm$ 12.20	255.88 $\pm$ 7.02
Subiculum (S)	239.98 $\pm$ 12.04	226.65 $\pm$ 10.53	221.74 $\pm$ 11.20	217.73 $\pm$ 6.72
Superior colliculus (SC)	254.18 $\pm$ 13.53	246.46 $\pm$ 8.80	240.89 $\pm$ 10.46	249.47 $\pm$ 8.05
Substantia nigra (SN)	214.80 $\pm$ 8.68	207.29 $\pm$ 8.24	211.66 $\pm$ 11.57	209.81 $\pm$ 6.72
Red nucleus (R)	250.37 $\pm$ 12.02	251.90 $\pm$ 13.05	234.69 $\pm$ 13.86	257.29 $\pm$ 12.34
Ventral tegmental area (VTA)	97.29 $\pm$ 1.32	99.91 $\pm$ 5.86	88.06 $\pm$ 3.55	96.05 $\pm$ 5.11

Means showing an individual group effect are boldfaced.

generally increased interregional correlation of cytochrome oxidase activity, specifically in a positive direction (i.e., MB resulted in more “redness” in the heat maps). This is true particularly in the sham condition (Figure 3). The result of MB treatment in the 2VO condition is not as obvious, though still apparent (Figure 4). One can also compare the left sides of Figures 3, 4 to observe an apparent decrease

in interregional correlation of cytochrome oxidase activity as a result of 2VO surgery. The most dramatic differences in interregional correlation of cytochrome oxidase activity appear in the outlined boxes in Figures 3, 4 (also represented in larger form in Figure 5), which represent connectivity between prefrontal and visual cortex ROIs, and amygdala and hippocampal ROIs. Figure 5 shows stronger interregional correlation of cytochrome

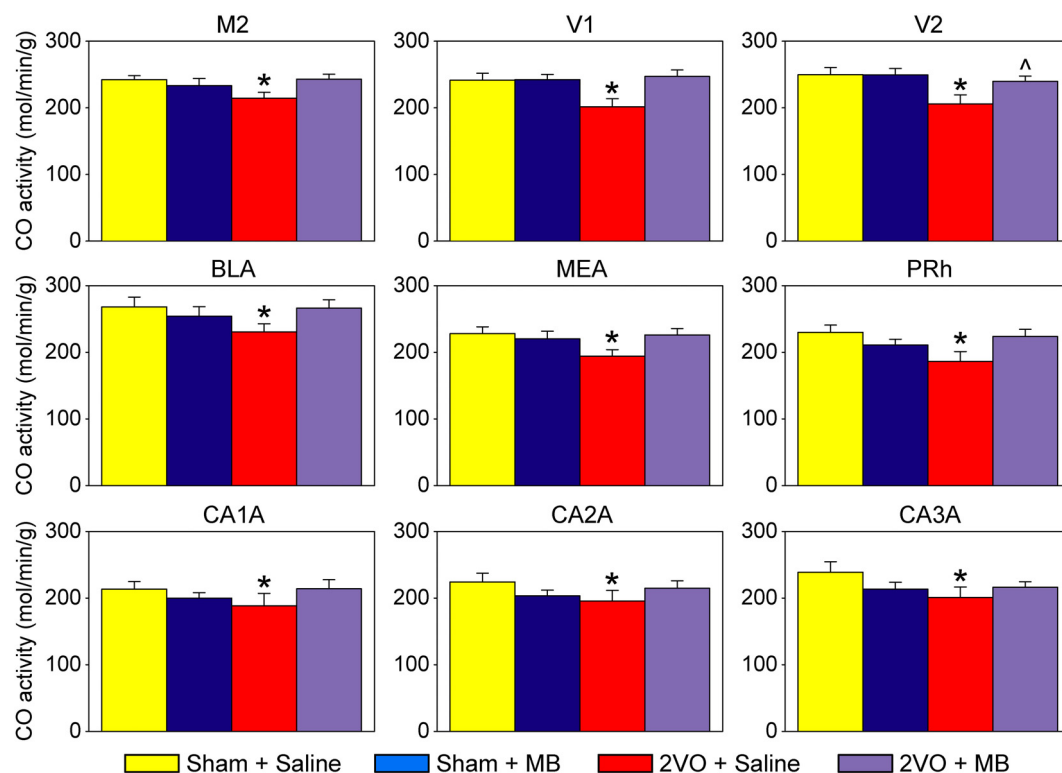


**FIGURE 2 |** Regions of interests showing significant effects. In these regions, 2VO surgery (red) resulted in a decrease in cytochrome oxidase activity, which was prevented by MB treatment (violet). M2, secondary motor cortex; V1, primary visual cortex; V2, secondary visual cortex; BLA, basolateral amygdala; MEA, medial amygdala; PRh, perirhinal cortex; CA1A, anterior hippocampus CA1; CA2A, anterior hippocampus CA2; CA3A, anterior hippocampus CA3. \*Significant surgery by drug interaction ( $p < 0.05$ ); ^Significant main effect of surgery ( $p < 0.05$ ).

oxidase activity in the sham animals given MB as compared to saline. Importantly, it appears that the connectivity between cortical, amygdala and hippocampal ROIs is decreased in subjects that received 2VO, but connectivity is restored in 2VO subjects treated with MB.

To further explore the effects of cerebral hypoperfusion and MB treatment on interregional correlation of cytochrome oxidase activity, bivariate correlation comparisons for each ROI were conducted (1) between the sham + saline group (control subjects) and 2VO + saline group, and (2) between the 2VO + saline group and the 2VO + MB group (Figure 6). The first group of comparisons essentially reveals which interregional correlations were significantly strengthened or weakened as a result of cerebral hypoperfusion. The second group of comparisons reveals which interregional correlations were significantly strengthened or weakened as a result of MB treatment during cerebral hypoperfusion.

As shown in the left panel of Figure 6, interregional correlation of cytochrome oxidase activity between visual cortices and basal forebrain, hippocampal and midbrain ROIs was weakened as a result of cerebral hypoperfusion. However, interregional correlation of cytochrome oxidase activity between cortical regions—particularly between secondary somatosensory cortex and prefrontal ROIs—was strengthened as a result of cerebral hypoperfusion. This could potentially be evidence of a

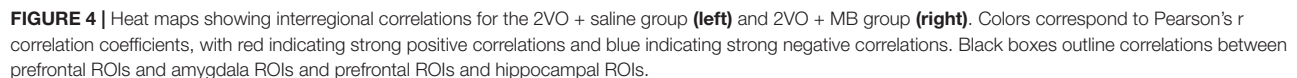
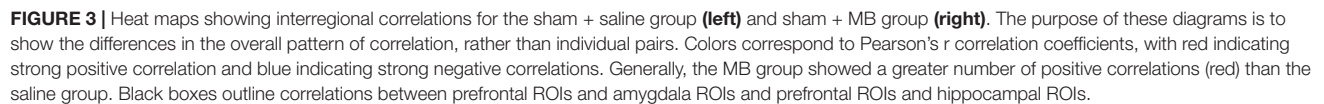
compensatory mechanism activated in response to the functional disconnection between regions involved in the visual network.

As shown in the right panel of Figure 6, interregional correlation of cytochrome oxidase activity between visual cortices and hippocampal ROIs—which was weakened in 2VO subjects—was strengthened as a result of MB treatment. Additionally, MB treatment resulted in increased interregional correlation of cytochrome oxidase activity between amygdala and cortical ROIs, and in midbrain ROIs with visual cortices and hippocampus.

## Neurodegenerative Lesions

Figure 7 illustrates the procedure for obtaining a conservative measure of neurodegenerative lesion area per section. About one third of subjects who received 2VO surgery ( $n = 3/9$  in the 2VO + saline group and  $n = 3/8$  in the 2VO + MB group) showed conspicuous anatomical lesions (Figure 8). Though there was quite a bit of heterogeneity in lesion size between subjects, the location of the lesions were categorically delimited, and thus were classified into 4 types: neocortical (occurring unilaterally or bilaterally in prefrontal regions and extending into primary motor, somatosensory and visual cortices;  $n = 2$ ), striatal (occurring unilaterally in the caudate and putamen;  $n = 6$ ), hippocampal (occurring unilaterally through the rostrocaudal extent of CA1, CA2 and CA3 subfields;  $n = 2$ ), and perirhinal (occurring unilaterally or bilaterally in





performance, indicating that the greater the overall lesion volume, the worse subjects performed on the VWT (**Figure 8**). Second, though the number of subjects displaying lesions is



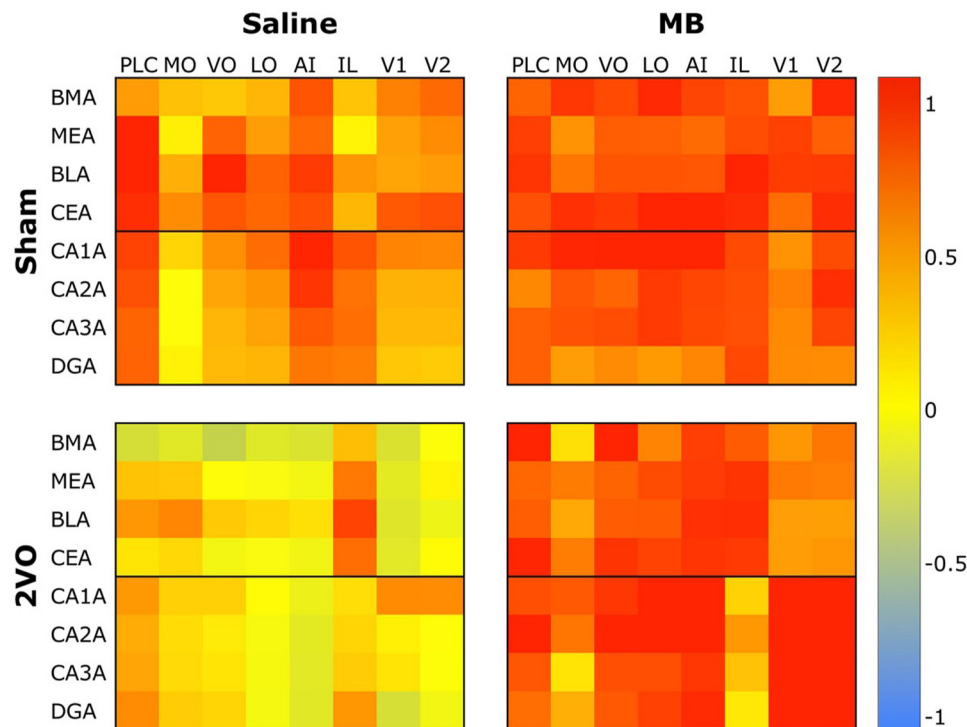


**FIGURE 5 |** Heat map comparing interregional correlation of cytochrome oxidase activity between prefrontal ROIs and amygdala and hippocampal ROIs in each experimental condition. Colors correspond to Pearson's  $r$  correlation coefficients, with red indicating strong positive correlations and blue indicating strong negative correlations.

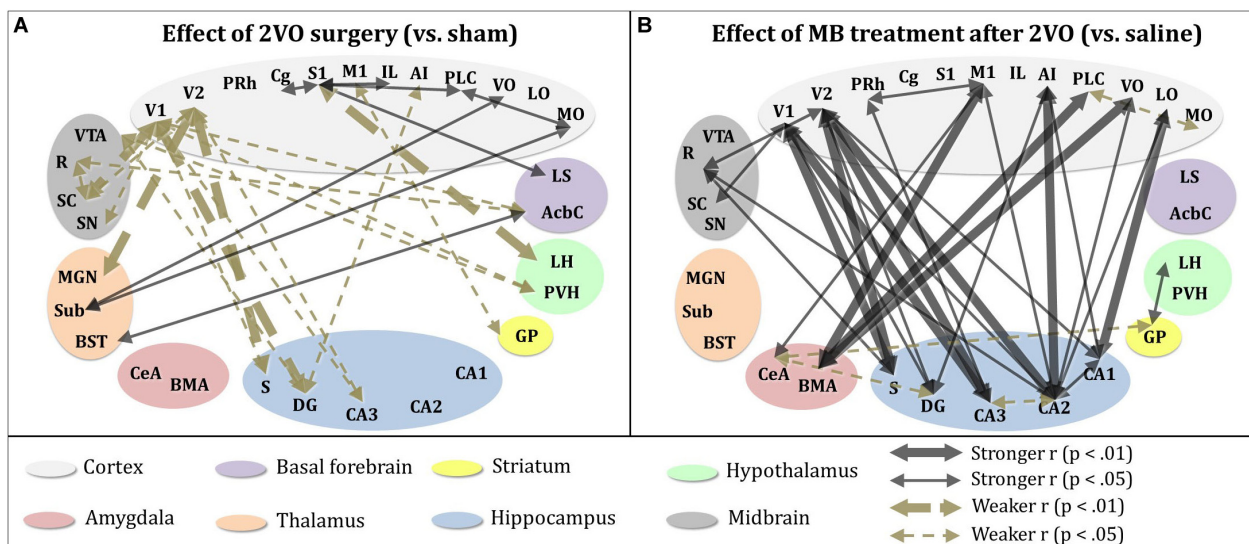


**FIGURE 6 |** Significant differences in interregional correlation of cytochrome oxidase activity due to 2VO surgery and MB treatment. **(A)** Comparison between control subjects (sham + saline group) and 2VO subjects (2VO + saline). 2VO surgery resulted in weaker interregional correlation of cytochrome oxidase activity (1) within ROIs involved in the visual pathway (V1, V2, SC), and (2) between visual ROIs and hippocampus (CA3, DG, S). Stronger interregional correlation of cytochrome oxidase activity was observed within cortical ROIs (MO, VO, PLC, IL, S1, Cg). **(B)** Comparison between 2VO subjects treated with saline and those treated with MB. In 2VO subjects, treatment with MB resulted in stronger interregional correlation of cytochrome oxidase activity (1) within ROIs involved in the visual pathway (V1, V2, SC), (2) between visual ROIs and hippocampus (CA1, CA2, CA3, DG, S), (3) between cortical ROIs (LO, VO, AI, M1) and hippocampus (CA1, CA2, DG), and (4) between cortical ROIs (VO, PLC, M1) and amygdala (BMA, CeA). Mildly weaker interregional correlation of cytochrome oxidase activity was observed between the amygdala (CeA), hippocampus (DG), and striatum (GP).

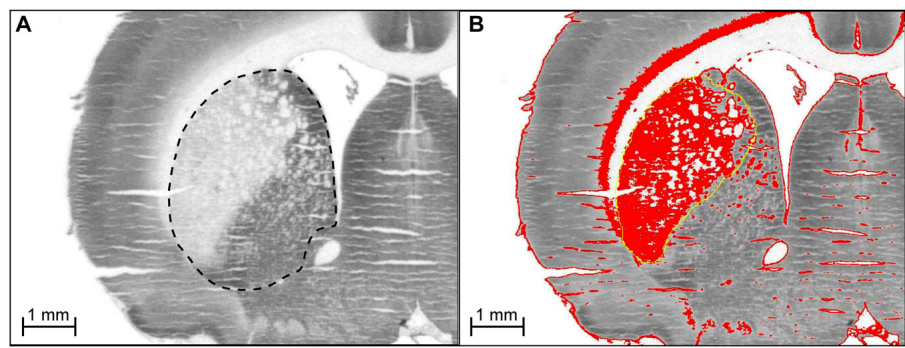


**FIGURE 7 | (A)** Delineation of region of interest for CO measurement. For regional CO activity measures, when 2VO-induced lesions were present within the ROI, both the affected and surviving tissue were included in the outlined ROI (i.e., the ROI was defined using the brain atlas, not the lesion). **(B)** Determination of 2VO-induced lesion volume in rat brain. For every coronal section showing a lesion (e.g., lateral side of striatum), a threshold was applied to highlight (in red) tissue with optical density (OD) values between that of white matter and healthy gray matter tissue (medial side of striatum). For each section showing a lesion, the area of the highlighted tissue within the approximate lesion outline (in yellow) was used as A in the equation to calculate lesion volume,  $V = \Sigma A \times d$ , where d is the distance between sections. The sections were stained for CO activity by the quantitative enzyme histochemistry method of Gonzalez-Lima and Jones (1994). We are showing the actual digitized images we used for the densitometric quantification of CO activity. Microphotographs with high contrast are not suitable for demonstration of a linear staining reaction product resulting from graded CO enzymatic activity as explained in our book on quantitative CO enzyme histochemistry with more details on this topic (Gonzalez-Lima, 1998). Briefly, digitized images with low contrast showing a linear gray level range are necessary to perform densitometric computer analysis of quantitative differences in CO activity from histochemically stained frozen brain sections and CO activity standards.

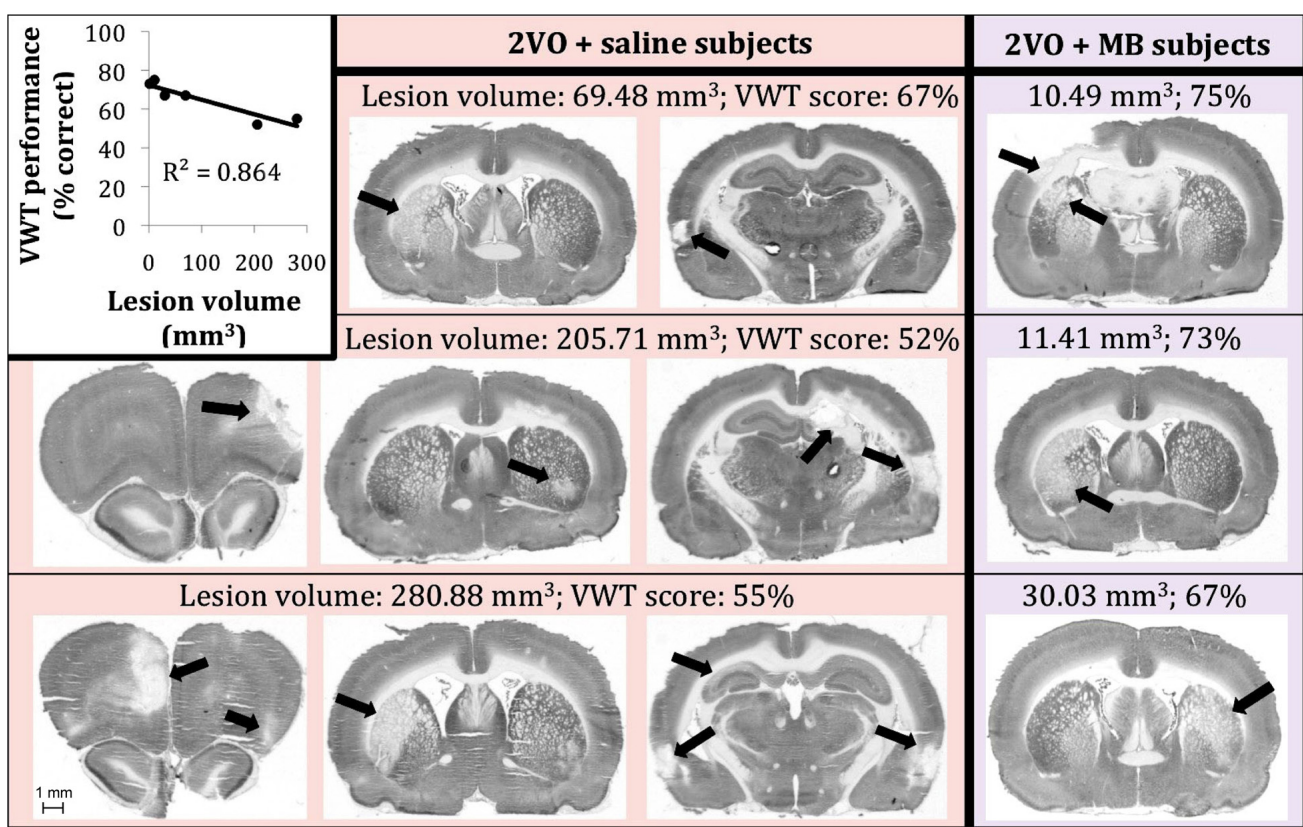


**FIGURE 8 |** Six 2VO subjects showed neurodegenerative lesions ( $n = 3$  saline-treated [pink background],  $n = 3$  MB-treated [purple background]). There was a negative linear correlation between lesion size and VWT performance (top left). We are showing actual examples of digitized images of CO-stained coronal sections used for the determination of lesion volume.

small, it appears that the emergence of the lesions followed a specific pattern. In subjects with the smallest lesion volumes, lesions were limited to striatum. In more severe cases, neocortical and perirhinal lesions appeared (**Figure 8**). Subjects with the largest lesion volumes showed striatal, neocortical, perirhinal and hippocampal lesions. Finally, though both carotid arteries were ligated in the 2VO surgery, when subjects had smaller lesions, the lesions were limited to either the right or the left cerebral hemisphere. Bilateral lesions only appeared in the most severe cases (in which subjects showed lesions in multiple locations, including hippocampus). Perhaps the most interesting observation in subjects displaying lesions was the impact of MB treatment. Though the same number of subjects showed lesions in each 2VO group, lesions in subjects treated with MB were smaller and more localized (i.e., only unilateral and only in/near striatum) than lesions in saline-treated 2VO subjects. The lesion volumes for each of the six subjects (as well as treatment group means) are shown in **Figure 9**.

## Brain–Behavior Correlations

Like the behavior performance for the elemental discrimination alone (Auchter et al., 2014), a univariate ANOVA—with the composite VWT performance score as the dependent variable and the surgery and drug treatment conditions as independent variables—revealed a surgery by drug treatment interaction,  $F(1,31) = 8.961$ ,  $p = 0.006$ . *Post hoc* pairwise comparisons demonstrated that subjects who received 2VO surgery performed worse than sham subjects (decreased percent correct responses), but this was ameliorated by MB treatment (**Figure 10**).

Visual water task performance scores were correlated with CO activity for a number of individual ROIs. Regions that showed significant positive brain-behavior correlations were perirhinal cortex,  $r(35) = 0.526$ ,  $p = 0.001$ , prelimbic cortex,  $r(35) = 0.353$ ,  $p = 0.038$ , secondary motor cortex,  $r(35) = 0.461$ ,  $p = 0.005$ , primary visual cortex,  $r(35) = 0.432$ ,  $p = 0.035$ , secondary visual cortex,  $r(35) = 0.410$ ,  $p = 0.047$ , caudate/putamen  $r(35) = 0.343$ ,  $p = 0.043$ , medial amygdala,  $r(35) = 0.368$ ,  $p = 0.030$ , anterior CA1,  $r(35) = 0.455$ ,  $p = 0.006$ , anterior CA2,  $r(35) = 0.390$ ,  $p = 0.021$ , and anterior CA3,  $r(35) = 0.435$ ,  $p = 0.009$ . There were no significant negative correlations between CO activity and VWT performance.

To assess whether correlations between regional CO activities and VWT performance were specifically driven by subjects showing lesions, brain-behavior correlations were also conducted excluding subjects who displayed lesions. When lesioned subjects were excluded, perirhinal cortex,  $r(29) = 0.397$ ,  $p = 0.033$ , secondary motor cortex,  $r(29) = 0.409$ ,  $p = 0.027$ , medial amygdala,  $r(29) = 0.424$ ,  $p = 0.022$ , primary visual cortex,  $r(29) = 0.533$ ,  $p = 0.0323$ , and secondary visual cortex,  $r(29) = 0.471$ ,  $p = 0.049$  still showed significant positive correlations between CO activity and behavioral performance. Hippocampal regions, prelimbic cortex and caudate/putamen no longer showed significant correlations. Interestingly, significant correlations emerged in agranular insular cortex,  $r(29) = 0.392$ ,  $p = 0.035$ , and lateral orbital cortex,  $r(29) = 0.435$ ,  $p = 0.018$ , when lesioned subjects were excluded. That many correlations persisted when lesions were absent suggests that the lesions are not

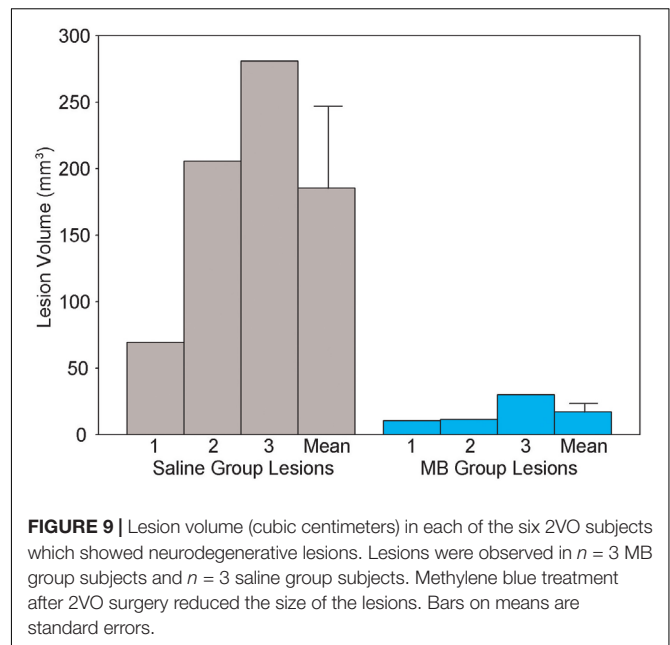


**FIGURE 9 |** Lesion volume (cubic centimeters) in each of the six 2VO subjects which showed neurodegenerative lesions. Lesions were observed in  $n = 3$  MB group subjects and  $n = 3$  saline group subjects. Methylene blue treatment after 2VO surgery reduced the size of the lesions. Bars on means are standard errors.

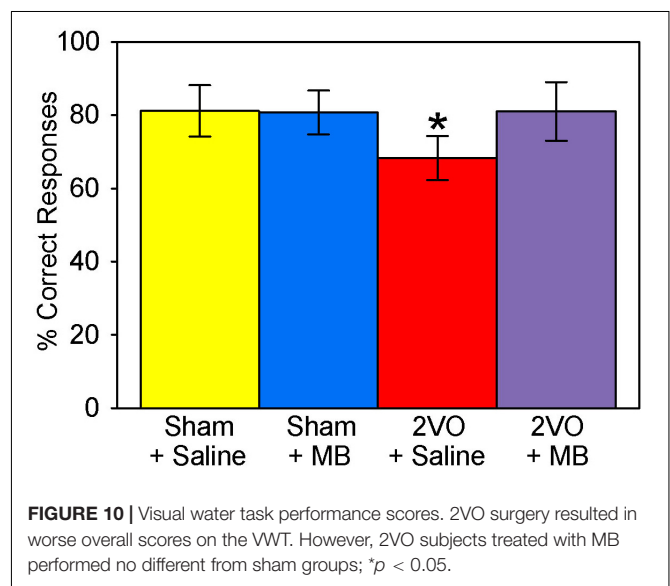


**FIGURE 10 |** Visual water task performance scores. 2VO surgery resulted in worse overall scores on the VWT. However, 2VO subjects treated with MB performed no different from sham groups; \* $p < 0.05$ .

entirely responsible for the observed brain-behavior correlations. However, correlations were not completely independent of lesions either, since some correlations disappeared when lesioned subjects were excluded. Further, since additional correlations appeared in non-lesions subjects (in ROIs that did not show lesions in lesioned subjects), the functional impact of lesions extended beyond the lesioned areas themselves.

## DISCUSSION

Brain cells rely on the circulatory system to supply the necessary glucose and oxygen needed for mitochondrial respiration, oxidative phosphorylation and ATP synthesis (Erecinska and



Silver, 1989). Cytochrome oxidase (CO)—a transmembrane protein localized in the inner mitochondrial membrane—is the terminal enzyme of the electron transport chain (Wong-Riley, 1989). It is well-known that chronic cerebral hypoperfusion results in impaired ATP synthesis (Plaschke, 2005; Briede and Duburs, 2007), mitochondrial dysfunction and a reduction in CO activity (de la Torre et al., 1997; Cada et al., 2000). There is also evidence that this mitochondrial dysfunction is paralleled by deficits in learning and memory (de la Torre et al., 1997; Cada et al., 2000). Here, we used a model of chronic cerebral hypoperfusion, bilateral carotid occlusion (2VO), the neuropathological effects of which have been well-characterized and resemble those of age-related progression of mild cognitive impairment (MCI) and Alzheimer's disease (AD) (de la Torre, 2016). We aimed to: (1) characterize the whole-brain regional and interregional correlation of cytochrome oxidase activity changes that result from 2VO surgery, (2) describe how these changes are ameliorated via treatment with the neurometabolic enhancer USP methylene blue (MB), and (3) correlate brain CO activity with performance on the visual water task (VWT).

## Regional Changes in Cytochrome Oxidase Activity

Regional changes in cytochrome oxidase activity as revealed by univariate analyses for each ROI were observed in cortical regions (secondary motor cortex, perirhinal cortex, primary visual cortex and secondary visual cortex), amygdala (basolateral and medial) and hippocampus (the anterior portions of CA1, CA2, and CA3). Though the neuropathological changes in hippocampus (Shang et al., 2005), retina (Lavinsky et al., 2006), and optic tract (Farkas et al., 2004) as a result of 2VO have been documented, regional differences in cortical areas specific to visually guided movements have only been documented one other time (Cada et al., 2000); and regional differences in the amygdala are novel findings.

Additionally, we show here that chronic cerebral hypoperfusion can affect regional cytochrome oxidase activity in two ways. First, regions susceptible to hypoperfusion show decreases in CO activity without developing anatomical lesions. This is evidenced by the fact that we observed univariate differences in CO activity as a result of 2VO surgery in regions that did not show lesions (e.g., in basolateral and medial amygdala). Interregional correlation of cytochrome oxidase activity changes observed in response to 2VO surgery in regions that do not show anatomical lesions further support this notion. Second, in about one third of subjects, 2VO surgery resulted in lesions, as indicated by absence of histochemical CO staining and presence of tissue damage. Studies comparing the CO method and other histological methods show that CO activity is a good proxy for cell density (Nelson and Silverstein, 1994; Wong-Riley and Welt, 1980; Riha et al., 2005). Thus we can infer that regions showing complete absence of CO activity in discrete identifiable regions are in fact damaged. Since this happens in less than half of the subjects and that lesion sizes vary so widely suggests that subjects are differentially susceptible to developing lesions during cerebral hypoperfusion after 2VO. This differential susceptibility not only results in variable lesion sizes, but greater

lesion sizes are also highly correlated to impaired behavioral performance in the VWT.

Additionally, that lesions appear in regions where CO activity is particularly involved in visual discrimination learning (Fidalgo et al., 2014)—and that CO activity in these regions were also correlated with VWT performance—brings about the question of whether the lesions caused the behavioral deficits, or whether the intensive behavioral training facilitated the lesions. In one likely scenario, we see the appearance of lesions as a result of certain regions being particularly vulnerable to cerebral hypoperfusion. The lesions would then lead to an inability of these subjects to master the VWT task. However, in an alternative scenario, the VWT itself may have resulted in increased CO activity demand in particular regions preceding neurodegeneration. In this case, cerebral hypoperfusion could result in increased oxidative stress in regions involved in learning the VWT task, and thus would result in “customized” lesions in brain regions involved in a particular task. Though both scenarios may have contributed in some way to the appearance of lesions, we believe that the former scenario is the most plausible, primarily because similar regions have been previously identified as susceptible to cerebrovascular ischemia. Additionally, since CO activity in the medial amygdala is correlated with VWT performance, if lesions resulted from the demanding VWT training, then we should also expect to see amygdala lesions, which we did not. The potential emergence of task-specific lesions can be further addressed in future investigations by (1) comparing mitochondrial lesions in trained vs. untrained subjects experiencing cerebral hypoperfusion, and/or (2) training subjects on a different task involving different brain regions (e.g., an auditory rather than visual task), and exploring whether the lesion location changes (e.g., to auditory rather than visual cortices).

## Interregional Correlations of Cytochrome Oxidase Activity

2-vessel occlusion surgery resulted in weakened interregional correlation of cytochrome oxidase activity in several regions. The most obvious decoupling occurred between visual cortices (primary and secondary) and hippocampus (CA3, dentate and subiculum). 2VO subjects also showed weaker interregional correlation of cytochrome oxidase activity between visual cortex and the superior colliculus, further implicating 2VO surgery in the pathogenesis of the visual system. There were also some noteworthy increases in interregional correlation of cytochrome oxidase activity, namely between the subthalamic nucleus and prefrontal cortex (ventral and medial orbital cortex), between the bed nucleus of the stria terminalis and nucleus accumbens, and between several cortical regions (medial orbital cortex, prelimbic cortex, infralimbic cortex, cingulate, and primary somatosensory cortex). Because these increases in interregional correlation of cytochrome oxidase activity seemed to appear mostly in regions that were not significantly affected by 2VO surgery (as indicated by univariate analyses), this strengthened interregional correlation of cytochrome oxidase activity may indicate a compensatory mechanism that occurred in response to the weakened interregional correlation



of cytochrome oxidase activity in visual and hippocampal regions. There is some evidence of compensatory mechanisms in 2VO, however most of this evidence concerns global normalization of cerebral blood flow via vascular changes, such as collateral perfusion and angiogenesis (Choy et al., 2006). Therefore, there is the possibility that MB may have preserved CO activity and memory by partly alleviating hypoperfusion in the ischemic brain, e.g., by increasing blood supply via the vertebral arteries after occluding the carotid arteries. Our own fMRI studies of cerebral blood flow indicate that MB can enhance blood flow under hypoxic conditions (Huang et al., 2013). To verify the existence of compensatory mechanisms in blood flow and metabolic activity, further investigation is needed.

## Biological Underpinnings of the Interregional Correlations of Cytochrome Oxidase Activity

At the cellular level, CO enzymatic activity reflects neuronal synaptic activity because CO is a rate-limiting enzyme in cellular respiration for ATP production, and ATP is required to sustain neuronal electrophysiological responses (Wong-Riley, 1989). Specifically, neuronal membranes depolarized by synaptic excitatory transmitters require ATP for repolarization to maintain electrophysiological responses. Moreover, at the transcriptional molecular level, there is a coupling of genes for CO enzymatic activity with genes for neuronal synaptic excitation (Wong-Riley, 2012). Specifically, the transcriptional regulation of CO genes is coupled with the transcription of nuclear respiratory factor genes, such as NRF-1 and NRF-2, which in turn are coupled with transcription of excitatory neurotransmitter receptors, such as NMDA receptor subunit genes for glutamatergic excitatory synaptic activity (GluN1 and GluN2) (Dhar and Wong-Riley, 2009; Wong-Riley, 2012; Nair and Wong-Riley, 2016). Therefore, all ten nuclear CO genes and the three mitochondrial CO transcription factors are transcribed in the same “transcription factory” that is neuronal activity-dependent (Wong-Riley, 2012). This makes quantitative CO histochemistry of individual brain regions an important metabolic index of neuronal activity (Gonzalez-Lima, 1998). Specifically, CO histochemical activity after 2VO provides insight into the metabolic history of brain regions during chronic brain hypoperfusion, as brain regions that are progressively less active will show reduced CO activity relative to regions with preserved neuronal activity (Cada et al., 2000).

Metabolic mapping techniques like quantitative CO histochemistry make it possible to gather functional data from most brain regions. However, most analyses of metabolic mapping data are limited to the comparison of mean regional activity between groups. This is like treating each brain region as if it were separate from the rest of the brain. However, the interactions between regions likely affect higher-order neurobiological functions underlying neural network communications and associative learning functions (Gonzalez-Lima and McIntosh, 1995). Differences in *regional* mean CO activity after chronic 2VO reflect differences in the cumulative neuronal activity of specific brain regions, whereas differences

in *interregional* correlations of CO activity reflect cumulative differences in functional synaptic coupling among brain regions. At the interregional physiological level, CO activity is critical for the coordinated functioning of brain regions because aerobic cellular respiration is the main way neurons obtain metabolic energy to communicate via synapses. Hence, interregional correlations of CO activity represent a functional connectivity index of the metabolic history of interactive neuronal synaptic activity among brain regions (Gonzalez-Lima, 1998). However, the biological underpinnings of CO interregional correlations are very different from other metabolic markers such as uptake of 2-deoxyglucose or fluorodeoxyglucose, or c-fos gene/protein expression, all of which reflect evoked or immediate neuronal activity. As explained in detail by Sakata et al. (2000), interregional correlations of CO activity represent functional “traits” rather than an acute “state.”

In our study, differences in the magnitude of interregional CO correlations after chronic 2VO and MB reflected the metabolic history of functional synaptic relationships between brain regions that were part of specific neural networks. Although interregional CO effects need to happen via anatomical synaptic connectivity, anatomical and functional connectivity are not synonymous. For example, two regions may be similarly connected anatomically in the saline groups and the MB groups, but differences in their interactive synaptic activity would lead to different interregional correlations of CO activity. Specifically, we found different interregional correlations in CO activity among prefrontal and limbic brain regions within groups of subjects treated with saline or MB from sham and 2VO groups. We then established the patterns of statistical significance for each condition of treatment (saline/MB) and surgical (sham/2VO) groups and interpreted these results as differences in the metabolic history of functional synaptic connections between brain regions due to each condition.

Horwitz et al. (1992) reviewed the first studies that introduced the analysis of functional network interactions using interregional correlations of metabolic mapping data in the 1980s. This network approach became popular to analyze the relationships of blood oxygen level dependent (BOLD) signals from multiple brain regions in fMRI, and Friston (1994) called it functional connectivity analysis. The only difference in these analytic techniques is the type of metabolic data used. However, all these network computational techniques are based on the same assumption that brain regions that function together have correlated activities. Gonzalez-Lima and McIntosh (1994) explicitly stated this assumption as the principle of neural interaction: “It states that if neural regions are synaptically connected, the disturbance in the postsynaptic action potentials of a region is passed on to another. In other words, brain regions do not merely act locally, they interact with one another in complex neural networks. Therefore, brain activity is interdependent on the actions and reactions of the components that form the neural networks.” (Gonzalez-Lima and McIntosh, 1994, p. 24).

Interpreted in terms of neural network analysis, an interregional correlation of CO activity represents the degree to which the neuronal synaptic activity between two regions are

related to one another, or how they vary together (covariance). As explained by McIntosh and Gonzalez-Lima (1994), a high interregional correlation between regions A and B means that if region A increases its activity, so too will B, in the case of a positive correlation. The brain is unique among other organs in that it is made of interconnected elements critically dependent on CO activity for synaptic communication, from the local synaptic activity of neurons, to interregional connections among ensembles of neurons across brain regions. Communication among neural elements, whether neurons or ensembles, is along these interconnections, and these network communications represent a large-scale biological underpinning of brain function. In other words, a change in interregional CO activity correlations between neural regions comes about through a change in the synaptic influences of one or more input pathways. Therefore, we identified changes in network interactions after 2VO and MB interventions by examining the interregional correlations of CO activity within regions of the brain. As brain regions became progressively less active after 2VO, their synaptic communications became weaker, resulting in a reduced number of significant interregional correlations. As MB facilitated CO activity in brain regions, so the interregional synaptic communications were stronger, resulting in a higher number of significant interregional correlations.

## Methylene Blue Preserves Cytochrome Oxidase Activity and Prevents Neurodegeneration in Chronic Cerebral Hypoperfusion

The enzymatic activity of CO is responsible for the consumption of oxygen by catalyzing the reaction that reduces oxygen into water in the process of oxidative phosphorylation that generates ATP (Erecinska and Silver, 1989). By preserving CO activity MB can improve oxygen consumption even under hypoxic conditions. For example, Huang et al. (2013) demonstrated that MB has a stronger effect under mild hypoxic conditions by comparing normoxia and hypoxia MB effects *in vivo*. MB under hypoxia induced greater stimulus-evoked fMRI responses and oxygen consumption as compared to normoxia. They concluded “Such enhanced potentiation during hypoxia could be one of the mechanisms that accounts for MB’s neuroprotective effects in metabolically stressed conditions reported in the literature (see review Rojas et al., 2012). For example, the higher the metabolic demand for oxygen consumption, the higher the respiratory chain electron flow produced by MB’s electron cycling action in mitochondria (Rojas et al., 2012). Therefore, MB’s effects during hypoxia may potentiate fMRI responses by further increasing mitochondrial electron transport. We predict that more severe (i.e., 9–12% O<sub>2</sub>) hypoxia could evoke a larger MB effect.” Furthermore, MB has been shown to protect against brain injury after cardiac arrest, which produces hypoxia-reperfusion injury demonstrated by a decrease in the plasma level of protein S-100Beta, an astroglial marker of hypoxic brain injury (Miclescu et al., 2006).

While it is outside the scope of this paper to provide a comprehensive review of all the properties and effects of MB, we refer the reader to a recent paper that reviews ways in

which MB may be neuroprotective by preserving mitochondrial function (Tucker et al., 2018). Similarly, more recently other MB studies have also shown MB’s protective action in multiple models and tissues. For example, Tian et al. (2018) showed that MB protects the lungs from ischemia-reperfusion injury by attenuating mitochondrial oxidative damage. Bhurtel et al. (2018) showed that MB protects dopaminergic neurons against MPTP-induced neurotoxicity by up-regulating brain-derived neurotrophic factor and Biju et al. (2018) showed that MB reduces motor deficits and olfactory dysfunction in a chronic MPTP-probenecid mouse model of Parkinson’s disease. Relevant to our study, Huang et al. (2018) investigated chronic oral MB treatment in a rat model of focal cerebral ischemia-reperfusion. However, the present study is the first to investigate MB neuroprotective effects on mitochondrial CO activity in the pathogenesis of chronic brain hypoperfusion.

When administered during chronic cerebral hypoperfusion, MB preserved mitochondrial CO activity in affected brain regions (secondary motor cortex, perirhinal cortex, primary visual cortex, basolateral amygdala, medial amygdala and hippocampus). This effect was so robust that only one region (secondary visual cortex) that showed decreased CO activity as a result of 2VO was not restored by MB treatment. Additionally, though the same number of subjects showed lesions as a result of 2VO surgery, subjects treated with MB displayed smaller, more localized lesions than subjects treated with saline.

One potential explanation for the appearance of lesions in some subjects and not in others is the induction of necrotic vs. apoptotic mechanisms in response to chronic cerebral hypoperfusion. Necrosis is a form of neuronal cell injury caused by external cellular factors (e.g., toxins or trauma) that result in autolysis, unregulated and detrimental digestion of cellular components. Apoptosis is programmed or targeted cell death, the results of which can potentially benefit the organism. A key determinant of necrosis vs. apoptosis is the presence of intracellular ATP. In the weeks following 2VO surgery, there is a rapid depletion of ATP (Plaschke, 2005; Briede and Duburs, 2007). This may lead to an induction of necrotic mechanisms in cells more vulnerable to ATP depletion. If this is indeed the case, then increases in ATP production as a result of MB treatment may explain why lesions were smaller and more localized in MB-treated subjects.

Methylene blue treatment in 2VO surgery also resulted in stronger interregional correlation of cytochrome oxidase activity between the same regions that were weakened in saline-treated subjects (i.e., between visual cortex and hippocampus and visual cortex and midbrain). MB treatment in sham and 2VO groups also resulted in widespread strengthened connectivity between hippocampus (CA1, CA2 and dentate) and prefrontal cortex (lateral orbital cortex, ventral orbital cortex and anterior insular cortex), as well as between amygdala (central and medial) and frontal cortex areas (ventral orbital cortex, prelimbic cortex and primary motor cortex). Widespread modulation of interregional correlation of cytochrome oxidase activity by MB has also been reported in the brains of healthy humans analyzed with fMRI (Rodriguez et al., 2017).

Though amygdala-cortical interregional correlation of cytochrome oxidase activity was not significantly affected by

2VO surgery, the strengthened interregional correlation of cytochrome oxidase activity between these regions likely assisted in the learning of the VWT. The amygdala has a modulatory role in both spatial and cued water maze tasks (Packard et al., 1994). The medial amygdala was also positively correlated with VWT performance, strengthening the likelihood that the increased amygdala-cortical interregional correlation of cytochrome oxidase activity we saw as a result of MB treatment was related to learning the VWT escape task.

It has been demonstrated before that low doses (1–4 mg/kg) of methylene blue (1) enhance cytochrome oxidase activity, (2) are neuroprotective, and (3) enhance learning and memory in animals and humans (Rojas et al., 2012; Telch et al., 2014; Echevarria et al., 2016; Rodriguez et al., 2016; Auchter et al., 2017; Zoellner et al., 2017). However, this is the first study to integrate all three of these implications to show that MB is neuroprotective by enhancing mitochondrial activity in regions specifically vulnerable to hypoperfusion. Additionally, functional networks that were specifically weakened by 2VO surgery were restored by daily MB treatment.

## CONCLUSION

This is the first study to characterize the functional changes in brain metabolic activity that result from chronic cerebral hypoperfusion, and show how treatment with MB ameliorates these changes, preventing neurodegeneration and memory impairment. Interregional correlation of cytochrome oxidase activity was weakened between regions specifically involved in visual discrimination learning, which likely resulted in decreased performance in the visual water task. Treatment with MB not only restored task-specific interregional correlation of cytochrome oxidase activity, but also restored average mitochondrial activity in regions specifically affected by 2VO surgery. These findings implicate MB as a potential prophylactic or therapeutic treatment for chronic cerebral hypoperfusion, including people at a high risk for or symptomatic of neurodegenerative disorders whose pathology is accompanied by cardiovascular disease or cerebrovascular hypoxia.

## REFERENCES

- Atamna, H., Nguyen, A., Schultz, C., Boyle, K., Newberry, J., Kato, H., et al. (2008). Methylene blue delays cellular senescence and enhances key mitochondrial biochemical pathways. *FASEB J.* 22, 703–712. doi: 10.1096/fj.07-9610com
- Auchter, A., Shumake, J., Gonzalez-Lima, F., and Monfils, M. H. (2017). Preventing the return of fear using reconsolidation updating and methylene blue is differentially dependent on extinction learning. *Sci. Rep.* 7:46071. doi: 10.1038/srep46071
- Auchter, A., Williams, J., Barksdale, B., Monfils, M. H., and Gonzalez-Lima, F. (2014). Therapeutic benefits of methylene blue on cognitive impairment during chronic cerebral hypoperfusion. *J. Alzheimers Dis.* 42, S525–S535. doi: 10.3233/JAD-141527
- Auchter, A. M. (2015). *Targeting Mitochondria via Methylene Blue: Implications in Memory Enhancement and Neuroprotection*. Ph.D. dissertation, University of Texas, Austin TX.

## DATA AVAILABILITY STATEMENT

The raw data supporting the conclusions of this article will be made available by the authors, without undue reservation, to any qualified researcher.

## ETHICS STATEMENT

This study was carried out in accordance with the recommendations of NIH Guide for the Care and Use of Laboratory Animals, Committee for the Update of the Guide for the Care and Use of Laboratory Animals. The protocol was approved by the Institutional Animal Care and Use Committee, University of Texas at Austin.

## AUTHOR CONTRIBUTIONS

FG-L, AA, and MM designed the experiment and interpreted the results. AA performed the surgery. AA and DB processed the tissue. AA and FG-L analyzed the data. AA, DB, and FG-L wrote the manuscript. FG-L revised and expanded it throughout the peer-review process. All authors contributed to manuscript revision, read and approved the submitted version.

## FUNDING

This study was supported by grants from the Oskar Fischer Project Fund to FG-L and the Darrell K Royal Research Fund to MM.

## ACKNOWLEDGMENTS

The authors thank Justin Williams and Bryan Barksdale for their assistance with the animal work. Some of this data was previously included as part of A. Auchter's dissertation at the University of Texas at Austin (Auchter, 2015).

- Bhurltel, S., Katila, N., Neupane, S., Srivastav, S., Park, P. H., and Choi, D. Y. (2018). Methylene blue protects dopaminergic neurons against MPTP-induced neurotoxicity by upregulating brain-derived neurotrophic factor. *Ann. N. Y. Acad. Sci.* 1431, 58–71. doi: 10.1111/nyas.13870
- Biju, K. C., Evans, R. C., Shrestha, K., Carlisle, D. C. B., Gelfond, J., and Clark, R. A. (2018). Methylene blue ameliorates olfactory dysfunction and motor deficits in a chronic MPTP/probenecid mouse model of Parkinson's disease. *Neuroscience* 380, 111–122. doi: 10.1016/j.neuroscience.2018.04.008
- Briede, J., and Duburs, G. (2007). Protective effect of cerebrocrast on rat brain ischaemia induced by occlusion of both common carotid arteries. *Cell Biochem. Funct.* 25, 203–210. doi: 10.1002/cbf.1318
- Bruchey, A. K., and Gonzalez-Lima, F. (2008). Behavioral, physiological and biochemical hormetic responses to the autoxidizable dye methylene blue. *Am. J. Pharmacol. Toxicol.* 3, 72–79. doi: 10.3844/ajptsp.2008.72.79
- Cada, A., de la Torre, J. C., and Gonzalez-Lima, F. (2000). Chronic cerebrovascular ischemia in aged rats: effects on brain metabolic capacity and behavior. *Neurobiol. Aging* 21, 225–233. doi: 10.1016/s0197-4580(00)00116-0



- Callaway, N. L., Riha, P. D., Bruchey, A. K., Munshi, Z., and Gonzalez-Lima, F. (2004). Methylene blue improves brain oxidative metabolism and memory retention in rats. *Pharmacol. Biochem. Behav.* 77, 175–181. doi: 10.1016/j.pbb.2003.10.007
- Callaway, N. L., Riha, P. D., Wrubel, K. M., McCollum, D., and Gonzalez-Lima, F. (2002). Methylene blue restores spatial memory retention impaired by an inhibitor of cytochrome oxidase in rats. *Neurosci. Lett.* 332, 83–86. doi: 10.1016/s0304-3940(02)00827-3
- Choy, M., Ganesan, V., Thomas, D. L., Thornton, J. S., Proctor, E., King, M. D., et al. (2006). The chronic vascular and haemodynamic response after permanent bilateral common carotid occlusion in newborn and adult rats. *J. Cereb. Blood Flow Metab.* 26, 1066–1075. doi: 10.1038/sj.jcbfm.9600259
- Cohen, J. (1988). *Statistical Power Analysis for the Behavioural Sciences*, 2nd Edn. New York, NY: Lawrence Erlbaum Associates.
- Conejo, N. M., Gonzalez-Pardo, H., Gonzalez-Lima, F., and Arias, J. L. (2010). Spatial learning of the water maze: progression of brain circuits mapped with cytochrome oxidase histochemistry. *Neurobiol. Learn. Mem.* 93, 362–371. doi: 10.1016/j.nlm.2009.12.002
- de la Torre, J. C. (1999). Critical threshold cerebral hypoperfusion causes Alzheimer's disease. *Acta Neuropathol.* 98, 1–8. doi: 10.1007/s004010051044
- de la Torre, J. C. (2000). Impaired cerebrovascular perfusion. Summary of evidence in support of its causality in Alzheimer's disease. *Ann. N. Y. Acad. Sci.* 924, 136–152. doi: 10.1111/j.1749-6632.2000.tb05572.x
- de la Torre, J. C. (2012). Cardiovascular risk factors promote brain hypoperfusion leading to cognitive decline and dementia. *Cardiovasc. Psychiatry Neurol.* 2012:367516. doi: 10.1155/2012/367516
- de la Torre, J. C. (2016). *Alzheimer's Turning Point: A Vascular Approach to Clinical Prevention*. Cham: Springer.
- de la Torre, J. C. (2018). The vascular hypothesis of Alzheimer's disease: a key to preclinical prediction of dementia using neuroimaging. *J. Alzheimers Dis.* 63, 35–52. doi: 10.3233/JAD-180004
- de la Torre, J. C., Cada, A., Nelson, N., Davis, G., Sutherland, R. J., and Gonzalez-Lima, F. (1997). Reduced cytochrome oxidase and memory dysfunction after chronic brain ischemia in aged rats. *Neurosci. Lett.* 223, 165–168. doi: 10.1016/s0304-3940(97)13421-8
- de la Torre, J. C., and Fortin, T. (1991). Partial or global rat brain ischemia: the SCOT model. *Brain Res. Bull.* 26, 365–372. doi: 10.1016/0361-9230(91)90008-8
- de la Torre, J. C., Fortin, T., Park, G. A., Butler, K. S., Kozlowski, P., Pappas, B. A., et al. (1992). Chronic cerebrovascular insufficiency induces dementia-like deficits in aged rats. *Brain Res.* 582, 186–195. doi: 10.1016/0006-8993(92)90132-s
- Dhar, S. S., and Wong-Riley, M. T. T. (2009). Coupling of energy metabolism and synaptic transmission at the transcriptional level: role of nuclear respiratory factor 1 in regulating both cytochrome c oxidase and NMDA glutamate receptor subunit genes. *J. Neurosci.* 29, 483–492. doi: 10.1523/JNEUROSCI.3704-08.2009
- Driscoll, I., Howard, S., Prusky, G., Rudy, J., and Sutherland, R. (2005). Seahorse wins all races: hippocampus participates in both linear and non-linear visual discrimination learning. *Behav. Brain Res.* 164, 29–35. doi: 10.1016/j.bbr.2005.05.006
- Echevarria, D. J., Caramillo, E. M., and Gonzalez-Lima, F. (2016). Methylene blue facilitates memory retention in zebrafish in a dose-dependent manner. *Zebrafish* 13, 489–494. doi: 10.1089/zeb.2016.1282
- Erecinska, M., and Silver, I. A. (1989). ATP and brain function. *J. Cereb. Blood Flow Metab.* 9, 2–19. doi: 10.1038/jcbfm.1989.2
- Farkas, E., Institoris, A., Domoki, F., Mihaly, A., Luiten, P. G., and Bari, F. (2004). Diazoxide and dimethyl sulphoxide prevent cerebral hypoperfusion-related learning dysfunction and brain damage after carotid artery occlusion. *Brain Res.* 1008, 252–258. doi: 10.1016/j.brainres.2004.02.037
- Farkas, E., Institoris, Á., Domoki, F., Mihály, A., and Bari, F. (2006). The effect of pre- and post-treatment with diazoxide on the early phase of chronic cerebral hypoperfusion in the rat. *Brain Res.* 1087, 168–174. doi: 10.1016/j.brainres.2006.02.134
- Farkas, E., Luiten, P., and Bari, F. (2007). Permanent, bilateral common carotid artery occlusion in the rat: a model for chronic cerebral hypoperfusion-related neurodegenerative diseases. *Brain Res. Rev.* 54, 162–180. doi: 10.1016/j.brainresrev.2007.01.003
- Farkas, E., and Luiten, P. G. M. (2001). Cerebral microvascular pathology in aging and Alzheimer's disease. *Prog. Neurobiol.* 64, 575–611. doi: 10.1016/s0301-0082(00)00068-x
- Fidalgo, C., Conejo, N. M., González-Pardo, H., and Arias, J. L. (2014). Dynamic functional brain networks involved in simple visual discrimination learning. *Neurobiol. Learn. Mem.* 114, 165–170. doi: 10.1016/j.nlm.2014.06.001
- Friston, K. J. (1994). Functional and effective connectivity in neuroimaging: A synthesis. *Human Brain Mapping* 2, 56–78. doi: 10.1002/hbm.460020107
- Gonzalez-Lima, F., and Bruchey, A. K. (2004). Extinction memory improvement by the metabolic enhancer methylene blue. *Learn. Mem.* 11, 633–640. doi: 10.1101/lm.82404
- Gonzalez-Lima, F., and Auchter, A., (2015). Protection against neurodegeneration with low-dose methylene blue and near-infrared light. *Front. Cell Neurosci.* 9:179. doi: 10.3389/fncel.2015.00179
- Gonzalez-Lima, F., and Cada, A. (1994). Cytochrome oxidase activity in the auditory system of the mouse: a qualitative and quantitative histochemical study. *Neuroscience* 63, 559–578. doi: 10.1016/0306-4522(94)90550-9
- Gonzalez-Lima, F. (ed.) (1998). *Cytochrome Oxidase in Neuronal Metabolism and Alzheimer's Disease*. New York, NY: Plenum Press.
- Gonzalez-Lima, F., and Jones, D. (1994). Quantitative mapping of cytochrome oxidase activity in the central auditory system of the gerbil: a study with calibrated activity standards and metal-intensified histochemistry. *Brain Res.* 660, 34–49. doi: 10.1016/0006-8993(94)90836-2
- Gonzalez-Lima, F., and McIntosh, A. R. (1994). Neural network interactions related to auditory learning analyzed with structural equation modeling. *Hum. Brain Mapp.* 2, 23–44. doi: 10.1002/hbm.460020105
- Gonzalez-Lima, F., and McIntosh, A. R. (1995). Analysis of neural network interactions related to associative learning using structural equation modeling. *Math. Comput. Simul.* 40, 115–140. doi: 10.1016/0378-4754(95)00022-x
- Haley, A. P., Forman, D. E., Poppas, A., Hoth, K. F., Gunstad, J., Jefferson, A. L., et al. (2007). Carotid artery intima-media thickness and cognition in cardiovascular disease. *Int. J. Cardiol.* 121, 148–154. doi: 10.1016/j.ijcard.2006.10.032
- Horwitz, B., Soncrant, T. T., and Haxby, J. V. (1992). "Covariance analysis of functional interactions in the brain using metabolic and blood flow data," in *Advances in Metabolic Mapping Techniques for Brain Imaging of Behavioral and Learning Functions*, Vol. 68, eds F. Gonzalez-Lima, T. H. Finkenstaedt, and H. Scheich (Dordrecht: Kluwer Academic Publishers), 189–217. doi: 10.1007/978-94-011-2712-7\_7
- Huang, L., Lu, J., Cerqueira, B., Liu, Y., Jiang, Z., and Duong, T. Q. (2018). Chronic oral methylene blue treatment in a rat model of focal cerebral ischemia/reperfusion. *Brain Res.* 1678, 322–329. doi: 10.1016/j.brainres.2017.10.033
- Huang, S., Du, F., Shih, Y. Y., Shen, Q., Gonzalez-Lima, F., and Duong, T. Q. (2013). Methylene blue potentiates stimulus-evoked fMRI responses and cerebral oxygen consumption during normoxia and hypoxia. *Neuroimage* 72, 237–242. doi: 10.1016/j.neuroimage.2013.01.027
- Lavinsky, D., Sarmento Arterni, N., Achaval, M., and Netto, C. A. (2006). Chronic bilateral common carotid artery occlusion: a model for ocular ischemic syndrome in the rat. *Graefes Arch. Clin. Exp. Ophthalmol.* 244, 199–204. doi: 10.1007/s00417-005-0006-7
- Lee, R. B., and Urban, J. P. (2002). Functional replacement of oxygen by other oxidants in articular cartilage. *Arthritis. Rheum.* 46, 3190–3200. doi: 10.1002/art.10686
- Liu, H. X., Zhang, J. J., Zheng, P., and Zhang, Y. (2005). Altered expression of MAP-2, GAP-43, and synaptophysin in the hippocampus of rats with chronic cerebral hypoperfusion correlates with cognitive impairment. *Brain Res. Mol. Brain Res.* 139, 169–177. doi: 10.1016/j.molbrainres.2005.05.014
- Liu, J., Jin, D. Z., Xiao, L., and Zhu, X. Z. (2006). Paeoniflorin attenuates chronic cerebral hypoperfusion-induced learning dysfunction and brain damage in rats. *Brain Res.* 1089, 162–170. doi: 10.1016/j.brainres.2006.02.115
- Martinez, J. L. Jr., Jensen, R. A., Vasquez, B. J., McGuinness, T., and McGaugh, J. L. (1978). Methylene blue alters retention of inhibitory avoidance responses. *Psychobiology* 6, 387–390. doi: 10.3758/bf03326744



- McIntosh, A. R., and Gonzalez-Lima, F. (1994). Structural equation modeling and its application to network analysis in functional brain imaging. *Hum. Brain Mapp.* 2, 2–22. doi: 10.1016/j.neuroimage.2009.05.078
- Miclescu, A., Basu, S., and Wiklund, L. (2006). Methylene blue added to a hypertonic-hyperoncotic solution increases short-term survival in experimental cardiac arrest. *Crit. Care Med.* 34, 2806–2813. doi: 10.1097/01.CCM.0000242517.23324.27
- Miclescu, A., Sharma, H. S., Martijn, C., and Wiklund, L. (2010). Methylene blue protects the cortical blood–brain barrier against ischemia/reperfusion-induced disruptions. *Crit. Care Med.* 38, 2199–2206. doi: 10.1097/CCM.0b013e3181f26b0c
- Nair, B., and Wong-Riley, M. T. (2016). Transcriptional regulation of brain-derived neurotrophic factor coding exon IX: role of nuclear respiratory factor 2. *J. Biol. Chem.* 291, 22583–22593. doi: 10.1074/jbc.M116.742304
- Nelson, C., and Silverstein, F. S. (1994). Acute disruption of cytochrome oxidase activity in brain in a perinatal rat stroke model. *Pediatr. Res.* 36, 12–19. doi: 10.1203/00006450-199407001-00003
- Ohtaki, H., Fujimoto, T., Sato, T., Kishimoto, K., Fujimoto, M., Moriya, M., et al. (2006). Progressive expression of vascular endothelial growth factor (VEGF) and angiogenesis after chronic ischemic hypoperfusion in rat. *Acta Neurochir. Suppl.* 96, 283–287.
- Packard, M. G., Cahill, L., and McGaugh, J. L. (1994). Amygdala modulation of hippocampal-dependent and caudate nucleus-dependent memory processes. *Proc. Natl. Acad. Sci. U.S.A.* 91, 8477–8481.
- Paxinos, G., and Watson, C. (1996). *The Rat Brain in Stereotaxic Coordinates*, 3rd Edn. San Diego, CA: Academic Press.
- Plaschke, K. (2005). Aspects of ageing in chronic cerebral oligoemia. Mechanisms of degeneration and compensation in rat models. *J. Neural Transm.* 112, 393–413. doi: 10.1007/s00702-004-0191-2
- Prusky, G. T., West, P. W., and Douglas, R. M. (2000). Behavioral assessment of visual acuity in mice and rats. *Vision Res.* 40, 2201–2209.
- Riha, P. D., Bruchey, A. K., Echevarria, D. J., and Gonzalez-Lima, F. (2005). Memory facilitation by methylene blue: dose-dependent effect on behavior and brain oxygen consumption. *Eur. J. Pharmacol.* 511, 151–158. doi: 10.1016/j.ejphar.2005.02.001
- Riha, P. D., Rojas, J. C., and Gonzalez-Lima, F. (2011). Beneficial network effects of methylene blue in an amnesic model. *Neuroimage* 54, 2623–2634. doi: 10.1016/j.neuroimage.2010.11.023
- Rodriguez, P., Singh, A. P., Malloy, K. E., Zhou, W., Barrett, D. W., Franklin, C. G., et al. (2017). Methylene blue modulates functional connectivity in the human brain. *Brain Imaging Behav.* 11, 640–648. doi: 10.1007/s11682-016-9541-6
- Rodriguez, P., Zhou, W., Barrett, D. W., Altmeyer, W., Gutierrez, J. E., Li, J., et al. (2016). Multimodal randomized functional MR imaging of the effects of methylene blue in the human brain. *Radiology* 281, 516–526. doi: 10.1148/radiol.2016152893
- Rojas, J. C., Bruchey, A. K., and Gonzalez-Lima, F. (2012). Neurometabolic mechanisms for memory enhancement and neuroprotection of methylene blue. *Prog. Neurobiol.* 96, 32–45. doi: 10.1016/j.pneurobio.2011.10.007
- Rojas, J. C., John, J. M., Lee, J., and Gonzalez-Lima, F. (2009a). Methylene blue provides behavioral and metabolic neuroprotection against optic neuropathy. *Neurotox. Res.* 15, 260–273. doi: 10.1007/s12640-009-9027-z
- Rojas, J. C., Simola, N., Kermath, B. A., Kane, J. R., Schallert, T., and Gonzalez-Lima, F. (2009b). Striatal neuroprotection with methylene blue. *Neuroscience* 163, 877–889. doi: 10.1016/j.neuroscience.2009.07.012
- Sakata, J. T., Coomber, P., Gonzalez-Lima, F., and Crews, D. (2000). Functional connectivity among limbic brain areas: differential effects of incubation temperature and gonadal sex in the leopard gecko, *Eublepharis macularius*. *Brain Behav. Evol.* 55, 139–151. doi: 10.1159/000006648
- Salaris, S. C., Babbs, C. F., and Voorhees, W. D. (1991). Methylene blue as an inhibitor of superoxide generation by xanthine oxidase: a potential new drug for the attenuation of ischemia/reperfusion injury. *Biochem. Pharmacol.* 42, 499–506.
- Sarti, C., Pantoni, L., Bartolini, L., and Inzitari, D. (2002). Persistent impairment of gait performances and working memory after bilateral common carotid artery occlusion in the adult Wistar rat. *Behav. Brain Res.* 136, 13–20.
- Schmidt-Kastner, R., Truettner, J., Lin, B., Zhao, W., Saul, I., Busto, R., et al. (2001). Transient changes of brain-derived neurotrophic factor (BDNF) mRNA expression in hippocampus during moderate ischemia induced by chronic bilateral common carotid artery occlusion in the rat. *Brain Res. Mol. Brain Res.* 92, 157–166.
- Shang, Y., Cheng, J., Oi, J., and Miao, H. (2005). Scutellaria flavonoid reduced memory dysfunction and neuronal injury caused by permanent global ischemia in rats. *Pharmacol. Biochem. Behav.* 82, 67–73. doi: 10.1016/j.pbb.2005.06.018
- Shen, Q., Du, F., Huang, S., Rodriguez, P., Watts, L. T., and Duong, T. Q. (2013). Neuroprotective efficacy of methylene blue in ischemic stroke: an MRI study. *PLoS One* 8:e79833. doi: 10.1371/journal.pone.0079833
- Smith, E. S., Clark, M. E., Hardy, G. A., Kraan, D. J., Biondo, E., Gonzalez-Lima, F., et al. (2017). Daily consumption of methylene blue reduces attentional deficits and dopamine reduction in a 6-OHDA model of Parkinson's disease. *Neuroscience* 359, 8–16. doi: 10.1016/j.neuroscience.2017.07.001
- Tachibana, H., Meyer, J. S., Okayasu, H., Shaw, T. G., Kandula, P., and Rogers, R. L. (1984). Xenon contrast CT–CBF scanning of the brain differentiates normal age-related changes from multi-infarct dementia and senile dementia of Alzheimer type. *J. Gerontol.* 39, 415–423.
- Telch, M. J., Bruchey, A. K., Rosenfield, D., Cobb, A. R., Smits, J., Pahl, S., et al. (2014). Effects of post-session administration of methylene blue on fear extinction and contextual memory in adults with claustrophobia. *Am. J. Psychiatry* 171, 1091–1098. doi: 10.1176/appi.ajp.2014.13101407
- Tian, W. F., Zeng, S., Sheng, Q., Chen, J. L., Weng, P., Zhang, X. T., et al. (2018). Methylene blue protects the isolated rat lungs from ischemia-reperfusion injury by attenuating mitochondrial oxidative damage. *Lung* 196, 73–82. doi: 10.1007/s00408-017-0072-8
- Tucker, D., Lu, Y., and Zhang, Q. (2018). From mitochondrial function to neuroprotection—an emerging role for methylene blue. *Mol. Neurobiol.* 55, 5137–5153. doi: 10.1007/s12035-017-0712-2
- Vélez-Hernández, M. E., Padilla, E., Gonzalez-Lima, F., and Jiménez-Rivera, C. A. (2014). Cocaine reduces cytochrome oxidase activity in the prefrontal cortex and modifies its functional connectivity with brainstem nuclei. *Brain Res.* 1542, 56–69. doi: 10.1016/j.brainres.2013.10.017
- Villarreal, V. S., Gonzalez-Lima, F., Berndt, J., and Barea-Rodriguez, E. J. (2002). Water maze training in aged rats: effects on brain metabolic capacity and behavior. *Brain Res.* 939, 43–51.
- Wong-Riley, M. T. (1989). Cytochrome oxidase: an endogenous metabolic marker for neuronal activity. *Trends Neurosci.* 12, 94–101.
- Wong-Riley, M. T. (2012). Bigenomic regulation of cytochrome c oxidase in neurons and the tight coupling between neuronal activity and energy metabolism. *Adv. Exp. Med. Biol.* 748, 283–304. doi: 10.1007/978-1-4614-3573-0\_12
- Wong-Riley, M. T., and Welt, C. (1980). Histochemical changes in cytochrome oxidase of cortical barrels after vibrissal removal in neonatal and adult mice. *Proc. Natl. Acad. Sci. U.S.A.* 77, 2333–2337.
- Wrubel, K. M., Riha, P. D., Maldonado, M. A., McCollum, D., and Gonzalez-Lima, F. (2007). The brain metabolic enhancer methylene blue improves discrimination learning in rats. *Pharmacol. Biochem. Behav.* 86, 712–717. doi: 10.1016/j.pbb.2007.02.018
- Zhang, X., Rojas, J. C., and Gonzalez-Lima, F. (2006). Methylene blue prevents neurodegeneration caused by rotenone in the retina. *Neurotox. Res.* 9, 47–57.
- Zoellner, L. A., Telch, M., Foa, E. B., Farach, F. J., McLean, C. P., Gallop, R., et al. (2017). Enhancing extinction learning in posttraumatic stress disorder with brief daily imaginal exposure and methylene blue: a randomized controlled trial. *J. Clin. Psychiatry* 78, e782–e789. doi: 10.4088/JCP.16m10936

**Conflict of Interest:** The authors declare that the research was conducted in the absence of any commercial or financial relationships that could be construed as a potential conflict of interest.

Copyright © 2020 Auchter, Barrett, Monfils and Gonzalez-Lima. This is an open-access article distributed under the terms of the Creative Commons Attribution License (CC BY). The use, distribution or reproduction in other forums is permitted, provided the original author(s) and the copyright owner(s) are credited and that the original publication in this journal is cited, in accordance with accepted academic practice. No use, distribution or reproduction is permitted which does not comply with these terms.



# PHF-Core Tau as the Potential Initiating Event for Tau Pathology in Alzheimer's Disease

Nabil Itzi Luna-Viramontes<sup>1,2</sup>, B. Berenice Campa-Córdoba<sup>1,2</sup>, Miguel Ángel Ontiveros-Torres<sup>3</sup>, Charles R. Harrington<sup>4</sup>, Ignacio Villanueva-Fierro<sup>5</sup>, Parménides Guadarrama-Ortiz<sup>6</sup>, Linda Garcés-Ramírez<sup>2</sup>, Fidel de la Cruz<sup>2</sup>, Mario Hernandez-Alejandro<sup>7</sup>, Sandra Martínez-Robles<sup>1</sup>, Erik González-Ballesteros<sup>1</sup>, Mar Pacheco-Herrero<sup>8\*</sup> and José Luna-Muñoz<sup>1\*</sup>

## OPEN ACCESS

### Edited by:

Rocío Martínez De Pablos,  
University of Seville, Spain

### Reviewed by:

Sylvia Eva Perez,  
Barrow Neurological Institute (BNI),  
United States  
Claude Wischik,  
TauRx Therapeutics Ltd, Singapore

### \*Correspondence:

Mar Pacheco-Herrero  
mpacheco@pucmm.edu.do;  
mm.pachecoherr@gmail.com  
José Luna-Muñoz  
jluna\_tau67@comunidad.unam.mx;  
jlunatau67@gmail.com

### Specialty section:

This article was submitted to  
Cellular Neuropathology,  
a section of the journal  
Frontiers in Cellular Neuroscience

**Received:** 29 April 2020

**Accepted:** 15 July 2020

**Published:** 10 September 2020

### Citation:

Luna-Viramontes NI,  
Campa-Córdoba BB,  
Ontiveros-Torres MÁ, Harrington CR,  
Villanueva-Fierro I,  
Guadarrama-Ortiz P,  
Garcés-Ramírez L, de la Cruz F,  
Hernandez-Alejandro M,  
Martínez-Robles S,  
González-Ballesteros E,  
Pacheco-Herrero M and  
Luna-Muñoz J (2020) PHF-Core Tau  
as the Potential Initiating Event for Tau  
Pathology in Alzheimer's Disease.  
Front. Cell. Neurosci. 14:247.  
doi: 10.3389/fncel.2020.00247

<sup>1</sup> National Dementia BioBank, Departamento de Ciencias Biológicas, Facultad de Estudios Superiores, Universidad Nacional Autónoma de México, Mexico City, Mexico, <sup>2</sup> Departamento de Fisiología, Escuela Nacional de Ciencias Biológicas, Instituto Politécnico Nacional, Mexico City, Mexico, <sup>3</sup> School of Engineering and Science, Tecnológico de Monterrey, Toluca, Mexico, <sup>4</sup> School of Medicine, Medical Sciences and Nutrition, University of Aberdeen, Aberdeen, United Kingdom, <sup>5</sup> CIIDIR, Instituto Politécnico Nacional, Becario COFAA, Durango, Mexico, <sup>6</sup> Departamento de Neurocirugía, Centro Especializado en Neurocirugía y Neurociencias México, CENNM, CDMX, Mexico City, Mexico, <sup>7</sup> Departamento de Bioingeniería, Unidad Profesional Interdisciplinaria de Biología y Biotecnología del Instituto Politécnico Nacional (UPIBI-IPN), Mexico City, México, <sup>8</sup> Neuroscience Research Laboratory, Faculty of Health Sciences, Pontificia Universidad Católica Madre y Maestra, Santiago de los Caballeros, Dominican Republic

Worldwide, around 50 million people have dementia. Alzheimer's disease (AD) is the most common type of dementia and one of the major causes of disability and dependency among the elderly worldwide. Clinically, AD is characterized by impaired memory accompanied by other deficiencies in the cognitive domain. Neuritic plaques (NPs) and neurofibrillary tangles (NFTs) are histopathological lesions that define brains with AD. NFTs consist of abundant intracellular paired helical filaments (PHFs) whose main constituent is tau protein. Tau undergoes posttranslational changes including hyperphosphorylation and truncation, both of which favor conformational changes in the protein. The sequential pathological processing of tau is illustrated with the following specific markers: pT231, TG3, AT8, AT100, and Alz50. Two proteolysis sites for tau have been described—truncation at glutamate 391 and at aspartate 421—and which can be demonstrated by reactivity with the antibodies 423 and TauC-3, respectively. In this review, we describe the molecular changes in tau protein as pre-NFTs progress to extracellular NFTs and during which the formation of a minimal nucleus of the filament, as the PHF core, occurs. We also analyzed the PHF core as the initiator of PHFs and tau phosphorylation as a protective neuronal mechanism against the assembly of the PHF core.

**Keywords:** tau protein, tau pathology, PHF core, truncation, phosphorylation, conformational changes, paired helical filament, neurofibrillary tangles

## INTRODUCTION

The elderly population is increasing globally, and this leads to the increased prevalence of neurodegenerative diseases typical of this age group. Moderate and severe Alzheimer's disease (AD) can be clinically diagnosed with a high degree of certainty. However, at a preclinical or early stage, symptoms shared with other neurodegenerative diseases make the diagnosis of AD difficult.

Clinically, AD is characterized by progressive memory loss and impaired cognitive functions (judgment, behavior, and language). Neuritic plaques (NPs) (**Figure 1A**) and neurofibrillary tangles (NFTs) (**Figures 1B–F**), which can be stained by thiazin red (TR) and thioflavin S (TS) (Kelenyi, 1967; Stiller et al., 1970; Mena et al., 1995; Luna-Munoz et al., 2008; **Figure 2**), are histopathological lesions in brains with AD (Perl, 2010). At a macroscopic level, decreases in brain size (**Figures 3A,B**), gray matter (**Figure 3B**, arrows), and white matter (**Figure 3B**, small arrows) are observed. A substantial increase in ventricular volume and significant atrophy in the brain convolutions and the hippocampus are also observed (**Figure 3B**). NFTs are associated with neuronal death in AD. They consist of abundant intracellular paired helical filaments (PHFs) whose main constituent is tau protein. To aggregate into PHFs, tau dissociates from microtubules, an event favored by specific modifications (Crowther and Wischik, 1985; Wischik and Crowther, 1986; Wischik et al., 1992). In this review, we discuss

the posttranslational mechanisms of the phosphorylation and truncation of tau protein that are associated with the formation of PHFs. We conclude from our review that pharmacological therapy for AD should not be directed against phosphorylated tau.

## NEURITIC PLAQUES

Neuritic plaques are made up of soluble or insoluble (**Figure 1A**) extracellular deposits of amyloid  $\beta$ -peptide ( $A\beta$ ). NPs are bordered by filiform structures that are the dystrophic neurites, which are part of the dendrites and axons of neurons (Guevara et al., 1998; Espinosa et al., 2001) and glial (**Figure 4A**; DaRocha-Souto et al., 2011; Serrano-Pozo et al., 2011) and microglial cells (**Figure 4B**; Hayes et al., 2002; Jekabsone et al., 2006; Lee and Landreth, 2010).  $A\beta$  is formed from the proteolytic processing of a transmembrane protein called the amyloid precursor protein (APP) (Kapaki et al., 2005).

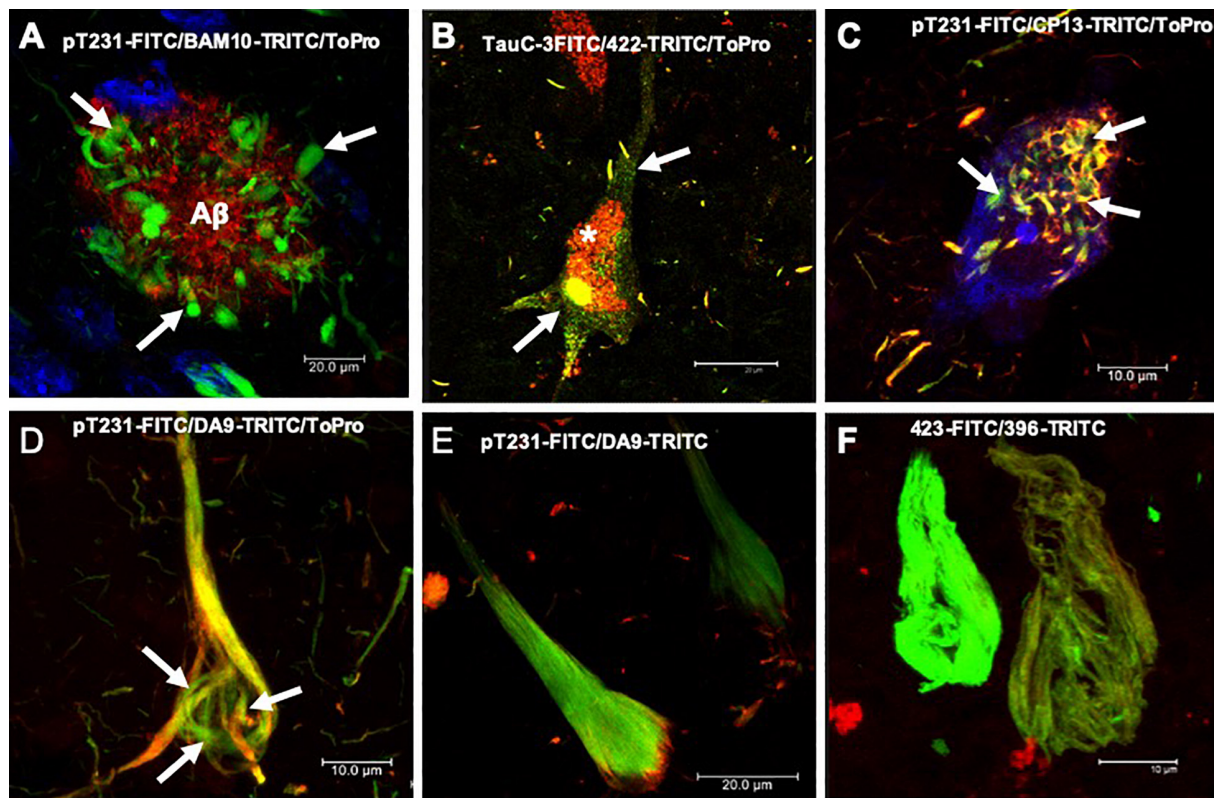


**FIGURE 1 |** Histopathological lesions in Alzheimer's disease (AD) brain. **(A)** Amyloid plaque stained using the BAM10 antibody (red channel), with associated dystrophic neurites (arrows), and nuclei stained with To-Pro (blue). **(B–F)** Evolution of the aggregation of the tau protein recognized by different antibodies directed against phosphorylated and truncated tau proteins. **(B)** Pre-neurofibrillary tangle (NFT) characterized by a diffuse granular staining in the neuronal soma (TauC-3, green channel; 423, red channel, arrows). Perinuclear immunoreactivity is observed. Lipofuscin is autofluorescent in the red channel (asterisk). **(C)** Small tangles (bead-like structures, arrows) visualized using two antibodies directed against the phosphorylated tau protein (pT231, green channel; CP13, red channel). **(D,E)** NFTs at different stages of aggregation. **(D)** NFT with a fibrillar structure in the form of a trabecula around the nucleus (arrows). **(E)** Compact NFT, where the PHFs have invaded the entire soma and displaced the nucleus from its original position, and visualised using pT231, which recognises a phospho-epitope within the mid domain (DA9). **(F)** Extracellular NFTs, the last stage of aggregation of the tau protein. In the neuronal soma, this structure is much looser, lacking a cell membrane and a nucleus. It consists of the minimum core of the filament (PHF core) and reacts with antibody 423, which recognizes truncation at Glu-391 (green channel) and phospho-tau S396 (red channel). Images obtained with a Leica SP8 confocal microscope.



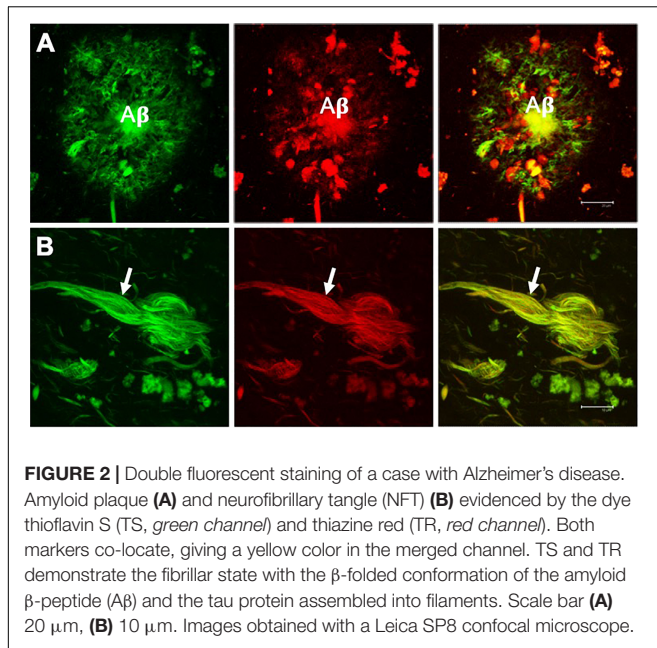


**FIGURE 2 |** Double fluorescent staining of a case with Alzheimer's disease. Amyloid plaque (A) and neurofibrillary tangle (NFT) (B) evidenced by the dye thioflavin S (TS, green channel) and thiazine red (TR, red channel). Both markers co-locate, giving a yellow color in the merged channel. TS and TR demonstrate the fibrillar state with the  $\beta$ -folded conformation of the amyloid  $\beta$ -peptide (A $\beta$ ) and the tau protein assembled into filaments. Scale bar (A) 20  $\mu$ m, (B) 10  $\mu$ m. Images obtained with a Leica SP8 confocal microscope.

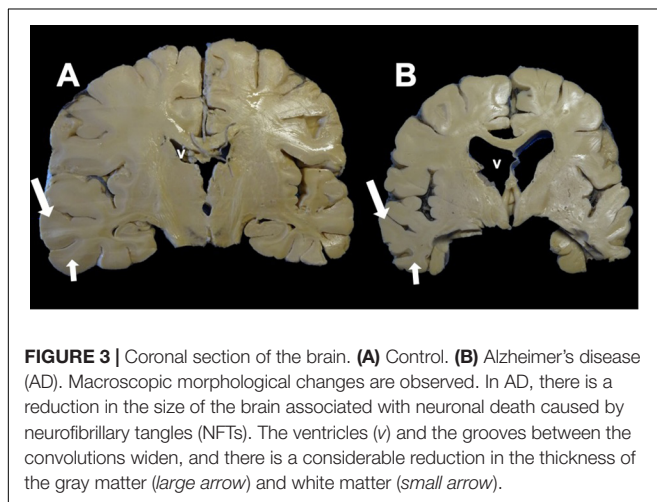


**FIGURE 3 |** Coronal section of the brain. (A) Control. (B) Alzheimer's disease (AD). Macroscopic morphological changes are observed. In AD, there is a reduction in the size of the brain associated with neuronal death caused by neurofibrillary tangles (NFTs). The ventricles (v) and the grooves between the convolutions widen, and there is a considerable reduction in the thickness of the gray matter (large arrow) and white matter (small arrow).

APP can be processed in two ways: one physiological or non-amyloidogenic and the other pathological or amyloidogenic. In the non-amyloidogenic pathway, APP is cleaved by  $\alpha$ -secretase in its N-terminal ectodomain (sAPP $\alpha$ ), leaving the C-terminal  $\alpha$ -CTF fragment anchored in the membrane. Subsequently,  $\alpha$ -CTF is cut by the action of  $\gamma$ -secretase, giving rise to fragments p3 and AICD (APP intracellular domain). In the amyloidogenic pathway,  $\beta$ -secretase initiates APP proteolysis by cutting the ectodomain called sAPP $\beta$  (soluble peptide APP $\beta$ ). The membrane-anchored fragment or  $\beta$ -CTF is subsequently cut by  $\gamma$ -secretase, generating A $\beta$ . While A $\beta$  peptides 1-40 and 1-42 are the main constituents of the NPs, A $\beta$ 1-42 is the first to be deposited and has greater ease of adding and polymerizing under physiological conditions (Jarrett et al., 1993; Iwatsubo et al., 1994). A $\beta$  undergoes post-translational modifications such as oxidation, phosphorylation, glycosylation, pyroglutamination,

isomerization, or racemization. These modifications may favor A $\beta$  polymerization, toxicity, and inflammatory activity observed in cases of AD (Polanco et al., 2018).

## NEUROFIBRILLARY TANGLES

The presence of NFTs in the hippocampus follows a stereotyped pattern described in six stages (Braak and Braak, 1991). In stages I and II, NFTs are observed in the transentorhinal cortex and the adjacent area of the entorhinal cortex II. They are considered the preclinical stages in the absence of clinical symptoms. In stages III and IV, NFTs have invaded mostly the entorhinal cortex II, subiculum, and CA1. At these stages, the first clinical symptoms, or memory loss, begin. Stages V and VI are characterized by a complete invasion of the hippocampus, layer IV of the entorhinal cortex, and the neocortex. These latter stages correspond to an advanced phase of AD. This pathological progression is important in the postmortem diagnosis of AD and characterization of the stages in its development.

## TAU PROTEIN

Tau protein belongs to the family of microtubule-associated proteins (MAPs) (Goedert et al., 1988; Lee et al., 1988; Himmler, 1989). In humans, tau is encoded by a single-copy gene located on chromosome 17q21.3 (Neve et al., 1986). This gene has 16 exons, of which exons 2, 3, 4A, 6, 8, 10, and 14 can be alternatively spliced (Figure 5). This processing generates six isoforms of tau in the central nervous system (CNS), ranging from 352 to 441 amino acids in length (Goedert et al., 1989b). Structurally, the tau molecule is highly elastic, without secondary structure (Schweers et al., 1994). It presents two domains: an amino terminal domain named "projection domain," composed of an acidic region and a proline-rich region. The carboxy-terminal domain consists of the "microtubule-binding domain," which contains three (3R) or four tandem repeats (4R) of 31 or 32 amino acids and a C-terminal tail. The additional repeat region is encoded by exon 10. It is the repeat domain of tau that is vital for its ability to polymerize into filaments, and it is highly sensitive to phosphorylation (Steiner et al., 1990). The tau isoforms differ in the presence of N-terminal inserts (0, 1, or 2) and the number of C-terminal repeats (3R or 4R). During the fetal and early developmental stages, 3R tau isoforms are predominant, whereas both the 3R and 4R isoforms can be found in adult brains (Goedert et al., 1989a; Andreadis et al., 1992). The 4R isoform is about 40-fold more efficient at binding microtubules than the 3R isoform. Thus, the 3R tau would allow greater cytoskeletal plasticity in the growing immature neurons of the fetal brain (Lindwall and Cole, 1984; Bramblett et al., 1993). It has been shown that the 4R/3R ratio in normal and AD brains are 1:1 and approximately 2:1, respectively (Goedert et al., 1989a). Alternative splicing of exon 10, which impacts on the expression of the 3R and 4R isoforms, could be related to the pathogenesis of tauopathies (Liu and Gong, 2008; Zhou et al., 2008). It has been demonstrated that the



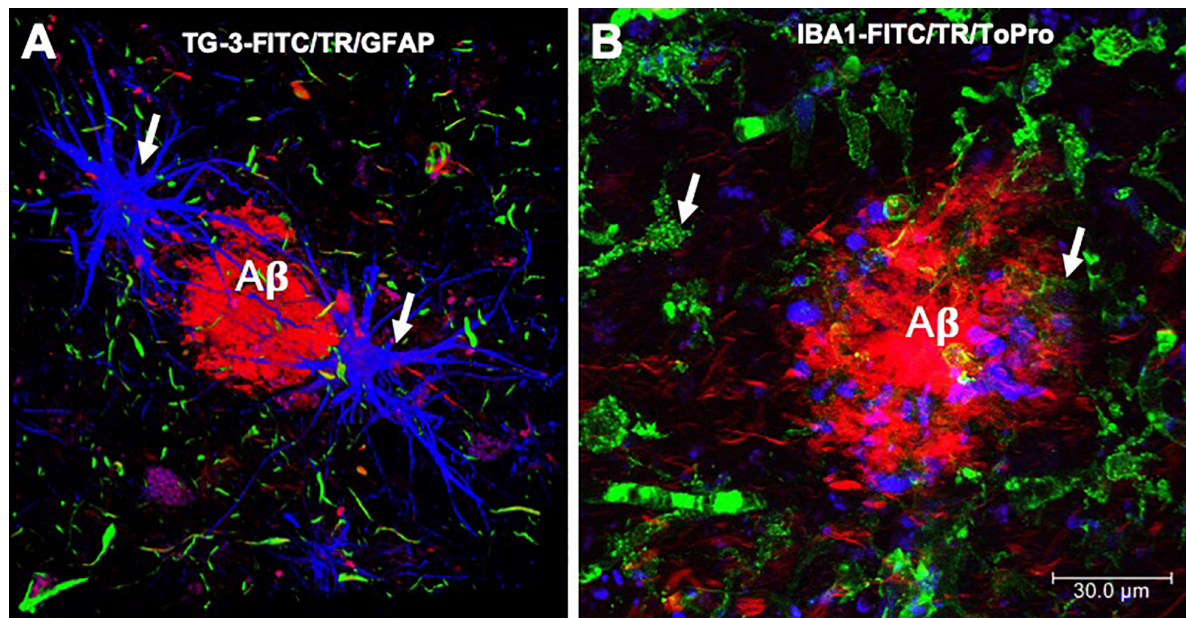


**FIGURE 4 |** Immunofluorescence of amyloid plaques. **(A)** Amyloid  $\beta$ -peptide ( $A\beta$ ) deposit recognized by thiazine red (TR, red color), which is bordered by glial cells (GFAP, blue color) and by dystrophic neurites, recognized by the antibody that reacts with phosphorylated tau protein (TG-3, green color). **(B)** Amyloid plaque is recognized by the TR dye (red color). At the periphery, microglial cells are recognized by the Iba-1 antibody (green color) and the cell nuclei with To-Pro (blue color). Images obtained with a Leica SP8 confocal microscope.

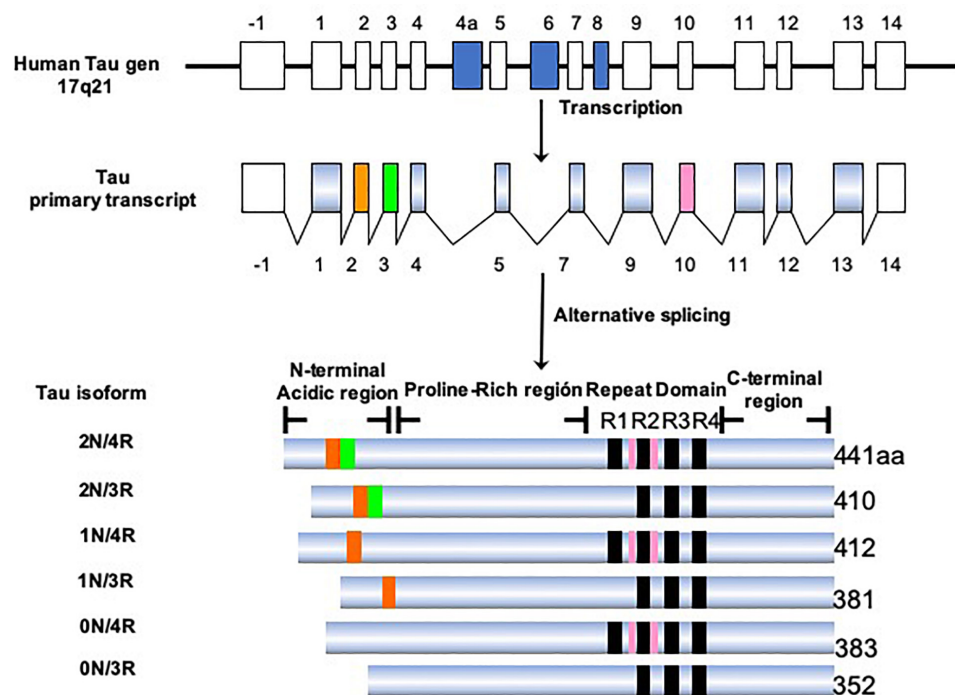


**FIGURE 5 |** Isoforms of the tau protein. The tau protein gene is located on the long arm of chromosome 17, which generates six isoforms by alternative processing. The longest isoform in the CNS is 441 amino acids and the shortest is 352 amino acids. The length depends on the presence/absence of inserts in the amino terminal portion and the presence of three or four repeated domains.

presence of these isoforms differs according to the type of tau deposit and corresponds to the morphological structure of NFTs (Ginsberg et al., 2006). For example, AD is characterized by 95% PHFs and 5% straight filaments (SFs), whereas in Pick's disease the filaments are predominantly SFs. Tau-positive neurons, which exhibit diffuse cytoplasmic tau without apparent fibrillary structures (pre-tangle neurons), appear to be 3R-negative/4R-positive. Intracellular NFTs with typical fibrillary structures contain equal amounts of 3R and 4R isoforms. Structures that are 3R-positive/4R-negative would correspond to extracellular ghost tangles. 3R tau-positive lesions are abundant in the areas in which tau deposition begins early and increase with disease progression (Ginsberg et al., 2006). In contrast, 4R tau-positive lesions appear in the regions in which tau deposition starts later. In this sense, an orchestrated regulation would change the tau isoform as the AD progresses (Jakes et al., 1991; Uchihara et al., 2012; Uchihara, 2014; Uematsu et al., 2018). It remains to be clarified how the synthesis of the different isoforms is regulated and exactly how the 3R and 4R tau isoforms affect the progression of AD.

## POSTTRANSLATIONAL MODIFICATIONS INVOLVED IN THE GENESIS OF PHFs

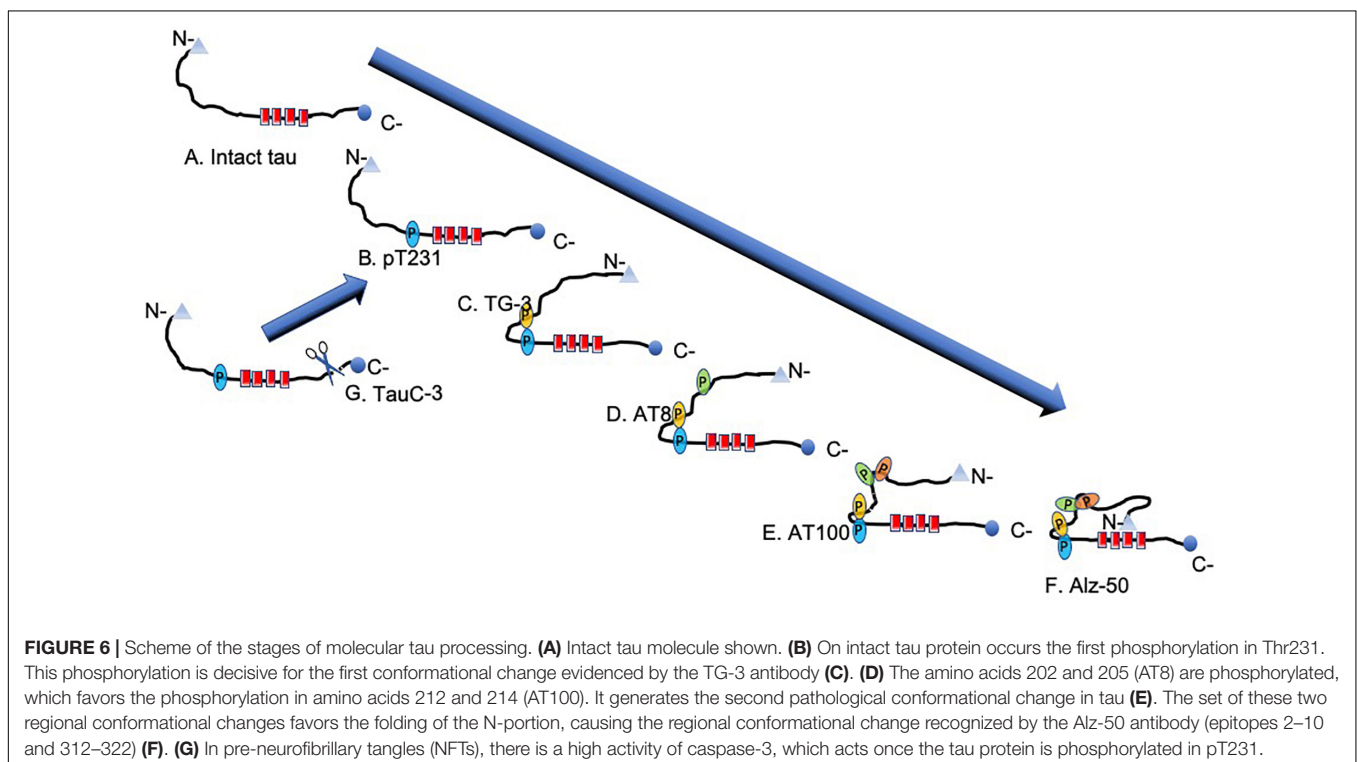
Tau protein undergoes a number of posttranslational modifications: phosphorylation, truncation, acetylation, methylation, glycosylation, nitration, glycation, and SUMOylation. The hyperphosphorylation and truncation of tau have been extensively studied in relation to the genesis of PHFs.

## Tau Hyperphosphorylation

The concentration of phosphorylated tau is increased by two to threefold in AD compared with healthy controls (Blennow et al., 1995; Vigo-Pelfrey et al., 1995). Tau protein has 85 feasible phosphorylation sites: 45 serine, 35 threonine, and five tyrosine residues. Of these, 30 sites appear to be abnormally phosphorylated (Figure 6). Phosphorylation causes tau to lose affinity for  $\beta$ -tubulin, microtubule depolymerization, and pathological aggregation (Noble et al., 2013; Ercan-Herbst et al., 2019). Phosphorylation of the serine residues 235, 262, 293, 324, and 356 favors detachment of tau from tubulin (Drewes et al., 1995; Liu et al., 2007). The main kinases involved in this process are the glycogen synthase kinase 3 beta (GSK-3 $\beta$ ), cell division protein kinase 5 (CDK5), AMP-activated protein kinase (AMPK), protein kinase A (Guillemin et al., 2005), and FYN (Mandelkow et al., 1992; Morishima-Kawashima and Kosik, 1996; Andorfer and Davies, 2000; Lee et al., 2004; Thornton et al., 2011; Mairret-Coello et al., 2013). The participation of these enzymes in neurodegeneration, however, remains to be established (Noble et al., 2013).

## Tau Truncation

Tau can undergo proteolysis by various enzymes *in vitro*: caspase-6, which cleaves tau between amino acids 13–14 and 402–403; caspase-3 (25–26 and 421–422); calpain (44–45, 230–231, and 242–243); ADAM10 (152–153); thrombin (155–156); and chymotrypsin (197–198) (Amadoro et al., 2020). For the identification of the truncation of tau at aspartate 421, Gamblin et al. (2003a) developed the monoclonal antibody TauC-3. Its characterization on AD brain tissue showed it to have a high



affinity for NFTs and dystrophic neurites (Guillozet-Bongaarts et al., 2005). Meanwhile, Rissman et al. (2004) recognized the same truncation using a polyclonal antibody, which showed reactivity in neurons lacking developed fibrillar structures. In contrast, the minimal nucleus, or PHF core, of the protease-resistant filaments (Wischik et al., 1985) is recognized by the monoclonal antibody 423. This PHF core consists of a fragment of the tau protein with 92–95 amino acids, ending at glutamate 391 (Glu-391). It is made up of three and a half tau domains, phase-shifted with respect to the tandem repeat domains, and is characterized by truncation at Glu-391 and, being highly insoluble, highly resistant to degradation by either formic acid or pronase (Novak et al., 1989; Wischik et al., 1992). Isolation and subsequent characterization of the PHF core showed it to have a C-shaped sub-domain repeating within a helical structure (Wischik et al., 1985, 1988a,b, 1992; Wischik and Crowther, 1986; Mena et al., 1996). Recently, the molecular structure of these C-shaped sub-domains of the PHF core has been established by cryo-electron microscopy (Fitzpatrick et al., 2017). It has been observed *in vitro* that the PHF-core tau is able to form PHFs (Al-Hilaly et al., 2017) and that its overexpression is capable of inducing cell death by apoptosis in COS cell cultures (Fasulo et al., 1998). In AD brains, the PHF core co-locates with intact tau and phosphorylated tau, from pre-NFTs to extracellular NFTs (Flores-Rodriguez et al., 2015). This structure is found in the different stages of the pathological processing of tau (intact, phosphorylated, and tau with conformational changes). It has been suggested that the PHF core favors the capture of intact phosphorylated tau molecules, preventing the neuron from perceiving the truncation in Glu-391 and its apoptosis (Fasulo et al., 1998, 2005).

## CONFORMATIONAL CHANGES OF THE TAU PROTEIN

### Regional Conformational Changes

Posttranslational pathological processing of the tau protein includes regional conformational changes dependent on phosphorylation (Jicha et al., 1997b; Zheng-Fischhofer et al., 1998) and structural changes (Carmel et al., 1996; Jicha et al., 1997a, 1999) dependent on these regional conformational changes (Luna-Munoz et al., 2005, 2007). Some regional conformational changes are characterized by phosphorylated amino acid residues. One of these conformational changes results from phosphorylation at position threonine 231 (Thr-231) and serine 235 (Ser-235), recognized by the TG-3 antibody (Wolozin et al., 1986; **Figure 6**). Meanwhile, the AT100 antibody also recognizes a regional conformational change dependent on the phosphorylation of amino acid residues 202 and 205 and, additionally, 212 and 214. Previous studies, using recombinant tau, determined that the phosphorylation of residues 202 and 205 (recognized by the AT8 antibody) occurs before the phosphorylation of amino acids 212 and 214. In contrast, if amino acids 212 and 214 are phosphorylated first, no regional conformational change occurs, and AT100 shows no reactivity (Zheng-Fischhofer et al., 1998). It has been observed that

the epitopes recognized by the TG-3 (phospho-tau 231–235) antibody are very stable during the evolution of the NFT, similar to pT396 (phospho-tau at amino acid 396), because they are closer to the contiguous portion of the PHF core.

### Structural Conformational Changes

There is a structural conformational change of tau that depends on an intact amino terminal (amino acids 2–10), and the third repeat (312–342). This conformation can be seen using Alz50, an antibody that has been associated with the initial stage of the pathological processing of tau (Jicha et al., 1997a).

## SEQUENCE OF MOLECULAR EVENTS DURING THE AGGREGATION OF TAU PROTEIN IN PHF FORMATION

Pathological aggregation of the tau protein follows a series of structural steps ranging from the formation of a pre-NFT to the formation of an extracellular NFT (**Figures 1B–F, 7**). The pre-NFT, characterized by a diffuse granular form in the cytoplasm (**Figure 1B**), results in a perinuclear staining recognized by some phosphorylated epitopes in the amino terminus and by an intact tau protein. This aggregation has no affinity for the TR dye as it is an assembly marker. The next stage is characterized by the presence of small dense aggregates of tau or small tangles (**Figure 1C**), which are related to the TR dye. These small packages converge and form a trabecula in the neuronal soma (**Figure 1D**). This structure fills the neuronal body, forming an intracellular NFT, which displaces the cell nucleus from its original central position toward the periphery (**Figure 1E**). Finally, these filaments are exposed as extracellular NFTs, which is only detected using the TR dye and the antibody 423 (truncation in Glu-391). This stage is characterized by a loose fibrillar structure in which the cell membrane and the nucleus have been lost (**Figure 1F**; Mena et al., 1991; Galvan et al., 2001; Luna-Munoz et al., 2007). At a molecular level, late events can be seen in NFTs, such as a structural conformational change or truncation in Asp-421 and Glu-391. Truncation at Asp-421 occurs after the conformational change recognized by the antibody Alz-50 (when the tau protein is perfectly assembled in the filament) and culminates with the presence of truncation at Glu-391 (Garcia-Sierra et al., 2003; Guillozet-Bongaarts et al., 2005; Basurto-Islas et al., 2008). However, this model does not take into account of phosphorylation state. The molecular events associated with tau phosphorylation follow a well-defined order (**Figure 6**). However, it is difficult to follow the phosphorylation of tau in the NFTs since, in these structures, the tau protein is found simultaneously in different states of expression and aggregation. Thus, the earliest events are studied in the pre-NFTs (**Figure 6A**). It has been suggested that the first step is the phosphorylation of the tau protein at Thr-231 (**Figure 6B**), followed by the phosphorylation of Ser-235, which leads to the first regional conformational change, detectable using the TG-3 antibody (**Figure 6C**). Subsequently, amino acid residues 202 and 205 become phosphorylated (epitopes recognized by the AT8 antibody) (**Figure 6D**). This modification involves a second



phase of phosphorylation at amino acids 212–214 and a second regional conformational change identified by the AT100 antibody (**Figure 6E**). These changes lead to a structural conformational change recognized by the Alz50 antibody (**Figure 6F**; Luna-Munoz et al., 2007), which requires an intact N-terminus (Carmel et al., 1996; Jicha et al., 1999). The truncation at Asp-421 is observed immediately after phosphorylation at Thr-231 (Luna-Munoz et al., 2007; **Figure 6G**). This suggests that the presence of the truncated tau protein at Asp-421 favors filament polymerization (Gamblin et al., 2003a,b; Yin and Kuret, 2006).

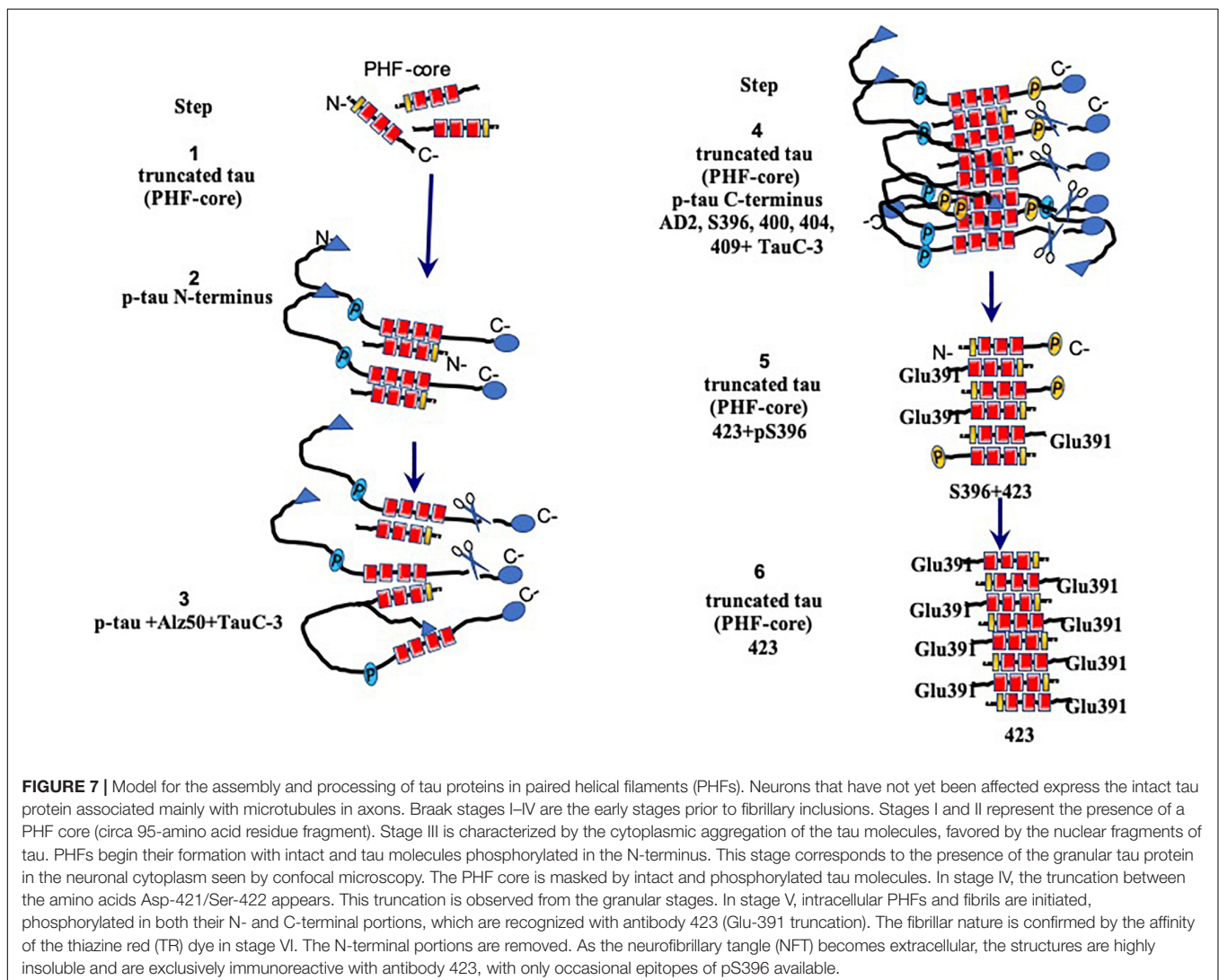
## TEMPLATE TAU PROTEIN IN PHF

We have been investigating the relationship between the different species of phosphorylated and truncated tau protein and the mechanism whereby tau assembles into insoluble and stable PHFs over a period of several years. We have been analyzing pre-tangle cells (**Figure 1B**, arrow), in which the first steps of non-fibrillary aggregation of the tau protein arise in AD. On the basis

of our morphomolecular analysis, we propose the following steps in PHF assembly (**Figure 7**).

- (1) The presence of a PHF core (297–391) is a highly toxic truncated tau species.
- (2) A specific cascade of phosphorylation on the N-terminus of the tau protein (**Figure 6**).
- (3) Truncation of the C-terminus by caspase-3.
- (4) Aggregation and oligomerization of all species of tau.
- (5) Assembly of tau protein in PHFs.

The first event that occurs in the formation of PHFs, and with it the NFTs, would be represented by the appearance (*via* an unknown origin) of subunits of the PHF core (**Figure 7**, step 1). The toxicity of the truncated tau (92–95 amino acids) is associated with the high affinity of the intact tau and the phosphorylated tau to this small fragment (**Figure 7**, step 2), which would trigger an immediate neuroprotective mechanism.





This would be reflected by the hyperphosphorylation of the tau molecule in a failed attempt to hide the PHF core and avoid the kidnapping of the molecules of intact tau. Unfortunately, in AD, the protective mechanism that might be involved in phosphorylated tau protein would only favor that there are more molecules available for its sequestration and the formation of PHF, which represents, finally, a polymer made up of fragments of tau in an intracellular NFT (**Figure 7**, steps 3 and 4). In extracellular NFTs, all phosphorylation is lost as a result of proteolysis, during which the PHF core becomes exposed (**Figure 7**, steps 5 and 6). There are findings suggesting that phosphorylation of the tau protein may have a protective role and be non-toxic (Castellani et al., 2008; Congdon and Duff, 2008; Luna-Munoz et al., 2013; Flores-Rodriguez et al., 2015). This implies that NFTs serve as a protective structure.

## FUTURE STUDY OF TAU PROTEIN

The complete functions of the tau protein remain to be elucidated. Tau is a stabilizing microtubule-associated protein. In the nucleus, this protein protects the DNA in situations of cellular stress; in the nucleolus, it favors the nucleolar function (Sjoberg et al., 2006), the process of mitosis (Flores-Rodriguez et al., 2019) and meiosis (Inoue et al., 2014). Tau has been previously observed in non-neuronal organs such as the heart, skeletal muscle, lung, or skin and in different states of non-pathological phosphorylation (Gu et al., 1996; Zhou et al., 2020). This suggests that tau phosphorylation may be involved in functions yet to be established. Therapeutic approaches to prevent tau phosphorylation could cause problems in these organs. Truncation at Glu-391 appears to be a good differential marker between AD and other neurodegenerative pathologies.

## CONCLUSION

The aggregation and polymerization of the tau protein has been suggested to be a response to pathological events that occur early in neurons and the brain. Tau phosphorylation and NFT formation seem to act as a protective event against the minimal nucleus of the filament (PHF core), which functions as a prion and is highly toxic. Taking into account that NFTs are closely correlated with the cognitive deterioration of patients, it is vitally important to look for other proteins that can define the early onset of AD. Whereas the development of drugs directed against the phosphorylation of the tau protein may involve certain risks, targeting the aggregation of tau proteins with compounds that fail to affect the normal association of tau with microtubules offers another therapeutic target (Wischik et al., 2014; Wilcock et al., 2018). Continued donation of tissue for research will be of utmost importance since it will allow a better understanding of these pathological events and,

ultimately, bring hope of discovering effective methods to both diagnose and cure AD.

## DATA AVAILABILITY STATEMENT

All datasets presented in this study are included in the article/supplementary material.

## ETHICS STATEMENT

The studies involving human participants were reviewed and approved by Ethics Committee, Facultad de Estudios Superiores UNAM. Written informed consent was obtained for the brain donation to National Dementia BioBank.

## AUTHOR CONTRIBUTIONS

MP-H and JL-M contributed to the idea formulation, writing, and revision of the manuscript. CH contributed to the writing and revision of the manuscript. NL-V and BC-C contributed to the images and revision of the manuscript. MO-T, IV-F, PG-O, LG-R, FC, SM-R, and EG-B contributed to the revision of the manuscript. All authors contributed to the article and approved the submitted version.

## FUNDING

This work was supported by Fondo Nacional de Ciencia, Tecnologia, FONDOCYT, from the Ministry of Higher Education, Science and Technology, Dominican Republic (2015-3A2-127 to MP-H and 2018-2019-2A3-208 to JL-M and MP-H).

## ACKNOWLEDGMENTS

We want to express our gratitude to the following: Dr. P. Davies (Albert Einstein College of Medicine, Bronx, NY, United States) and Lester I. Binder<sup>†</sup> (North Western, Chicago, IL, United States) for the generous gifts of mAbs TG-3 and Alz-50, and Tau-1, Tau-5, and Tau-7, respectively; Tec. Amparo Viramontes Pintos for the handling of the brain tissue; Samadhi Moreno-Campuzano for her technical assistance/support in the confocal microscopy unit of CIIDIR Durango, Instituto Politécnico Nacional; Union Medical University Clinic, Dominican Republic, for their support and collaboration in the development of this research project. We also want to express our gratitude to the Mexican families who have donated the brain of their loved ones affected with Alzheimer's disease and made our research possible. This work is dedicated to the memory of Professor Dr. José Raúl Mena López<sup>†</sup>.

<sup>†</sup>Deceased

## REFERENCES

- Al-Hilaly, Y. K., Pollack, S. J., Vadukul, D. M., Citossi, F., Rickard, J. E., Simpson, M., et al. (2017). Alzheimer's disease-like paired helical filament assembly from truncated tau protein is independent of disulfide crosslinking. *J. Mol. Biol.* 429, 3650–3665. doi: 10.1016/j.jmb.2017.09.007
- Amadoro, G., Latina, V., Corsetti, V., and Calissano, P. (2020). N-terminal tau truncation in the pathogenesis of Alzheimer's disease (AD): developing a novel diagnostic and therapeutic approach. *Biochim. Biophys. Acta Mol. Basis Dis.* 1866:165584. doi: 10.1016/j.bbadis.2019.165584
- Andorfer, C. A., and Davies, P. (2000). PKA phosphorylations on tau: developmental studies in the mouse. *Dev. Neurosci.* 22, 303–309. doi: 10.1159/000017454
- Andreadis, A., Brown, W. M., and Kosik, K. S. (1992). Structure and novel exons of the human tau gene. *Biochemistry* 31, 10626–10633. doi: 10.1021/bi00158a027
- Basurto-Islas, G., Luna-Munoz, J., Guillozet-Bongaarts, A. L., Binder, L. I., Mena, R., and Garcia-Sierra, F. (2008). Accumulation of aspartic acid421- and glutamic acid391-cleaved tau in neurofibrillary tangles correlates with progression in Alzheimer disease. *J. Neuropathol. Exp. Neurol.* 67, 470–483. doi: 10.1097/nen.0b013e31817275c7
- Blennow, K., Wallin, A., Agren, H., Spenger, C., Siegfried, J., and Vanmechelen, E. (1995). Tau protein in cerebrospinal fluid: a biochemical marker for axonal degeneration in Alzheimer disease? *Mol. Chem. Neuropathol.* 26, 231–245. doi: 10.1007/bf02815140
- Braak, H., and Braak, E. (1991). Neuropathological staging of Alzheimer-related changes. *Acta Neuropathol.* 82, 239–259. doi: 10.1007/bf00308809
- Bramblett, G. T., Goedert, M., Jakes, R., Merrick, S. E., Trojanowski, J. Q., and Lee, V. M. (1993). Abnormal tau phosphorylation at Ser396 in Alzheimer's disease recapitulates development and contributes to reduced microtubule binding. *Neuron* 10, 1089–1099. doi: 10.1016/0896-6273(93)90057-x
- Carmel, G., Mager, E. M., Binder, L. I., and Kuret, J. (1996). The structural basis of monoclonal antibody Alz50's selectivity for Alzheimer's disease pathology. *J. Biol. Chem.* 271, 32789–32795. doi: 10.1074/jbc.271.51.32789
- Castellani, R. J., Nunomura, A., Lee, H. G., Perry, G., and Smith, M. A. (2008). Phosphorylated tau: toxic, protective, or none of the above. *J. Alzheimers Dis.* 14, 377–383. doi: 10.3233/jad-2008-14404
- Congdon, E. E., and Duff, K. E. (2008). Is tau aggregation toxic or protective? *J. Alzheimers Dis.* 14, 453–457. doi: 10.3233/jad-2008-14415
- Crowther, R. A., and Wischik, C. M. (1985). Image reconstruction of the Alzheimer paired helical filament. *EMBO J.* 4, 3661–3665. doi: 10.1002/j.1460-2075.1985.tb04132.x
- DaRocha-Souto, B., Scotton, T. C., Coma, M., Serrano-Pozo, A., Hashimoto, T., Sereno, L., et al. (2011). Brain oligomeric beta-amyloid but not total amyloid plaque burden correlates with neuronal loss and astrocyte inflammatory response in amyloid precursor protein/tau transgenic mice. *J. Neuropathol. Exp. Neurol.* 70, 360–376. doi: 10.1097/nen.0b013e318217a118
- Drewes, G., Trinczek, B., Illenberger, S., Biernat, J., Schmitt-Ulms, G., Meyer, H. E., et al. (1995). Microtubule-associated protein/microtubule affinity-regulating kinase (p110mark). A novel protein kinase that regulates tau-microtubule interactions and dynamic instability by phosphorylation at the Alzheimer-specific site serine 262. *J. Biol. Chem.* 270, 7679–7688. doi: 10.1074/jbc.270.13.7679
- Ercan-Herbst, E., Ehrig, J., Schondorf, D. C., Behrendt, A., Klaus, B., Gomez Ramos, B., et al. (2019). A post-translational modification signature defines changes in soluble tau correlating with oligomerization in early stage Alzheimer's disease brain. *Acta Neuropathol. Commun.* 7:192.
- Espinosa, B., Zenteno, R., Mena, R., Robitaille, Y., Zenteno, E., and Guevara, J. (2001). O-Glycosylation in sprouting neurons in Alzheimer disease, indicating reactive plasticity. *J. Neuropathol. Exp. Neurol.* 60, 441–448. doi: 10.1093/jnen/60.5.441
- Fasulo, L., Visintin, M., Novak, M., and Cattaneo, A. (1998). Tau truncation in Alzheimer's disease: encompassing PHF core tau induces apoptosis in COS cells. *Alzheimers Rep.* 1, 25–32.
- Fasulo, L., Ugolini, G., and Cattaneo, A. (2005). Apoptotic effect of caspase-3 cleaved tau in hippocampal neurons and its potentiation by tau FTDP-mutation N279K. *J. Alzheimer Dis.* 7, 3–13.
- Fitzpatrick, A. W. P., Falcon, B., He, S., Murzin, A. G., Murshudov, G., Garringer, H. J., et al. (2017). Cryo-EM structures of tau filaments from Alzheimer's disease. *Nature* 547, 185–190.
- Flores-Rodriguez, P., Harrington, C. R., Wischik, C. M., Ibarra-Bracamontes, V., Zarco, N., Navarrete, A., et al. (2019). Phospho-tau protein expression in the cell cycle of SH-SY5Y neuroblastoma cells: a morphological study. *J. Alzheimers Dis.* 71, 631–645. doi: 10.3233/jad-190155
- Flores-Rodriguez, P., Ontiveros-Torres, M. A., Cardenas-Aguayo, M. C., Luna-Arias, J. P., Meraz-Rios, M. A., Viramontes-Pintos, A., et al. (2015). The relationship between truncation and phosphorylation at the C-terminus of tau protein in the paired helical filaments of Alzheimer's disease. *Front. Neurosci.* 9:33. doi: 10.3389/fnins.2015.00033
- Galvan, M., David, J. P., Delacourte, A., Luna, J., and Mena, R. (2001). Sequence of neurofibrillary changes in aging and Alzheimer's disease: a confocal study with phospho-tau antibody, AD2. *J. Alzheimers Dis.* 3, 417–425. doi: 10.3233/jad-2001-3409
- Gamblin, T. C., Berry, R. W., and Binder, L. I. (2003a). Modeling tau polymerization in vitro: a review and synthesis. *Biochemistry* 42, 15009–15017. doi: 10.1021/bi035722s
- Gamblin, T. C., Chen, F., Zambrano, A., Abrahama, A., Lagalwar, S., Guillozet, A. L., et al. (2003b). Caspase cleavage of tau: linking amyloid and neurofibrillary tangles in Alzheimer's disease. *Proc. Natl. Acad. Sci. U.S.A.* 100, 10032–10037. doi: 10.1073/pnas.1630428100
- Garcia-Sierra, F., Ghoshal, N., Quinn, B., Berry, R. W., and Binder, L. I. (2003). Conformational changes and truncation of tau protein during tangle evolution in Alzheimer's disease. *J. Alzheimers Dis.* 5, 65–77. doi: 10.3233/jad-2003-5201
- Ginsberg, S. D., Che, S., Counts, S. E., and Mufson, E. J. (2006). Shift in the ratio of three-repeat tau and four-repeat tau mRNAs in individual cholinergic basal forebrain neurons in mild cognitive impairment and Alzheimer's disease. *J. Neurochem.* 96, 1401–1408. doi: 10.1111/j.1471-4159.2005.03641.x
- Goedert, M., Spillantini, M. G., Jakes, R., Rutherford, D., and Crowther, R. A. (1989a). Multiple isoforms of human microtubule-associated protein tau: sequences and localization in neurofibrillary tangles of Alzheimer's disease. *Neuron* 3, 519–526. doi: 10.1016/0896-6273(89)90210-9
- Goedert, M., Spillantini, M. G., Potier, M. C., Ulrich, J., and Crowther, R. A. (1989b). Cloning and sequencing of the cDNA encoding an isoform of microtubule-associated protein tau containing four tandem repeats: differential expression of tau protein mRNAs in human brain. *EMBO J.* 8, 393–399. doi: 10.1002/j.1460-2075.1989.tb03390.x
- Goedert, M., Wischik, C. M., Crowther, R. A., Walker, J. E., and Klug, A. (1988). Cloning and sequencing of the cDNA encoding a core protein of the paired helical filament of Alzheimer disease: identification as the microtubule-associated protein tau. *Proc. Natl. Acad. Sci. U.S.A.* 85, 4051–4055. doi: 10.1073/pnas.85.11.4051
- Gu, Y., Oyama, F., and Ihara, Y. (1996). Tau is widely expressed in rat tissues. *J. Neurochem.* 67, 1235–1244. doi: 10.1046/j.1471-4159.1996.67031235.x
- Guevara, J., Espinosa, B., Zenteno, E., Vazquez, L., Luna, J., Perry, G., et al. (1998). Altered glycosylation pattern of proteins in Alzheimer disease. *J. Neuropathol. Exp. Neurol.* 57, 905–914. doi: 10.1097/00005072-199810000-00003
- Guillemin, I., Becker, M., Ociepa, K., Friauf, E., and Nothwang, H. G. (2005). A subcellular prefractionation protocol for minute amounts of mammalian cell cultures and tissue. *Proteomics* 5, 35–45. doi: 10.1002/pmic.200400892
- Guillozet-Bongaarts, A. L., Garcia-Sierra, F., Reynolds, M. R., Horowitz, P. M., Fu, Y., Wang, T., et al. (2005). Tau truncation during neurofibrillary tangle evolution in Alzheimer's disease. *Neurobiol. Aging* 26, 1015–1022. doi: 10.1016/j.neurobiolaging.2004.09.019
- Hayes, A., Thaker, U., Iwatsubo, T., Pickering-Brown, S. M., and Mann, D. M. (2002). Pathological relationships between microglial cell activity and tau and amyloid beta protein in patients with Alzheimer's disease. *Neurosci. Lett.* 331, 171–174. doi: 10.1016/s0304-3940(02)00888-1
- Himmler, A. (1989). Structure of the bovine tau gene: alternatively spliced transcripts generate a protein family. *Mol. Cell. Biol.* 9, 1389–1396. doi: 10.1128/mcb.9.4.1389
- Inoue, H., Hiradate, Y., Shirakata, Y., Kanai, K., Kosaka, K., Gotoh, A., et al. (2014). Site-specific phosphorylation of Tau protein is associated with deacetylation of microtubules in mouse spermatogenic cells during meiosis. *FEBS Lett.* 588, 2003–2008. doi: 10.1016/j.febslet.2014.04.021

- Iwatsubo, T., Odaka, A., Suzuki, N., Mizusawa, H., Nukina, N., and Ihara, Y. (1994). Visualization of A beta 42(43) and A beta 40 in senile plaques with end-specific A beta monoclonals: evidence that an initially deposited species is A beta 42(43). *Neuron* 13, 45–53. doi: 10.1016/0896-6273(94)90458-8
- Jakes, R., Novak, M., Davison, M., and Wischik, C. M. (1991). Identification of 3- and 4-repeat tau isoforms within the PHF in Alzheimer's disease. *EMBO J.* 10, 2725–2729. doi: 10.1002/j.1460-2075.1991.tb07820.x
- Jarrett, J. T., Berger, E. P., and Lansbury, P. T. Jr. (1993). The C-terminus of the beta protein is critical in amyloidogenesis. *Ann. N. Y. Acad. Sci.* 695, 144–148.
- Jekabsone, A., Mander, P. K., Tickler, A., Sharpe, M., and Brown, G. C. (2006). Fibrillar beta-amyloid peptide Abeta1-40 activates microglial proliferation via stimulating TNF-alpha release and H2O2 derived from NADPH oxidase: a cell culture study. *J. Neuroinflammation* 3:24.
- Jicha, G. A., Berenfeld, B., and Davies, P. (1999). Sequence requirements for formation of conformational variants of tau similar to those found in Alzheimer's disease. *J. Neurosci. Res.* 55, 713–723. doi: 10.1002/(sici)1097-4547(19990315)55:6<713::aid-jnr6>3.0.co;2-g
- Jicha, G. A., Bowser, R., Kazam, I. G., and Davies, P. (1997a). Alz-50 and MC-1, a new monoclonal antibody raised to paired helical filaments, recognize conformational epitopes on recombinant tau. *J. Neurosci. Res.* 48, 128–132. doi: 10.1002/(sici)1097-4547(19970415)48:2<128::aid-jnr5>3.0.co;2-e
- Jicha, G. A., Lane, E., Vincent, I., Otvos, L. Jr., Hoffmann, R., Davies, P., et al. (1997b). A conformation- and phosphorylation-dependent antibody recognizing the paired helical filaments of Alzheimer's disease. *J. Neurochem.* 69, 2087–2095. doi: 10.1046/j.1471-4159.1997.69052087.x
- Kapaki, E., Liappas, I., Paraskevas, G. P., Theotoka, I., and Rabavilas, A. (2005). The diagnostic value of tau protein, beta-amyloid (1-42) and their ratio for the discrimination of alcohol-related cognitive disorders from Alzheimer's disease in the early stages. *Int. J. Geriatr. Psychiatry* 20, 722–729. doi: 10.1002/gps.1351
- Kelenyi, G. (1967). Thioflavin S fluorescent and Congo red anisotropic stainings in the histologic demonstration of amyloid. *Acta Neuropathol.* 7, 336–348. doi: 10.1007/bf00688089
- Lee, C. Y., and Landreth, G. E. (2010). The role of microglia in amyloid clearance from the AD brain. *J. Neural Transm.* 117, 949–960. doi: 10.1007/s00702-010-0433-4
- Lee, G., Cowan, N., and Kirschner, M. (1988). The primary structure and heterogeneity of tau protein from mouse brain. *Science* 239, 285–288. doi: 10.1126/science.3122323
- Lee, G., Thangavel, R., Sharma, V. M., Litersky, J. M., Bhaskar, K., Fang, S. M., et al. (2004). Phosphorylation of tau by fyn: implications for Alzheimer's disease. *J. Neurosci.* 24, 2304–2312. doi: 10.1523/jneurosci.4162-03.2004
- Lindwall, G., and Cole, R. D. (1984). Phosphorylation affects the ability of tau protein to promote microtubule assembly. *J. Biol. Chem.* 259, 5301–5305.
- Liu, F., and Gong, C. X. (2008). Tau exon 10 alternative splicing and tauopathies. *Mol. Neurodegener.* 3:8. doi: 10.1186/1750-1326-3-8
- Liu, F., Li, B., Tung, E. J., Grundke-Iqbal, I., Iqbal, K., and Gong, C. X. (2007). Site-specific effects of tau phosphorylation on its microtubule assembly activity and self-aggregation. *Eur. J. Neurosci.* 26, 3429–3436. doi: 10.1111/j.1460-9568.2007.05955.x
- Luna-Munoz, J., Chavez-Macias, L., Garcia-Sierra, F., and Mena, R. (2007). Earliest stages of tau conformational changes are related to the appearance of a sequence of specific phospho-dependent tau epitopes in Alzheimer's disease. *J. Alzheimers Dis.* 12, 365–375. doi: 10.3233/jad-2007-12410
- Luna-Munoz, J., Garcia-Sierra, F., Falcon, V., Menendez, I., Chavez-Macias, L., and Mena, R. (2005). Regional conformational change involving phosphorylation of tau protein at the Thr231, precedes the structural change detected by Alz-50 antibody in Alzheimer's disease. *J. Alzheimers Dis.* 8, 29–41. doi: 10.3233/jad-2005-8104
- Luna-Munoz, J., Harrington, C. R., Wischik, C. M., Flores-Rodriguez, P., Avila, J., Zamudio, S., et al. (2013). "Phosphorylation of Tau protein associated as a protective mechanism in the presence of toxic, c-terminally truncated Tau in Alzheimer's disease," in *Understanding Alzheimer's Disease*, ed. I. Zerr (London: IntechOpen), 89–107.
- Luna-Munoz, J., Peralta-Ramirez, J., Chavez-Macias, L., Harrington, C. R., Wischik, C. M., and Mena, R. (2008). Thiazin red as a neuropathological tool for the rapid diagnosis of Alzheimer's disease in tissue imprints. *Acta Neuropathol.* 116, 507–515. doi: 10.1007/s00401-008-0431-x
- Mairet-Coello, G., Courchet, J., Pieraut, S., Courchet, V., Maximov, A., and Polleux, F. (2013). The CAMKK2-AMPK kinase pathway mediates the synaptotoxic effects of Abeta oligomers through Tau phosphorylation. *Neuron* 78, 94–108. doi: 10.1016/j.neuron.2013.02.003
- Mandelkow, E. M., Drewes, G., Biernat, J., Gustke, N., Van Lint, J., Vandenheede, J. R., et al. (1992). Glycogen synthase kinase-3 and the Alzheimer-like state of microtubule-associated protein tau. *FEBS Lett.* 314, 315–321. doi: 10.1016/0014-5793(92)81496-9
- Mena, R., Edwards, P., Perez-Olvera, O., and Wischik, C. M. (1995). Monitoring pathological assembly of tau and beta-amyloid proteins in Alzheimer's disease. *Acta Neuropathol.* 89, 50–56. doi: 10.1007/s004010050215
- Mena, R., Edwards, P. C., Harrington, C. R., Mukaetova-Ladinska, E. B., and Wischik, C. M. (1996). Staging the pathological assembly of truncated tau protein into paired helical filaments in Alzheimer's disease. *Acta Neuropathol.* 91, 633–641. doi: 10.1007/s004010050477
- Mena, R., Wischik, C. M., Novak, M., Milstein, C., and Cuello, A. C. (1991). A progressive deposition of paired helical filaments (PHF) in the brain characterizes the evolution of dementia in Alzheimer's disease. An immunocytochemical study with a monoclonal antibody against the PHF core. *J. Neuropathol. Exp. Neurol.* 50, 474–490. doi: 10.1097/00005072-199107000-00008
- Morishima-Kawashima, M., and Kosik, K. S. (1996). The pool of map kinase associated with microtubules is small but constitutively active. *Mol. Biol. Cell* 7, 893–905. doi: 10.1091/mbc.7.6.893
- Neve, R. L., Harris, P., Kosik, K. S., Kurnit, D. M., and Donlon, T. A. (1986). Identification of cDNA clones for the human microtubule-associated protein tau and chromosomal localization of the genes for tau and microtubule-associated protein 2. *Brain Res.* 387, 271–280. doi: 10.1016/0169-328x(86)90033-1
- Noble, W., Hanger, D. P., Miller, C. C., and Lovestone, S. (2013). The importance of tau phosphorylation for neurodegenerative diseases. *Front. Neurol.* 4:83. doi: 10.3389/fneur.2013.00083
- Novak, M., Wischik, C. M., Edwards, P., Pannell, R., and Milstein, C. (1989). Characterisation of the first monoclonal antibody against the pronase resistant core of the Alzheimer PHF. *Prog. Clin. Biol. Res.* 317, 755–761.
- Perl, D. P. (2010). Neuropathology of Alzheimer's disease. *Mt Sinai J. Med.* 77, 32–42.
- Polanco, J. C., Li, C., Bodea, L. G., Martinez-Marmol, R., Meunier, F. A., and Gotz, J. (2018). Amyloid-beta and tau complexity - towards improved biomarkers and targeted therapies. *Nat. Rev. Neurol.* 14, 22–39. doi: 10.1038/nrneurol.2017.162
- Rissman, R. A., Poon, W. W., Blurton-Jones, M., Oddo, S., Torp, R., Vitek, M. P., et al. (2004). Caspase-cleavage of tau is an early event in Alzheimer disease tangle pathology. *J. Clin. Invest.* 114, 121–130. doi: 10.1172/jci200420640
- Schweers, O., Schonbrunn-Hanebeck, E., Marx, A., and Mandelkow, E. (1994). Structural studies of tau protein and Alzheimer paired helical filaments show no evidence for beta-structure. *J. Biol. Chem.* 269, 24290–24297.
- Serrano-Pozo, A., Mielke, M. L., Gomez-Isla, T., Betensky, R. A., Growdon, J. H., Frosch, M. P., et al. (2011). Reactive glia not only associates with plaques but also parallels tangles in Alzheimer's disease. *Am. J. Pathol.* 179, 1373–1384. doi: 10.1016/j.ajpath.2011.05.047
- Sjoberg, M. K., Shestakova, E., Mansuroglu, Z., Maccioni, R. B., and Bonnefoy, E. (2006). Tau protein binds to pericentromeric DNA: a putative role for nuclear tau in nucleolar organization. *J. Cell. Sci.* 119, 2025–2034. doi: 10.1242/jcs.02907
- Steiner, B., Mandelkow, E. M., Biernat, J., Gustke, N., Meyer, H. E., Schmidt, B., et al. (1990). Phosphorylation of microtubule-associated protein tau: identification of the site for Ca2(+)-calmodulin dependent kinase and relationship with tau phosphorylation in Alzheimer tangles. *EMBO J.* 9, 3539–3544. doi: 10.1002/j.1460-2075.1990.tb07563.x
- Stiller, D., Katenkamp, D., and Thoss, K. (1970). [Fluorescence histochemistry demonstration of amyloid with thioflavin S and acridine orange]. *Acta Histochem.* 38, 18–30.
- Thornton, C., Bright, N. J., Sastre, M., Muckett, P. J., and Carling, D. (2011). AMP-activated protein kinase (AMPK) is a tau kinase, activated in response to amyloid beta-peptide exposure. *Biochem. J.* 434, 503–512. doi: 10.1042/bj20101485

- Uchihara, T. (2014). Pretangles and neurofibrillary changes: similarities and differences between AD and CBD based on molecular and morphological evolution. *Neuropathology* 34, 571–577. doi: 10.1111/neup.12108
- Uchihara, T., Hara, M., Nakamura, A., and Hirokawa, K. (2012). Tangle evolution linked to differential 3- and 4-repeat tau isoform deposition: a double immunofluorolabeling study using two monoclonal antibodies. *Histochem. Cell. Biol.* 137, 261–267. doi: 10.1007/s00418-011-0891-2
- Uematsu, M., Nakamura, A., Ebashi, M., Hirokawa, K., Takahashi, R., and Uchihara, T. (2018). Brainstem tau pathology in Alzheimer's disease is characterized by increase of three repeat tau and independent of amyloid beta. *Acta Neuropathol. Commun.* 6:1.
- Vigo-Pelfrey, C., Seubert, P., Barbour, R., Blomquist, C., Lee, M., Lee, D., et al. (1995). Elevation of microtubule-associated protein tau in the cerebrospinal fluid of patients with Alzheimer's disease. *Neurology* 45, 788–793. doi: 10.1212/wnl.45.4.788
- Wilcock, G. K., Gauthier, S., Frisoni, G. B., Jia, J., Hardlund, J. H., Moebius, H. J., et al. (2018). Potential of low dose leuco-methylthioninium bis(Hydromethanesulphonate) (LMTM) monotherapy for treatment of mild Alzheimer's disease: cohort analysis as modified primary outcome in a phase III clinical trial. *J. Alzheimers Dis.* 61, 435–457. doi: 10.3233/jad-170560
- Wischik, C. M., and Crowther, R. A. (1986). Subunit structure of the Alzheimer tangle. *Br. Med. Bull.* 42, 51–56. doi: 10.1093/oxfordjournals.bmb.a072098
- Wischik, C. M., Crowther, R. A., Stewart, M., and Roth, M. (1985). Subunit structure of paired helical filaments in Alzheimer's disease. *J. Cell. Biol.* 100, 1905–1912.
- Wischik, C. M., Harrington, C. R., Mukaetova-Ladinska, E. B., Novak, M., Edwards, P. C., and McArthur, F. K. (1992). Molecular characterization and measurement of Alzheimer's disease pathology: implications for genetic and environmental aetiology. *Ciba Found Symp.* 169, 268–302. doi: 10.1002/9780470514306.ch16
- Wischik, C. M., Harrington, C. R., and Storey, J. M. (2014). Tau-aggregation inhibitor therapy for Alzheimer's disease. *Biochem. Pharmacol.* 88, 529–539. doi: 10.1016/j.bcp.2013.12.008
- Wischik, C. M., Novak, M., Edwards, P. C., Klug, A., Tichelaar, W., and Crowther, R. A. (1988a). Structural characterization of the core of the paired helical filament of Alzheimer disease. *Proc. Natl. Acad. Sci. U.S.A.* 85, 4884–4888. doi: 10.1073/pnas.85.13.4884
- Wischik, C. M., Novak, M., Thøgersen, H. C., Edwards, P. C., Runswick, M. J., Jakes, R., et al. (1988b). Isolation of a fragment of tau derived from the core of the paired helical filament of Alzheimer disease. *Proc. Natl. Acad. Sci. U.S.A.* 85, 4506–4510. doi: 10.1073/pnas.85.12.4506
- Wolozin, B. L., Pruchnicki, A., Dickson, D. W., and Davies, P. (1986). A neuronal antigen in the brains of Alzheimer patients. *Science* 232, 648–650. doi: 10.1126/science.3083509
- Yin, H., and Kuret, J. (2006). C-terminal truncation modulates both nucleation and extension phases of tau fibrillization. *FEBS Lett.* 580, 211–215. doi: 10.1016/j.febslet.2005.11.077
- Zheng-Fischhofer, Q., Biernat, J., Mandelkow, E. M., Illenberger, S., Godemann, R., and Mandelkow, E. (1998). Sequential phosphorylation of Tau by glycogen synthase kinase-3 $\beta$  and protein kinase A at Thr212 and Ser214 generates the Alzheimer-specific epitope of antibody AT100 and requires a paired-helical-filament-like conformation. *Eur. J. Biochem.* 252, 542–552. doi: 10.1046/j.1432-1327.1998.2520542.x
- Zhou, J., Yu, Q., and Zou, T. (2008). Alternative splicing of exon 10 in the tau gene as a target for treatment of tauopathies. *BMC Neurosci.* 9(Suppl. 2):S10. doi: 10.1186/1471-2202-9-S2-S10
- Zhou, R., Hu, W., Dai, C. L., Gong, C. X., Iqbal, K., Zhu, D., et al. (2020). Expression of microtubule associated protein tau in mouse pancreatic islets is restricted to autonomic nerve fibers. *J. Alzheimers Dis.* 75, 1339–1349. doi: 10.3233/jad-200101

**Conflict of Interest:** CH is an officer of TauRx Therapeutics Ltd. and an inventor on patents relating to tau-aggregation inhibitors.

The remaining authors declare that the research was conducted in the absence of any commercial or financial relationships that could construed as a potential conflict of interest.

Copyright © 2020 Luna-Viramontes, Campa-Córdoba, Ontiveros-Torres, Harrington, Villanueva-Fierro, Guadarrama-Ortiz, Garcés-Ramírez, de la Cruz, Hernandez-Alejandro, Martínez-Robles, González-Ballesteros, Pacheco-Herrero and Luna-Muñoz. This is an open-access article distributed under the terms of the Creative Commons Attribution License (CC BY). The use, distribution or reproduction in other forums is permitted, provided the original author(s) and the copyright owner(s) are credited and that the original publication in this journal is cited, in accordance with accepted academic practice. No use, distribution or reproduction is permitted which does not comply with these terms.



# Advantages of publishing in Frontiers



## OPEN ACCESS

Articles are free to read  
for greatest visibility  
and readership



## FAST PUBLICATION

Around 90 days  
from submission  
to decision



## HIGH QUALITY PEER-REVIEW

Rigorous, collaborative,  
and constructive  
peer-review



## TRANSPARENT PEER-REVIEW

Editors and reviewers  
acknowledged by name  
on published articles

## Frontiers

Avenue du Tribunal-Fédéral 34  
1005 Lausanne | Switzerland

Visit us: [www.frontiersin.org](http://www.frontiersin.org)

Contact us: [frontiersin.org/about/contact](http://frontiersin.org/about/contact)



## REPRODUCIBILITY OF RESEARCH

Support open data  
and methods to enhance  
research reproducibility



## DIGITAL PUBLISHING

Articles designed  
for optimal readership  
across devices



## FOLLOW US

@frontiersin



## IMPACT METRICS

Advanced article metrics  
track visibility across  
digital media



## EXTENSIVE PROMOTION

Marketing  
and promotion  
of impactful research



## LOOP RESEARCH NETWORK

Our network  
increases your  
article's readership